WOODHEAD PUBLISHING SERIES IN ENERGY

Steam Generators for Nuclear Power Plants

Edited by Jovica Riznic

WP
WOODHEAD PUBLISHING

Steam Generators for Nuclear Power Plants

Related titles

Nuclear Power Plant Safety and Mechanical Integrity: Design and Operability of Mechanical Systems, Equipment and Supporting Structures
(ISBN 978-0-12-417248-7)

Nuclear Corrosion Science and Engineering
(ISBN 978-1-84569-765-5)

Nuclear Corrosion Modeling: The Nature of CRUD
(ISBN 978-1-85617-802-0)

Woodhead Publishing Series in Energy

Steam Generators for Nuclear Power Plants

Edited by

Jovica Riznic

ELSEVIER

WP
WOODHEAD
PUBLISHING
An imprint of Elsevier

Woodhead Publishing is an imprint of Elsevier
The Officers' Mess Business Centre, Royston Road, Duxford, CB22 4QH, United Kingdom
50 Hampshire Street, 5th Floor, Cambridge, MA 02139, United States
The Boulevard, Langford Lane, Kidlington, OX5 1GB, United Kingdom

© 2017 Elsevier Ltd. All rights reserved.

No part of this publication may be reproduced or transmitted in any form or by any means, electronic or mechanical, including photocopying, recording, or any information storage and retrieval system, without permission in writing from the publisher. Details on how to seek permission, further information about the Publisher's permissions policies and our arrangements with organizations such as the Copyright Clearance Center and the Copyright Licensing Agency, can be found at our website: www.elsevier.com/permissions.

This book and the individual contributions contained in it are protected under copyright by the Publisher (other than as may be noted herein).

Notices
Knowledge and best practice in this field are constantly changing. As new research and experience broaden our understanding, changes in research methods, professional practices, or medical treatment may become necessary.

Practitioners and researchers must always rely on their own experience and knowledge in evaluating and using any information, methods, compounds, or experiments described herein. In using such information or methods they should be mindful of their own safety and the safety of others, including parties for whom they have a professional responsibility.

To the fullest extent of the law, neither the Publisher nor the authors, contributors, or editors, assume any liability for any injury and/or damage to persons or property as a matter of products liability, negligence or otherwise, or from any use or operation of any methods, products, instructions, or ideas contained in the material herein.

Library of Congress Cataloging-in-Publication Data
A catalog record for this book is available from the Library of Congress

British Library Cataloguing-in-Publication Data
A catalogue record for this book is available from the British Library

ISBN: 978-0-08-100894-2 (print)
ISBN: 978-0-08-100928-4 (online)

For information on all Woodhead publications
visit our website at https://www.elsevier.com/books-and-journals

ELSEVIER
Book Aid International
Working together to grow libraries in developing countries
www.elsevier.com • www.bookaid.org

Publisher: Joe Hayton
Acquisition Editor: Maria Convey
Editorial Project Manager: Ashlie Jackman
Production Project Manager: Omer Mukthar
Cover Designer: Greg Harris

Typeset by SPi Global, India

Contents

List of contributors xi
Preface xiii

Part One Design and manufacturing 1

1 Introduction to steam generators—from Heron of Alexandria to nuclear power plants: Brief history and literature survey 3
J. Riznic
1.1 Introduction 3
1.2 Brief history of steam generation 5
1.3 Splitting of the atom and emergence of nuclear power: Atoms join water and steam 11
1.4 Unique features of different steam generators 16
1.5 Steam generators literature survey 27
References 31
Further reading 33

2 Nuclear steam generator design 35
J.C. Smith
2.1 Introduction 35
2.2 Specifications 35
2.3 Tube bundle 36
2.4 Overall steam generator layout 40
2.5 Circulation 41
2.6 Other elements of the circulation system 46
2.7 Feedwater inlet 49
2.8 Pressure boundary design 50
2.9 Conclusions 53

3 Steam generator manufacturing 55
J.C. Smith
3.1 Introduction, manufacturers 55
3.2 Manufacturing scheduling 58
3.3 Main sub-assemblies 60
3.4 Major assemblies 68
3.5 Final assembly and preparation for shipment 73

3.6 Stress reliefs **77**
3.7 Inspection and testing **78**
3.8 Shipment **79**
3.9 Conclusions **80**

4 Thermalhydraulics, circulation, and steam-water separation in nuclear steam generators 81
S. Laroche
4.1 Introduction **81**
4.2 Recirculating steam generators **81**
4.3 Once-through steam generators **101**
Acknowledgments **104**
References **104**

5 WWER steam generators 107
L. Papp, J. Vacek
5.1 Description of WWER steam generators **107**
5.2 SGs degradation **107**
5.3 WWER SGs modifications **113**
5.4 Integrity of heat exchange tubes **117**
References **124**

Part Two Operation and maintenance 125

6 Steam-water cycle chemistry relevant to nuclear steam generators 127
A. Drexler
6.1 Introduction **127**
6.2 Water chemistry treatments **134**
6.3 Additional water chemistry measures for high SG performance **138**
6.4 Water chemistry monitoring and control program **149**
6.5 Summary **150**
References **151**

7 Corrosion problems affecting steam generator tubes in commercial water-cooled nuclear power plants 155
J.A. Gorman
7.1 Introduction **155**
7.2 Primary side stress corrosion cracking (PWSCC) **162**
7.3 Denting **165**
References **178**

8 Environmental degradations in PWR steam generators 183
I. de Curieres
Acronyms **183**
8.1 Introduction **183**

8.2 Primary side environmental effects **184**
8.3 Secondary side environmental effects **194**
8.4 Conclusions **207**
References **207**

9 Corrosion product transport and fouling in nuclear steam generators 215
C.W. Turner, K. Khumsa-Ang
9.1 Introduction **215**
9.2 SG design and the effect of fouling on performance degradation **216**
9.3 Corrosion product transport **221**
9.4 Fouling of nuclear SGs—plant experience **239**
9.5 Fouling mechanisms—fundamental studies and modeling **250**
9.6 Mitigating fouling of nuclear SGs—field studies **257**
9.7 Summary and conclusions **262**
References **263**

10 Hideout, hideout return and crevice chemistry in nuclear steam generators 273
C.W. Turner, M. Huang, A. McKay
10.1 Introduction **273**
10.2 Hideout and hideout return in flow-restricted regions **274**
10.3 Chemistry environment in flow-restricted regions **291**
10.4 Plant hideout return studies **303**
10.5 Summary and conclusions **315**
References **317**

11 Deposit accumulation in PWR steam generators 323
Robert D. Varrin, Jr.
11.1 Overview **323**
11.2 Deposit characterization **334**
11.3 Deposit management **344**
11.4 Mechanical cleaning of PWR SGs **345**
11.5 Chemical cleaning of PWR SGs **351**
11.6 Mild cleaning of PWR SGs **360**
References **363**

12 Thermal performance degradation and heat-transfer fouling 365
M. Kreider, G. White
12.1 Introduction **365**
12.2 Quantifying SG heat-transfer fouling **366**
12.3 Industry trends in SG thermal performance **373**
12.4 Causes of thermal performance changes **378**
12.5 Consequences of SG thermal performance loss **392**
12.6 Effects of corrosion deposit removal **393**
12.7 Conclusion **396**
References **398**

13 Flow-induced vibrations in nuclear steam generators 405
M. Hassan
13.1 Flow characteristics **405**
13.2 Tube vibration characteristics **406**
13.3 Excitation mechanisms **408**
13.4 Estimation of tube bundle integrity **421**
13.5 Recent challenges **430**
13.6 Summary **431**
References **431**

14 Structural integrity assessment of nuclear steam generator 435
S. Majumdar, S. Bakhtiari, Z. Zeng, C.B. Bahn
Acronyms **435**
Symbols **436**
14.1 Introduction **436**
14.2 Structural integrity prediction models **438**
14.3 Structural integrity of U-bends with flaws **454**
14.4 Application of equivalent rectangular crack method **459**
14.5 Conclusions and recommendations for future research **465**
Acknowledgment **467**
References **467**

15 Nuclear steam generator inspection and testing 471
T. Sollier
Acronyms **471**
15.1 Introduction **472**
15.2 ISI techniques and qualification methodology **472**
15.3 In-service inspection **473**
15.4 Water tightness of the tube bundle **485**
15.5 Hydrostatic pressure test **487**
15.6 Future trends for recirculating steam generator maintenance and inspection **488**
15.7 Conclusion **490**
Acknowledgments **490**
References **490**

16 Nuclear steam generator tube inspection tools 495
L. Obrutsky
16.1 Introduction **495**
16.2 Historical perspective **495**
16.3 Inspection tools **496**
16.4 Data analysis **503**
16.5 Technique qualification **504**
16.6 Data management **504**
16.7 Advanced and automatic analysis techniques **505**

16.8 Inspection requirements and scope **506**
16.9 Summary/Conclusions **507**
Acknowledgments **508**
References **508**

17 Nuclear steam generator fitness-for-service assessment 511
L.B. Carroll
17.1 Overview **511**
17.2 Repair criteria for steam generator tubes **511**
17.3 Steam generator tube degradation assessment **513**
17.4 Performance criteria for steam generator tubes **514**
References **522**

18 Regulatory requirements and considerations for nuclear steam generators 525
E.L. Murphy
18.1 Introduction **525**
18.2 Regulatory requirements and considerations for nuclear SGs in the United States **525**
18.3 Regulatory practices and tubing inspection requirements in Canada **541**
References **545**

Index 549

This page intentionally left blank

List of contributors

C.B. Bahn Pusan National University, Busan, Republic of Korea

S. Bakhtiari Argonne National Laboratory, Lemont, IL, United States

L.B. Carroll Canadian Nuclear Safety Commission, Ottawa, ON, Canada

I. de Curieres IRSN, Fontenay-aux-Roses, France

A. Drexler AREVA GmbH, Erlangen, Germany

J.A. Gorman Dominion Engineering, Inc., Reston, VA, United States

M. Hassan School of Engineering University of Guelph, Guelph, ON, Canada

M. Huang Canadian Nuclear Laboratories, Chalk River, ON, Canada

K. Khumsa-Ang Canadian Nuclear Laboratories, Chalk River, ON, Canada

M. Kreider Dominion Engineering, Inc., Reston, VA, United States

S. Laroche Canadian Nuclear Laboratories, Chalk River, ON, Canada

S. Majumdar Argonne National Laboratory, Lemont, IL, United States

A. McKay Tottenham, ON, Canada

E.L. Murphy CONSULTANT, Gaithersburg, MD, USA

L. Obrutsky B. Eng, CGSB ET Level 3 M&O Tech, Deep River, ON, Canada

L. Papp University of West Bohemia, Pilsen, Czech Republic

J. Riznic Canadian Nuclear Safety Commission Operational Engineering Assessment Division, Ottawa, ON, Canada

J.C. Smith Northern Nuclear Industries, Inc., Ayr, ON, Canada

T. Sollier Institut de Radioprotection et de Sûreté Nucléaire-IRSN, Paris, France

C.W. Turner Deep River, ON, Canada

J. Vacek University of West Bohemia, Pilsen, Czech Republic

Robert D. Varrin, Jr. Dominion Engineering, Inc., Reston, VA, United States

G. White Dominion Engineering, Inc., Reston, VA, United States

Z. Zeng Argonne National Laboratory, Lemont, IL, United States

Preface

As of Jan. 2017, there were 450 operational nuclear power plants producing about 392 GWe or 12% of total electricity around the world. Safe and reliable operation of the current fleet of nuclear power plants is essential to ensure continued growth of the nuclear industry despite declines in some traditional markets. In Asia and the Middle East, many new plants are being built, in most cases as a replacement to fossil fuel burning plants. China has an ambitious nuclear program, importing the latest designs, and at the same time emulating path of Japan and Korea by developing its own design alternatives of nuclear power plants. However, given the slow rate of new nuclear builds in North America and Europe, the technical focus there has shifted toward enhancement of power output (uprate), integrated planning, and organization to ensure shorter inspection and maintenance outages and consequently high capacity factors, as well as extending plant life. In an era of cheap natural gas and the lack of credit for noncarbon emitting electricity production, it is often easier and less costly to extend the life of existing power plant than to build new one. Thus, plant refurbishment (replacement of reactor internals and steam generators) continues to be a driver.

Today there are more than 1300 steam generators in good operational condition in those 450 nuclear power plants worldwide. Power plants have anywhere from 2 to 12 steam generators. Steam generator provides a heat sink to cool the reactor while producing steam, but its tubes (between 4000 and 13,000 tubes for a total length of 70–270 km, per steam generator) must also withstand pressure of more than 15 MPa, while maintaining safe and structurally sound barrier between the radioactive reactor coolant and the secondary water/steam flowing to the steam turbine. A steam generator is therefore not only large heat exchanger, but also a pivotal component, that controls dynamic behavior of the whole nuclear power plant, whether under normal operation or upset and incident transients, providing a protective barrier for stable operation and safe plant shutdown.

There has long been a need for a steam generator reference book suitable for working professionals from those working in power generation and utilities operations, to technical service providers, to those working in national and industry labs and other research and development establishments, to finally students, educators, and trainers. The aim of this book is to serve as a concise and timely resource for professionals involved in all phases of nuclear steam generation life cycle, from design, manufacturing, operation and maintenance, and long-term operation. The ultimate goal is to provide an open-domain resource that will enable those new to the nuclear industry, whether a young engineer, a manager, a technical and/or regulatory specialist, or a student, to improve their knowledge of steam generators in nuclear power plants and prepare to continue their journey into more specific areas of interest and

specialization. We wrote this book with intent to cover fundamental engineering aspects and phenomena, as well as practical content, which typically does not appear in technical or scientific journals. The book is not intended to be a steam generator design guide or otherwise prescriptive reference book, but rather to describe technology and industry practices, its growth and what we have learn through operational experience, and current state-of-the-art. The book does not focus on any specific vendor-based technology but rather provides a broad generic technology overview across PWR, VVER, and PHWR nuclear power systems. Some of the most recognized experts worldwide contributed writing chapters from their field, and we sincerely hope that the book will be well received by the professional community at large, particularly among technicians, engineers, and researchers working on steam generators.

I started discussing the idea of this book several years ago with colleagues, experts, and pioneers who defined steam generators as a distinctive engineering and technological field. I am grateful to all contributors who graciously agreed to make their contributions to this book; they did outstanding work and, I alone should bear, as editor, critique for any deficiencies. Least, but definitely not last, on behalf of all contributors, we are grateful to Woodhead Publishing and Elsevier for inviting and providing us with the opportunity to work on this book, and for their continuous encouragement and support in bringing the book to the attention of readers.

I would like to invite readers to share their comments, suggestions, and critiques. This can be done through professional magazines and journals, social media, the publisher, or by sending them directly to me at jriznic@gmail.com.

J. Riznic
Ottawa, ON, Canada

Part One

Design and manufacturing

This page intentionally left blank

Introduction to steam generators—from Heron of Alexandria to nuclear power plants: Brief history and literature survey

1

J. Riznic
Canadian Nuclear Safety Commission Operational Engineering Assessment Division, Ottawa, ON, Canada

Acronyms

CANDU	Canadian deuterium uranium reactor
I600	Inconel 600
I800	Incoloy 800
IAEA	International Atomic Energy Agency
INIS	International Nuclear Information System
M400	Monel 400
NPP	nuclear power plant
OTSG	once-through steam generator
PHWR	pressurized heavy-water reactor
PRIS	power reactor information system
PWR	pressurized water reactor
PWSCC	primary water stress corrosion cracking
SG	steam generator
TSP	tube support plate
VVER	Vodo-Vodyanoj Energeticheskij Reaktor
WIPO	World Intellectual Property Organization

1.1 Introduction

Steam generators (SGs) are large shell and tube heat exchangers, containing several thousand tubes. They transfer heat from the primary reactor coolant to the secondary side to produce steam, which then powers turbine generators to produce electricity. Most nuclear power plants (NPPs) have anywhere from 2 to 6 SGs per reactor; however some designs have up to 12, with a total of more than 1300 SGs being in service in 357 of the total 450 reactors in the world. The performance of SGs is critical to the overall efficiency and safety of an NPP, particularly as plant ages. Operating

Steam Generators for Nuclear Power Plants. http://dx.doi.org/10.1016/B978-0-08-100894-2.00001-7
© 2017 Elsevier Ltd. All rights reserved.

experience has shown that overtime SGs become more susceptible to material degradations, which can affect plant life expectancy and overall safety. Generally, SG tubes must withstand more than 15 MPa of pressure from within the tube, while maintaining a safe and structurally important barrier between the primary and secondary side. Tube damage may decrease the integrity and lead to leakage and possible release of contaminants into the secondary side. The significance of these issues exemplifies the importance of maintenance, inspections, and testing of SG components, especially because of the safety significance of SG tubing (Revankar and Riznic, 2009). As of Jan. 2017, there were 450 operational nuclear reactors in the International Atomic Energy Agency's (IAEA) Power Reactor Information System (PRIS), representing 392 GW of electrical power. Aging is a relevant factor due to the fact that the majority of NPPs within the PRIS database are over 30 years of age. NPPs over the age of 30 are responsible for the highest total net electricity capacity of operational reactors, possessing 251,069 MW of the 392,012 MW of total operational net electricity capacity. However, many older NPPs use a variety of more corrosion-prone materials than used in modern plants, such as mill-annealed Inconel 600 (I600). For economic and safety reasons, a proper understanding of operating experience and plausible degradation mechanisms is of great importance. To understand the future of nuclear SGs, it makes sense to explore past development in steam technology and SGs, and their contribution to the advancement of society by providing carbon-free electricity.

A summary of the history of nuclear SGs was obtained from a variety of sources, with the purpose of detailing the origins of steam-powered technology through its development into NPP SG models (Cormier et al., 2016). The summary presented in this introductory chapter is not comprehensive of all advancements that were made through the development of the steam generation processes, systems, and engineered equipment for power applications; however, many of the milestones such as the first device to produce useful work, the first NPP connected to the grid, or the first patent on nuclear SGs are included. When discussing international experience with SGs, statistics and information are provided on various but most frequently used design types. Nuclear SG types discussed include the most common vertical U-tube design for pressurized water reactors (PWRs), combustion engineering and Korean AP1400 reactors, the straight-tube design of once-through steam generators (OTSGs), SGs for pressurized heavy-water reactors (PHWRs), as well as the horizontal SG design for Vodo-Vodyanoj Energeticheskij Reaktor (VVER) plants. Statistics on SGs were obtained using the IAEA's PRIS database. A search of patents was conducted on The World Intellectual Property Organization's (WIPO) Patentscope database, the purpose being to compare trends in the evolution of SGs. Furthermore, the growth of academic interest in SG related topics was tracked by conducting a literature survey of SG-related publications found in the IAEA's International Nuclear Information System (INIS) database, the Electric Power Research Institute's (EPRI) database, and Elsevier's SCOPUS database of scientific publications.

1.2 Brief history of steam generation

1.2.1 It began with water and steam

Water is source of life and energy. Since ancient times, people have used power derived from falling or fast-running water to support and improve their quality of life. Power extracted from various kinds of watermills and waterfalls has been the driving force for irrigation of agricultural lands and the operation of engineered devices such as grist and sawmills ore mills pumps, or lifting and load moving inventions of particular time. A Greek mathematician and scientist named Heron of Alexandria is readily credited with inventing the first SG back in 62 AD. It was named the Aeolipile, a word derived from *Aeolos* (the Greek god of the winds) and *pilos* (sphere) (Fig. 1.1). The device consisted of a sphere that received steam through tubing along its diameters. This tubing doubled as an axis of rotation for the sphere. The steam was generated in the cauldron and base of the device and released through the L-shaped tubes creating a reaction torque around the axis of rotation of the device. Although the Aeolipile did not produce useful work, it was a pivotal step toward the invention of the contemporary SG (Papadopoulos, 2007). Even today, the fundamental concept for industrial steam generation has remained the same: generate heat; use the heat to boil the water, and collect and use the steam.

1.2.2 The steam engine

Sixteen centuries after Heron of Alexandria, was a man named Jerónimo de Ayanz y Beaumont, who built the first modern steam engine in 1606. His invention was a steam-powered water pump used for draining flooded mines. Although it was probably the first example of steam-powered technology completing useful and practical tasks, Beaumont's innovation is often overshadowed by his more celebrated successors, Savery and Watt. The next notable progression for steam generation technologies was created by Giovanni Brance in 1629, when he experimented with a jet of steam, turning a modified water wheel. The wheel was successfully turned by the power of steam; however, not enough power was generated to do useful work. From there onward, many inventors experimented with steam-powered machines that were not necessarily what we would consider turbines.

Not long after, in 1698, the first steam-powered machine to produce useful work was invented by Thomas Savery. Savery constructed a steam engine whose function was to pump water using the vacuum created by condensing steam. Much like Beaumont's invention, Savery's steam engine was purposed to remove water from mines in Southern England. Later in 1705, Thomas Newcomen designed and constructed an atmospheric engine, which consisted of a piston connected to a large crossbeam. When steam was introduced into a cylinder, the pressure of the steam raised the piston. The process was then reversed by spraying cold water into the cylinder, condensing the steam and lowering the piston back in the cylinder. This up and down

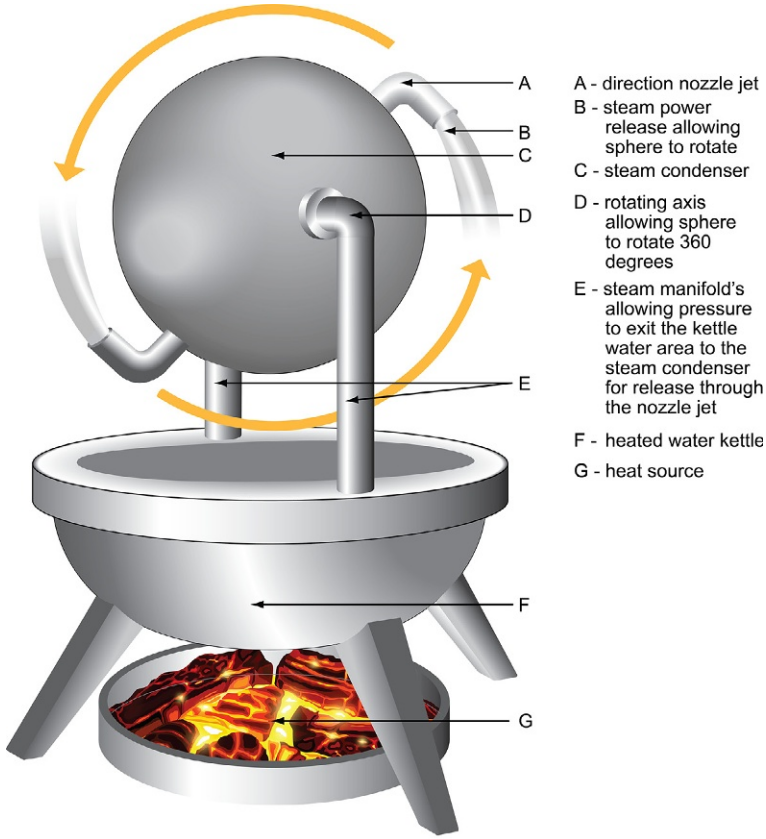

Fig. 1.1 Schematics of Heron's aeolipile.

motion on one end of the crossbeam caused the other end to move in the opposite direction. Such motion operated a pump, generating useful work. In 1765, this design was significantly improved by James Watt, who is often credited as "the father of the steam engine" for his contribution (Gopalakrishnan, 2009).

However, a true change on grand scale happens when people realized that energy derived from steam was much more powerful and versatile than the simple stationary inventions run in their local shops. Using steam is what enabled people to move and bring hydropower to places far from waterfalls and fast-flowing rivers. This period is known as the Industrial Revolution. The development and widespread applications of steam power were by far the greatest technological advances stemming from this period. The Industrial Revolution was the movement of gradual change from the agrarian, hand-labour economy to one driven by machine manufacture, use of steam power, and industrial production of goods. Although used earlier by French writers Louis-Guillaume Otto (1754–1817) and Jerome-Adolphe Blangui (1798–1854), the credit for popularising the term *Industrial Revolution* is attributed to the English

economic historian Arnold Toynbee, whose lecture in 1881 laid down a detailed account of the term (Encyclopedia Britannica, 2017). The year 1760 is generally accepted as the *eve* of the first Industrial Revolution (Encyclopedia Britannica, 2017), even though the economic and social changes occurred gradually and several historians rightfully argue that using the term "revolution" is a misnomer. To that extent, we may argue that this eve actually began more than 17 centuries before, with the very first discovery of potency of power from steaming water by Heron of Alexandria.

Watt's innovative ideas on steam power had large implications, which paved way for the Industrial Revolution. Watt's improvement on Newcomen's design involved altering the mechanism of spray water to increase efficiency. For an effective steam engine, Watt determined that the steam cylinder should be as hot as possible and that the condensation of steam should occur in a separate vessel, marking this birth of the condenser. In 1776, the first two steam engines became commercially operational. Without any doubt, Watt's design was revolutionary, even by today's standards. Because steam engines do not need to be operated on waterways like previous power generation inventions such as the water wheel, they could be set up anywhere. This innovative advantage, among others, established the foundation for the commercial applications of steam engines as the precursor for larger power plants later to come (Zink, 1996) (Fig. 1.2).

In 1680, Dr. Denis Papin (1647–1713), a French inventor, designed a steam digester for food processing, using boiling water under pressure higher than atmospheric. In order to control the buildup of steam pressure and to prevent explosion, Papin also invented the very first safety relief or overpressure protection valve. Papin is well known for his work on steam generation, and in 1690 he published his first work on steam engines in *De novis quibusdam machinis*. The purpose of his steam engine was to raise water to a canal between cities of Kassel and Karlshaven. He also

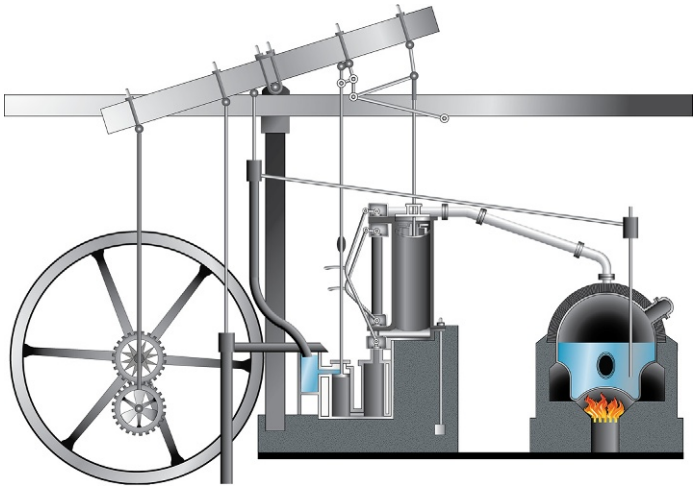

Fig. 1.2 Schematics of Watt's steam engine.

used a steam engine to pump water to a tank on the roof of a palace to supply water for the fountains in the grounds. In 1707, he wrote *The New Art of Pumping Water by using Steam*. To his credit, Papin was a visionary of integrated compact design, proposing the first SG with an internal firebox to burn coal. More than a hundred years later, we saw the development of locomotive SGs, or more commonly referred to as *boilers*.

1.2.3 The steam locomotive

The first successful steam-engine locomotive was invented by British engineer George Stephenson in 1814. The steam engine was capable of hauling up to 30 tons of coal at 6.5 kph (4 mph) going uphill. In 1825, Stephenson also created the first public railway for steam locomotives (Cavendish, 2014). Later in 1830, the locomotive was adopted in the United States of America. The first American steam locomotive was designed by Peter Cooper which hauled 36 passengers and went 18 mph (Franklin Institute, 1885). It is estimated that 176,000 steam locomotives were built for American railroads between 1831 and 1953. There was a peak in 1905, with 6365 engines ordered. As the requirement for larger and faster locomotives began, the size of SGs (boilers) increased. This period began in 1922, referred to as the super power era. In 1937, the fourth generation of locomotives began, which refined the super power machines. However, these machines were not commercially successful as America's railroads transitioned eventually to diesel-electric power (Lamb, 2003).

Those early boilers were direct fire tube boilers and as such limited in capacity. The invention of the locomotive and demand to make larger and faster boats required SGs that could withstand heavier pressure of increased steam capacity while being much safer by reducing the consequences of its explosion. John Cox Stevens invented a tube SG to be used on a Hudson River steam boat. Interestingly, at the end of 18th century, inventors had to go to England to obtain their patents since there were no similar laws to protect intellectual property in North America. John Stevens, being a lawyer, successfully petitioned the U.S. Congress, and in 1790 the U.S. Patent Law was born. In 1803, Stevens received the patent for his design of a water-tube boiler. Patent Law survived and evolved; however Stevens' design of water-tube boiler was short lived due to fundamental engineering problems with design, construction, and operation. Nevertheless, John Cox Stevens should receive proper credit since the basis of present U.S. Patent Laws grew out of the need to protect his design of a water-tube SG (Kitto and Stultz, 2005).

It took almost 50 years after Stevens' water-tube boiler patent was established for a new "disruptive" design solution to stir up and rejuvenate the steam-generation industry. Stephen Wilcox Jr. proposed a revolutionary new design of the water-tube SG, with inclined water tubes. The introduction of inclined tubes increased both the heat transfer surface within furnace and the water circulation inside tubes. Wilcox attached water tubes to collectors (headers) of cold and hot recirculating water and positioned a steam drum at the top of the construction. He partnered with his childhood friend George H. Babcock to create the first SG design and manufacturing company called

Babcock, Wilcox and Company in 1866. The very next year, the U.S. Patent No. 65.042 was granted to George H. Babcock and Steven Wilcox Jr., for their design of a water-tube boiler, which literally revolutionized the steam generation industry (Kitto and Stultz, 2005). The Babcock, Wilcox and Company changed names several times but survived the test of time and remained a true industry leader in the field of steam generation until today.

Sometimes in 1875, Babcock and Wilcox wrote *The Requirements of a Perfect Steam Boiler*. The list comprises 12 characteristics important for the design of a steam boiler. The list is comprehensive and amazingly still contemporarily relevant today for design of modern SGs operating in both fossil fuelled and NPPs. The *Requirements of a Perfect Steam Boiler* consists of the following (Kitto and Stultz, 2005):

> *Proper workmanship and simple construction; using materials that were shown to be the best through experience and to avoid early repairs.*
>
> *A mud drum is used to receive all impurities from the water.*
>
> *Have sufficient steam and water capacity to prevent fluctuation in pressure or water level.*
>
> *Contain a water surface for the disengagement of steam from water in order to prevent foaming.*
>
> *Maintain constant circulation of water through the boiler to ensure the temperature of all parts are the same.*
>
> *Ensure the water space is divided that should any section fail, no explosion will occur, and any destructive effects will be confined.*
>
> *The boiler must be free from strains due to unequal expansion.*
>
> *The combustion chamber must be arranged such that the combustion of the gases started in the furnace may be completed before the gases escape to the chimney.*
>
> *Have the heating surface at a right angle to the currents of heated gases and extract the entire available heat from the gases.*
>
> *For safety and economic reasons, have all parts accessible for cleaning and repairs.*
>
> *The steam boiler should be capable of working to its full rated capacity with the highest economy.*
>
> *Be equipped with the best gauges, safety valves, and other fixtures.*

1.2.4 Early steam boiler explosions

Watt's innovative steam-engine design brought forth many steam boiler designs with higher than atmospheric pressures. Although this was beneficial for efficiency, it carried significant risks that in many cases were not properly planned for or even considered. The first major boiler explosions occurred on steam boats as early as 1817, resulting in dozens of deaths. Despite this, there were no changes in legislation or law. The result of inaction leads to almost 500 deaths in 1838 in the United States alone, all as a result of steam boiler explosions (Burke, 1966). Some major steamboat boiler explosions included an explosion on the steamboat "Moselle," resulting in the

death of 151 citizens in 1938, and an explosion on the steamboat "Sultana," causing the death of over 1200 people (Petroski, 1996). Events like this led to eventual government interventation and the creation of the first codes (technical standards) dictating the design and operation of steamboat boilers; however, nothing was done for stationary steam boilers like those found in factories at the time.

Boiler explosions continued in stationary steam-generating plants; one such event occurred at the Grover Shoe Factory. In 1905, an old boiler at Grover Shoe Factory suffered a steam explosion, propelling it through three floors and the roof of the factory. This caused the factory to collapse and coal from the boiler started multiple fires, leaving workers trapped. In the end there were 58 deaths, 117 injuries, and the factory was completely destroyed (ASME, 2016a). Overall there were thousands of boiler explosions and thousands of deaths throughout the 1800s and early 1900s.

1.2.5 ASME boiler and pressure vessel code

The American Society of Mechanical Engineers (ASME) was initially founded in 1880. Its intention was to serve as a setting to discuss concerns caused by industrialization and mechanization, including boiler explosions. Following the Grover Shoe Factory accident in 1905, the state of Massachusetts formed a Board of Boiler Rules to write new boiler laws for the state, which were completed in 1908. In addition to the boiler laws, ASME sought to further protect the public against boiler accidents and formed a Boiler Code Committee in 1911. Four years later AMSE published their first Boiler and Pressure Vessel Code (BPVC), a single 114-page book (ASME, 2016b). Today, more than 100 years later, the ASME BPVC consists of 28 books with a total of over 16,000 pages. Since its initial publication, this code has been successfully incorporated into laws in most North American territories.

The ASME BPVC eventually found itself entangled in nuclear regulation, starting in 1947 with the creation of several ASME committees working with nuclear technology. Significant efforts began in 1954 when ASME appointed a task group of the Subcommittee on Power Boilers. This task group and later special committee worked closely with the Naval Reactors Program to produce codes and standards. In 1963, the ASME BPVC was expanded to include rules for the construction of NPP components, including reactor pressure vessels, containment, and SGs. Since then, the BPVC (including its nuclear standards) has been successfully incorporated into laws in most North American territories and is used internationally (Riznic and Duffey, 2017).

1.2.6 Development of central electricity generation stations

It was Thomas Edison's invention of the electric lightbulb in 1879 that resulted in the need for refinement of the steam engine and the development of steam turbines. To fill the electricity demands of the lightbulb, Edison's Pearl Street Station was the first central station built for generating electricity. Situated in New York, the plant featured six dynamos, each connected to a 750-hp steam engine. On Sep. 4, 1882, at 3:00 p.m., the plant began distributing electricity to its customers. Initially the station served

59 costumers a 73-kW load, but this load grew 10-fold in just 3 years. The viability of the Pearl Street Station resulted in a great demand for other centralized stations. However, the uneconomical nature of direct current (DC) transmission over large distances revealed the need for alternating current (AC) distribution. Nikola Tesla was already working on AC generation and transmission, albeit relying on hydro power. With all the advancements made in the field of SGs and power distribution, by the year 1900, numerous power generation stations delivering AC electricity were popping up through the western world.

The early steam engines were reliable but featured the drawbacks of being inefficient, large, and heavy. In order to increase efficiency and compact the size, development in steam turbine became the focus of nearly all electric equipment companies. In the United States, the first steam turbines were rated at 1.5 MW, a size much smaller than the average SG today. Between 1910 and 1920, larger units were appearing with 30–70 MW units being common. From then to 1945, little increase in size was observed with the median-sized SG unit being only 100 MW. It was not until around 1967 that a large increase in unit size was observed, where the median-size increased to 700 MW. Since then, the size of SGs has slightly decreased, due to technical factors but rather improved efficiencies and cogeneration. In 1996, steam turbines accounted for over 586 million kW of electrical capacity, which at the time was 78% of all power generation capability in the United States (Zink, 1996).

1.3 Splitting of the atom and emergence of nuclear power: Atoms join water and steam

After the splitting of the atom by Ernest Rutherford in 1917 in Montreal, and the discovery of the neutron in the early 1930s, the scientific community began to speculate that it might be possible to create elements heavier than uranium in the lab. A scientific race to confirm this began between Ernest Rutherford, at that time in Britain, Irene Joliot-Curie in France, Enrico Fermi in Italy, and the Lise Meitner and Otto Hahn team in Berlin. It was Lise Meitner and Otto Frisch who coined the term *nuclear fission* when they published *Disintegration of Uranium by Neutrons: A New Type of Nuclear Reaction* in the journal *Nature* on Feb. 11, 1939. Ironically, the peaceful uses of nuclear technologies such as NPPs to generate electricity were and still are greatly influenced by fear of atomic warfare. With threat of the Germans to develop atomic bomb, Albert Einstein signed the famous letter to Roosevelt that "it may become possible to set up a nuclear chain reaction in a large mass of uranium, by which vast amounts of power and large quantities of new radium-like elements would be generated." Einstein further explained that the phenomenon of nuclear reactions could lead to the construction of "extremely powerful bombs of a new type." With fear of the Germans developing a bomb of their own, Roosevelt reacted by forming an Advisory Committee on Uranium to oversee the research on nuclear fission. Scientists concluded that if the Germans had a nuclear bomb that "no shelters are available that

would be effective and that could be used on a large scale and the most effective reply would be a counter-threat with a similar bomb." (Frisch and Peierls, 1940). The Manhattan Project, originally known as the "Manhattan Engineering District," was launched in August 1942.

1.3.1 Chicago pile: The first energy from a nuclear reaction

A key part of the Manhattan Project, the Chicago Pile Experiment, was created to produce the first self-sustaining nuclear chain reaction. The history behind the Chicago Pile starts 3 years prior to the experiment itself in 1939, with the first thoughts of a nuclear chain reactor coming from a discussion between Enrico Fermi and Niels Bohr (Allardice and Trapnell, 1962). The following year, Fermi began work on potential reactor designs using a graphite moderator with uranium oxide or uranium metal as a fuel source. After 2 years of work, in 1942, Fermi chose a final design for a test pile made of pure graphite blocks to determine if a chain reaction could be sustained, and he was confident that measurements from the experimental designs provided enough information to choose a final test pile to build a prototype. Chicago Pile-1 was built underneath the stands at Stagg Field at the University of Chicago, and was described as "a pile of black bricks and wooden timbers, square at the bottom and a flattened sphere at the top. Up to half of its height, its sides were straight. The top half was domed, like a beehive." (Allardice and Trapnell, 1962). Shortly after construction was finished, on Dec. 2, 1942, testing started, and at 9:45 a.m., control rods were repeatedly withdrawn until 3:25 p.m. when they were finally held in place. It was then that the reactor became self-sustaining, and for the first time in history man had created a self-sustaining nuclear chain reaction.

1.3.2 The nuclear-powered submarines and Admiral Rickover

Following the Manhattan Project and the Chicago Pile Experiment, the world was now moving into the Atomic age. Submarines were diesel powered during the Second World War; however, with the invention of nuclear reactors, it was not long before nuclear-powered submarines were built.

Over the objections of many, the design and manufacturing of the world's first nuclear submarine was led by then Captain (later Admiral) Hyman G. Rickover, with the USS Nautilus, launched in Jan. 17, 1955 in Groton, Connecticut (Paine, 1997). The USS Nautilus was powered by a PWR with horizontal SGs, which allowed it to break a multitude of submarine records during its operation, solely because of the new addition of nuclear power as a propulsion source. These records included the longest submerged distance travelled, the highest underwater speed, the first vessel to reach the geographical North Pole, and the first vessel to successfully complete a submerged voyage around the North Pole. In combination with his work in the U.S. Navy, Rickover led the development and construction of the first nuclear power electricity generating station in the United States, located in Shippingport, Pennsylvania.

Following the Second World War, Rickover had a 6-month tour with the Manhattan Project, as well as several years working in nuclear ship propulsion. It was then that he planned the creation of the USS Nautilus, but his involvement in nuclear side of the navy did not stop there. He proceeded to exert an extremely large influence on the United States' growing nuclear fleet, being promoted to admiral, and becoming involved in multiple generations of nuclear-powered submarines and other naval vessels (Naval History, 2015). Rickover was preoccupied with quality, efficiency, and getting engineering correct by a wide margin of safety. His influence was so strong that he interviewed all potential officers that wanted to serve on a nuclear vessel and was known to "emotionally crush" many candidates (Langbert et al., 2008).

Admiral Rickover and his dedicated staff continued to drive forward in both the naval nuclear power and the commercial nuclear power (US Congress, 1971). He worked with several generations of nuclear-powered vessels, exerting significant control over their operation and leading to the U.S. nuclear navy having a total of zero nuclear accidents, a record still continuing to this day. Admiral Rickover was further involved in nuclear power by leading the development and construction of the first "atomic power station" in the United States. This happened in Shippingport, Pennsylvania, starting operation in 1957, the reactor being a PWR, much like those found in the vessels of the U.S. Navy, which was no doubt, because of Rickover's influence (Shippingport's reactor was meant to be used for the Navy).

1.3.3 Growth of commercial nuclear power

When looking at the first nuclear-produced propulsion steam, work was also proceeding on building the NPP to generate electricity for commercial use. On Jun. 27, 1954 the first nuclear electricity generation plant APS-1 was connected to the grid in Obninsk, Russia. The impact of the APS-1 is greater than simply being a 5-MW electricity source since it was also a demonstration of the peaceful use of nuclear technologies. This demonstration of peaceful use of atomic energy proved to be highly influential in motivating other countries to take suit in embarking on the development and construction of NPPs. The APS-1 had a thermal power of 30 MW with the electric power output from the turbogenerator of only 5 MW (Kotchetkov, 2004).

Continuing on past APS-1 in Obninsk, commercial nuclear power kept advancing. Much nuclear research was performed in Arco, Idaho. Both the first pressurized water reactor (a precursor to the reactor in the USS Nautilus) and the first boiling water reactor (BWR) were built in Arco. The first BWR was known as BORAX-I (BORAX meaning boiling water reactor experiment), and although it did not produce power for the grid it served as a precursor to later designs such as BORAX-II, III, IV, V, and arguably every modern BWR. BORAX-IV later became the first reactor to use thorium as fuel. The first reactor to supply commercial electricity in the United States was the BORAX-III boiling water reactor. In 1955, the BORAX-III reactor supplied 100% of Arco's power for over an hour, becoming the first reactor to fully supply a city's power (Marcus, 2010); it also powered the BORAX facilities and some other nearby testing facilities. This development was announced at the United Nations

conference on atomic energy. It has since been debated whether BORAX-III or APS-1 was the first commercial NPP to connect to the grid.

The first "full-scale" reactor connected to the grid was the Calder Hall I in Sellafield, United Kingdom, in 1956, being so defined as it produced approximately 50 MWe of power. This was significantly larger than other experimental or prototype power plants at the time and differentiated Calder Hall I from reactors such as APS-1 and BORAX-III. It is sometimes credited as the first reactor to produce "commercial quantities" of power (Marcus, 2010) due to its larger, more viable size. However, it is also sometimes discredited as a commercial plant due to its primary purpose being the production of plutonium for nuclear weapons. Calder Hall I was also unique with its Magnox design. The reactor used a graphite moderator with gas cooling, natural uranium fuel, and a magnesium fuel cladding which is the source of the term Magnox.

With reactors now being built for peaceful purposes, the United Nations established the IAEA in 1957. The main mission of the IAEA was and still is to work on an international level to prevent the proliferation of nuclear weapons and to promote the safe, secure, and peaceful use of nuclear technologies. Initially consisting of only 26 members, The IAEA has now expanded to a total of 168 member states (as of Jan. 2017). IAEA has been thoroughly involved in all forms of nuclear power including commercial, and in 1970 started work on the INIS, an information system on the peaceful uses of nuclear technology (including commercial NPPs).

Not long after the beginning of commercial PWRs and BWRs, the first CANDU (Canadian Deuterium) reactor prototype started to produce energy. This was the Nuclear Power Demonstration (NPD) reactor in Rolphton, Ontario, in 1962, which was the first PHWR in the world. NPD showed the feasibility of heavy-water technology, and the design was advanced to the Douglas Point reactor in 1967, becoming the first full-scale pressurized heavy-water reactor. These reactor designs differed from most other reactor designs at the time, and still today, by using pressure tubes instead of pressure vessels, a decision that was made because of the difficulties associated with machining the large pressure vessels by domestic manufacturers.

The first commercial nuclear plant designs now emerged, from General Electric (with the BWR) and Westinghouse (with the PWR), both of which had also contributed to the beginnings of the Navy Nuclear program. They, along with Babcock and Wilcox and combustion engineering (CE), produced factories for all the major components and fuel lines. The United States expanded its global cooperation, signing major commercial Nuclear Cooperation Agreements (NCAs) with France (Westinghouse with government-owned Framatome), Japan (Mitsubishi for PWRs, and Toshiba and Hitachi for BWRs), and South Korea (CE for PWRs). Commercial deals for nuclear collaboration, fuel supply, and licensed plants with France, Japan, and Korea were essential to founding their own national programs, provided they had agreed to the international Nuclear Nonproliferation Treaty (NPT). The global spread for peaceful uses caused many international developments in reactor technology with France, Japan, the United Kingdom, Canada, Germany, Korea, Sweden, Russia, India, Argentina, and most recently China to develop their own design variations of water- and liquid-metal-cooled reactors for commercial power production (Riznic and Duffey, 2017).

1.3.4 Current state of the nuclear industry

Overall there are currently 450 operating reactors of multiple designs, with over 1300 operational SGs. Roughly 13.5% of the world's power is generated from nuclear sources; the vast majority produced from burning fossil fuels in the form of coal or natural gas (62.3%) (Pioro and Duffey, 2015). Out of the largest 11 power stations in the world, 4 are nuclear plants, with the remaining 7 being hydro dams. Interest in the use of nuclear energy for electricity generation, as an essential and reliable energy source, free from "green-house" gases, is leading to new nuclear reactors being built in many countries, despite declines in some traditional markets. Safe and efficient operation of the current fleet of NPPs is essential, as is their life extension, for global sustainability and human well-being. These current generation reactors, largely water-cooled, have and are serving the world well. The challenges include advances in thermal efficiency, managing rare-event safety, fuel-cycle enhancements, improved economic competitiveness, and high-level waste management with full public and political participation.

Given the slow rate of new-builds in the North America and Europe, the technical focus has been on enhancing plant output and capacity factors, avoiding extended outages using integrated outage planning, and on extending plant life. These have been preoccupations for the utility industry, particularly as many operate in competitive power markets. As a result, increased operating efficiencies and lowered operating costs are a premium, without compromising safety. The lack of credit for noncarbon emissions and of guaranteed subsidies or power prices have left many plants commercially disadvantaged, and some have even been threatened by closure. In the era of cheap natural gas, it is often easier and cheaper to extend the life of an existing (already amortised or paid off) unit than build a new one. This is the case in many countries, such as Canada, Sweden, and Japan. Thus, the replacement of internals and SGs continues.

Meanwhile, in Asia and the Middle East, many new plants are being built, some to replace coal or oil-burning units. China has an ambitious new-build program, importing the latest designs, and at the same time emulating Korea by developing their own design variants. They are also exploring new liquid metal fast breeder reactors (LMFBR), high-temperature reactors (HTR), and other technologies.

The future also lies in the development of the next generation concepts and designs, including Generation-IV and other reactor applications, which offer potential solutions to many of these problems, including advances in the use of risk-informed decision-making and safety regulations. Radiation science and protection are integral to NPP design and operation, and critical to ensuring public and worker safety, by understanding and predicting health effects, enhancing industrial uses and medical therapy, and providing more realistic estimations and regulations of radiation risk using scientific advances. New reactor designs and regulations will incorporate the latest developments and understanding in this important engineering/scientific discipline. The emergence of Generation IV concepts in the 21st century promises perhaps the most promising technological advance and importantly involves significant international collaboration (Pioro, 2016).

1.4 Unique features of different steam generators

This section briefly introduces the different designs for currently operating SGs in NPPs. Recirculating steam generators (RSGs), designed by Westinghouse (USA), and CE (USA and Doosan (Korea) are described first, followed by the Babcock and Wilcox OTSG design along with the Canadian PHWR designs, and the Russian (WWER) designs.

Differing SGs contain some unique features and operational performance indicators. Table 1.1 displays various statistics by reactor type. The total number of NPPs, total number of SGs, and SG tube materials can be compared by different NPP types. Fig. 1.3 shows two pie-chart representations of the total number of operational SGs and those under construction. Quick analysis reveals that PWRs are both the most common operational and under construction nuclear reactor and SG types. Data were obtained from the IAEA PRISs database for nuclear power reactors. The database provides information on specifications and performance history data of reactors under construction, operational, and decommissioned reactors. The PRIS database contains information on NPPs from 48 countries worldwide. Looking at Table 1.1, it can be seen that the majority of operational SGs are from PWR plants, making up 58% operational SGs. With 290 and 274 SGs, PHWRs (22.2%) and VVERs (21%) plants host the second and third highest amount, respectively.

1.4.1 PWR vertical steam generators

Commercial NPPs with PWR reactors contain between two and four SGs depending on the design and plant size. A differential element of PWR SGs is that boiling occurs in the shell side of the heat exchanger rather than in the tubes. This is done in order to keep a high velocity of primary reactor coolant at high pressure to maintain effective heat transfer from reactor coolant to the low pressure steam system on the secondary side. The typical PWR SGs are of a vertical cylindrical vessel configuration with inverted U-tubes in the lower section and moisture or steam-water separators at the top of the tube bundle in the upper section.

In PWR SGs, high temperature (usually in the range of 585–605 K), high pressure (15 MPa) primary reactor coolant flows through U-tubes, where it rises in one-half of the SG referred to as the hot leg side and flows down the cold leg side to exit at approximately 560 K. Older plants have lower temperatures. The secondary system water (feedwater) is fed through a feedwater nozzle, to a feedring, and then into the downcomer, where it mixes with recirculating water draining from the moisture separators. The flow coming into the SG is typically directed first upward, through a “gooseneck” pipe assembly, and then downward into the feedring (sometimes called the feedwater header). This avoids risk of flow stratification in the feedwater inlet line, which can lead to high thermomechanical stressing of the feedwater piping system. The feedring typically has some type of J-tube vents on the top of it to prevent the feedring from draining and creating steam plugs during the SG operation. The downcomer water flows to the bottom of the SG, across

Table 1.1 **IAEA PRIS information on steam generators by reactor type, as of Jan. 2017**

Reactor type	Number of operational NPPs	Number of operational SGs	Number of NPPs under construction	Number of SGs under construction	SG tube materials
Pressurized water reactor (PWR)	233	705	36	113	Incoloy-800, Inconel-690, Inconel-600
Vodo-Vodyanoj Energeticheskij Reaktor	57	274	15	64	Austenitic Stainless Steel (08CH18N10T SS)
Once-through steam generator	6	12	0	0	Inconel 600 (I600), Incoloy 800
Pressurized heavy-water reactor	49	290	4	16	Incoloy-800, I600, Monel 400
Fast breeder reactor	3	5	1	2	ICR2MO
Light-water graphite reactor	15	68[a]	0	0	(Insufficient Information)
Gas-cooled reactor	14	76	0	0	BS3059/3 mild steel/9%CrMo steel/TP316 stainless steel, mild/chrome/ST, austenitic stainless steel & Cr/Mo, mild steel

[a]LGWRs use steam drums rather than steam generators.

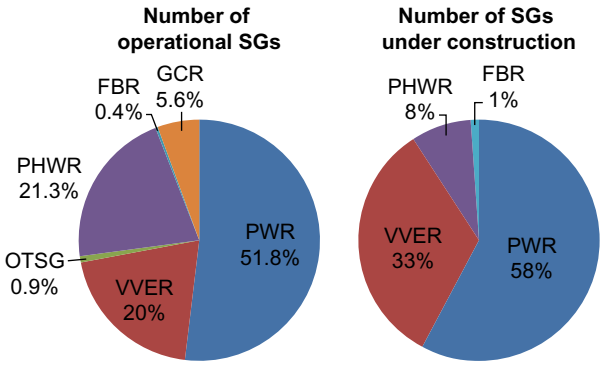

Fig. 1.3 Steam generators that are operational and under construction as of Jan. 2017.

the top of the tubesheet, and then up through the tube bundle where steam is generated. About 20%–25% of the secondary water is converted to steam on each pass through the generator, while the remainder of hot secondary water is recirculated. This configuration, as depicted in Fig. 1.4, does not have an integral preheater or economizer (IAEA, 2011).

An alternate design with an integral preheater (see Fig. 1.8 later in the text) brings the feedwater through a nozzle, located in the lower part of the vessel on the outlet or "cold leg" side of the tube bundle, near the tubesheet. This configuration does not have feedring and all incoming feedwater is forced to flow through the preheater, by cross flow over a number of baffle plates on the cold leg side. Auxiliary feedwater (AFW) is injected through a separate nozzle in the upper part of the vessel. The preheater uses heat from the primary fluid leaving the SG to increase the temperature of the feedwater to near saturation level before it is mixed with the recirculating water flowing down from the top of the tube bundle. Some plants use two separate feedwater nozzles: one as the AFW typically during the start-up operation and one as the main feedwater for ongoing operation. AFW could be provided either from a separate AFW tank (at ambient temperature) or from the feedwater tank (Siemens and Mitsubishi plants use this option to bring in warm feedwater).

The most recent Westinghouse type AP1000 units use two Delta 125 SGs, with thermally treated Alloy 690 tubes and ferritic stainless steel support plates. The tube support plates (TSPs) are broached with hole geometry to promote high velocity flow along the tube. The thermal sleeve and feedwater nozzles are fabricated from the thermally treated Alloy 690, which is highly resistant to erosion and corrosion. The Delta 125 SGs are rated at 1707.5 MWt and employ 210 modular primary separators with a riser diameter of 7 in. Double hook and pocket dryers are employed for collecting moisture. The steam quality is increased to a designed minimum of 99.75%. The design pressures of the primary and secondary sides are 17.13 and 8.17 MPa, respectively. The design primary reactor coolant inlet temperature is 321°C and of steam side is 315.5°C. These newly designed SGs introduce a sludge collector, located at the bottom of the steam separator deck, but above the U-bend section of the tube bundle with the inlet at box center and outlet at brim. Some of the recirculated water, joined with

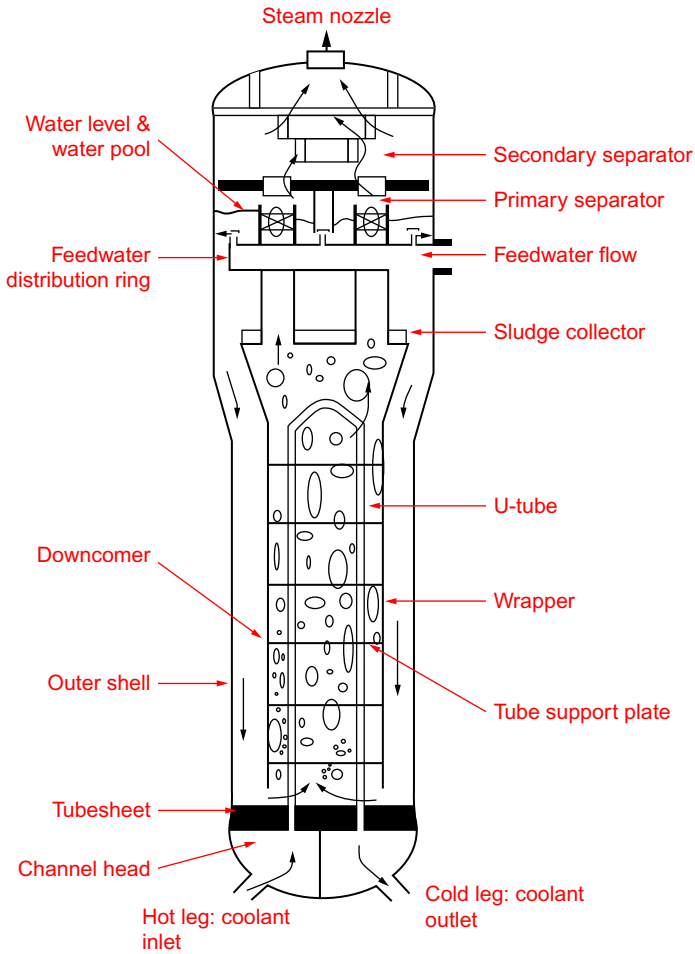

Fig. 1.4 Recirculating PWR steam generator.

the feed water, could get into the sludge collector and flow in a radial direction. With the flow velocity decreasing, the sludge particles carried by the water could settle down by gravity, which could be removed at outage. The sludge collector provides a passive device for sludge settling before the fluids and impurities reach the tube supports and top of the tube sheet region. Almost all new replacement SGs have some kind of sludge collectors to reduce the sludge accumulation on the tubesheet, which should prevent or minimize progression of various corrosion degradations (IAEA, 2011).

CE system 80 PWRs are slightly different from other PWR vendors by having two hot legs, four cold legs, four primary reactor coolant pumps, and only two SGs. CE SGs employs unique "square" instead of typical U-shaped tubes bundles with two

90-degree bends. The Korean Standard Nuclear Plant and the later OPR 1000 (optimized power reactor 1000 MWe) are based on CE System 80 technology, with over 8200 tubes per SG, made of I600. CE System 80 and OPR 1000 tubes have a 0.75″ outer diameter—a standard size for PWR U-tubes. Newly manufactured and replacement SGs for OPR 1000 are made of Inconel 690 tubes, with a 16.96 mm (0.668″) inner diameter and a wall thickness of 1.07 mm (0.042″).

Current generation of the APR 1400 SG represents the uprated and evolutionary design from the CE and OPR 1000 operating SGs in Korea. Reactor coolant enters the inlet plenum through the primary inlet nozzle at 597 K, flows up through the tubesheet and U-bend tubing, and returns through the tubesheet to the outlet plenum and exits through the two outlet nozzles at 564 K. Feedwater with 505 K enters the preheater region at the tubesheet on the cold leg side of the tube bundle. Above the flow distribution plate, feedwater flows upward in axial counter flow, being heated by forced convection to near saturation conditions at the top of the economizer. At this elevation, heated feedwater mixes with cold leg downcomer water and secondary fluid from the hot leg side in the evaporator section of the tube bundle. Heat transfer by nucleate boiling occurs in the evaporator as the secondary fluid flows upward continually increasing in steam quality. Steam separators mounted on a deck plate at the top of the tube bundle shroud separate the steam from the two-phase mixture. Separated steam (about 25%) flows through the dryers and out the steam nozzles while the water (about 75%) returns to the downcomer. The 10% of total feedwater flow is mixed with the recirculated water in the downcomer to condense any steam carry under which may eventually find its way downstream.

Major design enhancements for the APR 1400 include a modified primary outlet nozzle angled to improve the mid-loop operation, automatic control of stream generator water level for all operating ranges, design improvement to prevent the flow induced vibration (El Bouzidi et al., 2015; Hassan and Riznic, 2014), and employing Alloy 690 thermally treated tubes. For maintenance and inspection, the internal structures inside the SG are accessible via manways and handholes. The design pressures of the primary and secondary sides are 17.2 and 8.27 MPa, respectively. The design temperatures of the primary and secondary sides are 616 and 572 K, respectively (IAEA, 2011). The Palo Verde plant in U.S. (with RSG designed by CE and manufactured by Ansaldo) and Korean APR 1400 units in Korea and United Arabic Emirates have the largest SGs in the current nuclear fleet (Fig. 1.5).

1.4.2 PWR once-through steam generators

The Babcock and Wilcox OTSGs use straight heat exchanger tubes with tubesheets at both the top and bottom of the SG, as shown in Fig. 1.6 (Green and Hetsroni, 1995). OTSGs are smaller in size than other PWR SGs since they do not have moisture separators. The OTSG works by having the primary reactor coolant pumped through the tubes from the top to the bottom, while the secondary coolant moves outside the tubes from bottom to top in a counter-flow direction (Singhal and Srikantiah, 1991). The secondary-system water enters a feed annulus above the ninth TSP level where it mixes with steam aspirated from the tube bundle area and is preheated to saturation.

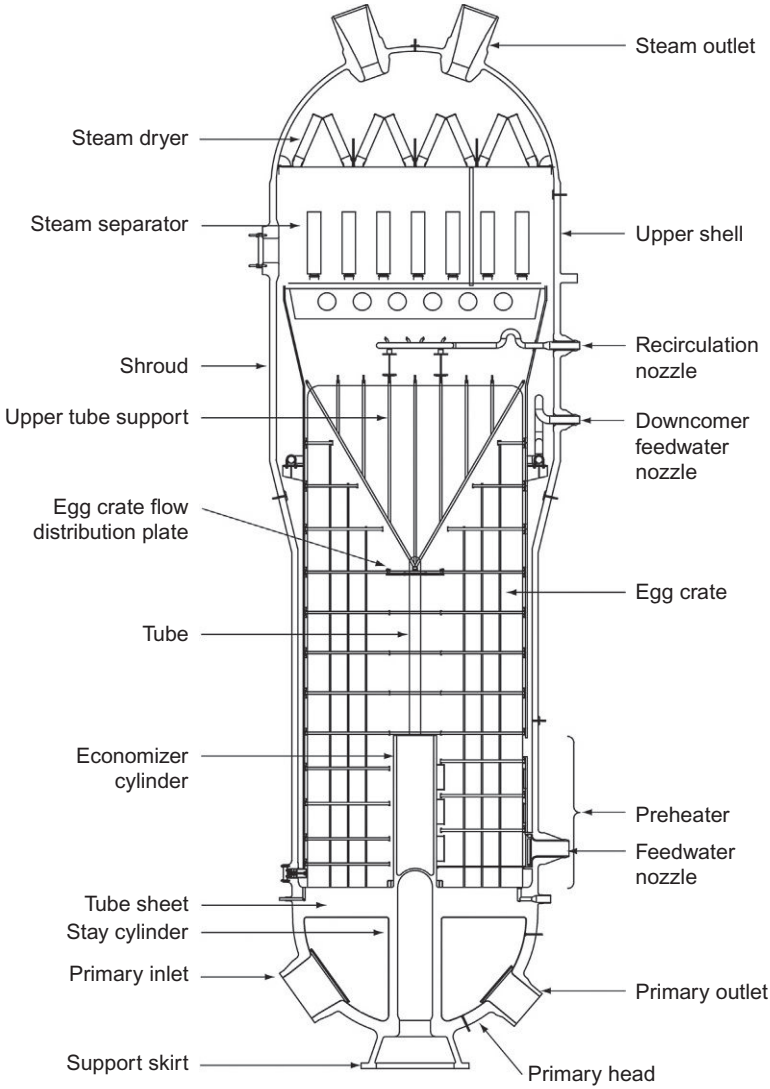

Fig. 1.5 Korean recirculating steam generator (Doosan Heavy Industry model) (IAEA, 2011).

The saturated water flows down the annulus, across the lower tubesheet, and up into the tube bundle where it becomes steam. This superheated steam flows radially outward and then down the annulus to the steam outlet connection. Most of the secondary coolant is completely evaporated in a single pass through the SG.

Tubing of OTSGs undergoes a different heat treatment process. The heat treatment includes high mill-annealing temperatures (1338 K) followed by holding the

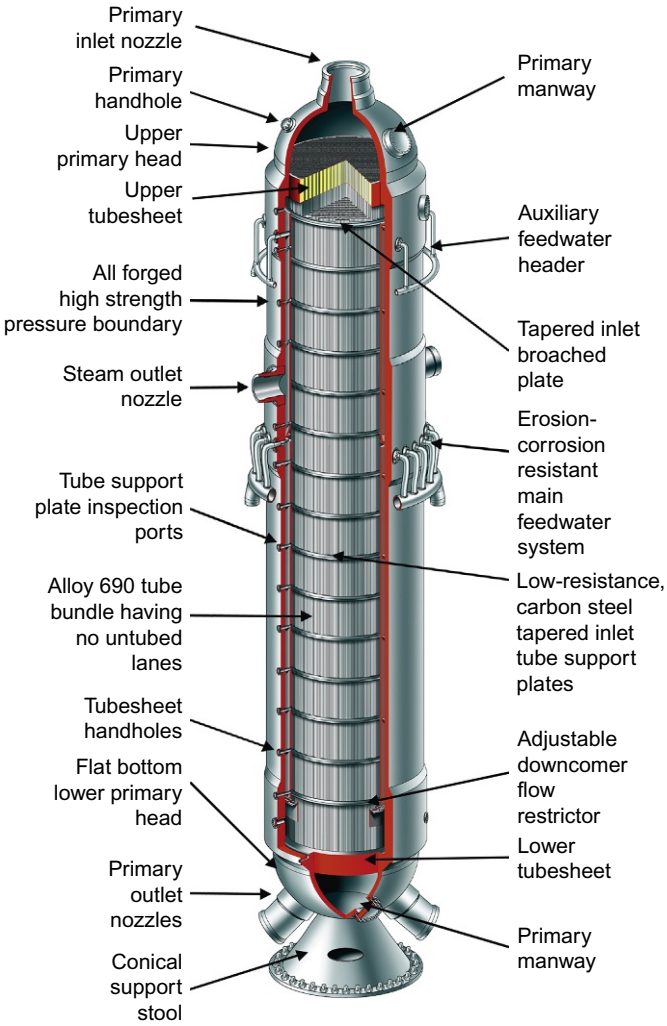

Fig. 1.6 B&W advanced series PWR replacement OTSG courtesy of B&W Canada.

SG at 893 K after assembly for 10 h. This process provides relief of residual stresses in the tubing and results in large quantities of intergranular carbides in the tubing. This process makes OTSG tubes highly resistant to primary water stress corrosion cracking (PWSCC). Although the heat treatment is successful at protecting OTSG tubing from PWSCC, it causes depletion of chromium in the grain boundary making both the primary and secondary sides susceptible to attack by sulfur species. Sulfur species attacks have occurred at two Babcock and Wilcox plants (Shah et al., 1990).

1.4.3 PWR VVER steam generator

VVERs, transliterated from water-water energetic reactors, are a series of PWRs developed in Russia. In addition to Russia, countries operating VVERs include Armenia, Bulgaria, China, Czech Republic, Finland, Hungary, India, Iran, Slovakia, and Ukraine. Unique features of VVERs include hexagonal fuel assembly cassettes and horizontal SGs. The SGs used in the WWER-440 and WWER-1000 plants are horizontal shell-and-tube heat exchangers manufactured by Gidropress (Russia) and Skoda Vitkovice (Czech Republic). They consist of a SG vessel, a horizontal heat exchange tube bundle, two vertical primary collectors and a feedwater piping system, moisture separators, and a steam collector. A sketch of a WWER-1000 SG is shown in Fig. 1.7 (IAEA, 2011).

Primary coolant enters the SG through a vertical collector, travels through the horizontal U-shaped submerged stainless steel tubing, and exits through a second vertical collector. The tube ends penetrate the collector wall, which performs the same function as the tubesheet in a PWR SG, and are expanded using either a hydraulic or explosive expansion process and then welded at the collector inside wall surface. The WWER-440 collectors are made of Ti-stabilized austenitic stainless steel. The WWER-1000 collectors are made of low-alloy steel cladded with stainless steel. The WWER-440 tubes are arranged in line (corridor), while the WWER-1000 tubes are staggered. Tube supports are made of stainless steel bars and stamped wave-like plates, with a typical distance between the tube supports being 700–750 mm. The SG vessel is made of a carbon steel (WWER-440) or low-alloy bainitic steel (WWER-1000) designed as horizontal cylinder consisting of forged shells, stamped elliptical

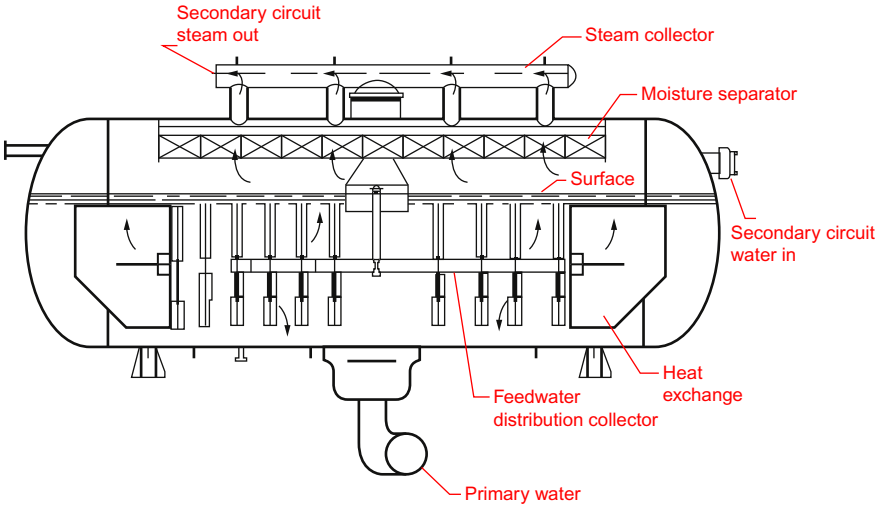

Fig. 1.7 VVER steam generator.

ends and stamped branch pipes and hatches welded together. The vertical hot and cold primary coolant collectors penetrate the vessel near its mid-point. Feedwater is supplied to the middle of the WWER-400 tube bundle by perforated piping. In the WWER-1000 SGs, the feedwater is supplied from the top of the hot leg of the tube bundle under a submerged perforated sheet. The tube bundle is completely submerged in both designs. The WWER-440 and WWER-1000 SG designs are similar except for the (a) size (the WWER-1000 SG is about 4 m longer), (b) tube arrangement (corridor vs staggered), (c) collector material, (d) feedwater supply location, (e) submerged perforated top plate (WWER-1000 only), (f) steam dryer arrangement, (g) emergency feedwater distribution system (WWER-1000 only), (h) steam header arrangement, and (i) vessel material. The most recent design of the WWER-1200 SG (PGV-1000MKP) is similar to PGV-1000 M except its bigger vessel diameter (4200 mm) and corridor tube bundle arrangement (IAEA, 2011).

Many similarities can be drawn between the VVER and Western PWRs such as the use of low-enriched uranium oxide fuel, and their light water coolant and moderator. Even though similar in many ways, early designs of VVERs plants lack a number of safety features that are standard for the Western PWRs, such as a fire protection system, an emergency core cooling system, and a strong containment system (Trunov et al., 2008). Nevertheless, some of the advantages of using horizontal rather than vertical SGs in VVER have been exemplified over many years of operating experience. Advantages include:

- moderate steam load (steam outflow rate from the evaporation surface of around 0.2–0.3 m/s)
- moderate velocity of the medium within the second loop (up to 0.5 m/s) which prevents danger of vibrations of the heat exchanger tubes
- validated serviceability of 08Kh18N10T austenitic steel tubes for up to 38 years in a PGV-440 and 23 years in PGV-1000
- vertical arrangement of the first-loop collectors, preventing accumulation of sludge deposits on their surfaces, reducing the danger of corrosion damage to the heat exchanger (Trunov et al., 2008)

There are currently two large issues with horizontal SGs in operation: defects in weld joints and SG tube degradations. It is important to note that these issues affect vertical PWRs as well, and to an even larger magnitude. VVER SG tubes have been plugged in almost an order of magnitude than that of vertical SG counterparts (Trunov et al., 2008).

1.4.4 PHWR CANDU steam generators

The first Canadian prototype reactor, the NPD plant, used a horizontal steam drum as opposed to the current, vertical SGs. Finished in 1962, the NPD SG was based on U.S. navy designs of SGs in nuclear submarines, but the reactor itself was meant to be a demonstration of CANDU power. Although NPD succeeded in producing power and showing the CANDU cycle to be viable, I-600 SG tubes were experiencing extensive fretting, which only worsened over time until shutdown. The initial success of the NPD led to the construction of the Douglas Point reactor. Like the NPD, Douglas Point

used horizontal steam drums, but they were made of Monel 400 (M400) tubing instead. The design consisted of 80 vertical hairpin heat exchangers connected to four steam drums, and drilled hole plates were used for tube supports (Dyke and Garland, 2006). During operation, Douglas Point experienced extensive fretting as well as rising radiation fields from corrosion products (Taylor, 1997) and eventually shutdown in 1984. Pickering A was meant to be a direct upscaling of the previous Douglas Point reactor (Pon, 1978). The SG design ended up being a vertical RSG with a vertical steam drum, the first of its kind for CANDU. There were 12 of these SGs, made of M400. At the time Pickering A was unique in the way that it used a lattice bar system for tube supports, whereas the typical design for PWR SGs was with drilled holes. The lattice bars were not initially designed properly but after a redesign and repair the lattice bars proved to be very effective and Pickering A SGs had very good operational results (Dyke and Garland, 2006). Pickering B is very similar in design to Pickering A, but the tube supports are broached hole plates instead of lattice bars. The design of Bruce A differed in several ways from Pickering A since it was decided to go back to a horizontal steam drum design, which underwent significant stresses during operation and kept Bruce A at reduced power for some time. Bruce A used I600 as the tube material. Bruce B returned to the vertical, integral steam drum design, much like Pickering, but consisting of only eight SGs. Bruce B continued to use broached hole plates for tube support, and the tubes were still I600. Darlington was designed at the same time as Bruce B, and the designs ended up much different. Darlington abandoned broached hole plates in favor of lattice bars for tube support, which provided some of the world's best boiler performance (Tapping et al., 2000). Darlington was also improved through the use of Incoloy 800 (I800) for tubes and only had a total of four SGs. Apart from the main nuclear generating stations in Ontario, Quebec, and New Brunswick, CANDU reactors can be found around the world. A variety of CANDU 6 units can be found in Argentina, Korea, Romania, and China. These are typically similar designs with four vertical SGs consisting of I800 tubes, with either broached plates or lattice bars for tube supports.

Essentially, operating CANDU SGs are vertical RSGs built by Babcock & Wilcox Canada Ltd. The only exception is the Wolsong 1 unit in the Republic of Korea, which uses similar SGs, but built by Foster Wheeler. CANDU RSGs are very similar to the PWR RSG with some subtle differences in size, materials, operating temperatures, and tube support structure. Fig. 1.8 depicts the SG with integral preheater used in the Darlington Generating Station, which has all of the most current features of CANDU RSGs (Kozluk et al., 2006). Although the size of CANDU RSGs has escalated greatly with successive reactor designs, they are generally smaller than PWR RSGs and operate at lower temperatures (563–583 K primary reactor coolant inlet temperatures). The lower temperatures generally delay the onset of thermally activated corrosion processes such as PWSCC or intergranular stress corrosion cracking. Because the primary coolant in a CANDU reactor is heavy water (D_20), relatively small tube sizes (12.7 mm (1/2″) OD and, in more recent units, 15.9 mm (5/8″) OD) have been used to minimize the heavy water inventory. The nominal tube wall thickness ranges from 1.13 to 1.2 mm, depending on the type of tube alloy used (e.g., Alloy 800 M has a lower thermal conductivity than Alloy 600, requiring thinner

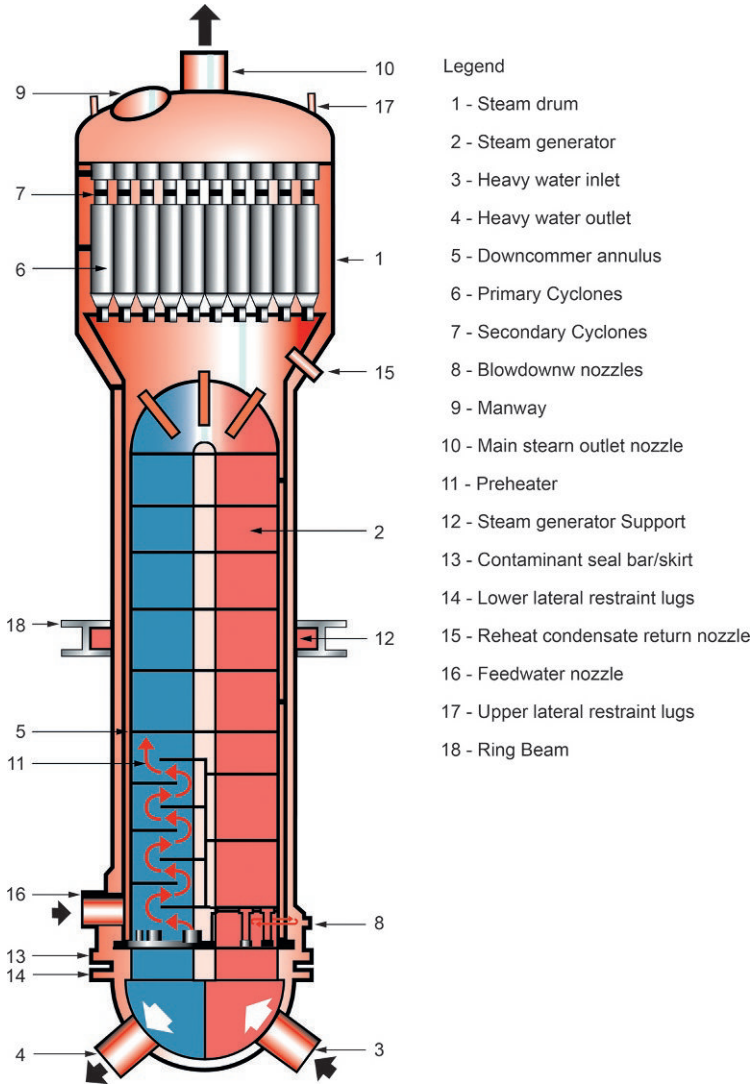

Fig. 1.8 CANDU recirculating SG with integral preheater used at the Darlington station.

tubes). The most important area of diversity in the CANDU design is in the choice of tube material. The CANDU SGs currently operate with tubes such as the high-temperature mill-annealed Alloy 600, the M400, and the titanium-stabilized Alloy 800. As CANDU SGs evolved, they greatly increased in size from many (12) low input (515 MWe) of the Pickering A & B design, to the Darlington design of 4 SGs of 880 MWe output.

1.5 Steam generators literature survey

A literature survey of nuclear SG related publications was conducted on various databases. The databases used include the IAEA INIS database, the Electric Power Research Institute (EPRI) database, and Elsevier's Scopus database. To ensure the usefulness and relevance of results, a certain level of discretion in the search queries had to be taken. This discretion stems from the fact that the INIS database specifically searches for "nuclear" entries, whereas the Elsevier's Scopus, the EPRI, or databases used by universities do not have exclusively "nuclear" content. Additionally, the variation of "keywords" that result in a "hit" between databases can result in discrepancies. Each database presents different challenges in order to retrieve an accurate representation of publications per specific field of study. In order to overcome these challenges, various search queries and actual results were tested in each database to ensure that the most appropriate search string was used for the desired literature survey. The interchangeability of the words "boiler" and "SG" may also be the cause for the apparent discrepancy of data outputs when conducting literature searches. When searching for publications from a specified year, publications that had sources cited to that specific year had the potential to be included in the search results as well. Despite the discretion put into these searches, it should be noted that there still may be some measure of inaccuracy, stemming from the differences in the way each database indexes publications. For example, searching a keyword in one database may not result in all of the expected results simply because of database coding. Let us briefly describe databases used in the search for the status and growth of SG-related publications.

The IAEA INIS is a database dedicated to hosting a collection of published information on the peaceful uses of nuclear science and technology. Over 3.6 million documents make up the INIS collection. Being a nuclear-dedicated database, all searches within it are relevant to nuclear technologies; the word "nuclear" does not need to be included to conduct the desired search. Searching "SG" was sufficient at retrieving references on nuclear SGs due to the fact that INIS is a nuclear-specific database.

The Electric Power Research Institute (EPRI) is a nonprofit organization, which conducts research on the generation, delivery, transmission, and use of electricity. EPRI has a search engine on their webpage with different accessible power-related publications. What makes EPRI's database most different from that of the INIS is that it has a smaller collection of publications. Although smaller in scale, a literature survey of the EPRI database was still useful at generating information, particularly since the EPRI provides strong technical support to utilities operating power plants (Table 1.2).

The distribution of publications in the INIS databases displays a parabolic trend, peaking at around 1990. Looking at Fig. 1.9, it is seen that before 1971, there were not many documents published, but shortly after there is a sharp increase. The strength of this database is its consistent distribution of publications after the year 1971, whereas a weakness is its lack of publications before 1971.

The number of SG and nuclear-specific SG-related publications from the EPRI database has grown sharply and consistently since 1996 continues to show signs of

Table 1.2 Search details

Database	Search date	Number of hits	Year of earliest publication	Year of most recent publication
IAEA INIS	2017-01-11	29,560	1960	2016
EPRI	2017-01-11	1742	1977	2016
Scopus	2017-01-19	17,639	1960	2017

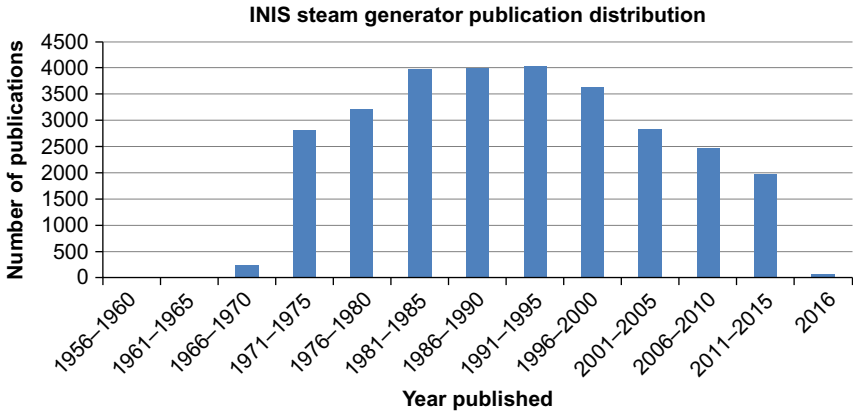

Fig. 1.9 Number of steam generator publications on the INIS database as of Jan. 2017.

future growth based on the 149 SG and 92 nuclear-specific SG publications published in 2016 alone. A weakness in the database is the lack in documents prior to 1996. To compare, the total number of publications before 1996, relating to both SGs and nuclear-specific SGs, is less than the number of publications that were published for both topics from 1996 to 2000.

Fig. 1.10 displays a comparison of nuclear-specific and all SG publications. An example of inaccuracy of the search query is shown. When using the search query of "nuclear SG," the search was too restrictive and many relevant publications are omitted resulting in only 74 results. When the search query was changed to "nuclear" "SG," the number of results sky rocketed to 742. Therefore, for accurate data collection purposes, the search query of, "nuclear" "SG," was used to analyze the distribution of nuclear SG-related publications.

The SCOPUS database is the largest abstract and citation database of peer-reviewed literature; it contains over 57 million records. This includes records in health sciences, life sciences, social sciences, and physical sciences. A SCOPUS search was performed after the previously mentioned data. It can be seen in Fig. 1.11 that the SCOPUS data do follow a similar trend by year for total publications over time, excluding the 2011–2015 data which is much larger than the rest.

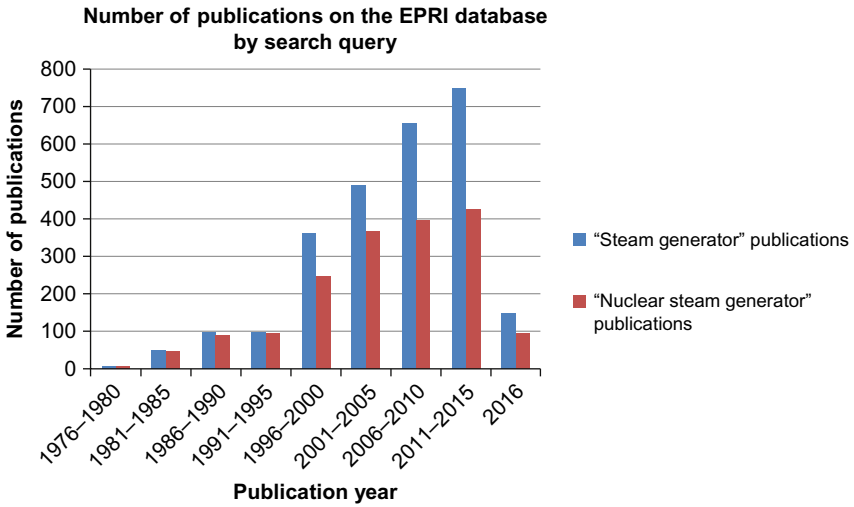

Fig. 1.10 Number of publications from the EPRI database by search query, as of Jan. 2017.

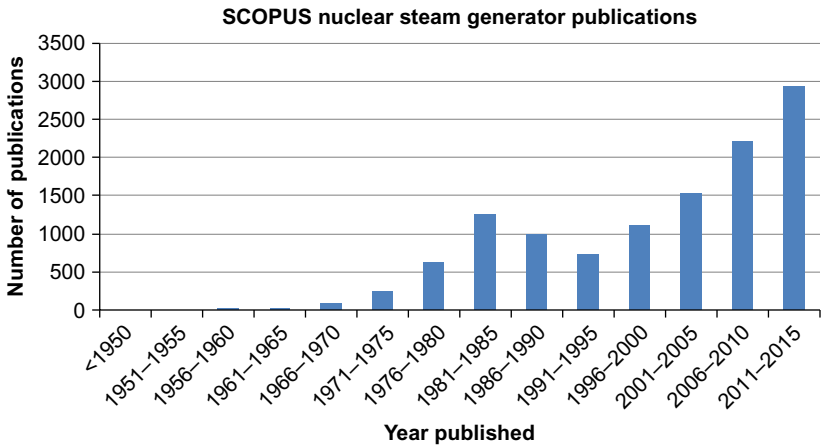

Fig. 1.11 SCOPUS nuclear steam generator publications.

1.5.1 Steam generator patents

The WIPO is a comprehensive source for worldwide information on intellectual property. Established in 1967, WIPO is a global forum for intellectual property (IP) services, policy, information, and cooperation. Existing under the umbrella of the United Nations, WIPO has 188 member countries and works with governments and businesses all over the world. WIPO assists in shaping international IP laws, provides global services to protect IP internationally, builds infrastructure to connect IP systems and share knowledge, uses cooperation and programs to enable all countries to use IP to their

benefit, and acts as a reference source for IP information (WIPO, 2015). Its Patentscope database is an online resource, which provides a search of over 46 million international patent documents. When comparing the number of nuclear-specific SG patents in Fig. 1.12, it is interesting to notice the sharp peak in patents from 1986 to 1990. In general, a growth is seen in number of nuclear-specific SG patents from 1981 to 1995, but much growth has not been seen since then.

With the information gathered, there is strong evidence that building new NPPs was a driving force for the large increase in engineering and scientific publications on SGs from the 1950s onward. The great interest put into nuclear SGs translates to the interest of further improvements of SGs in general. A visual representation of this conclusion can be seen in Fig. 1.13, which combines SG publication data (from

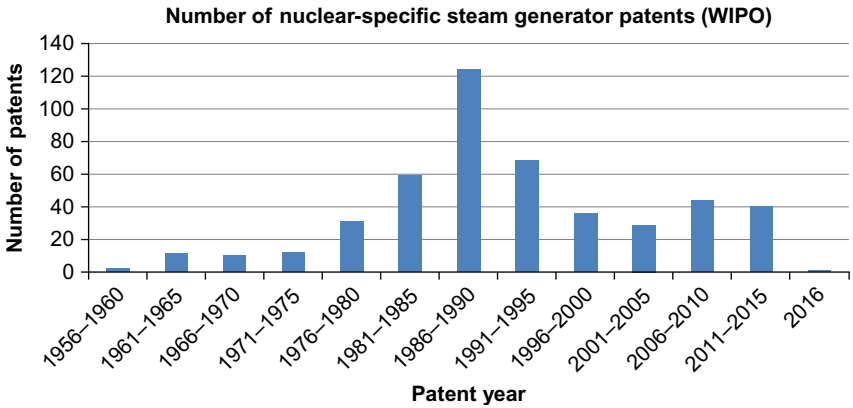

Fig. 1.12 Number of nuclear-specific steam generator patents, as of Jan. 2017.

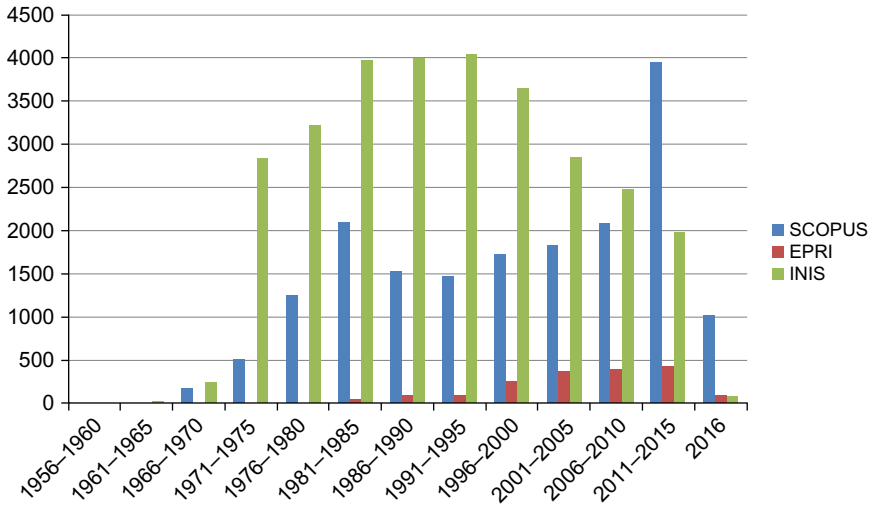

Fig. 1.13 Number of nuclear-specific steam generator publications by database, as of Jan. 2017.

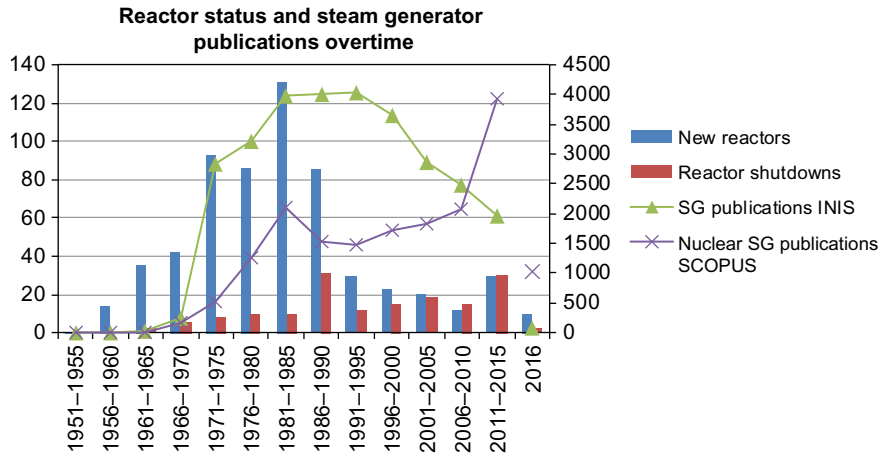

Fig. 1.14 Reactor status and distribution of steam generator-related publications overtime.

IAEA INIS, EPRI, and Elsevier's Scopus) and plots it alongside the number of new reactors and reactor shutdowns in each time period. Generally it appears that the major growth of the nuclear industry in the 1970s and 1980s resulted in a similar growth in publications. The decline of the industry from the 1990s to the early 2000s had a corresponding decrease in publications. An alternative view of this data can be seen in Fig. 1.14, with publications and reactor data shown as cumulative totals over time, which provides an easier trend comparison.

References

Allardice, C., Trapnell, E.R., 1962. The first pile. IAEA Bull. 4, 41–47.

ASME, 2016a. The History of ASME's Boiler and Pressure Vessel Code. https://www.asme.org/engineering-topics/articles/boilers/the-history-of-asmes-boiler-and-pressure. Retrieved August 10th 2016, American Society of Mechanical Engineers, New York, NY.

ASME, 2016b. About ASME—Engineering History. https://www.asme.org/about-asme/engineering-histor. Retrieved August 18th 2016, American Society of Mechanical Engineers, New York, NY.

Burke, J.G., 1966. Bursting boilers and the federal power. Technol. Cult. 7 (1), 1–23.

Cavendish, R., 2014. George Stephenson's first steam locomotive. Hist. Today. 64 (7). Available from: http://www.historytoday.com/richard-cavendish/george-stephensons-first-steam-locomotive. (Accessed 24 January 2017).

Cormier, K., Rivet, M., Riznic, J., 2016. Nuclear Steam Generation: History and Literature Survey. OEAD Report, Canadian Nuclear Safety Commission, e-docs# 4823545, Ottawa, Ontario, Canada.

Dyke, J.M., Garland, W.J., 2006. Evolution of CANDU Steam Generators—A Historical View. Canteach Candu Owners Group-COG, Toronto, ON. Available from: www.canteach.candu.org. (Accessed 20 January 2017).

El Bouzidi, S., Hassan, M., Riznic, J., 2015. A comprehensive flow-induced vibration model to predict crack growth and leakage potential in steam generator tubes. Nucl. Eng. Des. 292, 17–31.

Encyclopedia Britannica the Editors of Industrial Revolution, [On Line- Last Updated: 12-8-2016]. Available at: https://www.britannica.com/event/Industrial-Revolution. (Accessed 10 January 2017).

Franklin Institute, 1885. Journal of the Franklin Institute. Pergamon Press, Philadelphia.

Frisch, O.R., Peierls, R., 1940. Memorandum on the Properties of a Radioactive "Super-bomb" (Frisch-Peierls Memorandum). March 1940, Atomic Archive, Available at: http://www.atomicarchive.com/Docs/Begin/FrischPeierls.shtml. (Accessed 16 January 2017).

Gopalakrishnan, K., 2009. James Watt: father of steam power. Resonance 14 (6), 522–529.

Green, S., Hetsroni, G., 1995. PWR steam generators. Int. J. Multiphase Flow 21 (Suppl.), 1–97.

Hassan, M., Riznic, J., 2014. Evaluation of the integrity of steam generator tubes subjected to flow induced vibrations. ASME J. Press. Vessel Technol. 136, 051305-1–051305-11.

IAEA, 2011. Assessment and Management of Ageing of Major Nuclear Power Plant Components Important to Safety: Steam Generators, Tecdoc-1668. International Atomic Energy Agency, Vienna.

Kitto, J.B., Stultz, S.C. (Eds.), 2005. Steam, Its Generation and Use, 41st ed. Babcock & Wilcox Company, Barberton, OH.

Kotchetkov, L., 2004. Obinisk: number one. Nucl. Eng. Int. 49, 14–17.

Kozluk, M., Mills, B., Pagan, S., 2006. Darlington Steam Generator tube Fretting Fitness-for-Service: Operating Experience and Structural and Leak-rate Tests. In: 5th CNS International Steam Generator Conference, Canadian Nuclear Society, Toronto, Canada, November 26–29.

Lamb, J.P., 2003. Perfecting the American Steam Locomotive. Indiana University Press, Bloomington, IN.

Langbert, M., Stanchina, M., Grunewald, F., 2008. Howard Roark and the ghost of Admiral Rickover. Int. J. Cross Cult. Manag. 15 (2), 194–216.

Marcus, G.H., 2010. Nuclear Firsts: Milestones on the Road to Nuclear Power Development. American Nuclear Society, La Grange Park, IL.

Naval History and Heritage Command, 2015. Hyman Rickover (SSN-709), July 21, 2015. Available at: http://www.history.navy.mil/research/histories/ship-histories/danfs/h/hyman-rickover-ssn-709.html. (Accessed 18 September 2015).

Paine, L.P., 1997. Ships of the World—An Historical Encyclopedia. Houghton Mifflin Harcourt Publishing, Boston, MA.

Papadopoulos, R., 2007. Heron of Alexandria (c. 10–85 AD). In: Distinguished Figures in Mechanism and Machine Science. Springer Netherlands, Athens, pp. 217–245.

Petroski, H., 1996. Harnessing steam. Am. Sci. 84, 15–19.

Pioro, I. (Ed.), 2016. Handbook of Generation IV Nuclear Reactors. Woodhead Publishing, Duxford.

Pioro, I., Duffey, R., 2015. Nuclear power as a basis for future electricity generation. J. Nucl. Eng. Radiat. Sci. 1 (1), 1–18.

Pon, G., 1978. Evolution of CANDU Reactor Design, Atomic Energy of Canada Limited. Chalk River Nuclear Laboratories, Chalk River, ON.

Revankar, S.T., Riznic, J.R., 2009. Assessment of steam generator tube flaw size and leak rate models. Nucl. Technol. 167 (1), 157–168.

Riznic, J., Duffey, R., 2017. 60 years in motion—short history of nuclear engineering division. ASME J. Nucl. Eng. Radiat. Sci. 3 (1), 1–13.

Shah, V., Lowenstein, D., Turner, A., Ward, S., Gorman, J., MacDonald, P., Weidenhammer, G., 1990. Assessment of primary water stress corrosion cracking. Nucl. Eng. Des. 134 (2–3), 199–215.

Singhal, A., Srikantiah, G., 1991. A Review of thermal hydraulic analysis methodology for pwr steam generators and ATHOS3 code applications. Prog. Nucl. Energy 25 (1), 7–70.

Tapping, R., Nickerson, J., Speke's, P., Mariska, C., 2000. CANDU steam generator life management. Nucl. Eng. Des. 197 (1–2), 213–223.
Taylor, G., 1997. Heat Exchanger Tubing Materials for CANDU Nuclear Generating Stations, Atomic Energy of Canada Limited. Chalk River Nuclear Laboratories, Chalk River, ON.
Trunov, N., Lukasevich, B., Veselov, D., Dragunov, Y.G., 2008. Steam generators—horizontal or vertical (which type should be used in nuclear power plants with VVER?). Atomic Energy 105 (3), 165–174.
US Congress, Hearing of the Joint Committee on Atomic Energy, 1971. The Naval Nuclear Propulsion Program. In: 92nd Congress, Testimony of Vice Admiral H.G. Rickover, March 10. US Government Printing Office, Washington, DC.
WIPO, 2015. Inside WIPO, World Intellectual Property Organization. Available at: http://www.wipo.int/about-wipo/en/#connecting. (Accessed 13 July 2015).
Zink, J.C., 1996. Steam Turbines Power an Industry. PennWell Corporation, Tulsa, OK.

Further Reading

Bergunker, V.D., 2011. Integrity of the tubes used in vertical and horizontal steam generators. Therm. Eng. 58 (3), 232–239.
Cirincione, J., 2007. Bomb Scare: The History and Future of Nuclear Weapons. Columbia University Press, New York, NY.
Goldschmidt, B., 1982. The Atomic Complex. American Nuclear Society, Hinsdale, IL.
IAEA, 2015. What is PRIS. International Atomic Energy Agency, Vienna. Available at: https://www.iaea.org/PRIS/About.aspx. (Accessed 15 June 2015).
Pagan, S., Duan, X., Kozluk, M., Mills, B., Goszczynski, G., 2009. Characterization and structural integrity tests of ex-service steam generator tubes at Ontario power generation. Nucl. Eng. Des. 239 (3), 477–483.
Revankar, S.T., Wolf, B., Riznic, J.R., 2013. Investigation of subcooled water discharge through simulated steam generator tube cracks. Multiph. Sci. Technol. 25 (2–4), 249–285.
Wolfe, R., 2015. Field Experience with Steam Generator Tubing Materials in the United States. In: International Nuclear Components Conference, Mississauga, Canadian Nuclear Society, November 1–4, 2015, Mississauga, Ontario, Canada.

This page intentionally left blank

Nuclear steam generator design

2

J.C. Smith
Northern Nuclear Industries, Inc., Ayr, ON, Canada

2.1 Introduction

In the previous chapter, the concept of a nuclear steam generator was introduced. For purposes of the ongoing discussion in this chapter, a steam generator for a nuclear power plant will be summarized as: part of the heat transport system in either a pressurized water reactor (PWR) or a pressurized heavy-water reactor, which is a vertical heat exchanger, using an inverted "U-tube" bundle of small diameter tubes, separating the high-pressure reactor coolant inside the tubes from the medium pressure light water outside the tubes, which boils the light water to steam within a heavy pressure vessel. The steam and water are separated into pure steam for the turbine-generator, and pure water which is recirculated within the confines of the steam generator shell. From this starting point, the design process is laid out in this chapter.

2.2 Specifications

Before beginning the design process, it is essential to have full specifications of the design requirements. The steam generator will receive reactor coolant at flow rate, temperature, and pressure requirements which are determined from the reactor system analysis. The steam generator must produce steam at a prescribed flow rate and pressure as required by the steam system. Design conditions must be specified which are consistent with overall plant safety criteria. All plant operating transients must be fully described in the specifications to be consistent with all anticipated operating cycles over the life of the plant. However, the main criteria required to get the design process underway are:

Full power reactor coolant flow (kg/s), and fluid (heavy or light water)
Full power reactor coolant pressure (MPa)
Full power reactor coolant temperature at the steam generator Inlet (°C)
Full power reactor coolant outlet temperature from the steam generator (°C) (or alternately heat transferred at full power)
Steam pressure at full power (MPa)
Variation in steam pressure with power level[1] (MPa)
Full power steam flow rate (kg/s)
Feedwater temperature (°C)
Primary and secondary side design pressures (as defined by ASME)

With the operating parameters specified, the design process can begin.

[1] Heavy-water reactors are usually constant steam pressure, while PWRs are variable pressure.

Steam Generators for Nuclear Power Plants. http://dx.doi.org/10.1016/B978-0-08-100894-2.00003-0
© 2017 Elsevier Ltd. All rights reserved.

2.3 Tube bundle

The steam generator will be designed from the inside outward. At the heart of the steam generator is the tube bundle. It is necessary to decide:

- number of tubes
- tube size
- tube material
- tube heating surface

The designer will try several combinations before an optimum is selected.

Tube sizes are based on several considerations:

- Heat transport system pressure drop considerations. (A small number of tubes will result in high pressure loss, reduced overall flow in the heat transport system, etc.)
- Overall plant containment geometry. (A small number of tubes will result in a very tall tube bundle to achieve desired heat transfer rate, an excessively tall steam generator which could force an excessively tall containment.)
- Generally steam generators are 20–23 m tall, and use of smaller diameter tubes tends to make tube bundles shorter but larger in diameter, so tube diameter factors into overall plant containment design.
- Use of certain "standard" tube sizes helps to assure that "standard" tube inspection probes can be used for eventual in-service inspections.
- In heavy-water reactors there is a tendency to use smaller diameter tubes in an attempt to minimize heavy-water volume, as pure heavy water is quite costly.

Common tube sizes used in the past in steam generators are:

$7/8'' \times 0.050''$ tube wall (22.2 mm × 1.27 mm) (older Westinghouse and licensee designs)
$3/4'' \times 0.043''$ tube wall (19.05 mm × 1.09 mm) (Westinghouse Model D, E, and Combustion Engineering designs)
$11/16'' \times 0.040''$ tube wall (17.5 mm × 1.02 mm) (Westinghouse Model F and some replacement PWR steam generators)
$5/8'' \times 0.0445''$ tube wall (CANDU steam generators, CANDU 6, and Darlington)
$1/2'' \times 0.044''$ tube wall (older CANDU steam generators, Pickering, Bruce)

Note that the tube walls of the CANDU steam generators are similar to those of PWR steam generator tubes, while the diameters of the CANDU tubes are smaller. This would suggest that the pressures of the CANDU reactor coolant must be higher than that of PWRs. In fact, the opposite is true. CANDU tubes have traditionally used the higher-wall thickness as additional margin against corrosion conditions.

For an overall steam generator height of 20–23 m, it is expected that the tube bundle will be in the range of 9.5–10.5 m in height, and pressure drop from inlet to outlet for the reactor coolant will be in the range of 250 kPa. With these numbers in mind, an optimum number of tubes is selected.

Selection of tube material is much more about long-term corrosion performance than immediate heat transfer performance. This chapter will not go into the discussion of tube corrosion and degradation. The reader is referred to Chapter 8 for this discussion. Suffice it to say that the main tube materials used in nuclear steam generators in the past have been:

Alloy 600, mill annealed quite unsatisfactory, most of the steam generators with this tube material have been replaced.
Alloy 600, thermally treated, significant improvement over mill annealed, but certain of these steam generators are now being replaced. Alloy 600 was first adopted for nuclear use by the US Navy in the 1950s.
Alloy 800, used first in Germany and then in CANDU steam generators, significant improvement in performance over alloy 600. However, alloy 800 has a lower thermal conductivity and (per ASME code rules) a lower strength than alloy 600. Alloy 800 has had excellent corrosion performance in operation in most cases (with several notable exceptions) but can be shown in laboratory testing to still have corrosion susceptibility. Alloy 800 continues to be used in CANDU (replacement) steam generators.
Alloy 690, developed around 1980, seems impervious to all forms of steam generator tube corrosion. It is the material of choice for virtually all new and replacement PWR steam generators. Compared to alloy 800 it has higher resistance to corrosion, higher thermal conductivity, and higher strength.

When the tube material is chosen, final decisions can be made about tube wall thickness (function of tube diameter, strength, and fluid pressures inside and outside of the tubes).

Finally, the tube heating surface must be determined.

To show how this is done, a very simple type of steam generator is used, representative of typical PWR steam generators without integral preheaters. Integral preheaters will be described later in this chapter.

First, for the typical simple PWR steam generator, the operating pressure on the primary side is 15.7 MPa, at which water saturation temperature is 344.4°C. The water is heated in the reactor to something approaching saturation temperature, but seldom exceeding 326°C. As it turns out, the corrosion of the tubing is a strong function of exactly what this maximum temperature of the reactor coolant is.

The pressure of the steam produced in the steam generator will typically be in the range of 5.5–7 MPa, with a corresponding saturation temperature of 269–285°C.

Basically, the tube bundle is immersed in a pool of water at steam cycle saturation temperature, and as the heat transport fluid passes through the tubes, heat is released which cools the heat transport fluid while causing the steam cycle water to boil at constant temperature. This pattern is shown in the following temperature diagram. A single tube is assumed to be straightened out so that the left side represents the tube inlet and the right side represents the tube outlet. The temperature of the fluid inside the tubes drops from inlet to outlet, whereas the temperature of the fluid outside the tubes is constant at saturation temperature (Fig. 2.1).

At the Inlet end of the tubes, the temperature difference is (325–270) = 55°C, and at the outlet end of the tube the temperature difference is (285–270) = 15°C. Therefore, it is to be expected that the heat transfer rate (per square meter of heating surface) will be highest at the inlet end and lowest at the outlet end of the tube. The average rate of heat transfer over the bundle is determined using a log-mean temperature difference approach. For this particular set of temperature conditions, the log-mean temperature difference is:

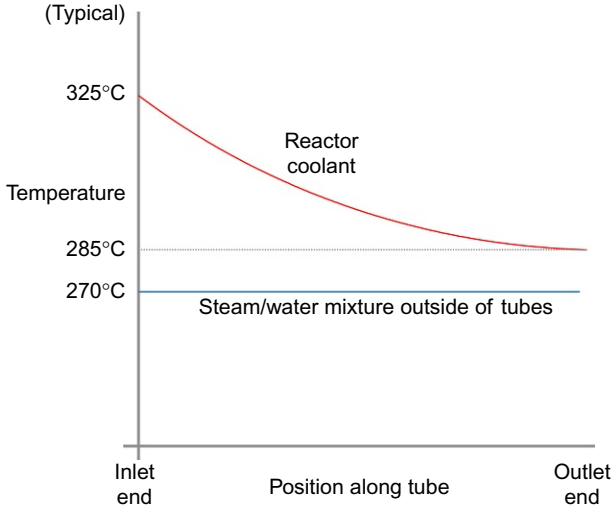

Fig. 2.1 Temperature diagram.

$$\Delta T_1 = 55°\text{C}, \quad \Delta T_2 = 15°\text{C}$$

$$\text{LMTD} = \frac{\Delta T_1 - \Delta T_2}{\ln(\Delta T_1/\Delta T_2)} = 30.8°\text{C}$$

In other words, the average temperature difference driving heat flow between the fluid inside the tube and the fluid which is boiling on the outside of the tube is 30.8°C.

Total heat flow rate from the reactor coolant to the boiling water outside the tubes is determined by simple thermodynamics:

For a total massflow M,

$$\text{Heat flow } Q = M(h_{\text{inlet}} - h_{\text{outlet}})$$

where h represents fluid enthalpy.

This is calculated and also used to verify that the same heat flow rate will generate sufficient steam on the outside of the tubes.

Once verified that the heat flow rate is correct, it is observed that:

$$Q = U_{\text{o}} \times A \times \text{LMTD}$$

Therefore, calculation of the surface area depends on the known LMTD and heat flow rate Q, plus the overall heat transfer coefficient U_{o}, which remains to be calculated.

The overall heat transfer coefficient for the tube bundle is determined from a series of resistances to heat transfer, specifically:

- resistance inside the tube, essentially 1/heat transfer coefficient of the fluid inside the tube
- resistance of the tube metal to heat transfer, this is where tube metal conductivity and wall thickness become important

- resistance to heat transfer from any fouling or foreign materials that accumulate on the tube surface over years of operation
- resistance to heat transfer from the boiling process on the tube outside surface

There are adjustments made to these resistances to normalize all calculations to the tube outside surface dimension. For example, the inside fluid heat transfer coefficient is applied at the inside surface, which is smaller than the outside surface area (say, per meter of tube length), and so the inside resistance to heat transfer must be increased to normalize it to the outside surface dimension.

Generally, the inside, tube metal, and fouling resistance are straightforward calculations using standard textbook correlations. The most complex of the calculations is the boiling heat transfer correlation on the outside of the tubes.

First, without going into a detailed dissertation on two-phase flow, the conditions on the outside surface of the tube have been described as a boiling container of water. We want pure steam going to the turbines, so does the water all turn to steam around the tube bundle, and if so does it somehow invalidate the boiling water assumption? In fact, as will be described later in this chapter, there is a constant flow of water past the tube bundle on the outside of the tubes, starting at the bottom of the tube bundle, and flowing upwards around the tubes. The quality of two-phase mixture is zero at the bottom of the tube bundle, and typically only a maximum of 40% as this flow leaves the top of the tube bundle. The steam and water are separated in the separators in the steam drum (see Fig. 2.3), and only the pure steam leaves the steam generator. The saturated water is recirculated in an annulus to pass through the tube bundle again for more boiling. The mass of steam taken out is matched by the mass of feedwater put into the steam generator over any period of constant power operation. So long as the quality of the two-phase mixture surrounding the tubes is less than 40%, the outside heat transfer process will be nucleate boiling.

There are many heat transfer correlations available for nucleate boiling, some of which were developed specifically for water where the boiling action is the dominant mode of heat transfer over any contribution of pure convection. All of these correlations have one common characteristic: they are highly dependent upon the boiling heat transfer film temperature differential. To understand this, imagine a tube with fluid flowing inside it at temperature T_{inside}, transferring heat into the tube wall, through a fouling layer on the outside of the tube, and then to a boiling fluid at T_{sat}. There is a continuous temperature pattern as shown in Fig. 2.2. There is a "boiling film temperature" where the temperature at the surface, where the boiling fluid contacts the tube wall, where the temperature is higher than saturation, and where the formation of bubbles or steam pockets originates. As this boiling film temperature gets larger, there is more bubble formation and hence more heat transfer.

In simple form, the boiling heat transfer coefficients will state that:

$$H_{\text{boiling}} = K \cdot (\Delta T_{\text{film}})^2$$

As overall heat flux Q/A is based on $H \cdot \Delta T$, Q/A is then proportional to $(\Delta T_{\text{film}})^3$, usually requiring iterative solutions.

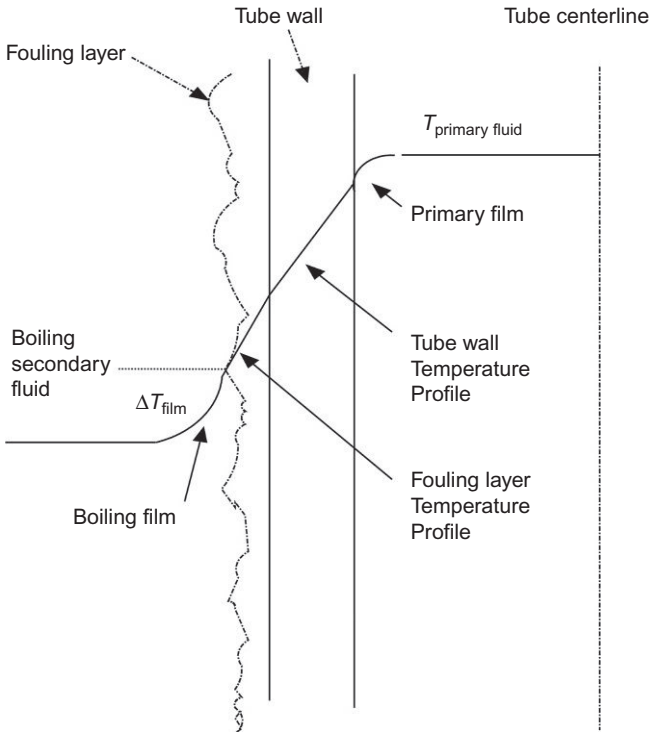

Fig. 2.2 Temperature profile around tube wall.

The outside heat transfer coefficient is quite large, meaning that the boiling heat transfer is very effective. In very rough numbers, in a PWR steam generator, surface area will average out in the range of 15 m^2/MWe. In other words, in a 1200 MWe 4-loop PWR (300 MWe per steam generator), the expected surface area of the tube bundle in each steam generator would be in the range of 4500 m^2. Using higher steam pressure will tend to require more surface as the net ΔT between the primary and secondary fluids will become less as steam saturation temperature goes up. Use of higher conductivity tubing will require less surface area as metal resistance to heat transfer goes down.

2.4 Overall steam generator layout

At this point, with the tube bundle essentially set, the rest of the steam generator can be sketched around the bundle. The overall steam generator will generally appear as in Fig. 2.3. This drawing is deliberately generic in order to avoid focusing on design specifics of any one steam generator designer and instead shows the common features of

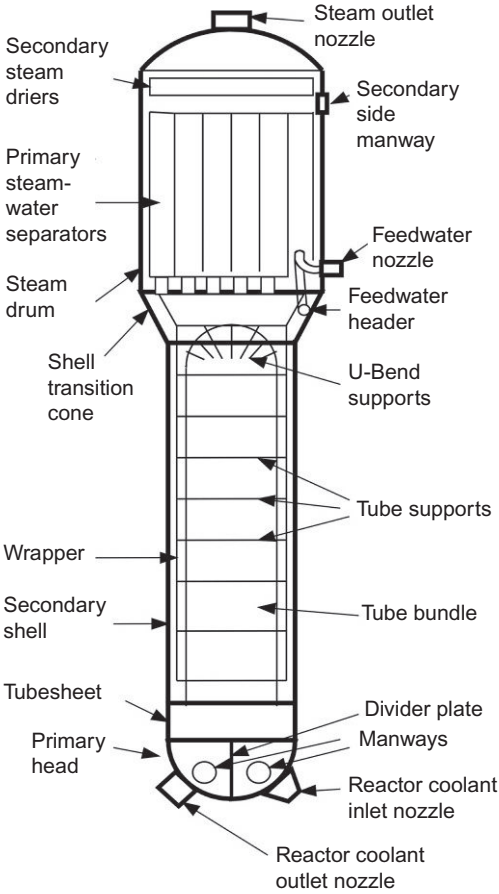

Fig. 2.3 Steam generator general arrangement.

all designs. The balance of this discussion revolves around completing the details of the design.

2.5 Circulation

Most of the steam generators used in PWRs worldwide are vertical *recirculating* steam generators as are all of the steam generators used in CANDU reactors. Notable exceptions in PWRs are Russian reactors which use horizontal steam generators, and certain US PWRs which use once-through steam generators. However the vast majority are recirculating type which will be the basis of this discussion.

Note in Fig. 2.3 that the tube bundle is surrounded by an "inner shell" referred to as the wrapper. The wrapper creates an annular gap inside the secondary shell. The secondary side water fills the steam generator up to a water level which is located in the

area of the primary steam-water separators. As bubbles form in the water immediately adjacent to the tube surfaces, the density of the fluid (steam-water mixture) around the outside of the tubes begins to drop. However, the density of the fluid in the annular space remains constant at saturated liquid density. Therefore, as the boiling goes on, the hydrostatic pressure head of the secondary fluid around the tube bundle begins to drop, while the hydrostatic pressure head at the bottom of the annulus region remains constant, higher than that of the fluid in the bundle region. The pressure differential causes the fluid from the annulus to begin flowing into the tube bundle region, and the two-phase mixture around the tubes must flow upward. All of the secondary side upward flow then enters the steam-water separators, the steam exits the top of the separators and goes through driers, and then out through the steam outlet nozzle. The water which is separated from the steam is released into the drum and is ready to recirculate again down the annulus.

The amount of recirculation in a steam generator is described by a normalized "circulation ratio." The total amount of flow moving up through the tube bundle region of the steam generator is divided by the steam flow.

$$\text{Circulation ratio} = \frac{\text{Total mass flow rate rising through tube bundle region}}{\text{Steam flow rate leaving steam generator}}$$

Most steam generators are designed to have a circulation ratio in the range of 3–6. In other words, most of the *mass* flow moving up through the tube bundle region is actually water. At a circulation ratio of 6, 5 parts out of 6 are water. However, note that this can still represent a *void fraction* of the mixture as much as 85%–90%. It is pointed out that this circulation flow is referred to as "natural circulation." It is caused by the hydrostatic head differentials, i.e., it is not driven by pumps and outside forces.

Calculation of the exact circulation ratio which a steam generator will operate at requires detailed knowledge of the pressure drop characteristics of elements in the flow path. As the flow rises through the tube bundle, it encounters tube supports, the design of which will be described later in this chapter. The tube supports must be solid enough to restrain the tubes against vibration, but yet at the same time be open enough to allow this very high flow of two-phase mixture to pass through them. The two-phase flow enters the primary separators, and the two phases are stripped apart. This causes further pressure loss. The single-phase flow is returned down the annulus and experiences flow friction losses, entrance and exit losses, etc. The exact circulation ratio of a steam generator is determined by calculating the hydrostatic head differential (pumping head) between the annulus region (saturated water) and the tube bundle region (two-phase mixture), and equating them to total flow pressure drop around the circulating loop.

One important concept to observe is the following:

As the flow moves upward through the tube bundle region, it starts as saturated water entering the tube bundle region from the annulus, and as it gains heat from the tubes, bubbles form and move along with the flow. The further the flow moves up in the bundle region, the more steam bubbles are gathered. Above the tube bundle,

just before entering the separators, the flow is a two-phase mixture of average quality χ. The circulation ratio is total flow divided by steam flow, but total flow is $m_{st}+m_{liq}$.

$$CR = \left(m_{st} + m_{liq}\right)/m_{st}$$

For a perfectly mixed flow, the quality of the mixture is:

$$\chi = m_{st}/\left(m_{st} + m_{liq}\right)$$

Note that the *average quality of the two-phase mixture leaving the tube bundle is the inverse of the circulation ratio*. If the circulation ratio is 6, the average quality of the two-phase mixture leaving the tube bundle is 16.7%. Note, however that there is usually a range of qualities in the U-bend region. These qualities must be determined using 3D computer models such as the ATHOS computer code. The quality and flow velocity values determined by 3D codes are very important for tube vibration analysis, design of U-bend supports, and long-term resistance of the steam generator to having dry regions and regions of excessive deposits on the tube outside surfaces.

Detailed calculation of the circulation ratio in any steam generator is an iterative process. It is the result of balancing of the hydrostatic pressure differential between the liquid in the annulus vs the two-phase mixture in the bundle region (pumping head) against the circuit pressure losses.

Regarding pumping head, if we first assume that the steam generator will circulate with a circulation ratio of 5, we can calculate the pumping head by calculating the density of the two-phase mixture throughout the bundle region. Usually this is done by developing a detailed quality distribution, as local qualities are important in a number of calculations, such as the individual tube support pressure losses. The average quality leaving the tube bundle is the inverse of the circulation ratio, i.e., 1/5 or 20%. If we then calculate pumping head for a circulation ratio of 6, the average quality leaving the tube bundle will be 1/6 or 16.7%. Qualities will typically be lower throughout the tube bundle, making the average density of two-phase mixture around the tube bundle higher, the hydrostatic pressure at the bottom of the bundle region higher, and therefore the hydrostatic pressure *differential* between the bottom of the annulus and the bottom of the bundle region lower. Therefore, pumping head decreases with increasing circulation ratio.

As the steam generator circulates with higher and higher circulation ratios, the pressure losses through tube supports, separators, etc., can be expected to increase dramatically, approximately by flow rate squared. Note that these calculations have to be done in detail taking into account two-phase flow effects, etc., but the flow squared proportionality concept is reasonable.

The final effect comes from the following: It was stated earlier that the water level creating the hydrostatic pressure at the bottom of the annulus was "somewhere in the range of the primary separators." In fact, this level can fluctuate, and so if the water level goes up, it creates more hydrostatic pressure at the bottom of the annulus and hence tends to force higher circulation ratios. The following three figures illustrate determination of circulation ratio.

In Fig. 2.4A, the iterative process is shown. First, an assumed circulation ratio (iteration 1) is selected. The quality distribution throughout the tube bundle region is calculated, giving the hydrostatic pressure differential or pumping head, and all of the circuit pressure losses are calculated. The circuit losses are lower than the pumping head, so it can be concluded that the circulation ratio must be higher than the assumed number in iteration 1. In iteration 2, a higher circulation ratio is assumed. Note that the pumping head is lower due to lower average qualities throughout the tube bundle. However, the circuit pressure losses at this higher circulation ratio now exceed the pumping head, and so it can be concluded that the actual circulation ratio must be lower than the assumed value in iteration 2. In iteration 3, there is an exact balance of the circuit losses against pumping head. This therefore represents the stable circulation ratio of the steam generator, for the power level and water level analyzed.

As mentioned earlier, the hydrostatic pressure created at the bottom of the annulus depends on exactly where the water level is in the steam drum area. In Fig. 2.4B we see that for decreasing water level, there is a set of ever decreasing pumping head lines, which cross the flow losses line at ever decreasing circulation ratios. The conclusion is that lower water levels, all else being equal, will result in lower circulation ratios.

Finally, we refer back to the concept of average quality leaving the tube bundle region being the inverse of circulation ratio. If one imagines a steam generator at zero power level, both the annulus and the area around the tube bundle are full of saturated liquid. With the addition of a very small amount of heat from the tube bundle, a small handful of bubbles form in the bundle region and start moving upward. The quality of two-phase mixture is very low due to the limited number of steam bubbles. As power increases, there is an ever increasing amount of steam with the water, full circulation is established, and quality continues to increase as power level continues to increase. However, circulation ratio is the inverse of quality exiting the bundle. Therefore it makes sense that the circulation ratio vs power level curve for a steam generator will be as per Fig. 2.4C.

As power level goes down, the circulation ratio goes up. Remember, however, that circulation ratio is the ratio of total flow moving up through the bundle region divided by steam flow. As power level goes down, so also does steam flow. The question becomes, is the maximum flow rate through the tube bundle achieved at 100% power or at some lower power level? Analysis of most steam generators suggests that the maximum flow rate through the steam generator usually occurs at a lower than 100% power level, somewhere in the 60%–80% range, but this maximum flow rate is usually within 10% of the total flow rate through the tube bundle region at 100% power. Nevertheless, this condition of higher flow at lower power must be carefully considered in tube vibration analysis.

Finally the question arises, what is a "good" circulation ratio to strive for and why? To avoid deposition on the tube surfaces, a target of maximum 40% quality has been shown to be effective. At the top of the tube bundle, where quality of the two-phase mixture is maximum, a quality of 40% would seem to imply that a circulation ratio of $1/0.4 = 2.5$ would suffice. However, a quality of 1/CR is only a bulk average. Some steam generators with circulation ratios in the range of 2.5 have shown signs of having localized regions in the U-bend with qualities of 90% or higher. There will be a brief

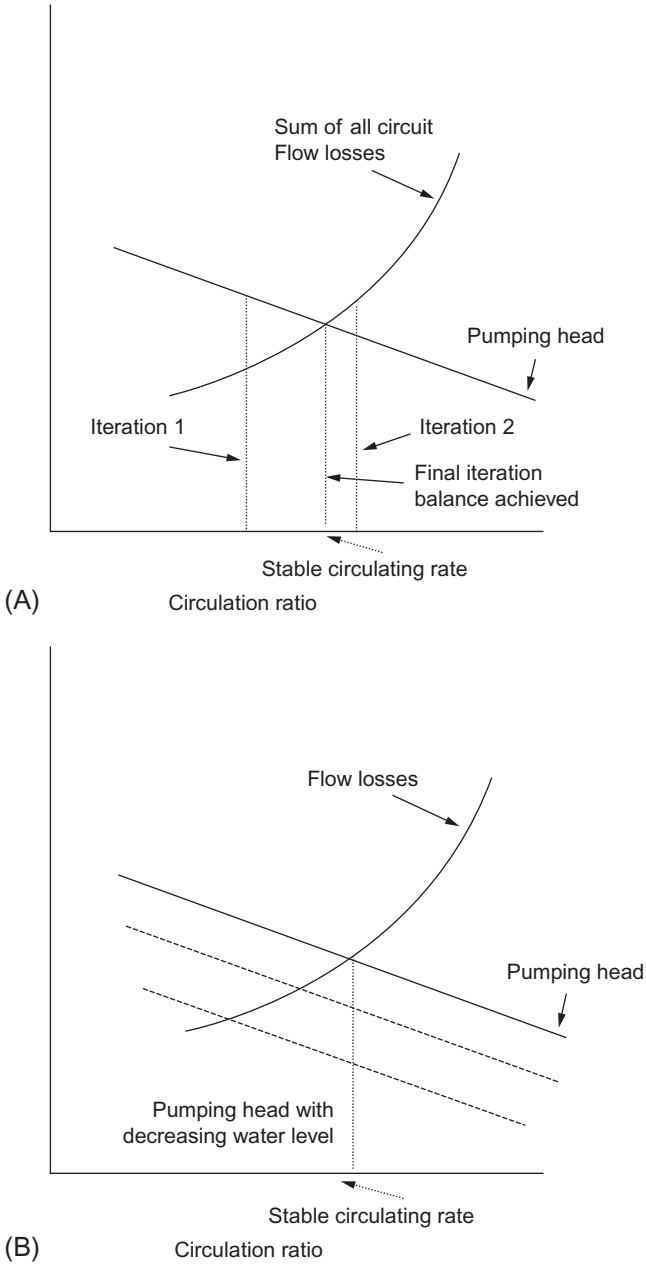

Fig. 2.4 (A) Circulation iterations. (B) Effect of water level on circulation ratio.

(Continued)

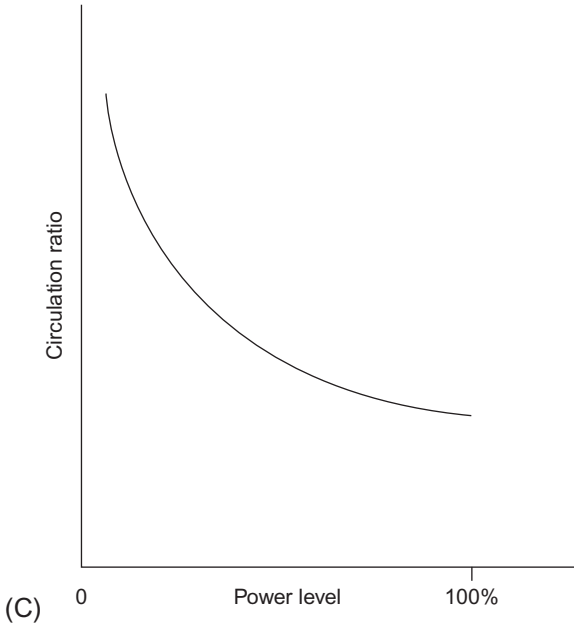

Fig. 2.4, cont'd (C) Circulation ratio vs power level.

discussion of tube vibration analysis later in this chapter, and a full chapter (Chapter 14) dedicated to this topic, but suffice it to say at this point that at very high qualities, the damping effects of the water in a two-phase mixture disappear, dramatically increasing potential for tube vibration and fretting wear.

CANDU steam generators have traditionally targeted a circulation ratio of 6 as a design target, and Westinghouse licensees generally targeted 4–4.5. Combustion Engineering targeted lower values, in their very large steam generators. Over the long term in operation, the CANDU steam generators survived well. The only adverse affect of the high circulation ratio was occasional tube fretting in the U-bend region, but the steam generators remained very clean in operation, due in large part to the relatively high flow rates and low mixture qualities throughout the steam generator. Circulation and its analysis are very important aspects of the steam generator design regardless of which model is selected.

2.6 Other elements of the circulation system

From this point, the remainder of the steam generator is designed around the tube bundle and the basic circulating loop.

The first key consideration is tube supports. There are two main types of tube supports in use currently: broached plates and lattice grids.

Tube supports are intended to restrain tubes against vibration, but at the same time allow the upward flow of two-phase mixture to pass through them in operation. The more metal that can be removed from the support, the more open it will be to flow, but at the same time it will lose its structural strength. The key to design is to pick the optimum balance between strength and minimum flow loss. Shown below are views of broached plates and lattice grid tube supports.

The broached plate starts with a solid disc of stainless steel, roughly 32 mm thick and slightly larger in diameter than the tube bundle. The tube pattern which is used in the tubesheet is also used to initially drill all of the required holes for the tubes (2 holes per tube) in the plate. Then broaching tools are pulled through each hole in order to open up the flow areas as shown in Fig. 2.5A. Flow passes through these areas and sweeps the tube surface as it goes through. The broached plate shown is for a triangular pitch tube bundle. There is a similar design but with four flow areas used for square or "quatrefoil" pitch broached plates.

Fig. 2.5B shows a typical lattice grid section. Rather than starting with a solid plate and machining away much of the metal, the lattice grid is made using strips of stainless steel material, assembled into a grid. There are plusses and minuses to each design. Broached plates have been used exclusively by most of the major PWR suppliers, with the exception of Siemens. Siemens used lattice grids in the KWU PWR plants. CANDU steam generators have used both broached plates and lattice grids at various points in time. All CANDU steam generators built since 1980 have used lattice grid tube supports, and replacement PWR steam generators sold in the United States which were based on CANDU steam generator technology also used lattice grids. Lattice grids will typically have lower pressure losses than broached plates, particularly at lower bundle pitch to tube diameter ratios, and hence have been preferred for high circulation ratio CANDU steam generators.

The next major element in the circulation loop is the steam-water separators. The separators must perform several functions:

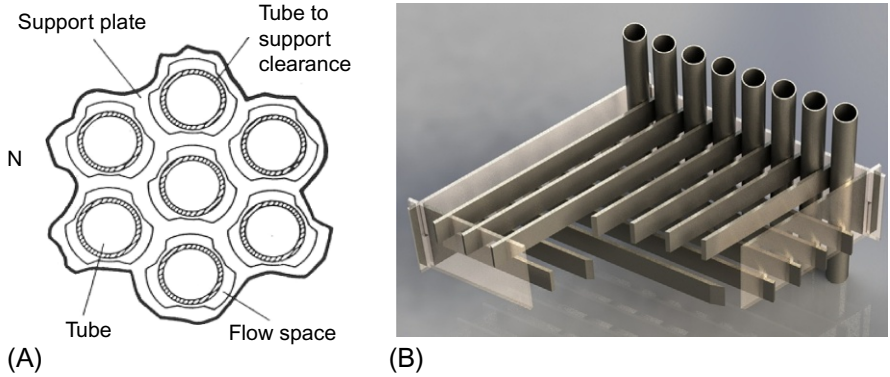

Fig. 2.5 (A) Broached plate tube support. (B) Lattice grid tube support.
Photo courtesy of BWXT Canada Ltd. © 2016 BWXT Canada Ltd. All rights reserved.

- The entire two-phase flow coming from the tube bundle enters the separators and is separated into steam, which exits and is directed toward the steam outlet nozzle, and water which is directed to return to the annulus for recirculation. The separators must perform this operation with high efficiency and low-pressure drop. The steam exiting the primary separators will have quality very close to 100%, and then the steam is passed through final driers, where the quality will be 99.9% or higher heading to the turbine. The remaining moisture, referred to as carryover, is not permitted to be higher than 0.1%. Steam generator suppliers can meet this requirement consistently.
- The separators must remove all of the steam from the recirculated water. This entrained steam, called carry-under, can cause a significant reduction in circulation ratio as a small amount of steam in the annulus water significantly reduces density of the water.
- The separators must operate effectively over a range of pressures, loads, water levels, etc.
- Separators will be discussed in more detail in Chapter 4. Each steam generator supplier has their own design of separators, largely tested and proven in operation or in full scale lab testing. The testing will verify a design loading permissible for each separator type, and the designer then sets a drum design based on the required number of separators and required range of water levels for operation.

Another major design consideration is the U-bend supports. At this point in the design process, the steam generator is almost complete, and so detailed thermal hydraulic analysis (ATHOS, etc.) can be performed, detailed fluid velocities and qualities throughout the tube bundle can be established (see Chapter 4). Then tube vibration analysis is performed.

There are three general types of forcing functions for steam generator tube vibration:

- *Vortex shedding:* It is not common, only possible at the entrance region of the tube bundle and in single-phase flow.
- *Fluid-elastic instability*: This can occur anywhere in the tube bundle, single- or two-phase flow, but will most likely occur in areas of high crossflow velocities. These include bundle entrance regions, the U-bends, and if the steam generator is an intergral preheater type, at several locations in the preheater. Fluid-elastic instability is unique in that it can change from very minor vibration to major vibration with very little change in fluid flow conditions.
- *Turbulent buffeting*: This is a general shaking of tubes caused by statistical turbulence. It can occur in either single- or two-phase flow and increases proportionately to flow (i.e., lacks the sudden dramatic increases possible with fluid-elastic instability).

The response of the tubing to the excitation or forcing functions is calculated using tube models which correctly calculate natural frequencies, tube stiffness, attached mass, and damping. True tube responses in terms of mean amplitudes of vibration and fretting loads against tube supports are calculated. This sort of analysis allows the designer to ensure having adequate numbers of U-bend supports.

The areas of the tube bundle most likely to exhibit tube vibration are the entrance region immediately above the tubesheet, the U-bend region, and in the vicinity of the preheater if the steam generator is an integral preheater type. Integral preheaters are used in most CANDU steam generators and have been used in some older Westinghouse designs, as well as some Siemens designs. Most of the Westinghouse integral preheater steam generators have been replaced, but more because of tube material

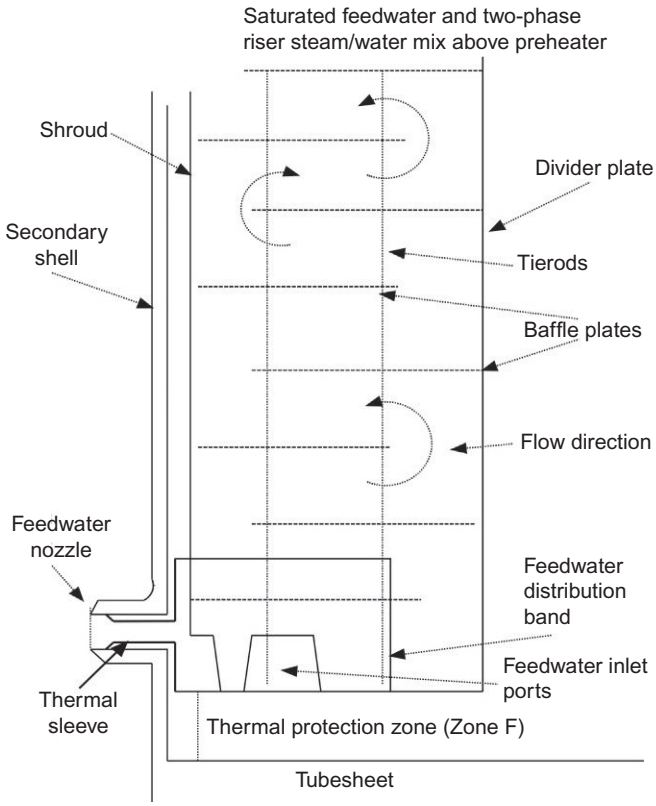

Fig. 2.6 Layout of integral preheater.

issues rather than preheater issues. In an integral preheater design of steam generator, the lower end of the outlet side of the tube bundle is segmented and isolated to become a heat exchanger. This enhances the heat transfer efficiency of the steam generator, allowing use of less heat transfer surface in the tube bundle. A typical integral preheater arrangement is shown below. Integral preheaters use stainless steel drilled baffle plates for both flow direction and tube support against vibration (Fig. 2.6).

2.7 Feedwater inlet

As steam is produced in the steam generator, it leaves the steam generator via the steam outlet nozzle. The mass flow rate of steam exiting is balanced by the mass flow rate of feedwater entering the steam generator. For a steam generator which is not an integral preheater type, the feedwater enters via a feedwater nozzle

typically located in the side of the steam drum (see Fig. 2.3). For an integral preheater type steam generator, the feedwater nozzle is on the outlet or "cold leg" side of the tube bundle, near the tubesheet. The integral preheater system directs all incoming feedwater to flow through the preheater. The nonpreheater designs direct the incoming feedwater flow into a feedwater header, typically a pipe bent into a circular form and located in the annulus. The flow coming into the steam generator is typically directed first upward, through a "gooseneck" pipe assembly, and then downward into the feedwater header. This avoids risk of flow stratification in the feedwater inlet line, which can lead to high stressing of the feedwater piping system. The feedwater header itself generally has some form of J-tube outlets on the top of it to prevent the header from draining and creating steam pockets while the steam generator operates.

At this point, the details of the steam generator internals are complete, and dimensions are essentially fixed. However, the entire set of internals is contained within a pressure boundary which must be designed next.

2.8 Pressure boundary design

The pressure boundary of a nuclear steam generator is designed to the highest level of national pressure vessel codes specifically for nuclear vessels. In the United States and many other countries, that code is the ASME code, Section III Division 1, section NB for Class 1 components. The design process to be used under this section of the code is "design by Analysis," in other words the vessel is required to have a full stress analysis of all sections of it to be a registered and approved design.

The steam generator has two distinct pressure zones: the primary side and the secondary side, separated by both the tubesheet and the tubes. Although the tubes are internal to the steam generator, they still represent the pressure boundary between the primary and secondary fluids and hence are also subject to stress analysis. The design of the steam generator pressure boundary is completely analyzed, typically by finite element stress analysis, and must be shown in every respect to have stresses, stress ranges, stress intensity factors, and fatigue usage factors within the range specified by ASME as "allowable." Code acceptance criteria include evaluation for failure due to net-section collapse (local and global), incremental collapse, fatigue, and nonductile failure from a variety of load sources experienced from the plant design.

Although "internals" of the steam generator might not be pressure retaining parts, they serve various safety-related purposes for the pressure boundary and must therefore also be subjected to analysis to prove their ability to prevent loss of integrity. An example is tube supports and baffles. If they collapse in burst pipe accidents and can potentially cause tube puncturing or rupture when they collapse, their design is regarded as unacceptable.

The steam generator shell is all-welded. There are bolted closures such as manway covers, inspection port covers, etc. The bolted covers must be fully analyzed,

including strength of the bolts, and their ability to maintain sufficient load on gaskets to ensure sealing during all transient conditions. The code requirements for welds are such that they are effectively one continuum of metal with the shell. The welds have the same properties as the parent steel pieces they are joining together. There are no differences in thickness, strength, stiffness, etc.

Shown below are some of the graphics of typical steam generator stress analysis (Figs. 2.7).

Bolted closures are particularly challenging to analyze, but these analyses are also required as shown below. What makes the analysis so challenging is that during transients, large temperature differences develop between the bolts and the rest of the structure. These temperature differences can result in relaxation of bolt preloads on gaskets, and resultant leakage, or in some cases overstressing of the bolts.

Finally large sections of the vessel are analyzed as integral assemblies, as shown below, when there are limited highly stressed discontinuities. A discontinuity would be a geometric feature such as the corner joint between the shell and the conical

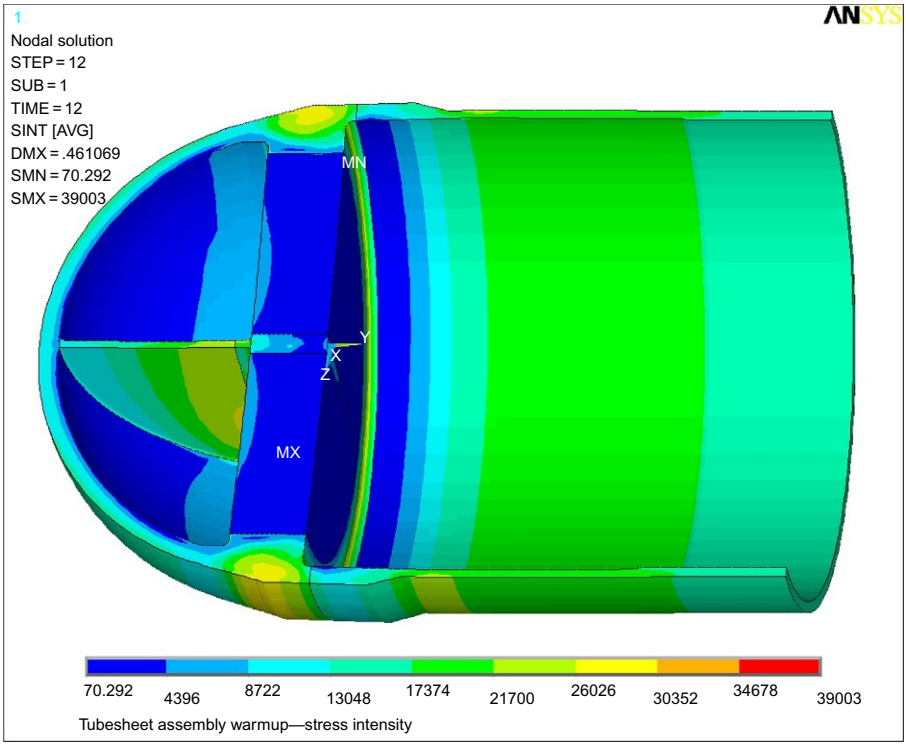

Fig. 2.7 Stress intensities, primary head, tubesheet, lower secondary shell at end of warm-up transient.
Photo courtesy of BWXT Canada Ltd. © 2016 BWXT Canada Ltd. All rights reserved.

section. All of this is factored into the finite element model. The resultant shell thicknesses, even using high strength materials, are in the range of:

Primary side design pressure	17.5 MPa
Primary head thickness	13–15 cm
Tubesheet thickness*	55–60 cm
Secondary side design pressure	5.6–7.7 MPa
Secondary shell thickness	8–10 cm
Drum and drum head thickness	10–12 cm

*The tubesheet, by virtue of being drilled, is a flat, porous plate, very prone to stresses when exposed to differential pressure. The shell and the primary divider plate are used as stiffeners and supports for the tubesheet, or its thickness could be much higher than the values shown (Fig. 2.8).

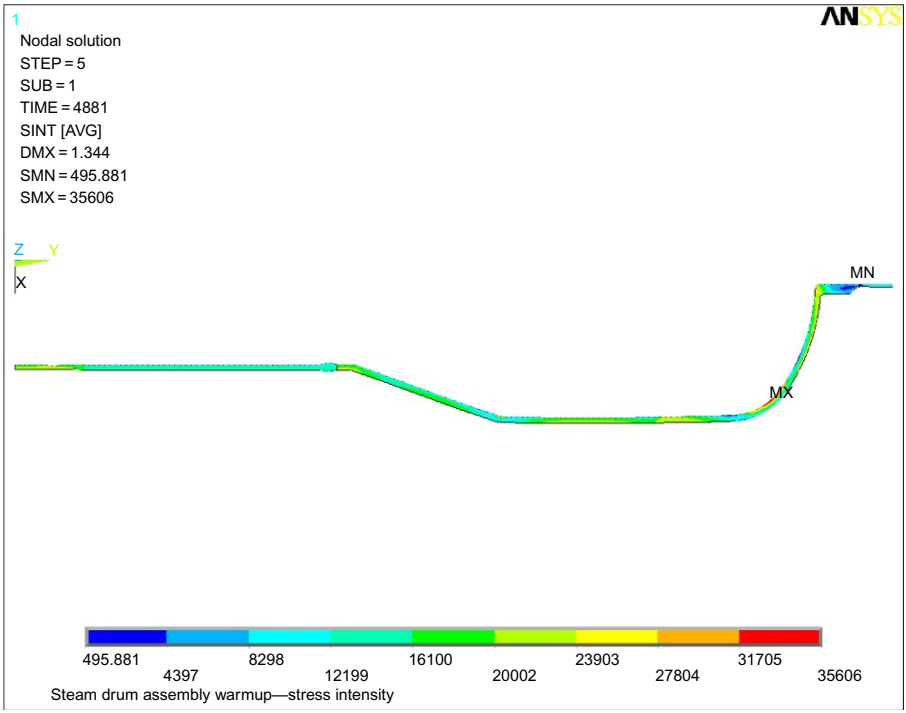

Fig. 2.8 Stress intensities in shell, transition cone, drum, and head at the end of a transient.
Photo courtesy of BWXT Canada Ltd. © 2016 BWXT Canada Ltd. All rights reserved.

With the pressure boundary sized and fully analyzed, the design is complete.

Shown below are several typical PWR and CANDU steam generator sizes including the Once Through steam generators for comparison (Fig. 2.9).

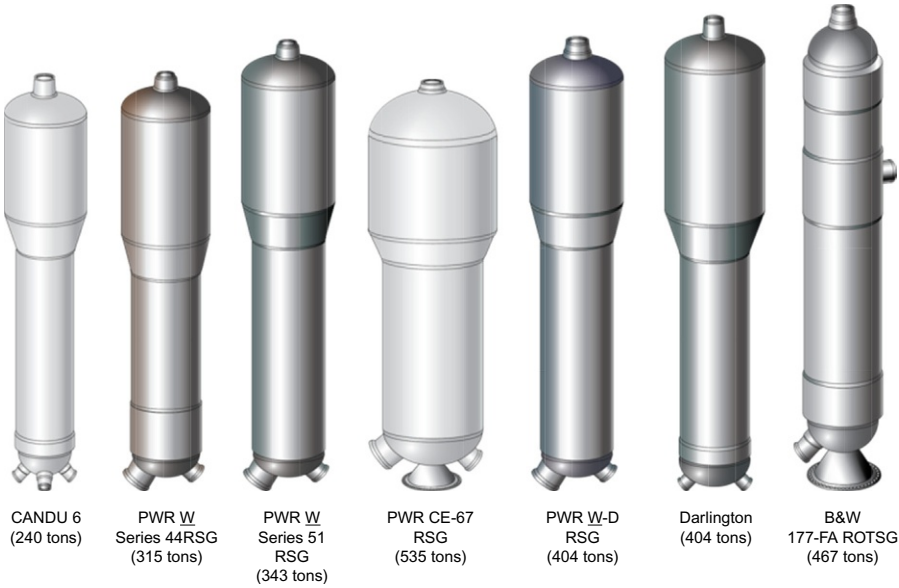

Fig. 2.9 Steam generator sizes, typical PWR and CANDU plants.
Photo courtesy of BWXT Canada Ltd. © 2016 BWXT Canada Ltd. All rights reserved.

2.9 Conclusions

Steam generators of the vertical recirculating type are widely used in both PWR and CANDU reactors. This is not the only type of steam generator used (some horizontal in Russian plants and some once-through steam generators in US PWRs), but still the dominant type used. These steam generators are typically 20–23 m tall and weigh in the range of 300–500 tons each. Some (C-E System 80) weigh as much as 800 tons. Newer steam generators for the AP1000 reactors weigh in the range of 600 tons each. These designs use inverted U-bend tubes, and current trends are to use mainly alloy 690 tubing although alloy 800 is still occasionally used. Both broached plate and lattice grid type tube supports are used, always made of stainless steel. The technology of steam generators is mature, in that failures of steam generators, such as catastrophic tube failures, are becoming quite rare. This chapter has explained how steam generators are designed, and from here we move to the manufacturing.

This page intentionally left blank

Steam generator manufacturing

3

J.C. Smith
Northern Nuclear Industries, Inc., Ayr, ON, Canada

3.1 Introduction, manufacturers

We have now examined in detail how a steam generator is designed; how critical materials are selected; how the design is verified through analysis for stress, tube vibration, thermal performance, etc. Now we look at how this vessel is assembled, and how certain of the assembly steps are developed specifically to ensure that they meet design objectives. For example, if the designers require certain tolerances of fit between tubes and tubes supports, it is one thing to talk of a 0.1 mm clearance on paper, but quite another to achieve this tolerance in a 400–600 ton steam generator. Manufacturing people describe steam generators as "400 ton Swiss Watches," but long-term reliability of the product depends on achieving these requirements.

Around the world there are numerous companies which have some level of nuclear steam generator manufacturing experience:

China—with the rapidly expanding program of PWR manufacturing in China, there are now four steam generator manufacturers, which are also PWR reactor vessel and pressurizer fabricators, in some cases with their own forging capabilities. Shanghai Nuclear Electric Power Co. is focusing on Westinghouse AP1000 type equipment, Dongfang Boiler Group on Areva EPR equipment, China First Heavy Industries on Domestic Chinese designs, with some work by Harbin Boiler Company as well. These plants have not produced CANDU steam generators. The steam generators for Qinshan Phase 3 were produced through a cooperative effort between BWXT Canada[1] and Doosan of South Korea.

South Korea—Doosan is a well-established supplier capable of making steam generators of up to 800 tons, PWR reactor vessels and pressurizers, etc. Doosan has its own forging capability. Doosan produces all of the heavy components for Domestic Korean PWR's, has produced many of the components for the Wolsong and Qinshan (China) CANDU plants, as well as components for Westinghouse AP1000 PWR's in the United States and China. Doosan has also produced replacement PWR steam generators for Westinghouse for the United States and South Korea. The Korean domestic PWR program is based originally on technology from Combustion Engineering in the United States. They have 1000 and 1400 MWe reactors, with only two steam generators of 650–800 tons each per reactor. Korea has also sold four of these reactors to the United Arab Emirates, with all steam generators and heavy components coming from Doosan. The four Westinghouse AP1000s currently (in 2016) under construction in the United States have all of their heavy components, including steam generators, coming from Doosan in South Korea. Doosan has CANDU

[1] As of Jul., 2015, B&W Canada has been renamed BWXT Canada as part of a Corporate reorganization in the United States. This is still the company that has supplied nearly all of the CANDU steam generators and 46 PWR replacement SG's, about 300 steam generators in total.

Steam Generators for Nuclear Power Plants. http://dx.doi.org/10.1016/B978-0-08-100894-2.00004-2
© 2017 Elsevier Ltd. All rights reserved.

steam generator experience through cooperation agreements with BWXT Canada and shared manufacturing on Wolsong 2, 3, and 4 and Qinshan Phase 3 in China.

Japan—Mitsubishi Heavy Industries (MHI) has a large plant in Kobe which produces steam generators for domestic Japanese PWRs, as well as replacement steam generators for the United States and France. MHI started as a licensee of Westinghouse and, in recent years, has developed technology independent of Westinghouse.

France—Areva has a large factory at Chalon/St. Marcel which has produced close to 300 steam generators, mostly new and replacement steam generators for PWRs in France. Areva has also provided some new and replacement steam generators internationally. Areva's predecessor company Framatome started out as a Westinghouse licensee but developed technology independent of Westinghouse starting in the 1980s. Areva has produced no CANDU steam generators. Areva owns forging capability through Creusot Forge at another location in France.

Spain—ENSA of Spain has a medium-sized shop which has produced steam generators (build to print) for Westinghouse, Siemens, and Areva. The last domestic Spanish activity at ENSA was to produce 12 replacement steam generators for 4 Westinghouse reactors in Spain. In that case the replacement steam generator design came from Siemens. Recently ENSA has been producing some replacement steam generators for the United States for Westinghouse. ENSA has no heavy forging capability.

Italy—Ansaldo has produced some PWR replacement steam generators, including 850 ton (2 for 1400 MWe) replacements for Palo Verde in the United States. Ansaldo has no heavy forging capability at the Milan facility.

India—There are two steam generator manufacturers in India: Larson and Toubro, which began building a design based on Douglas Point (CANDU) in the 1970s, and BHEL which is making steam generators for the domestically designed 700 MWe series PHWRs.

Canada—BWXT Canada is the dominant and only active steam generator manufacturer in Canada, which made all of the remaining CANDU steam generators (in some cases in cooperation with others such as Doosan), as well as 46 replacement steam generators for US PWRs and 32 replacement steam generators for Bruce A. In total, BWXT Canada has supplied more than 300 steam generators. BWXT Canada is a wholly owned subsidiary of BWXT United States and is not a licensee of any other supplier. BWXT Canada has developed its own unique technology for both the design and manufacturing of nuclear steam generators. BWXT Canada generally does not license its technology but rather develops project-specific cooperation agreements to share manufacturing with a recipient, as was done with Doosan.

Germany—The German company MAN used to manufacture steam generators for Siemens/KWU but ceased this work in the 1990s.

Belgium—Belgian company Cockerill used to manufacture steam generators under license from Westinghouse but ceased this work in the 1980s.

Russia—Russia has one main steam generator shop for PWR plants of their own design.

Argentina—has one steam generator shop (IMPSA) which has done some work under license from Siemens for the Atucha plant and has produced the replacement steam generators for Embalse under a cooperation agreement BWXT Canada.

Romania—has a large shop (IMGB) which was State owned and developed to make components for Russian PWRs and CANDU plants during the Communist era. This plant is now privately owned. There are some license agreements in place from the Cernavoda 1&2 construction era, but very limited CANDU manufacturing experience.

Eastern Europe—there were several shops in Eastern Europe (Czech Republic, former Yugoslavia) set up to make components, including steam generators for earlier Russian reactors, but this work has largely gone back to Russia since the breakup of Comecon.

The United States—In the 1960s and 1970s, during the period of massive expansion of nuclear in the United States, there were as many as five US shops making steam generators. Westinghouse had two in Florida, Combustion Engineering had one in Tennessee, and Babcock & Wilcox had two: one in Ohio and another in Indiana. The B&W shops were primarily for work on smaller PWRs for the US Navy, but the Mount Vernon, Indiana shop also did B&W commercial PWRs, of which six are currently operating in the United States. The six B&W PWRs all use a unique design of Once-Through Steam Generators. Of these shops, only the B&W shops are still in operation as a result of the Navy work. Combustion Engineering Nuclear was sold to ABB and closed the Tennessee shop and ultimately was resold and became part of Westinghouse. Westinghouse closed their Florida shops in the 1990s.

The United Kingdom—In the United Kingdom, there were numerous suppliers involved in the Magnox and AGR program where steam generators are entirely different designs. The only PWR presently operating in the United Kingdom is Sizewell B, where the steam generators were designed by Westinghouse and fabricated by Babcock Power in Scotland. Although more PWRs are planned in the United Kingdom, the plans for steam generator fabrication are unclear. Sizewell C is to be Areva EPR reactors, and AP1000 (Westinghouse) reactors are also planned for the United Kingdom. Babcock Power in the United Kingdom is now owned by Doosan and has been renamed Doosan Babcock.

3.1.1 Overview and manufacturing objectives

In this chapter we look at the entire process of manufacturing nuclear steam generators. Different manufacturers have slight variations on the manufacturing sequence, but overall the sequence and methods are very similar, both for PWR and CANDU steam generators. Key aspects of the process such as material purchasing, scheduling, Quality Assurance (QA) and inspection, stress relieving, and final shipment will also be examined.

The basic objective in manufacturing of the steam generators is to successfully translate the design and materials requirements from the engineering office to a piece of hardware that meets all of the exacting requirements, built correctly, verified by detailed inspection and testing, and delivered to the end user on schedule and on budget. This is a difficult undertaking, but with the experience of making 300 such pieces of equipment, it can be done dependably and consistently.

3.1.2 QA requirements for nuclear manufacturing

Nuclear manufacturing, in particular of steam generators built to the requirements of ASME Code Section III Division 1, must be done under an established and approved QA program specific to the facility where the work is being done. Every aspect of the work, starting from the review and acceptance of client technical documentation

which forms the basis of the contract, is addressed under the QA program. Key typical blanket programs for QA under which steam generators are commonly fabricated are:

ASME NQA-1 Regulatory Standard created and maintained by the ASME
US 10CFR 50 Appendix B (US Law regarding nuclear QA programs, administered by US Nuclear Regulatory Commission)
ASME N-Stamp (ASME issued stamp placed on finished vessels by the manufacturer certifying that every aspect of the vessel manufacturing has been performed and verified as being fully in accordance with the manufacturer's QA program)

There are similar programs and requirements in other countries where the pressure vessel codes include specific nuclear codes. However, most of the focus of this chapter will be on ASME requirements as an example.

3.2 Manufacturing scheduling

The supply of nuclear steam generators is typically at or near the critical path of either new reactor construction or replacement of steam generators. Therefore it is critical that the steam generators are delivered reliably on schedule. A typical steam generator has more than 10,000 parts, which must be ordered, obtained in accordance with applicable QA requirements in a sequence supporting the schedule, machined, welded, assembled, and tested. Insofar as the manufacturing of a steam generator is in a specific sequence, just one wrong or missing part can stop the entire process. Prevention of such an occurrence starts with understanding both the manufacturing sequence and the schedule which comes from it.

In essence, the first step is to create major sub-assemblies, which are the tubesheet, the primary head, the secondary shell, the tube supports and shroud, the separators and separator assemblies, and the steam drum shell.

Then, a major assembly of tubesheet and secondary shell is welded together and goes to the nuclear clean room. (There is a variation of this sequence used by BWXT in Canada which will be explained later). In the clean room, the shroud and tube supports are installed in the shell, and then the tubes are installed, with U-bend supports being added as the tubes are installed. Then, the primary head is added. In parallel, the separator assemblies are installed in the drum shell. Finally, the secondary shell and drum shell are welded together, a local stress relief is performed on this "closing weld," and the vessel receives final inspections and testing, including hydrostatic testing of the primary and secondary sides, and the vessel is prepared for shipping. A steam generator can take 2–3 years to fabricate. As contracts are for groups of steam generators, it is also necessary to understand constraints and bottlenecks in the shop which will determine the stagger between steam generators. Usually, the biggest constraint is the drilling of the tubesheet. This will create a stagger of about 1 month to 6 weeks between steam generators. The critical path at the front end of the schedule is determined by the time required to get certain key forgings, and due to their "custom order" nature, this can take up to 6 months. So, if the fabrication of one steam generator takes 2 years, the forging delivery time on the front end is 6 months, the stagger

between each of four steam generators is 1 month, and final delivery time to site is 1 month, the total delivery span for four steam generators will be:

Engineering to prepare ordering documents for forgings	2 months
Delivery time of first critical forging	6 months
Fabrication of first steam generator	24 months
Completion of fourth steam generator relative to first	3 months
Delivery to site	1 month
Total	36 months

Three-year delivery is typical for a set of steam generators by any manufacturer in the world. It can take longer depending on the size of the steam generators (and hence fabrication time for one) (see Fig. 3.15).

3.2.1 Material purchasing to support schedule

As can be seen from the above section, it is critical to get materials ordered. They must be ordered so as to meet quality and engineering requirements and be delivered so as to be available to go into production almost as soon as they arrive at the shop. This requires a very high level of cooperation between the Purchasing Department, as well as Engineering, QA, the material supplier, and Project Management. The deliveries are to support a shop schedule, and so the shop or Manufacturing Department is also a key element in the process.

The most critical orders are for the forgings required for the first manufacturing operations. These are the tubesheet, the primary head, and the secondary shell. The common practice with PWR secondary shells is to use cylindrical and conical forgings for the shell. This eliminates risk of out of roundness and reduces the amount of in-service ultrasonic inspection (UT) required but has a higher cost than plate. The stainless steel bars for the tube supports (lattice grids and U-bend supports) are another critical material to order. Alternately, if broached plates are used, the stainless steel discs are also critical custom orders. As the tubing is not required until later in the manufacturing process, it is not, typically a critical path item for ordering. However, the preproduction sampling process must be started early in the steam generator schedule to ensure that the tubing does not become critical path.

In order to limit the amount of time required to get forgings ordered, typically the designer will perform certain engineering work, such as finite element analysis of the tubesheet/primary head area, to get exact dimensions and designs of the tubesheet and head forgings. These forgings on occasion are preordered to get a “jump” on the schedule. In some cases enough work is done ahead of time with the material vendor to allow forging orders to be placed literally the day that the steam generator order is received, eliminating the 2 months of document time at the front end of the job.

Another key consideration in the purchasing of materials is the condition at time of delivery. For example, the tubes have very specific bend radii and lengths, for specific tube locations in the steam generator. The tubes go into the steam generator in a very

specific order. Therefore, the tubes have to be specified to be packed into boxes which will yield tubes in the exact order in which they go into the steam generator. Therefore there is no unpacking and sorting. The tubes will go straight from the box into the steam generator. Every tube is identified and traceable from the tube supplier to exact heat and lot numbers, via bar coding on the plastic sleeve which is on each tube. The manufacturer will record the location of each tube as the tubes are moved from the box to installed position in the steam generator.

In some cases materials such as forgings are ordered with some work done on them at the forging facility. Every forging has some machining done, and this can include machining details such as weld preparations. In a PWR, the inside of the primary head is clad with stainless steel by a strip welding process. BWXT Canada typically subcontracts this work to the forging vendor. As a result, the forging vendor also has to be an N-Stamp supplier.

3.3 Main sub-assemblies

The work on the steam generators starts with parallel efforts on several main sub-assemblies. These are:

- Tubesheet (in some cases including secondary side thick shell)
- Primary head
- Secondary shell
- Drum shell

Also in parallel, work is initiated to fabricate the tube supports, separators, and shroud.

Fig. 3.1 shows an assembled steam generator, which will be broken down into sub-assemblies.

3.3.1 Tubesheet/thick shell

The tubesheet/thick shell assembly is welded together using a full-penetration weld which is inspected and the assembly is machined, particularly on the primary face of the tubesheet. The tubesheet is a solid disc of low alloy steel at this point, typically 0.4–0.6 m thick. Some tubesheets, for example, for larger steam generators for PWRs, will weigh as much as 80 tons at this point. Note that in some cases (particularly steam generators without integral preheaters) the thick shell will be made part of the

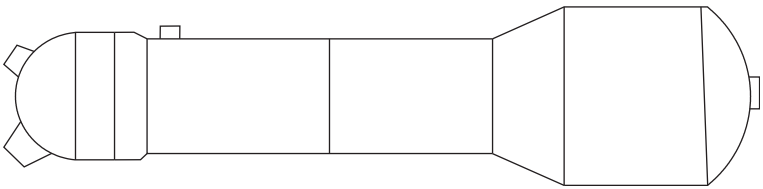

Fig. 3.1 Assembled steam generator.

secondary shell, making the thick shell to tubesheet weld the closing weld. This is an option which sometimes shortens schedule and simplifies assembly (Fig. 3.2).

The primary face of the tubesheet is then given a coating of inconel cladding. The cladding is deposited by a welding process, in 3–4 layers. Each layer of cladding material is machined before adding the next layer. The cladding is to facilitate high-quality welding of the tubes to the tubesheet. The use of inconel as a cladding material both dilutes any carbon which may enter the weld from the tubesheet metal, contaminating the weld, and it allows for the weld to be a proper pressure boundary weld without stress relief. The tube to tubesheet weld will not see a stress relief cycle. We will see this in subsequent sections of this chapter. The final thickness of the cladding is typically about 8 mm. The cladding is ultrasonically inspected to a very high standard to ensure that there are no inclusions in the cladding which could impact the integrity of the tube to tubesheet seal welds.

Next, the tubesheet/thick shell sub-assembly is drilled. As the tubes are U-tubes and will penetrate the full thickness of the tubesheet, for each tube there are two precisely placed holes, in a very distinct pattern of holes, going through the entire tubesheet. It is essential that the holes are precise in location and straightness.

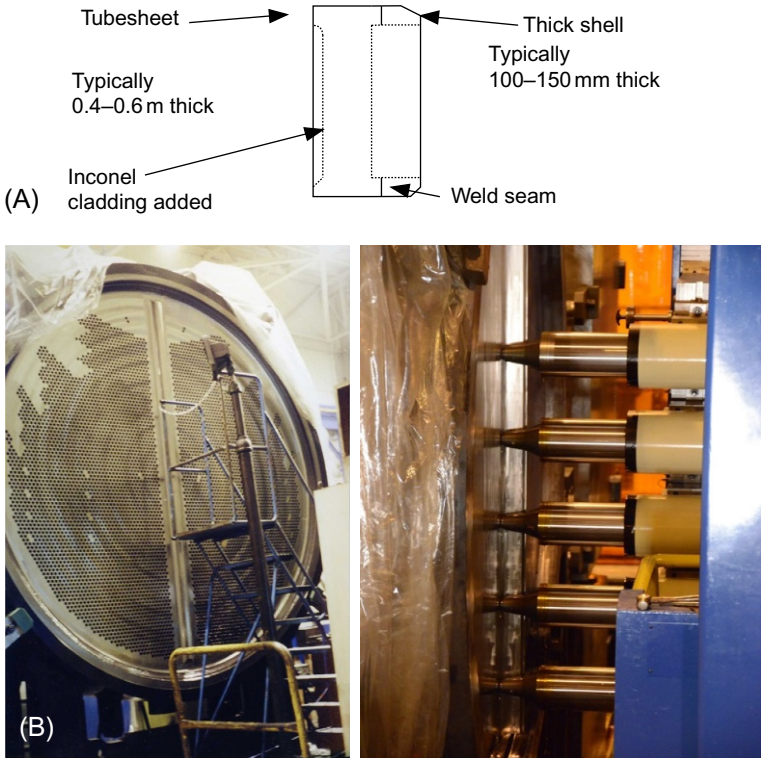

Fig. 3.2 (A) Tubesheet/thick shell sub-assembly. (B) Drilling of tubesheet.
Photos courtesy of BWXT Canada Ltd. © 2016 BWXT Canada Ltd. All rights reserved.

Specialized machines are used for this drilling. The pattern for drilling is programmed into the machine, which can drill as many as five holes simultaneously. Two drilling processes have been used for this step:

Gundrilling: The drill bits have hollow center and a v-notch in the side of the drill. Cutting fluid is carried to the drill tip through the hollow center, and the v-notch carries the drill cuttings as well as cutting fluid out from the hole.
BTA/STS (Boring and Trepanning Association/Single-Tube System): The center of the drilling tool is hollow and carries drill cuttings out of the hole through the middle of the cutting tool.

The results are comparable. Some believe that there is an advantage to BTA in terms of not scratching the inside of the holes with the drill cutting chips. Both processes are highly accurate in hole location and lack of "drift" of the holes in the tubesheet (gradual bending of the drill resulting in the location exiting the tubesheet being different from location entering the tubesheet). Avoiding drift is primarily a function of having perfectly homogeneous steel in the forging (no hard spots) and having very sharp drills (drill tools must be changed and sharpened frequently).

Some of the larger PWR tubesheets will have as much as 25 tons of steel drilled out of them, one chip at a time. Drilling is always done from the primary face to ensure that the exact pattern and exact hole location is maintained at the location where seal welding is to occur. The tubes will also be hydraulically expanded into the tubesheet holes. The drilled holes must be only in the area of 0.05 mm larger than the tube diameter in order to minimize the residual tube stresses left by the hydraulic expansion process. Typically, this high-precision process is on the critical path of steam generator fabrication, and so it is done on a 24/7 basis. Drilling of one tubesheet, 24/7, can take 4–6 weeks.

3.3.2 Primary head

The primary head sub-assembly is as shown in Fig. 3.3. The head itself is a forging, generally a low alloy material with 80 ksi ultimate strength. CANDU primary heads generally have the base of the nozzles formed into the head, with nozzle extensions butt welded to the bases. Some PWR steam generators have the entire nozzle formed as part of the head, so there is no welding. This is typical for Westinghouse-type steam generators. This practice originated from Westinghouse in older steam generator designs using castings for the head rather than forgings. As the primary head assembly is developed, other features such as manway openings, the base of the primary divider plate and vertical supports are added. The entire sub-assembly is machined upon completion of welding and carefully checked against required dimensions and tolerances. PWR steam generators require a completely stainless steel primary side in contact with the reactor coolant. For this reason the inside of the primary head is clad with stainless steel, as well as the inside of the nozzles. If the nozzles are welded to the primary head, the inside surface of the weld joint is back-clad. Westinghouse-type PWR plants use solid stainless steel primary piping, and hence use stainless steel "safe ends" (stainless steel extensions on the ends of the nozzles) to allow stainless to stainless welding of the steam generator to the pipes in the field. The primary

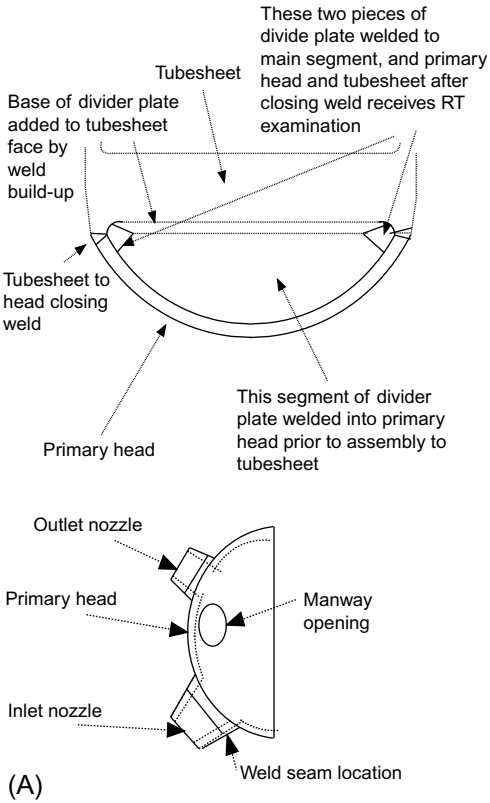

Fig. 3.3 (A) Schematic of primary head sub-assembly. (B) Primary head sub-assembly. Photo courtesy of BWXT Canada Ltd. © 2016 BWXT Canada Ltd. All rights reserved.

divider plate is added at this point, but segments have to be left out to allow inspection of the primary head to tubesheet weld. Most steam generator divider plates are solid welded in designs. These designs can help in keeping the thickness of the tubesheet down by reinforcing the tubesheet against pressure loading.

When this assembly is complete, it is machined largely to final dimensions, and the weld preparation for the head to tubesheet weld is machined. Weld preparations at the ends of the nozzles are generally not final machined at this point as high pressure caps will be welded to the heads at a later stage for hydrostatic testing, following which final machining will be done.

3.3.3 Secondary shell

The secondary shell assembly usually consists of the cylindrical shell courses plus the conical section. In certain cases, the conical section is made part of the drum shell, but this makes separator installation in the drum more complicated and hence is avoided where possible. The shell courses can be either plate material or forgings. Plate material is less costly than forgings but introduces longitudinal welds. Plate shells tend to have greater "out of roundness" than forgings, as forgings are precisely machined to final dimensions. If a forging is used for the cone, it usually includes a cylindrical section (maybe 150 mm long) on both the top and bottom ends so that the welds to the shell and drum are butt welds vs "corner" welds, and hence are easier to inspect (by RT, UT, etc.).

There have been cases where only partial conical sections are added to the shell, generally in replacement steam generators. The diameter of the partial conical section at the top end is based on the maximum size which can fit into reactor containment equipment hatches. This is decided on a case-by-case basis, so we will only address the "standard" case of a shell with cylindrical courses.

The individual shell cans are prepared, including the cone, and these sections are welded together. Then, after careful measurement, other features such as vessel external supports, water level taps, handholes, and inspection ports are added. The shell is not stress relieved at this point as it will be stress relieved with the tubesheet and primary head attached later (Fig. 3.4).

It is of critical importance at this point to ensure that the shell is very precise dimensionally, and in terms of straightness. Weld preparations are machined in order to be precisely square with the cylinders so that there are no "bends" between shells. Lasers are used to ensure dimensional correctness, including the locations of the attachments. Even factors such as weld "shrinkage" have to be factored in to ensure dimensional correctness.

3.3.4 Drum shell

The drum shell is assembled although it is much less on the critical path than the other sub-assemblies. The drum head is either formed plate or sometimes a forging depending on the shape and features to be included. In PWR steam generators, the steam outlet nozzle is commonly made an integral part of the head forging in order

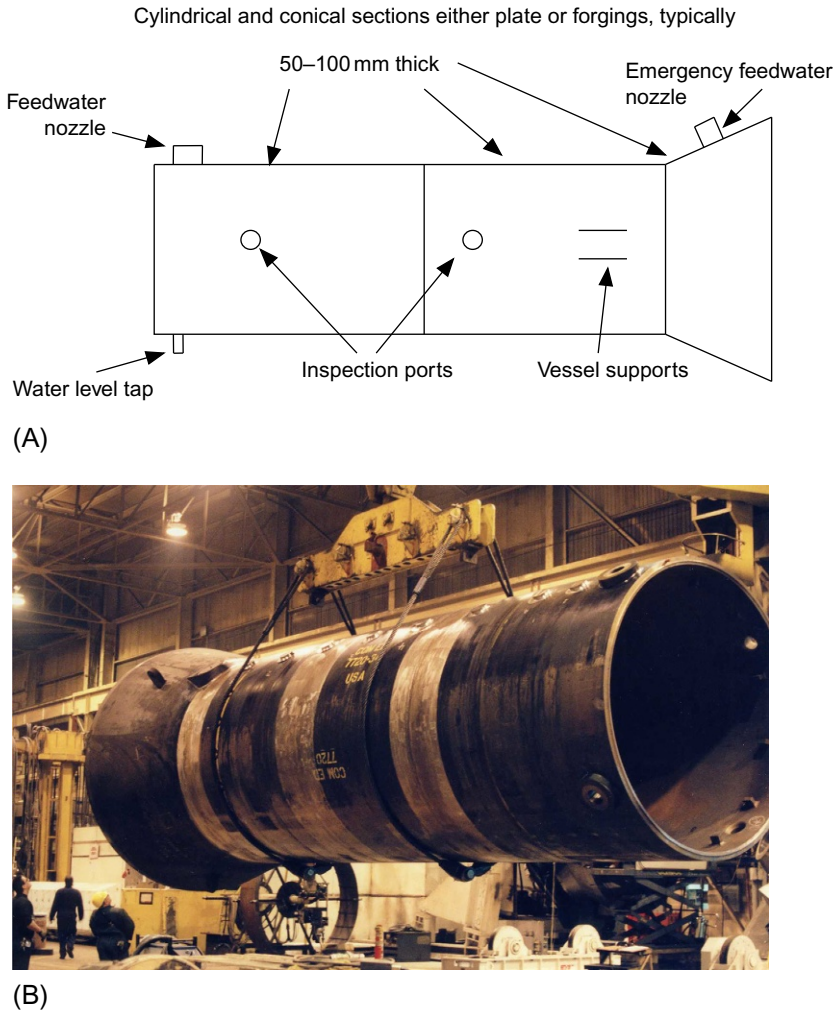

Fig. 3.4 (A) Secondary shell assembly. (B) Secondary shell sub-assembly.
Photo courtesy of BWXT Canada Ltd. © 2016 BWXT Canada Ltd. All rights reserved.

to accommodate venturi flow restrictors used to limit steam flow in a steam-line break accident. Most CANDU steam drum heads have been made of formed plate pressed or spun into their final shape. The drum cylindrical sections can be plate or forgings. The sub-assembly includes the steam outlet nozzle, water level taps, and the steam drum manways. PWR manways are commonly in the side of the drum (as shown in the photo later). This sub-assembly is stress relieved prior to final machining. Final machining of manway gasket surfaces must be done after stress relief to ensure flatness and surface quality (Fig. 3.5A and B).

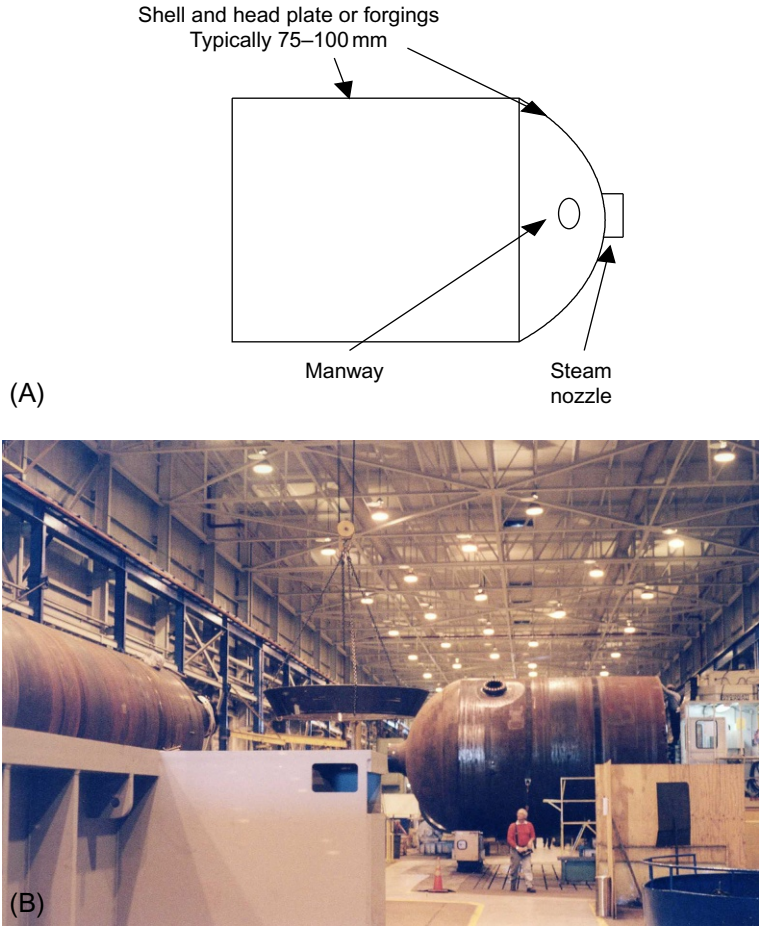

Fig. 3.5 (A) Schematic of steam drum shell. (B) Steam drum shell.
Photo courtesy of BWXT Canada Ltd. © 2016 BWXT Canada Ltd. All rights reserved.

3.3.5 Separator sub-assembly

Individual separators are fabricated and are then assembled onto a deck structure. This assembly is generally done vertically. The deck assembly ensures that all secondary side flow is directed into the separators and provides structural strength against seismic and steam-line break loadings. The secondary separators are also assembled into a structure which ensures all flow goes through the secondaries without bypass, and any water stripped from the steam is returned to the reservoir of liquid in the steam drum. The secondary separator deck must also maintain integrity of the separators in a steam-line break and a seismic loading situation.

There is considerable flexibility in how the separator decks are designed, depending on the particular design case. For example, replacement steam generators have been designed where new separators are installed as modules into the original drums, which are then welded onto the new lower steam generator sections in the field. The modules are typically made up of both primary and secondary separators in an integral module including drains from the secondaries. In some C-E separators, the modules had to be designed to fit into the original steam drums in five interlocking pieces. The key is to ensure complete sealing between the pieces and with the drum to ensure no flow bypasses, and that structural strength is designed into the separator decks. Recent designs of separator deck for both PWR and CANDU projects have also included "sludge traps" on the top of the primary separator deck to try to avoid having sludge accumulation on the top of the tubesheet (Fig. 3.6).

3.3.6 Tube supports and shrouds

In parallel with the heavy sub-assemblies, the tube supports (lattice grids, U-bend supports, preheater baffle plates, divider plates, etc.) are fabricated and stored in the clean room. The tube supports require extensive machining and fitting, and the U-bend supports are welded structures requiring stress relief in a specialized electric furnace in the clean room. This part of the work involves literally thousands of parts, which must be carefully controlled and documented. Each lattice grid must be very carefully tested for dimensional tolerancing in order to ensure that the tubes will pass smoothly into the steam generator and yet will fit with very small clearances into the spaces in the lattice grids (Fig. 3.7).

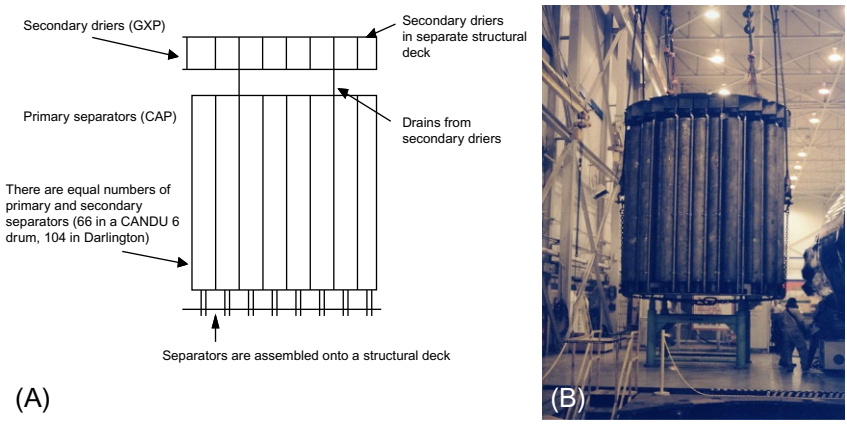

Fig. 3.6 (A) Schematic of separator sub-assembly. (B) Separator sub-assembly. Photo courtesy of BWXT Canada Ltd. © 2016 BWXT Canada Ltd. All rights reserved.

Fig. 3.7 Lattice grid tube supports being assembled. Photo courtesy of BWXT Canada Ltd. © 2016 BWXT Canada Ltd. All rights reserved.

3.4 Major assemblies

With the major sub-assemblies taking shape, we are now ready for major final assemblies. First is the primary head/tubesheet/secondary shell.

There have been three different approaches taken to this particular assembly. Typically, the traditional PWR approach has been to attach the tubesheet sub-assembly to the shell sub-assembly; add the internals and tubing; and after the tubing is installed, add the primary head and perform a local postweld heat treatment of the head to tubesheet weld. There is concern that the local postweld heat treatment can damage the tubing.

A second approach, used in steam generators designed by Siemens, was to weld an extra ring forging to the primary side of the tubesheet and still install the remainder of the primary head after tubing. By adding this ring forging, the location of the closing weld is moved from immediately at the tubesheet to a distance from the tubesheet determined by the length of the ring forging. This reduces the risk of damage to the tubing due to local postweld heat treatment considerably.

There is a third approach, which is a unique process only done by BWXT Canada, both for CANDU and for PWR replacement steam generators. The objective of this manufacturing method is to avoid having any exposure of the tubing to stress relief operations, whether general or local. Stress relief has no metallurgical benefit for alloy 800 and could even be detrimental. It has no advantage to alloy 690 which has already

been thermally treated. While there is a theoretical advantage in terms of relieving residual stress in the tube expansion in the tubesheet, this is not necessary if low stress hydraulic tube expansion is used.

In the BWXT process, the primary head, tubesheet/thick shell, and the secondary shell are welded together, and then furnace stress relieved. This assembly will receive no further stress relief, either full or local. There are cover plates placed over the faces of the drilled tubesheet, and inert gas is used in an effort to keep the drilled hole surfaces clean during the furnace stress relief. This stress relief operation is done at 607°C.

Note that this assembly, once verified for dimensions and cleaned, goes to the nuclear clean room for further work. The shell is empty at this point, so it is possible to walk up the length of the shell (right to left in Fig. 3.8A) to the secondary face of the drilled tubesheet.

Once in the clean room, the next stage of fabrication is the installation of the shroud or wrapper, baffle plates if the design has an integral preheater, and the tube supports. Lattice grid tube supports do not require tierods for support in the out-of-plane direction, but broached plates and the preheater baffle plates (if applicable) do, so the

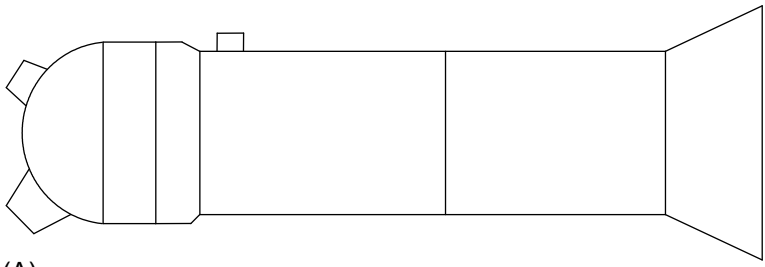

(A)

(B)

Fig. 3.8 (A) Schematic of primary head/tubesheet/secondary shell assembly. (B) Primary head/tubesheet/secondary shell assembly.
Photo courtesy of BWXT Canada Ltd. © 2016 BWXT Canada Ltd. All rights reserved.

tierods are added where needed as part of the "cage" assembly of tube supports inside the shroud or wrapper. The shroud has a series of threaded pins which are tightened outward against the inside of the shell and adjusted to allow very precise alignment and concentricity and squareness of the shroud in the shell. Once position is confirmed, the pins are welded to the inside of the shroud and the position is secured. There are additional shroud supports near the tubesheet which lock the vertical position of the shroud.

Note that it is imperative at this point to have exceptionally good alignment of each tube support to the drilled hole pattern in the tubesheet. Tubes will be installed from right to left (see Fig. 3.9), and at this point the only access to the tubing as it enters the steam generator is at the uppermost lattice grid. The tubes must be free to slide through typically 8–10 tube supports, plus preheater baffles where applicable, and then enter and pass through to the primary face of the tubesheet. The tubes must never end up in the wrong tube opening in any tube support. Hence, extreme care is taken as each tube support is installed to check alignment against the drilled holes in the tubesheet. This is done with optical and laser alignment devices. Once each tube support is verified for alignment, its position is held by use of welded blocks and wedges, and then the wedges are welded to the lattice grid rings and the inside of the shroud.

With all alignment confirmed, the assembly is ready for tubing.

Tubes are installed (see Fig. 3.10A diagram) from right to left. The tubes are received from the tube vendor in plywood boxes, individually sleeved in plastic, with identifying bar codes on each sleeve. The tubes are placed in the boxes in the order in which they will go into the steam generator. The entire tube sleeve for an individual tube is removed, other than the identifier bar code piece which is at the U-bend end. The steam generator is oriented so that the untubed lane is vertical in orientation (in other words, Fig. 3.10A is a view from above the steam generator, looking vertically downward in the clean room). The tubes are installed in layers, from the smallest to the largest bend radius tube in each layer. In order to minimize the risk of a tube going off direction during installation, "bullet nose" plugs are installed in the open ends of the

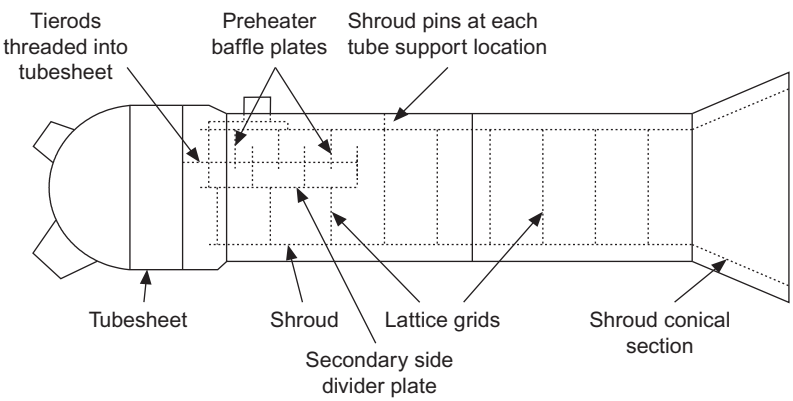

Fig. 3.9 Shell with shroud, preheater baffles, and lattice grids installed.

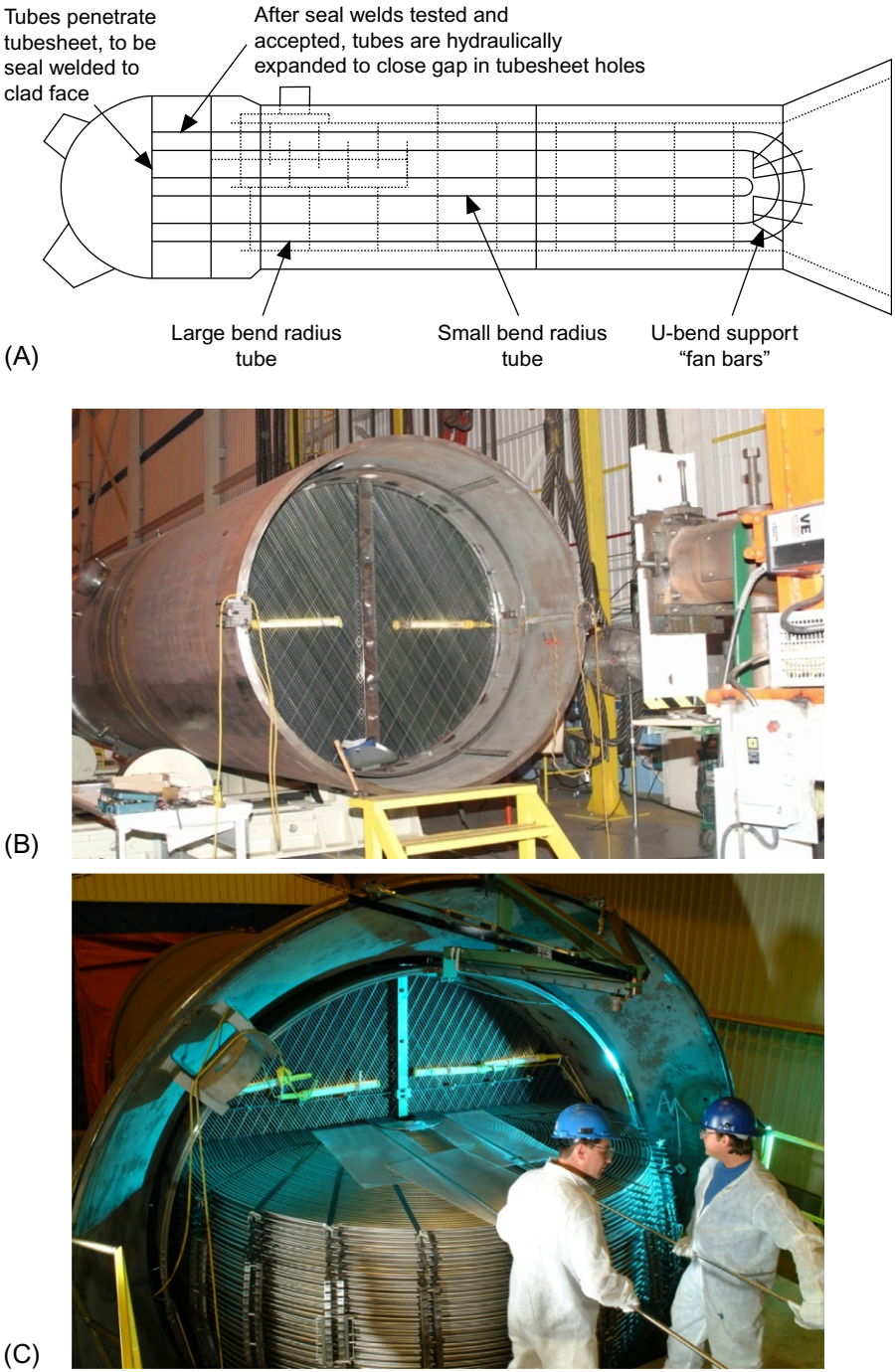

Fig. 3.10 (A) Tubing installation. (B) Assembly ready for tubing. (C) Secondary side receives tubing.
Photo courtesy of BWXT Canada Ltd. © 2016 BWXT Canada Ltd. All rights reserved.

tubes before pushing them through the uppermost tube support. That way even the slight sag of the tube due to gravity as it passes from one tube support to the next is compensated for. Once a tube has been pushed all the way into the steam generator, the bullet nose plugs are removed at the primary face of tubesheet. The exact location of the U-bend relative to all of the neighboring tubes is confirmed, the exact amount by which the tube extends beyond the primary face of the tubesheet is confirmed, and then the tube is lightly expanded into the tubesheet hole (tack expanded) to maintain its position.

As each layer of tubes is installed, U-bend support "fan bars" are laid on top of the tube layer. Assembling the steam generator this way avoids a risk that U-bend supports shoved into the steam generator between tube layers after tubing could end up in the wrong location, leading to improperly supported tubes. This actually happened in Japan, (Mihama Nuclear Plant), and the layer-by-layer assembly sequence has been essentially universally adopted in the industry as a result.

When all tubes have been installed, the tube to tubesheet seal welding begins. There are two styles of seal weld used in the industry. Traditionally, all CANDU seal welding is fillet weld style. PWRs use predominantly flush-type seal welds (Fig. 3.11).

There is a slightly higher primary side pressure drop associated with fillet weld due to the protruding tube end. However, there is no risk of the weld extending into the open part of the tube, thereby inhibiting eddy current probe entry into the tube. The "minimum leak path" of the fillet weld is 1¼× the tube thickness "*T*," and hence risk of leakage through the seal weld is less. Typically for a flush weld the minimum leak path is roughly 0.8 T. It was traditionally felt that there was a risk associated with fillet seal welds which had to do with loose parts of the primary system getting into the primary head of the steam generator in operation and battering the protruding tube

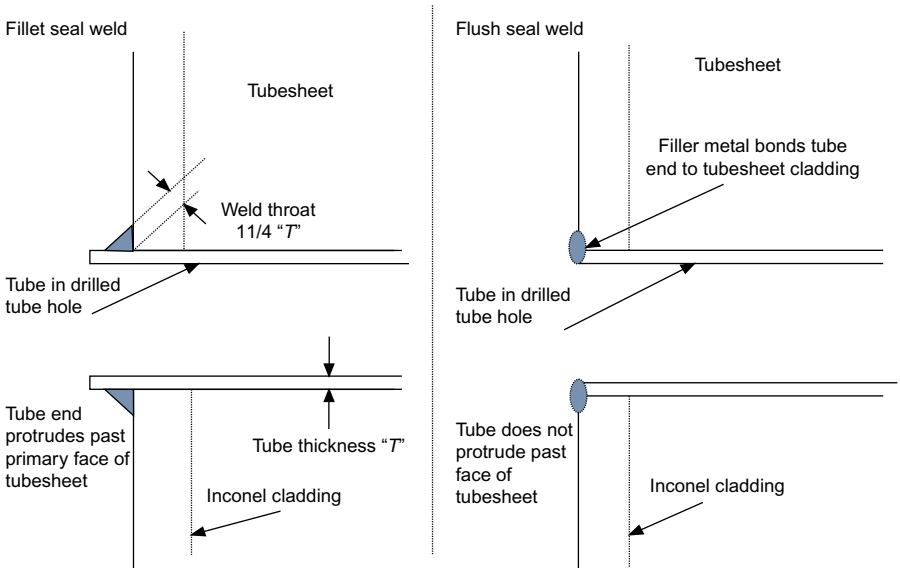

Fig. 3.11 Fillet and flush seal welds.

ends. Experience has generally shown that in loose parts situations, the fact that the tube end takes the damage makes for simpler repairs. A damaged tube end can be cut off or refinished and repaired with a flush weld. Flush welds damaged by loose parts are considerably more difficult to repair as the entire weld has to be cut out and replaced, which involves cutting into the tubesheet cladding.

The seal welds are made with the tube "tack" expanded into the tubesheet. Inspection of seal welds has been traditionally a hotly debated topic. For one thing, as there is a "crack" between the tube and the tubesheet, the root of the seal weld automatically has a "crack" or stress concentration. The geometry of the seal weld makes it highly difficult to inspect, and given the automatic existence of the crack at the tube to tubesheet discontinuity, inspections can be meaningless in any case. It is common practice, nevertheless in Europe to perform radiographic (RT) examination on each seal weld. North American practice is to perform Liquid Penetrant Examination on the seal welds once completed, plus helium leak test on all of the seal welds. In situ cases of seal weld leakage have been extremely rare, so this method is accepted as quite sufficient for seal weld inspection. If the weld machine parameters such as current and voltage are carefully monitored during performance of highly automated and repetitive seal welds, any deviations of the parameters will quickly give indication of developing problems. Defective seal welds can be cut out and replaced, even if this means using a flush weld to replace a fillet weld. Steam generators are liquid penetrant examined at this point but await final assembly for further testing.

The last major sub-assembly is the steam drum/separator sub-assembly. The separators are assembled into "decks" (see Fig. 3.12) in the vertical orientation and secured together structurally. The exact nature of how they are secured together varies from one project to the next considering seismic loading, whether the separators are to be assembled into the drum in the shop or the field (sometimes field assembly of separators is required as part of steam generator replacement projects), whether the separator modules can be one or multiple pieces, etc. In the shop, the primary and secondary separators usually end up as one assembled vertical module, and the drum is picked up by a heavy crane and lowered over the separator module. The structural supports connecting the separators to the drum are completed, and sealing strips preventing any bypass of steam around the secondary separators are put in place. Access to the separators at this point is limited to the secondary side manways. From the open end at the bottom of the steam drum access is very limited due to the primary separator deck. The separator modules have built into them access "tunnels" which will allow for personnel to enter the secondary side manways, climb down the tunnels, open a door in the primary separator deck, and access the tube bundle during outages. At this point in assembly the door is open.

3.5 Final assembly and preparation for shipment

Basically, the final assembly is the joining of the tubed lower section of the steam generator with the finished steam drum assembly. However, there are multiple steps in finalizing the steam generator and preparing for shipment (Fig. 3.13).

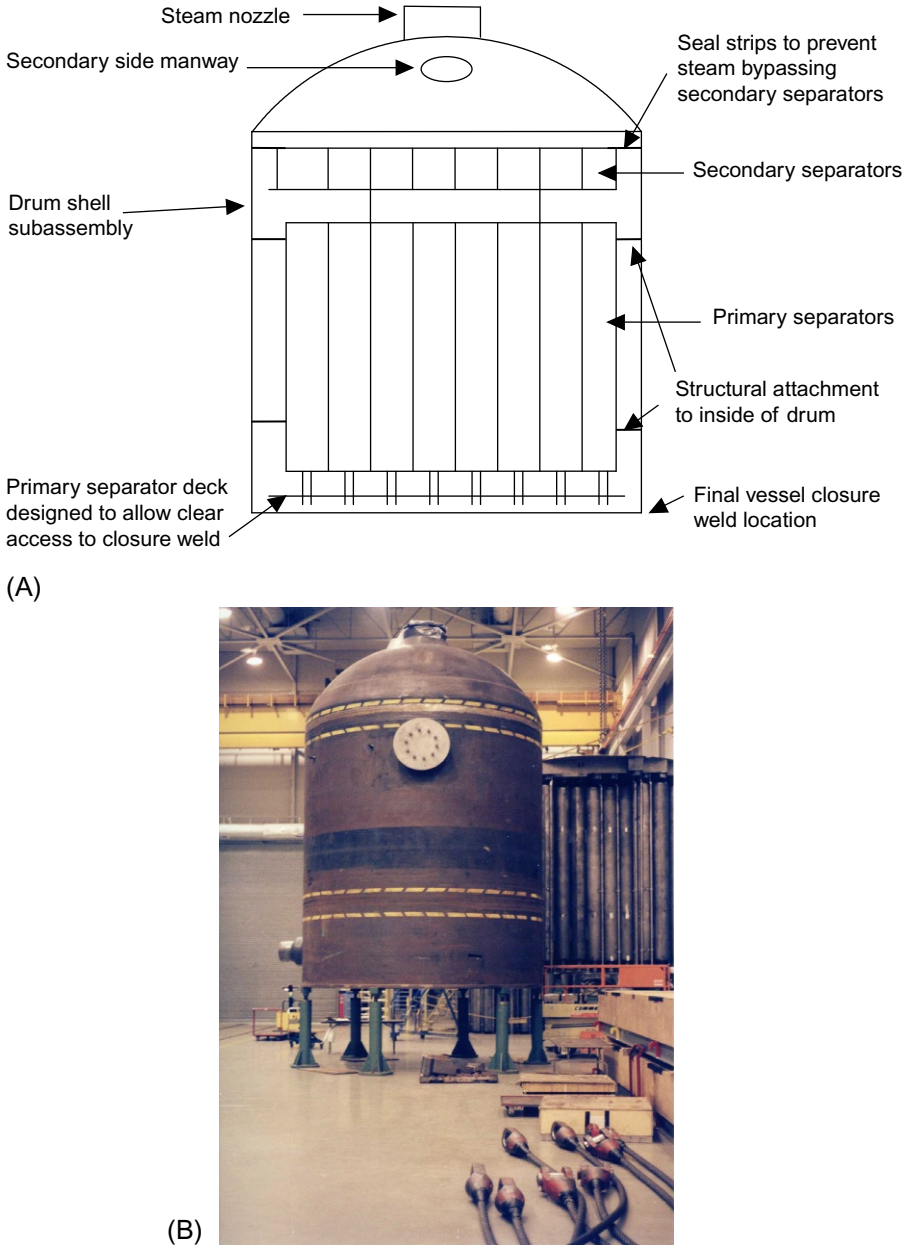

Fig. 3.12 (A) Schematic of Steam drum/separator assembly. (B) Steam drum/separator assembly (Courtesy of BWXT Canada).
Photo courtesy of BWXT Canada Ltd. © 2016 BWXT Canada Ltd. All rights reserved.

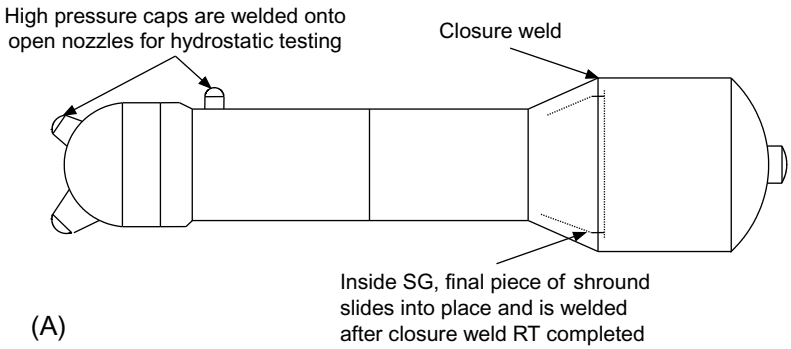

Fig. 3.13 (A) Schematic of Final assembly. (B) Final assembly.
Photo courtesy of BWXT Canada Ltd. © 2016 BWXT Canada Ltd. All rights reserved.

There is a movable piece required to complete the shroud connection placed inside the steam generator adjacent to the closure weld. The closure weld is made, ground to finished condition, and given a local stress relief. Following local stress relief, the weld is RT examined. The movable piece of the shroud is left out of place initially to allow access to the inside of the closure weld, required for some of the welding, and for placing of the RT film. Following RT, the final piece of the shroud connecting the shroud cone to the separator deck is installed.

All secondary side openings such as handholes, etc., which have their own covers are closed and bolted. Hydrostatic test caps are welded to the open nozzles. This is to seal the secondary side so that helium leak testing of the seal welds can be performed. The secondary side is pressurized with helium, and a device labeled a "sniffer" seeks even miniscule signs of helium at the primary face of the tubesheet, which would indicate seal weld leakage. This test is deliberately performed before tube expansion into the tubesheet to remove any possibility of the expanded joint sealing the tube against helium leakage and allowing a bad seal weld to pass the test. Once the seal welds are verified leak-tight, the tubes are hydraulically expanded into the tubesheet holes. The expanded joint starts at the secondary face of the tubesheet and can be a depth of anywhere from 125 mm long to the full depth of the tubesheet. Once hydraulic tube

expansion is completed, any remaining pieces of the primary divide plate are welded in place, the primary manway covers are installed, and final primary head cleanup is completed. The hydrostatic test caps are welded to the primary nozzles.

Both the primary and secondary sides of the steam generator receive hydrostatic tests, using very high purity demineralized water. All possible sources of leakage, especially around gasketed joints such as manways and handholes, are searched out and verified as leak-tight.

Final preparations for shipment include installing "shipping frames" in the U-bend region to prevent any damage due to shipping motions, shifting of parts, etc. These frames can be removed through the secondary side manways and access tunnels through the separators. Bolted covers are fitted with shipping gaskets. The vessel is vacuum dried and back-filled on both primary and secondary sides with nitrogen to prevent any oxide formations. Exterior surfaces are prepared as specified by the customer for shipment. These preparations can include primer paint, dry-strippable coatings, or shrink wrapping (Fig. 3.14).

The entire schedule for a set of steam generators is essentially as shown in Fig. 3.15. One of the interesting things to note about this schedule is the critical nature of getting the forgings on order (mainly the tubesheet, thick shell, and primary head). Also of interest is that the tubing ordering is not critical path. Insofar as the tubing is delivered ready to install in the steam generator, and this occurs nearly 2 years into the schedule, the 12–14 month tube procurement time is still not critical path. A set of four steam generators will typically be fabricated on 1 month staggers. In other words, the start and finish date of fabrication for each steam generator is staggered to 1 month later than its predecessor. The first steam generator finishes after 32 months, the second 33, third 34, and fourth 35 months after contract award. The last month is spent in delivery. In certain circumstances, extraordinary steps can be taken to shorten

Fig. 3.14 Steam generator ready for rail shipment.
Photo courtesy of BWXT Canada Ltd. © 2016 BWXT Canada Ltd. All rights reserved.

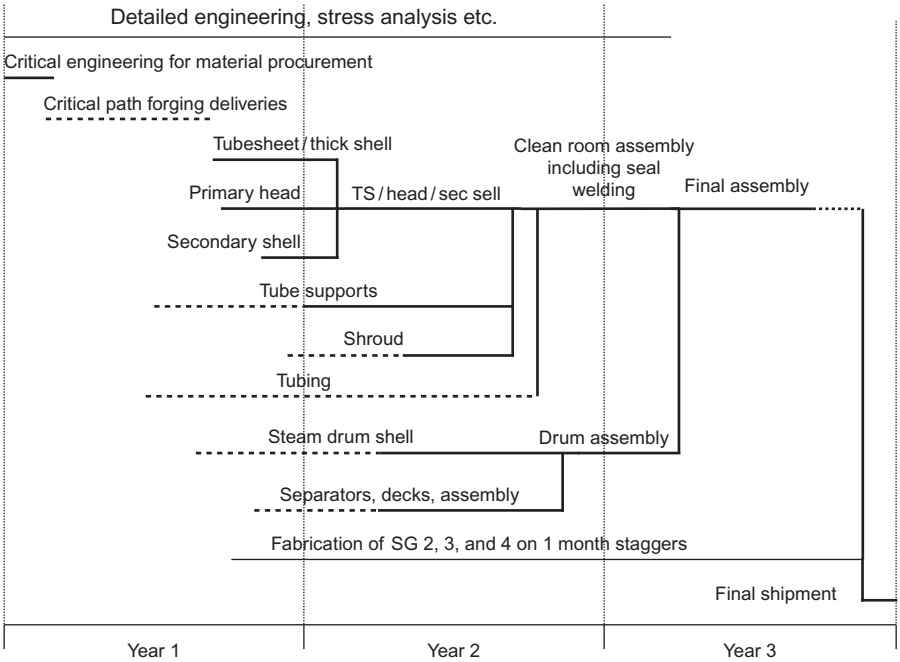

Fig. 3.15 Sample schedule.

delivery. For example, for Cernavoda Unit 1, steps were taken to procure tubesheets very early. Fabrication began in the shop only 2 months after contract award, and the first set of four steam generators was delivered (to the dock in Toronto) in only 29 months from Contract Effective Date. The second set of four steam generators was scheduled to be delivered 35 months after Contract Effective Date. The work was scheduled as effectively eight steam generators, at 1 month stagger and the second set was actually delivered 1 month early.

3.6 Stress reliefs

The stress reliefs in a steam generator are planned very carefully to ensure the following:

- All pressure boundary welds will receive a stress relief at 607°C.
- Nonpressure boundary welds and certain inconel welds can be exempted from stress relief.
- Heat-up and cool-down rates are established to preclude excessive stressing of the shell during stress relief.
- Stress reliefs are developed which preclude any heating of the tubes during the operation. This avoids metallurgical alteration of the tubing which might decrease resistance to corrosion and eliminates the risk of damaging tubing through distortion of the surrounding tube supports during stress relief.
- A local stress relief is as effective for a weld seam as a full-furnace stress relief as long as upper temperature, heat-up, and cool-down rates are met.

Major full-furnace stress reliefs are performed on the primary head/tubesheet/thick shell/secondary shell assembly, and on the steam drum shell assembly. Local stress relief is performed on the closing (shell to drum) weld. Other final welding inside the steam generator, such as the primary divider plate, the separators and separator assemblies, and the shroud closure, are exempted from stress relief.

3.7 Inspection and testing

Nuclear steam generators are subject to numerous tests and inspections to absolutely ensure the highest possible quality of the end product. The following are many of the inspections and tests performed.

Forgings: The entire volume of the forging is ultrasonic examined to ensure no tiny defects in the metal. Defects can be caused by impurities. To eliminate impurities, the steel is made from remelted steel, which was already purified once. In the pouring of a forging ingot, the impurities tend to migrate to the ends of the ingot, and so the ends of the ingot are "cropped" prior to forming. The forging is formed in such a way as to allow "coupons" or pieces to be taken for destructive examination, verifying the chemistry, homogeneity, and properties of the steel. Once heat treated and machined, the entire forging is 100% UT examined.

Plate: If plate material is used, it is 100% UT examined and the edges are PT (liquid penetrant) tested.

Tubing: Tubing is both 100% Eddy current tested (ECT) and UT examined at the tube mill. It receives numerous other tests to ensure dimensional correctness, material properties, proper recording to heat and lot numbers, etc. In the steam generators, the tubing will receive further eddy current testing, in some cases in the shop, and in some cases in the field after shipping but before installation. Often the tubing receives further "benchmark" preservice ECT as a reference for future in-service ECTs. There is extensive verification of dimensions after bending (the bend radius, parallelness of the two straight sections, and length of the straight sections).

Pressure boundary welds: Weld preparations are machined and/or ground to ensure ideal shape for automated welding. The weld preparations are magnetic particle (MT) or PT examined to ensure that there are no "latent" material defects in the heat-affected zone. The weld surface is periodically MT tested as a precaution against unexpected weld defects (slag inclusions, etc.) The finished weld, prior to stress relief, is given a complete UT examination to preclude any unwanted surprises after RT. By Code rules, the governing volumetric inspection (RT) must be done after stress relief, or post weld heat treatment. On the rare occasion that a defect is found in a pressure boundary weld, it must be ground out and rewelded using an approved repair procedure. Pressure boundary welds are made using fully automated processes and rarely result in defects. The repair procedures are manual welds which are much more likely to result in defects than the automated procedures. Even after RT, the pressure boundary welds are given, in some cases a preservice reference UT examination. This preservice UT forms the basis or "benchmark" for in-service inspection (ISI) UT

Fig. 3.16 RT examination of a steam generator weld, Linatron accelerator vault.
Photo courtesy of BWXT Canada Ltd. © 2016 BWXT Canada Ltd. All rights reserved.

examinations of all pressure boundary welds which is performed every 10 years once the steam generators go into operation.

Lighter internal structures such as separators, tube supports where welded, etc., are given only visual inspections or surface PT examinations.

The entire vessel is given a hydrostatic test for each of the primary and secondary sides. With the main vessel test done, the vessel may receive extra hydrostatic tests with the system tests at site. The vessel stress report will confirm vessel capability of taking up to 10 hydrostatic tests (Fig. 3.16).

3.8 Shipment

Finally, it is necessary to get the steam generators shipped. The steam generators were designed to operate in the vertical position, so shipping in the horizontal orientation introduces loadings and stresses which the steam generators normally do not see. In some cases (e.g., the U-bends of the tubes) shipping frames are added just to give the added support against these unusual loads.

Most international steam generator shops have access to ocean shipping, i.e., they are on the waterfront and have barge or ship loading capability on their own property. Alternately rail shipping can be used for most steam generators. This can be by multiaxle rail cars or “Schnabel cars,” where the steam generator effectively becomes

part of the car. Very large frames are attached to each end of the steam generator, allowing the steam generator to travel only a few centimeters above the rail tracks. There is a rail car in front of and one behind the steam generator, each carrying half of the load. These rail cars also use swivel bolsters to allow for turns in the track. In some cases the load can be shifted laterally to compensate for "banking" in the tracks or to get around obstacles such as posts near the tracks. BWXT had one bad experience with a Schnabel car, having it roll over due to not properly compensating for banking in a track in Ohio. However, with carefully engineered shipments, rail is very effective for all steam generator sizes. If necessary, due to limitations on rail access or barge landing access at the reactor site, road transporters can be used as well.

For international shipments, the rail shipped steam generators can be transferred to ocean vessels at major ports, or to barges for inland waterway shipment.

The steam generators are typically fitted with accelerometers during shipment to ensure no damage has occurred due to dropping, or other shock loads which can happen. After meticulous inspection of steam generator which rolled over in Ohio (including 100% eddy current examination of the tubing), it was deemed satisfactory to put into service and has now operated problem free for about 20 years.

3.9 Conclusions

Steam generator manufacturing is a mature technology used in many countries. The methods of manufacturing are largely the same in all such factories. There are small differences in assembly sequence, and in some cases in welding methods, but the overall results are very similar in all cases. This chapter has been about what amounts to the universal manufacturing method for all steam generators.

Thermalhydraulics, circulation, and steam-water separation in nuclear steam generators

4

S. Laroche
Canadian Nuclear Laboratories, Chalk River, ON, Canada

4.1 Introduction

In the steam generator, the primary fluid is transported through tubes while its heat is transferred from the primary fluid to the secondary fluid in the shell. Inside the shell, the secondary fluid temperature increases to its saturation temperature and steam is produced. This steam exits the steam generator and drives the turbine generator before condensing and returning to the steam generator as feedwater.

There are two main types of vertical steam generators in nuclear power plants: recirculating steam generators and once-through steam generators. The thermalhydraulics, specific design features, and flow-affected phenomena that lead to degradation are discussed for both types of steam generators.

4.2 Recirculating steam generators

The thermalhydraulics for recirculating steam generators will be described in the following sections.

4.2.1 Flow paths

The flow paths for the primary and secondary fluids are described as primary fluid flows through the tubes transferring heat to the secondary fluid in the shell.

4.2.1.1 Primary fluid

The primary fluid enters the primary fluid inlet plenum of the steam generator and flows into the inverted U-tubes on the hot-side, or hot-leg, of the steam generator as shown in Fig. 4.1 by the dashed lines. This fluid exits the tubes on the cold-side, or cold-leg, through the primary fluid outlet. In pressurized water reactor (PWR) steam generators, the primary fluid temperature is between 315°C and 330°C at the tube inlet and 280°C and 295°C at the tube outlet. For CANDU steam generators, the primary fluid enters the steam generator with a temperature between 290°C and 310°C with a low steam quality, typically <5%, and exits with a temperature between 250°C and 265°C (IAEA, 1997).

Steam Generators for Nuclear Power Plants. http://dx.doi.org/10.1016/B978-0-08-100894-2.00006-6
© 2017 Elsevier Ltd. All rights reserved.

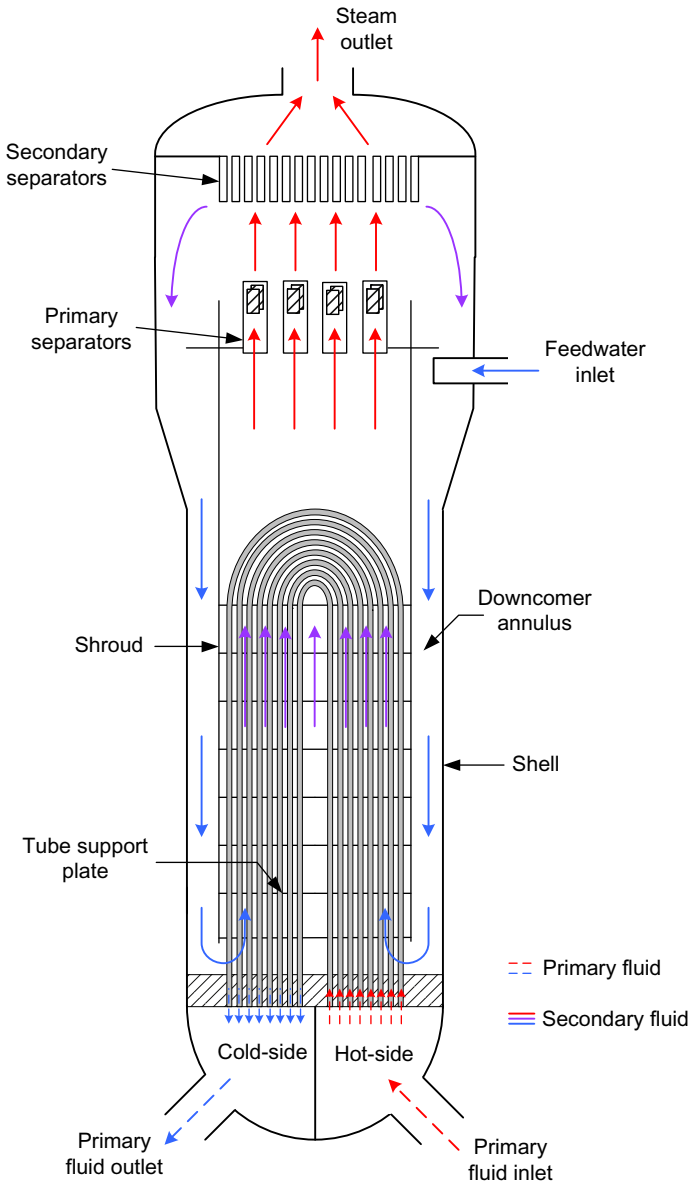

Fig. 4.1 Sketch of fluid flow path in PWR recirculating steam generator.

The operating pressure of the primary fluid pressure is significantly higher than the secondary fluid pressure. If a tube leaks, the primary fluid is released into the secondary fluid.

4.2.1.2 Secondary fluid

The feedwater fluid enters the steam generator as a subcooled fluid through the feedwater inlet and mixes with the recirculating secondary fluid. The solid lines in Fig. 4.1 show the flow path for the secondary fluid in PWRs.

An example of the secondary fluid velocity for a PWR steam generator plane of symmetry is shown in Fig. 4.2 as predicted by Atomic Energy of Canada Limited (AECL) steam generator thermalhydraulic code, THIRST (Carver et al., 1981). Theoretical approaches used to solve the thermalhydraulics are discussed in Section 4.2.8. In Fig. 4.2, the secondary fluid velocity on the hot-side is predicted to reach roughly 7 m/s. On the cold-side, this velocity is predicted to be 4 m/s only. The secondary fluid velocity is higher on the hot-side of the steam generator than the cold-side due to its higher void fraction and lower fluid density.

In PWR steam generators, the feedwater mixes with the saturated liquid from the moisture separators in the downcomer annulus. This resulting mixture flows down through the downcomer annulus toward the tubesheet and enters the tube bundle through downcomer windows. The fluid is then directed across the tubesheet and rises up through the tube bundle, known as riser flow. The fluid is heated as it flows over the tubes and becomes quickly saturated and then steam is produced. Between 20% and 40% of this riser mass flow rate is converted to steam in the tube bundle while the remainder of

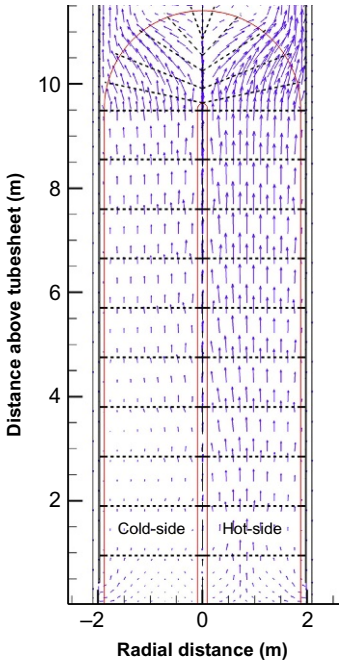

Fig. 4.2 Predicted secondary fluid relative velocities at the plane of symmetry for PWR steam generator.

the flow is recirculated via the downcomer as recirculating flow. The water-steam mixture passes through the primary and secondary separators to reduce its moisture content before almost pure saturated steam exits the steam generator. Any moisture removed by the separators is returned to the recirculating flow in the downcomer annulus.

Most CANDU and some PWR steam generators include an internal, or integral, preheater that heats the secondary fluid (discussed in Section 4.2.6). A simplified sketch of the secondary fluid flow path is shown in Fig. 4.3. In this steam generator design, the feedwater enters the preheater to flow perpendicular to the tubes as the

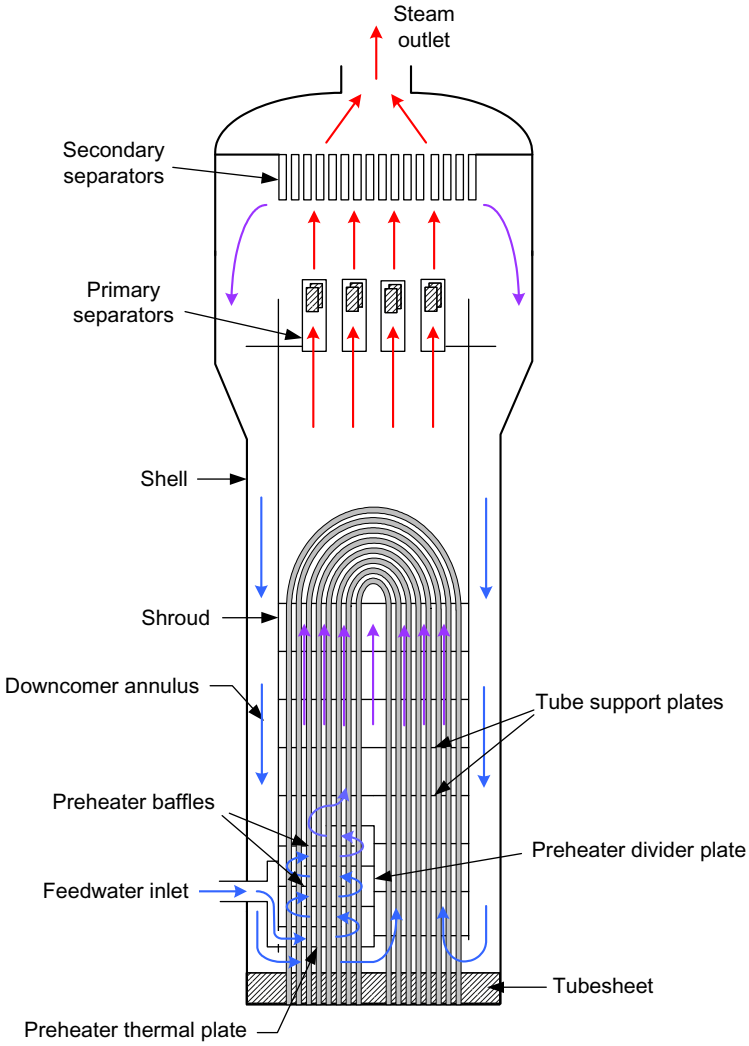

Fig. 4.3 Sketch of secondary fluid flow path in CANDU steam generator with an internal preheater.

fluid passes back and forth through the preheater. This flow path in the preheater is known as crossflow. At the top of the preheater, the feedwater mixes with the riser flow from the hot-side of the steam generator. In a similar way as in steam generators without preheaters, the steam produced in the tube bundle passes through the primary and secondary separators where entrained liquid droplets are removed. These liquid droplets are returned to the recirculating flow in the downcomer annulus. The recirculating flow is directed into the tube bundle at the tubesheet through the downcomer windows.

An example of the velocity at the steam generator plane of symmetry is shown in Fig. 4.4 as predicted by AECL's THIRST code. On the hot-side of the steam generator, the secondary fluid velocity is predicted to reach roughly 6 m/s while this velocity is

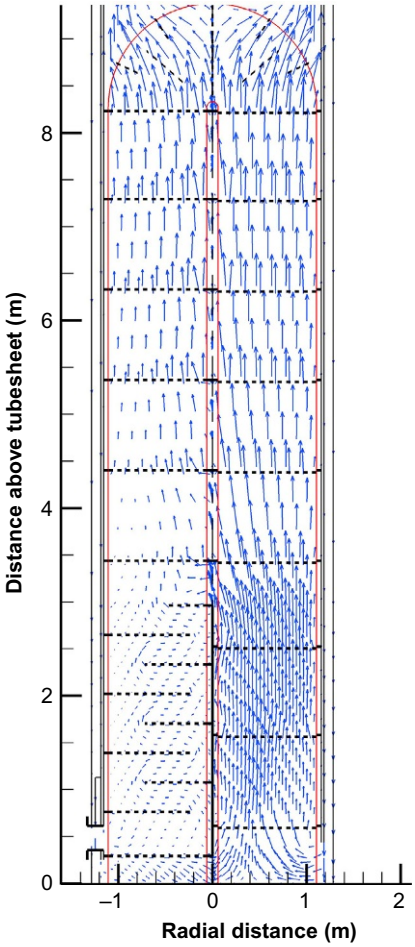

Fig. 4.4 Predicted secondary fluid relative velocities at the plane of symmetry for CANDU steam generator with an internal preheater.

predicted to be only 4 m/s on the cold-side. The secondary fluid velocity in the lower section of the steam generator is higher on the hot-side of the steam generator than on the cold-side due to the presence of the preheater and different flow conditions.

Recirculating steam generators remove a small percentage fluid, 1% or less, of their steam mass flow rate at their tubesheet on an intermittent or continuous basis. This flow is known as blowdown. The objective of blowdown is to limit the build-up of impurities in the recirculating flow.

The recirculation ratio (*RR*) is an overall indicator of the downcomer or riser flow rate and heat transfer to the secondary fluid. This ratio is important during the design and operation phase as the ratio indicates the maximum steam quality in the tube bundle. The *RR* is influenced by several steam generator design elements and can be used to estimate separator loading, steam flow, tube bundle exit steam quality, downcomer flow rates, and system pressure losses. These parameters cannot be directly measured in the steam generator (Duffey, 1981).

The *RR* of the recirculating fluid is defined in Eq. (4.1) as:

$$RR = \frac{\text{downcomer mass flow rate}}{\text{steam mass flow rate}} \tag{4.1}$$

The *RR* is related to the circulation ratio (*CR*), which is the ratio of the riser mass flow rate to the steam mass flow rate, given in Eq. (4.2) as:

$$CR = RR + 1 \tag{4.2}$$

For high overall heat transfer rate, high fluid velocities and high *RR* are needed. However, to minimize the effects of flow-affected degradation mechanism, a moderate to low fluid velocities and *RR* are required. Therefore, the *RR* should be optimized to ensure high overall heat transfer rate while having negligible effects on flow-affected degradation mechanisms. The effects of flow-affected phenomena on degradation mechanism will be discussed in more detail in Section 4.2.7.

4.2.2 Heat transfer

In the steam generator, the secondary fluid is heated by the primary fluid. Due to the large volume of secondary fluid in the steam generator in comparison to the primary fluid inventory, the secondary fluid is able to store several times more energy than the primary fluid. As a result, the natural circulation of the primary fluid will allow this fluid to act as the heat source while the secondary fluid is the heat sink under accident scenarios.

The boiling regimes for the secondary fluid are shown in Figs. 4.5 and 4.6 for PWRs and CANDU steam generators, respectively. At the tubesheet, the secondary fluid is primarily a subcooled liquid. In steam generators with preheaters, subcooled liquid is also present in the majority of the preheater. The steam quality increases as the fluid flows up through the tube bundle with the saturated nucleate boiling and turbulent saturated boiling producing turbulent and bubbly flow in most of the tube bundle. The fluid can become annular flow as the steam quality continues to increase as

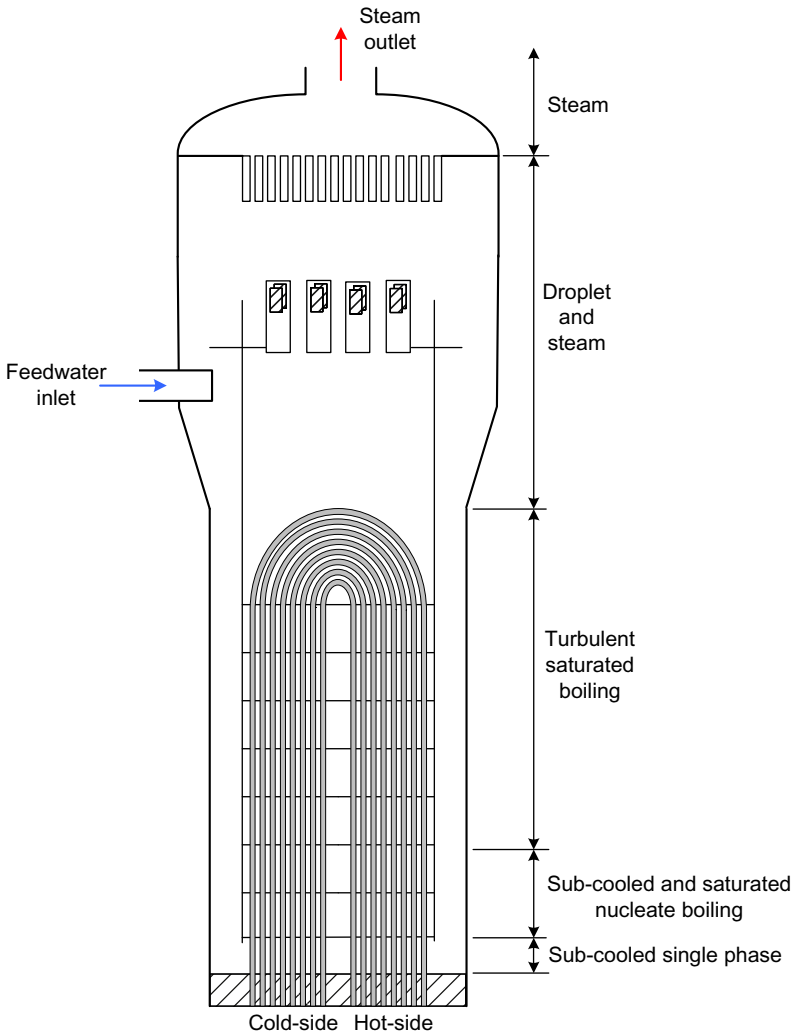

Fig. 4.5 Secondary fluid flow regimes in typical recirculating steam generator.

flow goes up through the tube bundle. In the separators, water droplets are removed from the fluid and relatively dry steam exits the steam generator.

At the top of the tube bundle, the two-phase steam quality reaches 20%–40%. Fig. 4.7 shows the predicted steam quality at the plane of symmetry for a CANDU steam generator with an internal preheater, as predicted by the AECL's THIRST code. For an as-designed, clean steam generator that operates with a *RR* of about 5, the maximum steam quality indicated in Fig. 4.7 is 25% with this maximum located at the hot-side of the tube bundle in the U-bend region.

In the tube bundle, the tube supports causes local changes, an increase and reduction, in the fluid velocity. In these regions, localized nucleation and boiling can occur

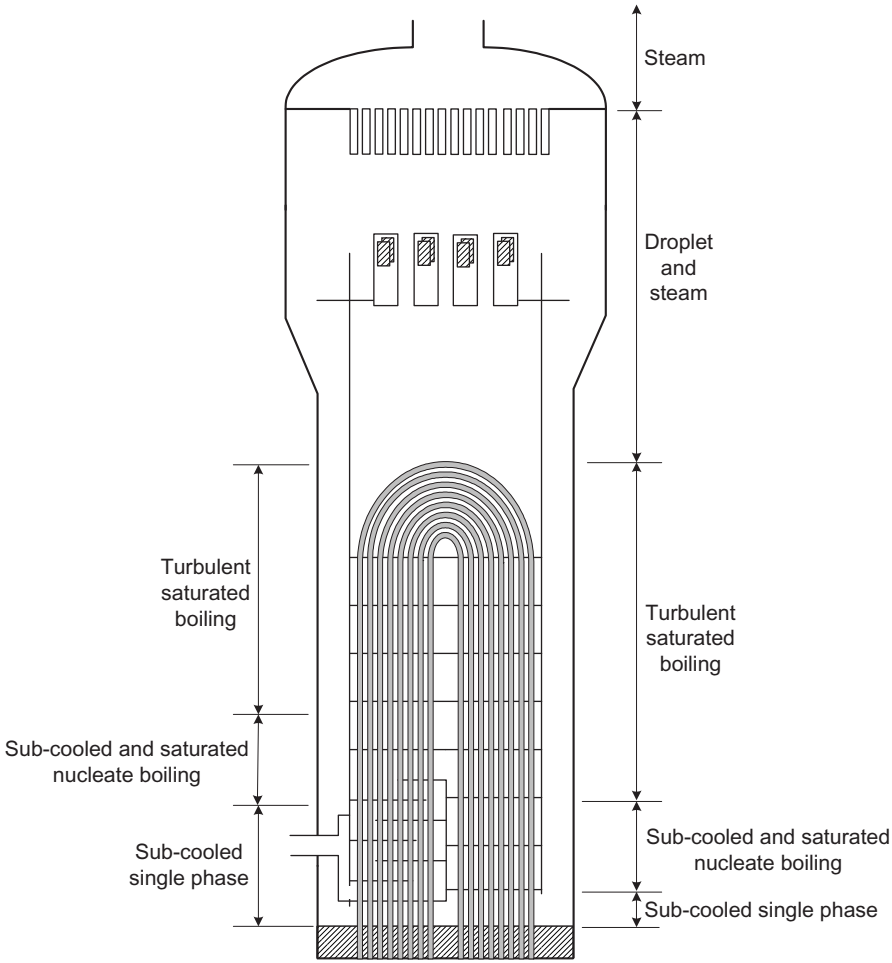

Fig. 4.6 Secondary fluid flow regimes in a CANDU steam generator with an internal preheater.

that might result in the local concentration of impurities and increased particle deposition. This phenomenon will be discussed in Section 4.2.7.

The thermal performance degradation of the steam generator results from tube fouling, separator fouling, primary divider plate leakage and preheater thermal plate leakage, and tube plugging (Yetisir et al., 2000). These effects are discussed below.

4.2.2.1 Fouling

Tube fouling in the steam generator reduces the heat flux from the primary to secondary fluid (Turner, 2013; Klimas et al., 2004). Primary-side deposits increase the thermal resistance for heat transfer to the secondary fluid. Initially, secondary-side deposits enhance heat transfer as the porous layer provides additional sites for bubble nucleation when the tube surface is covered by a thin layer of deposit. However, these secondary-side deposits

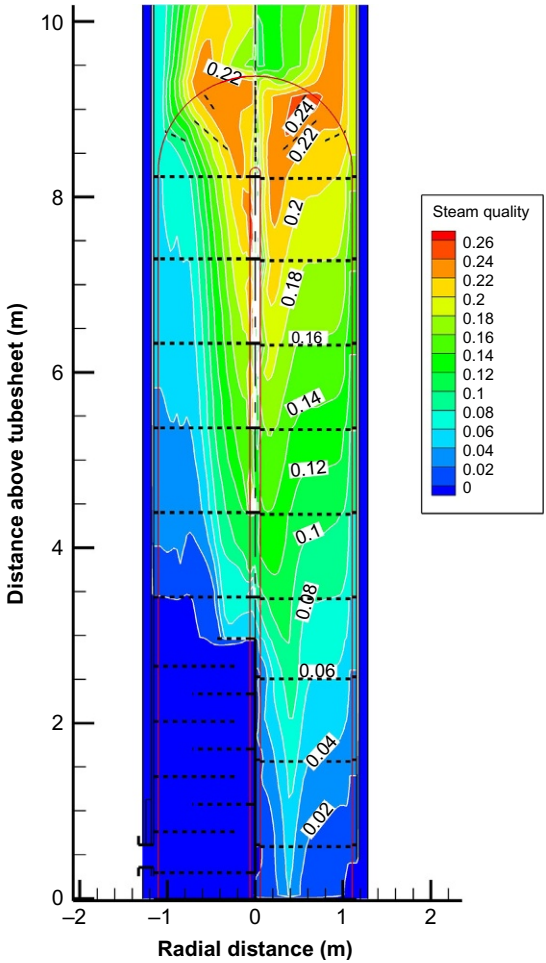

Fig. 4.7 Predicted steam quality at plane of symmetry for a CANDU steam generator.

consolidate over time, increasing their heat transfer resistance. In both cases, the increase in thermal resistance of the primary- or secondary-side deposits decreases the heat transfer rate in the steam generator, reducing its efficiency. This decreased efficiency results in higher primary fluid temperature exiting the steam generator and reduces the steam flow rate available to the turbine.

In an attempt to mitigate fouling, a small mass of fluid is removed from above the tubesheet as blowdown. This flow helps to limit the tubesheet fouling and local impurities but has a negligible effect on the thermal performance of the steam generator.

4.2.2.2 Divider plate leakage

In the primary head of the steam generator, the primary fluid inlet and outlet are separated by a divider plate. Leakage through or around this divider plate occurs when primary fluid leaks from the inlet, through the divider plate, to the outlet without

transferring its heat to the secondary fluid. Due to the pressure drop across the divider plate, this leakage has a high velocity and flow-accelerated corrosion (FAC) of the divider plate can occur if this divider plate is made of carbon steel. Over time, this leakage rate can increase and contribute to thermal degradation of the steam generator.

4.2.2.3 Preheater thermal plate leakage

The integral preheater with crossflow usually includes a thermal plate that separates the feedwater from the recirculating flow from the downcomer flow entering the tube bundle. There is a small clearance gap between the tubes and the thermal plate and leakage is possible through this gap. The leakage rate and its direction are dependent of the pressure drop across the thermal plate with higher pressure drops resulting in higher leakage rates. If the feedwater leaks from the preheater into the recirculating flow, the preheater efficiency and steam generator thermal output are reduced as a fraction of the feedwater mixes with the hot recirculating flow below the thermal plate. If the recirculating flow leaks into the preheater, the hot riser flow mixes with the feedwater inside the preheater, thus reducing heat transfer to the feedwater. The lower heat flux reduces the thermal efficiency of the preheater.

4.2.2.4 Tube plugging

Tubes must sometimes be plugged to mitigate tube material degradation and leaks from the primary to secondary fluid. Plugging tubes decreases the heat transfer area of the steam generator and increases the primary-side tube velocity in the remaining tubes. Lowering the heat transfer area reduces the thermal efficiency of the steam generator, even though increased flow velocity in the tubes increases the heat transfer coefficient.

4.2.3 Steam-water separation

Steam-water separation occurs in the primary and secondary separators where liquid water is removed from the secondary fluid mixture. This separation occurs in three steps. The primary separators perform the initial separation by centrifugal force. Distance between the primary and secondary separators allows the gravity to separate the water droplets from the steam. Finally, chevron-type or corrugated-shaped secondary separators perform the final separation (Green and Hetsroni, 1995).

The performance of the separators affects the exit steam quality and *RR*. As the mass flow rate in the separators increases, there is a rapid increase in moisture carryover that adversely affects the turbine blades and its structures. A low pressure drop in the separators increases the *RR*; however, a high pressure drop can also create water level oscillations, or flow instabilities, in the steam generator (Green and Hetsroni, 1995). These water level oscillations are discussed in Section 4.2.7.

4.2.4 Carryover and carryunder

Moisture carryover in the steam exiting the steam generator is the ratio of mass flow rate of liquid water to mass flow rate of steam. Liquid water, in the form of droplets, is reentrained from the surfaces in the steam drum and also results from the imperfect separation of liquid droplets from the steam. Moisture carryover is an indicator of the efficiency of the steam generator and less carryover results in improved steam generator performance. Carryover should not exceed 0.25%; however, this limit may not be low enough to minimize turbine damage. Advanced separators can achieve a carryover below 0.1% (Green and Hetsroni, 1995).

The ratio of steam mass flow rate in the downcomer flow to recirculating mass flow rate is known as carryunder. Steam bubbles are carried in the recirculating flow into the downcomer due to imperfect separation of the liquid and gas phases by the separators. These bubbles saturate the recirculating water and increase the pressure drop of the recirculation loop in comparison to this pressure drop for unsaturated water in the downcomer annulus.

4.2.5 Effect of primary fluid on steam generator thermal performance

Heavy water (D_2O) is used as the primary fluid in pressurized heavy water reactors, such as CANDU reactors. The thermal properties of heavy water are similar to those for light water (H_2O) (Kestin et al., 1984). For example, the density of heavy water is $\sim$10% greater than the density of light water and the boiling point for heavy water is 101.4°C at atmospheric pressure. This higher density of heavy water means this fluid has a greater potential for transporting heat.

In CANDU steam generators, the primary fluid may contain a small percentage of steam. Typically, the inlet contains $<$5% steam quality which increases the heat available to be transferred to the secondary fluid.

4.2.6 Use of preheater

Preheaters or economizers improve the thermal efficiency of the steam generator by transferring heat from the primary fluid before leaving the tubes to the feedwater. These preheaters may be internal, or integral, to the steam generator. In axial flow preheaters, the feedwater flow is parallel to the tubes, or axial. In crossflow preheaters, feedwater flow is perpendicular to the tubes. The thermalhydraulics for internal preheater designs will be discussed in the following sections.

4.2.6.1 Axial flow preheaters

Feedwater enters the steam generator through a feedwater distribution ring and is mixed with about 10% of the recirculated flow as the feedwater is directed down the bundle wrapper toward the tubesheet (Teller, 2010). The feedwater is heated by

its mixing with the recirculating fluid before the mixture enters the tube bundle of the axial preheater as shown in Fig. 4.8. At the tubesheet, the remaining 90% of the recirculating flow is directed into the tube bundle on the hot-side. Inside the preheater, the flow is predominately parallel to the tubes and axial to the tube support plates, which do not change the direction of the flow. After leaving the preheater, the flow joins the hot-leg riser flow.

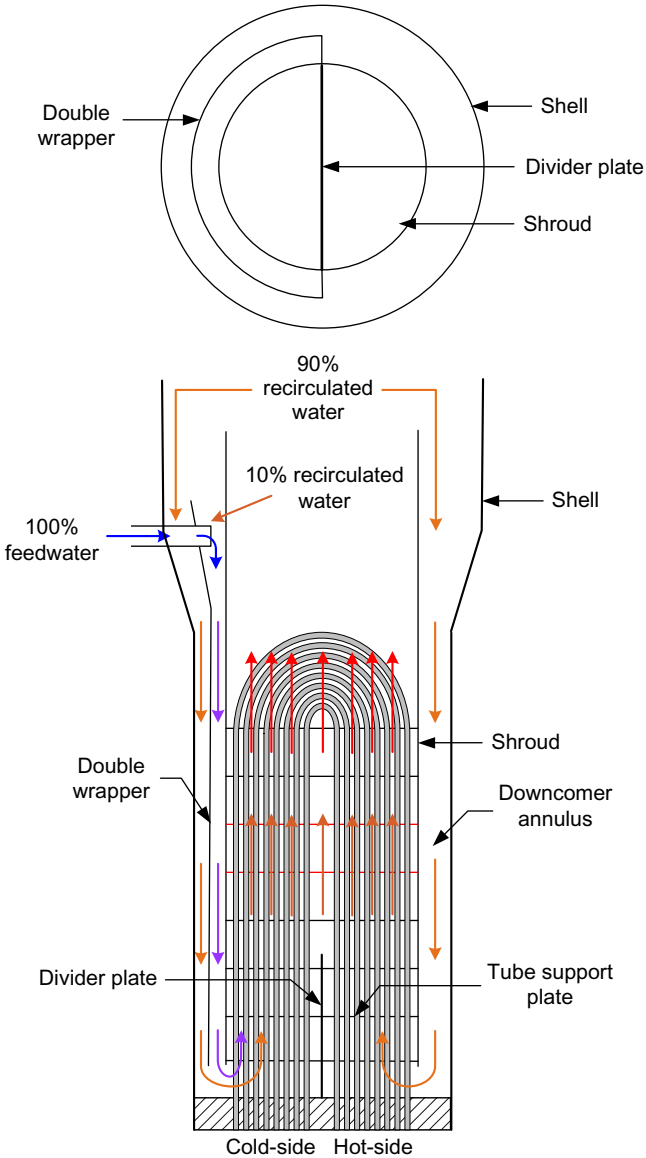

Fig. 4.8 Simplified sketch of axial flow preheater—horizontal (top) and vertical (bottom) cross-sections.

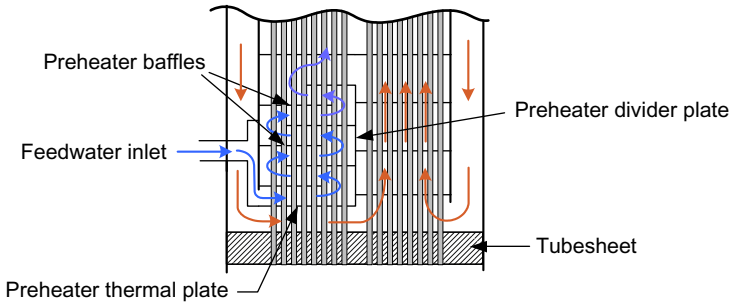

Fig. 4.9 Simplified integral preheater with crossflow.

4.2.6.2 Crossflow preheaters

In integral preheaters with crossflow, the feedwater enters a feedwater distribution box above the tubesheet on the cold-side of the steam generator as shown in Fig. 4.9. Heat from the primary fluid leaving the steam generator is transferred to the feedwater. The preheater baffles force the feedwater to flow mostly perpendicular to the tube bundle through the preheater. This crossflow path increases the heat transfer and increases the temperature of the feedwater to roughly its saturation temperature when the feedwater mixes with the riser flow at the top of the preheater (IAEA, 1997).

4.2.7 Flow-affected phenomena leading to degradation

Thermalhydraulics play an important role in thermal and material degradation within the steam generator. Thermal degradation results in a reduction in the ability to transfer heat from the primary fluid to the secondary fluid over the lifetime of the steam generator. Material degradation, especially tube degradation, can limit the operation of the steam generator. These flow-affected phenomena are described in the following sections.

4.2.7.1 High fouling rates on tubes in regions with high steam quality

Fouling on the primary and secondary sides of steam generator tubes reduces the thermal performance of the steam generator. These deposits provide thermal resistance to the heat transfer from the primary to secondary fluids. The fouling rates are generally low in the presence of low steam quality. However, above a steam quality of 35%, this fouling rate increases by up to three orders of magnitude in experiments simulating steam generator operating conditions (Klimas et al., 2004). To operate the steam generator under low deposit rates, a high *RR* is recommended to reduce the average and maximum local steam quality in the secondary fluid (Turner, 2013).

4.2.7.2 Sludge accumulation on the tubesheet

Low horizontal, or crossflow, velocity of the secondary fluid above the tubesheet results in a low steam quality in the middle region of the tubesheet. This steam quality can typically be <5%. The low fluid velocity and boiling are conducive for particle deposition and the accumulation of deposits on the tubesheet. The presence of these deposits can create local environments where boiling can concentrate corrosive impurities to create aggressive chemistry. This local aggressive chemistry might increase the susceptibility to localized degradation, such as stress corrosion cracking (SCC) (IAEA, 1997; Green and Hetsroni, 1995). High horizontal fluid velocities above the tubesheet allow the flow to penetrate deeper into the tube bundle, avoid or reduce boiling, and thus result in lower sludge deposition on the tubesheet.

4.2.7.3 High concentration rate of chemicals in crevices

Impurities in the secondary fluid preferentially stay in the liquid phase and are concentrated at high steam qualities, which occur at lower *RR*s. Localized boiling can also occur in the clearance gap between the tubesheet or tube support structure and the tube. This gap is known as a crevice where the heat flux concentrates nonvolatile ionic impurities and creates environments that increase the susceptibility to localized degradation (e.g., SCC).

4.2.7.4 Cavitation erosion

In crossflow preheaters, subcooled boiling might occur in the clearance gap between the preheater baffle plate and the tube. In this gap, there is secondary fluid flow due to the pressure difference across the baffle plate coupled with a temperature difference between the primary and secondary fluids. The temperature difference can cause water in this narrow gap to boil and vapor bubbles can form. These steam bubbles can collapse when they mix with the subcooled feedwater at the exit of the clearance gap. If these bubbles violently collapse in the vicinity of the tube, material damage can occur and is known as cavitation erosion (Laroche et al., 2014).

4.2.7.5 Water level oscillations

The pressure drop in the recirculation loop is determined primarily by the pressure drop of the downcomer and riser flow. In the downcomer, flow is primarily single-phase flow while in the riser, the flow is two-phase flow. This recirculating loop is stable if the ratio of the pressure drop in the riser, two-phase flow region, to the pressure drop in the downcomer, single-phase flow region, does not exceeds a critical value. If the steam quality in the tube bundle is high, this critical value can be exceeded and flow instabilities can occur. These flow instabilities can result in large water level oscillations that can be in the order of 1 m or more. These oscillations result from

inherent flow instabilities from the hydrodynamics of natural recirculating two-phase flow systems.

As the steam generator ages, sludge deposits accumulate on tube support plates and these deposits increase the pressure drop in the two-phase flow thereby reducing the *RR*. As the two-phase flow pressure drop increases, the probability of water level oscillations also increases.

4.2.7.6 Flow-induced vibrations

There is two-phase flow with high steam qualities in the upper region of the tube bundle and these conditions result in high fluid velocities. These flow characteristics in the U-bend region of the tube bundle produce high crossflow which increases the potential for the vibration of a single or multiple tubes. This flow-induced vibration (FIV) may result in fretting wear. Fretting wear is a mechanically induced material degradation that results from small amplitude, oscillatory motion at the contact between a tube and another tube or a tube and a tube support structure (IAEA, 1997).

In the steam generator shell, foreign objects can be transported by the flow. When these objects hit or vibrate against structures or tubes, degradation, such as fretting wear or dings, can result.

4.2.7.7 Fatigue

Fatigue is a phenomenon leading to material degradation under the repeated application of mechanical or thermal stresses. These stresses may result from local thermalhydraulics, such as thermal stratification, thermal striping, or thermal mixing, that were not typically considered during the design of the steam generator.

High cycle fatigue can result from cyclic thermal stratification and/or thermal mixing when the cold feedwater mixes with the hot saturated fluid in the downcomer. These thermalhydraulic conditions can result in the feedwater nozzle and thermal sleeve joint experiencing high cycle fatigue due to cyclic thermal stratification and/or thermal mixing (IAEA, 1997).

4.2.7.8 Flow-accelerated corrosion

High fluid velocities in the steam generator can cause FAC of carbon steel or low-alloy steel components or structures. This phenomenon occurs when water, unsaturated with magnetite, flows over the surface at a high velocity. The flow dissolves the protective iron oxide layer, typically magnetite, on the surface and results in material damage (IAEA, 1997). FAC degradation has been observed for carbon steel tube support structures, feedwater nozzles, and in the primary separators.

As an indirect contributor, the corrosion products generated by FAC inside the steam generator and those transported into the steam generator with the feedwater can accumulate on the tubesheet and on tube support structures. These deposits can

affect the thermalhydraulics and thermal performance of the steam generator by phenomena mentioned previously in this section.

4.2.8 Theoretical approach to solving thermalhydraulics

Theoretical approaches, based on conservation equations solved by numerical computations, have been developed to predict the detailed three-dimensional flow in steam generators. This knowledge has provided insight into the flow distribution within the steam generator that can then be used to improve the understanding of steam generator performance and flow-induced degradation (Duffey, 1981; EPRI, 1985).

The thermal power, Q, from the steam generator can be estimated using the simple heat transfer kinetics given in Eq. (4.3) for a steam generator without a preheater (Kreider et al., 1998):

$$Q = U \times A \times \Delta T_m = U \times A \times \frac{(T_{hot} - T_{cold})}{\ln\left[\frac{(T_{hot} - T_{sat})}{(T_{cold} - T_{sat})}\right]} \tag{4.3}$$

where A is the effective heat transfer area, ΔT_m is the log mean temperature difference, T_{hot} is the primary fluid temperature at the steam generator inlet, T_{cold} is the primary fluid temperature exiting the steam generator, and T_{sat} is the saturation temperature of the secondary fluid. The overall average heat transfer coefficient, U, and can be determined by Eq. (4.4):

$$U = \frac{1}{\left(\frac{1}{h_{pri}} + \frac{1}{U_{wall}} + \frac{1}{U_{foul}} + \frac{1}{h_b}\right)} \tag{4.4}$$

where h_{pri} is the primary-side heat transfer coefficient, U_{wall} is the tube wall thermal conductivity heat transfer coefficient, U_{foul} is the heat transfer coefficient of deposits on the tube, and h_b is the boiling heat transfer coefficient. All the heat transfer coefficients should be reduced to the same tube diameter as the effective heat transfer area.

In a PWR steam generator, the temperature profile for the primary and secondary fluid is shown in Fig. 4.10. In this figure, the rate of change in the primary fluid temperature at the inlet, T_{hot}, is greater at the inlet due to the higher temperature difference between the primary and secondary fluids than at the outlet. At the outlet, the primary fluid temperature, T_{cold}, is close to the secondary fluid saturation temperature, T_{sat}. The secondary fluid temperature is roughly at its saturation temperature as this fluid enters and exits the tube bundle.

For a steam generator with an internal preheater, the thermal power can use a similar approach using Eq. (4.3); however, this approach divides the steam generator into two regions: the preheater region and the remainder of the steam generator. The thermal power is calculated for each region separately and added for the whole steam generator as given in Eq. (4.5). The thermal power of the preheater, Q_{ph}, is given in

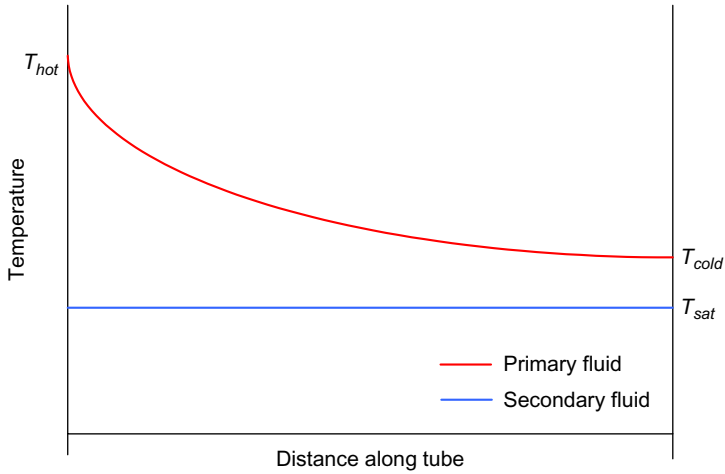

Fig. 4.10 Primary and secondary temperature profile in a PWR steam generator.

Eq. (4.6) and for the rest of the steam generator, Q_r, in Eq. (4.7). These equations assume that at the exit of the preheater, the feedwater temperature equals its saturation temperature:

$$Q = Q_{ph} + Q_r \tag{4.5}$$

$$Q_{ph} = U_{ph} \times A_{ph} \times \Delta T_m = U \times A_{ph} \times \frac{\left[\left(T_{ph} - T_{sat}\right) - \left(T_{cold} - T_{fw}\right)\right]}{\ln\left[\frac{\left(T_{ph} - T_{sat}\right)}{\left(T_{cold} - T_{fw}\right)}\right]} \tag{4.6}$$

where U_{ph} is the heat transfer coefficient in the preheater, A_{ph} is the effective heat transfer area in the preheater, T_{ph} is the primary fluid as it enters the preheater, and T_{fw} is the feedwater temperature.

$$Q_r = U \times \left(A - A_{ph}\right) \times \Delta T_m = U \times \left(A - A_{ph}\right) \times \frac{\left(T_{hot} - T_{ph}\right)}{\ln\left[\frac{\left(T_{hot} - T_{sat}\right)}{\left(T_{ph} - T_{sat}\right)}\right]} \tag{4.7}$$

The primary fluid temperature entering the preheater, T_{ph}, can be calculated from the heat balance for the preheater using Eq. (4.8):

$$Q_{ph} = \dot{m}_{fw} c_{p_fw}\left(T_{sat} - T_{fw}\right) = \dot{m}_{ps} c_{p_ps}\left(T_{ph} - T_{cold}\right) \tag{4.8}$$

where $\dot{m}_{fw}$ is the feedwater mass flow rate, c_{p_fw} is the specific heat for the feedwater, $\dot{m}_{ps}$ is the primary fluid flow rate, and c_{p_ps} is the specific heat for the primary fluid.

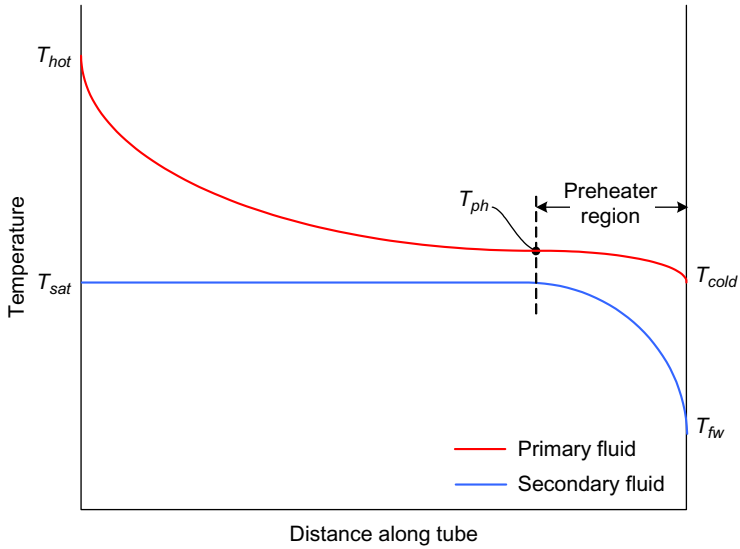

Fig. 4.11 Primary and secondary temperature profile for a CANDU steam generator.

The temperature profile for the primary and secondary fluids in a CANDU steam generator is shown in Fig. 4.11. The rate of change in the primary fluid temperature at the inlet, T_{hot}, is greater at the inlet due to the higher temperature difference between the primary and secondary fluids. In the preheater, the feedwater temperature, T_{fw}, increases until this feedwater reaches its saturation temperature, T_{sat}, at the exit of the preheater. The primary fluid temperature exiting the steam generator, T_{cold}, is close to the secondary fluid saturation temperature.

A heat balance can also be performed for the primary and secondary fluids according to Eqs. (4.9)–(4.13). These equations can be rearranged to solve for the steam flow rate for a given set of operating conditions. The steam flow rate and the feedwater flow rate are assumed equal for this simplistic heat balance:

$$Q = Q_{ps_in} - Q_{ps_out} = Q_{ss_out} - Q_{ss_in} \tag{4.9}$$

where Q_{ps_out} is the heat rate from the primary fluid exiting the steam generator, Q_{ps_in} is the heat rate from the primary fluid entering the steam generator, Q_{ss_out} is the heat rate of secondary fluid exiting as steam, and Q_{ss_in} is the heat rate entering as feedwater.

$$Q_{ps_out} = \dot{m}_p \times H_{ps_l}(T_{cold}) \tag{4.10}$$

where $H_{ps_l}(T)$ is the enthalpy of the primary fluid for liquid at the specified temperature, T.

$$Q_{ps_in} = \dot{m}_{ps} \times \left[x_{ps_in} \times H_{ps_g}(T_{hot}) - \left(1 - x_{ps_l}\right) \times H_{ps_l}(T_{hot})\right] \tag{4.11}$$

where x_{ps_in} is the inlet steam quality of the primary fluid and $H_{ps_g}(T)$ is the enthalpy of the primary fluid for the gas at the specified temperature.

$$Q_{ss_out} = \dot{m}_{steam} \times H_{ss_g}(T_{sat}) \tag{4.12}$$

where $\dot{m}_{steam}$ is the steam mass flow rate exiting the steam generator and $H_{ss_g}(T)$ is the enthalpy of the secondary fluid for the gas phase at the specified temperature, T.

$$Q_{ss_in} = \dot{m}_{fw} \times H_{ss_l}(T_{fw}) \tag{4.13}$$

where $H_{ss_l}(T)$ is the enthalpy of the secondary fluid for the liquid at the feedwater temperature, T_{fw}.

The numerical analysis is a common method that uses computer codes to solve the differential equations for mass, momentum, and energy balance of the secondary fluid. The heat balance equation for the secondary fluid is solved simultaneously with the heat balance for the primary fluid and together with the other differential equations.

The governing differential equations for a homogeneous two-phase flow mixture for the secondary fluid are given in Eqs. (4.15)–(4.19), respectively, for cylindrical coordinates (EPRI, 1985).

Conservation of momentum:

- Axial momentum

$$\begin{aligned}\frac{1}{\alpha}\left[\frac{\partial}{\partial x}(\alpha\rho u^2) + \frac{1}{r}\frac{\partial}{\partial r}(r\alpha\rho uv) + \frac{1}{r}\frac{\partial}{\partial\theta}(\alpha\rho uw)\right] &= -\frac{\partial P}{\partial x} - \rho g + R_x \\ + \frac{1}{\alpha}\left[\frac{\partial}{\partial x}\left(\alpha\mu_t\frac{\partial u}{\partial x}\right) + \frac{1}{r}\frac{\partial}{\partial r}\left(\alpha r\mu_t\frac{\partial u}{\partial r}\right) + \frac{1}{r}\frac{\partial}{\partial\theta}\left(\alpha\frac{\mu_t}{r}\frac{\partial u}{\partial\theta}\right)\right]\end{aligned} \tag{4.14}$$

- Radial momentum

$$\begin{aligned}\frac{1}{\alpha}\left[\frac{\partial}{\partial x}(\alpha\rho uv) + \frac{1}{r}\frac{\partial}{\partial r}(r\alpha\rho v^2) + \frac{1}{r}\frac{\partial}{\partial\theta}(\alpha\rho vw)\right] &= -\frac{\partial P}{\partial r} - \frac{\rho w^2}{r} + R_r \\ + \frac{1}{\alpha}\left[\frac{\partial}{\partial x}\left(\alpha\mu_t\frac{\partial v}{\partial x}\right) + \frac{1}{r}\frac{\partial}{\partial r}\left(\alpha r\mu_t\frac{\partial v}{\partial r}\right) + \frac{1}{r}\frac{\partial}{\partial\theta}\left(\alpha\frac{\mu_t}{r}\frac{\partial v}{\partial\theta}\right)\right]\end{aligned} \tag{4.15}$$

- Circumferential momentum

$$\begin{aligned}\frac{1}{\alpha}\left[\frac{\partial}{\partial x}(\alpha\rho uw) + \frac{1}{r}\frac{\partial}{\partial r}(r\alpha\rho vw) + \frac{1}{r}\frac{\partial}{\partial\theta}(\alpha\rho w^2)\right] &= -\frac{1}{r}\frac{\partial P}{\partial\theta} - \frac{\rho vw}{r} + R_\theta \\ + \frac{1}{\alpha}\left[\frac{\partial}{\partial x}\left(\alpha\mu_t\frac{\partial w}{\partial x}\right) + \frac{1}{r}\frac{\partial}{\partial r}\left(\alpha r\mu_t\frac{\partial w}{\partial r}\right) + \frac{1}{r}\frac{\partial}{\partial\theta}\left(\alpha\frac{\mu_t}{r}\frac{\partial w}{\partial\theta}\right)\right]\end{aligned} \tag{4.16}$$

where u, v, and w are the velocity components in the axial (x), radial (r), and circumferential (θ) direction, respectively; ρ is the mixture density; g is the acceleration due to gravity; P is the pressure; μ_t is the turbulent effective viscosity; and, R_x, R_r, and R_θ are the distributed resistance that represent resistance force per unit volume in each flow direction.

Conservation of energy:

- Secondary side

$$\frac{1}{\alpha}\left[\frac{\partial}{\partial x}(\alpha\rho u H_s)+\frac{1}{r}\frac{\partial}{\partial r}(r\alpha\rho v H_s)+\frac{1}{r}\frac{\partial}{\partial\theta}(\alpha\rho w H_s)\right]=S_H \\ +\frac{1}{\alpha}\left[\frac{\partial}{\partial x}\left(\alpha\Gamma_t\frac{\partial H_s}{\partial x}\right)+\frac{1}{r}\frac{\partial}{\partial r}\left(\alpha r\Gamma_t\frac{\partial H_s}{\partial r}\right)+\frac{1}{r}\frac{\partial}{\partial\theta}\left(\alpha\frac{\Gamma_t}{r}\frac{\partial H_s}{\partial\theta}\right)\right] \tag{4.17}$$

- Primary side

$$\frac{1}{\alpha_p}\left[\frac{\partial}{\partial x}(\alpha_p\rho_p u_p H_p)+\frac{1}{r}\frac{\partial}{\partial r}(r\alpha_p\rho_p v_p H_p)+\frac{1}{r}\frac{\partial}{\partial\theta}(\alpha_p\rho_p w_p H_p)\right]=S_P \tag{4.18}$$

where H_s and H_p are the enthalpy of the primary and secondary fluid, respectively; Γ_t is the eddy thermal diffusivity; S_H is the fluid-solid heat "source" as heat transfer rate per unit volume; α_P is the porosity of primary fluid domain and equals $(1-\alpha)$ if the volume of the tubes is neglected; u_p, v_p, and w_p are the primary fluid velocity components in the axial (x), radial (r), and circumferential (θ) direction, respectively; ρ_p is the primary fluid density; and S_P is the heat "source" of the primary fluid.

Continuity equation:

$$\frac{\partial}{\partial x}(\alpha\rho u)+\frac{1}{r}(\alpha\rho r v)+\frac{1}{r}\frac{\partial}{\partial\theta}(\alpha\rho w)=0 \tag{4.19}$$

The momentum source terms are dependent on the flow direction and steam generator structures that contribute to local frictional pressure gradients. In the tube bundle, the direction of the flow relative to the tubes, parallel or perpendicular, influences the pressure drop which must be estimated using suitable correlations. Structures in the steam generator affect the contraction or expansion of flow and thus affect the local pressure drop.

The computational domain is typically from the tubesheet to the bottom of the separators. The modeled region is treated as a continuum with the tube bundle being treated as a porous-media and structures being modeled as hydraulic resistance. Using closure criteria for void fraction, steam quality, relative velocity, and mixture density, the governing equations can be solved for this computational domain.

Once the differential equations have been solved, the pressure distribution, *RR*, void fraction distribution, and flow distribution within the steam generator will have been calculated. Traditionally, these models have been solved using homogeneous equilibrium model when examining global thermal performance (Duffey, 1981).

Steam generator thermalhydraulic codes use finite volume methods to solve the differential equations and predict the detailed three-dimensional thermalhydraulics for the shell-side of the steam generator. These past and present codes include:

- ATHOS/SGAP (EPRI) (EPRI, 1985; EPRI, 2012a)
- CALIPSOS (Combustion Engineering) (Green and Hetsroni, 1995; EPRI, 1985)

- FAUST (Korean Advanced Institute of Science and Technology) (Lee and No, 1986)
- FIT-III (Mitsubishi Heavy Industry (MHI)) (Hirao et al., 1991)
- FLOW-3 (Bettis Atomic Power Laboratory) (EPRI, 1985)
- GENEPI (Électricité de France (EdF)) (Yetisir et al., 2004)
- PORTHOS (EPRI)
- PORTHOS-MHI (MHI) (Kondo et al., 2000)
- THIRST (AECL and CANDU Owners Group (COG)) (Yetisir et al., 2004; Carver et al., 1981)
- THYC (EdF) (Tincq et al., 1995)

In 2012, EPRI began development of a new steam generator thermalhydraulic code, Triton (EPRI). This code will use modern numerical methods, empirical correlations, discretization techniques and up-to-date programming schemes to solve for steam generator thermalhydraulics (EPRI, 2012b).

4.3 Once-through steam generators

The thermalhydraulics for once-through steam generators (OTSGs) will be described in the following sections.

4.3.1 Flow paths

In an OTSG, the primary fluid enters at the top of the OTSG and flows down through the straight tubes before exiting at the bottom of the steam generator. As the primary fluid passes through the tubes, heat is transferred to the secondary fluid in the shell. The secondary fluid flows from the bottom of the steam generator shell to the top and is countercurrent to the primary fluid flow.

Fig. 4.12 shows the secondary fluid flow path. The feedwater enters an annulus above the ninth tube support plate where it mixes with steam aspirated from the tube bundle to preheat the feedwater to its saturation temperature (EPRI, 1985; EPRI, 1980). This saturated liquid flows down the annulus, across the lower tubesheet and up the tube bundle where it is converted first to saturated steam and then to superheated steam. This superheated steam exits the tube bundle radially at the top tubesheet and flows down the annulus to the steam outlet.

4.3.2 Heat transfer

During operation, superheated steam is produced at constant power over the OTSG power range. The temperature difference between the primary and secondary fluid at the OTSG outlet is similar to that at the outlet of the cold-leg of a recirculating steam generator (Green and Hetsroni, 1995). When the outlet steam pressure decreases, the feedwater flow rate increases proportional to the increased steam flow rate. At lower power levels (below 15%), the steam temperature at the outlet nozzle is approximately equal to the saturation temperature.

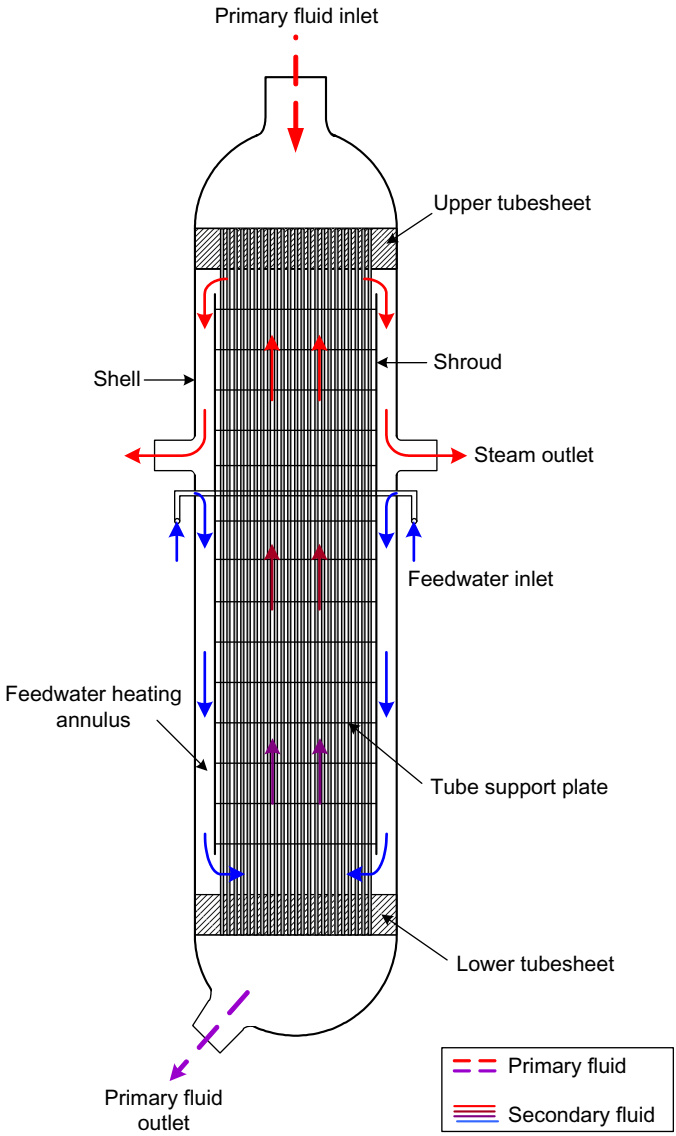

Fig. 4.12 Sketch of primary and secondary fluid flow paths in once-through steam generators.

In an OTSG, the secondary fluid is converted from a subcooled fluid to superheated steam as it passes through three different heat transfer zones (EPRI, 2012b). During nucleate boiling, the secondary-side heat transfer coefficient is at its maximum. Film dryout occurs when the steam quality reaches ~95% and the heat transfer coefficient is reduced in film boiling to produce steam. The temperature of the steam increases as

it is superheated in the upper region of the OTSG. In this superheated region, the tube area available for superheat varies inversely with the steam generator load.

4.3.3 Flow-affected phenomena leading to degradation

Thermalhydraulic conditions in OTSG can cause material degradation that is referred to as flow-affected degradation mechanisms. In most cases, these phenomena are similar to those observed in recirculating steam generators.

More specific to OTSG, FIVs can result and the evaporation of secondary fluid in film boiling region increases the concentration of impurities in the remaining water droplets. The steam flow carries these droplets to the upper tubesheet region where the droplets impinge on the tubes. With boiling, the concentration of these impurities increases and crevice corrosion coupled with cyclic vibrations can lead to localized material degradation (IAEA, 1997).

4.3.4 Theoretical approach to solving thermalhydraulics

The theoretical approach, including fundamental equations and relationships, are the same for OTSGs as for recirculating steam generators (see Section 4.2.8). These approaches have also been developed to predict the detailed three-dimensional flow that are based on conservation equations and provide insight into the flow structure within the OTSG.

The temperature profile for the primary and secondary fluid in an OTSG is shown in Fig. 4.13 where the primary and secondary fluid flow is countercurrent. In the OTSG, the rate of change in the primary fluid temperature at the inlet, T_{hot}, is greater at the inlet due to the higher temperature difference between the primary and secondary fluids than is observed in recirculating steam generators. For most of the OTSG, the secondary fluid temperature remains at its saturation temperature, T_{sat}, until all of

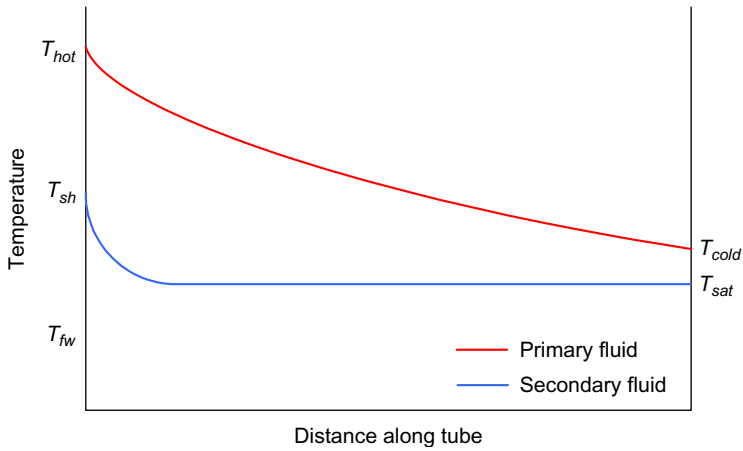

Fig. 4.13 Primary and secondary temperature profile in an OTSG.

the water evaporates and gas temperature approaches its superheated steam temperature, T_{sh}. When the primary fluid exits the OTSG, this temperature difference is similar to that observed on the cold-leg of a recirculating steam generator (EPRI, 1985).

The OTSG computational domain is from the upper tubesheet to the lower tubesheet and the tube bundle is modeled as a porous-media. Flow on the secondary side is modeled using a quasistatic continuum approach so porosity is modified to account for flow obstructions such as tubes and baffles.

Development of a code that predicts the three-dimensional thermalhydraulics for OTSG began with THEDA (EPRI, 2012b; Green and Hetsroni, 1995; EPRI, 1980). THEDA solved the two-phase flow equations using an algebraic slip model in the secondary fluid and support structures were modeled as distributed resistance (EPRI, 1980). Later, THEDA-2 was developed that allowed for helical tube bundle designs (Green and Hetsroni, 1995).

In 2012, EPRI began development of the Triton code which should be able to solve the OTSG thermalhydraulics using modern numerical methods, empirical correlations, discretization techniques, and up-to-date programming schemes (EPRI, 2012a).

Acknowledgments

The author would like to thank Dr. J.M. Pietralik for the technical discussions and his assistance in preparing this chapter, and Dr. P. Angell and Dr. S. Jaffer for their review of its contents.

References

Carver, M.B., Carlucci, L.N., Inch, W.W.R., 1981. Thermal-Hydraulics in Recirculating Steam Generators – THIRST Code User's Manual. AECL–7254, Atomic Energy of Canada Limited, Chalk River, ON. April.

Duffey, R.B., 1981. The thermal hydraulic of steam generators for PWRs. Heat Transfer and Fluid Flow in Nuclear Systems. Pergamon Press, New York, NY. pp. 463–496, Chapter 6.

EPRI, 1980. Thermalhydraulic Analysis of Once-Through Steam Generators. Report NP-1431, EPRI, Palo Alto, CA.

EPRI, 1985. Steam Generator Reference Book. EPRI, Palo Alto, CA.

EPRI, 2012a. Steam Generator Management Program: Thermal-Hydraulic Analysis of a Recirculating Steam Generator Using Commercial Computational Fluid Dynamics Software. EPRI, Palo Alto, CA. Product 1024838.

EPRI, 2012b. Nuclear Sector Roadmap. EPRI, Palo Alto, CA.

Green, S.J., Hetsroni, G., 1995. PWR steam generators. Int. J. Multiphase Flow 21 (Suppl.), 1–97.

Hirao, Y., Nakamori, N., Ukai, O., Kawanishi, K., Tsuge, A., Uneno, T., Kasakabe, T., 1991. Development of thermal-hydraulic computer code for steam generators. In: 1st JSME/ASME Joint International Conference on Nuclear Engineering, INIS, Vol. 23, No. 18.

IAEA, 1997. Assessment and Management of Ageing of Major Nuclear Power Plant Components Important to Safety: Steam Generators. IAEA TECDOC 981, IAEA, Vienna.

Kestin, J., Senger, J.V., Kamgar-Parsi, B., Leveit Sengers, J.M.H., 1984. Thermophysical properties of fluid D2O. J. Phys. Chem. Ref. Data. 13 (2), 601–609.

Klimas, S.J., Pietralik, J.M., Fruzzetti, K., Tapping, R.L., 2004. Fouling enhancement under flow boiling at elevated steam qualities. In: 2003 ECI Conference on Heat Exchanger Fouling and Cleaning: Fundamentals and Applications, Paper 36, Santa Fe, New Mexico, USA.

Kondo, Y., Hirao, Y., Suzuta, T., Ueno, T., Tomomatsu, K., 2000. Development of thermal-hydraulic code (two-fluid model) for steam generator (second report; verification results at low load conditions). In: Proceedings of 4th JSME-KSME Thermal Engineering Conference, Kobe, Hyogo, Japan, 2000 October 1–6.

Kreider, M.A., White, G.A., Varrin Jr. R.D., 1998. A Global Fouling Factor Methodology for Analyzing Steam Generator Thermal Performance, www.iaea.org/inis/collection/NCLCollectionStore/_Public/31/018/31018394.pdf.

Laroche, S.L., Sun, L., Pietralk, J.M., 2014. Numerical analysis of cavitation susceptibility for steam generator integral preheater tubes. AECL Nucl. Rev. 3 (1), 37–46.

Lee, J.Y., No, H.C., 1986. Three dimensional two-fluid code for U-tube steam generator thermal design analysis. Nucl. Technol. 75, 205–214.

Teller, A., 2010. The EPR Reactor Evolution to Gen III+ Based on Proven Technology. www.iaea.org/NIPRO/1st_Dialogue_Forum/15_Teller.pdf, Vienna, Austria, February 2.

Tincq, D., David, F., Rascule, P., 1995. THYC, A 3D Thermal-Hydraulic Code for Steam Generator, Heat Exchangers and Condensers: Recent Developments and Validation Tests. IAEA INIS Collection, IAEA, France, 1161-0611.

Turner, C.W., 2013. Fouling of nuclear steam generators: fundamental studies, operating experience and remedial measures using chemical additives. AECL Nucl. Rev. 2 (1), 61–88.

Yetisir, M., Turner, C.W., Pietralik, J., 2000. Contribution of steam generator degradation mechanisms to RIHT behaviour. AECL 12118, In: Proceedings of the 5th CNS International Conference on CANDU Maintenance, Toronto, Ontario, Canada, 2000 November 19–21.

Yetisir, M., Pietralik, J., Tapping, R.L., 2004. Steam generator analysis tools and modeling of degradation mechanisms. In: Proceedings of 12th International Conference on Nuclear Engineering, Arlington, Virginia, USA, 2004 April 25–29.

This page intentionally left blank

WWER steam generators

5

L. Papp, J. Vacek
University of West Bohemia, Pilsen, Czech Republic

5.1 Description of WWER steam generators

The WWER 440 and WWER 1000 steam generators (SGs) basically differ only in dimensions, materials of vessel and collectors, and heat exchange tube arrangement. They consist of a horizontal pressure vessel, horizontal heat exchange tube bundles, two cylindrical vertical collectors, feedwater system, and steam collector. A schematic sketch of WWER SGs is shown in Fig. 5.1A (side view) and B (top view).

The pressure vessel is a horizontal cylinder with elliptical heads made of a carbon steel 22 K (WWER 440) or a low alloy bainitic steel 10GN2MFA (WWER 1000). The WWER 440 collectors are made of austenitic stainless steel, and WWER 1000 collectors are made of low alloy bainitic steel with austenitic cladding on the primary side. Collectors are situated symmetrically to both horizontal axes of pressure vessel near to the vessel center.

Primary coolant enters the hot collector (HC) and through heat exchange tube bundles, and cold collector (CC) exits a SG.

Parameters of WWER 440 and WWER 1000 SGs are summarized in Table 5.1.

Chemical composition of used materials is given in Table 5.2.

Heat exchange tubes lie on 30 mm wide support plates (ensuring vertical distance) and wave plates which ensure horizontal distance between tubes. The horizontal distance between tube support plates is about 700–800 mm. The horizontal position of support plates with dominant vertical secondary water flow is a potential source of tubes corrosion problems. Tube support plates crevices are the places with restricted water flow, i.e., the concentration of salts is here much higher than that on the free length of tubes.

5.2 SGs degradation

The mechanisms of corrosion degradation of WWER SGs heat exchange tubes are the same or similar with vertical SGs, and they are described in many articles. Influence of bulk water chemistry on corrosion degradation was studied in depth, e.g., in Nuclear Research Institute, Rez (NRI), VÍTKOVICE plc, and another research institutes. Based on performed research results, requirements on feedwater chemistry were refined and, at present, integrity of SGs tubing is relatively trouble free. But, as will be shown later, nor the best feedwater chemistry guarantee sufficient condition for noninitiation and grows of corrosion cracks.

Erosion-corrosion damage of SGs feedwater distribution system occurred at all WWRE 440 NPPs. The feedwater tubing was originally manufactured from carbon

Steam Generators for Nuclear Power Plants. http://dx.doi.org/10.1016/B978-0-08-100894-2.00007-8
© 2017 Elsevier Ltd. All rights reserved.

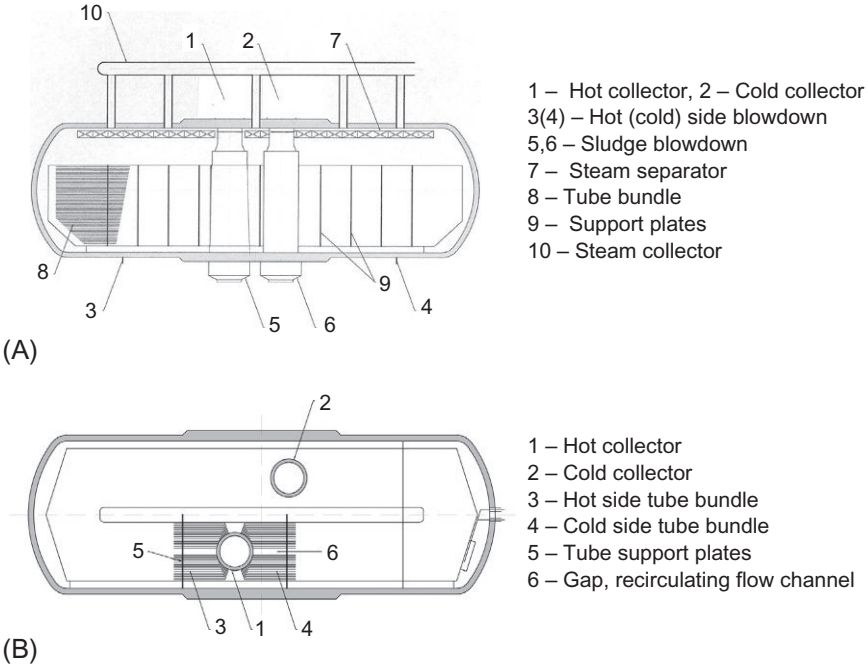

Fig. 5.1 (A) Sketch of WWER steam generators (SGs)—side view. (B) Sketch of WWER SGs—top view.

Table 5.1 Basic parameters of WWER steam generators

Parameters	SG 440	SG 1000
Thermal power (MW_t)	229	750
Steam capacity (kg s^{-1})	125	408
Steam pressure (MPa)	4.61	6.27
Steam temperature (°C)	258.9	278.5
Coolant temperature (inlet/outlet) (°C)	297/270	320/289
Coolant pressure (MPa)	12.26	15.7
Coolant flow rate (m^3 h^{-1})	7100	21,200
Feedwater temperature (°C)	164–223	164–220
Vessel internal diameter (m)	3.2	4.0
Vessel length (m)	11.6	13.4
Evaporation surface (m^2)	24	40
Vessel material	22 K	10GN2MFA
Collector material	08Ch18N10T	10GN2MFA
Heat exchange tube material	08Ch18N10T	08Ch18N10T
Tube diameter (mm)	16	16
Tube thickness (mm)	1.4	1.5
Number of tubes	5536	11,000

Table 5.1 Continued

Parameters	SG 440	SG 1000
Tubes arrangement	Corridor	Staggered
Average tube length	9.26	11.1
Heat exchange surface (m^2)	2577	6115
Weight (t)	169	328
Specific output (MW_t/t)	1.36	2.28
Number of SG/reactor	6	4

Table 5.2 Chemical composition of WWER steam generators materials

Material	C	Mn	Si	P	S	Cr	Ni	Mo	TI
08Ch18N10T	≤0.08	≤2.0	≤0.8	0.035	0.02	17–19	9–11		5xC
10GN2MFA	0.08 0.15	0.60 0.90	0.1 0.37	≤0.025	≤0.025	≤0.30	1.70 2.70	0.40 0.60	
22 K	0.19 026	0.75 1.0	0.2 0.4	0.030	0.030	≤0.3	≤0.3		

steel, and a feedwater was distributed from central pipe to center of heat exchange bundle via many rectangular turnings. The damaged feedwater systems were removed, and they were replaced using stainless steel pipes. At Loviisa and Paks (GIDROPRES solution) feedwater is distributed above tube bundles; at Dukovany, Bohunice, and Temelin submerged distribution (similar as original design) was implemented. After these modifications, the feedwater distribution system seems to be trouble free.

Corrosion cracks in collectors threaded holes (sealing of covers) occurred at many power plants. This damage requires replacement of the collector upper part which is a time-consuming operation. High level of tensile stress and splash of secondary water to holes are the basic reasons for this problem. The level of secondary water around HC is above the steam separators—Fig. 5.2A. Level at the cold side of SG is uniform and sufficiently low—Fig. 5.2B.

Difference in levels is given by different average void fraction in tube bundles. The average void fraction around HC is approximately 0.2 and around cold one is lower than 0.07 (Papp, 1996).

Difference between steam-water mixture levels near hot and CCs results from uneven steam performance along the heat exchange tubes—heat flux exponentially decrease with distance from HC.

The problem of level measurement can be explained using simplified model of SG shown in Fig. 5.3.

Static equilibrium of two-phase mixture in SG sections i,j is given by

$$H_i \cdot \overline{\rho_i} \cdot g = H_j \cdot \overline{\rho_j} \cdot g \tag{5.1}$$

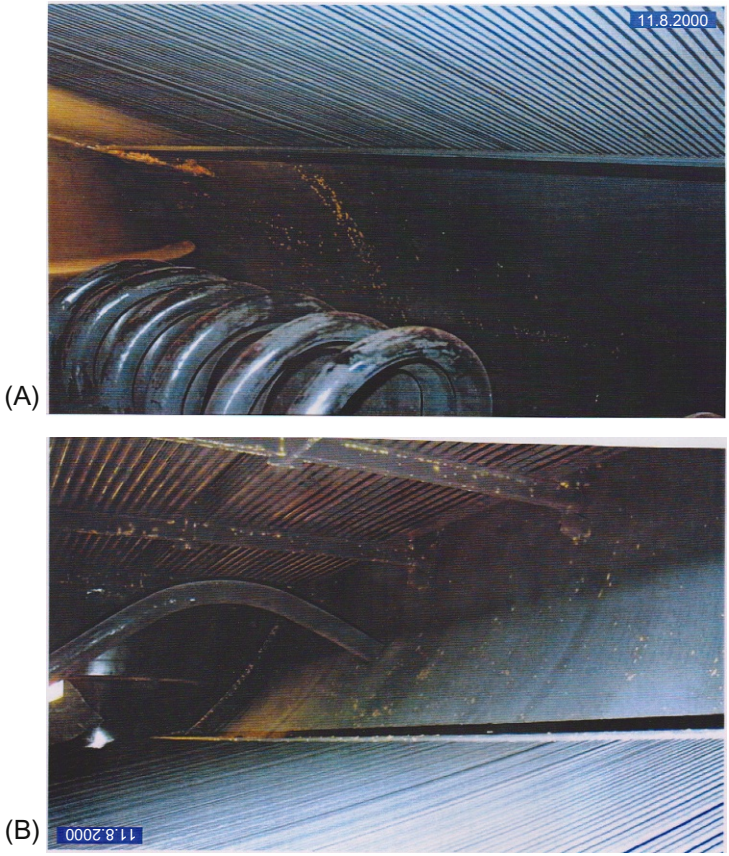

Fig. 5.2 (A) Trace of level, hot collector (HC), (B) trace of level, cold collector (CC).

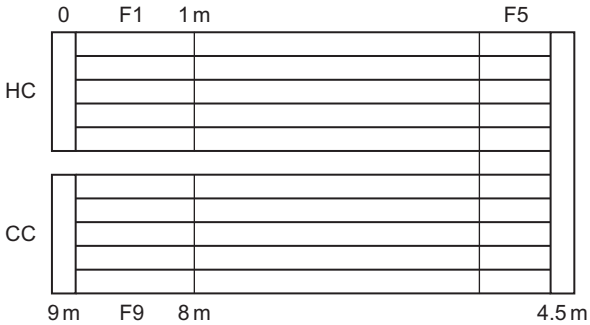

Fig. 5.3 Simplified model of SG.

and

$$\overline{\rho}_{i,j} = \overline{\alpha_{i,j}} \cdot \rho'' + \left(1 - \overline{\alpha_{i,j}}\right) \cdot \rho' \tag{5.2}$$

where ρ' and ρ'' are the density of water and density of steam and $\overline{\alpha_{i,j}}$ is the average void fraction in sections i and j.

Void fraction can be calculated from equation (Trunov et al., 2001; Kozlov, 1974)

$$\alpha_{out,i,j} = \frac{w''_{i,j}}{w''_{i,j} + a} \tag{5.3}$$

where $a = 0.65 - 0.0398p$ (MPa) and w'' is a reduced steam velocity above tube bundle

$$w''_{i,j} = \frac{Pv_{i,j}}{\rho'' \cdot F_{i,j}} \tag{5.4}$$

where $Pv_{i,j}\left(\mathrm{kg\,s^{-1}}\right)$ is the steam performance of section i,j and $F_{i,j}$ ($\mathrm{m^2}$) is the surface of section.

For average value of void fraction we assume linear function, i.e., $\overline{\alpha} = \alpha_{out}/2$.

For WWER SG 440 at operational condition is $p = 4.62$MPa, $\rho'' = 785\,\mathrm{kg\,m^{-3}}$, $\rho' = 23.28\,\mathrm{kg\,m^{-3}}$, $F_i = 1.7\,\mathrm{m^2}$, and $a = 0.467$. The steam performance of sections F1–F9 and adequate values for level height calculation are shown in Table 5.3.

The height of upper row of tube exchange tubes from bottom of SG is approximately 2.45 m.

With requirement that the level above tube bundle has to be higher as 0.1 m, the H_9 must be 2.55 m. From Eq. (5.1) H_1 will be

$$H_1 = \frac{2.55 \cdot 734}{625.8} = 3.0\mathrm{m} \tag{5.5}$$

This is only 0.2 m under top of SG, i.e., the two-phase mixture can reach the moisture separators (it is interesting that the result of very simplified calculation is in a good agreement with observed values).

The height of only water column H_w level will be

$$H_w = \frac{2.55 \cdot 734}{785} = 2.4\mathrm{m} \tag{5.6}$$

This level measurement is used at operated SG, too.

Table 5.3 Steam performance and calculated steam-water mixture level height

	F1	F2	F3	F4	F5	F6	F7	F8	F9
Pv ($\mathrm{kg\,s^{-1}}$)	13.3	11	9	7.5	6.2	5.1	4.2	3.4	2.9
w″ ($\mathrm{m\,s^{-1}}$)	0.336	0.278	0.227	0.19	0.157	0.129	0.106	0.086	0.073
$\overline{\alpha}(-)$	0.209	0.187	0.163	0.144	0.126	0.108	0.093	0.078	0.067
$\overline{\rho}$ ($\mathrm{kg\,m^{-3}}$)	625.8	624.6	660.8	675.3	689	702.7	714.2	725.6	734

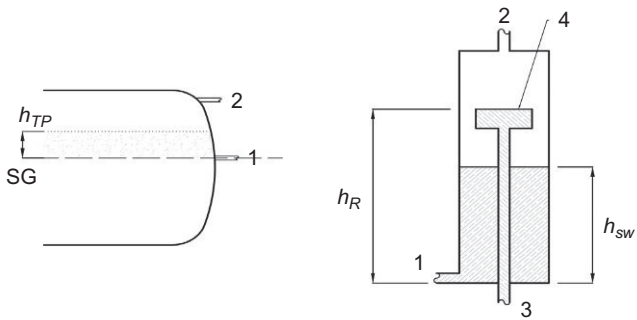

Fig. 5.4 Sketch of SG level measurement.

The schematic sketch of device for level measurement is shown in Fig. 5.4

Steam condensation in the measure vessel ensures the constant level h_R (4) in reference tube, and h_{SW} is

$$h_{SW} = \frac{h_R \cdot \rho' \cdot g - \Delta p_{1,3}}{\rho' \cdot g} \tag{5.7}$$

According to Eq. (5.1) the height h_{TP} of two-phase level above point 1 is

$$h_{TP} = h_{SW} \cdot \frac{\rho'}{\rho_{out}} \tag{5.8}$$

where ρ_{out} is calculated using Eqs. (5.2)–(5.4).

The additional device is installed in SG for direct measurement of level in given points with binary output—level is higher/lower. This method enables to adjust the level measurement at different operation regimes of SG.

To prevent the problem with steam-water level, the following measures were applied:

- change of screw lubricant
- change of sealing from nickel to graphite sealing which requires lower level of prestress
- installation of perforated plate around a HC for equalization of secondary water level
- elimination of the notch in the end of threaded hole (Fig. 5.5)

The replacement of upper part of SG collector was earlier performed manually with relatively high radiation load for personnel. At present, automatic welding device is qualified for this repair.

All problems mentioned above concerning especially WWER 440 SGs are basically repairable. Stress corrosion cracking of the WWER 1000 collectors is fatal and difficultly repairable.

The first damage of WWER 1000 SG collector was detected at South Ukraine NPP Unit 1 in 1986 about after 12,000 hours of operation (Trunov et al., 2001). Till

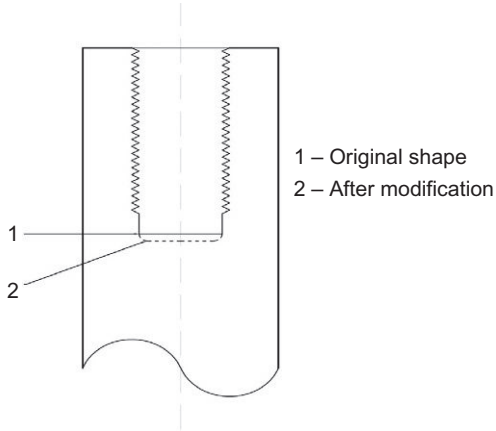

Fig. 5.5 Modification of threaded holes bottom.

1993, 33 SGs at WWER 1000 plants were replaced (Trunov et al., 2001). Only CCs were damaged.

The metallographic examination of cracks showed that cracks started at the crevice between the collector holes and nonexpanded tube and the cracks grew through ligaments, to adjoining hole.

Mechanism and causation of collector damage are described in detail in Trunov et al. (2001) and Berezanin (2001). Results of performed investigations and analysis of damage reasons can be summarized as follows:

- high residual stresses in collector holes after explosive expansion of tubes
- unprojected secondary water chemistry, especially low pH (quite often lower than 5)
- 10GN2MFA steel casting in air; high content of sulfur and phosphorus in collector materiál

After above mentioned accidents, these factors were eliminated during manufacturing of SGs (vacuum casting, hydraulic expansion of tubes in collectors, additional mechanical drilling of collector-tube crevices) and firm measures were taken for secondary water chemistry. After 10 years of operation (NPP Temelin) no collector crack indication was found.

Potential source of WWER 440SGs defects is the dissimilar weld between SG shell (22 K steel) and stainless steel collector (08CH18N10T)—Fig. 5.6.

The narrow pocket between the shell and collector is practically flow free (steady secondary water), and in this pocket sludge is concentrated. To minimize this problem, the sophisticated blowdown strategy is very important.

5.3 WWER SGs modifications

Modifications of SGs were started after damage of WWER 440 SGs collectors upper part and especially after damage of WWER 1000 collectors.

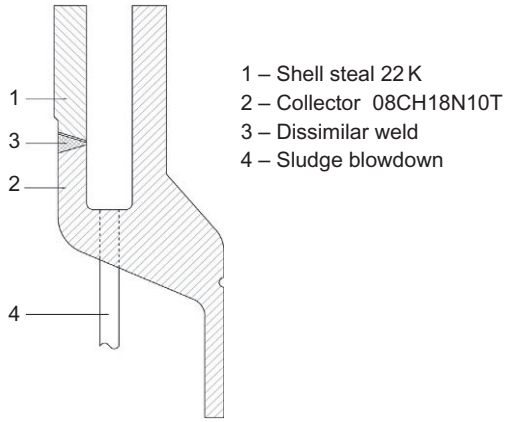

Fig. 5.6 (A) Dissimilar shell, (B) collector weld.

Removed WWER 1000 SGs were cut, and extreme impurities concentration around collectors were confirmed—dry crystalline salt deposits were found between heat exchange tubes of hot leg tube bundle (Trunov et al., 2001). The reason why only CCs were damaged was explained, too. Due to intensive heat flux near tube—HC crevices (250 kW m^{-2}), these crevices are plugged by salt, i.e., corrosion medium free. Heat flux in CC area is approximately 45 kW m^{-2}.

Calculations and sampling of secondary water on operated WWER 1000 power plants (Trunov et al., 2001) have shown that the highest concentration of impurities is around HC and is approximately three times higher than the concentration in blowdown. This value is questionable—it depends on time of sampling from time of sludge blowdown, on height of sampling point, etc. In places with dry deposits, the concentration was not measured.

The problem of impurities distribution in WWER SGs is specific problem of horizontal SGs and can be explained using Fig. 5.7A and B. In these figures are shown the extreme variants of WWER SGs blowdown strategy.

The concentration of impurities in blowdown in case of Fig. 5.7A is given by equation

$$C_b = C_F . M_F / M_b$$

(the salt content in steam is neglected)

where

- C_b is the concentration of impurities in blowdown
- C_F is the concentration of impurities in feedwater
- M_b is the blowdown flow rate (kg s^{-1})
- M_F is the feedwater flow rate (kg s^{-1})

For usual value of $M_F/M_b = 0.5\%$, the concentration of impurities in blowdown will be

$$C_b = 200.C_F$$

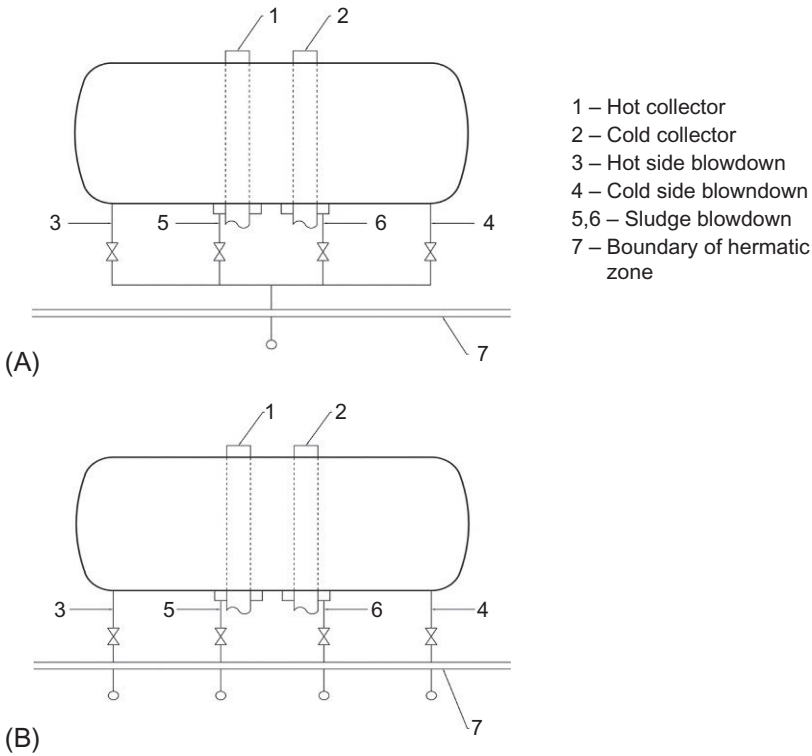

Fig. 5.7 (A) United blowdown, (B) separated blowdown.

and it is independent of feedwater distribution and distribution of blowdown between individual blowdown lines, i.e., we have no information about distribution of impurities in secondary water.

Blowdown according to Fig. 5.5B with measured individual flow rates and concentrations gives relatively full information about impurities distribution in SG and enables optimization of secondary water chemistry by management of flow rate from individual blowdown lines.

In original WWER 1000 SGs 10/16 of feedwater volume is distributed to the cold head side and 6/10 to the hot side, both in hot legs axis (Trunov et al., 2001). Within reconstruction, 5 feedwater distribution tubes from cold side were removed and 4 distribution tubes were added to hot head of SG. In this way, hot side of SG is overfeeded and "salt corner" was created near cold head of SG. The blowdown lines 3, 5, 6, and 4 were joined, and new blowdown line from the middle of cold head was installed (Trunov et al., 2001; Berezanin, 2001).

After this modifications, the impurities concentration in HC surrounding dropped by an order, and the maximal concentration (200. C_F) is located in salt corner, i.e., in blowdown.

The feedwater distribution system at Dukovany NPP SGs was basically not changed. About 35% of feedwater volume is distributed into the SGs hot side and about 65% into cold side of SGs. The vertical distribution pipes are submerged in the gap between hot legs and at about in the middle of vertical axis of SG the feedwater is horizontally directed to hot side of SG. This distribution creates salt corner near hot head of SG (Papp, 1995).

The influence of blowdown arrangement on impurities distribution in SG was tested at Dukovany NPP. Result of this test is shown in Fig. 5.8 (CB—cold side blowdown).

Where sampling points (all in collectors axes) are as follows:

1. blowdown
2. HC, cold side
3. CC, hot side
4. between CC and cold side

It is evident that due to assymetric feedwater distribution, salt corner near HC was created, and after closing of blowdown line from the cold side of SG, concentration of impurities around HC decreased 2.5 times.

Temelin WWER 1000 NPP SGs feedwater distribution system is almost the same as in Dukovany SGs with one difference. Vertical submerged feedwater distribution pipes are uniformly perforated, and feedwater is injected into gaps between hot leg bundles. The purpose of this distribution system is to enhance circulation on the secondary side of SGs by condensation of steam in gaps (recirculation channels).

Cold feedwater flow down can cause additional thermal stress in the collector wall, and therefore, the absorbing capacity of heat exchange tubes bundle was calculated. The method of calculation is described in Papp (1997), and there is shown that in case of 250 kW m^{-2} heat flux, above 0.5 m of the tube bundle height, the two-phase flow rate

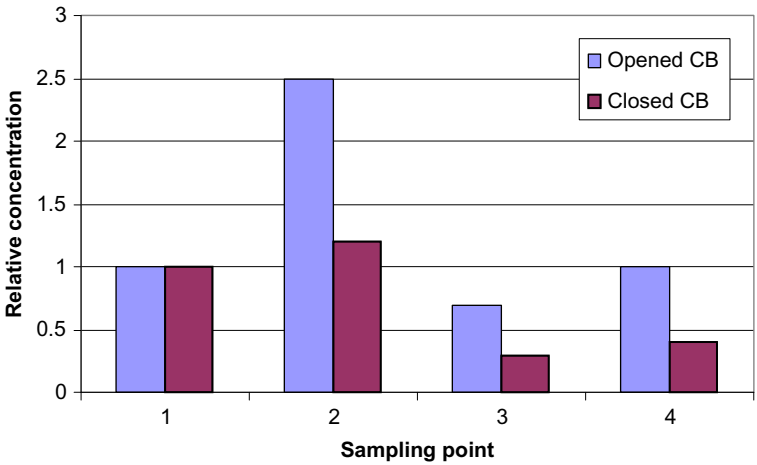

Fig. 5.8 Impurities distribution versus blowdown arrangement in WWER 440 SG.

in bundle decreases and steam-water mixture is pushed from bundle to circulation channels. This process results from the feature of two-phase flow pressure drop. With increasing void fraction and constant mass flow rate, the pressure drop increases. Therefore, only about 60% of feedwater is distributed by submerged pipes, and 40% is distributed above the submerged perforated plate situated under secondary water level.

5.4 Integrity of heat exchange tubes

Integrity of WWER SGs heat exchange tubes is up to now trouble free. The summary of ECT inspection results at Dukovany NPP for time period 1985–2000 is reported in Berezanin (2001). The maximum number of plugged tubes on 1 SG after 13 years of operation was 43, i.e., 0.78% of total number of SG tubes. At 168 operated SGs up to 1999 0.65% of tubes were plugged (Trunov et al., 2001).

Especially for WWER 440 NPP with 15% projected reserve of heat exchange tubes, these values are negligible.

Nevertheless, each leakage of primary water generates significant economic loss for NPP. To reduce this loss, the following issues have to be studied:

- accuracy of corrosion cracks detection
- burst pressure for tubes rupture
- probability of cracks detection
- crack growth rate

The eddy current method (ECT) is the basic method for heat exchange tubes testing. Tests of accuracy with laboratory prepared cracks, using bobbin coil and x-probe coils, were performed in 1996, and comparison of results is shown in Fig. 5.9.

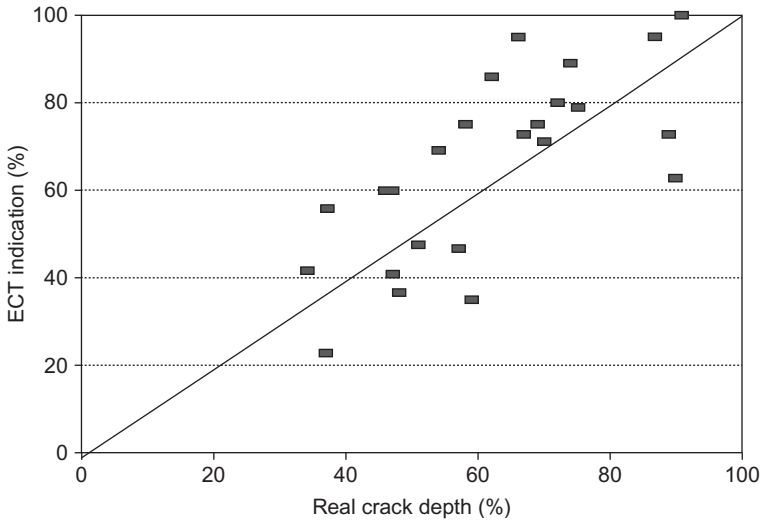

Fig. 5.9 WWER SG tubes ECT indication vs. real crack depth.

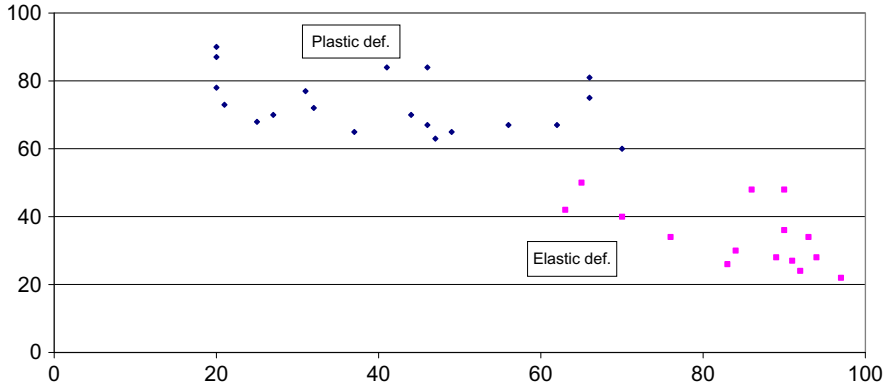

Fig. 5.10 WWER 440 tubes burst tests results.

The inaccuracy of detection for cracks depth lower than 60% of tube wall is about 15%. Due to improvement of technology, accuracy of ECT results will be now probably better.

Results of burst tests are shown in Fig. 5.10.

The burst pressure is for all tested tubes higher than 20 MPa, i.e., three times higher than operation conditions of WWER SGs. Important finding resulting from burst tests is the fact that rupture of tubes with ECT indication lower than 70% evokes plastic deformation of tube wall, i.e., huge leakage, and rupture of cracks with ECT indication higher than 70% results in elastic deformation in tube wall, i.e., in low leakage of primary water. The postburst test photos are shown in Fig. 5.11.

This finding was confirmed within leakage tests performed on 20 tubes with throw-wall cracks. Tests were performed on operational parameters (16 MPa, 320°C), and the leakage flow rate was lower than 12 L/hour.

Burst tests are the basis for heat exchange tubes plugging criteria determination. For this purpose, the lower limit curves have to be constructed (Little and Jebe, 1975).

In Fig. 5.12, the lower limit curve LLC P/X% represents that at probability level P/X% of next burst pressures will be above appropriate line.

For the determination of plugging criteria, the required pressure condition and probability level has to be done. For example, if we use the pressure $dp = p_p$ (loss of secondary pressure) and the crack growth rate 0.6%/month for the 48-month inspection period the plugging criteria will be:

I. for LLC 0.9/90% $100 - 48*0.6 - 15 = 56.2\%$
(100 is the intersection of LLC and $dp = p_p$ lines, 15 is the inaccuracy of ECT)
LLC 0.97/96% $79 - 48*0.6 - 15 = 35.2\%$

For $dp = p_p - p_s$ it will be:

II. for LLC 0.9/90% $120 - 48*0.6 - 15 = 76.2.2\%$
LLC 0.97/96% $89 - 48*0.6 - 15 = 45.2\%$

The difference of plugging criteria—35%/76%—is significant, and the choice is a matter for NPP and regulatory body.

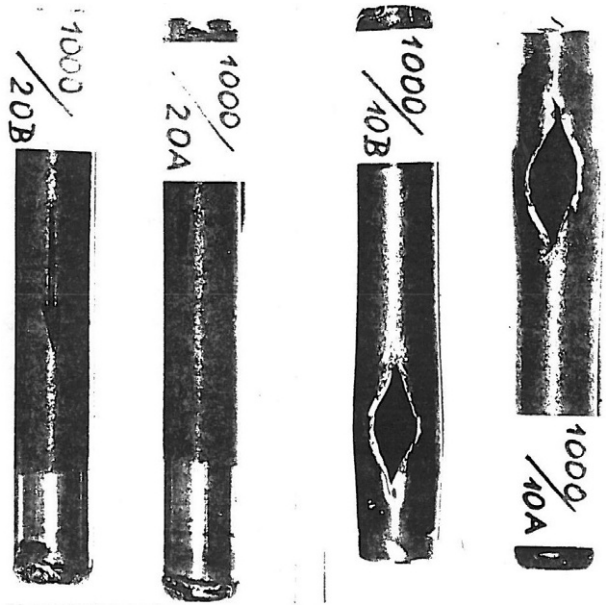

Fig. 5.11 Elastic (20A, 20B) and plastic (10A, 10B) deformation after burst tests.

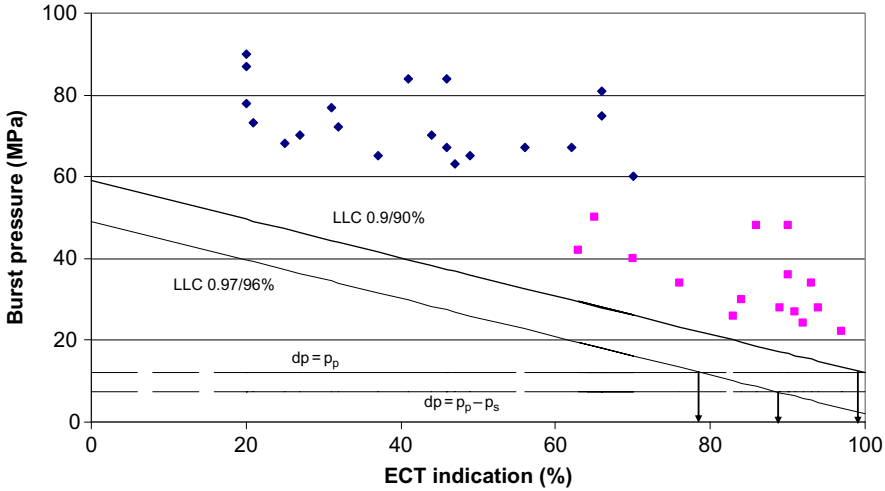

Fig. 5.12 Burst tests lower limit curves.

Especially for estimation of corrosion cracks growth rate, the probability of crack detection (POD curve) is important. For this examination were used 67 WWER 440 heat exchange tubes with ECT indication 10%–30% of tube wall degradation supplemented with 31 tubes without ECT indications (necessary for credibility of tests). Three teams took place in this test.

We will assume that analytical form of POD curve can be expressed as a linear logistic function of crack depth, i.e.,

$$p(x) = 1/\left(1 + e^{a+b.x}\right)$$

where p is the probability of detection, x is the relative crack depth [%], and a and b are the sought parameters. These parameters can be determined using maximum likelihood method (data are not normally distributed and mean square method is not applicable). The typical POD curve is shown in Fig. 5.13 ($a = 3.585$, $b = -0.1515$).

It is evident that the declared sensitivity of ECT method (20%) is very optimistic.

The corrosion crack growth rate was studied with 46 repeatedly tested tubes at Dukovany NPP. Due to cracks POD, tubes with ECT indication lower than 20% were excluded from evaluation. The correlation—crack growth rate/time is shown in Fig. 5.14.

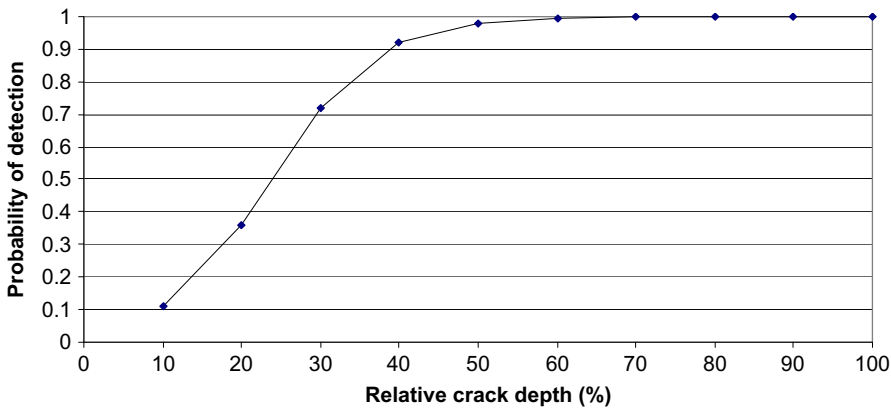

Fig. 5.13 Typical POD curve for WWER SG tubes.

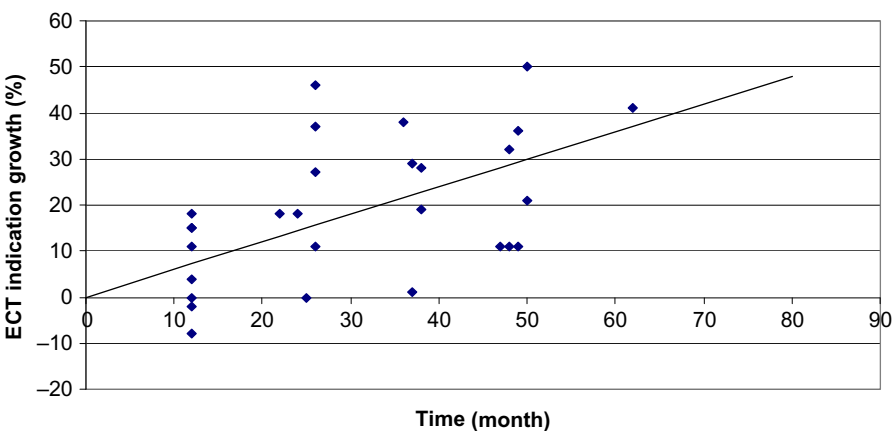

Fig. 5.14 Crack growth vs. time.

The estimated crack growth rate is approximately 0.6%/month, i.e., 28.8% for test period (4 years). Correlation is very weak and more tests would be necessary.

Nevertheless, from economic reasons and low number of plugged heat exchange tubes, all tubes with any ECT indication are usually plugged and, therefore, the study of crack growth rate is impossible.

Damages of SGs tubes can be divided into two basic groups on the basis of dominant mechanism of damage (Trunov et al., 2001):

1. Tubes, where the processes during SG manufacturing are the dominant cause of damage. Local contamination during manufacturing and tensile stresses arose from assembly are the typical examples of these causes. These damages appear in the relative short time, and their occurrence decreases with time.
2. Tubes, where the corrosion environment is the dominant cause of damage. Number of the damages increase with time.

Statistical evaluation of data enables to differentiate mechanisms of SG tubes damages occurred during SGs operation. The most frequently used distribution for description of time-dependence of corrosion failures is the Weibull distribution (Steahle, 2001). The probability density function $f(t)$ is given in Eq. (5.9)

$$f(t) = \left(\frac{\beta}{\theta^{\beta}}\right) t^{\beta-1} \exp\left[-\left(\frac{t}{\theta}\right)^{\beta}\right] \tag{5.9}$$

where

t = time

θ = scale parameter of the Weibull distribution

β = shape parameter

The cumulative distribution function $P(t)$ is given in Eq. (5.10):

$$P(t) = 1 - \exp\left[-\left(\frac{t}{\theta}\right)^{\beta}\right] \tag{5.10}$$

and the hazard function $h(t)$ which determines the probability that failure will occur in the next increment of time, dt, is given in

$$h(t) = \frac{\beta}{\theta^{\beta}} t^{\beta-1} \tag{5.11}$$

The value of the shape parameter β is the most important for the decision about the feature of tubes damage. According to Eq. (5.11), if:

$\beta < 1$, probability of new damages decreases with time

$\beta = 1$, probability of damage is independent of time

$\beta > 1$, probability of damage increases with time

For the available data sorting into the two groups mentioned above the following process was used:

- All available data were analyzed and a first Weibull function was fitted.
- If the value of the shape parameter β was near 1, the earliest data were excluded from the database data till the value of β significantly increased. The excluded data form the first group of tube damage.
- The remained data create the second group of tube damage.

Using this method the data of SGs 14 and 24 were analyzed.

Typical example of SG with sufficient amount of late damages and with negligible "earliest" damages is the SG 14. The graph of cumulative probability of damage is shown in Fig. 5.15.

We can see (Fig. 5.15) that the probable lifetime of this SG is approximately 55 years (the projected reserve of heat-exchange surface is 15%, i.e., $P(t) = 0.15$), the value of β is 2.83, and therefore, the dominant cause of damages is the environment.

The SG 24 is the examples of SG where the processes during manufacture have a dominant influence at tubes damage. The hazard function $h(t)$ with all available data taken into account is shown in Fig. 5.16.

As we can see in Fig. 5.16, the hazard function decreases with time ($\beta = 0.512$) in this case, i.e., in the data prevail damages caused by manufacture processes.

The earliest tube damages occurred mostly under tube support system in the first 8 years of SGs operation. This phenomenon can result from water chemistry in the crevices among the tube supports and tubes which depend on heat flux. The distribution of tubes defects under tube support plates (numbered from HC) is shown in Fig. 5.17.

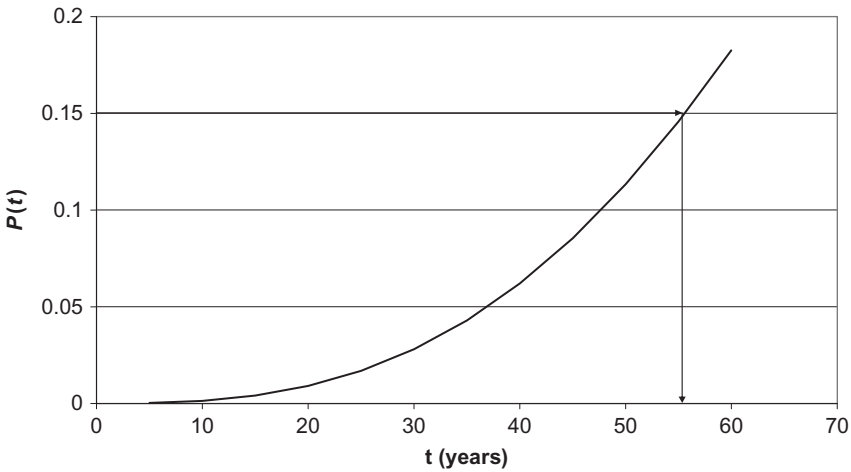

Fig. 5.15 Cumulative probability of SG14 tubes damage.

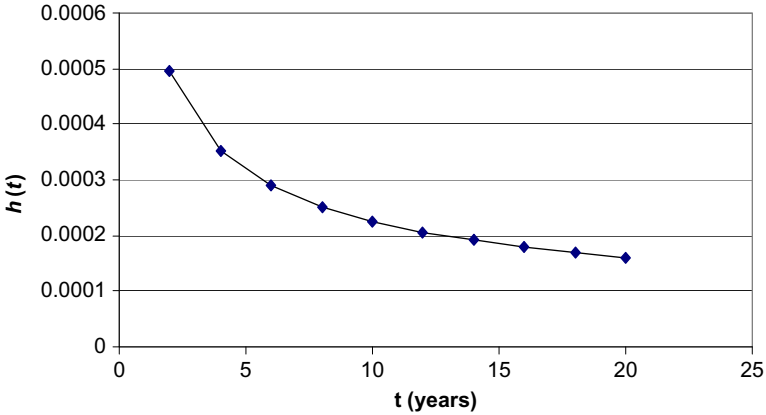

Fig. 5.16 SG24 hazard function.

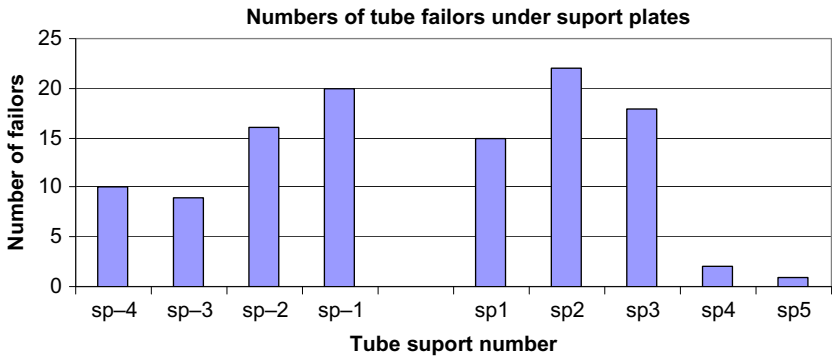

Fig. 5.17 Distribution of tube defects under support plates.

As the heat flux decreases with distance from HC, the number of tubes defects decreases, too.

5.4.1 Conclusions

The basic measures described in Section 5.1.2 essential for SG lifetime, related to material and design of WWER SGs, were described. Operational experiences from WWER NPPs confirmed that performed measures are satisfactory.

As was shown in Section 5.1.3, the SGs lifetime of operated SGs is determined only by feedwater-blowdown systems management.

Problems of eddy current tests (ECT) of heat exchange tubes are described in Section 5.1.4. It is evident that due to ECT inaccuracy and probability of crack detection, leakage-free operation of SGs cannot be guaranteed.

Up to now published data concerning to WWER SGs tubes plugging show that heat exchange tubes are trouble free, and they will not be the limiting factor for WWER SGs lifetime.

References

Berezanin, A.A., 2001. Opyt ekspluatacii i provedenija komplexa rabot po povyseniju resursa teploobmennych trubok na parogeneratorach Kalininskoj AES, Celostnost trubok parogeneratorov. ENIC VNIIAES, Moskva.

Kozlov, J.V., 1974. Rezultaty issledovanija I puti usovershenstvovanija separacii para v parogeneratorach i barabanach- separatorach AES. Trudy VTI, ENERGIA, Moskva.

Little, R.E., Jebe, E.H., 1975. Statistical Design of Fatigue Experiments. J. Wiley and Sons, New York.

Papp, L., 1995. Influence of feedwater and blowdown systems on the mineral distribution in WWER steam generator. In: Proceedings of the Third International Seminar of Horizontal Steam Generators, Lappeenranta, Finland.

Papp, L., 1996. Influence of heat transfer and feedwater distribution on corrosion damage of SG tubes. In: Proceedings of IAEA Specialist Meeting, Ostrava.

Papp, I., 1997. Feedwater Flow-in to Steam Generator Tube Bundle. In: Proceedings of the Fourth International Seminar on Horizontal Steam Generators, Lappeenranta, Finland.

Steahle, R.W., 2001. Bases for predicting the earliest penetrations due to SCC for alloy 600 on the secondary side of PWR steam generators. ANL, Washington, DC.

Trunov, N.B., et al., 2001. Gidrodinamiceskie I teplochemiceskie processy v parogeneratorach AES s VVER. Energoatomiydat, Moskva.

Part Two

Operation and maintenance

This page intentionally left blank

Steam-water cycle chemistry relevant to nuclear steam generators

6

A. Drexler
AREVA GmbH, Erlangen, Germany

6.1 Introduction

6.1.1 Objective of steam-water cycle water chemistry

Water and steam serve in the steam-water cycle as the energy transport and work medium. Under prevailing work conditions these fluids should have no negative influence on the construction materials and no consequences for the normal plant operation. In a more detailed form, the following criteria shall be met:

- The metal release rates of the structural materials shall be at minimum
- The probability of selective forms of corrosion shall be at minimum
- The deposition of corrosion products on heat transfer surfaces shall be minimized
- The formation of aggressive media shall be avoided

All these criteria are especially valid for the steam generators (SGs) as they are key components of pressurized (heavy) water reactors from the viewpoint of chemistry. Besides their major function of providing steam for the turbine (and the subsequent generator), the most important function of SGs from a safety point of view is being the barrier between the radioactive primary side and the nonradioactive secondary side. Any degradation mechanism, which impairs this barrier function, is a significant safety concern.

In order to fulfill the above requirements the water chemistry treatment of the various system of the steam-water cycle is specified. Water chemistry guidelines define a set of parameters with normal operating values, target values, or limit values which are linked to actions or countermeasure in case of deviations (Electric Power Research Institute, 2004; VGB PowerTech, 2006). The defined guideline values have to be monitored frequently by plant chemistry personnel.

6.1.2 Root causes for SG degradation

The main reason for SG tube failure is known to be the formation of deposits and accumulation of corrosive impurities (e.g., chloride, sulfate) contributing to formation of locally aggressive conditions in combination with the SG tubing alloy.

Corrosion products, i.e., mainly iron compounds, are transported toward the SG and can form deposits especially in flow-restricted areas on the tubesheet. Those

Steam Generators for Nuclear Power Plants. http://dx.doi.org/10.1016/B978-0-08-100894-2.00008-X
© 2017 Elsevier Ltd. All rights reserved.

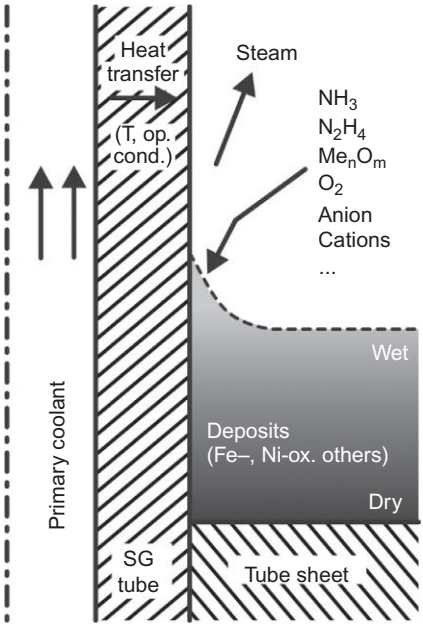

Fig. 6.1 Accumulation of deposits (Stellwag et al., 1993).

deposits in contact with the tube heat transfer surfaces will cause a local overheating and a dryout of the corrosion products. The surrounding water will keep the outer surface of the deposits wet. This water will evaporate as it penetrating the deposit, creating a dry-to-wet interface where a permanent boiling will take place (Fig. 6.1). This is commonly referred to as a nucleate boiling site.

This boiling will cause nonvolatile impurities to concentrate at the dry-to-wet interface up to very high local concentrations (Hide-out effect) in crevices or on top of tubesheet. Enrichment factors may achieve values in the range of 10^4–10^6 times the bulk concentration. In case of enrichment of ionic species the local pH value can be shifted into critical region from a corrosion point of view. The development of the local pH value with increasing enrichment factor depends on the nature of the impurities (e.g., sulfate shifts the pH into acidic regions). Under those conditions even tube material which is stable under normal operating conditions (e.g., Inconel 690 or Incoloy 800) can be put at risk from damage mechanisms such as corrosion or pit initiation.

In combination with hardening species, e.g., silicate, calcium, or aluminum, the situation becomes even worse as the formed hard deposits are in general nonremovable. In case of ionic impurity ingress (by a condenser leakage for instance) these hard deposits can promote the above described pH shift. They can also cause a damage mechanism called denting.[1]

[1] Denting of steam generator tubing refers to the reduction in tube diameter due to forces exerted by corrosion products on the outer diameter surface. This deformation increases the risk of stress corrosion cracking (SCC) due to the high stresses and cold work imparted to the tube.

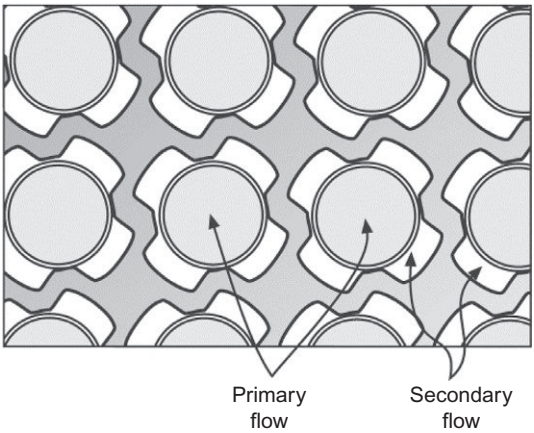

Fig. 6.2 Quatrefoil tube support structure (Staehle and Gorman, 2001).

Furthermore, deposits on the secondary side of SG tubes reduce the primary to secondary side heat transfer performance, called SG fouling. In pressurized heavy water reactors (PHWR) of the CANDU type also deposits on the primary side of the SG tubes are known, due to the material concept of the primary side.

Besides the reduction of the heat transfer efficiency the blockage of the tube support plate broached holes (Fig. 6.2) by corrosion products might became an issue (so-called SG clogging). It was observed by visual inspections that the gaps between the tube and tube support structure at the lower part of the broached holes are getting blocked (Fig. 6.3). SG clogging can interfere significant the flow distribution inside the SG causing for instance water level oscillations and vibrations of SG internals.

The origin of SGs deposits is not the SGs themselves but rather the whole steam-water cycle. Corrosion products generated by flow-accelerated corrosion in the moisture separator area for instance are transported toward the SG which acts as sink of all nonvolatile species[2]. In other words, high corrosion rates result in a high corrosion product inventory in the SGs. Chloride and sulfate can cause pitting and stress corrosion cracking (SCC) due to pH(T) shift in crevices and deposits. These degradation phenomena are enhanced by oxidizing conditions. Low transport of impurities into the SGs and reducing conditions consequently improves the safety margin to corrosion and other damage mechanisms in the SGs.

By minimizing the corrosion product load of SGs all degradation problems can be managed to the lowest risks for damage or performance issues, i.e., not only the corrosion but also the thermal efficiency and the thermo-hydraulic issues. This can be reached by minimization of generation and transport of corrosion products

[2] To counteract this phenomenon all steam generators are equipped with blow-down systems, which remove a defined fraction of steam generator water and is intended to maintain the impurity concentration below a certain level.

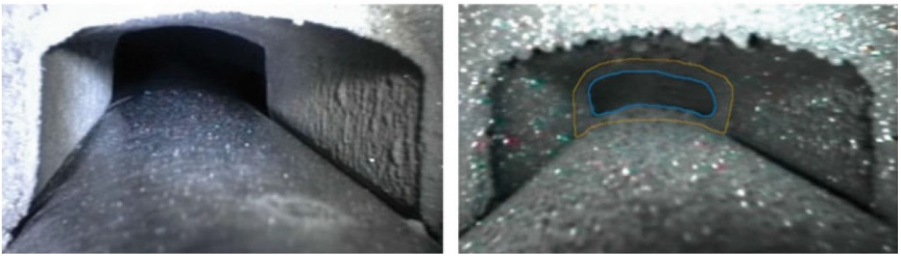

Fig. 6.3 Pictures of a clean (left) and a clogged (right) quatrefoil hole obtained by endoscopic inspection of upper tube support plates. On the right picture, the outer orange outline indicates the junction between the deposit and the quatrefoil hole edges. The inner blue outline delimits the surface area through which the secondary mixture flows. These pictures are taken from the top, and it can be observed that the deposit is located at the bottom of the hole. This is almost always the case for 51B type steam generators (SGs) (Girard, 2014).

(preventive) and/or by improvement of the removal of corrosion products from the SGs (curative).

This target can be summarized by "Keep the SG as clean as possible."

6.1.3 Corrosion product control by optimized pH

By operating the plant with adequate water chemistry the metal release of structural materials and the transport of corrosion products into the SG can be minimized. As carried out, deposits can support or even cause severe damages of SGs (e.g., denting, SCC, primary-to-secondary leakages). The fundamental water chemistry parameters which influence the corrosion rate (besides the present materials and the plant design) are pH-value and oxygen concentration throughout the steam-water cycle.

Structural components of the steam-water cycles are usually made of carbon steel. Additionally copper or copper alloys (e.g., for heat exchangers tubes or bearings), stainless steel, or titanium (e.g., for condenser tubes) can be present. The general corrosion rate of carbon steel, copper, and copper alloys depends strongly on the pH-value and the presence of oxygen.

The optimum pH value to protect carbon steel was derived by Goodstine and Kurpen (1973) to be approximately 12 at ambient temperature (Fig. 6.4). This value cannot be achieved by week amines, like ammonia or ethanolamine.

Copper and its alloys have their corrosion minimum at pH(25°C) of 8.8, but copper corrosion can significantly increase with increasing pH values if oxygen is present. Therefore all-ferrous plants can be operated at higher pH values than those with copper alloys. Copper-alloy plants are usually operated at a pH(25°C) in feed water of 9.2 as a compromise. The pH(25°C) in feed water has traditionally been used as a reference to assess the degree of alkalinity in the steam-water cycle. But the pH of interest is the pH at the real operating temperature at each location within the cycle.

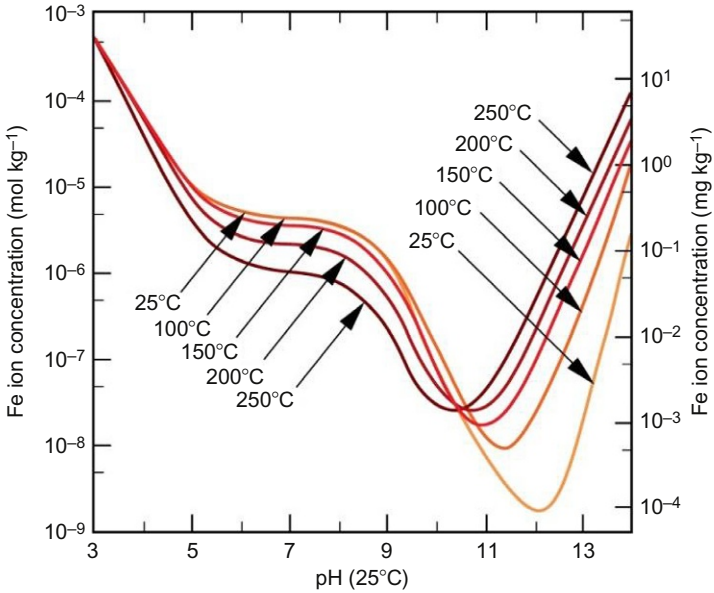

Fig. 6.4 Fe ion corrosion as rate for the corrosion of carbon steel as a function of pH(*T*) (Roumiguiere et al., 2012a).

At higher temperatures the necessary pH value (measured at 25°C) required for minimization of corrosion is around 10 at 250°C. Fig. 6.4 shows the iron ion concentration as rate for the carbon steel corrosion, i.e., low iron concentration represents low carbon steel corrosion.

Besides general corrosion also the degradation mechanism of flow-accelerated corrosion (or erosion-corrosion) affect carbon steel and contributes to the corrosion product transport into the steam generator. Flow-accelerated corrosion had major plant operational concerns in the past, e.g., incidents at NPP Surry Unit 2 (1986), Millstone (1990), or Mihama Unit 3 (2004). The mechanism and the importance of FAC are widely known within the plant operator community. The rate of FAC is determined by:

- Component material (especially chromium content)
- Thermodynamic criteria (flow velocity, media temperature, laminar, or turbulence flow)
- Design criteria (geometry which can cause turbulences)
- Chemistry criteria (pH value, oxygen concentration)
- Moisture content (two-phase FAC)

The easiest factor of the above list to be influenced is the pH value which is additionally very effective for suppression of FAC. It was shown that by increasing the pH-value in the water film on the surface, i.e., where flow-accelerated corrosion acts, from 9.5 to 9.6 the wall thinning rate was reduced by one order of magnitude (Fig. 6.5).

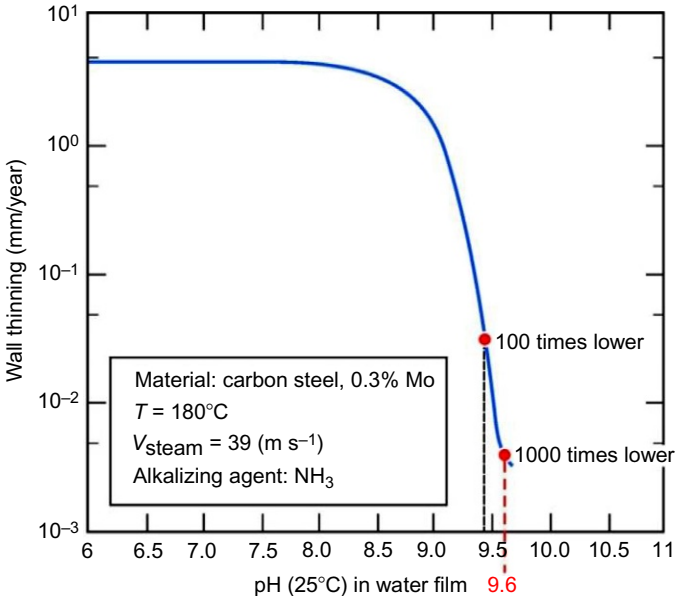

Fig. 6.5 FAC rate at 180°C vs. pH(25°C) at the water film in contact with the metal (Alkalizing agent: Ammonia) (Roumiguiere et al., 2012a).

The target of any conditioning agent of the water chemistry in steam-water cycle of nuclear power plants is to minimize both types of corrosion, i.e., general and flow-accelerated corrosion. This goal yields two simple questions:

- What kind of alkalizing agent should be dosed?
- Which amount alkalizing agent is required?

The alkalinization of the media of steam-water cycle is performed by dosing at minimum one amine (including ammonia) or by injection of an amine combination. For selection of optimum alkalizing amine(s) maintaining the pH(T) in the whole steam-water cycle two properties of the amines have to be considered:

- dissociation constants of used amine (basicity)
- distribution coefficients of used amine (volatility)

The dissociation constant and the distribution coefficient of the most applied amines are given in Figs. 6.6 and 6.7.

On the one hand amines having a relative high basicity at the application temperature are in principle the best choice to keep the pH as high as possible. On the other hand a high volatility of the amines is required to ensure a good distribution also in the steam systems and main condenser due to the injection point. This is usually located in the low-pressure, low-temperature region of PWRs, namely the condensate or feedwater system.

The selection of the best pH strategy depends not only on several influencing factors like plant design parameter and material concept but also on nontechnical factors as environmental protection law.

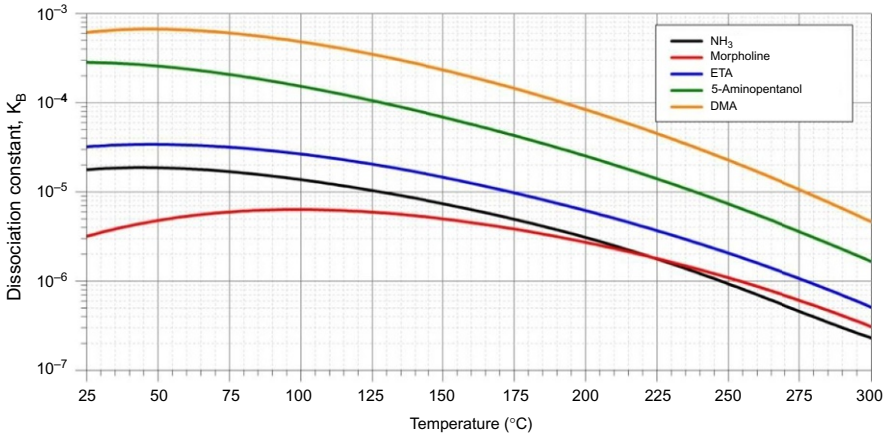

Fig. 6.6 Dissociate constants of five alkalizing amines.
Based on Drexler, A., Roumiguiere, F., Ramminger, U., Fandrich, J., 2012. Evaluation of the steam-water cycle condition for sustainable water chemistry operation. In: 3rd International Conference on NPP Life Management (PLIM) for Long Term Operations (LTO). Conference ID: 41982 (CN-194), Salt Lake City, Vienna.

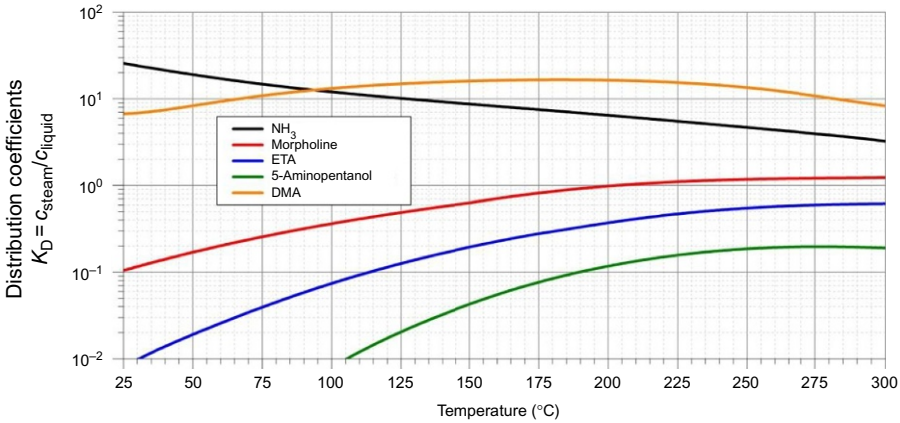

Fig. 6.7 Distribution coefficients of five alkalizing amines.
Based on Drexler, A., Roumiguiere, F., Ramminger, U., Fandrich, J., 2012. Evaluation of the steam-water cycle condition for sustainable water chemistry operation. In: 3rd International Conference on NPP Life Management (PLIM) for Long Term Operations (LTO). Conference ID: 41982 (CN-194), Salt Lake City, Vienna.

6.2 Water chemistry treatments

6.2.1 Historical evolution of steam-water cycle chemistry treatment

Historically most of the pressurized water reactor (PWR) units were using the Phosphate treatment based on fossil fired unit experience. This treatment is able to buffer ionic impurities entering the system and concentrating in the SG (see Section 6.1.2). The reason for the necessity of such a buffering effect was that the condenser tubes, historically made of copper alloys due to their high thermal conductivity, were not always tight. In the early 1970s (under phosphate chemistry treatment) Alloy 600 MA started to suffer from corrosion.

It has been considered first, that locally the chemistry was either too alkaline or too acidic respectively inducing SCC or wastage of the SG tubing. Several Na/PO_4^{3-}-ratios have been successively tried to avoid both type of corrosion but without success. In fact both environments were able to coexist in different local parts of the SG, it became obvious that it was impossible to avoid corrosion of Alloy 600 MA tubes, whatever which Na/PO_4^{3-} molar ratio was met (2.0–2.6).

Most of the PWR with Alloy 600 MA tubing effectively moved to all volatile treatment (AVT) chemistry. AVT typically involves using ammonia (NH_3) to raise pH and hydrazine (N_2H_4) to minimize oxygen. Due to copper containing materials still present in the steam-water circuit, the ammonia concentration was low. In the time of phosphate treatment, utilities were used to operate with rather high impurity levels, much higher than now, particularly for seawater-cooled plants. This has been the cause for the "denting" phenomenon. But the AVT chemistry, without any buffering effect, was unable to neutralize the acidity or alkalinity of cooling water ingresses or other pollutions, when they concentrate in the SGs. Accordingly denting phenomena induced extremely quick and severe degradation, requiring urgent steam generator replacements (SGR) in several PWR units in the United States, particularly high for seawater-cooled units.

The obtainable pH(T) applying the Low-AVT was not high enough to be a countermeasure to flow-accelerated corrosion (FAC) in main steam lines, for example. In various western countries different measures, like boric acid treatment or molar ratio control, were implemented to improve secondary side chemistry. Also other alkalization agents than ammonia, like morpholine, Ethanolamine (ETA), 3-methoxy-propyl-amine (MPA), or Di-methyl-amine (DMA), were used.

6.2.2 Ammonia and Hydrazine only (High-AVT)

The objective of introducing the High-AVT chemistry was to stop the FAC in two-phase flow steam systems for an improved feedwater corrosion product control. The High-AVT chemistry treatment is using ammonia (NH_3) for adjusting to the necessary pH-value (VGB PowerTech, 2006).

Applying High-AVT chemistry has the great advantage, that only one chemical has to be dosed to ensure on the one hand reducing conditions inside the SG and

on the other hand to maintain a sufficient high pH value in final feed water. For both purposes hydrazine (N_2H_4) is dosed into the main condensate which reacts with oxygen to nitrogen and water ($N_2H_4 + O_2 \rightarrow N_2 + 2H_2O$) at higher temperature. For that a hydrazine concentration of approximately 100 μg/kg is necessary. Besides the oxygen scavenging effect N_2H_4 decomposes also thermally into ammonia ($N_2H_4 \rightarrow xN_2 + yH_2 + zNH_3$).

Depending on plant conditions, the NH_3 concentration in feed water can achieve values of 5–10 mg/kg. This corresponds to pH(25°C) = 9.81–9.98 in feed water or pH(190°C) = 6.83–6.98. That means the hydrazine requirements satisfy simultaneously the need of high pH for general corrosion control. Typical feedwater concentrations are summarized in Table 6.1.

The advantage of this High-AVT chemistry is its simple application. It does not produce organic acids in the cycle, and therefore there is no cation conductivity increase, as some other chemical treatments do, due to production of organic acids. Therefore the cation conductivity can be easily used as an indicator of impurity concentration in final feedwater. High-AVT is field proven for its efficiency with respect to corrosion product control.

By applying High-AVT very low iron concentration values (taken as the key components for corrosion products) in the final feedwater are achievable. By rising the pH(25°C) > 9.8 in final feedwater iron concentration values even below of 1 μg/kg are achievable (Fig. 6.8).

This water chemistry treatment has been proven to be very effective to drastically reduce feedwater iron concentrations. For example, in older Siemens-KWU designed plants, SG tube fouling can be stopped after introducing High-AVT chemistry. At several plants operating on High-AVT since commissioning, the SG tube fouling was minimal after 25 years of operation. In this plants operated with High-AVT treatment, the feedwater iron transport is so low that the amount of sludge removed by annual tubesheet lancing became to be in the range of 2–3 kg/SG. Similar good field results were also experienced with High-AVT chemistry at plants of other OEM in Europe and Asia which introduced High-AVT treatment (Sugino et al., 2009). Also in VVER plants the pH was maintained historically only by hydrazine-ammonia treatment (with potential later addition of lithium hydroxide).

Table 6.1 Typical concentrations in feed water in PWRs applying H-AVT chemistry treatment

Parameter	Value
Ammonia (mg/kg)	5–15
Hydrazine (μg/kg)	20–150
pH (25°C)	>9.8
Specific conductivity (μS/cm)	15–35

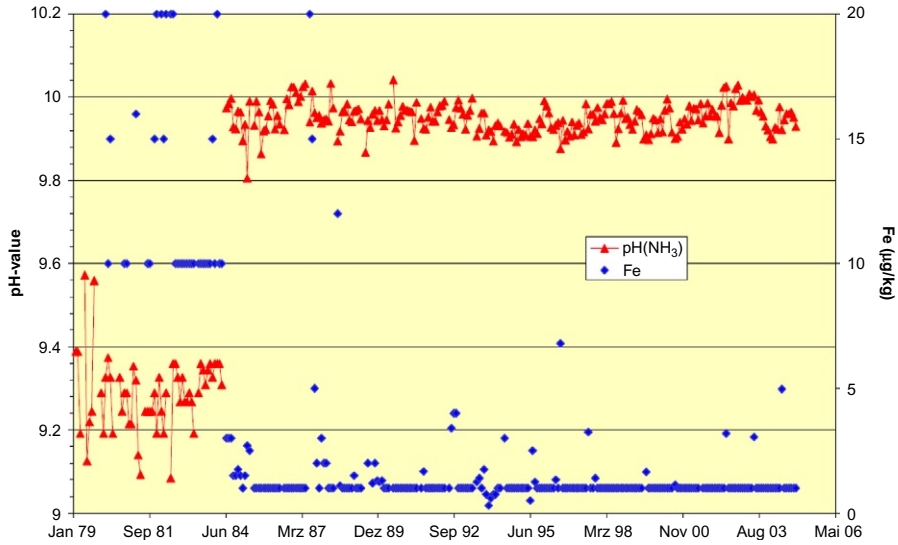

Fig. 6.8 Long-term feedwater iron concentration as a function of pH increase (Odar, 2004).

Although High-AVT treatment has several advantages some undesirable restrictions have to be mentioned. A prerequisite for High-AVT chemistry treatment is the absence of any copper materials in the steam-water cycle. This is a handicap from the commercial point of view because replacement of copper materials is quite expensive and time-consuming, especially if all heat exchangers are equipped with copper or copper-alloy (e.g., brass) tubing. Nevertheless plants in Japan and Spain replaced their components with copper tubing completely.

Another issue is the fact that High-AVT chemistry requires not to use condensate polishing system (CPS) during continuous operation. Due to the high ammonia concentration in the condensate the CPS resins would be exhausted after a short operating time. Nevertheless the CPS can be put in-service in case of condenser leaks which implied high ionic impurity load. Other limitation factors for applying High-AVT chemistry treatment might be special plant designs. Roumiguiere et al. (2012a) reported about a PWR with higher than normal condenser exhaust flow rate causing loss of considerable amounts of ammonia. In consequence, the remaining ammonia concentration was too low to maintain a sufficient pH in the system. For this plant the additional dosing of small amount of ethanolamine was recommended due to its lower volatility.

6.2.3 Alternative amines (Morpholine, Ethanolamine, and others)

Besides the use of ammonia obtained directly by thermal decomposition of hydrazine as alkalizing agent ammonia other alternative amines are used. The most commonly used amines are:

- Ethanolamine (ETA)
- Morpholine
- Di-methyl-amine (DMA)
- Methyl-propanol-amine (MPA)

They generally have a higher dissociation constant and a better distribution coefficient between the water and steam phase of two flow system, and therefore they might provide a better protection against FAC.

At temperature above approximately 200°C (see Fig. 6.7) morpholine is distributed evenly between steam and liquid phase in two-phase flow systems. This is the main advantage of morpholine having the ability to protect all of the steam-water cycle system surfaces against flow-accelerated corrosion even in the presence of copper alloys. A disadvantage of the morpholine treatment is the relative high concentration necessary for adjustment of a target pH in feed water above 9.5. For example the expected concentration in feed water of French PWR was set to 6 mg/kg morpholine and 100 μg/kg hydrazine (Staudt et al., 2002). The consequence of the higher concentration is a reduction of condensate polisher or blowdown resin service lifetime (as with ammonia at high pH). Another disadvantage may be the presence of organic acids due to thermal decomposition of morpholine in the system. This may affect sensitivity of the impurity monitoring by cation conductivity measurements.

In 2014 EDF is still operating 44 of 58 units with morpholine treatment. The pH(25°C) for those units with copper alloy in the steam-water cycle (14 units) is limited to 9.2 in order to avoid copper corrosion. The remaining 30 units with morpholine treatment are copper free, and the pH(25°C) can be therefore higher and is limited to 9.6. Based on a pH optimization study to derive the best alkalizing agent for their plants, EDF decided to introduce in all 58 plant the ethanolamine treatment by 2020 (Duchaussoy et al., 2014) with a target concentration in final feed water of 4 ppm of ethanolamine and 1.5 ppm of ammonia.

ETA is used in an increasing number of countries with PWR units. It is used in the majority US PWR units either alone or with other amine. It is applied at PWR and VVER plants in Europe, Russia, Korea, Japan, China, and South Africa. ETA was selected because the laboratory data were promising that pH(T) values would be more increased in wet steam areas and also organic acid production would be less when compared to morpholine. The distribution coefficient is <1 (see Fig. 6.7), i.e., ETA stays more in water phase, which will not give a constant concentration in the different parts of the secondary side system. This results in the possibility that the various portions of the system are not exposed to the optimum ETA concentration and therefore less protection may exist in some parts of the secondary system if ETA concentration is adjusted for other parts of the system. However, in the two-phase parts of the secondary system the liquid phase may have a higher ETA concentration.

In addition to morpholine or ETA, other reagents may be used, each of them has its own advantages and disadvantages. Moreover, some utilities with PWR made the interesting approach of using a mixing of amines with each one its own purpose, such

as protecting different part of the secondary side circuit against FAC or more efficiently reducing the corrosion products transport and deposition. The main considered amines are DMA and MPA. A disadvantage of such a mixing of amines is the higher complexity of dosing control and monitoring. Additional health and safety issues have to be considered, e.g., DMA is a colorless, flammable gas with an ammonia-like odor. The flash point is at −6°C and explosive limits between 2.8 and 14.4 vol.%. This induced high efforts in case of implementation of a DMA dosing in the steam-water cycle of PWRs.

6.2.4 Conclusion

The most effective approach of counteracting any degradation problems and thus of improving the SG performance is to keep them in clean conditions or to perform measures bringing them to clean conditions.

The level of SG cleanliness or in other word the amount of corrosion products transported toward the SG depends on three factors:

- Chemistry
- Plant design (including SG)
- Plant materials (including SG)

The most frequent cases of SG degradation caused or supported by incompatibility between these three factors. Plants having a good design and material concept can afford a less restrictive chemistry, and vice versa.

In existing plants the easiest, i.e., with lowest cost and workload achievable, control element is the water chemistry, namely, the pH strategy. Therefore the selection of the optimum water chemistry treatment is a key factor for low deposits load of the SGs. Each applied alkalizing agent, e.g., ammonia, morpholine, ethanolamine, etc., has its advantages and disadvantages.

When selecting a pH control strategy, plant design (e.g., material concept, purification system, feedwater tank), operation characteristics (base load or load-follow operation), and environmental law have to be carefully considered. Any strategy has to be tailored to the plant-specific needs and requirements. Owing to the complexity of the interrelated variables, the best way is to perform a modeling with a suitable computer code (Roumiguiere et al., 2012a,b).

6.3 Additional water chemistry measures for high SG performance

Within this chapter additional measures complementing an optimum pH strategy for low corrosion product generation are described.

6.3.1 Minimization of corrosion product generation and transport to SGs

6.3.1.1 Oxygen dosing

Oxygen can cause pitting or accelerate the SCC of the SG tubing material. Accordingly, oxygen and other species which produce oxidizing conditions such as copper oxides or hematite should be excluded inside the SGs (for this purpose hydrazine is added, see above).

On the other hand it is widely known that small amounts of oxygen can drastically suppress the flow-accelerated corrosion rate of carbon steels. One widely applied example is the AVT(O) treatment in conventional power plants (International Association for the Properties of Water and Steam, 2015); another the operation of BWR plants under neutral water chemistry conditions, where oxygen is produced due to radiolysis. The suppression of FAC is caused by the formation of hematite (Fe_2O_3) passive layers in the presence of oxygen. Hematite is much less soluble compared to magnetite (Fe_3O_4), which is built under reducing PWR and VVER operating conditions. Due to the lower solubility of hematite the amount of generated corrosion products are lower compared to surfaces with a magnetite layer. The influence of the redox potential on the iron solubility was calculated by Schneider et al. in 2004 (Fig. 6.9).

By adding small amount of oxygen the redox potential can be shifted from magnetite stable region into conditions where hematite is the stable phase. It has to be noted that all plants applying such an oxygenation treatment are operated with

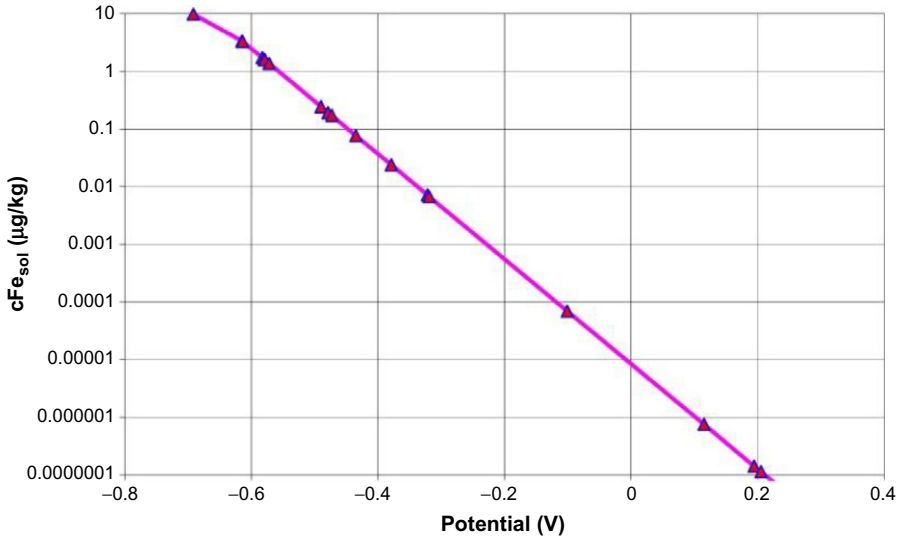

Fig. 6.9 Calculated iron solubility as a function of potential (Rühle et al., 2004).

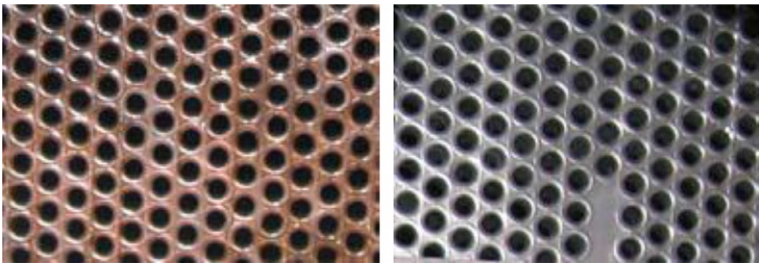

Fig. 6.10 High-pressure feedwater heater inlet (left) and outlet (right). Red color (Fe_2O_3) occurred due to few ppb O_2 still existing because of low reaction rate at lower temperature (T approximately 180°C). Black color (Fe_3O_4) indicates reducing conditions of feed water after (O_2 scavenging is approximately 150 times faster at $T > 220$°C).

all-volatile chemistry, i.e., ammonia and hydrazine only. The oxygen scavenging for reducing conditions inside the feed water is applied by

- mechanical degassing either in the feedwater tanks or by degasser in the feedwater train and
- chemical degassing by the hydrazine-oxygen reaction ($N_2H_4 + O_2 \rightarrow N_2 + 2H_2O$)

The chemical oxygen scavenging usually takes place in the area of the last high-pressure heater of the feedwater train (Fig. 6.10).

The injection of oxygen in order to counteract FAC in the carbon steel reheating steam tubes in the MSR was implemented in German PWRs since 1998. The first unit was Philippsburg Unit 2 where tube failures at the MRS were detected. Examinations at the pulled tube showed tube failure in the upper part of the reheating steam tube and accumulated significant magnetite deposits just down-stream tube failure. After mechanical tube cleaning by blasting technology the first oxygen injection was performed. Besides Philippsburg Unit 2 the German PWRs Isar Unit 2 and Biblis Unit A/B started oxygen injection in the heating steam of the MSR (Rühle et al., 2004).

In order to exclude oxidizing condition inside the SGs the oxygen concentration was monitored in the reheater condensate as well as in the final feed water at Phlippsburg. Due to the first-of-a-kind application the oxygen concentration measured in the reheater condensate was slowly increased over several months to the target concentration of 150 μg/kg (Rühle et al., 2004) (Fig. 6.11).

At NPP Isar Unit 2 the reducing conditions inside the SGs were ensured by additional redox potential measurements in reheater condensate and final feed water. It can be shown that only a small increase of the redox potential occurred, i.e., increase from −500 mV to −475 mV (Fig. 6.12). This clearly indicates that the requirement of reducing conditions inside the SG was not violated by adding small amount of oxygen in the reheater steam line.

Oxygen injection had been performed also at the Japanese PWR Tsuruga Unit 2 where wall thinning of carbon steel tubes was detected. The principle is similar to the application in German PWRs. Small amounts of oxygen are injected upstream of the FAC area in order to increase the redox potential into the stability phase of

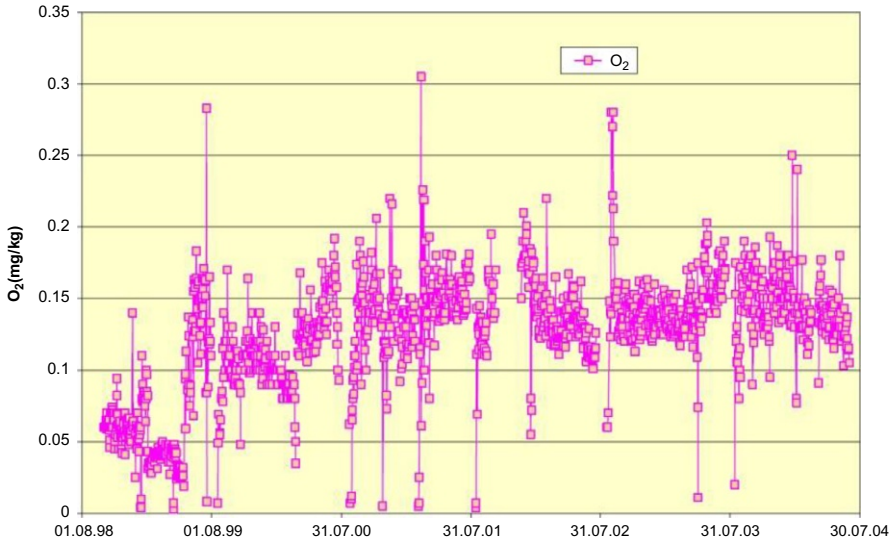

Fig. 6.11 Oxygen concentration in reheater condensate of Philippsburg Unit 2 (Rühle et al., 2004).

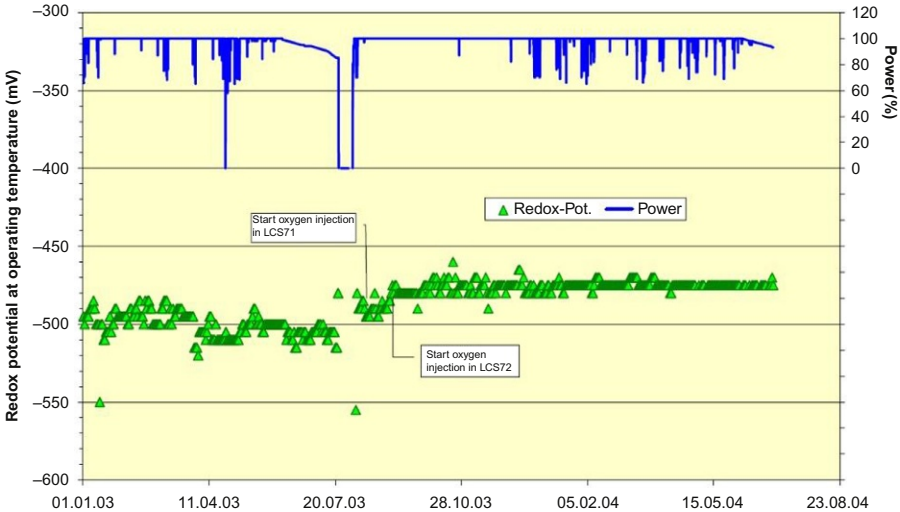

Fig. 6.12 Redox potential measured in final feed water of NPP Isar 2 prior and with oxygen injection in reheater steam (Rühle et al., 2004).

hematite. By the formation of a Fe_2O_3 oxide film the carbon steel surface is protected against FAC. The applicability and effectiveness had been proved by an in-plant test in 2007. Based on its promising results the so-called oxygenated water chemistry had been introduced in 2011 (Sugino et al., 2012). It was shown that FAC can be mitigated

- at low-AVT treatment (i.e., pH(25°C) > 9.3) by an oxygen concentration of 5 μg/kg and
- at high-AVT treatment (i.e., pH(25°C) > 9.8) by an oxygen concentration of 2 μg/kg.

6.3.1.2 Optimized plant lay-up and start-up

The outage phase and the subsequent start-up phase of power plants are as important for the SG cleanliness as the power operation phase. Loose corrosion products which might be generated by improper plant layup (and also other potentially corrosive impurities, see Section 6.3.3) can be transported toward the SG. This is usually reduced by an intensive flushing of the condensate and feedwater train.

An example of high ingress of corrosion products during the start-up phase is given in Fig. 6.13. The plant was started up at very high corrosion product level. More than half of the cumulative magnetite ingress during 7 months of operation was caused by two start-up operations.

The currently applied strategies for the minimization of corrosion product control are based on reduction and controlling of moisture or oxygen. By excluding one of those factors corrosion is impossible. For reaching this target special

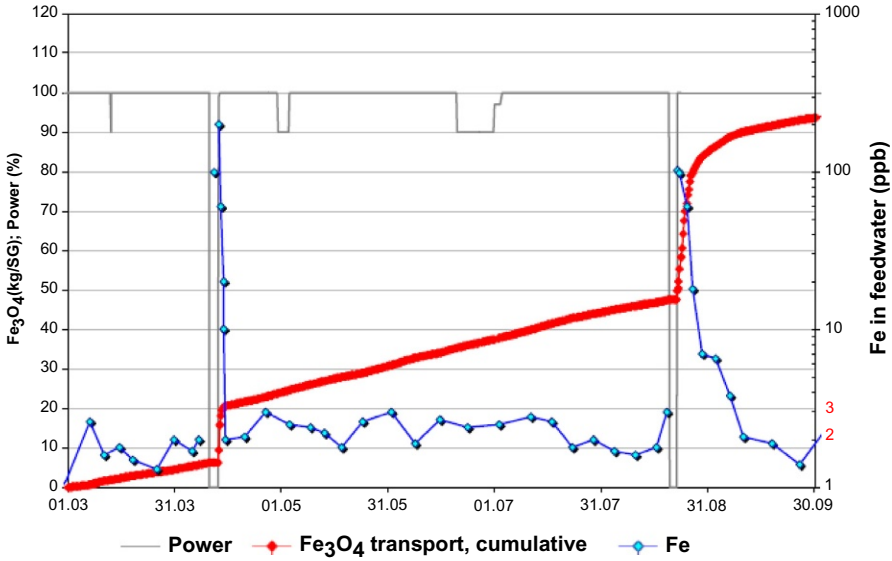

Fig. 6.13 High corrosion products transport toward the SG (International Atomic Energy Agency, 2011).

System	Layup method	Parameter	Frequency	Expected value	Limit value
Feed train, steam reheating system (tube and shell side), condenser (secondary side)	Drain and dry with dry air	Relative humidity (%)	Once per day until stable then three times per week	30	40
Steam generator	Drain and dry with dry air	Relative humidity (%)	Once per day until stable then three times per week	30	40
	Wet	Hydrazine (uncatalyzed) N_2H_4 (mg/kg)	Once per week	$\geq 75 + (7 \times J1)$ J1 = number of days in wet layup	75
		$pH_{25°C}$ obtained with an alkalizing agent (ammonia, ethanolamine or morpholine)	Once per week	9.8–10.1	9.7–10.3
Condenser (cooling side) *Copper and stainless steel tubes*	Drain, wash down, dry and open to atmosphere				
Condenser (cooling side) *Titanium tubes*	Drain, wash down, connect water recirculation in accordance with normal operation				
Stator cooling circuit	Keep in service and normal analytical surveillance maintained				

Fig. 6.14 EDF secondary system and SG conservation specifications (Alos Ramos et al., 2014).

requirements for the dry (empty systems) and wet (filled systems) have been fulfilled:

- Dry layup: Establishment of a dew point <10°C or <50% relative humidity usually achieved by blowing dry or hot air into the system/component. Disadvantages: Continuous drying with high workload required
- Wet layup: Oxygen elimination can only be achieved by addition of conditioning agents (usually hydrazine or carbohydrazide). Disadvantages: Hydrazine is toxic and carcinogenic

Besides the increased corrosion product transport localized corrosion can be a result of improper lay-up, which might lead to severe degradation modes. The importance of proper plant lay-up was emphasized by EDF in 2014: "EDF operational experience in this area confirms that damage to plant equipment from improper layup procedures is a cause of reduced plant reliability and availability and can increase the corrosion products ingress into the SG during start-up (Alos Ramos et al., 2014)." The current SG and steam-water cycle lay-up of EDF is given in Fig. 6.14.

6.3.2 Corrosion product removal from SGs

Even in case of adequate water chemistry the ingress of corrosion products and formation of deposits in SGs is a matter of fact. Of course amount, composition and characteristics of material ingress vary from plant to plant due to different water

chemistry, material concept, blowdown techniques and effectiveness, etc. Consequently, the amount of corrosion products, the deposition area, and the composition of this sludge are plant specific and can vary in a wide range. The main deposition areas can be differentiated into the tubesheet area, the upper tube bundle region, or general tube fouling.

There are two principle approaches applied by the community for reduction or removal of SG deposits:

- Mechanical cleaning technologies
- Chemical cleaning processes

Mechanical cleaning

Mechanical cleaning measures are principle based on high-pressure water jet in order to remove deposits from the surfaces inside the SG. These corrosion products are flushed out by the water and are removed from the SGs. Typical processes are:

(a) Tubesheet lancing
  - Removes deposit from tubesheet area high-pressure water lancing
  - Avoids corrosion by boil-out concentration effect of impurities
  - Reduces the secondary side oxide inventory

(b) Upper bundle flushing
  - Reduces clogging at tube support plates

(c) Inner-bundle lancing
  - Removes deposits by high-pressure water spray inside of the tube bundle
  - High deposit removal capability from inner tubesheet bundle area
  - Followed by normal lancing application to flush out the loose deposits

The approach to removal hard deposits is plant specific and needs to be developed on a case by case basis. This can include also processes which are designed to remove hard deposits (e.g., AREVA's Enhanced Inner Bundle Lancing). Mechanical cleaning is widely applied to remove SG deposits but cannot be discussed here in detail.

6.3.2.1 Chemical cleaning

Chemical cleaning processes provide a cleaning method for the whole SG, i.e., ranging from tubesheet to top of bundle. The basic principle is injecting a chemical or chemical compound into the SG which dissolves the iron-based deposits and scales on the tubesheet, tube support plates, tubes, etc. The usually applied basic chemicals are:

- Ethylen-diamine-tetra-acedic-acid (EDTA)
- Oxalic acid (OA)
- Citric acid (CA) & Ascorbic acid (AA)

Since each plant has its own history and design it is mandatory to tailor any treatment specifically to each plant individually for obtaining the optimum result. There are many processes available on the market, which are capable of removing a wide range of deposit amounts (i.e., 250–2000 kg/SG):

- ASCA, iASCA (Advanced scale conditioning agent), Westinghouse
- DART (Deposit accumulation reduction treatment), AREVA
- DMT (Deposition minimization treatment), AREVA
- EPRI SGOG
- HTCC (High-temperature chemical cleaning), formerly Siemens (now AREVA)
- PACCO (Preventive acid chemical cleaning operation), Comex Lainsa

Besides the capability of removing deposits, and if required reducing clogging phenomena, there are other aspects which have to be considered during selection of a suitable process:

- Corrosion of base material: Chemical cleaning agents are intended to dissolve chemically the present deposits, which imply that these agents can also be aggressive toward the base materials of the SG (and injection line). In general chemical cleaning processes are especially designed to minimize such base metal corrosion. For this purpose sometime corrosion inhibitors are required to be added to the cleaning agent, which make the cleaning compound also more complex.
- For establishing reducing conditions, required in some chemical cleaning processes, CMR (carcinogenic, mutagenic, and toxic to reproduction) chemicals have to be applied, e.g., hydrazine. This might impact the process application from a health, safety, and environmental perspective.
- It has to be kept in mind that any chemical cleaning process creates liquid waste, i.e., the chemical solvent containing the dissolved deposits, which is drained from the SGs. When selecting a chemical cleaning process not only the cleaning process effectiveness needs to be considered but also the waste treatment and disposal of residual waste materials. From this perspective cleaning agents which produce waste, which is either environmentally harmless or which can be easily decomposed on side, are favorable.

6.3.3 Corrosion product control by additives

6.3.3.1 Dispersants

The approach of dispersant injection into the steam-water cycle of PWRs is improving the corrosion product removal from the SGs via the blowdown system. The mode of functioning of dispersants (namely polyacrylic acid, PAA) is discussed as electrical repulsion due to adsorption of the dispersant on the corrosion particle (Electric Power Research Institute, 2001a).

The technology is originated in the fossil-fired power plants and was qualified by EPRI since 1998 (Electric Power Research Institute, 2001a,b, 2002). Nowadays EPRI differs between three application scenarios (Wolfe and Fruzzetti, 2015):

- Start-up application: Long-path recirculation clean-up process of the condensate and feedwater system during start-up
- Online application: Mitigation of SG fouling during operation
- SG wet lay-up application: During shutdown to remove some of the existing deposits and help remove hardness elements

Plants which had injected PAA reported an increased corrosion product load of the SG blowdown filter during the application and improved efficiency of sludge

lancing, e.g., Doel 3 (Laire et al., 2014). But besides all promising results it should also be noted that at both units of NPP Byron small changes (approximately 0.1%–0.2%) in feedwater flow indications were observed when PAA injection was started and stopped. KHNP reported about slightly (i.e., within the limit values) increase of corrosion of Alloy 690 and SA 106 Gr. B in case of increase of PAA concentration (Kwon et al., 2014). These issues support the importance of a plant-specific feasibility and compatibility study prior to any introduction or change of the chemistry regime. To cover this issue EPRI had issued a sourcebook (Electric Power Research Institute, 2012).

6.3.3.2 Film-forming amines

A method for further reduction of corrosion product generation is the application of surface active agents like film-forming amines. The principle of this technology is the formation of a protective ideally monomolecular film on the surface of either metal or metal oxides.

This adherent, nonwetable film acts like a barrier that limits the access of water and hydrated species to the metal or metal oxide surface. It lowers the corrosion rate by inhibiting the mass transfer between surface and solution (Figs. 6.15).

The origin of this technology is located in fossil-fired power plants, but it was also applied in steam-water cycle of VVERs. It was also recently applied in Western-type PWRs (Ramminger et al., 2012, 2013) and also in a CANDU plant (Ramminger et al., 2014). In contrast to the application in the VVER units the dosing in the Western PWRs as well as the CANDU plants was not applied continuous during the operation cycle but rather noncontinuous within a few weeks.

The results reported after the application of this technology in the Western PWRs are very satisfying. The plants operator reports: “FFA treatments mainly contributed to minimization of transport of corrosion products and other impurities into the SGs (…)” (Arias Alonso et al., 2014). By establishing the protective film during the FFA dosing other substances adsorbed or adhered on the surfaces (like colloidal iron-oxide deposits or ionic impurities) can be released at variable extent (cleaning effect).

Nevertheless prior to an application of this technology at a specific plant the compatibility and feasibility has to be evaluated. However, this statement is valid for any change of the water chemistry in operating plants.

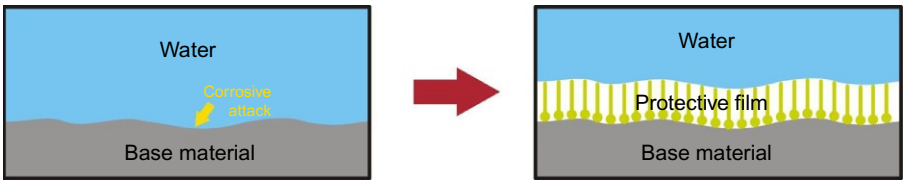

Fig. 6.15 Principle of the application of film-forming amine.

The FFA technology focuses not only on the power operation. It improves also the lay-up conditions during outages. In fact the cited application in the CANDU plant was performed due to a large refurbishment program linked with a standstill period for several month or even years. The FFA technology offers sufficient protection of the carbon or low-alloyed steel surfaces in the steam-water cycle without addition lay-up works.

6.3.4 Minimization of formation of aggressive environment in SGs

The main risks of hard deposits are on the one hand the enrichment of corrosive impurities, like chloride or sulfate, in the sludge pile or in crevices between tube and tubesheet causing local pit corrosion of the SG tubes and several other secondary side stress corrosion effects. On the other hand hard deposits promote the effect of denting in the areas of tubesheet. Denting is well known since the 1980s and is caused by the increase of the specific volume by the factor of 2 in case of oxidation of ferrite particles ($3Fe + 4H_2O \rightarrow Fe_3O_4 + 4H_2$) (Fig. 6.16).

As main source of corrosive impurities and hardening species should be considered:

- Make-up water supply system (e.g., silica slip or regeneration chemicals)
- Main condenser leakage
- Resins of CPS or SG blowdown system
- Chemical used for regeneration of ion-exchange resins (e.g., SG blowdown)
- Impurities in conditioning chemicals (e.g., hydrazine, amines)
- Outage works (e.g., aluminum and silica-based abrasives).

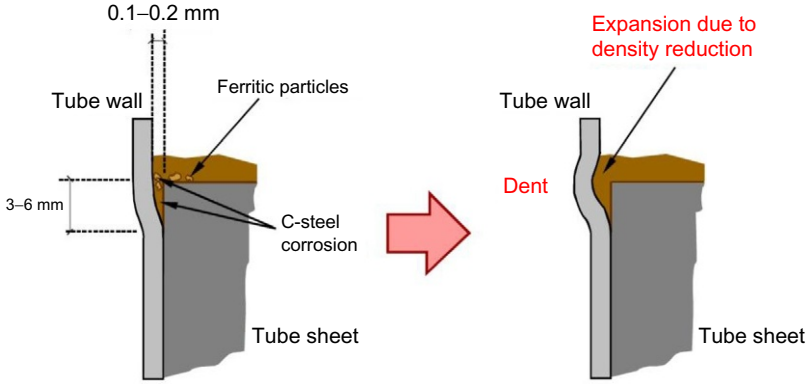

Fig. 6.16 Schematic scheme of tube denting mechanism (International Atomic Energy Agency, 2011).

From the above list the main measures for minimization of impurities ingress can be deduced:

- Minimize the risk of condenser leaks by selecting corrosion resistant material (e.g., titanium or stainless steel)
- Detect and repair immediately condenser leaks, e.g., by installing sensitive sodium online monitoring in main condenser hotwells. Helium leak test is an adequate technology to detect even small leaks
- Clearly evaluate the necessity of continuous operation of a CPS; it can even increase the impurity level in the steam-water cycle as reported in International Atomic Energy Agency (2011, p. 52ff)
- Establish specification as well as a quality and supervision system for chemical additives (e.g., hydrazine) and auxiliary products (e.g., tapes, abrasives etc.)[3], e.g., the EDF PMUC system or AREVA's QP-Database

Surveillance of ionic impurity ingress in steam-water cycle is state of the art (see Section 6.4). But even this measure cannot exclude an actual ingress like in Hamaoka Unit 5 (Tsukada et al., 2014) where in 2011 a large volume of seawater flowed into the reactor facilities due to damage to the main condenser tubes. This is of course a worst case example. However, even very small condenser leakages can gradually lead to severe SG conditions. A continuous small in-leakage of seawater for instance, which does not harm any action or limit value in the condensate feedwater train, can enrich the corrosive impurities inside of existing SG deposits leading to a shift the local pH value into a critical region or in combination with hard deposits to SCC.

Due to this risk the definition and surveillance of integrated exposure or accumulated values (e.g., for sodium) becomes more and more favorable. EPRI covers this issue within dedicated appendix in the "Pressurized Water Reactor Secondary Water Chemistry Guidelines" (Electric Power Research Institute, 2004). Also plants vendors specify accumulated limit value within Chemistry Guidelines for replacement SGs.

The interrelation between the above describes factors are summarized in Fig. 6.17.

It should be the target of each plant operator to reduce the risks for the SGs by establishing a chemistry program which focuses on reducing any ingress into

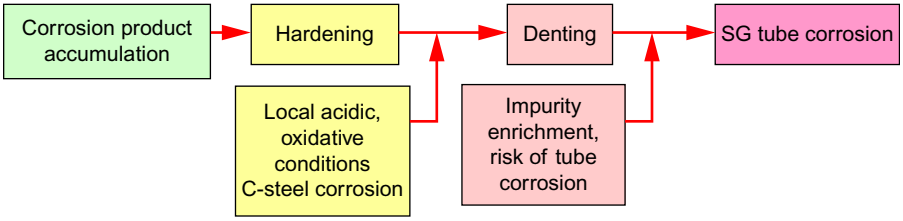

Fig. 6.17 Interrelation of corrosion product deposits, hardening, impurities, and tube corrosion (International Atomic Energy Agency, 2011).

[3]This is valid not only for the steam-water cycle than rather the whole nuclear plant systems.

the SG. This comprises either transport of corrosion products or impurities. By preventing its accumulation inside the SG the risk corrosion is minimized or even suppressed.

6.4 Water chemistry monitoring and control program

6.4.1 Water chemistry guidelines

As outline above water chemistry plays an important role in nuclear power plants, especially with respect to overall plant performance. In order to meet main targets of any water chemistry treatment (see Section 6.1.1), chemistry guidelines specify a set of parameters that allows an efficient and reliable plant operation. The chemistry guidelines serve as the basis for the associated chemistry monitoring program (see Section 6.4.2).

The specified chemistry parameters can be divided into control and diagnostic parameters. The VGB guideline (VGB PowerTech, 2006) defines control parameter as chemistry key parameters that determine the overall chemistry conditions. These parameters are chosen not only because of their importance but also because of the existence of good detection methods according to the state of the art as to reliability, sensitivity, and accuracy. Deviations could lead to corrosion of structural materials and its consequences. Diagnostic parameters complement the overall picture of the controlled water chemistry. They show trends of individual water chemistry aspects. Deviations do not lead to a risk of the structural materials; however they indicate chemistry anomalies. Therefore the identification and elimination of the anomaly are required. The diagnostic parameters are complementary to control parameters.

Due to their importance control parameters are accomplished by Action Levels and Limit Values. Action Levels are associated with chemistry deviations in connection with a maximum allowed duration and with regard to allowed plant power. For example in case of reaching Action Level 3, the VGB guideline (VGB PowerTech, 2006) stipulates to shut down the plant within the next 12 hours according to the plant operation manual. The concept of three action levels is enclosed also in the EPRI guideline (Electric Power Research Institute, 2004) and the current Japanese guidelines (Kawamura et al., 2014).

Due to the specified water chemistry treatment, the plant design and material concepts the specified set of parameter as well as the specified values differs between the guidelines.

6.4.2 Water chemistry surveillance

Any water chemistry measures implemented for increase of the SG reliability has to be controlled and evaluated. Therefore the chemistry treatment or guideline is any time accomplished by a water chemistry monitoring concept. For surveillance of the water

chemistry data online or laboratory analysis can be applied. Online monitoring in nuclear power plants should be considered as the preferred method for chemistry monitoring in two cases:

- applicable for control parameters or
- short-term corrective actions are required

Laboratory analysis should be considered

- if the value serves as a necessary complement for the diagnostics of chemistry-related issues
- to verify the accuracy and reliability of online measurement techniques
- in general if online measurement techniques are not available with a given reliability and cost-effectiveness.

The dedicated surveillance parameter, frequency, as well as limit values or actions levels depend on the water chemistry treatment as well as plant design and have to be developed plant specific. Nevertheless from the perspective of SG integrity the necessity of an adequate measurement of corrosion products in feed water should be emphasized. The established chemistry monitoring system, both the specification and the monitoring systems installed in the plant, should be regularly evaluated and updated (Drexler et al., 2014).

6.5 Summary

SGs are one of the most important components of pressurized (heavy) water reactors. Besides their major function of providing steam for the turbine (and the subsequent generator), the most important function of SGs from a safety point of view is being the barrier between the radioactive primary side and the nonradioactive secondary side. Any degradation mechanism, which impairs this barrier function, is a significant safety concern.

For a safe and reliable operation and optimum performance of the SGs the applied water chemistry is one of the key parameter. However, the optimum water chemistry treatment focuses not only on the SG but also the whole steam-water cycle. The water chemistry is influenced by

- various factors (e.g., cooling water in-leakages or condenser vacuum) and
- various plant systems (e.g., design and metallurgy) during
- all plant operation modes (start-up, power operation, shutdown, outages)

In order to optimize the SG performance and to derive an optimum treatment all these factors have to be considered. Keeping the SGs clean and in good shape is therefore not only an issue of the SGs themselves.

In summary, adequate water chemistry treatment is a prerequisite for optimum SG performance. A change of water chemistry parameter might yield to significant improvements of the SG health and performance. However due to several cross-link any changing has to be evaluated in advance.

References

Alos Ramos, O., de Maria Pablo, S., Wintergerst, M., Postic, A., Courtaudière, J.P., Fournier, C., Vialette, R., Waeber, J., Couturier, D., Robillart, P., 2014. Layup practices at EDF PWR fleet and future developments. In: Proceedings of the Nuclear Plant Chemistry Conference 2014, Sapporo.

Arias Alonso, C.J., Boned, U., Ramminger, U., Fandrich, J., Caris, N., 2014. Operating experience with improved water chemistry treatment in water-steam cycles of PWRs. In: Steam Generator Secondary Side Management Conference (SGMP 2014), Baltimore, Palo Alto.

Drexler, A., van Dijke, N., Sigrist, M., 2014. Concept study of steam-water cycle sampling system modernization at NPP Borssele. In: Proceedings of the Nuclear Plant Chemistry Conference 2014, Sapporo.

Duchaussoy, T., Alos Ramos, O., Qui, G., Knight, K., Fontan, G., Bretelle, J.-L., 2014. Outcomes and analyses of the secondary circuit water chemistry strategy for the French PWR fleet. In: Proceedings of the Nuclear Plant Chemistry Conference 2014, Sapporo.

Electric Power Research Institute, 2001a. Dispersants for Tube Fouling Control: Volume 2: Short-Term Trial at ANO-2. Electric Power Research Institute, Palo Alto, CA.

Electric Power Research Institute, 2001b. Dispersants for Tube Fouling Control: Volume 1: Qualification for a Short-Term Trial at ANO-2. Electric Power Research Institute, Palo Alto, CA.

Electric Power Research Institute, 2002. Dispersants for Tube Fouling Control: Volume 3: Qualification for a Long-Term Trial in a Replacement Steam Generator Tubed with Alloy 690 TT. Electric Power Research Institute, Palo Alto, CA.

Electric Power Research Institute, 2004. Pressurized Water Reactor Secondary Water Chemistry Guidelines, sixth ed. EPRI, Palo Alto, CA.

Electric Power Research Institute, 2012. Dispersants for Pressurized Water Reactor Secondary Side Fouling Control: Sourcebook for Online and Offline Applications. Electric Power Research Institute, Palo Alto, CA.

Girard, S., 2014. Physical and Statistical Models for Steam Generator Clogging Diagnosis. Springer International Publishing, Cham. p. sl.

Goodstine, S., Kurpen, I., 1973. Corrosion and corrosion product control in the utility boiler-turbine cycle. Combustion 44, 6–18.

International Association for the Properties of Water and Steam, 2015. Volatile Treatments for the Steam-Water Circuits of Fossil and Combined Cycle/HRSG Power Plants: Technical Guidance Document—2015 Revision. International Association for the Properties of Water and Steam, Stockholm.

International Atomic Energy Agency, 2011. Assessment and Management of Ageing of Major Nuclear Power Plant Components Important to Safety: Steam Generators. International Atomic Energy Agency, Wien.

Kawamura, H., Shoda, Y., Nishimura, T., Tsuzuki, Y., Watanabe, Y., Taked, K., Terachi, T., Ishihara, N., Takahashi, A., Hisamune, K., 2014. Primary water chemistry guidelines for Japanese PWR plants. In: Proceedings of the Nuclear Plant Chemistry Conference 2014, Sapporo.

Kwon, H., Lee, D., Sung, K., 2014. Dispersant Application During SG Wet Layup at SK Unit 1. In: Spring Meeting.

Laire, C., Bosmans, S., Delporte, R., Coart, S., Lecocq, R., Ceursters, D., 2014. First steam generator cleanup application with dispersant at Doel 3. In: Proceedings of the Nuclear Plant Chemistry Conference 2014, Sapporo.

Odar, S., 2004. Water chemistry measures to improve steam generator performance. In: Water, Steam, and Aqueous Solutions for Electric Power: Advances In Science and Technology. Proceedings of the 14th International Conference of the Properties of Water and Steam, Kyoto, Maruzen, pp. 531–544.

Ramminger, U., Hoffmann-Wankerl, S.D., Fandrich, J., 2012. The application of film-forming amines in secondary side chemistry treatment of NPPs. In: International Conference NPC 2012 on Water Chemistry of Nuclear Reactor Systems, Paris.

Ramminger, U., Fandrich, J., Roumiguiere, F., 2013. (AREVA GmbH) EP000002700075B1.

Ramminger, U., Fandrich, J., Sainz, R., Ovando, L., Herrera, C., Menizabal, M., Dumon, A., Chocrón, M., 2014. Qualification of FFA treatment for the water-steam cycle as an innovative lay-up strategy for the long term outage of a CANDU-6 reactor. In: Proceedings of the Nuclear Plant Chemistry Conference 2014, Sapporo.

Roumiguiere, F., Fandrich, J., Ramminger, U., Hoffmann-Wankerl, S.D., Drexler, A., 2012a. Secondary side water chemistry pH control strategy improvements. Power Plant Chem. 14, 658–670.

Roumiguiere, F., Fandrich, J., Ramminger, U., Hoffmann-Wankerl, S.D., Drexler, A., 2012b. Secondary side water chemistry pH control strategy improvements. In: International Conference NPC 2012 on Water Chemistry of Nuclear Reactor Systems, Paris.

Rühle, W., Neder, H., Holz, G., Schneider, V., 2004. Oxygen injection into reheating steam of moisture separator reheaters. In: Water, Steam, and Aqueous Solutions for Electric Power: Advances In Science and Technology.Proceedings of the 14th International Conference of the Properties of Water and Steam, Kyoto, Maruzen Co. Ltd, pp. 573–580.

Staehle, R.W., Gorman, J.A., 2001. Progress in understanding and mitigating corrosion on the secondary side in PWR steam generators. In: Proceedings of the Tenth International Symposium on Environmental Degradation of Materials in Nuclear Power Systems—Water Reactors, American Nuclear Society, Lake Tahoe, pp. 1–255.

Staudt, U., Odar, S., Stutzmann, A., 2002. Comparison of French and German NPP water chemistry programs. In: Proceedings Chimie 2002: International Conference "Water Chemistry in Nuclear Reactors Systems, Operation Optimisation and New Developments", Avignon, EURODOC SA.

Stellwag, B., Aaltonen, P., Hickling, J., 1993. Field experience with advanced methods of on-line monitoring of water chemistry and corrosion degradation in nuclear power station. In: IAEA Meeting on Influence of Water Chemistry on Fuel Cladding Behaviour, Rez, Czech Republic.

Sugino, W., Ohira, T., Nagata, N., Abe, A., Takiguchi, H., 2009. Effect of water chemistry improvement on flow accelerated corrosion in light-water nuclear reactor. In: Symposium on Water Chemistry and Corrosion in Nuclear power Plants in Asia: Proceedings, Nagoya, pp. 84–91.

Sugino, W., Fukuda, J., Kitano, Juya, Hisamune, Kenji, Meguro, Y., 2012. Effectiveness of oxygen treatment on flow accelerated corrosion mitigation on PWR secondary system. In: International Conference NPC 2012 on Water Chemistry of Nuclear Reactor Systems, Paris.

Tsukada, T., Egami, Y., Watanuki, Y., Mitani, K., Watanabe, T., 2014. Effect of seawater infiltration from main condenser, damaged by break on the reactor facilities, Hamaoka Unit 5. In: Proceedings of the Nuclear Plant Chemistry Conference 2014, Sapporo.

VGB PowerTech, 2006. Technische Vereinigung der Grosskraftwerksbetreiber, Richtlinie für das Wasser in Kernkraftwerken mit Leichtwasserreaktoren. VGB PowerTech, Essen.

Wolfe, R., Fruzzetti, K., 2015. Dispersant application and field experience. In: SGMP Workshop in Taiwan: Steam Generator Management Program, Taipower Maanshan Power Plant, Palo Alto, CA.

This page intentionally left blank

Corrosion problems affecting steam generator tubes in commercial water-cooled nuclear power plants

7

J.A. Gorman
Dominion Engineering, Inc., Reston, VA, United States

7.1 Introduction

This chapter contains a review of the main corrosion problems that have affected commercial PWR steam generators. The problems discussed in this chapter are mostly limited to those that have had significant impacts on steam generator life or reliability. It should be understood that there are numerous other modes of corrosion that have affected small numbers of tubes but that have not caused serious safety or operability concerns and thus are not covered in this chapter.

General corrosion on the primary side is not covered in this chapter since it has not been a corrosion mode that has damaged steam generator tubes. However, it should be understood that limiting the corrosion of wetted surfaces on the primary side is important for PWRs since corrosion products released from the tubing, especially nickel and iron, deposit on fuel rod surfaces and that these deposits, known as crud, can cause several problems. These problems include interfering with heat transfer, development of activated corrosion products that can be released and cause higher shutdown dose rates around the primary system, and crud-induced power shifts (also known as axial offset anomaly). Selection of tube materials and control of tubing fabrication processes need to takes these possible problems into account.

7.1.1 Overview of steam generator types covered in this chapter

This section provides a brief description of the types of steam generators discussed in this chapter.

7.1.1.1 Vertical PWR steam generators of the Westinghouse Electric (WE) and Combustion Engineering (CE) types

Steam generators designed by WE and CE and their licensees have U-bent or square bent tubes and are of the vertical recirculating type in which boiling water and steam on the secondary side rises through the tube bundle, water is removed from the

Steam Generators for Nuclear Power Plants. http://dx.doi.org/10.1016/B978-0-08-100894-2.00009-1
© 2017 Elsevier Ltd. All rights reserved.

two-phase mixture in moisture separators at the top of the tube bundle, and the water is returned to the bottom of the tube bundle via a downcomer region at the periphery of the tube bundle, as illustrated in Fig. 1.4. The configuration shown in Fig. 1.4 is for a feedring unit, which is also known as a nonpreheat unit, in which feedwater is added to the steam generator above the top of the downcomer region at the periphery of the tube bundle. An alternate configuration uses a preheater (also called an economizer) at the bottom of the cold leg, as shown in (Fig. 1.8). In this configuration, feedwater is added near the bottom of the cold leg and is heated by cross flow passes in the cold leg side until it reaches saturation temperature.

There have been four main tube alloy types used in WE and CE type recirculating steam generators. Early commercial nuclear power plant steam generators used either Type 304 or Type 316 stainless steel tubes. However, starting with the first large commercial units, San Onofre 1 and Conn Yankee in 1968, the tubes were mill-annealed Alloy 600 (600MA[1]), an alloy with about 72% nickel and 15% chromium. About 10 years later, in the early 1980s, the tubes in new steam generators were upgraded to be in the thermally treated (TT) condition, i.e., to 600TT, which resulted in an improved microstructure and lower residual stresses. Other steam generator design improvements, such as use of stainless steel supports, broached holes, and full depth hydraulic expansions in the tubesheet, were also introduced at the same time. Starting about 1989, the tube alloy was changed to Alloy 690TT, with a chromium content of about 30%. The corrosion experience with these four types of alloys (stainless steel, 600MA, 600TT, and 690TT) has been quite different, as summarized below.

- *Steam generators with stainless steel tubes*. In early (noncommercial) plants such as Shippingport and the New Production Reactor with horizontal steam generators, stress corrosion due to caustics or chlorides severely affected Type 304 stainless steel tubes and changes were made to use 600MA tubes (Bush and Dillon, 1973). However, experience at the three commercial WE plants built in the early to mid-1960s with Type 304 or Type 316 stainless steel tubes, Yankee Rowe, Chooz A, and Trino Vercellese, was generally satisfactory until the plants were permanently shut down for nonsteam generator reasons. Plugging of tubes at these plants was limited, with two of the plants plugging tubes only for fretting, while the other (Yankee Rowe) plugged limited numbers of tubes for phosphate-induced wastage, intergranular attack/stress corrosion cracking (IGA/SCC), pitting, and fretting (AECL, 1975–1992). The good experience at these plants with stainless steel tubes may have been due in part to the relatively low hot leg temperatures of these plants, 288°C, 302°C, and 298°C, respectively, as compared to the typical hot leg temperature of many later plants of about 323°C.
- *Steam generators with Alloy 600MA tubes*. WE and CE type steam generators with mill-annealed Alloy 600 tubes (600MA) have experienced a large variety of corrosion problems that initiated from both the primary side and secondary side of the tubes (e.g., Gorman et al., 2003; Staehle and Gorman, 2003). As a result of these problems, almost all of the original steam generators with 600MA tubes have been replaced or are scheduled to be replaced.

[1] Alloy 600MA tubing was used in two main conditions, a low temperature mill annealed (LTMA) condition typical of Westinghouse units and a high temperature mill annealed (HTMA) condition typical of Combustion Engineering units. The LTMA condition generally was more susceptible to both primary and secondary side corrosion problems than the HTMA condition.

The main corrosion modes that have affected 600MA tubes are illustrated in Fig. 7.1 and listed in Tables 7.1–7.3; it should be understood that other modes have also affected small numbers of tubes. More details regarding the main modes are provided in later parts of this chapter and in other chapters in this book. It should be noted that the corrosion mode identified as IGC or intergranular corrosion in Fig. 7.1 is more commonly called IGA or intergranular attack, and that the corrosion mode identified as LPSCC or low potential stress corrosion cracking in Fig. 7.1 is more commonly called PWSCC or primary water stress corrosion cracking.

- *Steam generators with Alloy 600TT tubes*. WE type steam generators with Alloy 600TT tubing have experienced much less corrosion than steam generators with 600MA tubing. The main experience with corrosion of 600TT tubes has been PWSCC in areas where there was significant cold work of the tubes during fabrication of the SGs, e.g., at kiss-rolled transitions (see Fig. 7.2) (EPRI, 1994). This has led to replacement of steam generators with 600TT tubes at several plants, and the planned replacement at many more in France (World Nuclear News, 2011). In the United States, there also have been significant numbers

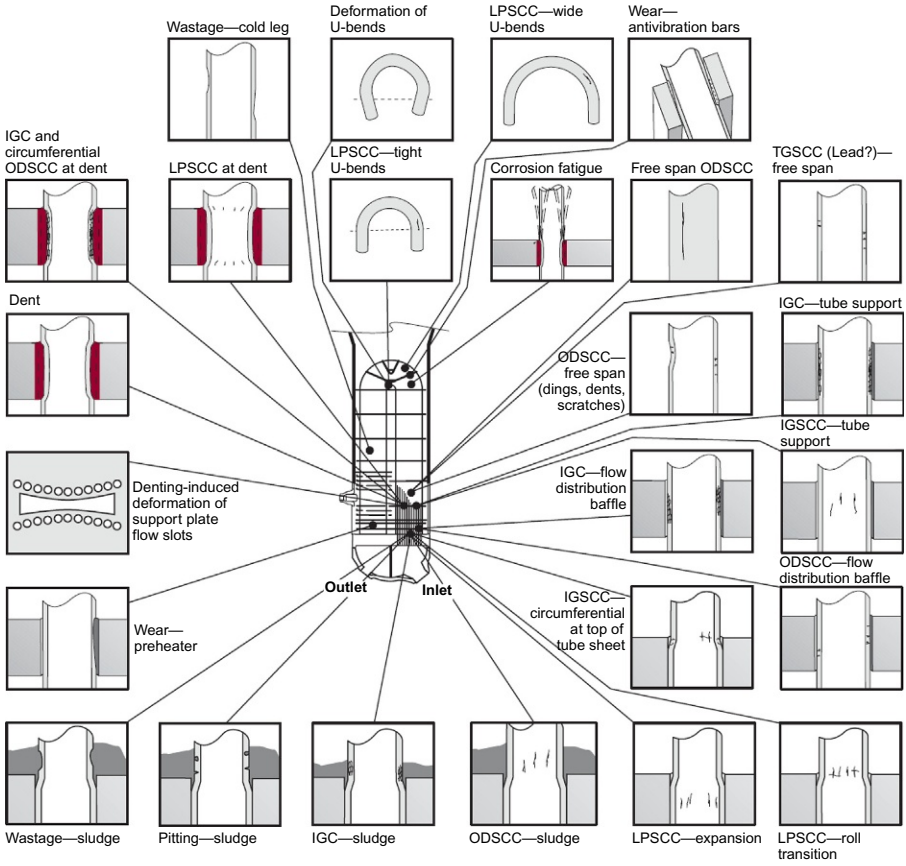

Fig. 7.1 Array of corrosion modes that have affected recirculating steam generators (Staehle and Gorman, 2003).

Table 7.1 Primary side corrosion modes affecting steam generators with Alloy 600MA tubes

Predominant location	Description
Hot leg bottom end	PWSCC of welds and bottom tack rolls
Hot leg and cold leg hard roll expansion overlaps	Axial and circumferential PWSCC of high stress deformed areas at overlaps of roll expansion passes
Hot leg and cold leg roll expansion transitions	Axial PWSCC of roll expansion transitions located deep in tubesheet in part depth roll units and at the top of the tubesheet (TTS) of full depth rolled or explosively expanded units
Hot leg sleeve joints	PWSCC of hot leg sleeve joints made using hydraulic expansions, explosive expansions, or welds
Hot leg and cold leg dents	Axial and circumferential PWSCC at dents at tube support plates (TSPs) and less commonly at the TTS
Hot leg free span dings	PWSCC at free span dings, mostly on the hot leg side
Top of U-bends	Axial PWSCC at top of U-bend, sometimes caused by denting-induced deformation, other times by as fabricated ovalization
Tight radius U-bends	Axial PWSCC at transitions of row 1 or row 2 U-bends at deformations and cold work associated with use of metal ball mandrels
Small radius U-bends	PWSCC of row 1 to 10 U-bends associated with cold work and stresses from bending

Table 7.2 Secondary side corrosion modes affecting steam generators using phosphate water chemistry

Predominant location	Description
Hot leg TTS and TSPs and hot leg deep tubesheet crevices	IGA/SCC caused by caustics associated with use of phosphate water chemistry in early PWRs
Hot leg TTS and TSPs	Wastage-induced wall thinning associated with use of phosphate water chemistry in early PWRs

of tubes affected by PWSCC at hot leg tube-to-tubesheet welds and in the bottom tack roll area (NRC, 2005); however, tubes with these indications are not considered to raise safety or performance issues and generally are allowed to remain without repair in accordance with alternate repair criteria that have been accepted by the U.S. NRC.

Steam generators with 600TT tubes have also experienced small amounts of secondary side corrosion. For example, in 2002 a number of tubes were detected with IGA/SCC at both hot leg and cold leg TSPs at Seabrook (NRC, 2013a), and a number of tubes have experienced IGA/SCC at the TTS in Vogtle 1 (NRC, 2008).

- *Steam generators with Alloy 690TT tubes*. WE and CE type steam generators with Alloy 690TT tubing have experienced no confirmed corrosion from either the secondary side or the primary side, with one possible exception. This possible exception is that there have

Table 7.3 Secondary side corrosion modes affecting steam generators using AVT water chemistry

Predominant location	Description
Hot leg deep tubesheet crevice	Axial SCC, also some IGA
Hot leg TTS crevices and deposit collars	Circumferential IGA/SCC, often most severe at edges of sludge piles
Hot and cold leg sludge piles on TTS	Pitting, often more severe on cold leg side than on hot leg side
Hot leg sludge piles	Axial and volumetric IGA/SCC
Hot leg TSPs and TTS	Denting caused by corrosion of carbon steel supports, low alloy steel tubesheets, and iron shot in the sludge pile
Lower elevation hot leg free spans	Axial SCC, often associated with presence of lead
Hot leg TSPs	Axial and circumferential SCC, often associated with some denting
Upper elevation hot leg free spans and supports	Axial IGA/SCC associated with accumulation of deposits in upper elevation regions of CE type SGs
Top TSPs and AVBs	Corrosion fatigue leading to large circumferential cracks
U-bend AVBs and supports	Fretting-induced wear at AVBs and flat supports in U-bend and square bend areas, probably with some corrosion-induced acceleration
Cold leg TSPs, generally at peripheral lower elevation locations	Wastage, generally attributed to accumulation of acidic sulfur species combined with fretting induced by tube vibration
Cold leg free spans in WE preheat units	Axial SCC, generally associated with lines of severe abrasion or scratching

some amounts of tube fretting wear experienced at AVBs and loose parts. While this wear might have some corrosion involvement, it is considered to be dominated by mechanical factors, i.e., flow-induced vibration (FIV) caused impacts and sliding, and not to be associated with the type of tubing alloy.

7.1.1.2 PHWR steam generators

PHWR steam generators are of the U-bend recirculating type. Some have a configuration similar to that shown in Fig. 1.4, without an integral preheater, while others have preheaters, similar to that illustrated in Fig. 1.8. Three types of tubing alloys have been used: Alloy 400, Alloy 600, and nuclear grade Alloy 800 (800NG).

- PHWR steam generators with Alloy 400 tubing. This type of steam generator is used at Pickering A, Units 1 and 4 (Units 2 and 3 have been laid up since 1997), and at Pickering B, Units 5–8. The main corrosion modes that have affected these units are as follows (Brennenstuhl et al., 2009; Pagan et al., 2007):

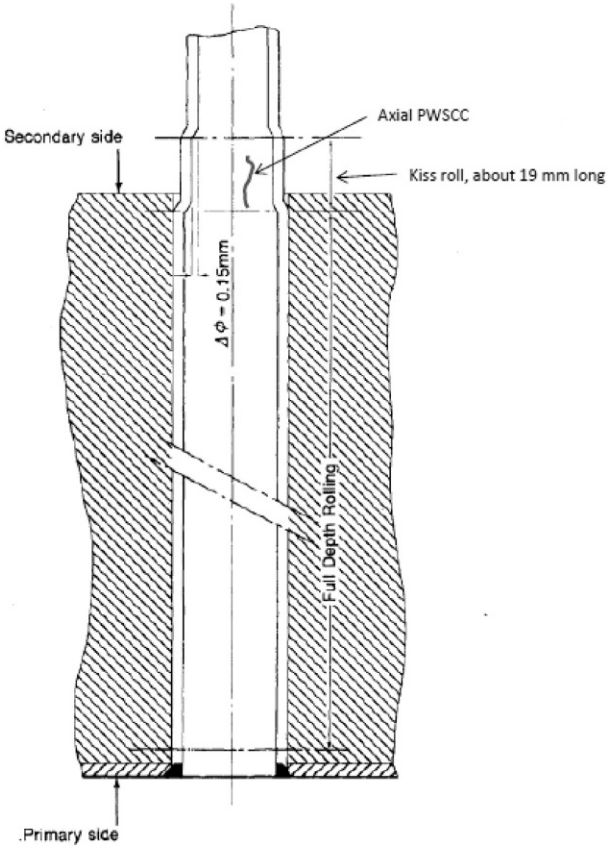

Fig. 7.2 PWSCC at kiss rolls (EPRI, 1994).

- The most significant corrosion mode is under deposit corrosion at the TTS and at supports, which has commonly been called pitting. It has most seriously affected Pickering B5, but Pickering A units have also been affected to a lesser extent.
- Pickering B has also been affected by an erosion-corrosion thinning mechanism at the top of broached hole TSPs.
- There have been some cases of secondary side IGA detected in Pickering A at under deposit locations.
- In addition, there has been some IGA detected on the primary side of tubes at Pickering Units 1 and 2 associated with high levels of boron at the grain boundaries.
- Several of the Pickering units have been affected by thinning at the top of the cold leg tubesheet and at supports.
- With the exception of a couple of tubes where cracks have occurred at manufacturing defects, the Pickering steam generator tubes have been free of detected SCC (Pagan et al., 2007).

• PHWR steam generators with Alloy 600SR tubing. This type of steam generator is used at Bruce A, Units 3 and 4 (Units 1 and 2 have been replaced with Alloy 800NG steam

generators), and Bruce B, Units 5–8. The tubing in these units is sensitized as a result of vessel stress relief heat treatments. The main corrosion modes that have affected these units are as follows (Warr et al., 1987; Roy, 1994; Clark et al., 1998, 2006; Nickerson and Maruska, 1998; Tapping et al., 2000; Durance, 2009):
  - Corrosion fatigue of U-bends in Bruce A.
  - IGA/SCC at U-bend supports in Bruce A associated with deformation and denting caused by deposit buildup and corrosion of carbon steel scallop bar type antivibration supports. This mode was aggravated at Bruce A2 by the ingress of lead.
  - Circumferential PWSCC and secondary side IGA/SCC at the TTS of Bruce A3 and A4.
  - Circumferential IGA evolving into IGA/SCC at the TTS of Bruce A4; this mode was essentially stopped by changes to shut down and start-up practices that minimized development of oxidizing conditions.
  - Fretting wear in Bruce B, especially Unit B8, associated with flow accelerated corrosion (FAC) of the upper TSPs.
- PHWR steam generators with Alloy 800NG tubing. This type of steam generator is used at CANDU 6 plants and at Darlington, and as replacements at Bruce 1 and 2. The main corrosion modes that have affected these units are as follows (Brennenstuhl et al., 2009; Gorman et al., 2009a; Luna et al., 2009):
  - Pitting and wastage at the TTS and supports at Point Lepreau associated with the use of phosphate water chemistry during its first years of operation. The other Alloy 800NG units have not experienced this problem since they have always used AVT water chemistry.
  - Fretting-induced wear at AVBs and due to loose parts. Fretting at Embalse was aggravated by FAC of carbon steel supports; this factor has not been involved at the other CANDU 6 units or at Darlington since they have stainless steel supports.

7.1.2 PWR steam generators of the KWU/Siemens/AREVA type with Alloy 800NG tubing

This type of steam generator has Alloy 800NG tubing and austenitic stainless steel supports. Both feedring and preheater type designs have been used. The main corrosion modes that have affected this type of unit include (Kilian et al., 2007, 2011; Gorman et al., 2009b; de Diego et al., 2014; Wallin et al., 2010; IAEA, 2011):

- Wastage-induced thinning at the TTS and supports in earlier units that operated using phosphate water chemistry.
- IGA/SCC in deep tubesheet crevices at two older units (Biblis A and Unterweser), and probable IGA/SCC at the top of the tubesheet and at supports at Unterweser.
- Circumferential IGA/SCC at the TTS at dents in sludge pile regions at two units with replacement steam generators in Spain.

7.1.3 PWR once-through steam generators (OTSGs) with Alloy 600SR tubing

This type of steam generator had mill-annealed Alloy 600 that was heat treated as part of the vessel's post weld stress relief heat treatment and is thus designated as Alloy 600SR. The Alloy 600SR tubing was sensitized by the stress relief heat treatment and is sometimes designated as Alloy 600Sen or Alloy 600SN. All units of this type have

been replaced with units with Alloy 690TT tubing. The geometry of this type of steam generator is illustrated in Figs. 1.6 and 9.2. The main types of corrosion that affected this type of steam generator were as follows (EPRI, 1994; Jones et al., 1983; Sherburne, 1998; Rochester and Eaker, 1999):

- Circumferential cracks at the upper tubesheet lower face and at the top TSP caused by corrosion fatigue associated with FIV.
- Erosion-corrosion-induced thinning of tubes at TSPs.
- Secondary side IGA/SCC in upper tubesheet crevices.
- Primary side IGA/SCC, mainly in the upper tubesheet area, associated with a sulfur ingress event at TMI 1 during its long layup following the TMI 2 accident in 1979.
- PWSCC of tubes in the roll transition region in the upper tubesheet.
- Secondary side axial IGA/SCC in the free span regions in the upper parts of the OTSG. The development of increasing amounts of this mode of tube degradation was the main driver for the replacement of the OTSGs with 600SR tubing with new units with Alloy 690TT tubes.

7.1.4 VVER[2] SGs with stabilized stainless steel tubes

This type of steam generator is used in all of the Russian design VVER PWRs, including the 440 and 1000 MWe size units. The steam generators are horizontal units with horizontal U-bent tubes that attach to hot and cold vertical collectors (large pipes that are also called headers). The general arrangement is shown in Fig. 5.1. The collector walls take the place of the tubesheet in vertical PWR and PHWR recirculating steam generators. The tubing material in these units is titanium-stabilized austenitic stainless steel with the designation 08X18Nl0T and is similar to AISI Type 321 stainless steel.

The main corrosion problems that have affected the tubing in VVER steam generators are as follows (Miroslav and Stefan, 1994; Rucsak et al., 1998; Kadenko et al., 2003; Trunov et al., 2010; Yurmanov et al., 2010; Kukushkin, 2010; IAEA, 2007):

- Pitting and SCC associated with deposit buildup on tubes as a result of corrosion product (Cu and Fe) ingress from the secondary system. The SCC often starts from the base of a corrosion pit.
- Pitting and SCC at support straps.
- The above pitting and SCC occurs predominantly in the region near the hot collector (also known as the hot header) and is generally attributed to chlorides aggravated by oxidizing conditions associated with ingress of copper.
- Limited general corrosion.

7.2 Primary side stress corrosion cracking (PWSCC)

Discussion of PWSCC in this chapter is limited since the next chapter (Chapter 8, "Environmental degradation of materials in nuclear steam generators") provides

[2] VVER is also written as WWER. The initials stand for the name in Russian and mean "water water energy reactor," indicating that the reactor is water cooled and water moderated.

an in-depth review of this topic. PWSCC is also known as LPSCC since it occurs at low electrochemical potentials near the hydrogen line in a Pourbaix diagram, rather than at the higher potentials associated with oxidizing conditions (Staehle and Gorman, 2003).

7.2.1 Types of steam generators affected, and locations affected by PWSCC

The types of steam generators that have been affected by PWSCC are those with 600MA, 600TT, and 600SR tubing.

600MA units. Steam generators with 600MA tubes have experienced the most severe amounts of PWSCC. The most severely affected locations in these units have been:

- Roll and explosive expansion transitions. This has most strongly affected hot legs, but cold legs have also been affected.
- Roll overlaps in hard rolled areas in the tubesheet. This has most strongly affected hot legs, but cold legs have also been affected.
- Areas in the tubesheet where tubes were rolled into machining irregularities (often called bulges).
- Dents caused by corrosion of carbon or low alloy steel at the top of the hot leg tubesheet and at both hot leg and cold leg support elevations.
- Dings and dents in free span areas.
- Tight radius U-bends. For many years this was limited to rows 1 and 2 but after about 20 years of operation, PWSCC started to be observed at rows up to about row 10 (NRC, 2003).
- Sleeve joints made by expansion methods or welding that were not stress relief heat treated.

600TT units. Steam generators with Alloy 600TT tubing have experienced significantly less PWSCC than those with 600MA tubing. The main locations affected by PWSCC in 600TT steam generators have been (EPRI, 1994; NRC, 2008):

- Kiss roll expansion transitions. This mode is limited to those steam generators that were fabricated using kiss rolls at the top of the tubesheet, e.g., many units in France. In response to the detection of this problem, peening was performed of the top of the tubesheet area of units with kiss rolls, which served to reduce the severity of the attack.
- Hard roll transitions in at the top of the tubesheet. This mode of PWSCC occurred in a Japanese plant with 600TT tubes that had been full depth hydraulically expanded and then also hard roll expanded for the full depth of the tubesheet. The affected steam generators have been replaced.
- Dented regions at the top of the tubesheet in Alloy 600TT units that have experienced denting in this region, probably as the result of the accumulation and subsequent corrosion of steel shot in the sludge piles on the tubesheet.
- Hot leg tube ends in 600TT units in the United States This mode has affected the tube-to-tubesheet weld and also the tack roll area at the bottom of the tubesheet (NRC, 2008).

600SR units. Steam generators with Alloy 600SR tubing have experienced relatively little PWSCC. The main occurrences have been as follows (Clark et al., 1998; Sherburne, 1998; Davis-Besse Nuclear Power Station, 2012):

- Circumferential PWSCC at the hot leg TTS at Bruce A.
- PWSCC in OTSGs at the upper (hot leg) tube end (tube to tubesheet weld), at the upper rolled area and at the upper roll expansion transitions.
- PWSCC in OTSGs at the lower (cold leg) tube ends and roll expansion transitions.

In addition to the above cases of PWSCC, TMI 1 experienced a severe occurrence of primary side IGA associated with a sulfur ingress event during its long layup after the TMI accident (Sherburne, 1998). The mechanism involved in this attack, IGA caused by reduced sulfur attack of sensitized grain boundaries at relatively low temperature, was very different from the high-temperature PWSCC discussed above.

800NG and 690TT units. There have been no reports of PWSCC affecting steam generator tubing made of Alloy 800NG or Alloy 690TT, despite units with these tube materials having been in operation since 1972 and 1989, respectively.

7.2.2 Conditions required for occurrence of PWSCC and factors that increase the rate of PWSCC

This topic is covered in depth in the next chapter. In summary, as for all SCC, a susceptible material, an aggressive environment, and tensile stresses are required for PWSCC. For this specific application, these factors are as follows (EPRI, 1994):

- *Material*. Tests and experience show that Alloy 600 ranges from low susceptibility to high susceptibility to PWSCC depending on its thermomechanical history and the resulting microstructure. The strongest correlation is with the carbide microstructure, with susceptibility increasing as the density of carbides on grain boundaries decreases and as the density of intragranular carbides increases. Susceptibility also tends to increase as strength levels and amounts of cold work increase.
- *Environment*. Normal primary coolant with lithium, boron, and hydrogen has been found to cause PWSCC. Variations in the concentrations of these species and in the resulting pH and potential affect the rate of PWSCC, but these effects are too complex to discuss here and are left to the next chapter.
- *Stress*. The time to occurrence of PWSCC is strongly affected by the total tensile stress at the wetted surface and is often modeled as decreasing as stress raised to the inverse fourth to seventh power.

7.2.3 Consequences of PWSCC and likelihood of future occurrence

The occurrence of PWSCC has been the main factor resulting in the replacement of steam generators in France, first for units with 600MA tubing and then for units with 600TT tubing. It has also been a factor in replacements of steam generators in the United States, Japan, and Korea although secondary side attack has generally been more important in these countries.

With regard to the likelihood of future occurrence of PWSCC, the situation is as follows:

- *600MA*. For those remaining steam generators with 600MA tubing, PWSCC is likely to be an important life limiting factor. This is the result of the high susceptibility of Alloy 600MA to PWSCC.

- *600SR*. For those few operating units with 600SR tubing (e.g., Bruce B), PWSCC may affect limited numbers of tubes but is not likely to be a life limiting factor.
- *600TT*. For 600TT units with kiss rolls, the occurrence of PWSCC has been found to be a life limiting problem. However, for those units that peened the kiss roll area before start of operation, the rate of PWSCC may be so slow that it does not impact lifetime. Similarly, units in the United States without kiss rolls seem likely to find that PWSCC will not strongly affect unit lifetime since the tube end area that is most affected by PWSCC has been granted relief using the H* criteria (e.g., NRC, 2013b).
- *690TT and 800NG*. The risk of PWSCC affecting units with these tubing materials is considered to be negligibly small.

7.3 Denting

The term "denting" is used to describe the situation where expansion of carbon steel corrosion products on the outside of a tube results in inward deformation of the tube. A typical dent is illustrated in Fig. 7.3. This type of denting occurs most readily if the hole in the tube support plate is a round drilled hole. However, denting has also occurred at broached hole supports and at lattice bar and flat plate supports.

7.3.1 Locations where denting has occurred

Locations where denting has occurred include:

- Drilled hole carbon steel tube support plates
- At the top of carbon or low alloy steel tubesheets in steam generators with part depth rolled tubes, i.e., where there are deep tubesheet crevices, and also in some steam generators with full depth expanded tubes
- At carbon steel lattice bar, scallop bar, and flat bar supports
- At carbon steel broached hole tube supports
- In sludge piles at the top of the tubesheet where carbon steel foreign material such as shot used for blasting has collected and corroded

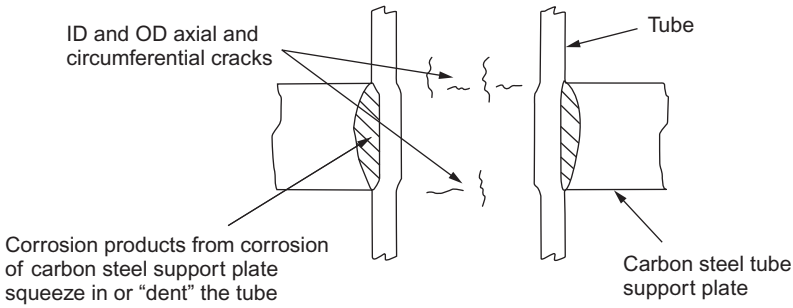

Fig. 7.3 Denting at tube support plate.

7.3.2 Types of steam generators affected by denting

The steam generators that have been most severely affected by denting are those with Alloy 600MA tubes. This is not a result of the tube material but rather the result of using carbon steel supports in these steam generators and the types of water chemistry used in these plants. There have been lesser amounts of denting in plants with 600TT, 800NG, and 690TT tubing. This is a result of the use of stainless steel supports in these units, together with improved water chemistry in the plants with these types of steam generators.

7.3.2.1 Materials and design features required for denting to occur

The essential features required for denting of a tube to occur include:

- A readily corrodible material such as carbon or low alloy steel in close proximity to the tube
- A crevice between the tube and the corrodible material in which impurities can concentrate and lead to aggressive conditions fostering corrosion of the carbon or low alloy steel
- Sufficient heat flux to cause boiling and concentration of chemicals in the crevice
- Water chemistry conditions conducive to the concentration of impurities to aggressive levels in occluded areas of the steam generators coupled with the presence of oxidants such as copper oxide. These adverse chemistry conditions were most commonly the result of condenser leaks at plants with salty cooling water, but also occurred in a few freshwater-cooled plants, e.g., as the result of ingress of condensate polisher resins

The most effective ways to prevent or minimize denting are to (1) use design features that minimize susceptibility, e.g., use stainless steel supports and design features that minimize crevices at the OD of tubes, such as lattice bar supports; (2) control of water chemistry conditions to minimize factors that aggravate denting, such as minimizing ingress of chlorides, copper, and resin particles; and (3) ensuring that reducing conditions are achieved early during start-ups. In addition, it is necessary to ensure that foreign materials such as iron shot from blasting operations are not allowed to enter the steam generators.

7.3.2.2 Consequences of denting and likelihood of future occurrence

The main consequences of denting are (1) the strains and stresses developed in the tube at the dents increase the likelihood of SCC occurring from both the primary and secondary sides of the tubes and (2) the deformation can interfere with inspection of the tube and require it to be plugged for that reason. As noted earlier, steam generators with 600TT, 800NG, and 690TT tubes have experienced less denting than units with 600MA tubes. The lower amount of denting, together with the increased resistance to cracking of these alloys, has resulted in there being relatively little or no denting caused SCC, and it is expected that this relative freedom from denting-induced SCC will continue in the future. However, since the tubesheet is low alloy steel, denting can and has occurred in these types of steam generators as

a result of corrosion at the top of the tubesheet crevice between the tube and tubesheet. In addition, denting could occur if iron foreign material is introduced into the steam generators and collects in the sludge piles on the tubesheet, e.g., as the result of blasting elsewhere in the secondary system. Thus, ensuring that denting does not occur requires good control of water chemistry conditions and effective foreign material exclusion practices.

7.3.3 Secondary side wastage

Wastage, also known as thinning or general corrosion, has occurred on the secondary side of steam generator tubes under some circumstances.

7.3.3.1 Locations where wastage has occurred

The most significant occurrences of wastage have been in units operating on phosphate water chemistry. This mode of corrosion affected WE and CE units with Alloy 600MA tubing until they converted to AVT chemistry in the mid to late 1970s (EPRI, 1994). KWU/Siemens/AREVA steam generators with Alloy 800NG tubes were also affected until most of the units were converted to AVT water chemistry in the 1980s (Bouecke and Odar, 1991). One CANDU PHWR plant with Alloy 800NG tubes that operated on phosphate water chemistry also experienced some limited wastage and pitting until it converted to AVT in 2000 (Gorman et al., 2009b). The wastage at all of these units mainly occurred in sludge piles on the tubesheet hot leg side and at hot leg tube supports and was attributed to development of aggressive phosphate species that developed in occluded areas as a result of concentration associated with boiling in the occluded areas.

Wastage to a limited extent has also occurred in steam generators operating on AVT chemistry. This includes some VVER steam generators with stabilized stainless steel tubes where the wastage is reported to have occurred under heavy sludge deposits on the horizontal tubes. It has also occurred at cold leg peripheral tube supports of vertical steam generators with Alloy 600MA tubing, where it appears to have been aggravated by fretting (EPRI, 1987), and in the sludge piles on the cold leg side of this type of plant, such as Point Beach 2.

7.3.3.2 Conditions required for wastage to occur

If phosphate water chemistry is used, wastage can occur in occluded areas as a result of the concentration of aggressive phosphate species, especially if low sodium to phosphate ratios are used to minimize risks of development of caustic conditions.

Wastage that has occurred in units operating on AVT chemistry is generally attributed to concentration of aggressive chloride and sulfur species that developed in occluded areas as a result of concentration of these species associated with boiling.

7.3.3.3 Consequences and likely future occurrence of wastage

Wastage has been brought under control such that it is now rarely important. This has been achieved by:

- Converting from phosphate water chemistry to AVT.
- Minimizing the rate of ingress of chlorides and sulfates by means of strict controls on water chemistry and by upgrading condensers.
- Minimizing the development of deposits of sludge on tubes, on tubesheets, and at supports by secondary system water chemistry controls that result in low ingress of iron and copper corrosion products. This has involved many factors, including elimination of copper alloys from secondary systems, use of advanced amines to allow higher pH values in the secondary system, etc.
- Removing deposits and sludge from the secondary side of steam generators by mechanical and/or chemical cleaning.

The current situation is that wastage is unlikely to occur to a significant extent in currently operating steam generators, regardless of the tubing material used. However, this could change if current stringent water chemistry practices were relaxed such that deposit buildup worsened and levels of impurity ingress increased.

7.3.4 Secondary side pitting

Pitting has seriously affected vertical steam generators at several PWRs and PHWRs and also has affected horizontal steam generators at many VVER plants, as discussed in the following sections.

7.3.4.1 Pitting in vertical PWR steam generators

The most seriously affected PWRs with vertical steam generators were Indian Point 3, Millstone 2, and Kori 1, all of which had 600MA tubing and salty cooling water (EPRI, 1994; Hwang et al., 2003). The pitting affected both the hot and cold legs but generally was worse on the cold leg. The pitting was attributed to development of sludge piles on the tubesheets coupled with ingress of aggressive chlorides and sulfur species and also with the ingress of oxidants such as copper oxides. The morphology of a typical pit is shown in Fig. 7.4. Susceptibility to this type of pitting has been resolved by:

- Significant upgrades to plant secondary systems to minimize ingress of corrosion products, aggressive anions, and oxidants
- Use of mechanical and chemical cleanings to remove accumulated deposits
- Replacement of steam generators

It is judged that pitting is unlikely to seriously affect any of the currently operating vertical PWR steam generators, assuming that current stringent water chemistry practices are maintained. In this regard, it should be understood that all of the tubing alloys, including 600MA, 600TT, 600SR, 690TT, 800NG, and stabilized stainless steel are susceptible to pitting if aggressive conditions are allowed to develop on the secondary side as the result of ingress of corrosion products, aggressive anions, and oxidants.

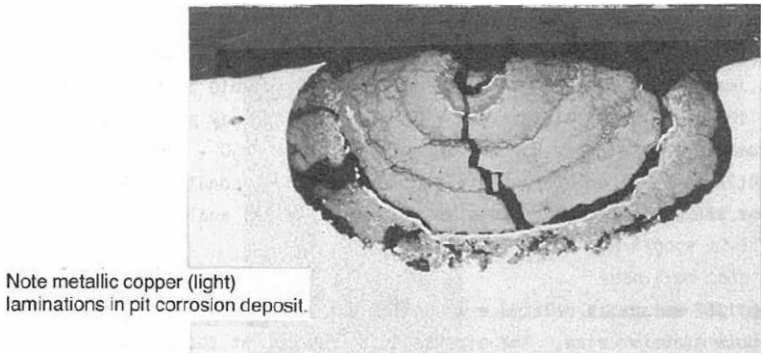

Fig. 7.4 Photomicrograph of pit from Indian Point 3 (EPRI, 1997).

7.3.4.2 Pitting in vertical PHWR steam generators

Pitting has affected the Alloy 400 tubing in several of the Pickering steam generators, with Unit B5 being the most seriously affected. The pitting has occurred mainly on the hot leg in the sludge pile region and has been attributed to the accumulation of deposits coupled with the presence of chlorides and sulfur species and oxidizing conditions associated with start-ups (Clark et al., 2006). This mode of corrosion has been brought under control by water chemistry improvements that minimize ingress of impurities and that also minimize development of oxidizing conditions (e.g., stricter control of hydrazine and minimizing condenser leaks), and chemical cleanings and sludge lancing to reduce the amount of deposits (Brennenstuhl et al., 2009).

7.3.4.3 Pitting in horizontal VVER steam generators

Early VVERs experienced significant amounts of pitting on the secondary side of the stabilized stainless steel tubing used in these units. This pitting sometimes led to development of stress corrosion cracks emanating from the base of the pits (Trunov et al., 2010). This mode of attack was generally most severe near the hot collector. The pitting was attributed to development of deposits and sludge piles on the horizontal tubes, coupled with ingress of aggressive chlorides and sulfur species and also the ingress of oxidants such as copper oxides. Susceptibility to this type of pitting has been largely resolved by:

- Significant upgrades to plant secondary systems to minimize ingress of corrosion products, aggressive anions, and oxidants
- Use of mechanical and chemical cleanings to remove accumulated deposits
- Replacement of steam generators at some plants

The above measures are reported to have brought the pitting and associated SCC situation under control such that they are unlikely to limit the lifetime of the steam generators. However, these modes of degradation remain active at low levels and require that current water chemistry, maintenance, and inspection practices be maintained at effective levels.

7.3.5 Secondary side intergranular attack

This mode of degradation, which is also known as IGC, has mainly affected steam generators with sensitized Alloy 600 tubing, i.e., Alloy 600SR. The "SR" in 600SR indicates that the tubing was stress relieved during steam generator construction, e.g., for about 12–15 hours at 593–621°C (Sherburne, 1998). The attack is generally attributed to corrosion associated with partially reduced sulfur species such as thiosulfates (Sherburne, 1998). This mode of attack, similar to wastage and pitting, does not require the presence of stresses to occur, although the consequences of IGA can be made more severe if significant tensile stresses are present, since it can lead to development of IGSCC as the depth of the IGA increases and stresses at the tip of the attack also increase. The morphology of typical IGA is shown in Fig. 7.5. It is characterized by fairly uniform attack of grain boundaries with little indication of there being a significant stress component to the attack.

7.3.5.1 IGA affecting OTSGs

Secondary side IGA affected several of the original OTSGs. The attack occurred at locations in the lower temperature (nonsuperheated) parts of the units and was attributed in some cases to attachment of particles of demineralizer resins, which contained sulfur species (EPRI, 1997). This problem never affected large numbers of tubes and has been resolved by replacement of the steam generators with new units with 690TT tubes, which are not susceptible to this mode of attack.

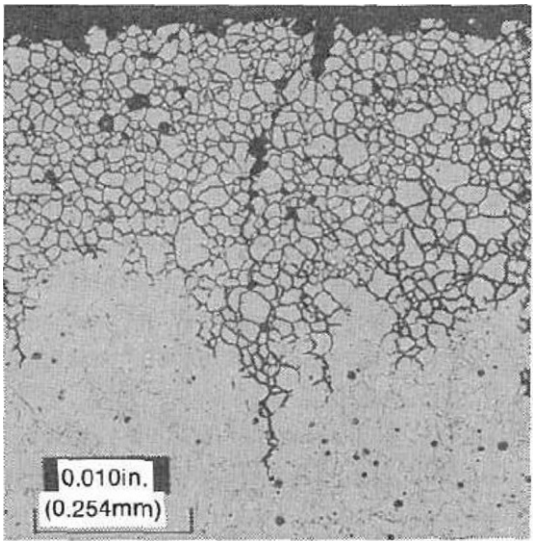

Fig. 7.5 Morphology of IGA of Alloy 600SR tube (EPRI, 1985).

7.3.5.2 IGA affecting PHWR Alloy 600 steam generators

IGA has also affected the Bruce A units, which have or had PHWR recirculating steam generators with Alloy 600SR tubes that were sensitized during steam generator fabrication. The IGA at the Bruce A units has mainly occurred at the hot leg top of tubesheet in sludge pile areas. In some cases, the IGA led to the development of IGSCC. The IGA and associated IGSCC have been attributed to reduced sulfur species attack of the sensitized tubing that occurred as the result of accumulation of sulfur in the sludge over the years of operation coupled with oxidizing conditions that developed during shutdowns and start-ups (Durance, 2009). The occurrence of this type of IGA and IGSCC appears to have been stopped by application of strict water chemistry controls during shutdowns and start-ups that limit exposures to oxidizing conditions.

7.3.5.3 IGA affecting Alloy 800NG tubes

Detailed failure investigation of the indications detected in the deep tubesheet crevice area of tubes in Biblis A indicates that the attack started as IGA due to the presence of aggressive sulfur species and then progressed to IGSCC (Kilian et al., 2011). Similar eddy current indications have been detected at Unterweser (Wallin et al., 2010) and presumably had the same root cause although this has not been confirmed by examination of pulled tubes.

7.3.5.4 Likelihood of IGA affecting new steam generators

It is considered that the tubing materials and design practices used with steam generators with Alloy 600TT, Alloy 800NG, Alloy 690TT, and stabilized stainless steel have high resistance to this mode of attack. However, the occurrence of IGA in the deep tubesheet crevices of two older units with Alloy 800NG tubes indicates that, if sufficiently aggressive crevice conditions develop, IGA and IGA/SCC are possible in this type of tubing.

7.3.6 Secondary side IGA/SCC

This mode of degradation was a major factor in the need to replace steam generators with Alloy 600MA tubes in many plants (Gorman et al., 2003) and remains an important reason for planning to replace the remaining units with Alloy 600MA tubes that are still operating. It also was a dominant reason for replacing OTSGs with Alloy 600SR tubing (Rochester and Eaker, 1999). A form of this type of attack was also a reason for the need to replace a limited number of steam generators with stabilized stainless steel tubes in VVER 1000 steam generators (Trunov et al., 2010). To date, it has only affected small numbers of tubes in units with Alloy 600TT tubing or Alloy 800NG tubing and is not reported to have affected any Alloy 690 tubing.

7.3.6.1 Steam generators with Alloy 600MA and Alloy 600SR tubing

The locations in Alloy 600MA and Alloy 600SR steam generators that have experienced secondary side IGA/SCC include at least the following (they are so numerous that it is difficult to cover them all):

- Deep tubesheet crevices on the hot leg side in units with part depth rolled tubes.
- Top of the tubesheet, both in sludge piles and in top of the tubesheet crevices and deposit collars outside of sludge piles. This attack has mostly occurred on the hot leg side, but some attack has also been observed on the cold leg side.
- In a few plants, freespan areas in the lower hot leg region. This mode of attack generally was associated with the presence of lead.
- Tube support plate crevices. This attack has mostly occurred on the hot leg side, but some attack has also been observed on the cold leg side.
- Upper bundle freespans and tube supports in CE design steam generators. This attack was generally associated with relatively heavy buildup of deposits on the tubes in the upper bundle region.
- Upper bundle freespan areas of OTSGs in the superheated region. This attack has sometimes been associated with the presence of lead deposits on the tube surface.
- Cold leg freespans in the preheater regions of Westinghouse preheat steam generators. This attack has been associated with lines of abrasion or scratches that are assumed to be the result of rubbing of the tubes against tube supports during insertion of the tubes.

7.3.7 Steam generators with Alloy 800NG tubing

There have been no reports of detected secondary side IGA/SCC of Alloy 800NG tubing in CANDU PHWRs. However, there have a few cases of IGA/SCC detected in Alloy 800NG tubing in PWR steam generators of KWU/Siemens/AREVA design, as follows (Kilian et al., 2007; Gorman et al., 2009b; de Diego et al., 2014; Wallin et al., 2010):

- IGA/SCC has been detected in the deep tubesheet crevices of steam generators at Biblis A and at Unterweser. For the most part, this IGA/SCC has been localized to tubes at the periphery of the tube bundle.
- Indications of possible IGA/SCC have been observed at the top of the tubesheet and at the first hot leg tube support at Unterweser. However, tubes have not been pulled to verify the mode of attack associated with the indications at these locations.
- Tubes with circumferential cracks at the top of the tubesheet have been detected at Almaraz 2 and Asco 1 in replacement steam generators at those units. These cracks have been associated with dents at the top of the tubesheet.

7.3.8 Vertical steam generators with Alloy 600TT tubing

Only limited numbers of tubes have been detected with IGA/SCC in units with 600TT tubing. The main occurrences have been as follows (NRC, 2013a and other NRC Information Notices referenced therein):

- Secondary side IGA/SCC was detected at Kori 2 early in life and was associated with denting at the top of the tube sheet and also the presence of lead (Song, 2006). This has led to plugging of more than 100 tubes. Other units in Korea with 600TT tubes have also reported the occasional detection of what appears to be secondary side IGA/SCC.
- Cracks were first detected at broached hole tube supports at Seabrook in 2002 and subsequently have been seen in limited numbers at one or two other U.S. units.
- In 2006 and continuing to the present, small numbers of tubes have been detected with top of the tubesheet IGA/SCC at Vogtle 1.
- In 2012 and 2013, cracks were reported to have been detected at dings and dents in freespan areas at Seabrook and Braidwood 2.

7.3.9 Horizontal steam generators with stabilized stainless steel tubing

IGA/SCC is reported to have initiated from pits in many VVER steam generators and to have affected enough tubes at a few plants to lead to steam generator replacement (Trunov et al., 2010). An example of pitting and associated IGA/SCC is shown in Fig. 7.6. This pitting and IGA/SCC has primarily occurred close to the hot collector and is reported to have occurred under heavy sludge deposits and at supports. Improved water chemistry controls coupled with periodic chemical and mechanical cleaning of the tubes is reported to have resulted in this problem currently affecting only small numbers of tubes and to not be a life limiting problem although continued attention to water chemistry and control of deposits is required.

7.3.9.1 Causes of secondary side IGA/SCC and methods to minimize its occurrence

The main cause of secondary side IGA/SCC is, with one exception, considered to be the accumulation of aggressive species to high concentrations in occluded areas as a result of boiling in the occluded areas. (The one exception to this rule seems to be that of cracks developed in Alloy 600MA tubes in cold legs of preheat units at lines of severe abrasion, where the cracking appears to have occurred in nonconcentrated secondary coolant.) While there is general agreement that secondary side IGA/SCC is

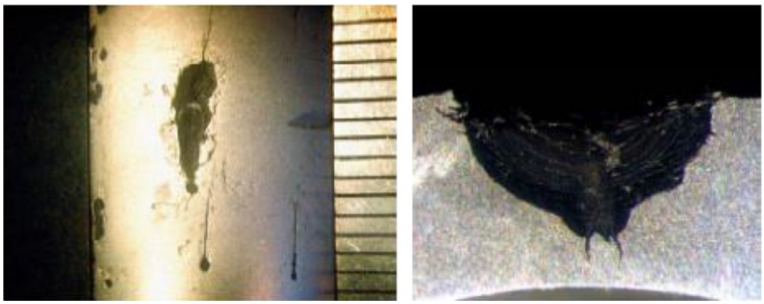

Fig. 7.6 Pitting and associated IGA/SCC in a VVER steam generator tube (IAEA, 2007).

mainly caused by the accumulation of aggressive species in occluded areas, there is uncertainty regarding what specific species are involved and regarding what other factors such as pH, ionic strength, or ECP are involved. In a few cases, the causes of secondary side IGA/SCC have been firmly identified, such as cases associated with ingress of large amounts of lead. However, for the most part, and despite many years of extensive research, firm conclusions have not been reached regarding the specific chemical species that have been involved in the IGA/SCC that has affected Alloy 600MA tubing.

Despite there being uncertainty regarding the chemical species involved in the secondary side IGA/SCC of 600MA tubing, some useful general observations have been developed regarding how to minimize its occurrence, as follows:

- Observation of strict limits on water chemistry during power operation and shutdown/start-up periods have successfully limited the rate of occurrence of secondary side IGA/SCC although they have not prevented continuing slow rates of occurrence. These limits include limits on ingress of species such as chlorides, sulfur species and sodium, and also limits on the ingress of oxidants such as oxygen and copper oxides.
- It has been found necessary to ensure that reducing conditions are maintained in steam generators when temperatures are over about 120°C. During power operation this is generally accomplished by addition of oxygen scavengers to the feedwater. During and following layup periods steps are taken to minimize the oxidation of species such as copper that could raise the potential during subsequent power operation (again using oxygen scavengers) and to reduce any oxides that did develop during the outage during the return to power phase of the start-up.
- Minimizing ingress of lead into steam generators is essential and requires strict observance of foreign material exclusion practices and minimizing the concentration of lead in materials used in components where wear or corrosion could result in the ingress of lead into the steam generators.
- Minimizing the presence of occluded areas where concentration of impurities can occur is important. This involves use of design features such as lattice bar supports that minimize built-in crevices and minimizing ingress and accumulation of deposits in the steam generator that can result in development of occluded areas.

7.3.10 Secondary side fatigue and corrosion fatigue

Fatigue and/or corrosion fatigue have caused the development of large circumferential cracks in tubes in both vertical recirculating steam generators and in vertical OTSGs. In some cases the cracks appear to have been initiated by corrosion mechanisms such as IGA/SCC, and for this reason the failures are covered in this chapter on steam generator tube corrosion problems. However, the fatigue crack growth rates in AVT water have been shown to not differ from those in air (NRC Bulletin, 1988). For this reason, the balance of this section will treat the cracks as "fatigue" rather than as "corrosion fatigue."

The only types of tubes that have been affected by fatigue failures are Alloy 600MA and Alloy 600SR. There have been no reports of fatigue failures in vertical steam generators with tubes made of Alloy 600TT, Alloy 800NG, or Alloy 690TT, and none have been reported as occurring in horizontal steam generators with stabilized stainless steel tubes.

Examples of circumferential fatigue cracks that have affected Alloy 600MA include the following:

- OTSGs (Sherburne, 1998): The original OTSGs had a missing row of tubes (known as the inspection lane) from the center of the tube bundle to the periphery. As a result of this missing row of tubes, moisture reached the top of the tube bundle in this region, despite the rest of the upper part of the tube bundle being superheated. In addition, steam flow rates were higher in the inspection lane region at the top of the tube bundle where the steam bends and flows toward the periphery of the bundle. These conditions led to FIV of the tubes near the inspection lane, especially toward the periphery of the tube bundle. These conditions led to development of circumferential cracks at the bottom of the top tubesheet and at the top of the 15th (top) support plate. This problem was addressed by preventive sleeving of tubes in the susceptible region close to the inspection lane.
- Bruce A (Clark et al., 2006): Fatigue failures caused by FIV occurred in a few tubes in the U-bend region early in the life of these steam generators. A few years later some more fatigue failures occurred due to flow changes associated with removal of secondary side deposits from the steam generators. At Bruce A2, more extensive failures occurred in the same region and were found to be the result of the accidental ingress of lead which aggravated occurrence of OD IGA/SCC at U-bend supports that acted as initiation sites for fatigue cracks. This was a factor involved in the shut down of the unit in 1995 which lasted until restart with new steam generators in 2012.
- Fatigue failures have led to large leaks at several vertical steam generators with Alloy 600MA tubes, including North Anna 1 in 1987 (NRC Bulletin, 1988), Indian Point 3 in 1988 (NRC, 1994), Mihama 2 in 1991 (Yashima, 1991), and Cruas 1 and 4 in 2004–06 (Bodineau and Sollier, 2015). These failures have been attributed to misplaced or poorly designed antivibration supports and/or to changes in flow rates associated with deposit buildup in the steam generators.

While the number of tubes affected by fatigue has been limited, these types of failure are nevertheless significant since they involve rapidly growing cracks and large leaks that are difficult to detect and prevent, and also since they raise safety concerns. The main protection against such failures is use of design features and maintenance practices that minimize the likelihood of their occurrence, combined with enhanced primary to secondary leak monitoring and response procedures. Some of the main lessons learned that need to be taken into account in this regard include:

- High levels of FIV are frequently involved and sometimes have been aggravated by the accumulation of deposits in the steam generators that increase flow rates in local areas and thus increase the driving force for FIV in the affected area. Minimizing accumulation of deposits in the steam generators is an important method for minimizing the risk of this type of failure.
- Denting at supports has been found to increase risks of fatigue occurring at the support. This is attributed to the denting (1) reducing the damping factor at the support, thus increasing amplitudes of vibration; (2) increasing the mean stress in the tube at the support thereby reducing margins to initiation of fatigue cracks; and (3) increasing the likelihood of IGA/SCC occurring at the support, which can act as a crack starter for fatigue. This last factor is the result of the high stresses and strains induced in the tube by the denting. The likelihood of denting can be minimized by use of stainless steel for supports, use of lattice bar supports, minimizing deposit buildup, and good control of water chemistry to minimize ingress of anions and oxidants.

Improper design or improper installation of U-bend supports has been a factor in some of the fatigue failures. This illustrates the need for high levels of quality assurance and control in the design and fabrication of steam generators.

7.3.11 Secondary side wear

Wear of steam generator tubes is driven by FIV that leads to sliding or impact type contact of tubes with support structures or between tubes, or between tubes and foreign objects, and thus is mostly the result of thermal-hydraulic and mechanical factors. However, environmental conditions such as temperature and water chemistry also affect wear rates, which indicates that corrosion processes are also involved (EPRI, 1998). For this reason, secondary side wear is covered in this chapter on corrosion.

7.3.11.1 Wear in vertical steam generators

All types of vertical steam generators have been affected by secondary side wear. Some of the main locations in vertical steam generators where wear has occurred are as follows:

- Wear has frequently occurred at antivibration bars and supports in the upper U-bend or square-bend areas. This is attributed to the cross flows and higher flow velocities that occur in this region. Wear has also been observed at the top horizontal tube supports in this region, which again is attributed to the cross flows and high-flow velocities that occur in this region.
- In vertical preheat steam generators, wear of tubes has occurred at baffles and supports in the preheater region as a result of cross FIV of the tubes.
- Significant amounts of wear have been detected due to tube-to-TSP contact and also due to tube-to-tube contact in some replacement OTSGs.
- Wear caused by contact with loose parts such as welding electrodes has occurred in many areas of steam generators, but mainly in peripheral areas close to the tube sheet where loose parts are introduced with the feedwater.

7.3.12 Wear in horizontal steam generators

While an IAEC document with guidance for inspection of horizontal steam generators includes a mention of wear scars (IAEA, 2007), wear has not been reported as causing significant problems in VVER steam generators (Trunov et al., 2010).

7.3.12.1 Long-term effects of wear

As plant designs have matured, rates of wear have generally decreased as a result of design improvements such as insertion of supplemental antivibration bars. However, experience has also shown that wear can become more severe under some conditions such that the potential for wear-induced problems must be considered as steam generators age and also as new designs are put into service. Two examples of wear problems that support this conclusion include:

- Some replacement OTSGs have experienced significant tube wear problems (e.g., as documented in Alley, 2006; NRC, 2012). The wear problems have required a variety of corrective actions to minimize future rates of wear.

- Severe amounts of wear were detected in replacement steam generators at San Onofre 2 and 3 (NRC, 2012; Dark Days for San Onofre, 2013). The end result of this problem was a decision by the utility to permanently shut down the two units.

7.3.13 Summary comments regarding control of corrosion of steam generator tubes

7.3.13.1 Primary side corrosion

The situation regarding primary side corrosion of PWR steam generator tubes can be summarized as follows:

- Industry experience and laboratory tests indicate that corrosion from the primary side is not likely to be a problem for tubes made using Alloy 690TT, Alloy 800NG, or stabilized stainless steel in either currently operating steam generators or new steam generators. In this regard, it is assumed that new PWR steam generators will be made using one of these three alloys.
- PWSCC has already affected or is likely to affect those remaining steam generators with Alloy 600MA tubing, and thus it is a corrosion mode that will require management. Over the long term it also may affect steam generators made using Alloy 600SR tubes at Bruce. With regard to steam generators that use Alloy 600TT, some amounts of PWSCC have already affected many of them, and it seems likely that additional amounts of PWSCC may occur, such that this possibility needs to be addressed in the life-cycle management of these steam generators.

7.3.14 Secondary side corrosion

The situation regarding secondary side corrosion of PWR steam generator tubes can be summarized as follows:

- *General*. Most or all of the secondary side corrosion modes, including pitting, IGA, and IGA/SCC, are aggravated by development of occluded areas caused by deposit buildups in steam generators, by the ingress and concentration of aggressive species such as chlorides, sulfates, sodium, and lead in occluded areas, and by the ingress of oxidants such as oxygen and copper oxides. Rigorous control of secondary water chemistry during both power operation and shutdown periods has been found to be essential and effective at minimizing the occurrence of these modes of secondary side corrosion. Meeting these water chemistry limits requires appropriate plant design features such as leak tight condensers, nonuse of copper alloys in secondary system heat exchangers, nonuse of lead containing materials in secondary system components, appropriate equipment for producing oxygen free makeup water, etc.
- *Wear*. The main degradation mode affecting new steam generators with corrosion-resistant tubing is wear at supports and at foreign objects (loose parts). Methods to minimize such problems include:
  - Use of steam generator design features that minimize FIV and thus wear at supports
  - Use of plant design features coupled with implementation of water chemistry practices that minimize the ingress and accumulation of deposits in the steam generators so that deposit buildup does not cause changes to flow patterns that result in excessive FIV

  - Use of steam generator design features that minimize the ingress of foreign objects, coupled with implementation of strict foreign material exclusion practices at manufacturing facilities, during plant construction, and during plant repair and maintenance activities
  - Performance of optimized foreign object search and removal practices (FOSAR) to detect and remove foreign objects that have entered the secondary side of the steam generators
- *Deposits*. As indicated above, accumulation of deposits in steam generators is a main factor involved in both secondary side corrosion problems and in the occurrence of FIV caused wear. For this reason it is important that plant designs and operating practices minimize the introduction of corrosion products into the steam generators. In addition, the accumulation of secondary side deposits needs to be regularly monitored and appropriate actions taken to remove deposits such as by sludge lancing and chemical cleaning. Minimizing accumulation of deposits in the steam generators also is expected to minimize the degradation in thermal performance that can be caused by accumulation of deposits.

References

AECL, 1975–1992. "Steam Generator Performance Report" for various years, report numbers AECL-5013 dated 1975, AECL-5242 dated 1975, AECL-5625 dated 1976, AECL-6095 dated 1978, AECL-6410 dated 1979, AECL-6582 dated 1980, AECL-7251 dated 1981, AECL-7689 dated 1982, AECL-8179 dated 1983, AECL-8268 dated 1864, AECL-9107 dated 1986, AECL-9724 dated 1988, and AECL-10000 dated 1992.

Alley, C.T., 2006. Duke Energy—Oconee Nuclear Station Steam Generator Wear Root Cause Update with NRC. Meeting Slides Available at NRC Accession No. ML061140370.

Bodineau, H., Sollier, T., 2015. "Tube support plate clogging up of French PWR steam generators" Eurosafe. (available on NRC website at ML15161A223).

Bouecke, R., Odar, S., 1991. Siemens/KWU strategies for high steam generator performance. In: International Power Generation Conference, San Diego, CA, ASME, October 6–10, 1991.

Brennenstuhl, A., et al., 2009. State-of-the-art review of OPG steam generator tubing degradation mechanisms. In: Proceedings, 6th CNS International Steam Generator Conference, Toronto, Ontario, Canada, Nov. 8–11. Paper No. 5.04.

Bush, S.H., Dillon, R.L., 1973. Stress corrosion in nuclear systems. In: Proceedings of "Stress Corrosion Cracking and Hydrogen Embrittlement of Iron Base Alloys," Conference Held at Unieux-Firminy, France, June 12–16. NACE, pp. 61–79.

Clark, M.A., et al., 1998. Top of tube sheet boiler tube cracking at BRUCE-A NGS—recent experience. In: Proceedings of the Third International Conference on Steam Generators and Heat Exchangers, Held in Toronto, Canada, June 1998. Ontario Hydro Technologies, pp. 422–437.

Clark, M., et al., 2006. Some recent observations on steam generator tubing degradation. In: 5th Annual CNS International Steam Generator Conference Proceedings, Toronto, Ontario, Canada, November 26–29. Paper No. 50, CNS.

Dark Days for San Onofre, 2013. Nucl. Eng. Int. 58(702), 16–19.

Davis-Besse Nuclear Power Station, Docket No. 50–346, License No. NPF-3, Technical Specification 5.6.6 Steam Generator Tube Inspection Report. November 30, 2012, NRC Accession No. ML12339A071.

de Diego, G., et al., 2014. Examination of steam generator Alloy 800 NG tube from the Almaraz Unit 2 NPP. In: Proceedings of the International Symposium, Fontevraud 8, Contribution of Materials Investigations and Operating Experience to LWRs' Safety, Performance, and Reliability, Avignon, France, September 15–18, SFEN.

Durance, D., 2009. FFS issues for steam generator tube (top of tubesheet) intergranular attack/stress corrosion cracking. In: Proceedings of the 17th International Conference on Nuclear Engineering—ICONE17, Brussels, Belgium, Jul. 12–16. ASME. Paper No. ICONE17-75599.

EPRI, 1987. Steam Generator Cold Leg Thinning in Operating Plants. EPRI, Palo Alto, CA. NP 5140.

EPRI, 1994. Steam Generator Reference Book, Revision 1, Volume 1. EPRI, Palo Alto, CA. TR 103824.

EPRI, 1997. Analysis of Steam Generator Tubing from Crystal River, Unit 3. EPRI, Palo Alto, CA. TR-106483.

EPRI, 1998. PWR Steam Generator Tube Fretting and Wear Characteristics. EPRI, Palo Alto, CA. TR-103506.

EPRI/SGOG, 1985. Steam Generator Reference. EPRI/SGOG.

Gorman, J.A., et al., 2003. Secondary side corrosion of 600MA tubing in PWR steam generators—causes, implications for alloys 600TT and 690TT, and needed research. In: Eleventh International Conference on "Environmental Degradation of Materials in Nuclear Power Systems-Water Reactors, Volume 1: Papers 1–60," Held in Stevenson, Washington, August 10–14. Paper No. 34, ANS.

Gorman, J.A., et al., 2009a. Performance based inspection plan for steam generators at point Lepreau. In: Proceedings 6th CNS International Steam Generator Conference Proceedings, Toronto, Ontario, Canada, Nov. 8–11. Paper 1.02. CNS.

Gorman, J.A., et al., 2009b. Alloy 800 steam generator tube performance. In: Proceedings 6th CNS International Steam Generator Conference Proceedings, Toronto, Ontario, Canada, Nov. 8–11. Paper 3.02, CNS.

Hwang, S.S., et al., 2003. Degradation of Alloy 600 steam generator tubes in operating pressurized water reactor nuclear power plants. Corrosion 59 (9), 821–827.

IAEA, 2007. Strategy for Assessment of WWER Steam Generator Tube Integrity. IAEA. IAEA-TECDOC-1577.

IAEA, 2011. Assessment and Management of Ageing of Major Nuclear Power Plant Components Important to Safety: Steam Generators. 2011 update, IAEA. IAEA-TECDOC-1668.

Jones, R.L., et al., 1983. The origin of the extensive cracking of the steam generator tubing at TMI Unit 1. NACE. Corrosion 83. Paper No. 141.

Kadenko, I., et al., 2003. Evaluation and reliability enhancement for ET data of VVER steam generator tubes. In: Steam Generator Management Program: 22nd EPRI Steam Generator NDE Workshop, held in Hilton Head, SC, June 30–July 2, 2003. EPRI, Palo Alto, CA. 1009215.

Kilian, R., et al., 2007. Operating experience with Alloy 800 SG tubing in Europe. In: 13th International Conference on Environmental Degradation of Materials in Nuclear Power Systems, Whistler, B.C., Canada, August 19–23, CNS.

Kilian, R., et al., 2011. Detailed root cause analysis of SG tube ODSCC indications within the tube sheets of NPP Biblis Unit A. In: Proceedings 15th International Conference on Environmental Degradation of Materials in Nuclear Power Systems Water Reactors, Colorado Springs, CO, TMS, Aug. 7–11.

Kukushkin, A.N., 2010. The impact of ODA microadditions into secondary system on corrosion rate reduction in VVER steam generators. In: Nuclear Plant Chemistry Conference 2010 Proceedings and 8th International Radiolysis Workshop Proceedings (Also Known as the 15th International Conference on Water Chemistry of Nuclear Reactor Systems), held in Quebec City, Canada, Oct. 3–7, CNS. Paper 1.13.

Luna, P., et al., 2009. Embalse steam generators—status in 2009. In: Proceedings 6th CNS International Steam Generator Conference, Toronto, Ontario, Canada, Nov. 8–11. Paper 3.03, CNS.

Miroslav, H., Stefan, C., 1994. In-service inspections of steam generators in NPP with VVER 440 at NPP Bohunice. In: Proceedings of the Specialists Meeting on Steam Generator Problems and Replacements, Madrid, Spain, 13–16 December 1993, Session C+D No. 2, IAEA.

Nickerson, J., Maruska, C., 1998. Steam generator management at Ontario Hydro Nuclear Stations. In: Proceedings of the Third International Conference on Steam Generators and Heat Exchangers, Held in Toronto, Canada, June 1998. Ontario Hydro Technologies, pp. 57–68.

NRC, 1994. NRC Information Notice 94-62. Operational Experience on Steam Generator Tube Leaks and Tube Ruptures.

NRC, 2003. NRC Information Notice 2003–13. Steam Generator Tube Degradation at Diablo Canyon. NRC.

NRC, 2005. NRC Information Notice 2005–09. Indications in Thermally Treated Alloy 600 Steam Generator Tubes and Tube-to-Tubesheet Welds.

NRC, 2008. NRC Information Notice 2008–07. Cracking Indications in Thermally Treated Alloy 600 Steam Generator Tubes. NRC, ML080040353.

NRC, 2012. NRC Information Notice 2012-07. Tube-to-Tube Contact Resulting in Wear in Once-Through Steam Generators.

NRC, 2013a. NRC Information Notice 2013–11. Crack-Like Indications at Dents/Dings and in the Free Span Region of Thermally Treated Alloy 600 Steam Generator Tubes NRC, ML13127A236.

NRC, 2013b. H. B. Robinson Steam Electric Plant, Unit No. 2—Issuance of an Amendment to Revise the Steam Generator Program Inspection Frequencies and Tube Sample Selection and Application of Permanent Alternate Repair Criteria (H*) (TAC No. ME9448). NRC Accession No. ML13198A367.

NRC Bulletin, 1988. Rapidly Propagating Fatigue Cracks in Steam Generator Tubes.

Pagan, S., et al., 2007. Assessment of crack-like flaw in ex-service Monel 400 steam generator tube removed from Pickering unit 4 steam generator 12. In: 2nd International Symposium on Nuclear Power Plant Life Management, Held in Shanghai, China, Oct 15–18, 2007. Paper No. IAEA-CN-155-077.

Rochester, D.P., Eaker, R.W., 1999. Laboratory examination results from Oconee nuclear station once through steam generator tubes. In: Proceedings of the Ninth International Symposium on Environmental Degradation of Materials in Nuclear Power Systems—Water Reactors, Newport Beach, CA, Aug. 1–5, TMS, pp. 639–648.

Roy, S., 1994. Steam generator performance and life management decisions in Bruce A nuclear generating station. In: Proceedings of a Conference on Steam Generators and Heat Exchangers, Toronto, June 1994, v1p1.47, Monenco AGRA.

Rucsak, M., et al., 1998. Tube corrosion damage and local VVER steam generator water chemistry. Approach to modeling. In: Contribution of Materials Investigation to the Resolution of Problems Encountered in Pressurized Water Reactors, Proceedings of the International Symposium, Fontevraud IV, vol. 1, Sept. 14–18, SFEN, pp. 719–730.

Sherburne, P., 1998. OTSG materials performance—25 years later. In: Contribution of Materials Investigation to the Resolution of Problems Encountered in Pressurized Water

Reactors, Proceedings of the International Symposium, Fontevraud IV, vol. 1, Sept. 14–18, SFENpp. 529–539.

Song, M.H., 2006. Regulatory activities on steam generator tubes in Korean nuclear power plants. In: 5th Annual CNS International Steam Generator Conference Proceedings. Toronto, Ontario, Canada, CNS, November 26–29. Paper No. 47.

Staehle, R.W., Gorman, J.A., 2003. Quantitative assessment of submodes of stress corrosion cracking on the secondary side of steam generator tubing in pressurized water reactors: Parts 1, 2 and 3. Corrosion, v59n11p931-994, v60n1p5-63, and v60n2p115-180. NACE, Nov. 2003, Jan. 2004 and Feb. 2004.

Tapping, R.L., et al., 2000. Technical note: CANDU steam generator life management. Nucl. Eng. Des. 197 (1–2), 213–223.

Trunov, N., et al., 2010. Pressing problems of managing the service life of tube bundles used in steam generators at nuclear power stations equipped with VVER reactors. Therm. Eng. 57 (5), 361–369.

Wallin, K., et al., 2010. Validation of statistical assessment method for optimization of the inspection need for nuclear steam generators. In: Contribution of Materials Investigations to Improve the Safety and Performance of LWRs. Proceedings of the International Symposium, Fontevraud VII, SFEN, Sep. 26–30. Paper O07-A021-T06.

Warr, B.D., et al., 1987. Operating experience and laboratory studies with fatigue and stress corrosion cracking of Inconel 600 steam generator tubes at Ontario Hydro. In: International Conference on Nuclear Power Plant Aging, Availability Factor and Reliability Analysis, San Diego, CA, 8–12, July 1985. ASM International, pp. 205–208.

World Nuclear News, 2011. EDF Orders 44 Steam Generators. World Nuclear News.

Yashima, S., 1991. Recent operating experience with steam generators in Japan. In: NEA/CNSI—UNIPEDE, Specialist Meeting on Operating Experience With Steam Generators, Brussels, Belgium, 16–20 September. Paper 2.2.

Yurmanov, V.A., et al., 2010. Corrosion product behavior in VVER secondary systems. In: NPC 2010—Nuclear Plant Chemistry Conference 2010 Proceedings and 8th International Radiolysis Workshop Proceedings (Also Known as the 15th International Conference on Water Chemistry of Nuclear Reactor Systems), Held in Quebec City, Canada, Oct. 3–7, CNS. Paper 6.12.

This page intentionally left blank

Environmental degradations in PWR steam generators

8

I. de Curieres
IRSN, Fontenay-aux-Roses, France

Acronyms

PWSCC	primary water stress corrosion cracking
NDE	nondestructive examination
SGTR	steam generator tube rupture
SG	steam generator
EFPY	effective full power years
DMW	dissimilar metal welds
HAZ	heat affected zone
IGSCC	intergranular stress corrosion cracking
C&LAS	carbon and low-alloy steels
BAC	boric acid corrosion
ODSCC	outer diameter stress corrosion cracking
IGA	intergranular attack
TSP	tube support plate
TTS	top of the tubesheet
PbSCC	Pb-induced stress corrosion cracking
S^y-SCC	sulfur-induced stress corrosion cracking
pH_T	pH in the high-temperature environment
ECP	electrochemical corrosion potential
AVT	all volatile treatment (conditioning of the secondary side water with amines)
RSG	replacement steam generator
FAC	flow-accelerated corrosion
EAC	environmentally assisted cracking
SICC	strain-induced corrosion cracking

8.1 Introduction

From the very early designs, steam generators have faced issues related to environmental effects, in particular corrosion. These various phenomena have led to many improvements, in the design of the components, the materials used, or the specified water chemistry. This chapter aims to review various environmental effects affecting steam generators, from corrosion degradation to corrosion product release.

Steam Generators for Nuclear Power Plants. http://dx.doi.org/10.1016/B978-0-08-100894-2.00010-8
© 2017 Elsevier Ltd. All rights reserved.

Although it cannot be fully exhaustive due to the wide range of the history of corrosion, this chapter reviews the main phenomena encountered worldwide, and it includes some operating experience and phenomenology to understand the challenges associated to the chemical environment of steam generators.

The chapter is basically divided into two parts: phenomena on the primary side of the equipment and phenomena on the secondary side. For each phenomenon, a review of the operating experience is made, prior to indicating the associated state of the art and modeling capabilities. Apart from obvious leaking circumstances, such damage and their follow-up or characterization are closely related to the nature, quality, and extent of associated NDE methods. Thus, the reader is advised to read Chapters 14 and 15 from this book containing relevant inputs completing the phenomenological ones described hereafter.

This chapter will deal only with main equipment, whereas damage concerning repair solutions, e.g., tube plugs or sleeves, are out of the scope of this chapter, even though they were globally the same as those affecting tubes (PWSCC, IGA/ODSCC, or wastage). In addition, this chapter essentially deals with phenomena affecting PWR and CANDU components. Some very limited information is provided for VVER-type reactors. If information for VVER reactors is wanted, the reader is advised to consider the previous chapter which contains more detailed data for this type of reactors.

8.2 Primary side environmental effects

8.2.1 (PW)SCC mechanisms

The main environmental issue on the primary side of steam generators is stress corrosion cracking of Ni-based alloys, which is in this instance called PWSCC, standing for Primary Water Stress Corrosion Cracking. This damage has required large expenditures on repair or replacement of components in the nuclear industry. The alloys susceptible to this damage are alloy 600, and its parent weld metals 182, 132, and 82. Hitherto, no crack has been detected in alloy 690 or its parent weld metals 52 and 152. Accordingly, this section focuses on low-chromium grades although some testing is performed to determine the susceptibility of alloy 690 to PWSCC of thick-walled materials.

8.2.1.1 Operating experience

SG tube bundles in alloy 600 (1972–2016+)

The tube bundle of steam generators is the most common location for the occurrence of corrosion, since thousands of cracks have been detected on the primary side of bundles in alloy 600 over the last four decades. In every country where alloy 600 has been used for SG tubes, PWSCC cracks have been detected. Alloy 600 was used for manufacturing SG tube bundles from the late 1960s to the mid-1980s. Since then, alloys 690TT or 800 have been used for manufacturing new steam generators. Currently, a few dozens of plants worldwide still have steam generators with bundles in alloy 600, though these equipments are being progressively replaced. The first cracking event in alloy 600 was reported in 1971, and each year, new PWSCC cracks

were and are still being discovered. To date, no crack has been reported on the primary side of tubes either in alloy 690TT or in alloy 800.

PWSCC occurs in all kinds of alloy 600 tubes, either in the mill-annealed or thermally treated conditions. Chapter 6 provides with a comprehensive review of the various types of cracking met, and references Flesch et al. (1990), de Curieres and Meunier (2010), USNRC (2008), and Hwang et al. (2013) are examples of reviews available on this specific topic. Basically, it can be briefly summarized by the following points:

- PWSCC cracks are usually entirely intergranular. They initiate at grain boundaries and propagate along them.
- The driving forces for PWSCC cracks are essentially the manufacturing residual stresses, such as tube-to-tubesheet expansion, U-bend forming, or welding. Deformations due to scratches, dings, or dents because of loose-parts may also promote cracking. The contribution of operating stresses to PWSCC is negligible.
- Cracks are oriented perpendicularly to the main stresses, which have given rise mainly to axial cracks, except in some specific circumstances:
  - Axial cracks are detected when their length is about 2 mm.
  - From experience, all axial cracks are through-wall when their length is 6 mm or more.
- The hot leg of the bundle is more affected than the cold leg, as may be expected from a thermally activated phenomenon (where the activation energy for crack initiation is about 180 kJ/mol[1]).
- The crack propagation rate observed in SG tubing is in the range of 0.1 to more than 2 mm/year, depending essentially on the alloy microstructure: TT heats are more likely in the lower range of cracks growth rates, whereas MA heats are in the upper range (see Mathon et al., 2014 for details).
- A microstructure where carbides are mostly intergranular has been observed to postpone crack initiation and slow down crack propagation. Such a microstructure is called an "optimized" one although it was not always obtained by the manufacturing sequence.
  - Alloy 600TT, although globally more resistant than alloy 600MA, is also susceptible to PWSCC; all fleets with alloy 600TT tubes worldwide have been affected by PWSCC.
- Treatments such as shot-peening of the expanded area before the first commercial operation, or stress relieving heat treatments of small bend radii, have proved efficient in inhibiting or delaying PWSCC in the tubes.

Cracking of a tube may lead to a steam generator tube rupture (SGTR) which is of high safety significance. To a lesser degree, cracking begets primary to secondary leakage which is a loss of integrity of the second containment barrier. Accordingly, this location is quite intensively inspected.

Partition plates

Apart from the tube bundle, some cracks were detected, to a limited extent, in other locations of SGs. In 2002, some indications were detected in a divider plate made of alloy 600 of a French steam generator (Bibollet et al., 2006; Bamford et al., 2009).

[1] In field experience-oriented analysis, crack initiation is often considered as the NDE detection threshold, which induces some discrepancies in the published activation energies.

These indications proved later on to be PWSCC cracks. Afterward, similar flaws were discovered in 11 partition plates in France.

The individual cracks were only of a few millimeters long, but many of them were aligned over distances up to 2 m long. Their depth was less than 2 mm. They were located in the partition stub runner, parallel to the weld connecting the stub and the divider plate (Fig. 8.1).

Destructive examination on a retired steam generator revealed that the cracks were located in a cold-worked surface layer generated by grinding and did not propagate beyond it. These locations were not entirely unexpected, since the concerned welds are the last ones performed during the manufacturing of the SGs lower head of the steam generator and its connection to the rest of the component. If the two parts are not properly aligned, then hydraulic jacks are used to pull them into alignment before the weld is made, resulting in nonnegligible residual stresses.

The origin of the cracking is considered to be the joint presence of weld shrinkage and manufacturing strains as well as local plastic strains occurring during the hydro-pressure tests performed before the first commercial start of the plant.

Though of lesser safety significance considering its current location (middle of the stub runner), these instances of cracking are a reminder that alloy 600 is susceptible to SCC in hot primary water whatever its location.

Steam generator bowl drains (1988–2008)

Steam generators lower heads contain nozzles used for the complete drainage of the bowl, in particular to permit access for inspections. There are different types or designs of drains, for instance:

- Unique vertical drains, located at the bottom end of the bowl, with a small "mouse hole" connecting the hot and cold boxes. One schematic view of such a design is represented below, from reference (Bamford et al., 2009).
- A set of two drains, located each in a water box of the lower head. These drains are usually obliquely oriented.
- Some drainage nozzles in the manhole cover (Fig. 8.2).

PWSCC cracks were discovered in the aforementioned locations, in the United States, France, Sweden, and Korea (Bamford et al., 2009; Duisabeau et al., 2010; USNRC, 2005a; Hwang et al., 2009a,b; Efsing et al., 2005), over the period 1988–2008.

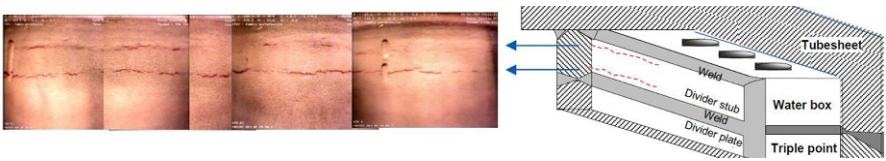

Fig. 8.1 PWSCC indications in a divider plate/stub in a French steam generator.
From Deforge, D., et al., 2010. Learnings from EDF investigations on SG divider plates and vessel head nozzles, paper A117-T04. Proceedings of the International Conference "Fontevraud 7", SFEN (Ed.), September.

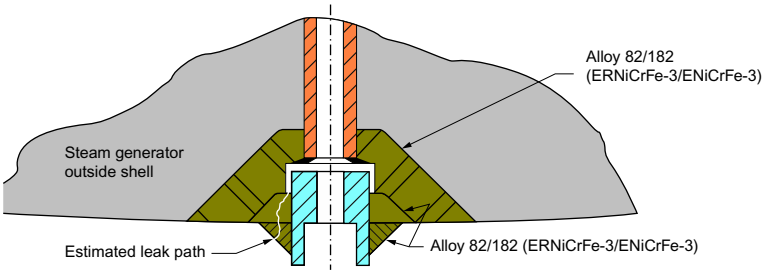

Fig. 8.2 Schematic view of the unique vertical drain of steam generators.
From Bamford, W.H., et al., 2009. Service experience with alloy 600 and associated welds in operating PWRs, including repair activities and regulatory and code actions. In Proceedings of the 14th International Conference on Environmental Degradation of Nuclear Reactors, Virginia Beach, VA, USA, August.

In the American, French, and one Korean cases, the lower heads concerned contain one vertical drain, made in alloy 600 and welded to the lower head by alloys 82 and 182. In the United States, the first event happened in 1988, after 1 year of operation of the plant. A few other cases happened until 2005, very often detected by the presence of boric acid leaks below the seal weld. In France, one single defect was reported. It was discovered in 2008 during a visual inspection of the component and has been detailed by the utility (Duisabeau et al., 2010). In all these cases, the defects were identified as PWSCC cracks, located in the Nickel-based alloys weld metals.

Two other occurrences on lower head drains were discovered in 2007 and 2008 in Korea, affecting two components (Hwang et al., 2009a,b), after 11 EFPY (Effective Full Power years) of operation. In this case, the lower heads of these SGs contain two drain nozzles, one in each box of the head. The drain in the hot box is made of alloy 690, whereas the one in the cold box is made of alloy 600. Some leaks were detected in the cold box ones, in alloy 600. Destructive examination revealed that the leaks were due to PWSCC of the base metal of the drain itself (Fig. 8.3).

Eventually, in 2004 in a Swedish plant, some leaks were detected on the drainage nozzles of the SG manhole covers (Efsing et al., 2005). The drain pipes are made of stabilized stainless steel, welded to the lower dome of the equipment by a J-groove weld made in alloy 82. The expertise showed that this leakage was due to PWSCC of the alloy 82 weld metal and is one of the very few unequivocal evidence of PWSCC initiating in alloy 82 as distinct from propagating in alloy 82 from alloy 182.

The risk associated with such events is not only a radioactive primary fluid leak. Such leaks may induce boric acid corrosion of the carbon steel lower head either from the inside (see Section 8.2.3) or from the outside, as occurred in a PWR pressurizer bottom head (EPRI, 2001a), or on the reactor vessel head in another plant where through-wall wastage of the low-alloy steel was found (USNRC, 2005b). This would result in a severe loss of integrity of the second containment barrier, with a potential significant breach, which is of high safety significance.

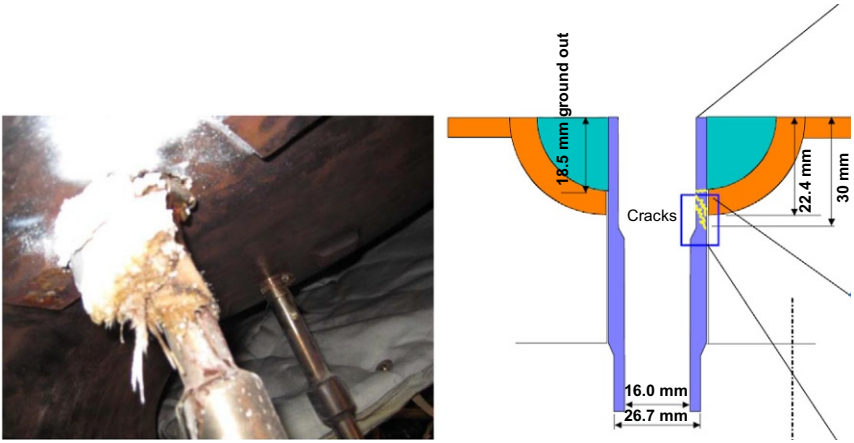

Fig. 8.3 Photograph from a leaking drain from a Korean steam generator (*left*) and schematics of the cracking path (*right*).
From Hwang, S.S., et al., 2009. Steam Generator Management Strategies in Korea. IAEA, Vienna.

Safety nozzles welds

Steam generators are connected to the main coolant pipes by a safe-end nozzle in austenitic stainless steel. The junction between the safe-end nozzle and the SG nozzle in low-alloy steel is ensured by a dissimilar metal weld, either in Nickel-based alloy or in stainless steel.

In the last two decades, PWSCC cracks were detected in this DMW in Japanese reactors (Bamford et al., 2009) in the inlet nozzle to safe-end junction. In their design, the DMW is made with alloy 82 or alloy 132 (alloy close in composition to the alloy 182). These cracks are typical of PWSCC, confirming laboratory assessment that the weld metals alloys 182 and 132 are equally susceptible to this damage. There may be as many as 10 axial cracks, with a maximum depth of about 10 mm, in these welds. As a result of these findings, the Japanese utilities used (i) more PWSCC-resistant weld metals when they replaced the SGs and (ii) applied some shot-peening to mitigate PWSCC in the susceptible welds by inducing compressive stresses on the surface in contact with the primary water.

The shot-peening process requires a preliminary inspection to verify the absence of already existing flaws. It is noteworthy that during one such inspection in 2007, a Japanese utility discovered cracks not only in the Nickel-based alloy of a SG after 92,000 hours of operation but also in the 316 stainless steel safe-end (Shoji et al., 2010; Matsubara et al., 2010; Yonezawa et al., 2014). There were a few cracks, with a maximum depth of 1.7 mm, in the HAZ and oriented parallel to the two welds of the safe-end. Destructive examination of some of the nozzle indicated that these cracks were of IGSCC,[2] i.e., purely intergranular stress corrosion cracks. Contrary to

[2] Although begetting intergranular cracks, this phenomenon in stainless steels is named IGSCC, and not PWSCC, as the latter is used specifically for Nickel base alloys.

PWSCC cracks in the Nickel-based alloy welds, these cracks were circumferentially oriented which, in addition to being an unexpected finding, made it more likely to induce a circumferential line-break of the primary circuit.

Destructive examination also indicated that these IGSCC cracks were located in a heavily cold-worked layer due to an intensive grinding performed during the manufacturing sequence.

The latter event emphasizes the fact that SCC cracking is not solely a matter of coupling a material to an environment, but also a matter of how a material is processed and a component manufactured. A material, usually very resistant to SCC for service in the PWR primary fluid, could become susceptible to it, should it be improperly processed.

8.2.1.2 Modeling

The extent of cracking and the associated risks prompted strong incentives to develop predictive capabilities. It led to two approaches. On the one hand, research efforts concentrated on determining the physical and chemical mechanisms inducing PWSCC in alloy 600 and its associated weld metals. On the other hand, some engineering models were developed to assist utilities in establishing component life management and maintenance strategies. These two approaches are developed below.

Damage modeling

Stress Corrosion Cracking phenomena gave birth to various physical models, usually depending on the type of physical and chemical parameters considered of primary importance. Thus, models have been based on:

- Slip-dissolution interactions (Ford, 1992)
- Hydrogen and plasticity interactions (Magnin, 1992)
- Film-induced cleavage (Cassagne, 1992)

Although each of these models applies satisfactorily to many material/environment couples, none seemed to really explain PWSCC affecting alloy 600 in PWR primary water, especially the thermodynamic and kinetic trends. The latter damage has been extensively studied worldwide and dozens of presentations are available in the complete sets of “Environmental Degradation” and “Fontevraud” conferences since the early 1980s.

In the early 1990s, another model was proposed by the nuclear industry, specifically for PWSCC of alloy 600 (Scott and Le Calvar, 1993). This model considers grain boundary “internal” oxidation as the main phenomenon governing PWSCC. It assumes that PWSCC propagation proceeds by oxidation of grain boundaries of the alloy. Some recent refinement of the model tends to indicate that the propagation itself seems to be due to preferential oxidation of chromium at the grain boundaries (Laghoutaris et al., 2011). This model agrees with many microscopic examinations performed on pulled components or after laboratory testing (Olszta et al., 2011). However, some very detailed scientific questions still remain unanswered. This refinement somewhat explains the better resistance of TT heats with respect to MA ones by the preferential oxidation of grain boundary carbides which would slow down the global grain boundary oxidation rate.

As for crack initiation, it is assumed that the precursors to crack embryos are micrometric grain boundary oxides (Fournier et al., 2011). Under the local stress or strain fields, these oxides break and so initiate an intergranular crack.

Hitherto, the "internal oxidation" model remains the most likely to assess the physical and chemical phenomena governing PWSCC although some mechanistic questions still remain unanswered.

Engineering basic tools

From an engineering perspective, PWSCC damage is usually assessed by two means: time to failure (t_f) and crack growth rate. Among the first tools, most were dedicated to SG tubes, which are described hereafter.

Time to failure[3] is often described as

$$t_f = C \cdot \frac{\sigma^{-4}}{I_m} \cdot e^{-\frac{Q}{RT}}$$

where C is a constant, σ is the stress (MPa), I_m is an index reflecting the alloy microstructural dependence, Q is the apparent activation energy (~180 kJ/mol), R is the gas constant, and T is the temperature (°K).

As for crack propagation, the following law was derived from tests and field experience (Scott, 1991):

$$\frac{da}{dt} = D \cdot (K - 9)^n$$

where D is a parameter depending on the temperature, K is the stress intensity factor (MPa.$\sqrt{m}$), and n is usually between 1 and 2.

In the propagation law, the value "9" in the equation is often mistakenly considered as an initiation threshold. This is however a false idea, since PWSCC essentially initiates on smooth surfaces, where K is theoretically zero. This value is in fact a linear-elastic criterion for long crack arrest in case of a decrease in the mechanical loading.

Lastly, these models can be complemented by introducing the primary fluid dissolved hydrogen (DH) dependence of initiation time and crack growth rate. A few research works have clearly demonstrated that these data vary with a concave curve for initiation time and a concave curve for crack growth rate, when DH increases see Richey et al. (2007) for instance. Such dependencies may be implemented to cope with specific plant chemistries.

PWSCC phenomenology is quite well characterized, and some industry documents provide disposition curves for PWSCC crack propagation, either in thick-wall alloy 600 base metal (EPRI, 2002) or in its associated weld metals (EPRI, 2004). Nonetheless, the basic mechanism is not yet clearly established although some extensive parametric studies have been performed, e.g., Daret (2005).

[3] Time to failure is defined as the time for detection by NDE, as initiation of PWSCC is usually the time limiting step of the damage.

Component-scale modeling

The main goal of component-scale modeling is twofold: (i) predicting the damage evolution at the component's scale and (ii) assessing a residual lifetime based on this evolution. As for SGs, the traditional assessment made is the evolution of detectable tube cracking, since it leads to tube plugging. Because the life and operational efficiency of a steam generator is directly connected to the amount of plugged tubes, many modeling efforts have been put in predicting the evolution of SG tube cracking by PWSCC.

Each SG contains 3000–10,000 tubes, hence statistical methods are relevant options, in particular the Weibull method (Stavropoulos et al., 1991; Staehle et al., 1994). This statistical approach is well adapted for large populations of tubes subject to a cumulative damage. It is quite simple to process, and once the first tubes have cracked, the evolution kinetics at the tube bundle scale can be globally assessed. Fig. 8.4 hereafter shows one application of the Weibull statistics to PWSCC in one SG (green line).

As can be seen above, the damage trend is quite well captured, albeit predictions can be imprecise, especially for the early precursors or for the long term where the Weibull-fit overestimates the actual damage evolution. This sometimes leads the industry to define more accurate prediction tools for finer economical predictions. One such improvement was made by the French industry (de Curieres and Meunier, 2010; Scott et al., 1995; de Curieres et al., 2010a). A statistical approach

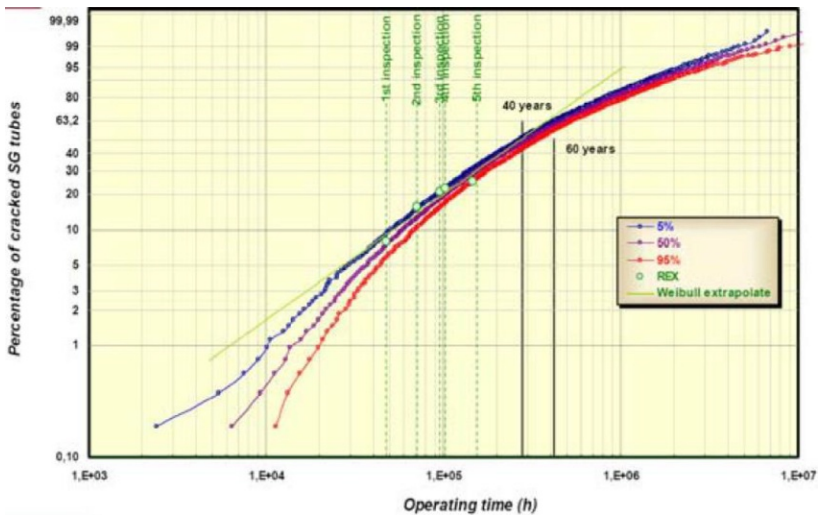

Fig. 8.4 Extrapolation of the cumulative number of tubes cracked by PWSCC in a steam generator. *Green* dots: results of NDE during various outages. *Green* line: Weibull extrapolation. *Blue*, *purple* and *red* lines: new model predictions.
From de Curieres, I., Meunier, M.-C., 2010. SCC of steam generator tubes made of alloy 600TT: analysis of operating experience, paper A126-T06. Proceedings of the International Conference "Fontevraud 7", SFEN (Ed.), September.

at the bundle scale was developed, also integrating tube manufacturing data (e.g., carbon content, type of expansion process in the tubesheet). This model is based on some indices reflecting the PWSCC phenomenological dependencies to temperature, stress, and microstructure. The results of the model are presented in the figure above, on the same set of data than the Weibull-fit. As is evident in the figure, it enables more accurate predictions of the evolution of the number of tubes affected by PWSCC. However, although precise, it is a more complicated model as it requires many manufacturing data concerning the affected component, such as surface finish, carbon content, temperature, and duration of the thermal treatment.

Once such models are applied, they may be completed with crack propagation mechanical laws to achieve a complete assessment of the tube plugging criteria. Such methods have been developed from the early 1990s (Scott, 1991) and may be used from an industrial and engineering perspective by vendors or utilities (de Curieres et al., 2010a; Mathon et al., 2014).

In addition to tube bundles, predictive models may also be applied for other locations at the steam generators, namely thick-walled components. For instance, the French operator, confronted with the events of partition plate cracking reported in Section 8.2.1.1, developed a physical model to both understand and determine the possible extent of cracking through a partition plate (Couvant et al., 2010). It integrates engineering, manufacturing, and physical data. Though strictly used for a partition plate, it could be applied to other parts of steam generators.

Eventually, one should also consider a sophisticated probabilistic PWSCC modeling developed by the US industry in the late 2000s (Fyfitch et al., 2015). It is a global PWSCC predictive tool, based on initiation models and propagation laws relying on the previously mentioned disposition curves. It is in particular dedicated to predicting the probability of occurrence of PWSCC in thick-walled components and through-wall cracking. Though not developed specifically for steam generators, this industry-born model could be used for drains, partition plates, or nozzle welds assessment.

Thus, a few models exist allowing trends of either initiation or propagation of PWSCC in a steam generator to be predicted. They range from simple models to complex ones, allowing all utilities to be able to access predictive tools according to their engineering capabilities. However, it should not be forgotten that these models provide trends or probabilistic time to failure, and consequently, their use does not absolutely ensure prevention of leaks or cracking. It is nevertheless a useful tool for risk-informed approaches.

8.2.2 SG corrosion products release

One of the main preoccupations of operating a nuclear power plant is managing the radiation field in the plant itself. The radiation dose is primarily due to the activation of dissolved corrosion products entrained with the coolant when they pass through the reactor core.

Major contributors to the radiation dose are the isotopes of cobalt, one of them being the ^{58}Co, produced by the Nickel corrosion products under the radiation flux

from the core. The essential contributors to the dissolved Nickel corrosion products are Nickel-based alloys and primarily the steam generators tube surfaces. Once released, the corrosion products flow with the coolant, become activated, and are then deposited on surfaces of the primary circuit. This induces an activity build-up in the plant and an exposure of workers to radiation doses during maintenance operations. Hence, dose reduction is a strategic aim for utilities for reasons of human radiological protection.

Dissolved corrosion product species release into the primary coolant is a natural and nonavoidable process; however, the industry has undertaken many improvements to minimize the corrosion products (cation) release rate.

Two ways of mitigating this issue are undertaken by the industry. First, by modifying the primary water chemistry in order to minimize the cation release from SG tubes. This may be achieved by optimizing the water chemistry: injecting small quantities of zinc to the primary fluid (EPRI, 2001b), and/or having a so-called high pH (IAEA, 1992). The other way is to directly alter the tube surface cation release rate. This may be achieved either by implementing a "smoother" internal surface of the tubes (Seo et al., 2014) or by applying a prepassivating treatment during the hot functional tests before the first commercial start of the equipment. Some noncomprehensive examples of such improvements and their promising results can be found in references (Clauzel et al., 2008; Engler et al., 2008).

From an industrial perspective it is complicated to practically assess precisely the efficiency of such processes. However, reports of operating experience from the industry (EPRI, 2006; NEA, 2014) indicate that the manufacturing processes do indeed influence the activity of a plant, in particular the ^{58}Co oxygenation peak.[4]

8.2.3 Miscellaneous—Undercladding boric acid corrosion

In 2011, an event was reported by an American vendor to the whole nuclear power industry: the finding of a cavity in the low-alloy steel of the lower head of a "nondomestic" steam generator, due to corrosion under the cladding, after 24 years of operation. The event was officially reported by a regulator in 2013 (USNRC, 2013).

In all steam generators with a recirculating design, the shells and heads are made of low-alloy steel, for the sake of mechanical properties and are clad on the primary side by a stainless steel layer. Accordingly, carbon and low-alloy steels (C&LAS) in steam generators are normally not exposed to the primary fluid and its corrosion. In the affected component, the stainless steel cladding of the lower head appeared to contain flaws giving access of the fluid to the base metal.

The resulting cavity was measured by ultrasonic examination to have a maximum length of 75 mm and a maximum depth of 28 mm. The corrosion is assumed to have occurred essentially during drained outages periods when boric acid could be

[4] During the oxygenation stage occurring during a shutdown, many corrosion products, often activated, are solubilized, inducing a sudden increase in the volumetric activity of the primary coolant. Afterwards, due to the purifications systems of the primary circuit, the global activity decreases anew. The result is the occurrence of an activity peak, especially of ^{58}Co, during the oxygenation of shutdown operation stages.

concentrated by an evaporation process. This assumption implies a corrosion rate of the order of magnitude of 2.7 mm/year. Considering only the outage time, estimated to be 5% of the duration of a fuel cycle, this means a corrosion rate of about 40–50 mm/year which is quite substantial and in the highest range obtained in laboratory tests (USNRC, 2005b).

In spite of research works dedicated to reproducing this extent of corrosion (Lister et al., 2015), this elevated corrosion rate remains unexplained. Furthermore, the cause of the cladding defects is not established either. Should it have been nondetected, this cavity could have grown until becoming possibly through-wall, leading to a breach in the pressurized primary circuit. The structural and reactor coolant pressure boundary integrity was affected.

This event is a first-of-a-kind in steam generators, but not in the nuclear industry. The NRC indeed reported in 1994 (USNRC, 1994) a similar event happening to a clad steel pump casing exposed to primary water in which an even larger cavity was discovered, after cracking of the cladding occurred. Hence, this event should not be considered as singular or specific event, but rather as a precursor emphasizing the need for a good cladding quality and a regular surveillance of its integrity.

8.3 Secondary side environmental effects

Secondary side corrosion phenomena were the first environmental issues faced by these components. Since the late 1950s, SCC problems occurred in SG tubing and prompted changes in the tube material grades: initially from stainless steel to alloy 600 (MA then TT) and then from alloy 600 to either alloy 690TT (since 1989) or 800NG. Henceforth, only alloys 690TT and 800NG are used for manufacturing new steam generators.

8.3.1 SG tube bundle

The tube bundles of steam generators have been affected by many corrosion problems: Stress corrosion cracking (SCC), Intergranular attack (IGA), wastage, pitting, or denting. The next paragraphs will detail these damages, giving a specific focus on SCC, IGA, and denting.

8.3.1.1 ODSCC/IGA—Operating experience (1957–2016+)

Outer Diameter Stress Corrosion Cracking (ODSCC) and IGA have been the main damage affecting the tube bundle of steam generators worldwide (Fig. 8.5). Until the early 2000s, ODSCC was the primary cause for SG tube plugging, literally plaguing the components, as can be seen on the graph below, from reference (Diercks et al., 1999).

Therefore, these phenomena have been extensively studied and reviewed, especially during the 1990s. References (Staehle and Gorman, 2003, 2004a,b; Scott et al., 2008) contain good historical review of the problem, as well as the status of

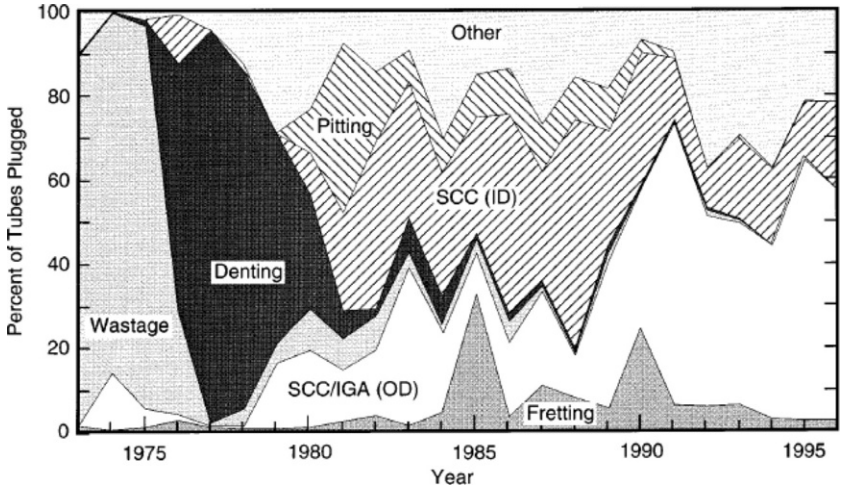

Fig. 8.5 World causes for SG tube plugging until 1996.
From Diercks, D.R., et al., 1999. Overview of steam generator tube degradation and integrity issues. Nucl. Eng. Des. 194, 19–30.

the operating experience and research works until the year 2000. Since then, new events of ODSCC have occurred which would require an update of these reviews. Currently, the operating experience may be summarized as follows:

- *Stainless steel tubes*: used in the late 1950s and encountered some ODSCC due to caustic or chloride-induced SCC (Staehle and Gorman, 2003). The replacement by Nickel-based alloys was elected to improve resistance to chloride-induced corrosion.
- *Alloy 600MA*: used for manufacturing from the early 1960s, this alloy suffered significantly from IGA/ODSCC worldwide. Corrosion occurred in various locations (Staehle and Gorman, 2003, 2004a,b; Scott et al., 2008; IAEA, 2011; Thebault et al., 2010; King, 2007):
  - Circumferentially and axially at the top of the tubesheet or in the crevice between the tube and the tubesheet.
  - *In the absence of denting* at the tube support plate (TSP elevation), cracks are axially oriented in the tube-tube support plate contact crevices. In 2009, the only circumferential crack at the TSP level without denting was found, to the knowledge of the author, in a French 900 MWe plant, after nearly 30 years of operation (Thebault et al., 2010). The damage consisted of a mixture of IGSCC and deep IGA. *When tubes are dented*, circumferential cracking has very often been encountered.
  - In the freespan of tubes, in the case of dings, dents, or scratches.
  - In the radii of U-bends. Cracks may be both axial and circumferential. In CANDU reactors, in particular, there have been essentially circumferential and shallow cracks, located at U-bend support intersections.
- *Alloy 600TT*: used for manufacturing from the mid-1970s to the late 1980s. The first instance of ODSCC occurred in Korea in 1990 (Staehle and Gorman, 2004a). Since then, ODSCC and IGA developed significantly in Korea (Hwang et al., 2009b), since 2002 in the United States (USNRC, 2008; IAEA, 2011; Wolfe, 2015) and since 2011 in France

(Boccanfuso et al., 2015). ODSCC clearly occurs in 600TT tubes, albeit crack indications are much less numerous than in 600MA tubes. Only a few hundreds of crack indications are currently reported worldwide. In most cases, at least one of the following causes was present (but not all of them at the same time):

- A "non-optimized" microstructure with non-purely intergranular carbide precipitation in the tube
- Some stresses higher than expected due to straightening after the final heat treatment or some denting
- Presence of lead or sulfur

  In 600TT tubes, cracks are essentially located at the top of the tubesheet or in the tube-to-tubesheet crevices. A few cracks were detected at the TSP level due to higher residual stresses mentioned earlier.

– *Alloy 800NG*: For power reactors, alloy 800NG has been used since the very early 1970s. It performed quite well from a corrosion perspective although it appears not to be immune. Indeed, in 2009, 135 cracks were reported to the IAEA (IAEA, 2011). Since then, some new cracks were detected, in particular at least 78 affected tubes with NDE indications in Spain in 2009. Although very few in comparison to the number of events befalling alloy 600 bundles, some cases of ODSCC were encountered, either in Germany (Kilian et al., 2007) or in Spain (Kilian et al., 2015) after about 10 years of operation in a replacement steam generator. Cracks were detected at different locations, in the gap between the tube and the tubesheet, in the sludge pile above the tubesheet, or at the tube support grids. Destructive examination of pulled tubes showed that the presence of sulfur and/or top-of-tubesheet denting or hard sludge deposits were aggravating factors in the most recent cases.
– *Alloy 690TT*: First start of a SG with such tubes occured in 1989. Hitherto, not a single indication has been reported.

In terms of phenomenology, ODSCC in alloy 600 is essentially intergranular. A few transgranular cracks have been encountered and each time in the presence of a substantial Pb pollution (Hwang et al., 2009b; Staehle and Gorman, 2004a). Since ODSCC cracks are in many cases circumferential, they pose a greater threat to safety than the PWSCC as there is a greater risk of SGTR with a guillotine rupture of the tubes. Furthermore, such cracks appear on the outer surface of tubes in locations where the NDE signals may be disrupted by deposits (copper), sludge, or transition at edges of tubesheet and tube support plates. ODSCC is thus a more serious damage (Figs. 8.6 and 8.7).

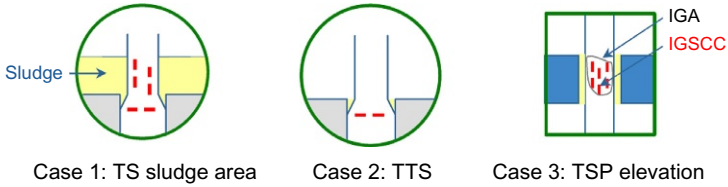

Fig. 8.6 Schematic representation of IGA/ODSCC in alloy 600.
From Buisine, D., et al., 2010. French steam generator tubes: an overview of degradations, paper A164-T06. Proceedings of the International Conference "Fontevraud 7", SFEN (Ed.), September.

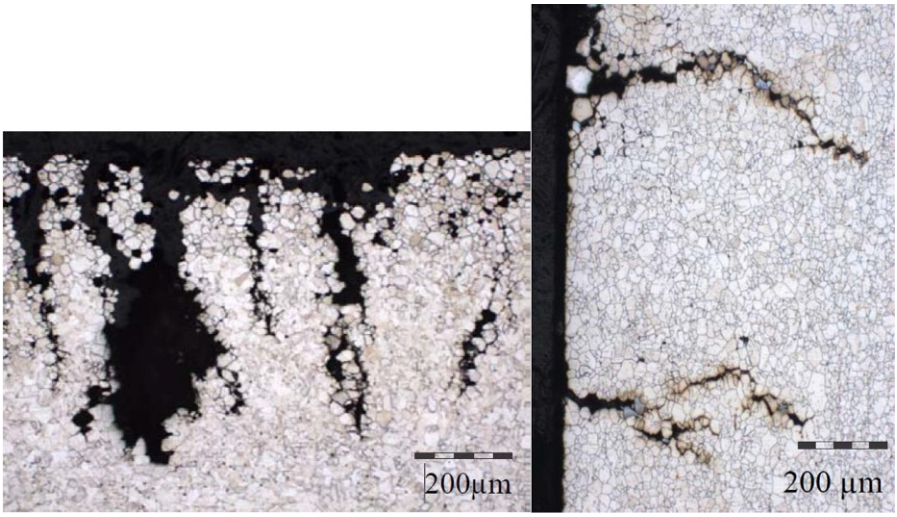

Fig. 8.7 IGA (*left*) and ODSCC (*right*) affecting alloy 600MA SG tubes, destructive examinations by EDF.
From Thebault, Y., et al., 2010. Experience of steam generator tube examination in the hot laboratory of EDF: analysis of recent events concerning the secondary side, paper A166-T06. Proceedings of the International Conference "Fontevraud 7", SFEN (Ed.), September.

It is considered that stresses above 50% of the yield stress are sufficient to induce ODSCC in alloy 600, depending on the local environments. Stresses are not required for IGA to occur, in contrast to ODSCC. Nonetheless, the two phenomena are closely related.

These examples of corrosion damage occur mostly in confined areas, where the chemistry is everything but nominal: tube-plate gaps or in sludge piles, for instance. In such locations, the boiling conditions, confined geometries, or the presence of magnetite crud induce very concentrated impurity chemistries, in comparison to the secondary bulk fluid (with concentration factors between 10^3 and 10^6). Indeed, analyses from utilities indicate:

- Alkaline or acidic crevice chemistries
- Elevated ionic concentrations in crevices (e.g., sodium, chloride, sulfate, magnesium) detected during hide-out-return when the plant is cooled down and there is no longer a heat flux to retain impurities in the confined areas
- Substantial concentrations of normally nondetectable impurities (lead, arsenic, etc.)
- Different compositions of the surface films on tubes in the confined areas than on the freespan ones (Cattant et al., 1994), with the presence of aluminosilica gels, different oxide compositions, for instance (Fig. 8.8)

In addition to these compounds, when sludge deposits are present on the tubesheet or on the tube support plate crevices, their chemical analyses reveal significant amounts of pollutants, especially lead and in some circumstances sulfur or copper (de Curieres et al., 2010b). The sponge-like ability of the sludge deposits with respect to some

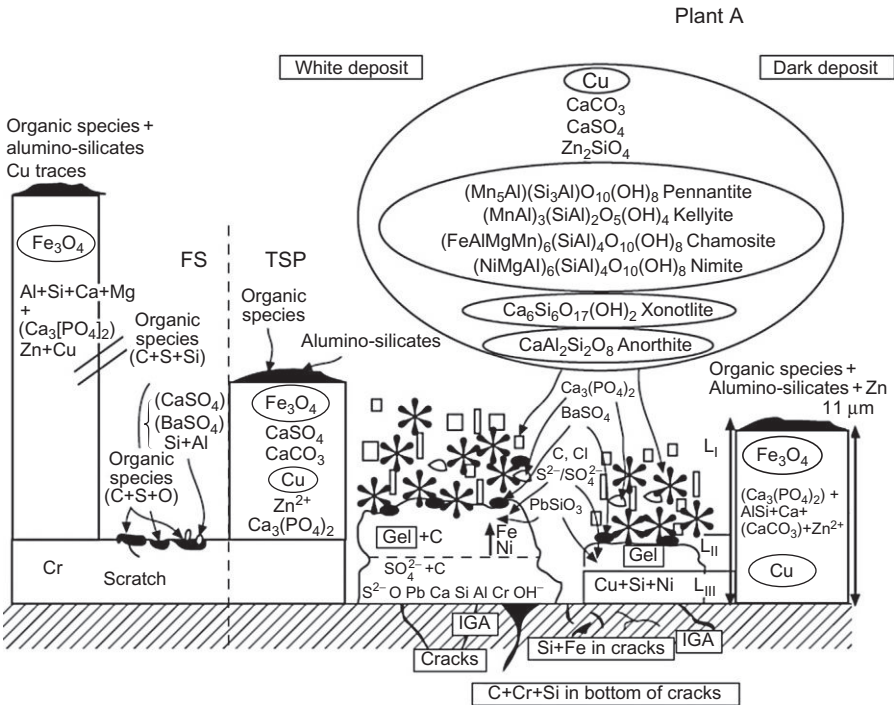

Fig. 8.8 Analysis of surface films of a pulled tube from a plant, after 83,300 hours of operation. *FS*, freespan; *TSP*, tube support plate.
From Cattant, F., et al., 1994. Analyses of deposits and underlying surfaces of the secondary side of pulled out tubes from a French plant. Proceedings of the International Conference "Fontevraud 3", vol. 2, SFEN (Ed.), September, pp. 469–480.

impurities has been confirmed by laboratory studies (Nasrazadan et al., 2007). Such results imply that, over time, some chemical species, even though below the detection threshold, may build up in the sludge and reach substantial amounts.

Today, the pollutants which could be considered as the most deleterious ones for secondary side corrosion are:

- Copper: originates mainly from brass or bronze condenser tubes. Its main effect is to induce oxidizing conditions when present as copper cations in solution.
- Sodium: comes from the make-up water, also from raw or brackish water when condensers leaks occur. It tends to induce very alkaline local conditions when concentrated.
- Lead: may originate from foreign objects (loose parts), residues from lubricants, or as traces in the water. Its role on corrosion is not well understood yet, but it has been found to greatly increase the susceptibility of SG tube alloys to IGA/ODSCC.
- Sulfur: may come from water leaks at the condenser or traces from various products. Its role is not clear either, but it has been determined to increase the susceptibility of SG tube alloys to corrosion, either localized or general, in some local chemistries.
- Aluminosilicates: they may originate from the make-up water and have a detrimental effect on the passivity of SG tube alloys.

Chlorides, phosphates, and organic acids are also considered as detrimental species, but of a lesser importance.

The contribution of lead (Pb) and Sulfur (S) species to IGA or ODSCC was reassessed in 2005 when some high-resolution microscope analyses on 18 pulled tubes in alloy 600 showed that in 14 of them, the damage could be ascribed to Pb or S although no specific pollution or chemistry excursion had been observed for the concerned steam generators (Staehle et al., 2006). This renewed interest in Pb and S effects led to a dedicated workshop (EPRI, 2005), whose proceedings, hitherto, remain one of the most detailed reviews. Cracking due to Pb pollutions is called PbSCC and that due to the influence of reduced sulfur species is called S^y-SCC. Contrary to what is usually believed, PbSCC of alloy 600 is essentially intergranular. It can be transgranular when the Pb pollution amount is important, but otherwise, it remains intergranular, as was shown after some pulled tubes analyses (Staehle et al., 2006).

Crevice conditions two decades ago were very far from the neutrality, with pH_T values estimated as low as 3 or as high as 10.5 (the neutral pH at 300°C is about 5.5). Henceforth, with stricter controls of the secondary side chemistry (in particular sodium impurity concentrations, lead or raw water/brackish ingresses, etc.), the crevice conditions are much less aggressive.

Currently, modifications to the design (tube material, tube support plates shapes and materials) or to the chemistry specifications (stronger limitations on sodium, etc.), secondary side cracking has become much less prominent. Nonetheless, IGA/ODSCC still occurs, emphasizing the remaining need to be able to determine vulnerability domains for SG tube alloys.

Recent events affecting some tubes in alloy 800NG after a relatively short period of operation are a reminder that immunity, on the secondary side of steam generators, is a delusion. Some alloys are very resistant but might be susceptible to IGA/ODSCC in case of chemistry excursions, nonoptimum cleanliness of the tubesheet, or if denting occurs.

8.3.1.2 ODSCC/IGA—State-of-the-art

Considering the discussion indicated above, it appears that, contrary to the primary side situation, it is not possible to produce a simple model for IGA or ODSCC, as local chemistries are too disparate. Moreover, one may understand the complexity of the situation by realizing that there are about 300,000 different crevices in a single SG, where chemistry may differ. Even the Weibull statistics satisfying for PWSCC situations is not always efficient in this case, reflecting the variations in local chemistries leading to ODSCC.

Moreover, field analysis clearly points the fact that tubes affected by PWSCC may not be susceptible to ODSCC or vice versa, in the same steam generator (Staehle and Gorman, 2004a), indicating that the damage mechanisms are different.

Many research efforts have been put into reproducing the IGA/ODSCC (Staehle and Gorman, 2003, 2004a,b; EPRI, 2005; Vaillant et al., 1995; Miglin et al., 1995; Kim et al., 2009; Pierson et al., 1995; Cullen et al., 1993; Sakai et al., 1991; Yamanaka, 1991; de Bouvier et al., 2001, 2005) and understanding the parametric effects of:

– pH (mostly caustic ones, with $pH_T > 10$, sometimes acidic ones with $pH_T < 4.5$ (Pierson et al., 1995; Cullen et al., 1993; Sakai et al., 1991; Yamanaka, 1991), or complex and neutral environments $5 < pH_T < 8$ (Staehle and Gorman, 2003, 2004a,b; de Bouvier et al., 2001, 2005)
– impurities, essentially Pb, S, Cu, and sometimes complex mixtures with aluminosilicates

Based on various series of testing, some utilities, in particular the French one, developed different models for secondary side corrosion of alloy 600 tubes, either in alkaline conditions (Bouchacourt et al., 1998) or neutral and polluted ones (Pavageau et al., 2001), models enabling the susceptibility of the alloy to be assessed according to its mechanical properties.

All those tests resulted in the conclusion that no alloy would be immune to either IGA or ODSCC in local crevice chemistries in the presence of off-normal chemistries, whatever the SG tube alloy. Testing also indicated that in highly caustic environments, the more corrosion-resistant alloys could behave worse than alloy 600, especially in the presence of pollutions of Pb (EPRI, 2005; Vaillant et al., 1995) (Fig. 8.9).

These tests were significant achievements since they indicated potential vulnerabilities and large-scale trends. However they do not reproduce the recent field experience as, obviously, alloys 800 or 690TT tubings do not suffer from more severe SCC than alloy 600 ones, as could be inferred from the plot above.

The discrepancy between the laboratory results and the field experience may be ascribed to the following causes:

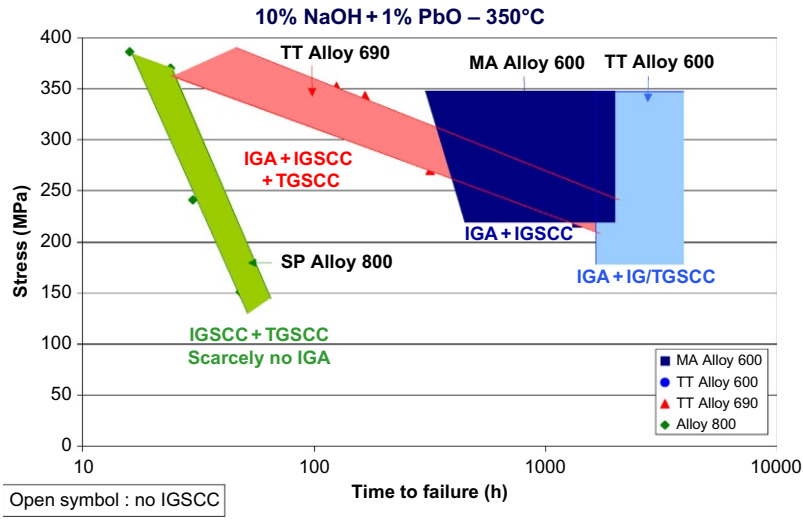

Fig. 8.9 IGA/SCC behavior of SG tube alloys in lead-caustic solutions, by EDF.
From de Curieres, I., Vaillant, F., et al., 2010. Lead pollution on the secondary side of steam generators: an overview, paper A127-T06. Proceedings of the International Conference "Fontevraud 7", SFEN (Ed.), September; Staehle, R.W., et al., 2006. Status and future of corrosion in PWR steam generators. Proceedings of the International Conference "Fontevraud 6", SFEN (Ed.), September, pp. 1225–1236.

- pH_T. Most of the past tests relied on estimated crevice pH values from the 1980s. Since then, the evolution of chemistry (lower sodium content) certainly allowed for less alkaline conditions in crevices. Moreover, pH_T often used to be:
  - estimated by "molar ratio index," defined as the ratio of the concentrations of cations (Na and K) and anions (Cl and excess SO_4) measured during hide-out-return
  - calculated by chemical computation codes integrating the output data from hide-out-return

  These methods have some drawbacks. Some research works have shown that the actual pH_T also depends on the presence or absence of solid magnetite acting as a buffering agent. For the same hide-out-return chemistry, there may be a 1.5 pH unit difference between the situation with or without magnetite deposits (Ulaganathan et al., 2015). Moreover, some other recent studies have shown that if not only classical impurity ions, but also aluminosilicate-derived ones, are considered, there may be a pH difference of up to 3 units (de Curieres, 2016) with a slight variation in aluminosilica species. Hence, the actual pH in crevices is difficult to precisely estimate, to say the least
- Electrochemical corrosion potential (ECP). The ECP may vary in crevices depending on whether they are occluded or not, the local hydrogen production, or diffusion from the primary side as well as the presence of oxidizing compounds. Tests have shown that a simple ECP change may inhibit IGA to favor ODSCC, or vice versa, or even inhibit both (Vaillant et al., 1995)
- Nature of species. The chemical state of species may influence the extent of corrosion. Sulfur species are a worthy example of it. They are known to be all the more detrimental when they are in a reduced state (EPRI, 2005). In the secondary side, although sulfates are measured at the blowdown of SGs, this element may be at various reduced states according to the presence of magnetite or hydrazine whose effect is to reduce sulfates (Staehle and Gorman, 2004a,b; Mansour et al., 2007; Delaunay et al., 2012). Thus, locally, sulfates, sulfides, or other reduced sulfur species could be present.

Based on this information, it appears utopian to try and establish a unified model for all secondary side corrosion phenomena, even though a tentative theoretical approach was proposed in the United States (Staehle, 2002). This is why since the early 2000s, laboratory tests have opted for a different approach that is more based on accessible chemistry data (e.g., hide-out-return, sludge analysis) and/or determining domains of susceptibility of alloys with respect to pH_T or ECP (de Curieres, 2016; Lu, 2007; Lu et al., 2008; Aublant et al., 2013; Wolfe et al., 2013; Turi et al., 2015). Such tests still show some potential susceptibilities even for corrosion-resistant alloys (de Curieres, 2016). One example of such obtained approach for CANDU reactors is presented below, from Lu (2007) (Fig. 8.10).

Rather than simple modeling, as is the case for PWSCC damage, this type of approach is likely to be the most crucial development to be made as it directly permits plant chemists to assist an operating plant.

8.3.1.3 Denting

Although not directly linked to the tubes, denting is another type of damage that affected the SG tubes. It can be defined as deformation of a tube due to bulging deposits or corrosion products on its outside surface.

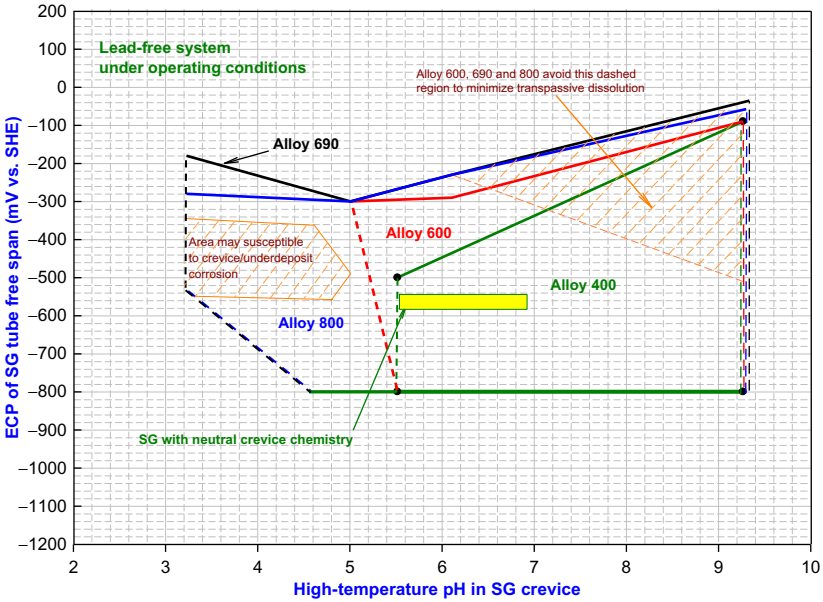

Fig. 8.10 Safe zones for SG tube alloys in CANDU SG operating conditions. Courtesy of Canadian Nuclear Laboratories (CNL).

Two locations of denting have been encountered:

- At the TSP elevation. This was historically the location of the first occurrences since 1975. The TSPs used to be drilled carbon steel plates. They corroded naturally during operation and the gap between the tube and the TSP filled with corrosion products. Since the volume of the corrosion products is more than twice that of the corroded steel, these products exerted a pressure on the tube resulting in deformation with slow straining. The kinetics of occurrence of denting could be high as impurities, such as copper, chlorides, or sulfur species penetrated the gap and accelerated the corrosion rate of the TSP mild steel. In this case, denting could be detected after a few fuel cycles following the pollutant ingress. TSP denting was tackled by changing the TSP design to broached stainless steel plates (Staehle and Gorman, 2003, 2004a,b).
- At the TTS location. SG tubes are expanded into tubesheets of A508 grade 3 class 1 steel. A narrow crevice remains between the tube and the tubesheet in order to minimize the residual stresses in the tube after expansion. In this crevice, the same phenomenon as was described immediately above may occur, leading to a bulge in the tube. In addition, when sludge deposits build up on the tubesheet, they may also impose a pressure on the tube, especially if they contain some iron particles, as was discovered in a plant nearly three decades ago (Scott et al., 1993) (Fig. 8.11).

Denting was a significant issue in the late 1970s at the TSP elevation, leading to a large number of tubes plugged. This was one of the consequences of the transition from a phosphate chemistry to the AVT one. Phosphates had a buffering effect in the crevices, limiting C&LAS corrosion, which is not the case for AVT chemistry. Improving

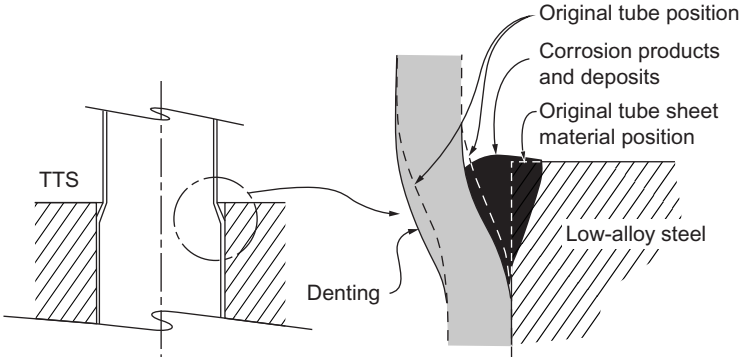

Fig. 8.11 Schematic representation of TTS denting.
From Staehle, R.W., Gorman, J.A., 2004. Quantitative assessment of sub-modes of stress corrosion cracking on the secondary side of steam generator tubing in Pressurized Water Reactors—part 2. Corrosion 60.

the AVT chemistry to a high purity one practically solved the issue by preventing most of the impurity ingress accelerating the corrosion in the crevices. At the TTS location, denting continued to occur during the 1980s, but to a lesser extent (Choi et al., 2014). It is noteworthy that currently, even replacement steam generators with highly corrosion-resistant alloys (800 and 690TT) have some tubes dented (Choi et al., 2014; Fernandez-Saavedra et al., 2014).

Limiting pollutants ingress enabled denting to be nearly completely suppressed by preventing fast corrosion in crevices. However, corrosion of carbon steel is a natural process, and accordingly, it could recur in the long-term operation of steam generators. The mechanism of denting is quite well established and can be found for instance in references (Staehle and Gorman, 2003, 2004a,b; Scott et al., 1993; Choi et al., 2014; Fernandez-Saavedra et al., 2014).

Apart from the tube deformation itself, denting may induce SCC in the tube. It used to induce SCC in alloy 600 tubes (Flesch et al., 1990; Staehle and Gorman, 2003; Choi et al., 2014) and even favored ODSCC in alloy 800 tubes (Kilian et al., 2007, 2015; Fernandez-Saavedra et al., 2014). It is worth mentioning that denting is more detrimental than a single mechanical deformation of the tube. Indeed, it is an evolving process, thus inducing slow strain rate deformation in the tube. Such continuous mechanical straining is more detrimental to SG tubes than a pure constant deformation; it could even be detrimental to alloy 690TT tubes (although no SCC has been reported yet in alloy 690TT dented tubes). Accordingly, it should not be disregarded.

8.3.1.4 Wastage

The final damage mechanism for SG tubes described here is wastage. This may be described as the generalized corrosion of the tube wall (Staehle and Gorman, 2003, 2004a,b; IAEA, 2011), i.e., a loss of wall thickness. It initially occurred in the first

steam generators with a phosphate chemistry and a low sodium to phosphate molar ratio. In these cases, under the sludge piles, some local very acidic conditions could develop, generating generalized corrosion either in alloy 600 or 800. The problem was solved by implementing flow distribution plates in the SGs (to limit the development of sludge piles) and a change to AVT chemistry.

Nevertheless, even with high purity AVT chemistry this phenomenon could occur in crevices if acidic conditions are present with sulfate additions (Cullen et al., 1993). Moreover, based on some laboratory tests, some authors have raised the possibility to have significant generalized corrosion in modern alloys (690TT and 800) in neutral or mildly alkaline conditions in the presence of Pb (Kilian et al., 1993).

Wastage has not been reported for decades. It is however worth citing as it indicates that in crevices or occluded areas, SCC may not be the only potential risk for tubing materials.

8.3.2 Carbon and low-alloy steels (C&LAS)

Apart from the tube bundle, the secondary side of steam generators is essentially made of carbon and low-alloy steels. In the past, these materials have also experienced some corrosion issues.

8.3.2.1 Generalized corrosion and flow-accelerated corrosion (FAC)

C&LAS naturally corrode in normal secondary side environments. This corrosion is sustainable for the life of the component, its rate being normally lower than 10 μm/year in deaerated high-temperature stagnant water. In case of high velocity or turbulent flowing conditions, the corrosion rate can be increased substantially, up to a few mm/year in the worst cases.

This phenomenon, called FAC, is well established, and precise modeling or phenomenology can be found in the literature (EPRI, 1996; Trevin, 2012). This damage is conditioned to specific situations (turbulent flow, medium range temperature, pH, etc.) and may result in local severe loss of thickness. FAC mostly affects carbon steel pipings in the secondary circuit, sometimes with lethal consequences after sudden fracture. In steam generators, the conditions are rarely fulfilled for severe FAC, with the exception of a few parts: some feedwater injection tubes, called J tubes, and feedrings (IAEA, 2011) as well as some moisture separators and blowdown pipes (EPRI, 1998) have experienced significant wall thinning.

For the steam generators themselves, the essential consequence of general corrosion and FAC of C&LAS in the secondary circuit is the presence of corrosion products in the water. They contribute to the following phenomena:

- Deposit build-up on the tubesheet or tube support plates
- Fouling of the steam generator tubes
- TSP blockage

These phenomena beget problems, such as:

- Loss of thermal power due to fouling of tubes
- Denting and SCC at the TTS location
- Vibration fatigue of SG tubes due to TSP blockage causing flow instabilities

The two former problems have already been dealt with in this chapter. The latter however is a mechanical problem which induced near SGTR in some tubes (Le Calvar et al., 2009), therefore with a significant safety impact for a plant. Moreover, because of such deposits, fouling and clogging events, whole campaigns of chemical cleanings were and continue to be performed, which are no trivial operations.

These phenomena are a reminder that the environmental behavior of materials in a steam generator must be well mastered in order to avoid long-term detrimental effects and heavy industrial maintenance and associated costs.

8.3.2.2 Localized corrosion and environmentally assisted cracking (EAC)

Apart from typical general corrosion, C&LAS have experienced direct degradation in the secondary side fluid, namely cracking and pitting. In the early 1980s, some cracks were discovered in some low-alloy steel shells of steam generators in a plant in the United States. It began by the discovery of a leak in a cone girth weld during an outage (USNRC, 1982). Extended ultrasonic examinations of the concerned weld in all the plant's steam generators revealed that about 170 cracks had initiated in each SG. One crack was through-wall, and the others had a typical depth of about 15 mm (3/4 in.). This prompted extended examinations in various plants and some other steam generator shells were found to be cracked. In the late 1990s, a total of eight plants (six in the United States and two in Europe) were affected by this problem (USNRC, 1982, 1985, 1990). The cracks were due to a mixture of corrosion-fatigue and stress corrosion cracking. Examination also showed extensive pitting in the areas of cracking and that cracks had initiated from the pits.

In addition to these cracking events, some other defects were detected in some German PWR SG parts, namely small bore diameter instrumentation lines (Roth et al., 2006). The German incidents were detected either by NDE or by small leaks. They consisted of pitting and sometimes cracking.

Apart from these PWR events, it is worth mentioning that similar incidents also befell some VVER steam generators (Zazantsev et al., 2013; Shutikov et al., 2014).

The cracking of C&LAS steels in hot water is generically designated by Environmentally Assisted Cracking (EAC), encompassing three different degradation modes:

- corrosion-fatigue (cyclic mechanical loadings)
- stress corrosion cracking (constant applied load)
- strain-induced corrosion cracking (SICC, cracking under monotonic dynamic local strains)

Field experience gave way to some detailed studies (Zazantsev et al., 2013; Shutikov et al., 2014; Czajlkowski, 1983; EPRI, 1993) which emphasized the following points as the contributors to the field events (although not all are necessary at the same time):

- presence of high residual stresses in the weld due to a too low-temperature post-weld heat treatment
- potential presence of geometrical stress raisers (e.g., weld defects, root notches)
- high or dynamic mechanical loads such as:
  - thermal stratification stresses
  - weld residual stresses
  - thermal stresses during start-up, shutdown, or hot standby
  - previous weld repairs
- presence of an oxidizing environment:
  - residual oxygen
  - presence of oxidizing impurities such as copper cations
- local nonnominal chemistry:
  - presence of chlorides under deposits, for instance
- previous localized corrosion (pitting) as an aggravating factor, serving both as a potential stress raiser and as an occluded area with a nonnominal chemistry

The important number of parameters aforementioned certainly explains the relatively small number of cracking instances worldwide. Nevertheless, the existence of oxidizing conditions, even transitory ones, was identified as the main factor permitting pitting and cracking. Were it needed, this is a reminder that avoidance of oxidizing conditions in the secondary side of steam generators is a sine qua noncondition to suppress localized corrosion and cracking in C&LAS.

Rapidly, laboratory tests confirmed the susceptibility of C&LAS to pitting and/or cracking in hot water (>100°C) when even small amounts of residual oxygen are present (sometimes 0.16 ppm was enough to trigger localized corrosion) (Mizuno et al., 1983; Szlarska-Smialowska et al., 1994) and the role of the MnS inclusions from the steel as initiation sites for pitting or cracking (Kuniya et al., 1992). Lastly, EAC has been extensively studied in laboratories (Seifert and Ritter, 2008a,b; Seifert et al., 2008; NUREG, 2004), with static, dynamic, or cyclic loading. One major conclusion is that EAC of C&LAS should not be possible under nominal secondary side conditions. However, as soon as some deviations exist, e.g.:

- chloride ingresses, even locally
- oxygen ingresses, even residuals or locally
- previous pitting is present

then EAC becomes possible. In this frame, meticulous and sustained care should be paid to outage and start-up stages of operation when oxidizing conditions may occur in the secondary circuit.

In the case of SICC, it appears that the most favorable situation exists for intermediate temperatures (100°C $< T <$ 150°C) with low oxygen concentrations (>30 ppb). It is worth noticing that the cracking domains for C&LAS in hot water correspond to the transition between hematite and magnetite (Kuniya et al., 2008).

In spite of the few incidents reported, cracking of C&LAS steels is of substantial safety significance as it directly impairs the availability of critical components required for safety.

8.4 Conclusions

Steam generators are a critical component for nuclear power plants, both in terms of operability and safety. They serve to cool the primary circuit and hence the nuclear fuel core. They also produce the steam activating the electricity generating turbines. From a safety perspective, the risks associated with damage in these components are loss of containment of the second barrier (SGTR, leaks at drains or tubes, bowl wastage), or impairment of the cooling of the fuel by unavailability of the steam generator. By design, it is a component facing quite harsh operating conditions, with heat fluxes, heat exchanges, boiling environments, crevice conditions, and thin materials for the tube bundle. Not surprisingly, corrosion, with various modes of occurrence, has been a major issue for these components, with high industrial and safety stakes.

These issues have prompted many evolutions in steam generator design (e.g., tube support plate geometry and steel grade, depth of crevices, tube-to-tubesheet expansion process, material grades for tubing) and operating practices with more stringent chemistry specifications over time. Such evolutions have postponed corrosion damage to later stages of operation, albeit the immunity of steam generators to corrosion cannot be fully guaranteed.

Significant efforts have been put into understanding the phenomenology of the various potential corrosion damages, without currently bringing solutions to all of them. Much research work is still needed to assess the critical elements required to deal with these issues on the secondary side. A renewed interest in research for steam generators degradation seems to be emerging, in connection with new field-reported-events or long-term operation concerns.

Eventually, the most efficient solution to prevent corrosion from happening in Steam Generators remains a good manufacturing design and quality, and to control accurately both the chemistry and the cleanliness of secondary side components. In particular, having more tolerant or resistant design and materials cannot lead to water chemistry specification relaxation for long-term operation. Finally, as operating experience constantly reminds us, immunity is an illusion as far as corrosion is concerned. Accordingly, the aforementioned precautions must be complemented with reliable and regular nondestructive examination.

References

Aublant, E., de Curieres, I., et al., 2013. Lead induced corrosion in SG tubing material. In: Proceedings of the 16th International Conference on Environmental Degradation of Nuclear Reactors, NACE, Asheville, USA, August 2013.

Bamford, W.H., et al., 2009. Service experience with alloy 600 and associated welds in operating PWRs, including repair activities and regulatory and code actions. In: Proceedings of the 14th International Conference on Environmental Degradation of Nuclear Reactors, Virginia Beach, VA, USA, August 2009.

Bibollet, C., et al., 2006. EDF field experience on steam generator divider plate examinations. Paper A0138-T04. In: SFEN, (Ed.), Proceedings of the international conference "Fontevraud 6," September 2006.

Boccanfuso, M., et al., 2015. The first two occurrences of external damage on alloy 600TT tubes in France. In: Proceedings of the 17th International Conference on Environmental Degradation of Nuclear Reactors, CNS, Ottawa, Canada, August 2015.

Bouchacourt, M., et al., 1998. Modélisation de l'IGA/IGSCC dans les générateurs de vapeur des centrales REP d'Electricité de France. In: SFEN, (Ed.), Proceedings of the International Conference "Fontevraud 4," Vol. 1 September 1998, pp. 663–674.

Buisine, D., et al., 2010. French steam generator tubes: an overview of degradations. Paper A164-T06. In: SFEN, (Ed.), Proceedings of the International Conference "Fontevraud 7," September 2010.

Cassagne, T., 1992. Le modèle de clivage induit par un film. In Corrosion sous Contrainte—phénoménologie et mécanismes—Bombannes 1990. Les éditions de physique, pp. 373–396.

Cattant, F., et al., 1994. Analyses of deposits and underlying surfaces of the secondary side of pulled out tubes from a French plan. In: SFEN, (Ed.), Proceedings of the International Conference "Fontevraud 3," Vol. 2, September 1994pp. 469–480.

Choi, S., et al., 2014. PWR steam generator tube denting at top of tubesheet. Paper 10137. In: Proceedings of the International Conference on Nuclear Power Chemistry, Sapporo, Japan.

Clauzel, M., et al., 2008. Correlation between Ni base alloys surface conditioning and cation release mitigation in primary coolant. In: Proceedings of the international conference on Nuclear Power Chemistry, Berlin.

Couvant, T., et al., 2010. PWSCC of steam generator divider plates in alloy 600. Paper A004-T04. In: SFEN, (Ed.), Proceedings of the international conference "Fontevraud 7," September 2010.

Cullen, W.H., et al., 1993. Corrosion of alloys 600&690 in acidified sulfate and chloride solutions. In: Proceedings of the 6th International Conference on Environmental Degradation of Nuclear Reactors, TMS, San Diego, USA, August 1993.

Czajlkowski, C.J., 1983. Investigation of Shell Cracking on Steam Generators at Indian Point Unit No. 3: USNRC Report NUREG/CR 3281.

Daret, J., 2005. Initiation of SCC in alloy 600 wrought materials: a laboratory and statistical evaluation. In: Proceedings of the 12th International Conference on Environmental Degradation of Nuclear Reactors, TMS, Salt Lake City, USA, August 2005.

de Bouvier, O., et al., 2001. Effect of copper species on IGA/SCC of alloy 600 in neutral sulfate environments. In: Proceedings of the 10th International Conference on Environmental Degradation of Nuclear Reactors, NACE, Lake Tahoe, USA, August 2001.

de Bouvier, O., et al., 2005. Stress corrosion cracking of Nickel alloys in "complex" (liquid and vapour) environments. In: Proceedings of the 12th International Conference on Environmental Degradation of Nuclear Reactors, TMS, Salt Lake City, USA, August 2005.

de Curieres, I., 2016. Domains of susceptibility of SG tube alloys in realistic secondary side crevice environments, private communication.

de Curieres, I., Meunier, M.-C., 2010. SCC of steam generator tubes made of alloy 600TT: analysis of operating experience. Paper A126-T06. In: SFEN, (Ed.), Proceedings of the international conference "Fontevraud 7," September 2010.

de Curieres, I., et al., 2010a. Residual life assessment of steam generators with alloy 600TT tubing: method and application. J. Eng. Gas Turb. Power 132 (10), 102902. ASME.

de Curieres, I., Vaillant, F., et al., 2010b. Lead pollution on the secondary side of steam generators: an overview. Paper A127-T06. In: SFEN, (Ed.), Proceedings of the International Conference "Fontevraud 7," September 2010.

Deforge, D., et al., 2010. Learnings from EDF investigations on SG divider plates and vessel head nozzles. Paper A117-T04. In: SFEN, (Ed.), Proceedings of the international conference "Fontevraud 7," September 2010.

Delaunay, S., et al., 2012. Prediction of sulfur speciation in secondary circuit conditions—influence of magnetite and hydrazine at 275°C. Paper 237-P2-15. In: Proceedings of the international conference on Nuclear Power Chemistry, Paris, France.

Diercks, D.R., et al., 1999. Overview of steam generator tube degradation and integrity issues. Nucl. Eng. Des. 194, 19–30.

Duisabeau, L., et al., 2010. EDF experience on 182 J-groove welds on CRDMs and SG channel head nozzles. Paper A118-T04. In: SFEN, (Ed.), Proceedings of the international conference "Fontevraud 7," September 2010.

Efsing, P., et al., 2005. Root cause analysis of failed J-groove welds in steam generator drainage nozzles. In: Proceedings of the 12th International Conference on Environmental Degradation of Nuclear Reactors, TMS, Salt Lake City, USA, August 2005.

Engler, N., et al., 2008. Optimization of SG tubes prefilming process to reduce Nickel release. In: Proceedings of the International Conference on Nuclear Power Chemistry, Berlin.

EPRI, 1993. Review of Steam Generator Girth Weld Cracking: Technical report TR-103498. EPRI, Palo Alto, CA.

EPRI, 1996. Flow-Accelerated Corrosion in Power Plants: TR-106611. EPRI, Palo Alto, CA.

EPRI, 1998. Correlation of Flow-Accelerated Corrosion (FAC) of Steam Generators Internals With Plant Water Chemistry: Technical report TR-111113. EPRI, Palo Alto, CA.

EPRI, 2001a. Boric Acid Corrosion Guidebook—Revision 1: Technical report TR-1000975. EPRI, Palo Alto, CA.

EPRI, 2001b. Overview report on Zn addition in PWR: Technical report 1001020. EPRI, Palo Alto, CA.

EPRI, 2002. Crack growth rates for evaluating PWSCC of thick-wall alloy 600: EPRI document MRP-55. EPRI, Palo Alto, CA. revision 1, ID 1006695.

EPRI, 2004. Crack growth rates for evaluating PWSCC of alloy 82, 182 and 132 welds: EPRI document MRP-115. EPRI, Palo Alto, CA. ID 1006696.

Proceedings 2005 EPRI/ANL/NRC Workshop on effects of Lead (Pb) and Sulfur (S) on the performance of the secondary side tubing of steam generators in PWRs, EPRI Report No 1012780, December 2005.

EPRI, 2006. Benchmarking Shutdown Chemistry Control Recommendations in the Pressurized Water Reactor Primary Water Chemistry Guidelines: Technical report TR-1011780. EPRI, Palo Alto, CA.

Fernandez-Saavedra, R., et al., 2014. Hard sludge and denting on the secondary side of PWR steam generators. Paper 10120. In: Proceedings of the International Conference on Nuclear Power Chemistry, Sapporo, Japan.

Flesch, B., et al., 1990. Contraintes en service et sur-contraintes de denting dans les zones de transition des générateurs de vapeur des réacteurs 900MWe et 1300MWe. In: SFEN, (Ed.), Proceedings of the international conference "Fontevraud 2," September 1990. p. 268.

Ford, F.P., 1992. Slip dissolution model. In Corrosion sous Contrainte—phénoménologie et mécanismes—Bombannes 1990, Les éditions de physique, pp. 307–344.

Fournier, L., et al., 2011. Grain boundary oxidation and embrittlement prior to crack initiation in alloy 600 in PWR primary wate. In: Proceedings of the 15th International Conference on Environmental Degradation of Nuclear Reactors, TMS, Colorado Springs, USA, August 2011.

Fyfitch, S., et al., 2015. Dissimilar Weld Metal PWSCC initiation model refinement for xLPR: part I. In: Proceedings of the 17th International Conference on Environmental Degradation of Nuclear Reactors, Ottawa, Canada, August 2015.

Hwang, S.S., et al., 2009a. PWSCC in the steam generator drain nozzle of a PWR. In: Proceedings of the 14th International Conference on Environmental Degradation of Nuclear Reactors, Virginia Beach, VA, USA, August 2009.

Hwang, S.S., et al., 2009b. Steam generator management strategies in Korea. IAEA, Vienna.

Hwang, S.S., et al., 2013. SCC of alloy 600 tubes from a retired steam generator. J. Nucl. Mater. 440, 129–135.

IAEA, 1992. Coolant Technology of Water Cooled Reactors—Volume 3: IAEA-TECDOC-667. IAEA, Vienna.

IAEA, 2011. Assessment and Management of Ageing of Major Nuclear Power Plant Components Important to Safety: Steam Generators: IAEA-TECDOC-1668. IAEA, Vienna.

Kilian, R., et al., 1993. Influence of lead on the SCC behavior of SG tubing materials. In: IAEA Specialists Meeting on Steam Generator Problems and Replacement, Madrid, Spain, p. 137.

Kilian, R., et al., 2007. Operating experience with alloy 800 SG tubes in Europe. In: Proceedings of the 13th International Conference on Environmental Degradation of Nuclear Reactors, CNS, Whistler, Canada, August 2007.

Kilian, R., et al., 2015. Examination of ET-indications of steam generator tubes from the Almaraz unit 2 NPP replacement steam generator SG3. In: Proceedings of the 17th International Conference on Environmental Degradation of Nuclear Reactors, CNS, Ottawa, Canada, August 2015.

Kim, D.G., et al., 2009. Oxides formed on steam generator tubing in lead containing high temperature aqueous solutions. In: Proceedings of the CNS International SG Conference, CNS, paper 5-11, Toronto, Canada, November 2009.

King, P.J., 2007. Examination of oxides and deposits on the tubes removed from Bruce units. In: Proceedings of the 13th International Conference on Environmental Degradation of Nuclear Reactors, CNS, Whistler, Canada, August 2007.

Kuniya, J., et al., 1992. Susceptibility of low-alloy carbon steel to pitting and stress corrosion cracking in steam generator conditions. Corrosion 48 (4), 419–425.

Kuniya, J., et al., 2008. Consideration on the existence of a threshold for SCC initiation of low alloy steel and carbon steel in simulated BWR environmen. In: Proceedings of "The SCC Initiation Workshop", Beaune, France, September 2008.

Laghoutaris, P., et al., 2011. Stress Corrosion Cracking of alloy 600 in PWR primary water: influence of chromium, hydrogen and oxygen diffusion. In: Proceedings of the 15th International Conference on Environmental Degradation of Nuclear Reactors, TMS, Colorado Springs, USA, August 2011.

Le Calvar, M., et al., 2009. Build-up of deposits in steam generators: a safety issue. In: Proceedings of the 14th International Conference on Environmental Degradation of Nuclear Reactors, Virginia Beach, VA, USA, August 2009.

Lister, D., et al., 2015. Boric-acid corrosion of carbon steel below perforated stainless steel cladding. In: Proceedings of the 17th International Conference on Environmental Degradation of Nuclear Reactors, CNS, Ottawa, Canada, August 2015.

Lu, Y., 2007. Define optimum conditions for Steam Generator tube integrity and extended Steam Generator life. In: Proceedings of "15th International Conference on Nuclear Engineering", Nagoya, Japan, April 2007.

Lu, B., et al., 2008. Roles of Film Rupture in Lead-Induced Stress Corrosion Cracking. Beaune, France, 2008.

Magnin, T., 1992. Les modèles liés à la plasticité. In Corrosion sous Contrainte—phénoménologie et mécanismes—Bombannes 1990, Les éditions de physique, pp. 345–372.

Mansour, C., et al., 2007. Behaviour of sulfur species in steam generator conditions of PWRs. In: Proceedings of the 13th International Conference on Environmental Degradation of Nuclear Reactors, CNS, Whistler, Canada, August 2007.

Mathon, C., et al., 2014. Predicting tube repair at French nuclear steam generators using statistical modeling. Nucl. Eng. Des. 269, 299–305.

Matsubara, N., et al., 2010. Research programs on SCC of cold-worked stainless steel in Japanese PWR N.P.P. Paper A099–T03. In: SFEN, (Ed.), Proceedings of the international conference "Fontevraud 7," September 2010.

Miglin, M.T., et al., 1995. SCC of alloy 600 in complex caustic environments. In: Proceedings of the 7th International Conference on Environmental Degradation of Nuclear Reactors, Breckenridge, USA, August 1995, pp. 277–290.

Mizuno, T., et al., 1983. Corrosion and stress corrosion cracking of carbon steel in oxygenated, high-purity water at elevated temperatures. In: Proceedings of the 1st International Conference on Environmental Degradation of Nuclear Reactors, Myrtle beach, USA, 1983.

Nasrazadan, S., et al., 2007. Lead (Pb^{2+}) adsorption on magnetite (Fe_3O_4) at 200°C. In: Proceedings of the 13th International Conference on Environmental Degradation of Nuclear Reactors, CNS, Whistler, Canada, August 2007.

Report NEA/CRPPH/R(2014)2, Radiation protection aspects of primary water chemistry and source term management, JT03360680, April 2014.

NUREG/CR-4667, Vol. 35, Environmentally Assisted Cracking in LWR, annual report, December 2004.

Olszta, M., et al., 2011. Electron Microscopy characterization and Atom Probe Tomography of Intergranular Attack in alloy 600 exposed to PWR primary water. In: Proceedings of the 15th International Conference on Environmental Degradation of Nuclear Reactors, TMS, Colorado Springs, USA, August 2011.

Pavageau, E.-M., et al., 2001. Secondary side corrosion modeling of alloy 600 for steam generator tubes based on laboratory tests in sulfate environments. In: Proceedings of the 10th International Conference on Environmental Degradation of Nuclear Reactors, NACE, Lake Tahoe, USA, August 2001.

Pierson, E., et al., 1995. How to simulate acid corrosion of alloy 600 steam generator tubes. In: Proceedings of the 7th International Conference on Environmental Degradation of Nuclear Reactors, Breckenridge, USA, August 1995, pp. 303–316.

Richey, E., et al., 2007. SCC initiation testing of Nickel-based alloys in high temperature water. In: Proceedings of the 13th International Conference on Environmental Degradation of Nuclear Reactors, CNS, Whistler, Canada, August 2007.

Roth, A., et al., 2006. Degradation of carbon steel and low alloy steel small diameter pipes due to localized corrosion and environmentally assisted cracking in German PWR plants. Paper A052-T07. In: SFEN, (Ed.), Proceedings of the International Conference "Fontevraud 6," September 2006.

Sakai, T., et al., 1991. Lead-induced stress corrosion cracking of alloy 600 and 690 in high temperature water. In: Proceedings of the 5th International Conference on Environmental Degradation of Nuclear Reactors, TMS, Monterey, USA, August 1991.

Scott, P.M., 1991. An analysis of Primary Water Stress Corrosion Cracking in PWR Steam generators. In: Specialist meeting on Operating Experience with Steam Generators, Brussels, Belgium, paper 5-6, UNIPEDE.

Scott, P.M., Le Calvar, M., 1993. Some possible mechanisms of intergranular stress corrosion cracking of alloy 600 in PWR primary water. In: Proceedings of the 6th International Conference on Environmental Degradation of Nuclear Reactors, TMS, San Diego, USA, August 1993.

Scott, P., et al., 1993. Factors affecting PWR steam generator tube denting above the tubesheet. In: Proceedings of the 6th International Conference on Environmental Degradation of Nuclear Reactors, San Diego, USA, August 1993, pp. 227–232.

Scott, P.M., Benhamou, C., Meyzaud, Y., 1995. Plant Ageing and Life Prediction of Corrodible Structures. NACE, Sapporo. pp. 285–294.

Scott, P., Cattant, F., de Curieres, I., Raquet, O., 2008. Matériaux pour les tubes de GV de réacteurs à eau pressurisée et leur résistance à la corrosion sous contrainte en service. In: SFEN, Paris. ST2 commission.

Seifert, H.P., Ritter, S., 2008a. Stress corrosion cracking of low-alloy reactor pressure vessel steels under boiling water reactor conditions. J. Nucl. Mater. 372, 114–131.

Seifert, H.P., Ritter, S., 2008b. Strain-induced corrosion cracking of low-alloy steels under boiling water reactor conditions. J. Nucl. Mater. 378, 312–329.

Seifert, H.P., et al., 2008. Crack initiation due to environmentally assisted cracking in carbon and low-alloy steels in high-temperature water—part 1: overview of results from laboratory tests. In: Proceedings of "The SCC Initiation Workshop", Beaune, France, September 2008.

Seo, M.J., et al., 2014. Influence of surface roughness on the corrosion behavior of alloy 690TT in PWR primary water. Nucl. Eng. Des. 280, 62–68.

Shoji, T., et al., 2010. Effect of cold-work and stress on the oxidation and SCC behavior of stainless steels in PWR primary water environments. Paper A103-T03. In: SFEN, (Ed.), Proceedings of the international conference "Fontevraud 7," September 2010.

Shutikov, A.V., et al., 2014. Maintaining of the integrity of the weld assembly of the coolant header weld to the DN1200 nozzle of PGV-1000 steam generators. Paper 77-T06. In: Proceedings of the International Conference "Fontevraud 8," September 2014.

Staehle, R.W., 2002. Approach to predicting SCC on the secondary side of steam generators. In: SFEN, (Ed.), Proceedings of the International Conference "Fontevraud 5," Vol. 2, September 2002, pp. 1019–1035.

Staehle, R.W., Gorman, J.A., 2003. Quantitative assessment of sub-modes of stress corrosion cracking on the secondary side of steam generator tubing in Pressurized Water Reactors—part 1. Corrosion 59, 931–994

Staehle, R.W., Gorman, J.A., 2004a. Quantitative assessment of sub-modes of stress corrosion cracking on the secondary side of steam generator tubing in Pressurized Water Reactors—part 2. Corrosion 60, 5–63

Staehle, R.W., Gorman, J.A., 2004b. Quantitative assessment of sub-modes of stress corrosion cracking on the secondary side of steam generator tubing in Pressurized Water Reactors—part 3. Corrosion 60, 115–180

Staehle, R.W., Gorman, J., et al., 1994. Application of statistical distributions to characterizing and predicting corrosion of tubing in steam generators of pressurized water reactors. In: Life Prediction in Corrodible Structures conference, NACE and JSCE, Houston, USA, pp. 1374–1439.

Staehle, R.W., et al., 2006. Status and Future of Corrosion in PWR Steam Generators. In: SFEN, (Ed.), Proceedings of the International Conference "Fontevraud 6," September 2006, pp. 1225–1236.

Stavropoulos, K.D., et al., 1991. Selection of statistical distributions for prediction of steam generator tube degradation. In: Proceedings of the 5th International Conference on Environmental Degradation of Nuclear Reactors, TMS, Monterey, USA, August 1991.

Szlarska-Smialowska, S., et al., 1994. Susceptibility of low-alloy carbon steel to pitting and stress corrosion cracking in steam generator conditions. Corrosion 50 (4), 279–289.

Thebault, Y., et al., 2010. Experience of steam generator tube examination in the hot laboratory of EDF: analysis of recent events concerning the secondary side. Paper A166-T06. In: Proceedings of the International Conference "Fontevraud 7," September 2010.

Trevin, S., 2012. Nuclear corrosion science and engineering. In: Feron, D. (Ed.), Woodhead Publishing, Sawston, Cambridge. Chapter 7.

Turi, M.-L., et al., 2015. Stress corrosion cracking of alloy 800 in secondary side crevice environment. In: Proceedings of the 17th International Conference on Environmental Degradation of Nuclear Reactors, CNS, Ottawa, Canada, August 2015.

Ulaganathan, J., et al., 2015. Mitigating effect of magnetite buffering on alloy 800 tubing degradation in acidic, sulfate-dominated, environments at 300°C. In: Proceedings of the 17th International Conference on Environmental Degradation of Nuclear Reactors, CNS, Ottawa, Canada, August 2015.

USNRC, 1982. Cracking of the Upper Shell-to-Transition Cone Girth Welds of a Steam Generator at an Operating Pressurized Water Reactor: Information Notice 82-37. USNRC, Rockville, MD.

USNRC, 1985. Crack Growth in Steam Generator Girth Welds: Information Notice 85-65. USNRC, Rockville, MD.

USNRC, 1990. Cracking of the Upper Shell-to-Transition Cone Girth Welds in Steam Generators: Information Notice 90-04. USNRC, Rockville, MD.

USNRC, 1994. Boric Acid Corrosion of Charging Pump Casing Caused by Cladding Cracks: Information Notice 94-63. USNRC, Rockville, MD.

USNRC, 2005a. Pressure boundary leakage identified on steam generator bowl drain: USNRC Information Notice 2005-02. USNRC, Rockville, MD.

USNRC, 2005b. Boric Acid Corrosion of Light Water Reactor Pressure Vessel Materials: NUREG/CR-6875, annual report. USNRC, Rockvile, MD.

USNRC, 2008. Cracking indications in thermally treated alloy 600 steam generator tubes: USNRC Information Notice 2008-07. USNRC, Rockville, MD.

USNRC, 2013. Steam Generator Channel Head and Tubsesheet Degradation: Information Notice 2013-20. USNRC, Rockville, MD.

Vaillant, F., et al., 1995. Comparative behavior of alloys 600, 690 and 800 in caustic environments. In: Proceedings of the 7th International Conference on Environmental Degradation of Nuclear Reactors, Breckenridge, USA, August 1995. pp. 219–232.

Wolfe, R., 2015. Field experience with steam generator tubing materials in the United States. In: Proceedings of the International Nuclear Components Conference, Mississauga, Canada, November 2015.

Wolfe, R., et al., 2013. PbSCC of alloy 690TT and 800NG steam generator tubing in alkaline conditions. In: Proceedings of the 16th International Conference on Environmental Degradation of Nuclear Reactors, NACE, Asheville, USA, August 2013.

Yamanaka, K., 1991. Straining electrode behavior and corrosion resistance of Nickel base alloys in high temperature acidic solution. In: Proceedings of the 5th International Conference on Environmental Degradation of Nuclear Reactors, TMS, Monterey, USA, August 1991.

Yonezawa, T., et al., 2014. The effect of cold-working on SCC growth rate of 316 stainless steels in simulated PWR primary water. Paper 57-T03. In: SFEN, (Ed.), Proceedings of the International Conference "Fontevraud 8," September 2014.

Zazantsev, A., et al., 2013. Stress corrosion cracking in steam generator SG 1000 under low-rate strain. In: Proceedings of the Transactions SMiRT-22, San Francisco, CA, USA, August 2013.

This page intentionally left blank

Corrosion product transport and fouling in nuclear steam generators

9

C.W. Turner[*], *K. Khumsa-Ang*[†]
[*]Deep River, ON, Canada, [†]Canadian Nuclear Laboratories, Chalk River, ON, Canada

9.1 Introduction

The function of the steam generator (SG) in an indirect cycle nuclear power plant (NPP) is to generate steam from the nuclear heat produced by fission reactions in the core during operation at power, and to act as a heat sink to remove decay—heat from fission products during both normal reactor shut down and for a postaccident scenario in the event that reactor core cooling has been impaired. Situated at the boundary between the nuclear (radioactive primary coolant system) and conventional (nonradioactive secondary coolant system) sides of the plant, the SG plays two safety-critical roles:

1. Provides a barrier to prevent the release of radioactivity from the primary reactor coolant to the secondary coolant where it can be released to the environment
2. Removes heat from the primary coolant to the secondary coolant to maintain a safety margin during power operation and some postaccident scenarios

Thus, the integrity of the SG and its internal components is vital for assuring the safe, economical, and reliable performance of the NPP (IAEA, 1997; Riznic, 2006).

Despite improvements in materials, designs, and water chemistry, degradation affecting the safety and performance of the SG continues to be a major concern within the nuclear industry (Tapping et al., 2000; Staehle et al., 2006). Every SG design has a multitude of crevices at the tube/tube-support intersections which, when partially filled with deposit, become concentration sites for impurities which, in turn, increases the risk of corrosion, and in particular stress-corrosion cracking (SCC) and/or pitting on the outer surface of the SG tube. Understanding the relationships between deposit accumulation, the development of aggressive (corrosive) chemistry environments and the impact of these environments on the risk of SG degradation must remain a key focus area for the industry, especially in light of the 60-year plus lifetimes that are now expected for SGs to meet the economic needs of NPPs. Almost without exception, the degradation of the SG is related in one way or another to the accumulation of deposits on various components on the secondary side of the SG, e.g., the tube

Steam Generators for Nuclear Power Plants. http://dx.doi.org/10.1016/B978-0-08-100894-2.00011-X
© 2017 Elsevier Ltd. All rights reserved.

bundle,[1] tube-support structure, tubesheet, and steam separators.[2] A corollary of this statement is that a properly designed SG should not fail by either of the above-mentioned degradation mechanisms provided that the SG remains clean, i.e., free of deposit. Thus, the key to minimizing degradation of the SG is the ability to mitigate the accumulation of unwanted deposit, or fouling, on the surfaces of critical components within the SG.

9.2 SG design and the effect of fouling on performance degradation

Detailed discussions of the various designs of SGs used at NPPs are presented in Chapters 1 and 4 of this Handbook. In the following sections, three basic designs will be briefly reviewed to provide context for the subsequent material presented in this chapter.

9.2.1 Recirculating SG

For all nuclear SGs considered in this Handbook, the primary reactor coolant flows on the inside of the SG tubes and boils water, i.e., the secondary coolant, on the outer surface, or shell side, of the tubes. In the vertical Recirculating Steam Generator (RSG) design, feedwater (FW) enters the SG either through a feed ring at the top of the tube bundle or via an integral preheater located at the base of the cold leg, as shown in Fig. 9.1. The FW is mixed with separated water from the steam separators and then flows up through the tube bundle where steam is generated. About 25 wt% of the water is converted to steam on a single pass through the tube bundle. The remainder is separated from the steam/water mixture in the steam separators and recirculated through the tube bundle via the downcomer, while the separated steam is sent to the turbine generator. A small flow of water known as blow down (BD), corresponding to 1% or less of the main steam mass flow rate, is removed from the SGs on a continuous basis to limit the accumulation of impurities in the recirculating water.

9.2.2 Once-through SG

For the Once-Through Steam Generator (OTSG) design, shown in Fig. 9.2, the secondary water enters the SG at about the tenth tube-support plate (TSP) and is heated while it drains via the downcomer to the tubesheet, where it enters the tube bundle. The OTSG is divided into two regions; the boiling region between the tubesheet and the tenth TSP where the FW is converted entirely to steam, and the super heater section above the tenth TSP, where the steam is superheated before being sent to the

[1] Precipitation fouling on the inside surface of the tube bundle as a result of the use of carbon steel for the feeder pipes and reactor coolant piping also leads to a loss of thermal performance in CANDU SGs.

[2] One exception is fretting wear associated with an improperly designed tube support structure which can cause high tube failure rates resulting from an excessively high fretting wear rate early in the life of the SG. Flow accelerated corrosion of carbon steel internal components, such as tube supports and separators, is another degradation mechanism that is not strictly linked to deposit formation.

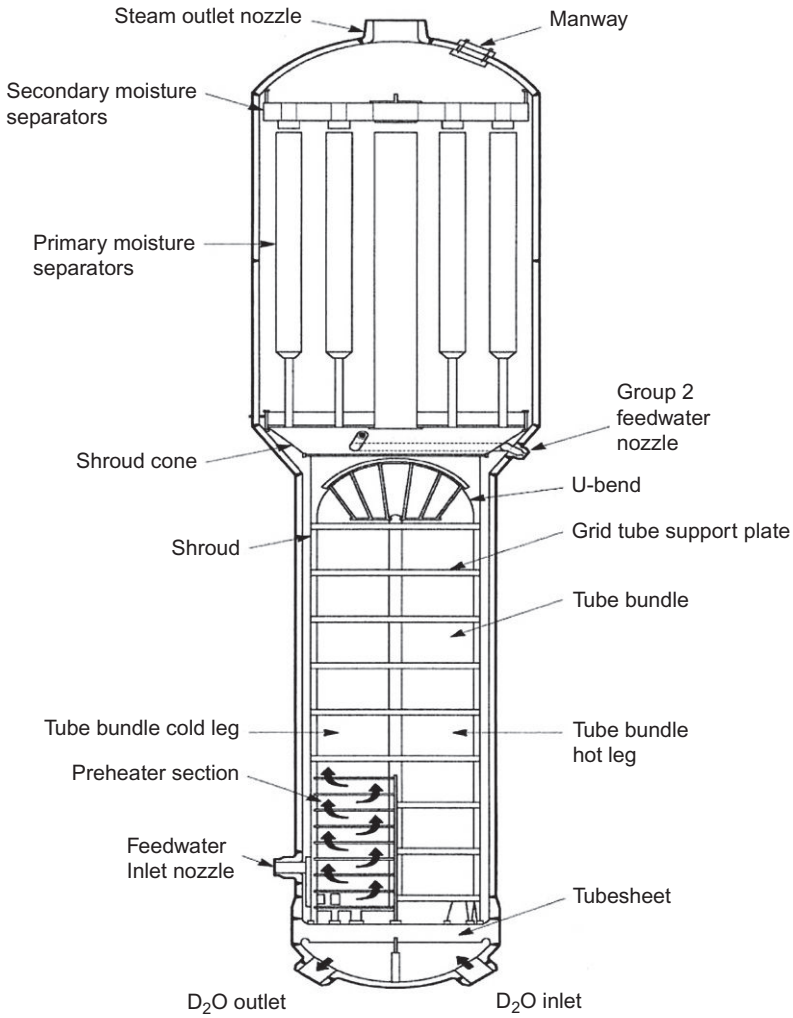

Fig. 9.1 Illustration of a vertical u-tube recirculating steam generator (RSG) with integral preheater (Turner, 2013).

turbine generator. In both the RSG and OTSG designs, after passing through the turbine generator the steam is condensed and returned to the SGs via a series of FW heaters that are heated using steam extracted from the high-pressure (HP) and low-pressure (LP) turbines.

9.2.3 Horizontal SG

For the horizontal SG (Trunov et al., 2006), primary coolant enters the SG via a vertical header, flows through the horizontal SG U-tube bundle, and exits via a second vertical header. The inlet and outlet primary coolant headers perforate the SG shell near the middle of the shell. FW is supplied to the shell side of the tube bundle at

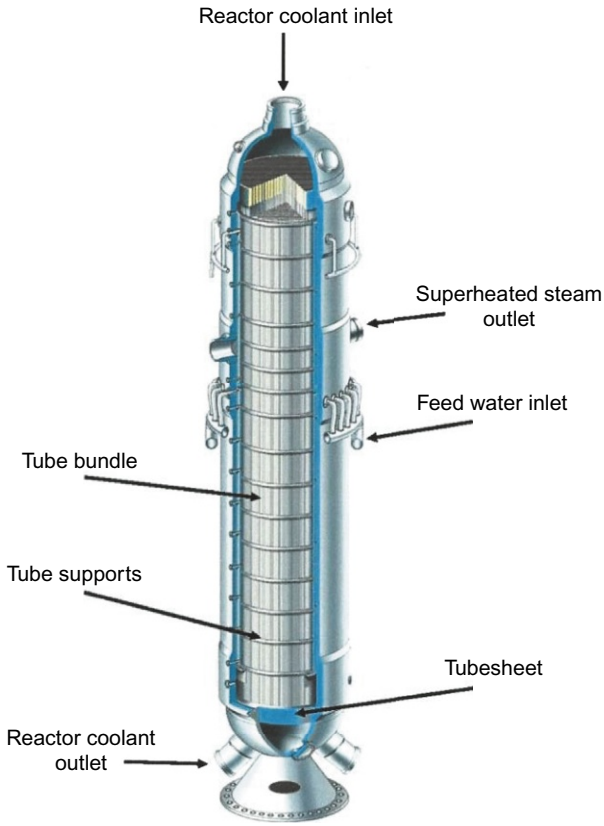

Fig. 9.2 Illustration of a vertical once-through steam generator (OTSG). Courtesy of BWXT Canada, Ltd.

the middle of the tube bundle via perforated piping under a perforated sheet. The tube bundle is entirely submerged in the secondary coolant.

9.2.4 Effect of fouling on SG performance degradation

Fouling was originally a descriptive term used in the oil industry to refer to the accumulation of undesirable deposit on heat-exchanger surfaces that increases the resistance to heat transmission (Taborek et al., 1972). The accumulation of corrosion products on the internal surfaces of a nuclear SG can severely degrade SG performance and increase the risk of materials degradation as a result of:

1. Formation of a resistive layer of deposit on the tube surface that could reduce the rate of heat transfer from the primary to the secondary coolant and decrease the safety margin,
2. Accumulation of ionic impurities to form concentrated solutions that are aggressive to tube integrity under thick deposits or in deposit-filled crevices between the tubes and the tube-support structure,
3. Restriction of the movement of the tubes caused by deposit accumulation on the tube-support structure; tube "lock-up" leading to high-cycle fatigue,

4. Blockage of the flow passages of the tube-support structure, resulting in several operational and materials degradation problems discussed below, and
5. Accumulation of a thick sludge pile on the tubesheet that becomes increasingly consolidated with time, with deleterious consequences for tube integrity.

The formation of a layer of corrosion product on the boiling side of the SG tube has two separate effects on heat transfer. The outer porous layer provides additional sites for bubble nucleation and, thus, reduces the wall superheat required for bubble nucleation. This is manifested by an improvement in heat transfer as the bare tube surface becomes covered with a thin layer of porous deposit. As deposits grow thicker, however, they develop a layered structure, with a dense inner layer that is resistive to heat transfer and a porous outer layer that enhances heat transfer (Turner et al., 2000). The net result is that many RSGs show a net improvement in thermal performance during the first few years of operation, followed by a steady deterioration in thermal performance as thicker deposits build up on the tube bundle (Lovett and Dow, 1991). Other factors, such as changes in primary and secondary coolant flow rates, separator fouling, and SG divider plate leakage to name a few, have also been shown to contribute to the degradation of SG thermal performance, and so a systematic approach must be taken to quantify all contributions to thermal performance degradation before taking any remedial action (Yetisir et al., 2000; Kreider et al., 1998).

The accumulation of deposit on the heat transfer surface also raises the risk of under-deposit corrosion, especially in crevice regions at the tubesheet, top of the sludge pile, and at the tube/tube-support intersections (IAEA, 1997) where high concentrations of impurities can accumulate during power operation through a process known as "hideout" (Balakrishnan et al., 1996; Balakrishnan, 1999). Hideout is driven by the evaporation of liquid within the pores of the deposit. As the liquid within the pores evaporates it is replaced by fresh solution that is drawn into the deposit by capillarity. The fresh solution brings with it additional nonvolatile ionic species, thus increasing the concentration of the solution in the pores. As the concentration of the solution increases selected compounds will precipitate, depending on their solubility. The pH of the solution that remains in equilibrium with the precipitate is determined by the relative concentrations of ionic species that remain in solution. Thus, the pH in fouled crevice regions and within the pores of thick deposits is not determined by the amine that is added for pH control in the steam cycle. The crevice pH is ultimately determined by the relative concentrations of soluble impurities that are transported to the SG with the FW and by the solubility and composition of the compounds that precipitate in the crevices under boiling heat transfer conditions. Electric Power Research Institute (EPRI) and Atomic Energy of Canada Limited (AECL) have developed codes to predict the high-temperature crevice pH that results from hideout and precipitation of nonvolatile soluble ionic species based on equilibrium models of crevice chemistry. This information, combined with measurements of the electrochemical corrosion potential (ECP) of SG tubes in various crevice environments, has been used to establish two-dimensional maps of pH and ECP at 25°C, 150°C, and 300°C where the risk of localized crevice corrosion and pitting of SG tubes is predicted to be at a minimum (Lu, 2007).

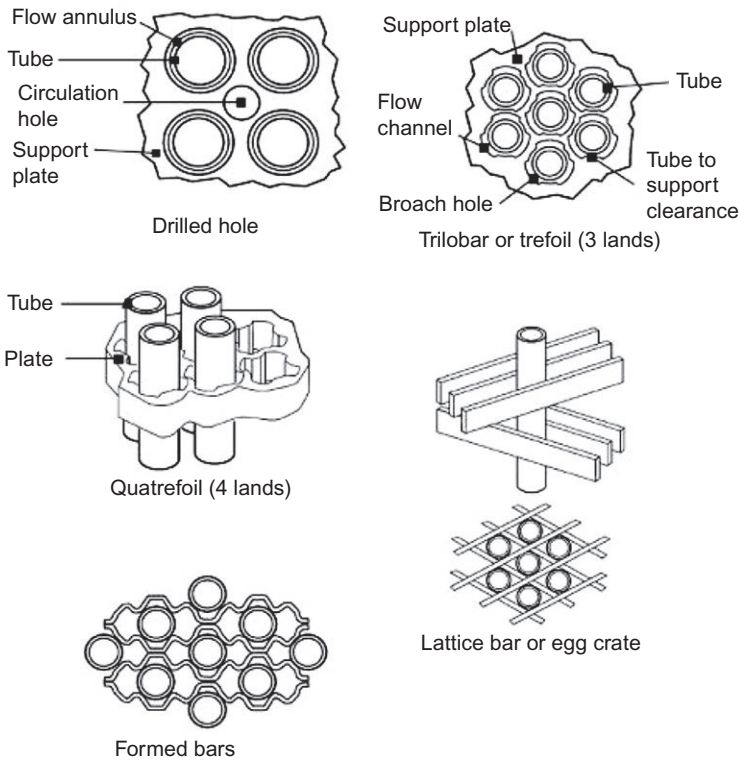

Fig. 9.3 Illustrations of different tube-support designs used in nuclear steam generators (Rummens et al., 2004).
Courtesy of the American Nuclear Society, La Grange Park, IL. Copyright 2004.

Accumulation of deposit on the SG tube-support structure can lead to both operational problems affecting the performance of the SG and degradation of the support structure and the SG tubes. Examples of common tube-support designs used in nuclear SGs are shown in Fig. 9.3 (Rummens et al., 2004). The trefoil and quatrefoil TSP designs are particularly susceptible to deposit accumulation within the flow-holes of the TSP, which causes an increase in the pressure drop across the TSPs. Flow blockage tends to be higher on the hot leg side of the SG compared to the cold leg in the RSGs and increases in the boiling zone with increasing steam quality. The increased pressure drop across the TSPs has led to flooding of the aspirator ports in OTSGs designed by Babcock and Wilcox (Johnson, 1987; Thompson and Lammana, 1986; Thompson, 1992; Thompson and Gaudreau, 1995) and to the onset of density-wave oscillations in RSGs of both the Westinghouse (Stickel et al., 1994) and the Babcock and Wilcox (Dyck et al., 1990; Malaugh and Ryder, 1990) designs.[3] In both cases, the short-term remedial

[3] Density-wave oscillations can occur in a system if there is a higher pressure drop in the two-phase flow region than in the region where the flow is single-phase. Density wave oscillations in an RSG manifest themselves as oscillations in the water level in the SG.

solution was to operate the plants at reduced power until such time as the deposit could be removed from the flow passages of the TSPs by either water-slap or chemical cleaning. The SGs at Gentilly-2 Nuclear Generating Station also showed early signs of level oscillations prior to chemical cleaning (Plante, 2005).

Blockage of the quatrefoil TSPs in SGs at the Cruas NPP did not lead to density-wave oscillations, but instead to a redistribution of flow in the upper bundle region that caused flow-induced vibration (FIV) that was outside of the design basis of the SG. FIV ultimately resulted in failure of some tight-radius SG tubes by high-cycle fatigue (Bodineau and Sollier, 2008; Corredera et al., 2008). The problem was exacerbated somewhat by the SG design which included a tube-free region in the centre of the bundle. Interestingly, the heavy TSP blockage did not manifest itself in the onset of a density-wave oscillation, as observed in other RSGs with blocked trefoil or quatrefoil TSPs. However, thermal-hydraulic analyses concluded that the SGs were susceptible to the onset of a density-wave oscillation in response to certain transients, such as a 10% step in reactor power. A subsequent investigation concluded that the tube failures were caused by a combination of: (1) Blockage of the flow-holes of the quatrefoil TSPs that caused the steam/water mixture to be redirected toward tubes near the centre of the bundle with small-radius bends and (2) Tube lock-up, resulting from heavy fouling of the tube-TSP intersections, which increased the local stress intensity of the tubes.

Partial blockage of the trefoil TSPs on the hot leg and extensive degradation of the carbon steel TSPs on the cold leg were identified in 2004 by a visual inspection of the SGs at the Embalse NPP (Luna et al., 2006; Obrutsky et al., 2006). The degradation on the cold leg was attributed to flow-accelerated corrosion (FAC) of the low chromium (0.07–0.08 wt%) carbon steel TSPs. Partial blockage of the trefoil TSP on the hot leg, which led to a redistribution of the riser flow and relatively high fluid velocity on the cold leg, was identified as a contributing factor. FAC was also identified as the cause of extensive degradation of the carbon steel trefoil TSPs at Unit 8 of the Bruce NPP, with the low chromium content of the carbon steel (0.03–0.04 wt%) and relatively high local fluid velocity cited as exacerbating factors (Sedman et al., 2005). The highest damage rates at the Bruce Unit 8 SGs were found on the periphery of the hot leg. Although partial blockage of the TSPs at Bruce was observed, it was not cited as a possible contributing factor.

9.3 Corrosion product transport

9.3.1 Origin and transport of corrosion products to the SG

An illustration of a FW heating system used at a CANDU[4] pressurized heavy-water reactor (PHWR) is shown in Fig. 9.4. The system has many features in common with FW heating systems used at Pressurized Water Reactor (PWR) plants. The materials of construction for the FW heating system are typically carbon steel for the piping, condenser and heater shells and tubesheets, stainless steel or titanium for the

[4]CANDU® is a registered trademark of Atomic Energy of Canada Limited.

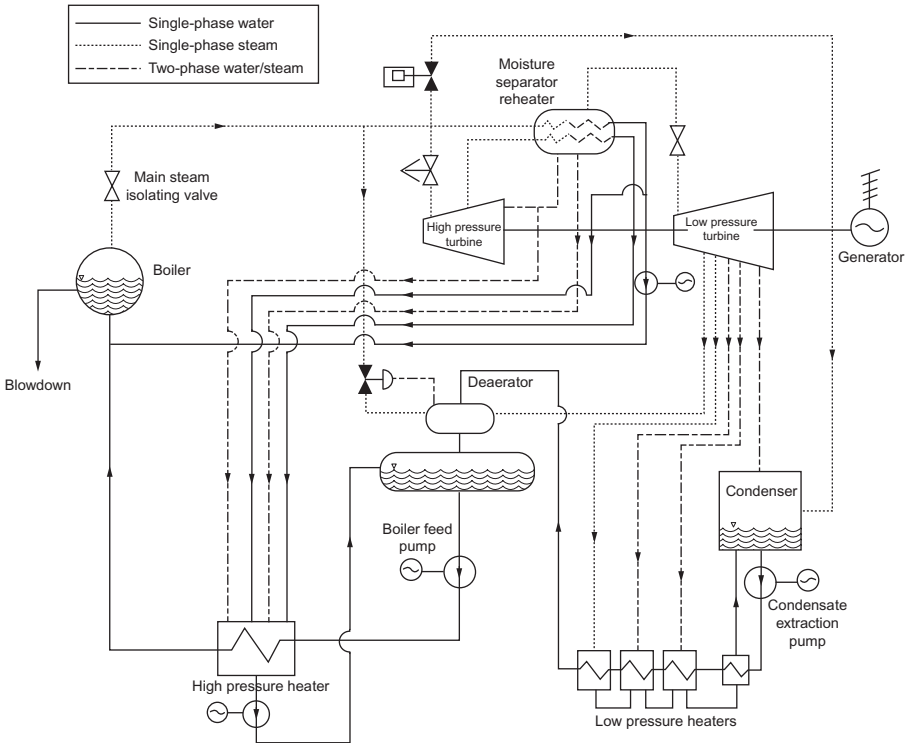

Fig. 9.4 Steam cycle of a CANDU6 pressurized heavy water reactor (Turner, 2011). Courtesy of the Minerals, Metals, and Materials Society. Copyright 2012.

condenser tubes, stainless steel for the LP FW heater tubes, and carbon steel for the HP FW heater tubes. A direct-contact steam-heated deaerator situated between the LP and HP sections of the FW heating system serves to both heat the FW and remove dissolved oxygen from the water before it is pumped forward to the HP section.[5] The condensate that drains from the heater shells is pumped back to either the deaerator storage tank (from the HP heaters and steam reheater drains) or to the condenser (from the LP heaters) to maximize system thermal efficiency. While maximizing thermal efficiency, the design of FW heating systems also ensures that corrosion products that are removed from the surfaces of carbon steel piping and components during operation are ultimately transported with the FW to the SGs where they can accumulate on internal structures such as the tube bundle, tube-support structure, and the tubesheet. Operating experience has shown that unless otherwise removed, the accumulation of

[5] Many PWR plants in the US, Europe and Asia have a Deaerator and Deaerator Storage Tank between the LP and HP sections of the feed water heating circuit such as that shown in Fig. 9.4. Plants that do not must provide an Auxiliary Feed Water Tank or Condensate Storage Tank to supply water for plant start-up operations.

corrosion products on these internal surfaces will eventually lead to degradation of the safety and performance of the SG (Turner, 2011).

Earlier designs of FW heating systems for NPPs tended to use copper alloys in the condensate and FW heating system to increase thermal efficiency. For example, it was common to find Admiralty Brass (70:30 copper:zinc alloy) tubes specified for the condenser and 90/10 copper/nickel alloy for the tubes in both the LP and HP FW heaters. Copper alloys were also used for the reheater tubes in the moisture separator reheater (MSR). This decision proved to be an unfortunate choice from the perspective of corrosion product transport to the SG because the optimum pH for minimizing the corrosion rate of copper does not coincide with the optimum pH for minimizing the corrosion rate of carbon steel. For example, the corrosion rates of copper alloys in the presence of dissolved oxygen tend to go through a broad minimum between $pH_{25°C}$ 8 and 9 at temperatures <100°C (Dooley et al., 1997; Resch and Zinke, 1980), whereas the corrosion rate of carbon steel in fast-flowing water that is under-saturated in dissolved iron[6] continues to decrease with increasing pH up to a $pH_{25°C}$ greater than or equal to 10 (EPRI, 1998). Thus, plants with copper alloys in the FW heating system have had to compromise by operating at an intermediate pH in the range of 8.9–9.2 in the FW which is nonoptimal for both copper and iron transport. Cu (I) and Cu (II) are powerful oxidizing agents (Greenwood and Earnshaw, 1984), and so it was not unusual for measurements of corrosion product transport to show evidence for copper ions released by corrosion of the condenser or LP FW heater tubing plating out on FW system piping surfaces concomitant with the release of iron according to the following reactions:

$$2Cu^{+} + Fe \rightarrow 2Cu + Fe^{2+} \tag{9.1}$$

$$Cu^{++} + Fe \rightarrow Cu + Fe^{2+} \tag{9.2}$$

Iron released from these locations is ultimately transported with other corrosion products to the SGs. Many plants have since removed copper alloys from the FW heating system as part of an initiative to reduce corrosion product transport to the SGs.

The rates of iron transport at various locations of the FW heating systems of PWRs and PHWRs have been investigated by determining the quantity of corrosion product that accumulates on a filter with a nominal pore size of 0.45 μm followed by a cation exchange membrane. These studies have concluded that the majority of the iron (typically about 90% of the mass) during power operation is transported to the SGs in the form of suspended particulate material with the remainder being a combination of dissolved iron and iron in colloidal form that passes through a 0.45 μm sample filter (Sawicki and Brett, 1993; EPRI, 2009). The particles in the FW have been reported to be primarily in the range of 0.1–1.0 μm (Sawochka, 2003). Iron transport results from

[6]The phenomenon of enhanced rate of corrosion of carbon steel in fast-flowing water that is under-saturated in dissolved iron is called Flow Accelerated Corrosion (FAC). Numerous investigations have shown that the rate of FAC of carbon steel decreases with increasing pH up to pH 10 or more and with increasing concentration of dissolved oxygen.

Table 9.1 Iron transport results from the 1984 corrosion product transport study at Point Lepreau Nuclear Generating Station during steady power operation (Plume et al., 1986)[a]

Sample location	Total iron (μg/kg)	Equivalent total iron transport (kg/day)	% Filterable[b]
CEP discharge	2.05	0.143	95
Boiler feed pump discharge	2.45	0.195	98
HP heater out	2.60	0.225	85
Reheater drain	1.07	0.077	63
Moisture separater drain	7.01	0.054	44
HP heater drain	6.13	0.106	44
BB SG/2	774	0.036	100
BD SG/4	640	0.022	100

[a]All values in the table are average of four samples taken daily for 4 consecutive days.
[b]A cation exchange membrane downstream of the filter with nominal pore size 0.45 μm allowed both filterable and nonfilterable fractions to be measured.

the corrosion product transport study at the Point Lepreau Nuclear Generating Station (PLGS) in 1984 for steady power operation are listed in Table 9.1 (Plume et al., 1986). The chemistry of the FW heating system during the sampling period was $pH_{25°C} = 9.2$ to 9.8 at the LP FW heater outlet, hydrazine from 100 to 195 μg/kg at the HP heater outlet, and dissolved oxygen from 5 to 7.5 μg/kg at the HP heater outlet. The FW heating system is all-ferrous with the exception of an aluminum bronze condenser tubesheet. The results listed in Table 9.1 are quite consistent with other plants with all-ferrous FW systems operating with pH in the range of 9.2–9.8, total iron concentrations of about 2–3 μg/kg in the LP and HP sections of the FW system with >85% of the iron in a form that is captured on a filter with nominal pore size of 0.45 μm. The iron concentrations are somewhat higher in the moisture separator drain (MSD) and HP heater drain, and the % filterable iron is markedly lower than in samples taken from the FW. The higher concentration of iron is consistent with the carbon steel components in the MSD and HP heater shell being wetted with condensed steam that is deficient in ammonia (from the decomposition of hydrazine) due to the high distribution ratio of ammonia between steam and water at elevated temperatures. A combination of lower pH and the condensed steam being deficient in iron will lead to a higher rate of FAC of carbon steel in these locations (EPRI, 1998) and higher concentrations of dissolved iron. The iron concentration in the final FW (HP heater outlet) results in an estimated annual transport of 82 kg of iron to the SGs. Some other conclusions deduced from this study are (the reader is referred to the original paper for the details): (1) an estimated 11–15 kg of iron and 1.1–2.2 kg of zinc[7] accumulate

[7]A probable source of zinc transport at PLGS was identified to be the Furmanite valve packing material used in several valves in the reheater section. No measurements of copper transport were made in this study.

Table 9.2 The percentage of magnetite in corrosion product samples collected from various sampling points in the steam cycle of PWR and PHWR plants during power operation

	CEP	FW	BD
Reactor type	**% Magnetite**	**% Magnetite**	**% Magnetite**
PWR[a]	25–65	30–84	50–96
PHWR[b]	37–65	14–59	44–83

[a]From a database of over 30 measurements (Millett and Sawochka, 1994).
[b]From a database of over 90 measurements (Sawicki et al., 1998).

annually in each SG, (2) BD efficiencies ranged from 29% to 45% for iron and 5.4%–7.7% for zinc, (3) mass balance for iron and zinc indicated that corrosion products were accumulating in the deaerator, and (4) the reheater drains contribute ~3% of the iron and ~50% of the zinc transported to the SGs.

Mossbauer analyses of the corrosion products filtered from water removed at various locations of the condensate/FW systems during power operation of PHWRs find primarily magnetite, hematite, and lepidocrocite, with goethite appearing in some samples as a minor constituent (Sawicki and Brett, 1993; Sawicki et al., 1998). Similar analyses of the material filtered from the condensate/FW system of PWRs find magnetite and hematite as major constituents, with relatively less lepidocrocite and more goethite than is generally found at PHWRs (EPRI, 2009; Millett and Sawochka, 1994). Iron transport investigations conducted at reaktor bolshoy moshchnosti kanalniy (RBMK) and water-water energetic reactor (VVER) plants also report magnetite, hematite, and lepidocrocite as being the major constituents of the corrosion products filtered from the hot water systems at these plants (Efimov et al., 1989). The results of these investigations are summarized in Table 9.2 by listing the range of % magnetite in the water samples filtered from three locations: the condensate extraction pump (CEP) discharge, final FW, and the SG BD. The % magnetite in the corrosion product samples varied widely from one plant to another and from one sampling location to another in the steam cycle. Note that the fraction of magnetite in the FW and BD at PWR plants tends to be higher than at PHWR plants. The lower fraction of magnetite at PHWRs compared to PWRs is likely a consequence of two main factors: (1) all PHWRs but one[8] have a steam-heated direct-contact deaerator between the LP FW heaters and the boiler feed pump that appears to act as a source of fully oxidized corrosion products to the FW and (2) high-temperature drains contribute a larger fraction of the total FW iron, mostly in the form of magnetite, at PWRs than at PHWRs.

Additional insights to the nature and formation of corrosion products in the secondary system of NPPs have been provided by the analysis of samples of corrosion products removed directly from the surfaces of piping and equipment during a

[8]Nucleoelectrica Argentina Sociedad Anonima (NASA) operates a CANDU PHWR plant at Embalse that does not have a deaerator in the condensate/feed water system.

maintenance outage. One such investigation was conducted at Bruce B. The FW system had been drained but not completed dried. As a result, some locations were still wet while others appeared to be completely dry. The results of this investigation are summarized as follows (Sawicki and Brett, 1993; Sawicki et al., 2005):

- High percentages of magnetite (Fe_3O_4) are found on carbon steel surfaces that are in contact with high-temperature steam, for example, the wall of the condenser above the water line and in the condensate steam discharge valve that discharges steam directly to the condenser.
- Lower percentages of magnetite mixed with lepidocrocite (γ-FeOOH) and hematite (α-Fe_2O_3) are found on carbon steel surfaces wetted by water, for example, the condenser wall and the condensate rejection tank below the water line.
- High percentages of hematite are found in samples taken from the deaerator storage tank.
- Maghemite (γ-Fe_2O_3) is only found in locations where the temperature does not exceed 40°C.
- Geothite (α-FeOOH) is found in locations where the temperature does not exceed 100°C.
- Lepidocrocite is found in low temperature parts of the feed train and is absent from locations where the temperature exceeds 150°C.

It has been suggested that the chemical phase of the corrosion products removed from the FW heating system during power operation can provide insights to the local chemistry conditions and, in particular, whether the local conditions are oxidizing or reducing (Sawicki et al., 1998; Millett and Sawochka, 1994). Whether the phase of corrosion products reflects local chemistry conditions or the conditions elsewhere in the circuit is a complex question. Corrosion products are produced over a wide range of conditions in the water/steam cycle reflecting differences in temperature, pH, and the concentrations of hydrazine and dissolved oxygen. Corrosion products produced in one location may be released and transported to another location where they may deposit and be released again to be transported to the SG. In the meantime, they may have undergone some phase transformation. Corrosion products produced during shutdown, when parts of the steam/FW/condensate system are open to the atmosphere for maintenance activities, may have a different phase than corrosion products produced at those same locations during power operation. Thus, it could be misleading to draw inferences regarding local chemistry conditions from the phases of corrosion products removed from the FW heating system during operation at power when corrosion products are being transported from one location to another.

Although the phase of the corrosion products may not be representative of the local chemistry conditions at the point of sampling, the phase should provide insight to the chemistry conditions that prevailed at the location at which the corrosion product was initially formed.[9] It has been hypothesized, however, that the phase of the corrosion products when first formed is determined not by the local oxidizing conditions but by the local pH (Turner and Chi, 2012). This hypothesis is based on the fact that all of the iron oxides present in the FW heating system can be synthesized in the laboratory under oxidizing conditions at temperatures between 25°C and 100°C, the main variable in the syntheses of different phases of iron oxide being the pH. For example,

[9] Implicit in this statement is the understanding that the location that the corrosion products first formed may not be the same location as the one where they were removed from the feed water heating system. The phase would provide insight to the chemistry environment at the location the corrosion products were formed provided the corrosion products have not subsequently undergone a phase transformation.

magnetite is prepared (Tsuchiya et al., 2005; David and Welch, 1956; Sugimoto and Matijevic, 1980) by oxidizing a solution of ferrous ions at pH 9 to 11, whereas lepidocrocite is prepared by oxidizing a solution of ferrous ions at a pH of approximately 7 (Cornell and Schwertmann, 1996; Ishikawa et al., 1993; Cho et al., 2000). Lepidocrocite will convert to magnetite by aging it in the presence of ferrous ions at pH 9. Hematite is prepared by aging the precipitate from a solution of ferric ions at pH 7 to 8 (Cornell et al., 1989; Schwertmann et al., 1999), while goethite is formed from a solution of ferric ions at pH from 12 to 13 (Schwertmann et al., 1999; Schwertmann and Murad, 1983). It has been proposed, therefore, that the phase of iron-based corrosion products in the secondary system of a NPP is determined primarily by the pH and not by the concentration of dissolved oxygen at the location at which the corrosion product was formed. Furthermore, it has been proposed that the fully oxidized phases of iron corrosion products, such as lepidocrocite and hematite, are formed not during power operation but, instead, are formed when the plant is shut down for a maintenance outage, during which time air ingress introduces carbon dioxide to the water that causes the low pH conditions (i.e., pH about 7) that are conducive to the formation of these phases. During operation at power, all locations in the water/steam cycle are at a pH sufficiently alkaline that magnetite should be the sole corrosion product formed regardless of the concentration of dissolved oxygen. Upon return to full power operation, both lepidocrocite and goethite will transform to hematite in the higher-temperature regions of the system. Lepidocrocite may also transform to magnetite at low temperature in the condenser hot-well, as noted above. The chemistry conditions favouring formation of selected phases of iron oxide by oxidation and hydrolysis of solutions of ferrous and ferric ions are summarized in Fig. 9.5.

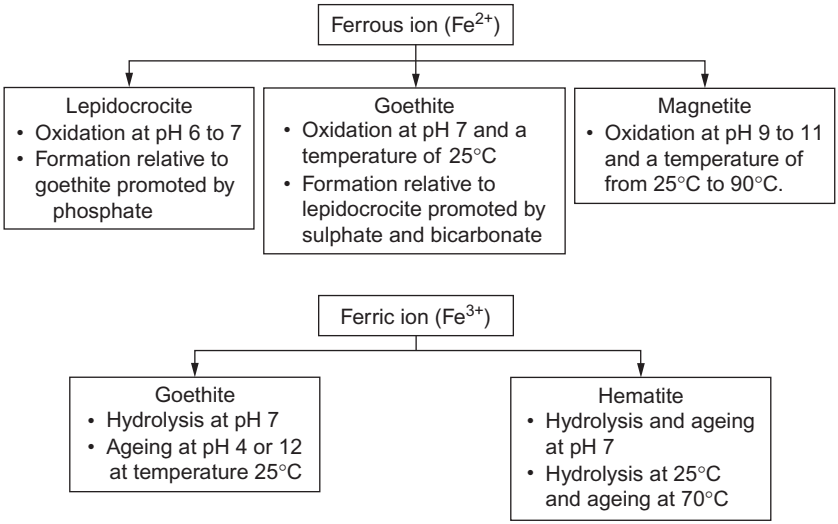

Fig. 9.5 Schematic showing chemistry conditions favouring formation of selected phases of iron oxide prepared by oxidation and hydrolysis of solutions of ferrous and ferric ions.

9.3.2 Corrosion product transport during start-up

It has long been noted that operations of a transient nature, for example, changes in reactor power, water flow rate, temperature, and chemistry, can initiate a release of corrosion product from the walls of piping and vessels, a so-called crud burst (Plume et al., 1986). The concentration of suspended particulate material during a "crud burst" is generally much higher than the concentration during steady operation. "Crud bursts," although of relatively short duration, can make a significant contribution to the accumulation of corrosion product in the SG. Therefore, it is important to understand the factors that contribute to the magnitude of the "crud bust" and to take steps to mitigate the effect of transient operations on the total levels of corrosion product transport to the SG.

Results showing the effect of both minor flow transients and start-up operations on iron concentrations at selected locations in the FW heating system from a corrosion product transport study at PLGS are listed in Table 9.3 (Plume et al., 1986). The minor flow transients that occurred during the sampling period were caused by MSR tests during which various sections of the reheater were isolated, reactor power was varied between 95% and 100%, the SG BD flow rate was varied, and the reheater drains were

Table 9.3 Iron transport results showing the effect of minor flow transients and start-up operations at Point Lepreau Nuclear Generating Station (Plume et al., 1986)

Sample location	Total iron (μg/kg)	Equivalent total iron transport (kg/day)	% Filterable#
Minor flow transients			
CEP discharge	86.0	5.03	100
Boiler feed pump discharge	26.0	2.22	98
HP heater out	31.8	2.71	95
Reheater drain	4.5	0.020	72
Moisture separator drain	12.7	0.102	67
HP heater drain	15.2	0.274	80
BB SG/2	11,980	0.476	–
BD SG/4	36,317	1.525	–
Start-up operations			
CEP discharge	272	8.4	95
Boiler feed pump discharge	338	15.4	95
HP heater out	262	11.9	98
Reheater drain	11.4	0.083	39
Moisture separater drain	140	1.09	24
HP heater drain	74	1.29	62
BB SG/2	53,659	2.46	–
BD SG/4	17,857	0.83	–

routed to the condenser for a period of time. During start-up, samples from the CEP discharge, boiler feed pump discharge, HP heater outlet, and BD were taken as reactor power was increased from 40% to 100%. The samples from the reheater, moisture separator, and HP heater drains were taken after the plant reached 100% reactor power. The results in Table 9.3 show that the severity of the transient influences the extent of the increase in iron concentration compared to values at steady power operation. The increase in iron concentration at every location is due almost entirely to the increase in amount of filterable corrosion product, which is consistent with the notion that the "crud burst" arises from the removal of previously deposited corrosion product and corrosion oxide layer from the walls of piping and equipment. The values for iron transport in Table 9.3 in units of kg/day are based on just one set of samples each for the minor and start-up flow transients, however, so these values may not be representative of iron transport throughout the entire transient. During plant start-up, it is neither known how much iron was transported to the SGs during the run-up from 0% to 40% power nor known for how many days the elevated iron levels persisted in the FW. From the one sample taken at 40% power, the amount of iron transported to the SGs during one day of start-up corresponds to 3.3% of the annual transport of iron to the SGs during steady operation.

An extensive investigation of corrosion product transport during start-up operations was conducted at the Bruce B site (Sawicka et al., 2000, 2001). The purpose of this investigation was to evaluate iron transport, concentrations, and oxidation state during start-ups and try to correlate the observations with operational and chemical parameters. The Bruce B Nuclear Generating Station consists of four 915 MW_e CANDU units. Each unit employs an all-ferrous secondary FW heating system. Corrosion products were analyzed during the start-up of one unit following a wet layup and for a second unit following a dry layup. The value of this investigation is that numerous samples were taken throughout the course of the start-up at reactor powers so that iron transport rates could be calculated throughout the start-up for reactor powers ranging from 0% to almost 85%. In addition to measuring iron concentration, each sample was analyzed using Mossbauer spectroscopy to determine the phase composition. Iron transport data and phase compositions determined from samples taken from the FW heating system of Unit 8 during start-up from a wet layup are listed in Tables 9.4 and 9.5, respectively. For the start-up of Bruce

Table 9.4 Maximum iron transport rates and corresponding iron concentrations measured at three locations of the feedwater heating system while reactor power was being raised from 40% to 70% during a start-up of Bruce B Unit 8 following wet layup (Sawicka et al., 2000)

Location	Iron concentration (μg/kg)	Iron transport rate (kg/day)
CEP discharge	80–120	5.2
FW	25	0.9
PHO[a]	10	0.5

[a]The PHO is an external preheater that heats the final feedwater using primary coolant before the feed water is sent to the SGs. External preheaters are used at all Bruce units.

Table 9.5 Phase composition of corrosion product samples at three locations of the feedwater heating system at reactor powers of 0% and >5% during start-up of Bruce B Unit 8 following wet layup (Sawicka et al., 2000)

Location	0% Reactor power			5% Reactor power		
	Magnetite (%)	Hematite (%)	Lepidocrocite (%)	Magnetite (%)	Hematite (%)	Lepidocrocite (%)
CEP	20–35	8–16	50–60	50–70	10–20	10–15
FW	20–30	8–16	55–65	60–65	20–30	10
PHO[a]	50–65	12–24	20–28	78–84	10–20	10–20

[a]The PHO is an external preheater that heats the final feedwater using primary coolant before the feedwater is sent to the SGs. External preheaters are used at all Bruce units.

B Unit 8 following wet layup, the iron transport rates at all sampling locations started to increase significantly when reactor power was raised from 5% to 30% (with a corresponding increase in FW flow rate) and continued to increase before going through a maximum value 24 h later at which point reactor power was about 70%. Although the transport rates began to subside while reactor power was held near 70% there was a second, smaller spike in iron transport rate when the reactor power was raised from 70% to 85%. Only the iron concentration at the CEP outlet went through a clear maximum when reactor power was raised from 30% to 70%. In contrast, the concentrations of iron at the FW and preheater outlet (PHO) locations diminished steadily throughout the start-up operations. The maximum iron transport rates and corresponding iron concentrations measured while reactor power was being raised from 40% to 70% are listed in Table 9.4. The iron concentration and transport rate at the CEP outlet are comparable to the values reported for the start-up at Point Lepreau at 40% reactor power (see Table 9.3), but the concentrations and transport rates at the FW and PHO are significantly lower than at the corresponding location at Point Lepreau, i.e., HP heater outlet. It is not clear why there is such a significant drop in iron concentration between the CEP and the FW/PHO. One can only conclude, if the data are representative, that there is a significant accumulation of corrosion product in the dearator storage tank during start-up.

Iron transport data and phase compositions determined from samples taken from the FW heating system of Unit 7 during start-up from a dry layup are listed in Tables 9.6 and 9.7, respectively. As with the start-up of Unit 8, an increase in iron transport rate was initiated when reactor power (and a corresponding increase in FW flow rate) was increased from 0% to 7%, having been held for the previous several days at 5%–7% reactor power with a single spike up to 30%. The iron transport rates at the three sampling locations continued to increase with the step increase in reactor power to 30% and went through a maximum the following day during which time the reactor power was raised from 30% to 70%. The transport rates diminished over the next several days while reactor power was raised incrementally from 70% to 85%. The latter increases in reactor power did not initiate a smaller crud burst as observed with the start-up of Unit 8. Neither the CEP iron nor the PHO iron concentrations go through a discernible maximum value as reactor power is increased; they both declined

Table 9.6 Maximum iron transport rates and corresponding iron concentrations measured at three locations of the feedwater heating system at 70% during a start-up of Bruce B Unit 7 following dry layup (Sawicka et al., 2000)

Location	Iron concentration (μg/kg)	Iron transport rate (kg/day)
CEP discharge	90–130	5.2
FW	180	8.2
PHO[a]	90	4.2

[a]The PHO is an external preheater that heats the final feedwater using primary coolant before the feedwater is sent to the SGs. External preheaters are used at all Bruce units.

Table 9.7 Phase composition of corrosion product samples at three locations of the feedwater heating system at reactor powers of 0% and >5% during start-up of Bruce B Unit 7 following dry layup (Sawicka et al., 2000)

Location	0% Reactor power			>5% Reactor power		
	Magnetite (%)	Hematite (%)	Lepidocrocite (%)	Magnetite (%)	Hematite (%)	Lepidocrocite (%)
CEP	36–60	15–30	15–30	30–48	18–20	30
FW	9–11	40–48	20–40	9–12	48–54	26–38
PHO[a]	15–40	20–40	26–42	40–55	45–55	8–10

[a]The PHO is an external preheater that heats the final feedwater using primary coolant before the feedwater is sent to the SGs. External preheaters are used at all Bruce units.

steadily throughout the start-up operations in contrast to the CEP iron concentration which peaked in value when reactor power was raised from 30% to 70%.

The results of the measurements of the phases of the corrosion products taken from the three sampling locations throughout the start-up operations are summarized in Tables 9.5 and 9.7 for start-ups following wet layup and dry layup, respectively. There is a lot of variation in the percentage phase compositions of the samples from location to location and with changing reactor power. The absence of more specific operating conditions, such as pH, water temperature, and flow rate during the sampling period, makes it difficult to interpret these results. One can observe, however, that the corrosion products were primarily in the form of magnetite in the final FW (outlet of the PHO) once reactor power reached greater than 5% for the start-up following wet layup, with only minor amounts of hematite and lepidocrocite. In contrast, for the start-up following a dry layup the corrosion products in the final FW (outlet of the PHO) consisted of about equal amounts of magnetite and hematite with a minor amount of lepidocrocite. If one accepts the hypothesis that the phase of the corrosion product is determined primarily by the pH at which it was formed (see Section 9.3.1), these results suggest that the pH of the water wetting the surfaces of carbon steel during "dry layup" was close to the neutral point, i.e., pH about 7, as a result of pickup of carbon dioxide from the air (Turner and Chi, 2012). If this is so, it emphasizes the importance of ensuring that all surfaces are rigorously dried during "dry layup."

A comparison between FW iron transport at PWR plants versus Boiling Water Reactor (BWR) plants during start-up operations concluded that iron transport is higher during start-up of PWR plants than that of BWR plants (Fruzzetti, 2012a). A survey of 21 PWR plants showed that iron transport during start-up operations ranged from a low of 2 kg to a high of 53 kg with a median value of 9 kg. Total iron transport during the cycle ranged from a low of 46 kg to a high of 316 kg with a median value of 136 kg. Thus, iron transport from a single start-up operation can provide anywhere from 2% to 20% of the total iron transport with a median value of 12%. Iron transport at BWR plants is generally much lower, with iron transport during start-up ranging from 0.5 to 5 kg. The survey noted significant differences in iron transport rates between plants of similar design and similar layup and start-up practices. A major source of iron transport appears to be the HP heater drains, but this can be plant specific. It was suggested that the transitions between oxidizing and reducing chemistry at PWR plants as they transition between the shutdown state to the full power state may be a contributing factor to the enhanced iron transport during start-up at PWR plants.

9.3.3 Mitigating corrosion product transport

Four methods for reducing the rate of corrosion product transport to the SGs will be considered in this section: pH optimization during operation at power, the addition of oxygen, filtration of corrosion products during operation at power, and FW cleanup prior to start-up operations following a maintenance outage.

It is well known that the rate of FAC of carbon steel decreases with increasing pH (EPRI, 1998), and this is now the basis for strategies to mitigate iron transport to the SGs

during power operation by attempting to raise the pH of the FW heating system, including the various drains that return water to the system. Amines with high base strength and low volatility ensure that carbon steel surfaces throughout the water/steam cycle remain protected, especially the heater drains and MSDs. Thus, some plants have replaced ammonia with morpholine because of its lower volatility at SG temperatures, while others have opted for ethanolamine (ETA) which is a stronger base and has lower volatility than morpholine. As discussed in Section 9.3.1, plants that have copper-bearing alloys in the FW heating system must compromise by operating at a pH lower than the optimum to minimize FAC of carbon steel. A compilation of iron corrosion product concentrations in the FW to the SG is listed in Table 9.8 (Shoda, 1997; Schwarz and Schneider, 1994; Pettus, 1994; Plume et al., 1986; Chocoron et al., 2000; Fellers et al., 1994; Ward, 1994; Brett et al., 1994; Splichal et al., 1994; Corredera et al., 2008). The data set is by no means complete and is heavily weighted toward plants with copper alloys in the FW heating system. Only data available in the open literature are included in this table. Many plants have conducted corrosion product transport studies and taken steps to reduce iron concentrations in the FW, but the results of these investigations are not always reported in the available literature. For plants with an all-ferrous FW heating system, maintaining a FW pH close to $pH_{25°C} \sim 10$ appears to be sufficient to maintain FW iron levels ≤ 1 μg/kg. The situation is more complicated in plants with a mixed iron/copper FW heating system. Ammonia is always present when hydrazine is added to the FW heating system as a result of the thermal decomposition of hydrazine. Ammonia exacerbates the release and transport of soluble copper from copper alloys as a result of the formation of the strong Cu(I)-ammonia complex (Trevani et al., 2001). Cu(I), in turn, will lead to increased corrosion of carbon steel by reaction (1), above, resulting in an increased concentration of iron-based corrosion products in the FW system. Organic amines such as morpholine and ETA form weaker complexes with copper ions than ammonia, hence organic amines should not have as deleterious an effect on copper transport as ammonia.

The addition of low concentrations of dissolved oxygen is known to be effective at reducing the rate of FAC of carbon steel (EPRI, 1998). This concept was introduced at Advanced Gas Reactor (AGR) plants in Britain to reduce the rate of FAC of flow-control orifices inserted into the SG tubes (Woolsey et al., 1989). In Germany, air was injected into the FW line at the Biblis-B plant to reduce the rate of FAC of the HP FW heater (Odar et al., 1986). The plant was operating with low pH ($pH < 9.5$) All Volatile Treatment (AVT), and this treatment continued until the plant switched to high pH ($pH > 9.5$) AVT. Oxygen was injected into the MSR reheating steam line at Philippsburg Unit 2 to arrest FAC which had caused a tube failure (Ruhle et al., 2006) and is being considered to arrest FAC of the FW heating system downstream of the deaerator at Tsuruga-2 (Takiguchi, 2008). A more comprehensive review of oxygen addition to arrest FAC and limit corrosion product transport in NPPs is found in Odar and Nordmann (2010).

Corrosion product transport studies have shown that heater drains and the MSDs are a significant source of corrosion product transport (Plume et al., 1986; Fruzzetti, 2012a), thus it stands to reason that filtration of the drains from these locations would reduce overall corrosion product transport to the SGs. The installation of

Table 9.8 Corrosion product transport data versus feedwater chemistry

Plant	FW pH	Amine	Corrosion products (μg/kg)	Comment
Japanese plants (Shoda, 1997) mixed iron/copper feedwater system	8.8–9.1	ammonia hydrazine	Fe: 9 Cu: < 3	Partial flow condensate polisher hydrazine 90–300 μg/kg
	9.2–9.3	ammonia hydrazine	Fe: 10 Cu: < 3	Partial flow condensate polisher hydrazine 270–600 μg/kg
	9.2–9.3	ammonia hydrazine	Fe: 4 Cu: < 3	Full flow condensate polisher hydrazine 270–600 μg/kg
	9.2–9.3	ammonia hydrazine	Fe: 7 Cu: < 3	Full flow condensate polisher hydrazine 340–570 μg/kg
German plants (Schwarz and Schneider, 1994) all-ferrous feedwater system	<9.5	ammonia hydrazine	Fe: 4	Low pH AVT
	10.0–10.2	ammonia hydrazine	Fe: 1	High pH AVT hydrazine 80–200 μg/kg
	10.0–10.2	ammonia hydrazine	Fe: 0.5	High AVT+filtration of drains
Callaway (Pettus, 1994) mixed iron/copper feedwater system	–	ammonia hydrazine	Fe: 6–8	–
	–	ethanolamine hydrazine	Fe: 2–4	–
PLGS (Plume et al., 1986) all-ferrous feedwater system	9.5	hydrazine	Fe: 2.6 Zn: 0.11	Hydrazine 100–200 μg/kg
Embalse (Chocoron et al., 2000) mixed iron/copper feedwater system	9.3–9.4	morpholine hydrazine	Fe: 5.1 Cu: 0.14 Zn: 0.13	morpholine 12–15 mg/kg hydrazine 2–4 μg/kg ammonia 0.6 mg/kg
Comanche Peaks (Fellers et al., 1994) all-ferrous, Ti condenser tubes	9.0–9.1	Morpholine hydrazine	7.6	morpholine 4–6 mg/kg
	9.2	morpholine hydrazine	2.6	morpholine 8-10 mg/kg
	8.9–9.1	dimethylamine hydrazine	0.95	dimethylamine 0.4–0.6 mg/kg

Continued

Table 9.8 Continued

Plant	FW pH	Amine	Corrosion products (μg/kg)	Comment
Oconee U2 (Ward, 1994) mixed iron/copper feed system	9.1–9.2	morpholine hydrazine	2.5	morpholine 5–10 mg/kg
	9.3–9.4	morpholine hydrazine	1.7	15–20 mg/kg morpholine
	9.4–9.6	ethanolamine hydrazine	1.6-2.0	3–5 mg/kg ethanolamine
	9.5–9.7	ethanolamine dimethylamine hydrazine	1.2	ethanolamine: 3–5 mg/kg dimethylamine: 0.5–1 mg/kg
Pickering U7 (Brett et al., 1994) mixed iron/copper feed system	~9.4	morpholine hydrazine	Fe: 2.0 Cu: 0.3 Zn: 2.4	morpholine 2–3 mg/kg hydrazine 0.1 mg/kg ammonia 1–2 mg/kg
VVER–440 Czech Republic (Splichal et al., 1994)	8.4–8.6	–	Fe: 25 Cu: < 5	ammonia: 0.1 mg/kg hydrazine: 0.020–0.060 mg/kg
	9.1–9.3	–	Fe: 12 Cu:< 5	ammonia: 0.2–0.8 mg/kg
Electricite de France (Corredera et al., 2008)	9.2	morpholine	Oxides: 7–12	–
	9.6	morpholine	Oxides: 3–6	–
	9.6	ammonia	Oxides: 3–8	–

mechanical filters on the MSDs and electromagnetic filters on the HP heater drains has been shown to reduce FW iron concentrations from 1.0 to 0.5 μg/kg (Schwarz and Schneider, 1994). A full flow permanent magnet filtration system has also been designed and tested for the removal of magnetic corrosion products, i.e., principally magnetite, from the FW system (Hayes, 1994). The developers predicted that if installed downstream of the HP heater it could be expected to remove from 85% to 90% of the suspended magnetite particles that would normally be transported to the SGs.

Studies have shown that a significant quantity of corrosion product can be transported to the SGs during start-up operations (Sawicka et al., 2000, 2001; Fruzzetti, 2012a) and that a significant fraction of the corrosion product transported during start-up may have been formed during layup. Thus, reducing the amount of corrosion product formed during layup of the FW heating system and subsequently transported to the SGs during start-up is an important aspect of the chemistry control program for the steam/water system. It is well known that the corrosion rate of carbon steel increases significantly with increasing relative humidity above 40%, so if the system is to be drained for maintenance it is imperative that the relative humidity be kept less than 40% to ensure that the corrosion rate of carbon steel remains acceptably low. Recirculation loops have been installed at many NPPs to permit the FW to be recirculated and filtered to remove corrosion products while the water chemistry is brought into specification prior to feeding forward to the SGs during start-up. Both the Gentilly-2 and Point Lepreau plants installed FW recirculation loops within several of years of first operation for this very purpose. Perhaps it is no coincidence that the deposit accumulation in these two plants, normalized to thermal power and the number of Effective Full Power Year (EFPY), is relatively low compared to other plants (see Table 9.9 and associated discussion in Section 9.4).

9.3.4 Corrosion product sampling

Although the results from corrosion product transport investigations at operating NPPs appear to be relatively consistent from one plant to another, how representative the samples are is still open to question. For example, long sample lines (up to 100 m in length) are used to deliver the sample stream to a centralized collection point, and almost invariably the sample is cooled before passing through the 0.45 μm filter to collect the suspended particles. Sampling nozzles have not necessarily been designed to ensure that the fluid entering the nozzle has the same velocity as the main stream, i.e., to ensure isokinetic sampling (Sehmel, 1970; Bird, 1984; Srisukvatananan et al., 2007). Thus, corrosion products sampled using existing sampling systems at NPPs are subject to the following uncertainties:

1. Precipitation of dissolved iron on cooling will result in the concentration of dissolved iron in the system being underestimated and the concentration of suspended particulate being overestimated. Precipitation on cooling may also affect the particle size distribution of the filtered sample.
2. Anisokinetic sampling could influence the measured concentration and bias the particle size distribution of suspended material in the sample stream.

3. Deposition and removal within the sample lines may affect the concentrations of both dissolved (by dissolution of existing deposit within the sample line) and suspended corrosion product.

Although the uncertainties introduced by anisokinetic sampling can be significant for an aerosol (Vitols, 1966), the importance of matching the sample and fluid velocities diminishes when sampling for suspended material in a liquid because the higher viscosity of the fluid makes it more likely for the particle to follow the fluid streamline. For example, simulations of the particle collection efficiency for 1 μm particles of magnetite suspended in 300°C water and in steam show that the sampling velocity has no discernible influence on the results for velocities ranging from 25% to 175% of the isokinetic velocity for the aqueous system but results in errors of up to 25% when sampling for those same particles entrained in steam (Srisukvatananan et al., 2008). As expected, the deviations become more significant with increasing particle size. Measurements of iron transport in the FW at the Winfrith[10] experimental Steam Generating Heavy Water Reactor (SGHWR) using capillary lines and isokinetic sampling found that dissolved iron constituted only ~1% of the mass of iron transported between the HP FW heaters, and ~0.5% of the mass of iron transported in the final FW (Bird, 1984). Measurements as a function of sample fluid velocity showed an absence of bias for fluid velocities between 75% and 125% of the isokinetic velocity. Deviations of +22% and −27% were reported for velocities of 30% and 200% of the isokinetic velocity, respectively. A study comparing hot filtration with filtration at ambient temperature using Ag and cellulose membrane filters, respectively, found no significant difference in particle size between the high-temperature and ambient-temperature samples (Stauffer, 1984). Interestingly, the concentrations of dissolved iron were relatively consistent from one sample to the next,[11] whereas the concentrations of filterable iron were three to six times lower in the samples filtered at ambient temperature compared to hot filtration. Although there are insufficient data to make a strong conclusion, particle deposition on the cooler may account for the lower concentration of filterable material in the sample filtered at ambient temperature.[12]

A sampling system to permit isokinetic sampling and hot filtration of particulates in the reactor coolant system of a PWR has been designed and commissioned (Palino et al., 2000) to provide representative samples to estimate particulate concentrations in the reactor coolant system at Diablo Canyon. The technology does not look complicated, and it would be beneficial if a similar system were implemented to collect more representative samples of corrosion products suspended in the FW systems of NPPs.

[10] The SGHWR was one of several experimental research reactors built at the Winfrith site in the United Kingdom.

[11] The database from this study is small: 3 samples filtered hot, of which one was compromised by a torn membrane, and 2 samples filtered cold. The results from the torn membrane were not used for this analysis.

[12] Particle transport down a temperature gradient leading to deposition on a cold surface is known as thermophoresis.

9.4 Fouling of nuclear SGs—plant experience

9.4.1 Overview of deposit loading and distribution

The SG tube bundle constitutes a large fraction of the total surface area of the primary coolant pressure-retaining boundary. All contaminants originating in the FW heating system, whether they be particulate or dissolved species, are transported with the FW to the SGs where they will either deposit or remain suspended where they can be removed with the BD flow. BD efficiencies[13] for soluble and suspended contaminants are often less than 10%, which means that more than 90% of the contaminants that are transported with the FW to the SGs accumulate; primarily on the tube bundle, the tubesheet and the tube-support structure. The impact of deposit accumulation on the performance of the SGs was reviewed in Section 9.2.4. The contaminants consist of a mixture of corrosion products and ionic impurities. The origin and transport of corrosion products was discussed in Section 9.3.2. The two major sources of ionic impurities are in-leakage of cooling water at the condenser and make-up water from the water treatment plant. Ionic impurities are not discussed further in this chapter other than to note that they are a constituent of the SG deposits. The accumulation of ionic contaminants in flow-restricted regions of the SG, such as crevices between the tubes and tube-support structure and within thick deposits on the tube bundle and tubesheet, and their effect on the localized chemistry conditions that develop within the flow-restricted regions will be discussed in Chapter 10 of this handbook.

Stations schedule periodic water lancing of the tubesheet and lower tube-support structures as well as flushing of the upper tube bundle during maintenance outages to limit the accumulation of deposit in these locations. Chemical cleaning is also required to remove deposit from tube surfaces, tubesheet, and tube-support structures. The cleaning program is scheduled for the following purposes: (i) for the removal of upper bundle corrosion products including bridge deposits and those that fill the gap between adjacent tubes, (ii) for the removal of bulk deposit on the tube bundle and tubesheet, and (iii) for the removal of crevice deposits in tube-support structure regions. Estimates have been made across the industry of the distribution of deposit within SGs based on visual inspections (Thompson and Lammana, 1986; Gay, 1994, 1997), chemical cleaning and water lancing campaigns (Dow, 1994, 1997; Wills, 1997), measurements of corrosion product transport (Plume et al., 1986; Sawicki et al., 1998; Millett and Sawochka, 1994; Chocoron et al., 2000; Sato et al., 1994; Wilson and Haskew, 1997), and measurements of tube deposit thickness (Turner et al., 1994; Varrin, 1996). Although plant-to-plant variations may be significant, the distribution of deposit within the SG appears to be roughly as follows: tube bundle including tube-support structure (~75%), tubesheet (~10%), and BD (~15%) (Sato et al., 1994; Turner, 2013).

For a 1000 MW_e plant operating with a thermodynamic efficiency of 33% and 1 μg/kg corrosion product in the final FW, the total amount of corrosion product

[13] The blow down efficiency for a particular contaminant is defined as the ratio of the rate of mass transport out of the SG with the blow down divided by the rate of mass transport into the SG with the feed water.

transported to the SGs in one EFPY is calculated to be ~60 kg.[14,15] Assuming one start-up per EFPY and an additional 12% corrosion product transport from one start-up operation (Fruzzetti, 2012a), the total corrosion product transported to the SGs in one EFPY becomes ~67 kg. For a BD efficiency of 15%, 10 kg will be removed from the SGs by BD per EFPY and the remaining 57 kg will accumulate on the tube bundle, tube-support structure, and tubesheet. Roofthooft (Roofthooft, 1994) noted that 1 μg/kg of magnetite in the FW can generate up to 18 kg of magnetite in each SG per year of operation. The mass of corrosion products removed from the SGs by chemical cleaning, however, can be more than one order of magnitude higher if corrosion product concentrations in the FW are significantly in excess of 1 μg/kg during operation.

Estimated deposit loadings on the tube bundle, tubesheet, and tube-support structure determined from the results of inspection and cleaning activities at specific NPPs can be used to estimate SG fouling rates, as discussed in more detail in the following sections.

9.4.2 Tube bundle fouling—external tube surface

Table 9.9 lists the estimated tube bundle deposit loading for selected RSGs and OTSGs based on data reported from selected chemical cleaning campaigns (Plante, 2005; Dow, 1997; Stanley, 2000; Roofthooft, 1994; Verma, 1996; Klimas and Semmler, 2007; Puzzuoli et al., 1997; Remark and Evans, 2000; Roofthooft et al., 1991; Paramithas et al., 1994; Harvey et al., 1997; Pendergrass, 1997; Fiola et al., 1997; King and Remark, 2000). The list in Table 9.9 is not meant to be exhaustive. Specific chemical cleaning campaigns were selected on the basis of there being sufficient details about the chemical cleaning available in the open literature to estimate a tube bundle fouling rate based on the amount of deposit removed. The number of EFPY of operation for many of the plants at the time of chemical cleaning was taken from Stanley (2000). For PLGS and Gentilly-2 the number of operating EFPYs was taken from Verma (1996) and Plante (2005), respectively. For the units at Pickering and Bruce, the number of EFPYs at chemical cleaning was calculated for each unit from data posted on the World Nuclear Association website. The deposit loadings on the tube bundle and tube-support structure were estimated by subtracting the amount of deposit removed by the preclean and postclean water lancing of the tubesheet from the total amount of deposit removed for each plant. In several cases the deposit loading was taken from Dow (1997) where it was noted that the total deposit removed by chemical cleaning did not include a contribution from sludge lancing.

[14] In this calculation, the final feed water flow rate is equated with the steaming rate. Thus, the relatively small blow down flow rate is ignored. A heat of vaporization equal to 1605 kJ/kg was used to convert thermal power to steaming rate.

[15] Deposit loadings in the SGs are generally reported as total mass of metal oxide, except for copper which is reported as the metal. Corrosion product transport data are generally reported as μg/kg metal. To convert the concentration of iron from units of μg/kg Fe (see, for example, Table 9.8) to μg/kg iron oxide one must multiply by 1.38. Thus, 1 μg/kg Fe is equivalent to 1.38 μg/kg iron oxide.

Table 9.9 Deposit loadings removed from nuclear SGs by chemical cleaning[a]

Plant	Year of chemical clean	Plant EFPY (Year)	Deposit removed[b] (kg)	Thermal power (MWt)	Deposit loading $\left(\frac{\text{kg}}{\text{MWt}\cdot\text{EFPY}}\right)$
PLGS (Verma, 1996)	1995	11.6	1112	2064	0.046
Gentilly-2 (Plante, 2005)	2005	21.5	1396	2064	0.031
Pickering-7 (Klimas and Semmler, 2007)	2003	14.8	2919	1656	0.12
Pickering-8 (Klimas and Semmler, 2007)	2002	12.0	3725	1656	0.19
Bruce-1 (Puzzuoli et al., 1997; Klimas and Semmler, 2007)	1995	12.1	8500	2240	0.31
Bruce-3 (Klimas and Semmler, 2007; Puzzuoli et al., 1997)	1994	12.4	6720	2240	0.24
Bruce-4 (Puzzuoli et al., 1997)	1993	11.1	6250	2240	0.25
Waterford 3 (Stanley, 2000; Evans et al., 2002)	2000	12.3	4400	3441	0.10
SONG 2 (Remark and Evans, 2000)	1996	10.1	10,425.5	3390	0.30
SONG 3 (Remark and Evans, 2000)	1997	8.6	11,614.5	3390	0.40
Callaway (Dow, 1997)	1996	8.6	8009	3565	0.26
Doel 4 (Roofthooft, 1994)	1992	7.0	2969.1	3170	0.13
Tihange 1 (Roofthooft, 1994; Roofthooft et al., 1991)	1988	11.4	4504	2873	0.14
Tihange 2 (Roofthooft, 1994; Roofthooft et al., 1991)	1989	6.1	1833	3064	0.10
Surry 1 (Stanley, 2000)	1994	14.6	8358	2441	0.23
Surry 2 (Stanley, 2000)	1994	13.9	6949	2441	0.20
Byron 1 (Fiola et al., 1997)	1994	7.7	6987	3411	0.27
Palo Verde 1 (Fiola et al., 1997)	1995	5.8	5251	3817	0.24
Palo Verde 2 (Paramithas et al., 1994)	1994	4.8	4828	3817	0.26
Palo Verde 3 (Dow, 1997)	1994	4.4	4413	3817	0.26
Sequoyah 1 (Harvey et al., 1997)	1995	7.5	9072	3441	0.35
Sequoyah 2 (Harvey et al., 1997)	1996	8.1	7419	3441	0.27
Wolf Creek (Pendergrass, 1997)	1996	8.2	3889	3565	0.13
CPSES 1 (Stanley, 2000)	1997	5.0	1551	3411	0.09
Salem 2 (King and Remark, 2000; Evans et al., 2002)	1999	9.1	6017	3423	0.19

[a]Oxide loadings do not include deposit removed by preclean and postclean water lancing of the tube sheet.
[b]Deposits removed composed of oxides of iron, nickel and zinc as well as metallic copper.

The total deposit removed was normalized for each plant to the EFPYs of operation at the time of chemical cleaning and to the total thermal power of the SGs to determine a deposit accumulation per EFPY per MW_t. For comparison, an average corrosion product concentration of 1 μg/kg in the FW is calculated to result in a deposit accumulation rate of 0.015 kg/MW_t/EFPY on the tube bundle and tube-support structure following the methodology outlined in Section 9.4.1. The normalization to plant thermal power is effectively a normalization to FW flow rate, and from the perspective of corrosion product transport is perhaps more useful than normalizations to tube bundle surface area or SG volume. The main contributions to differences in the normalized deposit loadings and deposit accumulation rates listed in Table 9.9 will be: (1) differences in the FW corrosion product concentration during operation at power and (2) differences in the total number of start-ups and the amount of corrosion product transported to the SGs during each start-up.

The two lowest deposit accumulation rates listed in Table 9.9 are for the SGs at the CANDU 6 plants, PLGS (Verma, 1996) and Gentilly-2 (Plante, 2005). Both plants installed FW recirculation loops within several of years of first operation to condition the water and remove corrosion products prior to feeding water forward to the SGs during start-up following a maintenance outage. Perhaps the relatively low deposit accumulation at these plants reflects, in part, a lower corrosion product transport rate to the SGs during start-up operations. There is very good agreement between the total deposit removed from the SGs by the cleaning operations, i.e., chemical cleaning plus sludge lancing, and the deposit loading estimated from corrosion product transport data in several cases where such data are available in the open literature. For example, corrosion product transport measurements predicted a deposit loading of 14,268 kg for the SGs at SONGS 2 compared to the total deposit removed equivalent to 14,243 kg (Remark and Evans, 2000). Similarly, the predicted deposit loading at SONGS 3 based on measurements of corrosion product transport was 18,153 kg compared to the total deposit removed equal to 17,690 kg. The predicted total deposit loading at Waterford based on corrosion product transport measurements was 6727 kg, and for comparison a combination of chemical cleaning and water lancing removed a total of 6912 kg (Stanley, 2000; Evans et al., 2002). The calculated deposit loading at the time of chemical cleaning for the tube bundle and support structure at PLGS, based on the iron concentration for PLGS listed in Table 9.8, is equal to 1238 kg,[16] which is in good agreement with the deposit loading listed in Table 9.9.

The deposit accumulation rates listed in Table 9.9 correspond to accumulations from 90 to 1200 kg/EFPY for a 1000 MW_e plant and equate to average corrosion product concentrations in the final FW ranging from 2 to 25 μg/kg based on the methodology outlined in Section 9.4.1.

[16]For this calculation the feed water flow rate for a steam temperature of 260°C was calculated from the thermal power using a heat of vaporization of 1661 kJ/kg. 75% of the corrosion product transported to the SG was assumed to deposit on the tube bundle and tube support structure, as per the discussion in Section 9.4.1.

9.4.3 Tube bundle fouling—internal tube surface (CANDU SGs)

The piping in the primary coolant circuit of a CANDU PHWR is made of carbon steel. Although the carbon steel is normally covered with a protective layer of magnetite that effectively reduces the iron release rate to a value in the order of 1 mg/dm^2·day (Gonzalez et al., 1997), significantly higher release rates occur in the feeder pipes that carry the hot primary coolant from the outlet of the reactor core to the SGs because the coolant exiting the core of the reactor is undersaturated in iron which results in FAC of the carbon steel. As the primary coolant flows through the SG tube bundle the coolant temperature decreases, causing iron to precipitate from solution onto the inside surface of the SG tube bundle (Burrill and Turner, 1994). The accumulation of a thick, thermally resistive layer of magnetite on the inside surface of the SG tube bundle has the effect of reducing the SG heat-transfer efficiency and interferes with the passage of nondestructive eddy current inspection probes (Husain and Krasznai, 2005).

Single-tube chemical cleans at PLGS and Gentilly-2 found single-tube deposit loadings of 0.185 kg/m^2 after 10 EFPY of operation (Yetisir et al., 2000). Ontario Hydro Technologies developed the Oxiprobe to measure the deposit loading at selected locations along the inside surface of a SG tube (Gonzalez et al., 1997). Deposit profiles have subsequently been measured for single tubes at the Pickering, Darlington, and Bruce Nuclear Generating Stations (Gonzalez et al., 1997; Husain and Krasznai, 2005). The profiles are similar in the Bruce and Pickering tubes; the deposit loading increases with distance from the tubesheet on the hot leg side of the tube bundle, passes through a maximum near the U-bend, and decreases toward the tubesheet on the cold leg side. The profile at Darlington is similar except the deposit loading increases again as the tube passes through the integral preheater on the cold leg. The measured deposit loadings are consistent with a model of precipitation fouling in the primary coolant of a CANDU reactor (Burrill and Turner, 1994). In this model, iron released from the carbon steel piping at the outlet of the core as the result of FAC precipitates onto the inner surfaces of the SG tubes as the primary coolant temperature decreases as a result of heat transfer from the primary to the secondary coolant in the SG. Deposit loadings measured at Pickering, Bruce, and Darlington by Oxiprobe inspection are listed in Table 9.10. The results are consistent with the deposit loading measured previously by single-tube chemical cleaning at PLGS and Gentilly-2.

Deposit profiles of magnetite deposited on the inside of the SG tubes of CANDU SGs have also been measured by eddy current probes (Lepine and Obrutsky, 2006). These profiles show the same general shape as those observed at Darlington by Oxiprobe measurements, with a sharp increase in deposit thickness within the integral preheater.

9.4.4 Tube-support structure fouling

Deposit accumulations within the broached-holes of trefoil and quatrefoil tube-support structures have resulted in significant operational problems at a number of NPPs operating with OTSGs (Johnson, 1987; Thompson and Lammana, 1986;

Table 9.10 Oxide loadings on the primary side of the tube bundle of CANDU SGs measured by oxiprobe inspection (Husain and Krasznai, 2005)

Station	EFPY	Magnetite loading (g/m^2)	Total oxide loading (g/m^2)
PNGS-A U1 SG8	14.5	20–143	21–147
PNGS-A U4 SG5	16.4	16–205	–
PNGS-A U1 SG8	16.7	53–217	–
BNGS-A U3 SG2	11.8	5–200	7–217
PNGS-B U6 SG7	13.9	98–389	–
PNGS-B U8 SG8	12.0	41–115	–
BNGS-B U5 SG5	8.1	38–209	60–250
DNGS U3 SG2	5.0	6–153	–
DNGS U2 SG1	7.3	16–244	–
DNGS U3 SG4	7.7	20–120	–

Thompson, 1992) and RSGs (Stickel et al., 1994; Dyck et al., 1990; Malaugh and Ryder, 1990; Bodineau and Sollier, 2008; Corredera et al., 2008; Luna et al., 2006; Obrutsky et al., 2006; Sedman et al., 2005), as discussed in Section 9.2.4.

In the OTSGs at the Crystal River plant, the blockage was reported to be greatest at the fourth TSP, decreasing to moderate at the third and fifth TSP, and light at the first and sixth TSP. The degree of blockage was greater at the inlet than the outlet of the broached-hole, and the deposit was described as "lips" protruding from the TSP toward the tube surface (Thompson, 1992). What is striking about the deposit is that it appears to grow primarily from the tube-support structure toward the SG tube. Rippled deposit is also observed on the surface of the TSP inside the broached-hole. In the RSGs at the Bruce A plant, the extent of the blockage was reported to increase with increasing TSP elevation and was greater on the hot leg than the cold leg. Restriction of the flow passages reached 100% on the hot leg of the seventh TSP and was as low as 20% on the cold leg. In all cases, the deposits were reported to be brittle with porosity ranging from 0% to 5%, and to have the form of a "lip" on the inlet to the flow passages of the TSP (Malaugh and Ryder, 1990).

The rate of flow-hole blockage in SGs operating with trefoil and quatrefoil TSPs appears to be lower in SGs operating with higher pH in the FW system. For example, the rate of rise of operating pressure and downcomer water level at Crystal River-3 was reduced to manageable levels by increasing the FW pH from between 8.9 and 9.2 to between 9.2 and 9.4 with ammonia, and by eventually replacing ammonia with morpholine (Thompson and Gaudreau, 1995). The Bruce A SGs operated at a FW pH of 8.9 with morpholine/hydrazine chemistry and experienced severe broached-hole blockage in Units 1 and 2 within 9 years of operation. In contrast, the SGs at Bruce B which operate with ammonia/hydrazine chemistry at a pH of 9.4 have not reported blockage of the trefoil broached-hole support plates to date. Like the Bruce A units,

Surry Units 1 and 2 operated with a FW pH of 8.9 and noted level oscillations caused by blockage of the flow holes in the upper bundle stainless steel support plates within 13 years of operation following SG replacement (Stickel et al., 1994). It is noteworthy that although blockage of the TSPs was not observed in Bruce B SGs operating with a FW pH of 9.4, the carbon steel support plates in the SGs of Unit 8 did undergo severe degradation due to FAC (Sedman et al., 2005). This experience is in contrast to the Bruce A SGs operating at a FW pH of 8.9, where the TSPs showed heavy blockage of the broached flow holes but FAC of the carbon steel TSPs was not reported to be an issue.

Both Embalse and Gentilly-2 have Admiralty Brass condenser tubes and operated their FW heating systems on morpholine chemistry at an intermediate pH (~9.3–9.5) with very low concentrations of ammonia and correspondingly low copper transport to the SGs (see data for Embalse in Table 9.8). Tube-support blockage proceeded at a relatively low rate in the SGs at both plants, with level oscillations just starting to be manifested at Gentilly-2 when the plant was taken off-line for chemical cleaning after 21.5 EFPY of operation (Plante, 2005). An inspection of the SGs at Embalse in 2005 showed heavy blockage (described as partial to complete blockage) of the top TSPs on the hot leg side of the SG after 23 years of operation. Severe degradation of the U-bend supports and TSPs was also observed on the cold leg side of the SG (Luna et al., 2006), so rather than chemically clean a decision was made to replace the SGs.

Following the SG tube leakage events at Cruas (Bodineau and Sollier, 2008; Corredera et al., 2008), Electricite de France (EdF) launched an investigation to determine if there was a correlation between FW chemistry and the rates of TSP blockage at their fleet of NPPs. Chemistry parameters examined in the investigation included FW pH, dissolved oxygen, hydrazine, morpholine, ammonia, dissolved and suspended corrosion products, and impurities such as silica, calcium, and sulfate. The rate of TSP blockage was assessed by a combination of visual inspection, wide-range level pressure measurements, and eddy current inspection. For the 900 MW plants operating with 51 B or 51 B1 SGs, TSP blockage rates were medium to high on the hot leg and cold leg for plants operating with a FW pH of 9.2, compared to TSP fouling rates that were medium to none on the hot leg and low to none on the cold leg for those plants operating with a FW pH of 9.6. The investigators concluded that low FW pH was an aggravating factor, but they could not conclude that it was a required condition for blockage to develop. No other chemistry parameters were found to have a direct influence on the rate of TSP blockage although impurities were considered to be a second-order aggravating factor.

The remedial action required for excessive blockage of the flow holes of trefoil and quatrefoil tube supports is to reduce the blockage by either water lancing or chemical cleaning. Simulations of SG operation with partially blocked flow holes suggest that the aggregate blockage of the upper TSPs of the Bruce A SGs would have to be reduced to 70% to allow operation at full power without level oscillations (Malaugh and Ryder, 1990). Similar analyses showed that level oscillations would occur for blockage of the quatrefoils at Kori and Yonggwang SGs in excess of 62% and 68%, respectively (Lee et al., 2006).

9.4.5 Tubesheet fouling

Most, if not all, NPPs now include water lancing of the SG tubesheets as one of their regular maintenance activities to mitigate tube corrosion at the tubesheet (Persed and Eybergen, 2005). Relatively few quantitative results from water lancing campaigns are reported in the open literature, but when they are they can be used to estimate a tubesheet fouling rate provided the operating period between water lancing campaigns is reported as well. Chemical cleaning operations which include preclean and postclean water lancing of the tubesheet also yield valuable data to estimate tubesheet fouling rates, subject to the uncertainties discussed below.

Results from tubesheet water lancing campaigns from several NPPs are listed in Table 9.11. At South Texas, for example, water lancing was focused on the sludge zone adjacent to the T-slot where eddy current inspection revealed circumferential cracking indications at the top of the tubesheet (Baker and Concklin, 1997). The sludge removed was primarily soft deposit that had not yet consolidated, and the mass reported is assumed to represent wet sludge. At the time these results were reported, it appears that an average of 27 kg of wet sludge was being removed from the SGs at South Texas for each water lancing campaign. Results of the water lancing campaigns conducted from 1995 to 2000 at Darlington NPP are also listed in Table 9.11 (Seppala et al., 1995; Jelinski, 2000). From the 1995 eddy current inspection at Darlington Unit 4 it was estimated there was about 3 mm of sludge accumulation on the

Table 9.11 Tubesheet deposit removed by water lancing during maintenance and refueling outages

Plant	Date in service	Water lancing campaign	Mass of wet sludge removed from all SGs (kg)
South Texas Unit 1 (Baker and Concklin, 1997)	August 1988	1RE01 1RE03 1RE05 1RE06	11 40 38 18
South Texas Unit 2 (Baker and Concklin, 1997)	June 1989	2RE04	26
Darlington Unit 1 (Jelinski, 2000)	1992	May 1996 April 2000	16 12
Darlington Unit 3 (Jelinski, 2000)	1993	June 1999	36
Darlington Unit 4 (Seppala et al., 1995; Jelinski, 2000)	1993	May 1995	16
Kori Unit 4 SG C (Lee, 1997)	1986	1986–96	99 (Cumulative over 8 campaigns)

tubesheets. The tubesheets of all Darlington SGs are water lanced every 4 years with removals averaging 20 kg of wet deposit from all four SGs on a unit per campaign. Water lancing of the tubesheets of the SGs at Kori Units 1 to 4 was regularly performed during maintenance outages using conventional technology since first commercial operation. However, eddy current inspection in 1996 revealed sludge accumulation on the tubesheet of SG C at Kori Unit 4 of up to 3 in. in height that had not been removed by previous water lancing (Lee, 1997). The first application in 1996 of intertube water lancing at HP removed an additional 42 kg of sludge from SG C over and above the cumulative total of 57 kg removed during all previous campaigns using conventional technology. This increased the cumulative total of tubesheet deposit removed by water lancing of SG C at Kori-4 over a 10-year period of operation to 99 kg. If the tubesheet deposit accumulation for SG C is representative of the other two SGs on the unit, the estimated deposit accumulation for all three SGs over the 10-year operating period is approximately 300 kg. For the purpose of comparison with the other units in Table 9.11, if the 300 kg of deposit had been removed with equal efficiency for each of the eight water lancing campaigns conducted between 1986 and 1996, the average amount removed per campaign would have been 37 kg.

Thus, the average mass of wet sludge removed from the tubesheets of all SGs on a single unit by water lancing campaigns at South Texas, Darlington and Kori are as follows: South Texas: 27 kg, Darlington: 20 kg, Kori: 37 kg. In addition, two separate water lancing campaigns of the SGs at Waterford removed 45 and 54 kg of wet deposit from the tubesheets (Evans et al., 2002). These estimates of deposit removed per water lancing campaign are not strictly comparable because the operating intervals between water lancing campaigns are different for each plant, the concentrations of corrosion product in the FW at each plant are different and the FW flow rates carrying corrosion product to the SGs are also different. However, the spread of the numbers is not that great considering the uncertainties, and they do provide a rough estimate of the amount of corrosion product that accumulates on the tubesheets of nuclear SGs for the corresponding operating periods.

Estimates of the mass of wet sludge removed by preclean and postclean water lancing of the tubesheets of SGs as part of chemical cleaning operations at selected NPPs are listed in Table 9.12. For each unit cleaned, the amount of deposit removed from the tubesheets is also expressed as a percentage of the total deposit removed by lancing plus chemical cleaning operations. There are, again, uncertainties associated with the numbers in Table 9.12, especially if they are used to calculate a tubesheet fouling rate. Some of the tubesheet deposit not removed by the preclean water lancing will be dissolved by chemical cleaning. It is likely that dissolution of bridging material between individual particles during the chemical cleaning step contributes to a reasonable fraction of the additional deposit removed by the postclean water lancing. Another source of uncertainty in using the data in Table 9.12 to estimate a tubesheet fouling rate is that fragments of insoluble material from the tube bundle may settle onto the tubesheet during chemical cleaning and contribute to the mass of material removed by the postclean water lancing. Nevertheless, it is still instructive to compare the mass of corrosion product removed from the tubesheet by water lancing with the total mass removed from the SGs by water lancing plus chemical cleaning operations in order

Table 9.12 Tubesheet deposit removed by preclean and postclean tubesheet water lancing as part of SG chemical cleaning operations

Plant	Year	Preclean lancing (kg)	Postclean lancing (kg)	Total removed by lancing (kg)	TS deposit as % of total SG deposit
Tihange-1 (Roofthooft et al., 1991)	1988	–	–	793	15
Tihange-2 (Roofthooft et al., 1991)	1989	–	–	240	11
SONGS-2 (Remark and Evans, 2000)	1996	–	–	3290	24
SONGS-3 (Remark and Evans, 2000)	1997	–	–	5516	32
Callaway (Dow, 1997)	1996	–	–	812	9
Waterford (Stanley, 2000; Evans et al., 2002)	2000	–	–	2090[a]	32
Salem-2 (King and Remark, 2000; Evans et al., 2002)	1999	–	–	559	8.5
PNGS-7 (Klimas and Semmler, 2007)	2003	420	500	920	24
PNGS-8 (Klimas and Semmler, 2007)	2002	540	660	1200	24
Bruce-1 (Klimas and Semmler, 2007; Puzzuoli et al., 1997)	1995	2000	520	2520	23
Bruce-3 (Klimas and Semmler, 2007; Puzzuoli et al., 1997)	1994	1770	875	2645	28
Bruce-4 (Klimas and Semmler, 2007; Puzzuoli et al., 1997)	1993	–	–	2200	26

[a]Includes a contribution from upper bundle flushing.

to get a rough estimate of the rate of tubesheet fouling. From the results in Table 9.12, the mass of corrosion product removed from the tubesheet averages 21% of the total deposit loading in the SG. It should be noted, however, that the data in Table 9.12 are heavily weighted toward plants with high tube bundle fouling rates, generally in excess of 0.20 kg/MW_t/EFPY (see Table 9.9). Plants with copper-free FW heating systems and correspondingly lower rates of corrosion product transport may not have such a high proportion of corrosion product accumulating on the tubesheet.

9.4.6 Fouling of horizontal SGs

Heavy deposits have been reported on the horizontal tube bundle and tube-support structure (Splichal et al., 1994, 1997) as well as on the bottom of the SG vessel in "dead" flow zones (Osez, 2009). The deposits are composed primarily of iron and copper mixed with ionic FW impurities. Corrosion defects were detected on SG tubes characterized by high deposit thickness and enhanced concentrations of copper and chloride in the deposit. Tube deposit in the free span was up to 100 μm thick. Typical modes of degradation in horizontal SGs are SCC and pitting. Eddy current testing showed that 90% of the defects were located in regions of the TSP. Estimated deposit loadings on the tube bundle of a single horizontal SG on a VVER-440 NPP are listed in Table 9.13 (Splichal et al., 1994). It is not clear from the presentation how the deposit loadings were determined nor was the operating period reported with precision. The deposit accumulation rates are consistent, however, with those listed in Table 9.9 based on chemical cleaning of OTSGs and the SGs on PWR and PHWR units.

Table 9.13 Estimated tube bundle deposit loadings for a single horizontal SG on VVER-440 units (Splichal et al., 1994)

Unit	Years in service	Estimated deposit loading (kg)	Estimated deposit accumulation rate (kg/(MWt × year))
1	14	440.2[a]	0.24
2	12	314.4[a]	0.17
3	8	151.0[b]	0.16
4	8	123.2	0.07
5	7	142.8	0.09
6	7	170.9	0.11

[a]The amount of deposit estimated from 8 years of operation.
[b]The amount of deposit estimated from 4 years of operation.

9.5 Fouling mechanisms—fundamental studies and modeling

9.5.1 Tube bundle fouling

Fouling of the tube bundle by corrosion products and other impurities transported to the SG with the FW involves a combination of particle deposition and precipitation under flow-boiling conditions. Since corrosion product transport investigations have concluded that about 90% of the corrosion product transported to the SGs is in the form of small particles up to 1 μm in size (Sawicki and Brett, 1993; EPRI, 2009; Sawochka, 2003; Plume et al., 1986), investigations into the mechanism of fouling of the tube bundle have focused on particle deposition. Fundamental studies into the mechanisms governing particulate fouling have recently been the subject of an in-depth review (Turner, 2013), and so only a summary overview will be provided here. The reader is referred to Turner (2013) and the references therein for a more thorough treatment of this subject.

Particulate fouling of a heat transfer surface involves transport of the particles from the bulk fluid to the surface, attachment of the particles to the surface and subsequent removal of particles from the surface if the fluid hydrodynamic removal force is great enough to overcome the energy of adhesion of the particle to the surface. Transport and attachment are two steps acting "in series" and can be combined into a single step called "deposition" provided it is remembered that this step has two components contributing in series to the overall deposition rate. If boiling is taking place on the heat transfer surface, there will be an additional transport mechanism associated with the flow of water to bubble nucleation sites that will augment transport of particles to the surface by forced convection in the turbulent flow. In addition, boiling will cause precipitation of soluble species, including soluble corrosion products, at the heat-transfer surface onto existing particles that have previously deposited. It has been proposed that precipitation onto and within the pores of existing porous deposit serves to "cement" the particles into place and is thus an important contributing factor to the formation of dense, consolidated deposit found on the tubesheets, tube-supports, and tube bundle in nuclear SGs (Turner et al., 2002). A schematic illustrating the steps involved in particulate fouling and consolidation is shown in Fig. 9.6. In this figure, the steps of transport and attachment are combined into a single step called "deposition." The figure also illustrates the concept that only the porous (unconsolidated) outer layer of the deposit is subject to removal.[17]

Based on the concepts described above, a model for particulate fouling under flow-boiling conditions can be written in the following form (Turner et al., 2002):

$$m(t) = \frac{KC\rho}{\lambda}\left(t\lambda_c + \frac{\lambda_r}{\lambda}\left(1 - e^{-\lambda_t}\right)\right) \tag{9.3}$$

[17] Once the consolidated deposit layer becomes very thick, differential coefficients of expansion and contraction between the deposit and tube can lead to fracturing of the deposit and spalling. Fragments of deposit showing the curvature of the SG tube are often found in SGs during inspection, and provide evidence for spalling (Tapping et al., 1991).

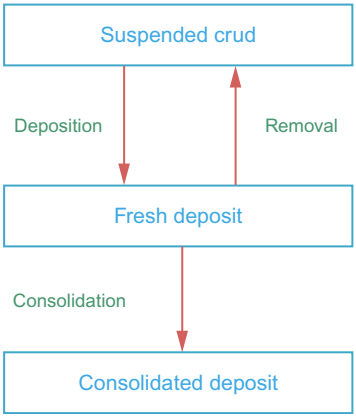

Fig. 9.6 Model of particulate fouling onto a heated surface illustrating the individual rate processes of deposition, removal, and consolidation (Turner, 2013).

where

$m(t)$ is the deposit mass at time t (kg/m^2),
K is the overall deposition rate constant (m/s),
C is the mass fraction of suspended particulate in the coolant (kg/kg),
λ is a rate constant $= \lambda_c + \lambda_r \left(s^{-1}\right)$,
λ_c is the rate constant for converting porous deposit to consolidated deposit (s^{-1}),
λ_r is the rate constant for removal of nonconsolidated, porous deposit (s^{-1}).

Under flow-boiling conditions, the deposition rate by forced convection is augmented by an additional flux of particles carried with the fluid toward bubble nucleation sites on the surface. Thus, the deposition rate constant K becomes:

$$K_{TP} = K_B + K_{FC} \tag{9.4}$$

where

K_{TP} = overall deposition rate constant in two-phase (TP) flow (m/s),
K_B = rate constant for deposition by boiling (m/s),
K_{FC} = rate constant for deposition by forced convection (m/s).

The rate constant K_B is equal to the boiling deposition coefficient (a_b) times the local boiling rate per unit area on the tube bundle. Thus, a_b can be understood as the fraction of the particles deposited per unit mass of water evaporated at a given location. It has been suggested that the deposition fluxes for boiling and forced convection should be combined in a way that takes account of the fractions of heat transferred by boiling and forced convection, respectively, thus (Najibi et al., 1997):

$$K_{TP} = \mathrm{NBF} \times K_B + (1 - \mathrm{NBF}) \times K_{FC} \tag{9.5}$$

where NBF is the fraction of heat transferred by nucleate boiling and can be calculated from any one of a number of correlations for boiling heat transfer.

The separate contributions from transport and attachment are related to the rate constant for deposition by forced convection through the following expression:

$$\frac{1}{K_{FC}} = \frac{1}{K_t} + \frac{1}{K_a} \tag{9.6}$$

where

K_t is the rate constant for the transport from the bulk to the surface (m/s),
K_a is the rate constant for the attachment of particles to the surface (m/s).

The term K_a is expressed as:

$$K_a = K_0 \times \exp\left(\frac{-E}{RT}\right) \tag{9.7}$$

where E is the activation energy for attachment and K_0 is the preexponential factor.

Fouling is a surface phenomenon. Thus, the susceptibility of a system to particulate fouling depends not only on the local thermal-hydraulic conditions but also on the surface chemistry of the particles and the solution chemistry as well. For example, results from high-temperature loop tests simulating local thermal-hydraulic conditions along the tube bundle of a nuclear SG show distinctly different fouling rates for the different phases of iron oxide particles that are transported with the FW to the SG (Turner et al., 2002; Turner and Klimas, 2001). The presence of a surface-active agent, such as a dispersant, has also been demonstrated to affect the fouling rate of particles under flow-boiling conditions (Balakrishnan et al., 1999; Burgmayer et al., 1998), as does the pH under conditions of forced-convective flow (Turner and Smith, 1992; Williamson et al., 1988; Turner et al., 1990), and subcooled nucleate boiling (Basset et al., 2000; Arbeau et al., 2004). A series of high-temperature loop tests demonstrated an effect of the amine used for pH control on the tube fouling rate under flow-boiling conditions (Turner et al., 1988, 1999; Klimas et al., 2002). Taken together, these investigations provide clear evidence for the importance of surface chemistry in determining the fouling rate of particles from flowing suspensions of particles under turbulent flow conditions, with and without heat transfer.

The effect of chemistry on the various steps of deposition, removal, and consolidation is contained in the parameters a_b, E, and λ_c, which must be determined by fitting the model described above to loop fouling data. The rate constants so determined have been incorporated into a three-dimensional transient model of the fouling behavior of an RSG (Turner et al., 1994). The relationship between the tube bundle fouling rate and BD efficiency is discussed in Section 9.5.4. This discussion sets the stage for understanding how the material presented in Sections 9.6.1 and 9.6.2 clearly demonstrates an effect of chemistry on SG fouling rates and SG performance in operating NPPs.

9.5.2 Tube-support fouling

With the trefoil and quatrefoil design, there is an abrupt reduction in the cross-sectional area to flow as the two-phase mixture on the secondary side of the SG enters the broached-holes of the TSP. This abrupt reduction in flow cross-sectional area results in separation of the fluid boundary layer from the surface of the TSP which causes the main flow to contract through a minimum cross-sectional area called the *vena contracta*. Associated with the *vena contracta* is a corresponding local maximum in fluid velocity, a local minimum in pressure and a local maximum in turbulence intensity. These localized phenomena at the entrance to the broached-holes have been verified by numerical modeling (Hirano et al., 2010) and measurements under single- and two-phase flow conditions (Rummens et al., 2004; Rummens, 1999). Measurements have also demonstrated that the localized phenomena are less pronounced with the more open lattice bar tube-support structure, and therefore this structure is predicted to be less susceptible to fouling.

The various phenomena that may contribute to the accumulation of deposit at the entrance to the broached-holes of the trefoil and quatrefoil TSP are identified in Fig. 9.7 (Rummens et al., 2004). The separation of the boundary layer from the surface of the TSP gives rise to three phenomena that act to promote the accumulation of deposit:

1. High turbulence intensity and mass transfer coefficient increase the rate of particle transport from the bulk fluid to the wall,
2. Particles transported into the low velocity circulation zone of the *vena contracta* will have little tendency to be removed because the hydrodynamic forces in this region will be very low, and
3. Precipitation of dissolved iron caused by flashing of the two-phase mixture at the *vena contracta* will contribute to deposit consolidation at this location.

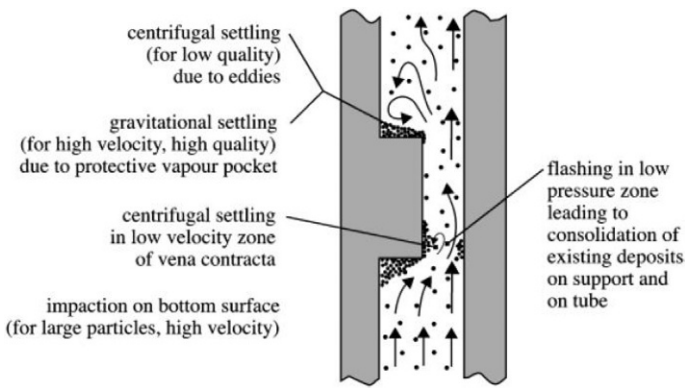

Fig. 9.7 Illustration of potential contributing factors to fouling of broached-holes in quatrefoil and trefoil tube-support plates under flow-boiling conditions (Rummens et al., 2004). Courtesy of the American Nuclear Society, La Grange Park, IL. Copyright 2004.

A detailed model based on the various hydrodynamic forces acting on a particle together with the phenomena described above was developed to account for the fouling of trefoil and quatrefoil tube-support structures in nuclear SGs. More recently, a model of TSP fouling was developed based on the work described in Rummens et al. (2004) and Rummens (1999) that takes account of changes in the fluid hydraulics as blockage of the TSPs progresses (Prusek et al., 2013).

An alternative mechanism for fouling trefoil and quatrefoil tube-supports has been proposed based on an investigation of pitting of aircraft slide and sleeve hydraulic servo valves (Beck et al., 1970) and the investigations of the blockage of flow orifices in boilers of AGRs (Woolsey et al., 1989; Robertson, 1986). This mechanism is based on the effect of the streaming potential that develops when a fluid accelerates past a charged surface. The fluid acceleration results in a streaming current gradient that must be matched by a balancing current from either anodic sites that develop on the surface or anodic reactions in the flowing solution. There has been a renewal of interest in the possible link between streaming potential and the accumulation of deposit in regions of accelerating flow in response to the experience of flow blockage of quatrefoils which lead to SG tube failures at some plants operated by EdF (Bodineau and Sollier, 2008; Corredera et al., 2008). Tests conducted in fast-flowing water have shown similar results to previous investigations of flow orifice blockage. The tests showed evidence for both precipitation and the deposition of fine particles within the flow orifice (Guillodo et al., 2004, 2009). The investigators proposed that pH and a redox potential were both important parameters, suggesting that a pHT in the vicinity of 5.7–5.9 and a redox potential more positive than −570 mV relative to an Ag-AgCl electrode promoted fouling of the orifice.

9.5.3 Tubesheet Fouling

Low velocity, high-steam quality regions on the tubesheet are recognized locations where deposit may accumulate as a result of gravitational settling. By comparing tubesheet deposit profiles with flow velocity and steam quality predictions from a thermal-hydraulic analysis code, a deposit criterion for tubesheet deposit accumulation was suggested as follows: steam quality > 0, liquid velocity < 0.4 m/s (Ayme, 1994).

An experimental investigation of tubesheet deposition was conducted in a loop operating at room temperature simulating the recirculating flow in an RSG (Burrill et al., 1994). From an analysis of gravitational settling from the thin liquid layer above the tubesheet it was concluded that all particles within the expected range of particle sizes in the SG would contribute to the tubesheet deposit by gravitational settling, i.e., no particles within the expected size range would be prevented from settling by the rising flow. Based on measured settling rates a deposit accumulation rate of 1 mm/y was estimated for SG operating conditions.

9.5.4 Relationship between fouling rate and BD efficiency

Corrosion products that are transported to the SGs either deposit somewhere or remain suspended where they can be removed by BD. Thus, BD and deposition can be thought of as the two main “sinks” for corrosion products that have been

transported to the SGs. A measure of the effectiveness of BD at limiting the accumulation of deposit in the SG is the BD efficiency, expressed as the percentage of the iron transported to the SG that is removed with the BD flow. The low BD efficiency of RSGs is primarily a consequence of the high surface area of the tube bundle, which makes deposition onto the tube bundle a more effective "sink" for particle removal than BD. The fact that fouling of the SG tube bundle is a more effective removal mechanism for corrosion products than BD is related to the relative time scales on which the two processes occur, as illustrated for the following simple relationships.

BD can only remove particles that are still in suspension, i.e., those particles that have not yet deposited. If BD was the only means of removal of particles in suspension from the SG then the half-mean-life for particle removal by BD would be equal to (Turner, 2011, 2013):

$$t_{1/2\,\mathrm{blowdown}} = 0.5 \times \mathrm{M/BD} \tag{9.8}$$

where the half-mean-life is the time that would be required to reduce the concentration of suspended corrosion products in the SG by one-half via BD. In this equation, M is the total mass of fluid in the SG and BD is the BD flow rate.

If fouling of the tube bundle were the only means to remove particles in suspension then the half-mean-life for particle removal by fouling would be:

$$t_{1/2\,\mathrm{tube-bundle\,fouling}} = 0.5 \times M/(\rho \times K_{\mathrm{TP}} \times A) \tag{9.9}$$

In this equation, ρ is the steam/water mixture density in the SG, K_{TP} is the particle deposition rate constant for tube bundle fouling under SG operating conditions (see Eq. 9.6), and A is the total surface area of the tube bundle.

For BD to be more effective at removing corrosion product than fouling of the tube bundle, the half-mean-life for removal by BD would have to be less than the half-mean-life for removal by fouling. Defining the ratio of the half-mean-life of BD relative to fouling as f, then:

$$f = \rho K_{\mathrm{TP}} A/BD \tag{9.10}$$

In the limit that tube bundle fouling is the dominant fouling mechanism in the SG, it can be shown that the BD efficiency is related to the ratio f by:

$$\text{Blow down efficiency } (\%) = (1 - f/(f+1)) \times 100 \tag{9.11}$$

Measures that either reduce the BD half-mean-life (e.g., by increasing the BD flow rate) or increase the deposition half-mean-life (e.g., by reducing the tube bundle deposition rate) will tend to increase the BD efficiency and result in a greater fraction of the corrosion products that have been transported to the SG being removed by BD.

BD efficiencies calculated using Eqs. (9.8)–(9.11) with different fouling rate constants and BD flow rates equivalent to 0.1% and 1.0% of the steaming rate are listed in

Table 9.14 Effect of fouling rate constant and blow down rate on blow down efficiency

Amine	ρK_{TP} (kg/m^{2}s)	$t_{1/2}$ Fouling (h)	f		Blow down efficiency (%)	
			0.1%	1.0%	0.1%	1.0%
Magnetite						
Morpholine	3.48×10^{-4}	5.7	3.86	0.39	21	72
Ethanolamine	5.52×10^{-4}	3.6	6.11	0.61	14	62
Dimethylamine	1.16×10^{-4}	17	1.29	0.13	44	89
Dodecylamine +Ethanolamine	0.70×10^{-4}	28	0.79	0.079	56	93
Hematite						
Morpholine	1.82×10^{-2}	0.11	200	20	<1	5
Ethanolamine	1.08×10^{-2}	0.18	122	12	<1	8
Dimethylamine	0.15×10^{-2}	1.29	17	1.7	6	37

Table 9.14.[18] Tube fouling rate constants under flow-boiling conditions were determined from an experimental investigation into the effect of alternative amines on the rate of tube bundle fouling under SG operating conditions (Turner et al., 1988, 1999; Klimas et al., 2002). The calculated BD efficiency of 21% for magnetite for a BD flow rate of 0.1% is bracketed by the BD efficiency of 13% calculated from the iron transport rates listed in Table 9.1 for the CANDU 6 SGs at PLGS and the range of BD efficiencies (i.e., 29%–45%) reported from that study (Plume et al., 1986). The results of this simple analysis are also consistent with the results of an analysis of the effect of BD flow rate and tube bundle fouling rate performed using a three-dimensional transient fouling code (SLUDGE) developed to simulate the fouling behavior of RSGs (Turner et al., 1994; Turner, 2013). For magnetite particles 1 μm in size and morpholine chemistry control, SLUDGE predicts BD efficiencies of 14% and 61% for BD rates of 0.1% and 1.0% of the steaming rate, respectively.

The results in Table 9.14 clearly illustrate the inverse relationship between BD efficiency and the fouling rate constant and the linear relationship between BD efficiency and BD flow rate. The results also illustrate that BD efficiencies are different for different particle types, e.g., magnetite versus hematite, and for different amines used for pH control. Both of these results reflect the importance of chemistry in determining particulate fouling behavior and BD efficiency in nuclear SGs. The material discussed in Sections 9.6.1 and 9.6.2 provides further evidence from operating NPPs of the importance of chemical effects in determining fouling rates.

[18] The calculations are done for a CANDU 6 SG with a tube-bundle surface area of 3600 m^2, steaming rate of 311 kg/s per SG and a water inventory in the SG of 50 Mg. The calculated half-mean-life for particle removal by blow down flow is 22 h and 2.2 h for blow down flow rates of 0.1% and 1.0%, respectively.

9.6 Mitigating fouling of nuclear SGs—field studies

9.6.1 Alternative amines

There are numerous papers in the open literature on the use of alternatives to ammonia to achieve lower iron transport rates to the SGs. These alternatives, e.g., morpholine, ETA, dimethylamine (DMA), methylpropylamine (MPA), are selected on the basis of their higher base strength and lower volatility at elevated temperature compared to ammonia to achieve higher pH and greater protection against FAC, especially in the MSR drains and the HP heater drains. The results are well documented in the literature, and the inverse relationship between pH and the rate of FAC is well established (EPRI, 1998). What has not been established in operating SGs, however, is whether there is an amine-specific effect on the rate of SG fouling such as has been observed in high-temperature loop tests (Turner et al., 1988, 1999; Klimas et al., 2002). A claim has been made for the efficacy of DMA at maintaining a more porous deposit structure which offers less resistance to heat transfer, higher rates of return of water-borne impurities such as silica and is more readily removed from the SG following soaks at reduced power and under wet layup conditions (Fellers et al., 1994; Trent and Fellers, 1997). The suggestion that DMA promotes a more porous deposit structure is consistent with observations regarding the effect of DMA on the fouling rate measured under flow-boiling conditions (Turner et al., 2002; Turner and Klimas, 2001), where it was noted that DMA appears to reduce the rate of deposit consolidation as illustrated by the data shown in Fig. 9.8. The graphs in the figure show Fe-59 radiotracing data for the deposition and removal of magnetite particles at a heat-transfer surface under flow-boiling conditions with the pH controlled by morpholine (top) and DMA (bottom). As disccused in Section 9.5.1, consolidation of a deposit is manifested by a reduction in the rate of particle removal (see Fig. 9.6), i.e., particles that have been consolidated are not subject to removal. The data in Fig. 9.8 show that the removal rate of magnetite particles that have deposited in the presence of DMA is significantly higher than the removal rate of particles that have deposited under morpholine chemistry control. Thus, the deposit that has formed under DMA pH control is less consolidated than the deposit that has formed under morpholine control, i.e., is more porous and more easily removed, which is consistent with the observations reported in Fellers et al. (1994) and Trent and Fellers (1997).

A study was conducted to determine if there was evidence from plant operating data to support a DMA-specific effect on the rate of FAC and the rate of SG fouling (Marks, 2009). This assessment covered nine plants operating in the United States that had initiated the addition of DMA after at least one cycle of operation. Based on trends of either the main steam pressure or the SG fouling factor, as determined by a global fouling factor analysis (Kreider et al., 1998), the conclusion of the assessment was that there was no evidence to support a DMA-specific effect on SG fouling. The assessment did not, however, include an analysis of the effect of DMA on BD efficiency which, as per the discussion in Section 9.5.4, would have provided a direct measure of the impact of DMA on the rate of deposit accumulation in the SG.

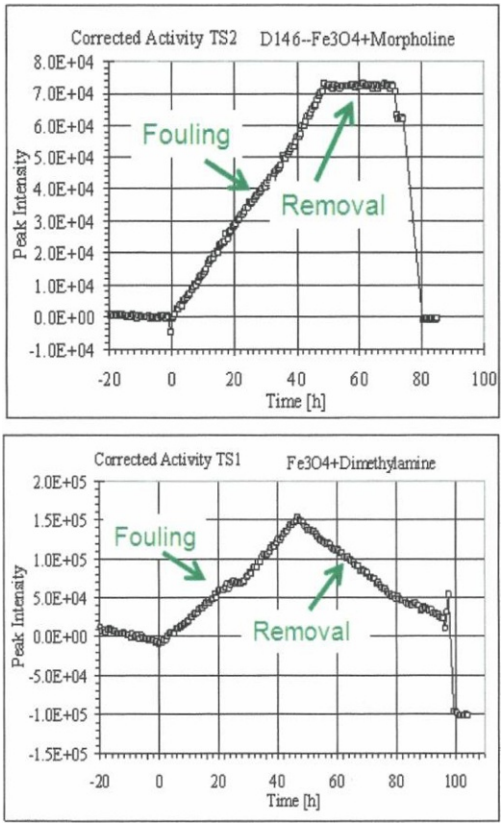

Fig. 9.8 Illustration of the effect of consolidation on the rate of particle removal from a heat-transfer surface under flow-boiling conditions; Top: High consolidation rate; Bottom: Low consolidation rate (Turner, 2013).

9.6.2 Surface-active agents: polymeric dispersants and film-forming amines

9.6.2.1 Polymeric dispersants

While polymeric dispersants have been used for decades to mitigate deposit accumulation in fossil-fuelled SGs, the nuclear industry was reluctant to introduce dispersants to nuclear SGs to mitigate fouling because of the possibility of introducing inorganic impurities (left over from the polymer synthesis) to the SGs and concerns regarding the impact of polymer decomposition products on crevice chemistry and materials. The CANDU Owners Group investigated the feasibility of applying dispersants to CANDU SGs in the 1990s and made preparations for a field trial of a low-molecular-weight polyacrylic acid (PAA) dispersant (Balakrishnan et al., 1999; Burgmayer et al., 1998), but the field trial did not come to fruition. Dearborn developed a high-molecular-weight PAA dispersant for application in nuclear SGs and following rigorous qualification (Fruzzetti et al., 2002a) the dispersant was approved for use: first in a short-term trial at ANO-2 (Fruzzetti et al., 2002b) and subsequently at a longer-term trial at McGuire 2 (Fruzzetti et al., 2008).

The short-term trial at ANO-2 and the longer-term trial at McGuire 2 both successfully demonstrated that the high-molecular-weight PAA could mitigate fouling in nuclear SGs. At ANO-2, PAA was added to the FW at a concentration of 2 μg/kg at the beginning of the trial and raised incrementally to 12 μg/kg by the end of the trial. BD efficiencies for both SGs increased from pretrial values of 1%–2% to average values of 20%–60% during the trial. There were no unexpected changes in secondary system chemistry that were attributed to PAA addition to the FW. Analysis of the thermal-hydraulic performance of the plant suggested that the FW venturis defouled during the injection of dispersant while the steam venturis appear to have fouled. The short-term trial at ANO-2 was followed by a longer-term trial at McGuire-2. PAA was injected into the FW to achieve a concentration ranging from 0.5 to 4 μg/kg. BD efficiency increased from a pretrial value of 5% to values in the range of 45%–50% when the PAA concentration was maintained between 2 and 4 μg/kg, i.e., roughly equivalent to the FW total iron concentration. None of the secondary system chemistry parameters were reported to be adversely affected during the trial. Exelon decided to implement online PAA dispersant technology at Braidwood Units 1 and 2 and at Byron Units 1 and 2. Preliminary results were encouraging, with iron BD efficiencies at both Braidwood and Byron increasing to more than 50% (Fruzzetti et al., 2010a,b) during the trial.

One apparently adverse effect of the dispersant addition was the sharp loss of thermal performance of the SGs during the last six weeks of the trial at ANO-2 (Fruzzetti et al., 2002b) that was only partially recovered when dispersant injection was stopped at the end of the trial. Two plausible causes of the loss of thermal performance were suggested: fouling of the moisture separators and loss of the porous outer layer of deposit on the tube bundle.[19] Of these two factors, loss of the porous outer layer was suggested to be the more likely (Fruzzetti et al., 2010a) although this explanation does not account for the observation that the loss took place primarily during the last six weeks of the trial. Fouling of both the moisture separators and the steam venturis is consistent with the high moisture carryover rate of 1% reported for the SGs at ANO-2. With BD iron concentrations averaging 14–32 times higher during the trial compared to pretrial values,[20] the fouling rates of any components exposed to the main steam will be correspondingly higher during PAA injection. The rate of moisture carryover at ANO-2 is anomalously high, and so the effect of elevated suspended iron concentration in the SG on the fouling of steam cycle components downstream of the SGs will be significantly higher at ANO-2 than at other plants. Fouling of steam-cycle components is not expected to affect performance at plants where the rate of moisture carryover is not an issue.[21]

The high-molecular-weight PAA qualified for use in the steam/water cycles of NPPs has since been applied for deposit removal during wet layup of SGs (Fruzzetti et al., 2010b; Anderson et al., 2011) and during long-path recirculation

[19] The outer porous layer reduces the wall superheat required for bubble nucleation, hence, acts to increase the rate of heat transfer. Only the dense inner layer offers a resistance to heat transfer.

[20] A log-mean average is reported in Fruzzetti et al. (2002b).

[21] Moisture carry-over rates at plants with properly functioning moisture separators are generally $< 0.25\%$.

and cleanup of FW prior to start-up following a refueling or maintenance outage (Fruzzetti et al., 2010b; Anderson and Marks, 2009). At TMI-1, 1.45 kg of deposit was removed from SG B to which PAA had been added to a concentration of 100 mg/kg compared to a removal of 0.045 kg from SG A to which no PAA was added. For the trial at Doel Unit 3, the amounts of deposit removed from two SGs that had been laid up with PAA added to a concentration of 6 mg/kg (26 and 17 g) were similar to the amount removed from the control SG to which no PAA had been added (20 g). At Braidwood, all four SGs on Unit 1 were put into wet layup with a concentration of 1 mg/kg PAA with the result that about 145 g of iron was removed from each SG. Although the affect of PAA on deposit removal under wet layup conditions appears to be modest, it was noted that removal of impurities such as calcium, aluminum, magnesium, and silica in the wet layup drain was consistently higher in the presence of PAA. Application of PAA at a concentration of 1 mg/kg during long-path recirculation cleanup at Byron Unit 1 was reported to have increased the amount of corrosion product removed by from 6 to 12 kg compared to previous cleanup operations without the addition of PAA. Iron transport rates during start-up operations can be significant, reportedly anywhere from 2 to 53 kg/day (Plume et al., 1986; Sawicka et al., 2001; Fruzzetti, 2012a). Thus, an enhanced removal of 6–12 kg during cleanup operations prior to feeding forward to the SGs during start-up has the potential to significantly reduce total iron transport to the SGs during start-up.

The EPRI has published a source book and guidelines to support utilities who are planning to use a dispersant to mitigate fouling of the SGs during power operation, wet layup, and start-up (Fruzzetti, 2012b).

9.6.2.2 Filming amines

Filming amines have used since the 1960s to mitigate corrosion in steam condensate systems in numerous industrial applications (Schuck et al., 1973; Obrecht, 1964), where their effectiveness is proposed to be related to the establishment of a non-wettable film on metal surfaces (Obrecht, 1964). The film is proposed to be a monolayer in thickness, and so its effectiveness does not increase with continued treatment beyond that required to maintain the monolayer coverage of the system surfaces. The most effective filming amines are those aliphatic amines with 10–18 carbon atoms in the chain. Octadecylamine (ODA) is a commonly used filming amine for the protection of industrial condensate systems.

The addition of ODA to mitigate corrosion in the secondary system and SGs of VVER plants is being investigated by a combination of experiments in autoclaves and tests in a pilot-scale SGs (Avdeev et al., 2010). Its effectiveness is being evaluated with respect to its ability to mitigate FAC in the steam cycle to reduce the level of corrosion product transport to the SGs during power operation, as well as to reduce the risk of chloride-cracking of the stainless steel SG tubes. The test program showed that ODA reduced the rate of chloride-cracking of stainless steel. It was postulated that its effectiveness was related to its adsorption onto the surface of the stainless steel, thus preventing access to the surface by chloride. Although the investigation was

to determine the effectiveness of ODA at mitigating corrosion, it was noted that the application of ODA to the Kola NPP increased the operating period between chemical cleanings. No other details were provided in the paper, so it is not clear whether the reduction in SG fouling was due to reduced corrosion product transport, reduced SG fouling, or some combination of the two. In other testing in the pilot-scale SG, the application of ODA reduced tube deposits from an average loading of 48 g/m^2 to an average loading of 17 g/m^2. Although few details were provided regarding deposit characterization, it appears that the application of ODA has been effective at removing deposit from the SG tube bundle under SG operating conditions.

Results from field trials of the use of filming amines to mitigate corrosion in the steam cycles of PWR plants have been reported recently (Ramminger et al., 2012). As with the ODA trial reviewed above, the motivation for adding the filming amine was the reduction of FAC in the steam cycle piping and, thereby, a reduction of the corresponding rate corrosion product transport to the SGs. Significantly, the field trial results showed both a reduction in FW iron transport to the SGs and an increase in the concentration of corrosion product in the SG BD, i.e., an increase in BD efficiency. This is a very important observation because it implies that the addition of the filming amine has reduced the rate of fouling of the SGs. Although it is possible that some of the increase in the concentration of corrosion product in the BD arises from the removal of deposit from within the SG, it is more likely that the major contributing factor is a reduction in the rate of tube bundle fouling.

The inference deduced from the above discussion that the addition of a filming amine can reduce the tube bundle fouling rate for a given input of iron to the SGs is consistent with results reported on the effect of another filming amine, dodecylamine (DDA), on the particle deposition rate under SG operating conditions (Klimas et al., 2004). As shown in Table 9.14, the fouling rate of magnetite particles measured in high-temperature loop experiments with pH control using a mixture of DDA and ETA was about seven times lower than the rate measured in the absence of DDA at the same high-temperature pH. Thus, filming amines may be a viable alternative to the use of the high-molecular weight PAA dispersant for fouling control in nuclear SGs, with the added advantage that the filming amine may also reduce the rate of iron transport to the SG by reducing the rate of FAC in the FW piping system.

Sludge collector

An important but relatively simple component to mitigate SG fouling is a sludge collector. Placed on the separator deck plate, the sludge collector processes water from the steam separators and removes a fraction of the suspended particles before directing the flow to the downcomer. Testing of a prototype design of sludge collector found that the sludge collector captured 66% of the injected sludge and reduced the concentration of suspended sludge and total deposition by a factor of 3 (Wilson and Haskew, 1997). In a field demonstration of the sludge collector at the V.C. Summer site, the sludge collector was estimated to have captured at least 50% of the corrosion product transported to the SG during an 18-month period of operation. Other field testing

found that the sludge collector removed from 14% to 63% of the sludge from the recirculating water (Takamatsu et al., 2000). Sludge collectors can be retrofitted to existing SGs.

9.7 Summary and conclusions

This chapter began with the statement that the key to mitigating degradation of the SG is reduction of the accumulation of unwanted deposit, or fouling, on the surfaces of critical components within the SG. The critical components include the tube bundle, the tube-support structure, and the tubesheet. Accumulation of thick deposits on these critical components has led to myriad of problems including loss of SG thermal performance, underdeposit corrosion, level oscillations in RSGs, rising water levels in the downcomer of OTSGs, and redirection of the riser flow in RSGs leading to FAC of carbon steel tube-supports and SG tube failure resulting from high-cycle fatigue.

It was noted that fouling deposits are composed primarily of corrosion products transported from the FW heating system to the SGs during both operation at full power and start-up operations, where start-ups could increase the amount of corrosion product transported to the SGs by anywhere from 5% to 20% of the amount transported during operation at full power. Corrosion product transport rates decrease with increasing pH due to the influence of pH on FAC, hence the introduction of amines with higher base strength and lower volatility at operating temperature has been instrumental at reducing the rates of corrosion product transport, especially from the moisture separator and heater drains. The elimination of copper alloys, thus allowing operation at higher pH, has also been a key factor at reducing rates of corrosion product transport to the SG.

Analysis of field data and the results of chemical cleaning campaigns suggest that about 75% of the corrosion products transported to the SGs end up accumulating on the tube bundle and tube-support structure, with another 10% accumulating on the tubesheet while about 15% is removed with the BD flow. This means that for a 1000 MW_e plant operating with a thermodynamic efficiency of 33% and 1 μg/kg corrosion product in the final FW, the total amount of corrosion product transported to the SGs in one EFPY (including additional transport from a single start-up) will be ~67 kg, of which ~50 kg accumulates on the tube bundles and tube-supports and ~7 kg accumulates on the tubesheets of the SGs. Deposit accumulation rates will be correspondingly higher in plants that have more than 1 μg/kg corrosion product in the final FW. The quatrefoil and trefoil broached-hole designs of tube-support are particularly susceptible to blockage by corrosion products as a result of the abrupt reduction in flow cross-sectional area accompanied by flow separation and a LP region developing at the entrance to the flow-hole. For this reason, the more open lattice bar design of tube-support structure is much less susceptible to fouling.

Fundamental studies have shown that the particle deposition rate under flow-boiling conditions can be influenced by water chemistry. Thus, there is the potential to mitigate the fouling rate of a nuclear SG through advanced water

chemistry programs. A simple analysis of the time scale on which fouling occurs versus the time scale on which particles are removed by BD shows that BD efficiency, i.e., the fraction of corrosion product transported to the SGs that is removed with the BD flow, can be significantly increased by reducing the tube bundle fouling rate. Investigations of fouling under flow-boiling conditions have demonstrated that alternative amines such as DMA as well as surface-active agents such as a filming amine, e.g., DDA or organic-based dispersants such as PAA are effective at reducing the rate of particulate fouling under flow-boiling conditions and, thus, should lead to increased BD efficiencies in operating nuclear SGs. Results from the introduction of a high-molecular-weight PAA to the FW at several NPPs in the United States and Europe during full power operation has shown conclusively that this is the case. Preliminary results from the introduction of the filming amine ODA to mitigate FAC in the FW heating system suggest that ODA may also lead to increased BD efficiency as well as a lower rate of iron transport to the SGs. Water treatment programs that have been shown to reduce the rate of tube bundle fouling under SG operating conditions may be even more effective when combined with a sludge collector designed to remove suspended corrosion product from the recirculation flow.

References

Anderson, C., Marks, C., 2009. The Use of Polymeric Dispersants in the Condensate/Feedwater Line During Long-Path Recirculation Cleanup at Pressurized Water Reactors: Electric Power Research Institute Report TR–1019237. EPRI, Palo Alto, CA.

Anderson, C., Marks, C., Kreider, M., 2011. Steam Generator Management Program: Generic Plant Qualification and Application Plan for Dispersant Use During Steam Generator Wet Layup. Electric Power Research Institute Report TR-1022826. EPRI, Palo Alto, CA.

Arbeau, N., Cook, W., Lister, D., 2004. The early stages of deposition of magnetite particles onto alloy-800 heat exchange surfaces under subcooled boiling conditions. In: Proceedings of the 2003 ECI Conference on Heat Exchanger Fouling and Cleaning: Fundamentals and Applications, Santa Fe.

Avdeev, A., Kukushkin, A.N., Repin, D.A., Omelchuk, V.V., Barmin, L.F., Yurmanov, V.A., Czempik, E., 2010. The impact of ODA microadditions into secondary system on corrosion rate reduction in VVER steam generators. In: Nuclear Plant Chemistry NPC 2010, Quebec City.

Ayme, H., 1994. Simulation of sludge deposition on tubeseheet: comparison with plant results. In: Proceedings of Steam Generator Sludge Management Workshop, Norfolk, Electric Power Research Institute Report TR-104212, July.

Baker, R., Concklin, J., 1997. Sludge lancing at South Texas project. In: Proceedings of Steam Generator Sludge Management Workshop, Myrtle Beach, Electric Power Research Institute Report TR-108047, July.

Balakrishnan, P.V., 1999. Hideout, hideout return and crevice chemistry in steam generators. In: Proceedings of the 13th International Conference on the Properties of Water and Steam, Toronto.

Balakrishnan, P.V., Pagan, S.M., McKay, S.M., Gonzalez, F., 1996. Hideout and Hideout Return: Laboratory Studies and Plant Measurements: CANDU Owners Group Report COG-95-555-I. CANDU Owners Group, Toronto, ON.

Balakrishnan, P.V., Klimas, S.J., Lepine, L., Turner, C.W., 1999. Polymeric Dispersants for Control of Steam Generator Fouling: Atomic Energy of Canada Limited Report AECL-11975. AECL, Chalk River, ON.

Basset, M., McInerney, J., Arbeau, N., Lister, D.H., 2000. The fouling of alloy-800 heat exchanger surfaces by magnetite particles. Can. J. Chem. Eng. 78, 40–52.

Beck, T.R., Mahaffey, D.W., Olsen, J.H., 1970. Wear of small orifices by streaming current driven corrosion. Trans. ASME J. Basic Eng. 92, 782–791.

Bird, E.J., 1984. Experience of continuous isokinetic sampling on the winfrith reactor. In: Proceedings of Workshop on Corrosion Product Sampling From Hot Water Systems, Electric Power Research Institute Report NP-3402-SR, March.

Bodineau, H., Sollier, T., 2008. Tube Support Plate Clogging Up of French PWR Steam Generators. Eurosafe Forum, Paris.

Brett, M.E., Kent, B.M., Sawicki, J.A., Fracalanza, E., 1994. The Effects of high hydrazine chemistry on corrosion product transport and feedwater electrochemical potential at Pickering NGS B, a mixed feedtrain station. In: 1st International Conference on Chemistry in Water Reactors, Nice.

Burgmayer, P., Crovetto, R., Turner, C.W., Klimas, S.J., 1998. Effectiveness of selected dispersants on magnetite deposition at simulated PWR heat-transfer surfaces. In: Proceedings of the 3rd Canadian Nuclear Society International Conference on Steam Generators, Toronto.

Burrill, K.A., Turner, C.W., 1994. Control of Reactor Inlet Header Temperature (RIHT) rise in CANDU. In: Proceedings of the 2nd Canadian Nuclear Society International Steam Generator and Heat Exchanger Conference, Toronto.

Burrill, K., Turner, C.W., Balakrishnan, P.V., 1994. Tubesheet fouling in nuclear steam generators. In: Chemistry in Water Reactors: Operating Experience and New Developments, Nice.

Cho, H., Kawasaki, H., Kumasawa, H., 2000. Formation of needle-like lepidocrocite fine particles by oxidation of an aqueous suspension of ferrous hydroxide in a bubble column. Can. J. Chem. Eng. 78, 842–846.

Chocoron, M., Fernandez, N., Sawicki, J., 2000. Crud transport and control at embalse. In: Proceedings of Steam Generator Sludge Management Workshop, Scottsdale, Electric Power Research Institute Report TR-114854, April.

Cornell, R.M., Schwertmann, U., 1996. The Iron Oxides: Structure, Properties, Reactions, Occurrence and Uses. VCH, Verlag GmbH, Weinheim. D-69451.

Cornell, R.M., Giovanoli, R., Schneider, W., 1989. Review of the hydrolysis of iron(III) and the crystallization of amorphous iron(III) hydroxide hydrate. J. Chem. Technol. Biotechnol. 46, 115–134.

Corredera, G., Alves Viera, M., De Bouvier, O., 2008. Fouling and TSP blockage of steam generators on EDF fleet: identified correlation with secondary water chemistry and planned remedies. In: International Conference on Water Chemistry of Nuclear Reactor Systems, Berlin.

David, I., Welch, J.E., 1956. The oxidation of magnetite and related spinels, constitution of γ-Fe_2O_3. Trans. Faraday Soc. 52, 1642–1650.

Dooley, R.B., Syrett, B.C., McCloskey, T.H., Tsou, J., Shields, K.J., Macdonald, D.D., 1997. State-of-Knowledge of Copper in Fossil Plant Cycles: Electric Power Research Institute Report TR-108460. EPRI, Palo Alto, CA.

Dow Jr., B., 1994. Overview of steam generator chemical cleaning experience. In: Proceedings of Steam Generator Sludge Management Workshop, Norfolk, Electric Power Research Institute Report TR-104212, July.

Dow Jr., B., 1997. Overview of steam generator chemical cleaning experience. In: Proceedings of Steam Generator Sludge Management Workshop, Myrtle Beach, Electric Power Research Institute Report TR-108047, July.

Dyck, R., Spekkens, P., Verma, K., Marchand, A., 1990. Operational experience with steam generators in Canadian nuclear plants. In: Proceedings of the Canadian Nuclear Society International Steam Generator and Heat Exchanger Conference, Toronto.

Efimov, A.A., Moskvin, L.N., Belozerskii, G.N., Kazakov, M.I., Gusev, B.A., Sempov, A.V., 1989. Mössbauer phase analysis of corrosion products dispersed in nuclear power station coolant. At. Energ. 67, 389–392.

EPRI, 1998. Flow-Accelerated Corrosion in Power Plants (Revision 1): Electric Power Research Institute Report TR-106611-R1. EPRI, Palo Alto, CA.

EPRI, 2009. Pressurized Water Reactor Secondary Water Chemistry Guidelines (Revision 7): Electric Power Research Institute Report TR-101655. EPRI, Palo Alto, CA.

Evans, S., Remark, J., Watson, S., Hengge, C., 2002. Review of steam generator chemical cleaning experiences 1998-2002. In: Proceedings of the 4th Canadian Nuclear Society International Steam Generator Conference, Toronto.

Fellers, B., Rose, G., Schenberger, D.S., 1994. Dimethylamine chemistry demonstration nuclear steam cycle application. In: International Water Chemistry Conference IWC 94–90, Pittsburgh.

Fiola, R.J., Jones, S.D., Palmer, C.D., Paramithas, P., Melton, M., Kerr, S., 1997. High temperature chemical clean of Byron 1 and Palo Verde 1. In: Proceedings of Steam Generator Sludge Management Workshop, Myrtle Beach, Electric Power Research Institute Report TR-108047, July.

Fruzzetti, K., 2012a. Feedwater iron transport during PWR (and BWR) startups. In: SGMP 2012 Steam Generator Secondary Side Chemistry Management Conference, Palo Alto, Electric Power Research Institute Report TR-1026545, December.

Fruzzetti, K., 2012b. Dispersants for Pressurized Water Reactor Secondary Side Fouling Control: Sourcebook for On-Line and Off-Line Applications: Electric Power Research Institute Report TR–1025317. EPRI, Palo Alto, CA.

Fruzzetti, K., Fratini, P., Robbins, P., Miller, A., Varin, R., Kreider, M., 2002a. Dispersant trial at ANO-2: qualification for a short-term trial prior to SG replacement. In: International Conference on Water Chemistry in Nuclear Reactor Systems, Avignon.

Fruzzetti, K., Fratini, P., Robbins, P., Miller, A., Varin, R., Kreider, M., 2002b. Dispersant trial at ANO-2: results from a short-term trial prior to SG replacement. In: International Conference on Water Chemistry in Nuclear Reactor Systems, Avignon.

Fruzzetti, K., Rochester, D., Wilson, L., Kreider, M., Miller, A., 2008. Dispersant application for mitigation of steam generator fouling: final results from the McGuire 2 long term trial and an industry update and EPRI perspective for long term use. In: International Conference on Water Chemistry in Nuclear Reactor Systems, Berlin.

Fruzzetti, K., Choi, S., Haas, C., Pender, M., Perkins, D., 2010a. PWR chemistry controls: a perspective on industry initiatives and trends relative to operating experience and the EPRI PWR water chemistry guidelines. In: Nuclear Plant Chemistry NPC 2010, Quebec City.

Fruzzetti, K., Anderson, C., Marks, C., Kreider, M., Walton, B., Reecher, W., Morey, D., 2010b. Dispersant application during steam generator wet layup and during long-path recirculation cleanup. In: Nuclear Plant Chemistry NPC 2010, Quebec City.

Gay, J., 1994. The role of visual inspections in managing steam generator sludge. In: Proceedings of Steam Generator Sludge Management Workshop, Norfolk, Electric Power Research Institute Report TR-104212, July.

Gay, J., 1997. Visual inspection capabilities, industry experience, new developments. In: Proceedings of Steam Generator Sludge Management Workshop, Myrtle Beach, Electric Power Research Institute Report TR-108047, July.

Gonzalez, F., Brennenstuhl, A.M., Palumbo, G., Dyck, R.W., 1997. Steam generator primary side fouling determination using oxiprobe inspection technique. In: Proceedings of the 4th Canadian Nuclear Society International Conference on CANDU Maintenance, Toronto.

Greenwood, N.N., Earnshaw, A., 1984. Chemistry of the Elements. Pergamon Press, Oxford.

Guillodo, M., Combrade, P., Dos Santos, B., Muller, T., Berthollon, G., Engler, N., Brun, C., Turler, G., 2004. Formation of deposits in HT water under high velocity conditions: a parametric study. In: Proceedings of the International Conference on Water Chemistry, San Francisco.

Guillodo, M., Muller, T., Barale, M., Foucault, M., Clinard, M.-H., Brun, C., Chahma, F., Corredera, G., de Bouvier, O., 2009. Singular deposit formation in PWR due to electrokinetic phenomena-application to SG clogging. In: Proceedings of the 6th Canadian Nuclear Society International Steam Generator Conference, Toronto.

Harvey, S., Hughes, D., Battaglia, P., 1997. Pressure pulse/chemical cleaning field experience. In: Proceedings: Steam Generator Sludge Management Workshop, Myrtle Beach, Electric Power Research Institute Report TR-108047, July.

Hayes, J.K., 1994. Development of full flow permanent magnet filters for power plant feed water systems. In: Proceedings of Steam Generator Sludge Management Workshop, Norfolk, Electric Power Research Institute Report TR-104212, July.

Hirano, H., Domae, M., Miyajima, K., Yoneda, K., 2010. Study on the mechanism of flow-hole blockage of steam generator tube support plates under PWR secondary conditions. In: Nuclear Plant Chemistry Conference NPC 2010, Quebec City.

Husain, A., Krasznai, J., 2005. CANDU steam generator primary side tube deposit: oxide characteristics and activity transport. In: Proceedings of the 26th Annual Conference of the Canadian Nuclear Society, Toronto.

IAEA, 1997. Assessment and Management of Ageing of Major Nuclear Power Plant Components Important to Safety: Steam Generators: International Atomic Energy Agency Report IAEA-TECDOC-981. IAEA, Vienna.

Ishikawa, T., Nishimori, H., Yasukawa, A., Kandori, K., 1993. Formation of γ-FeOOH in the presence of amines. J. Mater. Sci. Lett. 12, 1359–1361.

Jelinski, E., 2000. Darlington steam generator life management program. In: COG/WANO Steam Generator Aging Management Workshop, Toronto.

Johnson, L.E., 1987. Fouling in once-through steam generators. In: Paper 87-WA/NE-12 ASME Winter Annual Meeting, Boston.

King, R.F., Remark, J., 2000. Salem unit 2 chemical cleaning. In: Proceedings of Steam Generator Sludge Management Workshop, Scottsdale, Electric Power Research Institute Report TR-114854, April.

Klimas, S.J., Semmler, J., 2007. Rationale and method for selecting an optimal steam generator cleaning frequency: CANDU Owners Group Report COG-06-4065. CANDU Owners Group, Toronto, ON.

Klimas, S.J., Guzonas, D.A., Turner, C.W., 2002. Identification and Testing of Amines for Steam Generator Corrosion and Fouling Control: Electric Power Research Institute Report TR–1002773. EPRI, Palo Alto, CA.

Klimas, S.J., Fruzzetti, K., Balakrishnan, P.V., Beaton, E.D., Halliday, J., Lu, Y.C., Strati, G.L., Turner, C.W., 2004. Development of DDA as an amine additive for steam generator fouling mitigation. In: International Conference on Water Chemistry in Nuclear Reactor Systems, San Francisco.

Kreider, M., White, G., Varrin Jr., R., 1998. A global fouling factor methodology for analysing steam generator thermal performance. In: Proceedings of the 3rd Canadian Nuclear Society International Steam Generator and Heat Exchanger Conference, Toronto.

Lee, B., 1997. First use of CECIL in Korea. In: Proceedings of Steam Generator Sludge Management Workshop, Myrtle Beach, Electric Power Research Institute Report TR-108047, July.

Lee, J.Y., Yoon, D.J., Bae, H.S., 2006. Evaluation of SG hydraulic instability for Kori Units 3 & 4 and Yonggwang Units 1 & 2. In: Transactions of the Korean Nuclear Society Spring Meeting, Chuncheon.

Lepine, B., Obrutsky, L., 2006. The impact of magnetite deposits on steam generator inspections. In: Proceedings of the 5th Canadian Nuclear Society International Steam Generator Conference, Toronto.

Lovett, J.T., Dow, B.L., 1991. Steam Generator Thermal Performance Degradation: Electric Power Research Institute Report NP-7524. EPRI, Palo Alto, CA.

Lu, Y., 2007. Define optimal conditions for steam generator tube integrity and an extended steam generator service life. In: Proceedings of the 15th International Conference on Nuclear Engineering (ICONE-15), Nagoya.

Luna, P., Diaz, G., Sveruga, H., Sainz, R., 2006. Maintenance and life assessment of steam generators at Embalse nuclear station. In: Proceedings of the 5th Canadian Nuclear Society International Steam Generator Conference, Toronto.

Malaugh, J., Ryder, S., 1990. Bruce NGS—a support plate inspection and waterlancing. In: Proceedings of the Canadian Nuclear Society International Steam Generator and Heat Exchanger Conference, Toronto.

Marks, C., 2009. Steam Generator Management Program: Effects of Different pH Control Agents on Pressurized Water Reactor Plant Systems and Components: Electric Power Research Institute Report TR–1019042. EPRI, Palo Alto, CA.

Millett, P.J., Sawochka, S.G., 1994. Investigation of Redox conditions in the secondary system of PWRs. In: Proceedings of Chemistry in Water Reactors: Operating Experience and New Developments, Nice.

Najibi, S.H., Muller-Steinhagen, H., Jamialahmadi, M., 1997. Calcium carbonate scale formation during subcooled flow boiling. J. Heat Transf. 119, 767–775.

Obrecht, M.F., October, 1964. Steam and condensate return line corrosion—how to employ filming amines for its control. Heat. Piping Air Cond. 116–122.

Obrutsky, L., Cassidy, R., Cazal, M., Sedman, K., 2006. Eddy current assessment of support plate structures degradation in nuclear steam generators. In: Proceedings of the 5th Canadian Nuclear Society International Steam Generator Conference, Toronto.

Odar, S., Nordmann, F., 2010. PWR and VVER Secondary System Water Chemistry. Advanced Nuclear Technology International, Sweden.

Odar, S., Dorr, A., Shub, P., 1986. Stages of development of secondary water chemistry in pressurized water reactors. VGB Kraftwerkstechnik 66, 1059–1071.

Osez, J., 2009. Blowdown of VVER-440 Steam Generators in the Paks Nuclear Power Plant. VGB Power Tech 89, 54–56.

Palino, G.F., McNea, D., Kassen, W.R., 2000. Design of reactor coolant hot sampling panel for Diablo Canyon: Electric Power Research Institute Report TR-1000990. EPRI, Palo Alto, CA.

Paramithas, P., Knollmeyer, P., Jevec, J., 1994. Palo Verde nuclear generating station unit 2 SGs chemical cleaning. In: Proceedings of Steam Generator Sludge Management Workshop, Norfolk, Electric Power Research Institute Report TR-104212, July.

Pendergrass, G., 1997. High temperature steam generator cleaning of Wolf Creek. In: Proceedings of Steam Generator Sludge Management Workshop, Myrtle Beach, Electric Power Research Institute Report TR-108047, July.

Persed, R., Eybergen, D., 2005. Steam generator tube sheet waterlancing of Bruce B. In: Proceedings of the 7th Canadian Nuclear Society International Conference on CANDU Maintenance, Toronto.

Pettus, T., 1994. Steam generator pressure loss at Callaway. In: Proceedings of Steam Generator Sludge Management Workshop, Norfolk, Electric Power Research Institute Report TR-104212, July.

Plante, S., 2005. Steam generator secondary side chemical cleaning at Gentilly-2. In: Proceedings of the 7th Canadian Nuclear Society International Conference on CANDU Maintenance, Toronto.

Plume, G., Schneider, W., Stauffer, C., 1986. Corrosion product transport at Point Lepreau. In: Proceedings of Water Chemistry and Materials Performance Conference, Toronto.

Prusek, T., Moleiro, E., Oukacine, F., Adobes, A., Jaeger, M., Grandotto, M., 2013. Deposit models for tube support plate blockage in steam generators. Nucl. Eng. Des. 262, 418–428.

Puzzuoli, F.V., Leinonen, P.J., Lowe, G.A., Maruska, B., 1997. Steam generator cleaning campaigns at Bruce A 1993–1996. In: Proceedings of the 4th Canadian Nuclear Society International CANDU Maintenance Conference, Toronto.

Ramminger, U., Hoffmann–Wankel, S., Fandrich, J., 2012. The application of film forming amines in secondary side chemistry treatment of NPPs. In: Nuclear Plant Chemistry NPC 2012, Paris.

Remark, J., Evans, S., 2000. Chemical cleaning of SONGS unit 2 and unit 3 steam generators. In: Proceedings of Steam Generator Sludge Management Workshop, Scottsdale, Electric Power Research Institute Report TR-114854, April.

Resch, G., Zinke, K., 1980. Investigations relating to the effect of pH-value on the corrosion of brass. VGB Kraftwerkstechnik 60, 62–64.

Riznic, J., 2006. Some performance indicators of PWR steam generators. In: Proceedings of the 5th Canadian Nuclear Society International Steam Generator Conference, Toronto.

Robertson, J., 1986. Corrosion and Deposition Due to Electrokinetic Currents. Central Electricity Generating Board Report TPRD/L/3030/R86.

Roofthooft, R., 1994. Secondary side Chemical Cleaning of SGs. In: Proceedings of Steam Generator Sludge Management Workshop, Norfolk, Electric Power Research Institute Report TR-104212, July.

Roofthooft, R., Havard, P., Maquinay, J., Brognez, J., 1991. The Belgian experience of steam generator chemical cleaning. In: NEA/CSNI-UNIPEDE Specialist Meeting on Operating Experience with Steam Generators, Brussels.

Ruhle, W., Bolz, M., Neder, H., Holz, G., Schneider, V., 2006. Oxygen injection in the secondary side of German PWRs to counteract flow accelerated corrosion, up-date of field experience. In: International Conference on Water Chemistry of Nuclear Reactor Systems, Jeju Island.

Rummens, H.E.C., 1999. The Thermalhydraulics of Tube–Support Fouling in Nuclear Steam Generators. Carleton University, Ottawa, ON. PhD Thesis.

Rummens, H.E.C., Rogers, J.T., Turner, C.W., 2004. The thermal hydraulics of tube support fouling in nuclear steam generators. Nucl. Technol. 148, 268–286.

Sato, M., Ishimoto, S., Ando, K., Kitera, T., 1994. Recommended target value of FW iron concentration. In: Proceedings of Steam Generator Sludge Management Workshop, Norfolk, Electric Power Research Institute Report TR-104212, July.

Sawicka, B., Sawicki, J., Price, J., 2000. Sludge generation and transport during startup—Bruce B study. In: Proceedings of Steam Generator Sludge Management Workshop, Scottsdale, Electric Power Research Institute Report TR–114854.

Sawicka, B., Sawicki, J., Price, J., 2001. Crud oxidation and transport during startup. In: PWR/BWR Plant Chemistry Meeting, San Antonio, Electric Power Research Institute Report TR-1001489, May.

Sawicki, J.A., Brett, M.E., 1993. Mossbauer study of corrosion products from a CANDU secondary system. Nucl. Inst. Methods Phys. Res. B 76, 254–257.

Sawicki, J.A., Brett, M.E., Tapping, R.L., 1998. Corrosion Product Transport, Oxidation State and Remedial Measures: Atomic Energy of Canada Report AECL-11959. AECL, Chalk River, ON.

Sawicki, J.A., Price, J., Brett, M.E., 2005. Corrosion product inventory: the Bruce-B system. In: Proceedings of the 7th Canadian Nuclear Society International Conference on CANDU Maintenance.

Sawochka, S., 2003. Corrosion product transport. In: Proceedings of Steam Generator Secondary Side Management Conference, Palo Alto, Electric Power Research Institute Report TR-1008468, June.

Schuck, J.J., Nathan, C.C., Metcalf, J.R., 1973. Corrosion inhibitors for steam condensate systems. Mater. Protection Perform. 12, 42–47.

Schwarz, Th., Schneider, V., 1994. Influence of SG design and water chemistry on sludge accumulation in siemens steam generators. In: Proceedings of Steam Generator Sludge Management Workshop, Norfolk, Electric Power Research Institute Report TR-104212, July.

Schwertmann, U., Murad, E., 1983. The effect of pH on the formation of goethite and hematite from ferrihydrite. Clay Clay Miner. 31, 277–284.

Schwertmann, U., Friedl, J., Stanjek, H., 1999. From Fe(III) ions to ferrihydrite and then to hematite. J. Colloid Interface Sci. 209, 215–223.

Sedman, K.G., Galan, G.E., Dicks, B., 2005. Boiler tube support plate degradation in Bruce unit 8. In: Proceedings of the 7th Canadian Nuclear Society International Conference on CANDU Maintenance, Toronto.

Sehmel, G.A., 1970. Particle sampling bias introduced by an-isokinetic sampling and deposition within the sampling line. Am. Ind. Hyg. Assoc. J. 31, 758–771.

Seppala, D., Kiisel, E., Malaugh, J., Kamler, F., 1995. Steam generator tubesheet water lancing at DNGS. In: Proceedings of the 3rd Canadian Nuclear Society International Conference on CANDU Maintenance, Toronto.

Shoda, K., 1997. Studies of scaling problems in a program to reduce iron in the feedwater of Japanese PWRs. In: Proceedings of Steam Generator Sludge Management Workshop, Myrtle Beach, Electric Power Research Institute Report TR-108047, July.

Splichal, K., Burda, J., Ruscak, M., Zd'arek, J., Shejbal, J., 1994. Sludge deposits and effect on corrosion defect propagation. In: Proceedings of Steam Generator Sludge Management Workshop, Norfolk, Electric Power Research Institute Report TR-104212, July.

Splichal, K., Burda, J., Ruscak, M., Shejbal, J., Zambach, M., 1997. Crevice and free span surface deposits and steam generator corrosion. In: Proceedings of Steam Generator Sludge Management Workshop, Myrtle Beach, Electric Power Research Institute Report TR-108047, July.

Srisukvatananan, P., Lister, D.H., Svoboda, R., Daucik, K., 2007. Assessment of the sate of the art of sampling of corrosion products from water/steam cycles. PowerPlant Chem. 9, 613–626.

Srisukvatananan, P., Lister, D.H., Ng, C.E., Svoboda, R., Daucik, K., 2008. Corrosion product sampling in power plants under water/steam cycle conditions. In: Proceedings of the 15th International Conference on the Properties of Water and Steam, Berlin.

Staehle, R.W., Gorman, J.A., McIlree, A., Tapping, R.L., 2006. Status and future of corrosion in PWR steam generators. In: Proceedings of the International Symposium Fontevraud 6, Fontevraud Royal Abbey, Chinon.

Stanley, R., 2000. Chemical cleaning cost benefit analysis for Waterford 3. In: Proceedings of Steam Generator Sludge Management Workshop, Scottsdale, Electric Power Research Institute Report TR-114854, April.

Stauffer, C.C., 1984. Corrosion product sampling experience at Babcock and Wilcox: Electric Power Research Institute Report NP-3402-SR. In: Proceedings of Workshop on Corrosion Product Sampling From Hot Water Systems, March.

Stickel, M., Morgan, E., Hiu, M., Miller, H., Easterwood, J., 1994. Steam generator level oscillations from sludge-induced flow blockage. In: Proceedings of Steam Generator Sludge Management Workshop, Norfolk, Electric Power Research Institute Report TR-104212.

Sugimoto, T., Matijevic, E., 1980. Formation of uniform spherical magnetite particles by crystallization from ferrous hydroxide gels. J. Colloid Interface Sci. 74, 227–243.

Taborek, J., Aoki, T., Ritter, R.B., Palen, J.W., 1972. Fouling: the major unresolved problem in heat transfer. Chem. Eng. Prog. 68, 59–67.

Takamatsu, H., Matsunaga, T., Wilson, R.M., Kusakabe, T., 2000. Sludge collector performance in steam generators of pressurized water reactors. Nucl. Eng. Des. 200, 295–302.

Takiguchi, H., 2008. Oxygenated water chemistry for PWR secondary system—new approach to FAC. In: International Conference on Water Chemistry of Nuclear Reactor Systems, Berlin.

Tapping, R.L., Turner, C.W., Thompson, R.H., 1991. Steam generator deposits—a detailed analysis and some inferences. Corrosion 47, 489–495.

Tapping, R.L., Nickerson, J., Spekkens, P., Maruska, C., 2000. CANDU steam generator life management. Nucl. Eng. Des. 197, 213–223.

Thompson, R.H., 1992. Fouling of the crystal river 3 once-through steam generators after switchover to morpholine. In: Proceedings of the International Joint Power Generation Conference, Atlanta, ASME-NE, Vol. 8, pp. 29–38.

Thompson, R., Gaudreau, T., 1995. Modelling and field studies of fouling in once-through steam generators. In: Proceedings of the International Symposium on the Environmental Degradation of Materials in Nuclear Power Plants Water Reactors, Breckenridge.

Thompson, R.H., Lammana, L.S., 1986. Video inspection and sampling of the crystal river unit 3 once-through steam generators. In: Proceedings of the 47th International Water Conference, Pittsburgh.

Trent, R.L., Fellers, B.D., 1997. DMA technology to remove deposits and reduce fouling of nuclear steam generators. In: Proceedings of Steam Generator Sludge Management Workshop, Myrtle Beach, Electric Power Research Institute Report TR-108047, July.

Trevani, L.N., Roberts, J.C., Tremaine, P.R., 2001. Copper(II)-ammonia complexation equilibria in aqueous solutions at temperatures from 30 to 250°C by visible spectroscopy. J. Solut. Chem. 30, 585–622.

Trunov, N., Lukasevitch, B., Sotskov, V., Harchenko, S., 2006. The past and the future of horizontal steam generators. In: Proceedings of the 5th Canadian Nuclear Society International Steam Generator Conference, Toronto.

Tsuchiya, T., Miyake, Y., Shigehisa, T., Tomita, A., Watanabe, M., 2005. Kinetics of Magnetite Formation in a Three-Phase System. J. Chem. Eng. Jpn 38 (7), 509–515.

Turner, C.W., 2011. Implications of steam generator fouling on the degradation of materials and thermal performance. In: Proceedings of the 15th International Symposium on the Environmental Degradation of Materials in Nuclear Reactor Systems Water Reactors, Colorado Springs.

Turner, C.W., 2013. Particulate fouling of nuclear steam generators: fundamental studies and operating experience. AECL Nucl. Rev. 2, 61–88.

Turner, C.W., Chi, L., 2012. Formation of Corrosion Products of Carbon Steel under Condenser Operating Conditions. Nuclear Plant Chemistry NPC 2012, Paris.

Turner, C.W., Klimas, S.J., 2001. Modeling the effect of surface chemistry on particle deposition under flow-boiling conditions. In: Proceedings of Heat Exchanger Fouling: Fundamental Approaches and Technical Solutions, Davos.

Turner, C.W., Smith, D.W., 1992. A study of magnetite particle deposition onto alloy-800 and alloy-600. In: Baker, R.L., Harvego, E.A. (Eds.), Proceedings of Steam Generator Sludge Deposition in Recirculating and Once Through Steam Generator Upper Tube Bundle and Support Plates, ASME-NE, Vol. 8, pp. 9–17.

Turner, C.W., Klimas, S.J., Frattini, P.L., 1988. Reducing tube bundle deposition with alternative amines. In: Proceedings of the 3rd Canadian Nuclear Society International Steam Generator and Heat Exchanger Conference, Toronto.

Turner, C.W., Lister, D.H., Smith, D.W., 1990. The deposition and removal of sub-micron particles of magnetite at the surface of alloy 800. In: Proceedings of Canadian Nuclear Society International Steam Generator and Heat Exchanger Conference, Toronto.

Turner, C.W., Liner, Y., Carver, M.B., 1994. Modelling magnetite particle deposition in nuclear steam generators. In: Proceedings of the 2nd Canadian Nuclear Society International Steam Generator and Heat Exchanger Conference, Toronto.

Turner, C.W., Guzonas, D.A., Klimas, S.J., 1999. Surface Chemistry Interventions to Control Boiler Tube Fouling: Electric Power Research Institute Report TR-110083. EPRI, Palo Alto, CA.

Turner, C.W., Klimas, S.J., Brideau, M.G., 2000. Thermal resistance of steam-generator tube deposits under single-phase forced convection and flow-boiling heat transfer. Can. J. Chem. Eng. 78, 1–12.

Turner, C.W., Klimas, S.J., Guzonas, D.A., Frattini, P.L., Fruzzetti, K., 2002. New insights into controlling tube-bundle fouling using alternative amines. In: International Conference on Water Chemistry in Nuclear Reactor System, Avignon.

Varrin, R., 1996. Characterisation of PWR Steam Generator Deposits: Electric Power Research Institute Report TR-106048. EPRI, Palo Alto, CA.

Verma, K., 1996. Steam generator secondary side chemical cleaning at Point Lepreau using the siemen's high temperature process. In: Presented at the 4th Technical Committee Meeting on the Exchange of Operational Safety Experience of Pressurized Heavy Water Reactors, Kyong Ju.

Vitols, V., 1966. Theoretical limits of errors due to anisokinetic sampling of particulate matter. J. Air Pollut. Control Assess. 16, 79–84.

Ward, G., 1994. Steam generator feedwater nozzle fouling at duke power oconee unit 2. In: Proceedings of Steam Generator Sludge Management Workshop, Norfolk, Electric Power Research Institute Report TR-104212, July.

Williamson, R., Newson, I., Bott, T.R., 1988. The deposition of haematite particles from flowing water. Can. J. Chem. Eng. 66, 51–54.

Wills, L., 1997. Steam generator upper bundle cleaning: Electric Power Research Institute Report TR-108047. In: Proceedings of Steam Generator Sludge Management Workshop, Myrtle Beach, July.

Wilson, R., Haskew, J.T., 1997. Sludge collectors—their design and performance. In: Proceedings of Steam Generator Sludge Management Workshop, Myrtle Beach, Electric Power Research Institute Report TR-108047, July.

Woolsey, I.S., Thomas, D.M., Garbett, K., Bignold, G.J., 1989. Occurrence and prevention of enhanced oxide deposition in boiler flow control orifices. Water Chemistry of Nuclear Reactor Systems 5. British Nuclear Energy Society, London.

Yetisir, M., Turner, C.W., Pietralik, J., 2000. Contribution of steam generator degradation mechanisms to RIHT behaviour. In: Proceedings of the 5th Canadian Nuclear Society International Conference on CANDU Maintenance, Toronto.

This page intentionally left blank

Hideout, hideout return and crevice chemistry in nuclear steam generators

10

C.W. Turner[*], *M. Huang*[†], *A. McKay*[‡]
[*]Deep River, ON, Canada, [†]Canadian Nuclear Laboratories, Chalk River, ON, Canada, [‡]Tottenham, ON, Canada

10.1 Introduction

Localized corrosion originating on the outside surface of the steam generator (SG) tubes has been a major cause of SG incapability in the commercial nuclear power industry, with the predominant modes of attack being either stress corrosion cracking (SCC) or intergranular attack (IGA) (IAEA, 1997; Staehle and Gorman, 2003; Riznic, 2006). The concentrations of impurities in the feed water to the SG are generally sufficiently low that the bulk SG water is not aggressive to the tube material. In certain regions of restricted flow, however, such as crevices at the intersections of the SG tubes with the tube-sheet or tube-support structure, the sludge pile on the tube sheet and deposits on the outer surface of the tubes, boiling at the tube surface results in local concentrations of nonvolatile impurities that are orders of magnitude higher than in the bulk water. Depending on their composition and on chemical reactions between the various impurities, the highly concentrated solutions that develop in regions of restricted flow can be aggressive and cause localized corrosion. The accumulation of nonvolatile impurities in regions of restricted flow during operation at power is called "hideout." The release of these impurities to the SG bulk water during a power reduction or shut down is called "hideout return."

During operation, impurities may be introduced to the feed water heating system from one or more of the following sources: in-leakage of condenser cooling water, the water treatment plant and, for those plants that include these operating units, the condensate polishing plant and the blow down demineralizers. Many plants routinely perform hideout return studies at each shut down to monitor the effectiveness of their chemistry control program at mitigating impurity ingress and to evaluate the aggressiveness of the chemistry environment within crevice and deposit regions (Gonzalez and Pagan, 1990; McKay, 2002; Bates, 2007).

Considerable work has been done over the past several decades to understand and model the processes that lead to the accumulation of concentrated solutions of nonvolatile solutes within regions of restricted flow on the secondary side of nuclear SGs, and to the development of tools and methods that would enable the operators of nuclear plants to predict and manage the local chemistry environment within these regions to

Steam Generators for Nuclear Power Plants. http://dx.doi.org/10.1016/B978-0-08-100894-2.00012-1
© 2017 Elsevier Ltd. All rights reserved.

ensure that they are benign to the SG tubing material. Section 10.2 of this chapter begins with a review of work done to investigate and model the concentration processes that are operative in regions of restricted flow (Section 10.2.1), followed by a review of the results of experimental investigations of hideout and hideout return in fouled crevices (Section 10.2.2), tube-sheet sludge piles and in tube deposits (Section 10.2.3). Section 10.3 focuses on the chemistry that develops within flow-restricted regions during hideout and hideout return. Deterministic models and how they are used to predict chemistry within crevice regions are discussed in Section 10.3.1, followed by Sections that address the determination of crevice chemistry by direct sampling (Section 10.3.2) and by inference from plant and other experimental data (Section 10.3.3). Section 10.4 presents practical guidance for performing hideout return studies at operating plants, including guidelines for sampling, data evaluation and analysis, along with case studies involving hideout return studies for SGs of pressurized heavy water reactors (PHWRs) and pressurized water reactors (PWRs). Summary and Conclusions of this chapter are presented in Section 10.5, followed by references.

10.2 Hideout and hideout return in flow-restricted regions

10.2.1 Concentration processes in flow-restricted regions

The accumulation of high concentrations of nonvolatile impurities in crevices and deposits on the tube sheet and the surface of the tubes is ultimately a result of the high resistance to the transport of water into these regions compared to the relatively low resistance to the transport of steam out of these locations during SG operation. For nucleate boiling on the free surface of an SG tube, turbulent mixing of the bulk SG water with the concentrated solution that develops at the heat-transfer surface as a result of nucleate boiling limits the concentration factor of that solution to a value that is typically less than five and not greater than about twenty (Cohen, 1981). Thus, it appears that it is the isolation of the concentrating solution from the diluting effect of the bulk SG water that is responsible for the significantly high concentration factors of solutions found in flow-restricted regions.

Baum has provided an extensive discussion of the thermal-hydraulic processes and chemical conditions that lead to the formation of concentrated solutions in flow-restricted regions of a nuclear SG (Baum, 1987, 1989). The regions of interest in this discussion are crevices at the intersections of the SG tubes with the tube sheet and with the tube-support structure, including the antivibration bars. Two different concentration processes taking place in a heated crevice are described, with differing characteristics that depend on the local rates of heat and mass transfer. Near the entrance to the crevice, if the flow of water into the crevice is sufficient to maintain nucleate boiling and there is little or no entrainment of water droplets with the steam leaving the crevice, the concentration of solute will increase continuously by what Baum calls a hydraulic process. Further into the crevice the flow of water may not be adequate to maintain continuous nucleate boiling, in which case the heat-transfer

Table 10.1 Summary of thermal hydraulic and chemical concentration processes taking place in a flow-restricted region of a steam generator (Baum, 1987, 1989)

Zone[a]	Mode of heat transfer	Concentration process	Description
1	Nucleate boiling	Hydraulic	Flow of water adequate to maintain continuous nucleate boiling; steam and water highly separated
2	Transition boiling	Thermal	Flow of water insufficient to maintain continuous nucleate boiling; alternate wetting and drying
3	Conduction through steam	–	Water does not penetrate this region; steam blanketed

[a]Successive zones penetrate further into the crevice or flow-restricted region.

mode is transition boiling with alternate wetting and drying of the heat-transfer surface. Solute transported into a region of transition boiling is concentrated virtually instantaneously. Baum refers to this as a thermal concentration process. Further still into the crevice, the flow of water is insufficient to rewet the heat-transfer surface and the region becomes steam blanketed. The mode of heat transfer in the steam-blanketed region is conduction through the steam. The characteristics of the hydraulic and thermal concentration processes and the corresponding local thermal-hydraulic conditions in the crevice associated with these concentration processes are summarized in Table 10.1. The discussion to this point is completely general, and applies equally well to concentration processes taking place in so-called mechanical crevices (a line-of-contact crevice forms if an SG tube touches the tube-support structure), a deposit-filled crevice at either a tube support or the tube sheet, and in the sludge pile located on the tube sheet.

Whether concentrated by a hydraulic or a thermal process, the concentration of solute in a flow-restricted region will ultimately be limited by one of the following five phenomena:

1. *Boiling suppression*. The boiling temperature of a solution increases with increasing concentration, thus boiling and the driving force for concentration will cease when the boiling temperature of the solution equals the local wall temperature.[1]

[1]The difference between the wall temperature at the heat-transfer surface and the saturation temperature of the water at the pressure of interest is called the "superheat." A small superheat of several degrees Celsius is required on typical engineering surfaces to support bubble nucleation for heat transfer by nucleate boiling. Strictly speaking, boiling suppression occurs when the boiling temperature of the concentrated solution has increased to the point where there is insufficient superheat for bubble nucleation, thus heat transfer by nucleate boiling ceases.

2. *Precipitation*. The concentration of a given solute will be limited by precipitation if its solubility limit is reached at a temperature that is lower than the local wall temperature.
3. *Liquid-phase carryover*. Entrainment of droplets of concentrated solution by the steam exiting the flow-restricted region constitutes a removal process. A steady-state concentration will be reached if the rate of mass transport of solute out of the region is balanced by the rate of mass transport into the region.
4. *Solute volatility*. Depending on its volatility, the solute may have a finite concentration in the steam exiting the flow-restricted region. If the solute is sufficiently volatile, a steady-state concentration will be reached if the rate of mass transport of solute out of the region is balanced by the rate of mass transport into the region with the water.
5. *Diffusion*. Solute will be continuously removed from the flow-restricted region by diffusion under a concentration gradient. A steady-state concentration will be reached if the rate of diffusion of solute out of the region balances the rate of mass transport of solute into the region with the water.

The concentration limit imposed by boiling suppression is called the thermodynamic limit because the limit represents an equilibrium of the concentrated solution with the available wall superheat. The limiting concentrations imposed by precipitation and volatility are steady-state concentrations that are determined by a combination of mass flow rates and equilibrium constants for solubility in water and steam, respectively. Baum refers to these limiting concentrations as chemical limits. Finally, the limiting steady-state concentrations determined by liquid carry over and diffusion are determined by mass transfer rates and are called kinetic limits.

Further insight into the behavior of concentrated solutions in flow-restricted regions is provided through a parameter which Baum defines as the ratio between the boiling point elevation at the solubility limit divided by the local wall superheat, i.e., the local wall temperature in excess of the saturation temperature of water at the pressure of interest. Baum calls this parameter the solubility-superheat ratio (Baum, 1987, 1989). For a given solute, if the solubility-superheat ratio is greater than one then no precipitate will form as the solution concentrates, the concentration will ultimately be limited by boiling suppression and the resulting solution will be in thermodynamic equilibrium with the local wall temperature. As a consequence of this equilibrium, concentrated solution will migrate by either capillarity or gravity into regions which would otherwise be steam blanketed. Thus, a crevice that is initially steam blanketed will gradually fill with concentrated, nonboiling solution if the solubility-superheat ratio is greater than one. In contrast, if the solubility-superheat ratio is less than one then the solution will form a precipitate at a temperature that is lower than the available wall superheat, and in the presence of transition boiling the precipitate will be found at the edges of the region of alternate wetting and drying where the solution has concentrated to the solubility limit. A comparison of the evolution of the crevice temperature with time as a solute with solubility-superheat ratio greater than one accumulates in a packed crevice by a hydraulic and a thermal concentration process is shown in Fig. 10.1. The thermal concentration process occurs in a packed crevice where there is sufficient resistance to the flow of water to cause the heat-transfer surface to be initially steam blanketed. As concentrated solution migrates into the steam-blanketed region by the process described above, the steam

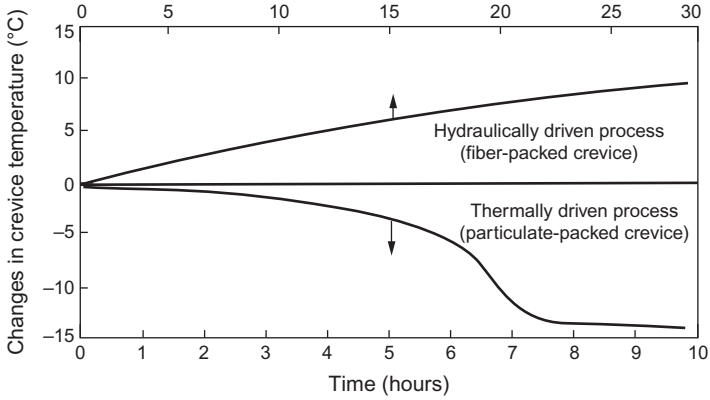

Fig. 10.1 Time histories of change in crevice temperature for hydraulically driven and thermally driven concentration processes (Baum, 1989).
Copyright 1989 by the American Society of Mechanical Engineers.

is gradually replaced with a nonboiling concentrated solution which is more thermally conductive than steam. Hence, the crevice temperature gradually diminishes with increasing time. For the hydraulically driven process, the packing is more open and the heat-transfer surface is fully wetted throughout the test. In this case, the crevice temperature gradually increases with time as a result of boiling point elevation as the solute gradually accumulates in the crevice. Other experimental and field data consistent with these descriptions of thermal and hydraulic concentration processes in a heated crevice are thoroughly discussed in Baum (1987, 1989).

Mathematical models have been developed on the rate of accumulation of concentrated solutions in porous deposit based on local rates of heat and mass transfer. Reviews of the heat and mass transfer processes in porous media under boiling conditions are found in Baum (1989), Cohen (1974), and Millett and Fenton (1990). The transport of a two-phase mixture through a porous medium is governed primarily by the capillary pressure and the morphology of the porous medium (Dullien, 1988), as characterized by:

1. Porosity (ε). Fraction of the volume of the porous medium occupied by pores.
2. Pore size and pore size distribution. A characteristic measure of the dimension of the pore in the plane perpendicular to flow and the number distribution of these values.
3. Permeability (κ). Reciprocal of resistance to fluid flow through a porous medium.
4. Tortuosity (τ). Effective path length through a porous medium.

The permeability is related to the geometric characteristics of the pore structure and has units of area. For a porous medium of porosity ε and composed of particles of diameter d_p, the intrinsic permeability can be estimated using the Blake-Kozeny equation (Bird et al., 1965):

$$\kappa = \left(d_p^2 \varepsilon^3\right) / \left(150 * (1-\varepsilon)^2\right) \tag{10.1}$$

For single-phase flow, the average velocity $\mathbf{U}$ of a fluid with dynamic viscosity μ, moving through a porous medium in response to a pressure gradient ∇P and the gravitational force $\rho\mathbf{g}$, is given by Darcy's law:

$$\mathbf{U} = -(\kappa/\mu)\cdot(\nabla P - \rho\mathbf{g}) \tag{10.2}$$

where ρ is density and $\mathbf{g}$ is acceleration due to gravity. For the flow of a two-phase mixture through a porous medium, equations analogous to Eq. (10.2) are written for each phase (Dullien, 1988). Thus, for steam-water flow:

$$\mathbf{U}_{\text{steam}} = -(\kappa\kappa_{\text{steam}}/\mu_{\text{steam}})\cdot(\nabla P_{\text{steam}} - \rho_{\text{steam}}\mathbf{g}) \tag{10.3}$$

$$\mathbf{U}_{\text{water}} = -(\kappa\kappa_{\text{water}}/\mu_{\text{water}})\cdot(\nabla P_{\text{water}} - \rho_{\text{water}}\mathbf{g}) \tag{10.4}$$

where κ_{water} and κ_{steam} are the relative permeabilities of the porous medium to the flow of water and steam, respectively. The relative permeabilities are functions of the contact angle and the fraction of the pore volume occupied by water.

When two fluids are present in a pore space, one of the fluids will be preferentially attracted to the surface of the pore compared to the other. The fluid that is preferentially attracted to the surface of the pore, i.e., the fluid with the smaller contact angle, is called the wetting fluid and the other is called the nonwetting fluid. In the case of a steam-water mixture in the pore space, water is the wetting fluid and steam is the nonwetting fluid. The steam and water are separated by an interface that is characterized by a surface energy (or surface tension) which is a measure of the work done to change the shape of the interface. The interface adopts a curvature to minimize the surface energy, with the accompanying pressure difference across the interface given by the Laplace equation (Adamson, 1982):

$$\Delta P = \sigma\cos\alpha(1/r_{c1} + 1/r_{c2}) \tag{10.5}$$

where r_{c1} and r_{c2} are the two principal radii of curvature of the interface, σ is the interfacial surface tension and α is the contact angle of the wetting fluid. The pressure is higher in the phase where the interface is concave, i.e., the nonwetting fluid. For the steam-water interface in a porous medium, therefore, the pressure will be higher in the steam phase and the difference between the steam pressure and the water pressure across the interface will be equal to the capillary pressure, as given by Eq. (10.5). For the transport of liquid and vapor in a porous medium, the pressure difference given by Eq. (10.5) must be large enough to overcome the difference in pressure between the liquid and vapor phases plus the energy losses associated with the flow of steam and water through the porous medium.

When steam is generated by a boiling process within a porous medium, such as a tube deposit, sludge pile or porous deposit within a crevice, water is drawn into the pores of the deposit by capillarity and flows toward the heat-transfer surface.[2] Steam

[2] In a porous medium, the wetting fluid is spontaneously imbibed into a sample saturated with a nonwetting fluid (Dullien, 1988).

generated at the heat-transfer surface will flow in the opposite direction toward the outside of the porous deposit. When the capillary number is low, i.e., the capillary force is much greater than the viscous force, the two fluids tend to flow in separate pore networks, with the wetting fluid preferentially occupying the smaller pores or distributing along the walls of pores penetrated by the nonwetting fluid while the nonwetting fluid preferentially occupies the central region of the larger pores (Dullien, 1988). In the case of steam-water flow in a porous deposit with low capillary number, water tends to flow in pores with smaller pore radii and the steam flows in pores with larger pore radii.

Macbeth developed a hydraulic model of mass flow through a porous body to account for the high rates of heat transfer that could be sustained on surfaces covered in porous deposit undergoing wick boiling (Macbeth, 1971). The process of wick boiling is described as one where water is drawn into a porous deposit by capillary forces and drawn to the heat-transfer surface where the water is evaporated. The steam escapes from the porous deposit through larger channels called chimneys. The model predicts the maximum flow rate of water to the heat-transfer surface for a given deposit morphology, from which the maximum heat flux that can be sustained by wick boiling is calculated by multiplying the flow rate of water by the heat of vaporization. Cohen developed a one-dimensional model of heat and mass transfer in porous deposit with chimneys that predicted the concentration factor of dissolved solute in porous deposit undergoing wick boiling as a function of distance normal to the heat-transfer surface (Cohen, 1974). Pan et al. expanded on the work of Cohen to develop a two-dimensional model of heat and momentum transfer in porous deposit with chimneys (Pan et al., 1985), which was later expanded to include the computation of concentration profiles of dissolved solute in porous deposit when wick boiling is the major mode of heat transfer (Pan et al., 1987). The two-dimensional model of Pan et al. predicts that the maximum concentration factor occurs at the chimney wall at the heat-transfer surface, and decreases with increasing distance from the chimney wall at a given axial distance and with increasing distance from the heat-transfer surface at a given radial distance from the center of the chimney. Moreover, the concentration factor increases approximately exponentially with heat flux and with deposit thickness, and increases with decreasing porosity, increasing chimney density and increasing pressure. Maximum concentration factors predicted by the two-dimensional model of Pan et al. ranged from 10^2 to 10^6 as porosity decreased from 0.8 to 0.3.[3] More recently, Henshaw et al. developed a one-dimensional model that coupled thermal hydraulics with water chemistry to investigate chemical reactions taking place within porous deposit under boiling heat transfer (Henshaw et al., 2006). Building on the work of Henshaw et al., ul Haq et al. developed a two-dimensional model of the heat and mass transport processes that allows the three mechanisms of heat conduction, advection and diffusion of solute as well as the diffusion of water to be modeled to investigate their aggregate effects (ul Haq et al., 2011).

[3] Other model parameters were: deposit thickness = 25 μm, chimney density = 3000 chimneys/mm^2, heat flux = 1.7 MW/m^2, radius of steam chimney = 2.5 μm, pressure = 15.5 MPa.

Millett and Fenton outlined a macroscopic mass-balance model for the concentration of solute in a crevice deposit (Millett and Fenton, 1990). The mechanism for mass transfer into the crevice is nucleate boiling and the removal mechanisms are droplet entrainment, volatilization and diffusion, as described earlier in this section. The nucleate boiling rate is proportional to the wetted length of the heat-transfer surface in the crevice deposit. The model assumes an average concentration for the pore solution throughout the deposit, and the accumulation rate decreases as the crevice solution temperature approaches the wall superheat. Millett and Fenton suggest that the macroscopic model could be improved by replacing the effective diffusion coefficient with one that takes account of the local steam void fraction in the pore solution. Thus:

$$\mathfrak{D}_{\text{steam-water}} = \mathfrak{D}_{\text{e}}(1-\theta)^n, \quad n = 1.5 - 5.0 \tag{10.6}$$

where $\mathfrak{D}_{\text{e}}$ is the effective diffusion coefficient of the solute in a porous medium and θ is the local steam void fraction. The effective diffusion coefficient is less than the diffusion coefficient in bulk water because of the increased path length (tortuosity) for mass transport through a porous medium and the reduction in diffusion rate caused by mass transport through channels of various cross-sectional areas (constrictivity) (Baum, 1989). Using the macroscopic mass-balance model described above with an effective diffusion coefficient given by Eq. (10.6) and average void fractions determined from a model of flow regimes in support-plate crevices (Baum and Greaney, 1981), Millett and Fenton were able to achieve reasonable agreement between the model predictions and experimental data for hideout of NaCl in a carbon-fiber packed heated crevice (Millett and Fenton, 1989).

Moving beyond the limitations of a mass-balance model and a uniform concentration of solution throughout the porous medium, Millett and Fenton developed a model that describes the concentration processes in fouled crevices and sludge piles starting from equations for the conservation of energy, mass, momentum and solute species within the pore solution of a porous deposit (Millett and Fenton, 1991, 1994). Heat transfer is by nucleate boiling unless the rate of ingress of saturated water is not sufficient to maintain a wetted heat-transfer surface, in which case the region becomes steam blanketed. The region of nucleate boiling is defined by the penetration depth of saturated water into the porous deposit, which is called the wetted length (Baum, 1989). Individual solute species accumulate in the nucleate boiling region. The species concentration in the pore solution is ultimately limited by either boiling suppression, volatilization or diffusion. The model does not take account of precipitation of species; so it is applicable only to concentrating solutions of highly soluble solutes such as sodium chloride, for example. A parametric study of the model predictions for the accumulation of sodium chloride in a porous crevice deposit or sludge provided some very useful insights. For example, the concentration of the pore solution was thermodynamically limited for dimensionless penetration depth (=penetration depth divided by crevice length) >0.2 for a wall superheat of 28°C and a crevice length of 5 mm, regardless of the bulk water concentration. A large reduction of either wall superheat (to <5°C) or crevice length (to <3 mm) was required to effectively reduce the concentration of solute in the crevice or sludge pile. The concentration profile in

the crevice was found to be only weakly dependent on the solute volatility for a distribution coefficient $>10^{-4}$. Even for a distribution coefficient of 0.9, the concentration near the bottom of the crevice (dimensionless penetration >0.9) was thermodynamically limited. The model is also shown to make realistic predictions of the wetted length and its dependence on deposit permeability and available wall superheat, and is in good agreement with available experimental data. Fig. 10.2 shows the development of the concentration profile of sodium chloride calculated by the model as a function of time for a fully wetted crevice. The concentration process first reaches the thermodynamic limit deep within the crevice, and as time proceeds the concentrated solution reaches the thermodynamic limit throughout the remainder of the crevice. Fig. 10.3 shows the wetted length of a packed crevice calculated by the model as a function of available superheat for selected packing permeability. These results illustrate that the thermal hydraulic requirements to support nucleate boiling become increasingly challenged with decreasing permeability and increasing wall superheat. For a fuller discussion of these results and additional insights into crevice concentration processes that are afforded by the model, the reader is referred to Millett and Fenton (1994).

As noted by Engelhardt et al. (1999), the crevice concentration model developed by Millett and Fenton (1991, 1994) based on the hydraulic concentration process does not take account of electrochemical effects. Thus, Engelhardt et al. combined the Millett and Fenton concentration model with the Macdonald and Urquidi-Macdonald coupled environment fracture model (Macdonald and Urquidi-Macdonald, 1991a,b) to develop a new coupled environment boiling crevice model (CEBCM) to calculate concentration and potential gradients in a boiling crevice. In the CEBCM model, transport of ionic species in the crevice takes account of convection and migration in a potential gradient in addition to molecular diffusion. The equations describing heat and momentum transport are taken from the boiling crevice model of Millett

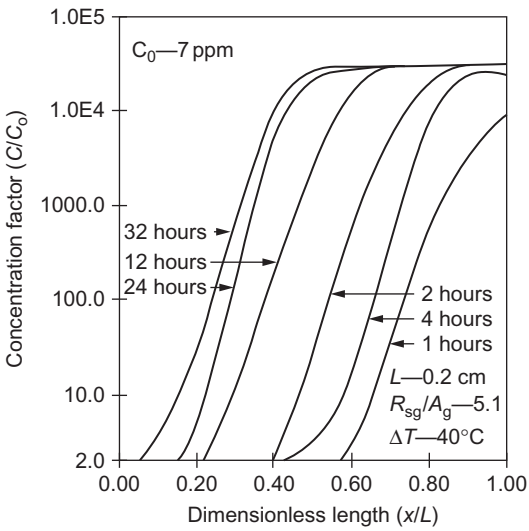

Fig. 10.2 Development of the concentration profile as a function of time for a fully wetted crevice (Millett and Fenton, 1994). Copyright 1994 by the American Nuclear Society, La Grange Park, Illinois.

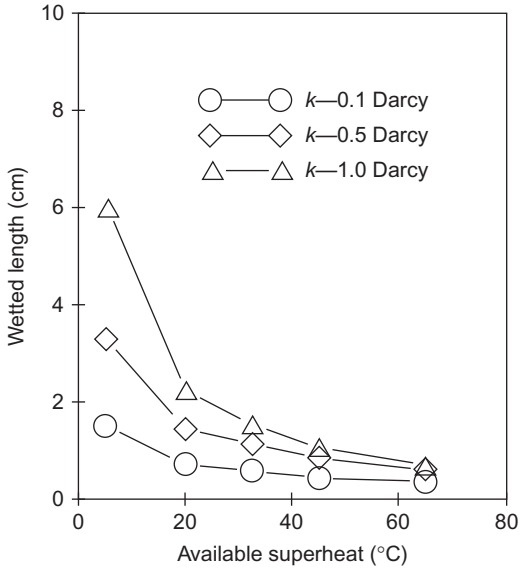

Fig. 10.3 Calculated initial wetted length as a function of heat flux for selected deposit permeability (Millett and Fenton, 1994).
Copyright 1994 by the American Nuclear Society, La Grange Park, Illinois.

and Fenton, and the four equations describing heat, mass, momentum and charge transfer are solved simultaneously. The model includes ionic species introduced to the crevice from the bulk solution as well as ionic species generated within the crevice by corrosion reactions. Calculations showed that the concentrations of all species eventually reach limiting values in the center of the crevice that do not depend on the corrosion potential in the external environment. A detailed discussion of the concentration and current profiles in the crevice for selected corrosion potentials and time intervals calculated by the CEBCM model and the implications for crevice corrosion are beyond the scope of this chapter and are thoroughly discussed in Engelhardt et al. (1999), Engelhardt and Macdonald (1999), and Abella et al. (2002).

10.2.2 Hideout and hideout return: Fouled crevice

There has been a significant amount of experimental work done investigating hideout and hideout return in fouled SG crevices. A typical setup used for such work is shown in Fig. 10.4. Its main components include a refreshed autoclave, a packed crevice assembly, a crevice heater, and electrodes for monitoring the pH, the potential, and the conductivity of both the bulk and the crevice environments. Parameters such as temperature, pressure, flow rate of the feed water, and the concentrations of added impurities in the feed water are monitored and controlled. A fine sampling tube is used to withdraw liquid samples from the crevice to measure the amount of solute that has accumulated during hideout. Various packing materials, such as magnetite, carbon fiber or carbon power, are added to the crevice to simulate the presence of a porous deposit. Crevice geometry can be an experimental variable as well.

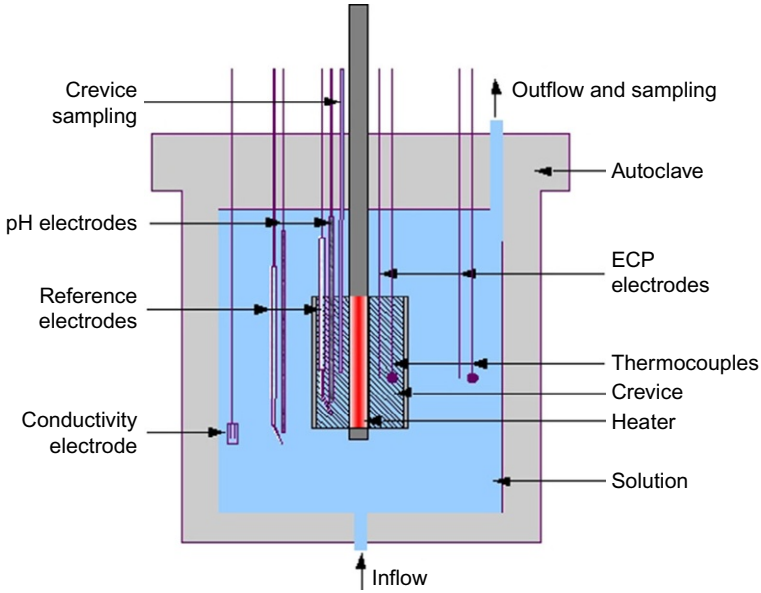

Fig. 10.4 Schematic of an experimental setup used for studies of hideout and hideout return from a heated crevice.

In a typical hideout and hideout return experiment the autoclave is heated, the flow established, and the water chemistry conditioned for a predetermined time to ensure that steady state has been achieved. The hideout phase is initiated either by heating the crevice with a cartridge heater or by flowing a hot coolant through the crevice SG tube. When using a cartridge heater as the heat source, the heater can be operated in constant heat flux or constant superheat mode. The conditions inside the autoclave are such that the additional heat is sufficient to cause boiling in the crevice, but not in the bulk. After hideout has proceeded for a predetermined period of time, the heat source is removed to initiate hideout return.

One of the earliest investigations of concentration of solutes on a surface undergoing nucleate boiling was that conducted by Picone et al. (1963). Using a ^{22}Na radiotracer, they found that solute concentration did not occur in the absence of nucleate boiling. On a clean surface, concentration does occur for a solute with retrograde solubility but not for a highly soluble solute. On a fouled surface, highly soluble solute will concentrate provided the deposit has a minimum thickness of 8 to 10 μm. Where concentration did occur, it appeared to be proportional to the rate of evaporation at the heat-transfer surface.

Mann and Castle (1983, 1984, 1987) investigated the hideout and hideout return from solutions of sodium chloride in a simulated heated crevice packed with carbon fiber. Some additional tests were done with a carbon-fiber packed crevice that had been corroded by exposure to a solution of ammonium chloride

(Mann and Castle, 1987). The tube surface temperature was monitored at several axial locations within the heated crevice to provide information on the mode of heat transfer. The concentration of sodium chloride in the bulk solution was monitored during hideout and hideout return by measuring the conductivity of the bulk solution. Wall temperature measurements showed that the carbon-fiber packed crevice was fully wetted along its entire length, whereas the corroded crevice was steam blanketed. The investigations by Mann and Castle found that sodium chloride accumulated in the heated crevice at a rate determined by both the bulk concentration and the rate of evaporation until an equilibrium concentration was reached. The total amount of salt that accumulated in the crevice was determined primarily by the available superheat. The hideout efficiency was from 80% to 100% in the fully wetted crevice, but was somewhat lower in the corroded crevice due to the steam blanketing. Salt diffused rapidly from the crevice when the heat flux was removed, although little salt was released if the power was not reduced to less than about 30% of its original value. When the heat flux was reduced to zero in the fully wetted crevice, all of the accumulated salt was released within 3 hours. Diffusion from the corroded crevice, however, was six times slower than from the fully wetted crevice.

Based on their experiments, Mann and Castle suggested a crevice concentration model for the fully wetted crevice that is illustrated in Fig. 10.5. They proposed that salt accumulates initially deep within the crevice. The concentration in this region increases rapidly until a small volume of solution reaches the thermodynamic limit, causing boiling to cease at that location. As accumulation continues in the boiling region of the crevice, the volume of nonboiling solution gradually increases and grows toward the mouth of the crevice. The boundary between the boiling and nonboiling solution is indicated by an abrupt increase in the tube wall temperature. The concentration of solution at the mouth of the crevice is kinetically limited by diffusion from the concentrated crevice solution to the bulk. The crevice concentration model suggested by Mann and Castle for the steam blanketed, corroded crevice is

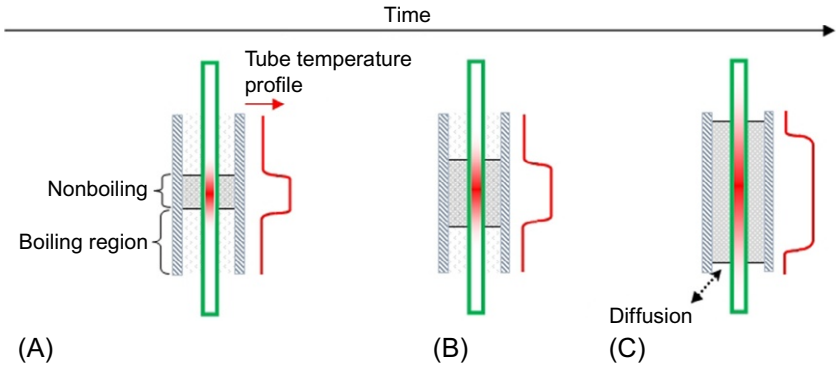

Fig. 10.5 Schematic illustrating the model for NaCl concentration in a heated crevice under nucleate boiling heat transfer packed with carbon fiber.

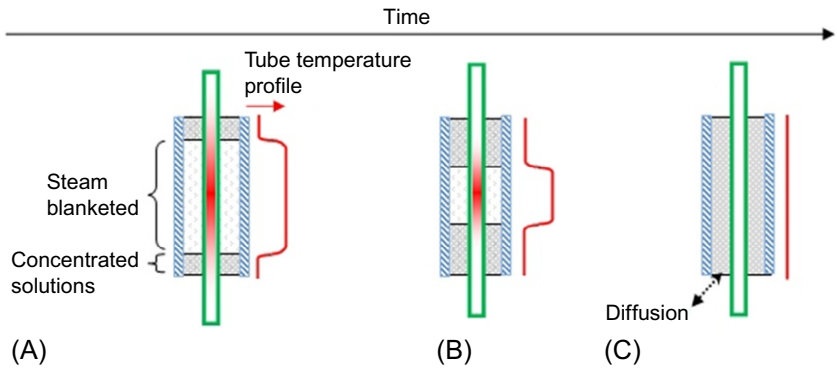

Fig. 10.6 Schematic illustrating the model for NaCl concentration in a heated crevice under nucleate boiling heat transfer packed with carbon powder.

illustrated in Fig. 10.6. In this case the concentration of solute occurs initially at the mouth of the crevice, the central region being steam blanketed. Concentrated solution at the thermodynamic limit gradually penetrates the steam-blanketed region by capillarity, as discussed by Baum (1987, 1989). The local wall temperature, therefore, gradually decreases as the steam blanket is replaced by a concentrated solution at the thermodynamic limit.

Studies of hideout and hideout return from solutions composed of mixtures of sodium hydroxide, sodium chloride and sodium carbonate were conducted by Brunet, Campan and Shoemaker using a single-tube model boiler incorporating a tube-support plate (TSP) crevice (Campan and Brune, 1987; Campan and Shoemaker, 1987) and a tube-sheet crevice (Campan and Shoemaker, 1987). The crevices were packed with either magnetite or carbon fiber to simulate a fouled crevice. Accumulation of sodium in the heated crevices was determined using a ^{24}Na radio tracer. The accumulation of sodium in the TSP crevice increased with the product of the bulk concentration and the accumulation time until the thermodynamic limit was reached. The total accumulation depended only on the available superheat, and was independent of the bulk concentration of sodium. Hideout return was rapid when the crevice heat flux was reduced to zero, but return was negligible when the bulk solute concentration was reduced to zero while continuing to apply the crevice heat flux. For the tube-sheet crevice the concentration kinetics depended upon the bulk sodium concentration, with accumulation starting at the mouth of the crevice at the lower solute concentration (5 mg/kg) and accumulation starting at the bottom of the crevice at the higher bulk concentration (50 mg/kg).

Balakrishnan investigated hideout and hideout return of sodium in heated crevices formed at the land and broach regions of a trefoil TSP geometry using the radio tracer ^{24}Na and a NaI gamma-ray detector (Balakrishnan, 1990). Fouled crevices were simulated by packing the TSP with stainless steel gauze, carbon cloth or magnetite to various packing densities. The studies were conducted in a high temperature, recirculating loop simulating conditions on the secondary side of a nuclear SG.

Balakrishnan observed that hideout was constant when the heat flux was applied, reaching concentration factors of 10^3 to 10^4 within 10 h of applying heat to the crevice. The concentration factor rapidly decreased when the heat flux was reduced. Following removal of either the heat flux or the bulk solute by ion exchange with heat flux still applied, all of the accumulated solute rapidly diffused from the crevice. No consistent hideout was observed in clean crevices. Instead, solute accumulation was sporadic, building up a little before being suddenly released to the bulk water.

Hideout from solutions composed of mixtures of sodium chloride, sodium sulfate and calcium chloride in heated crevices packed with either carbon fiber or carbon powder was investigated by Balakrishnan using a refreshed autoclave system (Balakrishnan, 1991). The concentrations of the individual solute species were measured in the influent and effluent of the autoclave using ion-selective electrodes. The tube wall temperature was measured at several axial locations within the heated crevice. The results of the hideout tests with the crevice packed with carbon fiber cloth were similar to those observed by Mann and Castle. The hideout efficiency was nearly 100%, suggesting that effectively all of the heat transfer from the crevice was by nucleate boiling. The tube temperature profile suggested that solute accumulation initiated deep within the crevice and spread toward the mouth of the crevice, as illustrated in Fig. 10.5. For the tests done with the carbon powder packing, the hideout efficiencies were lower (60%–80%), suggesting that regions of the packed crevice were initially steam blanketed. The tube wall temperature profile suggested that solute accumulation began at the mouth of the crevice with the interior of the crevice being steam blanketed, as illustrated in Fig. 10.6, consistent with the results of Mann and Castle for hideout in a corroded crevice (Mann and Castle, 1987). As hideout continued, solution at the thermodynamic limit migrated into the steam-blanketed region until the crevice was filled with nonboiling solution. No preferential hideout of any species was observed in either the fiber-packed or the powder-packed crevices. During hideout return, however, the pH of the effluent went through a maximum that was as high as pH 11 shortly following the maximum in the concentrations of the other species. The development of a highly alkaline return suggests that return of at least one of the anionic species is lagging behind the return of the cations. Adsorption of sulfate could contribute to a reduced rate of return for this species. The development of an alkaline return implies that the corresponding conditions in the crevice must be highly acidic during the period of alkaline return.

In a separate set of experiments, Balakrishnan used probes inserted into both the bulk and crevice solutions in a refreshed autoclave to measure crevice potential and pH relative to the bulk during hideout of a solution of sodium chloride (Balakrishnan, 1999). These measurements demonstrated that the crevice potential was +300 mV relative to the potential in the bulk solution when crevice corrosion occurred as a result of a small concentration of dissolved oxygen in the water entering the autoclave. The positive potential in the crevice (relative to the bulk) enhanced the migration of Cl^- and impeded the migration of Na^+ into the crevice during hideout, which resulted in an imbalance in the Na to Cl ratio and the development of an acidic crevice pH_T. During hideout return, the potential gradient caused the Cl^- to return from the crevice at a lower rate than the Na^+, causing the pH_T of the effluent from

the autoclave to go through a maximum. The addition of hydrazine to the bulk solution to remove the dissolved oxygen suppressed the crevice corrosion, equalized the crevice and bulk potentials, raised the crevice pH from 3.1 to 6.6 and resulted in Na^+ and Cl^- ions returning from the crevice at equivalent rates.

Lumsden et al. investigated the effect of available superheat, bulk water chemistry and packing porosity on the chemistry environment that develops in a heated crevice following concentration of highly soluble solutes such as sodium chloride and sodium hydroxide (Lumsden et al., 1997, 1999). The heated crevice packed with diamond dust was mounted in a refreshed autoclave system and instrumented to measure the tube axial temperature profile. Platinum electrodes were inserted to measure potentials in both the bulk water and the crevice solution. Both the bulk and crevice solutions could be examined by withdrawing solution for chemical analysis. Measurements of wall temperature at different axial locations indicated nucleate boiling, transition boiling and steam blanketing depending on the particular crevice geometry, i.e., closed bottom versus open ended, and the packing porosity. Accumulation of solute resulted in the steam-blanketed region and the region of transition boiling gradually being filled with nonboiling solution at the thermodynamic limit. The results of this investigation were found to be in good agreement with model predictions by MULTEQ and by the Millett-Fenton crevice concentration model (Millett and Fenton, 1994). The hideout return data from their experiments suggest a simple diffusion process following Fick's second law of diffusion. When added to the feed water, hydrazine concentrated in the crevice and lowered the crevice potential relative to the bulk solution.

10.2.3 Hideout and hideout return: Sludge pile and tube deposit

Gonzalez and Spekkens investigated the concentration processes taking place within a simulated sludge pile under boiling heat-transfer conditions (Gonzalez and Spekkens, 1987). Two different experimental setups were used. Series A experiments were done in an autoclave operating in the static mode with a heated test probe operating at constant heat fluxes of 40, 75, and 110 kW/m^2. Series B experiments were done with a heated test probe operating at a constant tube wall temperature from 310°C to 315°C in a refreshed autoclave, although the refresh rate was evidently so low that the autoclave operated effectively in the static mode. The bulk water temperature in both series of tests was 265°C. The effects of sludge pile height and heat flux on the concentration profiles of sodium chloride in the sludge pile were examined in the Series A tests, while the effect of porosity on the concentration profiles of sodium chloride within the sludge pile were examined in Series B. The concentration of chloride in the bulk water during hideout is shown in Figs. 10.7 and 10.8 for Series A and Series B experiments, respectively. The bulk water was eventually depleted in chloride for the Series A tests because the autoclave was run in static mode, whereas the chloride concentration diminished to a finite value in Series B because the autoclave was being constantly refreshed, albeit at an apparently low rate. Overall average concentration factors for chloride in the sludge pile ranging from 10^3 to 10^5 were measured after 30 h for heat fluxes ranging from 40 to 110 kW/m^2 in the Series A tests.

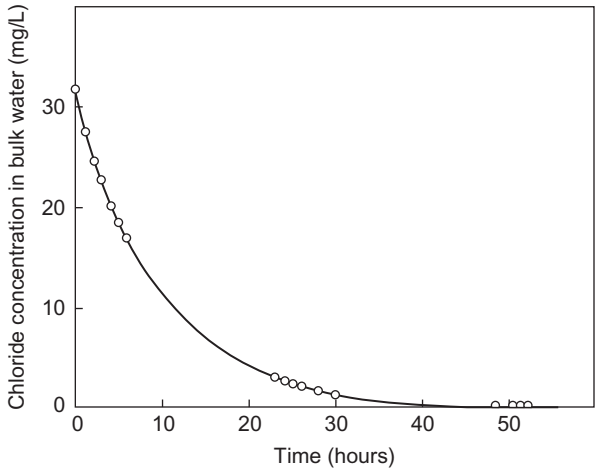

Fig. 10.7 Bulk water chloride concentration versus time for a typical Series A experiment (sludge pile depth: 100 mm; heat flux: 40 kW/m^2). Reprinted with permission of the author from Gonzalez, F., Spekkens, P., 1987. Concentration processes under tubesheet sludge piles in nuclear steam generators. Nucl. J. Can. 1, 121–140.

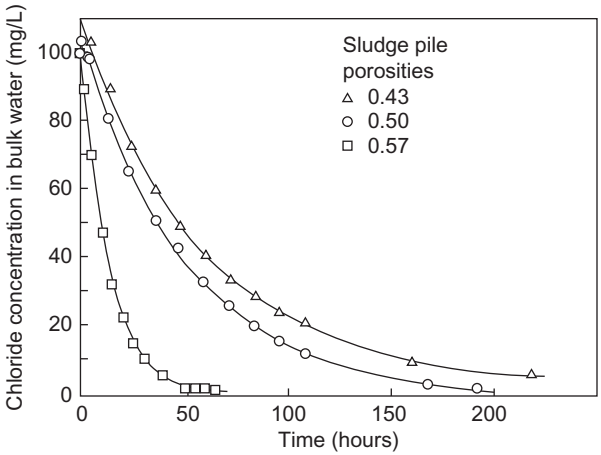

Fig. 10.8 Bulk water chloride concentration versus time for several sludge pile porosities (pile depth: 150 mm; heat flux: 20–25 kW/m^2). Reprinted with permission of the author from Gonzalez, F., Spekkens, P., 1987. Concentration processes under tubesheet sludge piles in nuclear steam generators. Nucl. J. Can. 1, 121–140.

The depletion of chloride in the bulk water from both series was compared to a model based on a mass balance of sodium chloride around the sludge pile. A parameter K, called the concentration coefficient, was included in the model to help explain the results, where K is equivalent to the fraction of the heat transferred that goes into the generation of steam. Factors that contribute to the value of K being less than one are heat transfer by conduction through the sludge pile and part of the heat-transfer surface being steam blanketed. Concentration coefficients determined for Series A and Series B tests are summarized in Tables 10.2 and 10.3, respectively. The results in Table 10.2 show that magnitude of K decreases with increasing pile height for a given heat flux, indicating that for deeper sludge piles an increasing fraction of the heat-transfer surface is steam blanketed and no longer contributes to the

Table 10.2 Sludge pile concentration coefficients for several sludge pile depths and heat fluxes (pile porosity 0.57)

Pile height (mm)	Heat flux (kW/m^2)		
	40	**75**	**110**
50	1.08	1.04	1.01
100	0.80	0.70	0.51
150	0.59	–	–

Reprinted with permission of the author from Gonzalez, F., Spekkens, P., 1987. Concentration processes under tubesheet sludge piles in nuclear steam generators. Nucl. J. Can. 1, 121–140.

Table 10.3 Sludge pile concentration coefficients for 150 mm sludge piles with varying porosities (heat flux 20–25 kW/m^2)

Pile porosity	0.43	0.50	0.57
Concentration coefficient	0.14	0.22	0.75

Reprinted with permission of the author from Gonzalez, F., Spekkens, P., 1987. Concentration processes under tubesheet sludge piles in nuclear steam generators. Nucl. J. Can. 1, 121–140.

concentration of sodium chloride. A similar trend was observed with increasing heat flux for constant pile height (Table 10.2) and with decreasing porosity for a given pile height and heat flux (Table 10.3). In general, the magnitude of K decreases in response to those changes in heat flux, sludge pile height, and porosity that would tend to reduce the flow rate of water to the heat-transfer surface such that it becomes insufficient to maintain nucleate boiling in deeper regions of the sludge pile.

The results of Spekkens and Gonzalez are generally consistent with the observations by Baum and Greaney from their study of the thermal and hydraulic transport processes occurring within sludge piles under SG secondary side conditions, where it was noted that nucleate boiling is only maintained within a relatively short distance from the top of the sludge pile, and beyond that distance, which they call the wetted length, heat transfer changes from nucleate boiling to liquid-deficient heat transfer (Baum and Greaney, 1981). By measuring the temperature distribution along the axis of a heated SG tube within sludge removed from two different operating SGs, Baum and Greaney reported that the wetted length is about 10 mm for heat flux between 70 and 380 kW/m^2 in typical SG sludge. For distances greater than the wetted length, the insulating effect of the steam blanket adjacent to the SG tube permits liquid to penetrate deeper into the sludge pile in the interstitial regions than at the tube surface (Baum, 1989).

Mann and Castle investigated hideout of sodium nitrate in a heated, stainless steel sinter simulating a tube deposit (Mann and Castle, 1983). Measurements were made in a static autoclave. The sinter had a thickness of 1.8 mm, porosity of 0.47 and had a pore size of 70 μm. The concentration of sodium nitrate in the bulk solution was

measured continuously by pumping the solution through a conductivity cell that had been calibrated against a solution of sodium nitrate. The bulk concentration of sodium nitrate decreased with the application of heat flux to the sinter and subsequently increased when the heat flux was removed, thus demonstrating hideout and hideout return. With the heat flux applied, the concentration of sodium nitrate decreased steadily before reaching a steady state after a period of many hours or days. The pore concentration was calculated by mass balance, and the concentration factor was defined as the ratio of the calculated pore concentration divided by the steady-state concentration in the bulk solution. The applied heat fluxes were rather low in this study, and the concentration factor so calculated increased from 25 to 32,000 with increasing heat flux from 2.3 to 84.9 kW/m^2.

Balakrishnan et al. investigated hideout of ionic impurities in porous deposits on SG tubes. In one investigation, measurements were made of hideout of a solution of sodium chloride in synthetic deposits of magnetite that had been deposited onto a length of Alloy 600 SG tubing (Balakrishnan et al., 1998). The thicknesses of individual synthetic deposits were from 23 to 72 μm with porosity ranging from 15% to 62%. Because the synthetic deposits were prepared under artificial conditions, they lacked the "wick boiling" morphology of deposit that has formed under boiling heat-transfer conditions. In a subsequent investigation, measurements were made of hideout of seawater impurities in thin ($<$10 μm) deposits on SG tubes removed from the Crystal River-3 nuclear power station (Balakrishnan et al., 1995). These latter deposits showed classic "wick boiling" morphology (Tapping et al., 1991). In both investigations, hideout and hideout return were measured using a high-temperature conductivity probe as well as by analysis of solutions removed periodically from the autoclave in which the experiments were done. Both investigations showed that significant hideout of ionic impurities does take place in SG tube deposit, reaching concentration factors of 2×10^3 for sodium chloride in the synthetic tube deposits and 1.3×10^4 in the tube deposit removed from a once-through steam generator (OTSG) at Crystal River-3. Hideout of sodium chloride was kinetically limited by back diffusion, reaching steady state within just a few hours depending on the magnitude of the heat flux.[4] Sodium chloride returned promptly from the porous deposits in both investigations once the heat flux was removed, whereas precipitates of calcium sulfate and magnesium hydroxide from hideout of seawater impurities returned more slowly, as expected. Hideout return studies at Crystal River-3 corroborated the results from the experimental investigation of the hideout of seawater impurities and concluded that hideout return at the Crystal River-3 plant is dominated by return from tube deposits (Balakrishnan et al., 1995).

Both investigations also provided insights into the importance of deposit morphology on hideout characteristics. For example, hideout tests conducted with a bare tube wrapped in one or two layers of 200-mesh stainless steel wire gauze

[4] Steady state was reached within 15 hours at a heat flux of 114 kW/m^2 (Balakrishnan et al., 1995) compared to approximately 5 hours and 3 hours at heat fluxes of 270 and 383 kW/m^2, respectively (Balakrishnan et al., 1998).

to simulate the presence of a porous deposit showed that hideout was disproportionately higher when the bare tube was double wrapped with wire gauze compared to a single wrap. This result suggests that the pore structure is a more important parameter than porosity for determining the extent of hideout in porous deposit (Balakrishnan et al., 1998). The pores in the single wrap of wire gauze would be essentially straight and normal to the surface and any solution concentrating under the wrap would be subject to facile release. In contrast the overlap of two layers of wire gauze would result in more tortuous paths in the pore structure, resulting in a significant reduction in the rate of diffusion from the pores to the bulk solution and a higher concentration of solution within the pores at steady state. For the synthetic deposits, the concentration factors for sodium chloride decreased with increasing deposit thickness. This result suggests that the concentration process was taking place within approximately the same volume, irrespective of deposit thickness (Balakrishnan et al., 1998). This implies that only a fraction of the pore volume within the deposit contains liquid under boiling heat-transfer conditions, with the remainder occupied by steam. Measurements of the thermal resistance of porous deposits that lacked the wick boiling morphology have led to the same conclusion, i.e., the pores of the deposit are filled with a mixture of steam and water under boiling heat-transfer conditions (Turner et al., 2000a). In both investigations, attempts were made to measure the distribution of hideout impurities within the deposit by quickly draining the autoclave while continuing to apply heat flux to the tube deposit. Deposits were subsequently examined by scanning electron microscopy (SEM) couple with energy dispersive X-ray (EDX) analysis to determine the concentration profiles of solute that had hidden out within the pores of the deposits. This method proved unsuccessful with the synthetic deposit because the concentration of solute within the deposit (estimated from the hideout data, deposit thickness and porosity) was below the limit of detection of EDX. For the tube deposit from Crystal River-3, however, elemental maps showed a relatively uniform distribution of sodium, chloride and sulfate across the deposit thickness. This result implies that boiling of the pore solution is occurring within the pores throughout the deposit and is not restricted to the heat-transfer surface itself.

10.3 Chemistry environment in flow-restricted regions

10.3.1 Predicting crevice chemistry using deterministic models

A significant amount of work has been done to investigate the chemistry environment that develops in flow-restricted regions using experimental setups simulating SG operating conditions. Real-time chemistry data inside the SG, however, are generally not available and may be significantly different for individual crevices, partly due to their locations in the SG and the extent to which individual crevices are fouled. In the absence of direct chemistry monitoring of SG crevice regions during plant operation, one approach is to try to calculate the chemistry environment within the crevice

regions of an operating SG using models based on thermodynamic data. Two different software packages developed within the nuclear industry to perform these calculations, ChemSolv[5] and MULTEQ,[6] and their methods of application are discussed in this section. It is noted that another code (MONA) was developed to calculate the chemistry that develops in the secondary water following the ingress of contaminants introduced by a condenser leak or released from demineralization resins (Nordmann, 1983).

10.3.1.1 ChemSolv

ChemSolv is a computer code that calculates the chemistry conditions throughout the steam cycle of a CANDU[7] reactor; it is based on a previous code developed to predict the impact of condenser leakage on SG crevice chemistry (Balakrishnan, 1980). ChemSolv models the transport of chemical species around the steam cycle and the interaction between the chemicals in each of the various parts of the steam cycle, including the feed water system components, SG bulk water and crevices within the SG, to calculate the local chemistry within each of these regions. ChemSolv sets up the differential equations describing the transport processes and the chemical reactions, and integrates the equations to obtain the concentrations of the chemical species considered in each region.

ChemSolv is able to perform three separate calculations: steam cycle chemistry, bulk water chemistry, and crevice chemistry. For the steam cycle chemistry calculation ChemSolv uses the heat balance diagram for the station, which provides the temperatures, flow rates and pressures for the steam cycle components, and the concentrations of volatile species at one location (typically at the condenser) to determine the concentrations of volatile species throughout the steam cycle. The calculation takes into account the thermal decomposition of organic amines and the oxidation of hydrazine. For the bulk water chemistry calculation, ChemSolv does a mass balance on chemicals entering and leaving the SG, taking into account the concentrations of each chemical species in the feed water, the feed water, blow down and steaming rates, and the volatilities of each species.

For the crevice chemistry calculation, ChemSolv could use the bulk chemistry concentrations calculated in the previous step, although in practice it is more usual to use the concentrations of each chemical species measured in the blow down during operation at power as input parameters. ChemSolv then sets up a mass balance

[5] ChemSolv is a trademark of Atomic Energy of Canada Limited (AECL). It was developed at Chalk River Laboratories, now called Canadian Nuclear Laboratories (CNL).

[6] MULTEQ is currently maintained by the Electric Power Research Institute (EPRI), Palo Alto, California, USA. It is based on a code developed by Bawden, Mann and Garnsey of the Central Electric Research Laboratory (CERL) in England under contract to EPRI (Bawden et al., 1984), and further developed by Oscarson and McBride at Brigham Young University (Oscarson and McBride, n.d.) and Alexander and Luu at S-Cubed (Alexander and Luu, 1989). Its redox option was developed at CNL by P.V. Balakrishnan.

[7] CANDU is a registered trademark of AECL.

between chemical species entering the crevice with the bulk water, those leaving the crevice with the steam and the amount of each species accumulating within the crevice solution as a function of time. The chemistry environment of the crevice solution is calculated by taking into account chemical reactions between species accumulating in the crevice and the volatility of each of these species. The flow rate of water entering the crevice and the flow rate of steam leaving the crevice are set equal to the crevice steaming rate, which is calculated from the local heat flux, the heat-transfer surface area within the crevice and the heat of vaporization. ChemSolv does not attempt to calculate the thermal-hydraulic conditions within the crevice. The crevice is assumed to have a fixed volume and to be filled with deposit of a given porosity, which are both input parameters to the model.

ChemSolv uses a numerical differential equation algorithm that simultaneously solves both kinetic and equilibrium equations to calculate crevice chemistry as a function of time, and reports the results at fixed time intervals. An advantage of this formulation is the ability to include kinetic equations (e.g., unimolecular decomposition of hydrazine to form ammonia, reaction of hydrazine with dissolved oxygen) that cannot be included in a purely equilibrium model. Individual species are drawn into the crevice as a result of nucleate boiling until their concentrations become limited by either volatility, precipitation or the concentrated crevice solution reaching the thermodynamic limit, at which point boiling (and the driving force for accumulation) within the crevice solution ceases. The concentrated crevice solution is in thermodynamic equilibrium with the steam leaving the crevice and with the precipitates that accumulate in the crevice in each time step.

The reactions considered in the calculation of crevice chemistry include:

1. Ionization (e.g., water, acid, base),
2. Hydrolysis,
3. Precipitation/dissolution,
4. Complex ion formation,
5. Oxidation/reduction (e.g., corrosion, oxygen/hydrazine reaction).

The individual chemical species considered in the calculation of crevice chemistry include:

1. Cations: sodium, potassium, magnesium, calcium, iron
2. Anions: chloride, sulfate, nitrate, carbonate, formate, acetate
3. Neutral molecules: hydrogen, oxygen
4. Amines: morpholine, ethanolamine, dimethylamine, ammonia, methoxypropylamine, 5-aminopentanol, and hydrazine.

Other chemical species can be added as the need arises.

ChemSolv was incorporated into AECL's plant chemistry monitoring and diagnostics software and installed in several Canadian and overseas CANDU plants to support the chemistry monitoring program (Turner et al., 2000b; IAEA, 2006). An example showing the predicted crevice chemistry for a plant operating with excess chloride in the SG blow down as a result of the thermal decomposition of organochloride compounds formed in the water treatment plant is shown in Table 10.4. In Case I the

Table 10.4 Calculated crevice pH for a plant operating with excess chloride in the feed water

Case	Na (μg/kg)	Ca (μg/kg)	Mg (μg/kg)	Cl (μg/kg)	SO_4 (μg/kg)	pH_N (–)	pH_T (–)	Precipitates
1	1	4	2	10	5	5.0	7.2	$CaSO_4$; $Ca(OH)_2$; $Mg(OH)_2$
2	1	1.5	0.5	10	5	5.0	6.5	$CaSO_4$; $Mg(OH)_2$; Na_2SO_4
3	1	1.5	0.5	2	5	5.0	7.3	$CaSO_4$; $Mg(OH)_2$; Na_2SO_4

crevice is well buffered by the hideout and precipitation of calcium and magnesium compounds, resulting in a crevice pH_T[8] that is alkaline despite the relatively high concentration of chloride in the blow down. This result is partially due to the fact that hydrochloric acid is not fully dissociated in high-temperature water, leading to some of the chloride that concentrates in the crevice solution being volatilized as hydrochloric acid. In Case 2, the concentrations of calcium and magnesium in the blow down are lower than in Case 1 but the crevice pH_T is still predicted to be higher than the neutral point. In Case 3, with a reduced chloride concentration relative to the other ionic species, the pH_T increases marginally. A mildly alkaline crevice is predicted in all three cases illustrated in Table 10.4, likely due to buffering by the calcium and magnesium precipitates.

10.3.1.2 MULTEQ

The MULTEQ code was developed to model the high-temperature chemistry of the concentrated solutions which form during operation in the flow-restricted regions of an SG. MULTEQ considers the same five types of reactions as ChemSolv, but only models equilibrium reactions and does not include rate-limited reactions such as those involved in the determination of the electrochemical corrosion potential (ECP) and corrosion rates. Reactions with the solid metal surface are represented by the addition of small amounts of metallic cations to the system. MULTEQ uses a more extensive chemical database than ChemSolv, including zinc, chromium, lead, silica, and selected calcium magnesium silicates (Gaudreau, 2005). MULTEQ is widely used within the nuclear industry, and the thermodynamic database that it employs is overseen by a database committee staffed by industry experts in high-temperature water chemistry (Millett, 2004).

[8] pH_T is the pH measured or calculated at the temperature of interest. In this example, the temperature of the concentrated crevice solution is the temperature of the primary reactor coolant.

Three models are available in MULTEQ to describe the conservation of mass as evaporation of water takes place in a water/steam/solid system (Millett and Paine, 1993): the static, flowing, and hideout return models. For the static and flowing models, there are options for both a closed system and an open system. For the static, closed-system model, all liquids, vapors and solids remain within the system, i.e., it is closed and all phases are in thermodynamic equilibrium. A concentration factor is introduced which is equal to the total number of moles of water in the system (i.e., the number of moles of liquid water introduced to the closed system is equal to the number of moles of water in the liquid phase plus the steam phase after evaporation) divided by the number of moles of liquid water remaining after evaporation. There are also static open-system models that allow removal of either steam or precipitates during the concentration process. For the open-system models, the concentration process takes place in a series of finite steps. For each step, the solid, i.e., precipitates, liquid and vapor phases are in thermodynamic equilibrium. After each step, either vapor or precipitates can be removed before proceeding to the next concentration step. In the flowing system model, water and steam enter and exit a control volume at equal rates. Solutes enter the control volume with the water and volatile species exit the control volume with the vapor. There is also an option for removing precipitates as with the static, open-system model. The third model is the hideout return model, which is similar to the static, closed-system model except that the liquid/vapor distribution coefficient for all species is set equal to zero. The rationale is that the hideout return is assumed to be representative of the inventory in fouled crevices and under deposits in the SG. When the heat flux is removed, the species in the concentrated solutions diffuse to the bulk water and the precipitates re-dissolve. Any volatile species that partitioned to the steam during operation are presumed to be not present in the hideout return. It is assumed, therefore, that a reasonable representation of the crevice chemistry during operation can be estimated by re-concentrating the hideout return inventory in the crevices using the static model with distribution coefficients set equal to zero.

Intergranular SCC and IGA have been serious problems for nuclear plants operating with I600 SG tubes (IAEA, 1997; Staehle and Gorman, 2003; Riznic, 2006). Although laboratory testing has shown that the initiation time for intergranular SCC/IGA of mill-annealed I600 tubing is significantly shorter in near-neutral water chemistry than in either strongly acidic or caustic environments, investigators did not find a strong correlation between the incidence of SCC/IGA at plants operating with I600 SG tubing and the high-temperature pH calculated by MULTEQ using the hideout concentration model (Paine et al., 1991). For this application, only the prompt return was used for input data to MULTEQ and no volatilization was allowed during the reconcentration process, as discussed above. The analysis showed that about 50% of the plants showing acidic or caustic crevices based on the MULTEQ hideout analysis did not have any tubes plugged for intergranular SCC/IGA.

It has been suggested that uncertainties regarding the crevice concentration mechanism and the inability to distinguish individual species hideout return from their respective locations, i.e., tube deposit, fouled crevices, sludge pile, make the determination of high-temperature pH from a deterministic model from hideout return data

impractical (Millett et al., 1995). Alternative indirect methods of inferring crevice chemistry conditions using evidence derived from plant operating data and data from experimental investigations are discussed in Section 10.3.3.

10.3.2 Verifying crevice chemistry by direct measurement

Some investigators have installed probes within the heated crevices of experimental facilities as well as sampling lines to withdraw solution directly from the crevice to interrogate the chemistry environment that develops within a fouled, heated crevice under boiling heat transfer using direct analytical methods. These measurements have provided valuable insights into the crevice chemistry that may develop under SG operating conditions, and have provided useful data for the further development of the deterministic codes for calculating crevice chemistry from thermodynamic data.

Balakrishnan and Strati reported the results of their investigation into the chemistry that develops from hideout of simple and complex mixtures of salts by analyzing samples that had been withdrawn from the crevice after a period of hideout (Balakrishnan and Strati, 2005). Hideout from simple mixtures of sodium and calcium chloride did not result in the formation of any precipitates in the crevice, as expected from thermodynamic data. The addition of sulfate to the mixture resulted in a concentrated solution at the end of the hideout phase of the experiment in which the concentrations of calcium and sulfate were lower than expected. Both calcium and sulfate were missing from the concentrated solution in equivalent amounts, indicating precipitation of calcium sulfate, again, as expected from thermodynamic data. Hideout from simple mixtures of sodium and magnesium chloride produced a concentrated solution in which the concentration of magnesium was lower than expected, which is consistent with the precipitation of magnesium hydroxide and is consistent with thermodynamic data. The addition of calcium and sulfate to the mixture, however, produced an unexpected result. In this case, the concentrations of both magnesium and sulfate were lower than expected while calcium appeared to have concentrated by the same amount as did sodium and chloride. In addition, both magnesium and sulfate were missing from the solution in equivalent amounts. This result suggests that magnesium and sulfate have precipitated as magnesium sulfate, but that calcium has not formed a precipitate with sulfate. When excess sulfate was added to the system, however, the concentrations of calcium, magnesium, and sulfate were all lower than expected, with the number of equivalents of sulfate missing from solution being equal to the total number of equivalents of missing calcium and magnesium. The conclusion from this investigation is that magnesium sulfate precipitates preferentially to calcium sulfate, but that sulfates of both calcium and magnesium will precipitate in the presence of excess sulfate.

Baum developed a test methodology based on measurements of temperature, impedance, pH and electrochemical potential distributions to investigate solute concentration processes within a deposit-packed heated crevice (Baum, 2002a,b). His investigations showed that there can be large temperature and chemistry variations within a heated crevice packed with porous deposit. By making simultaneous measurements of the tube wall temperature and the impedance of the crevice solutions,

Baum was able to determine the effect of the boiling regime within the crevice on the solute concentration distribution within the crevice as a function of time. For example, at a superheat of 10°C, the tube wall temperature profile indicated that the heat transfer regime was nucleate boiling throughout the crevice. Under this condition, the impedance measurements showed that the concentration of a soluble, nonvolatile salt increased steadily throughout the crevice and was accompanied by a corresponding increase in the temperatures of the tube wall and crevice solution, characteristic of a hydraulic concentration process (Baum, 1987, 1989) as illustrated in Fig. 10.1. Concentration maps generated from the impedance distribution indicated that there was a high radial concentration gradient between the heated tube wall and the wall of the crevice, with the highest solute concentrations developing at the tube surface. For tests conducted at superheats >20°C, tube wall temperature measurements indicated that the interior of the crevice was steam blanketed. In this case, the accumulation of a concentrated solution of highly soluble, nonvolatile solute resulted in a decrease in tube wall temperature as the steam-blanketed region was gradually replaced by concentrated solution, characteristic of a thermally driven concentration process (Baum, 1987, 1989) as illustrated in Fig. 10.1. Different behaviors were observed depending on the solubility and volatility of the solute as well as the magnitude of the superheat. For example, accumulation of seawater at a wall superheat of 11°C resulted in the development of an acidic crevice solution, as expected (Balakrishnan, 1980), for concentration of the solute by a hydraulic process. An abrupt increase in the wall superheat to 22°C and thereafter to 36°C, however, caused the crevice pH to increase toward that of a neutral solution. Baum suggested that this result is consistent with the volatilization of chloride from the crevice at the higher wall superheat. As hideout of seawater progressed, the pH started to trend back toward its value before the increase in wall superheat. Application of this test methodology to the accumulation of complex solutions in a heated crevice resulted in a wide range of responses reflecting the interactions between boiling regime, the solubility and volatility of bulk solutes and the presence of residual solutes in the crevice, and has been demonstrated to be capable of revealing new insights into the chemistry that develops in heated, deposit-filled crevices.

You et al. developed an experimental facility to investigate the thermodynamic equilibrium between the solid and liquid and the liquid and vapor phases while a solution is slowly being concentrated (You et al., 1998, 2005). Concentration takes place, however, in a heated autoclave in which constant liquid volume is maintained by balancing the flows of water and steam at the inlet and the outlet of the autoclave. Solutes in the solution flowing into the autoclave gradually concentrate in the autoclave solution until they either form precipitates or leave as volatile species with the steam. Although the facility does not represent the heat-transfer conditions that may prevail in a deposit-filled crevice, as per the previous discussion, investigations in the facility can be used to identify species which precipitate from complex mixtures of solutes and verify or expand existing thermodynamic databases that are used to predict the chemistry of highly concentrated solutions.

Takamatsu et al. (1991) and Kawamura and Hirano (1998) investigated the localized chemistry that develops in clean, heated crevices under the heat-transfer

conditions of alternate wetting and drying. Takamatsu et al. conducted their investigations using an on-site model boiler that was fed continuously with boiler blow down as the test solution. Fine sampling tubes were installed at the bottom of a simulated crevice in the model boiler to withdraw samples for chemical analysis. Measurements of tube wall temperature verified that the heat-transfer mode within the crevice was alternate wetting and drying. The results of Takamatsu et al. showed that for alternate wetting and drying heat transfer, the concentration factor of the nonvolatile soluble cations Na^+ and K^+ was at least 10^4 and independent of concentration over a concentration range in the bulk water from 0.1 to 100 μg/kg. For the soluble anion Cl^-, however, the concentration factor was 10^3 for low bulk water concentration, i.e., from 0.1 to 10 μg/kg, but increased to 10^4 for bulk water concentrations between 10 and 100 μg/kg.[9] The concentration factor for SO_4^{2-} was shown to be about 5×10^4 for bulk water concentrations of from 1 to 10 μg/kg and for boron the concentration factor was about 10. With additional testing, it was shown that the crevice pH_T calculated for a concentration factor of 10^5 using a proprietary computer program correlated well with the ratio of the total number of equivalents of cations in the crevice solution divided by the total number of equivalents of anions (Tsuruta et al., 1995). Kawamura and Hirano measured the concentration factors of solutions of sodium hydroxide and sulfuric acid in a heated crevice by relating changes in the corrosion potential of an Alloy 600 electrode to changes in crevice pH (Kawamura and Hirano, 1998). In separate measurements, the investigators showed that the pH response of the electrode followed very closely the hydrogen line. For tests with a solution of sodium hydroxide, the potential of the Alloy 600 electrode decreased in a step-wise fashion corresponding to incremental increases in pH as the applied heat flux was increased incrementally from 57 to 229 kW/m^2. Measurements of wall temperature showed that the heat-transfer mode in the crevice was alternate wetting and drying for heat fluxes >116 kW/m^2. Similar measurements with solutions of sulfuric acid showed that the pH decreased incrementally with incremental increases in heat flux. The concentration factors measured in this way for sodium hydroxide were relatively independent of both heat flux[10] and temperature, and ranged from approximately 10^3 to 10^5 as the sodium hydroxide bulk concentrations increased from 1 to 10^3 mg/kg. The concentration factors for solutions of sulfuric acid followed similar trends with concentration and heat flux as with sodium hydroxide, but the upper limit of the concentration factor decreased from 10^5 at 100°C to 10^4 at 200°C to 10^3 at 270°C.

Lumsden et al. measured the crevice chemistry that developed in a heated crevice facility using blow down from Ohi-1 for the feed solution to the autoclave (Lumsden et al., 1998). The heated crevice facility was identical to one used for previous laboratory investigations of a similar nature (Lumsden et al., 1997, 1999). Packing the

[9] Takamatsu et al. report a concentration factor of 10^3 throughout the concentration range for Cl^-, but their data in Fig. 7 of Takamatsu et al. (1991) show a concentration factor of 10^4 for concentrations above 10 μg/kg.

[10] Kawamura and Hirano report that the concentration factor increases with increasing heat flux, but data plotted in Figs. 6-1 and 6-2 in Kawamura and Hirano (1998) suggest that the concentration factors are independent of heat flux.

crevice with diamond dust resulted in a crevice that was steam blanketed in the central region. Accumulation of solute occurred initially at the mouth of the crevice, with concentrated solution gradually penetrating the steam-blanketed region. Direct sampling of the crevice showed that all inorganic solutes concentrated with the same hideout efficiency within an order of magnitude. There was no indication that after 1221 hours of hideout the concentrations of calcium, magnesium, and sulfate were sufficiently high to cause precipitation. Of particular interest is the fact that the hideout efficiencies of sodium and chloride were effectively the same throughout the test period, which is consistent with the results reported by Balakrishnan (1991) for hideout in both fully wetted and steam-blanketed heated crevices.

An instrumented, heated crevice facility was installed at the Bohunice NPP to monitor the crevice environment and provide insights to the risk of localized corrosion of the SG tubes (Hojna et al., 2010). The facility was equipped with seven SG tubes and the secondary side was fed with SG blow down which would concentrate in the heated crevice regions during operation. The SG tubes were heated with steam on the primary side, and the primary and secondary temperatures were controlled at 275°C and 260°C, respectively. Liquid samples were periodically extracted from the secondary side bulk water and crevice regions for chemical analyses, and the primary coolant temperature was periodically reduced to simulate hideout return under zero power hot conditions. An analysis using the hideout return data as input to MULTEQ predicted an alkaline high-temperature pH (7.8 and 9.4 for two difference data sets) in the crevice. Direct crevice sampling was also performed during hideout, and using these data as input to MULTEQ resulted in the prediction of a somewhat acidic crevice pH_T, with values ranging from 3.0 to 4.9 from four different sets of data. After 6000 operational hours, the facility was shut down and the SG tubes were removed for analysis. Although detailed results were not provided in Hojna et al. (2010), surface analysis of the SG tube in the crevice region revealed precipitates of calcium sulfate, copper metal and magnetite.

10.3.3 Inferring crevice chemistry from experimental and operating data

As noted previously, numerous studies have indicated that the initiation rates and crack growth rates of mill-annealed Alloy 600 are significantly reduced in a near-neutral chemistry environment compared to rates in either an acidic or a caustic environment (Paine et al., 1991; EPRI, 1993), but that a correlation between the incidence of SCC/IGA at plants operating with mill-annealed Alloy 600 SG tubes and the pH_T calculated by MULTEQ using input data from the analyses of hideout return from those same plants has not been clearly demonstrated (Paine et al., 1991). Differences between pH_T calculated from hideout return data and from direct sampling of a heated crevice during operation (Hojna et al., 2010) continue to challenge our understanding of how best to predict the chemistry environment within a fouled, heated crevice using deterministic equilibrium models.

An alternative methodology for assessing crevice pH_T from blow down chemistry data collected during operation and hideout return was developed by EPRI using the

molar ratio index (MRI). The methodology is based on the assumption that the crevice pH will be near neutral if the ratio of the concentrations of strong-base cations to strong-acid anions in the crevice is close to one (Millett et al., 1995). A ratio greater than one, therefore, implies an alkaline or even a caustic crevice, and a ratio less than one is indicative of an acidic crevice. If the relationship between the molar ratio in the bulk water to the corresponding molar ratio in the crevice is determined, then changes can be made to the molar ratio in the bulk water to control the crevice pH. The hideout MRI is defined as:

$$\mathrm{MRI} = (\mathrm{Na} + \mathrm{K})/(\mathrm{Cl} + \text{excess } \mathrm{SO_4}) \tag{10.7}$$

where the inputs to Eq. (10.7) are the number of equivalents of each species returned from the crevice regions as determined from an analysis of the hideout return. Only the equivalents of SO_4 in excess of those required to form a precipitate of calcium sulfate are used to calculate the MRI. A similar relationship is used to calculate the operational MRI from concentrations in the SG bulk water during operation at full power. Sodium-to-chloride molar ratios determined from hideout return are generally reported to be higher than the molar ratios calculated for operation at power (Sawochka et al., 1996). This has been attributed to the volatility of chloride in the crevices, especially as the crevice pH decreases.[11] Therefore, molar ratio control (MRC) generally involves a combination of sodium source reduction with the addition of ammonium chloride or some other source of chloride to the feed water to reduce the operating MRI to a value suitably less than one to achieve a crevice MRI of approximately one.

The hideout MRI is calculated using only the return from crevice regions; therefore, application of MRC requires a methodology to separate the hideout return from crevices from hideout return from other sources, such as tube deposits, sludge piles and from species that were adsorbed. Return during power reduction is thought to come primarily from tube surfaces; therefore hideout return data measured during power reduction are not used to calculate the hideout MRI. Return from crevice regions at zero power hot is presumed to follow a rate law associated with long-path diffusion from fouled crevice regions. Return of sulfate is complicated by the fact that sulfate adsorbs onto surfaces (Sawochka, 2005; Balakrishnan and Strati, 2005); thus its rate of return is affected by the dissolution kinetics of precipitates, i.e., calcium and magnesium sulfate, long-path diffusion through a deposit-filled crevice and the kinetics of adsorption/desorption as it migrates from deposits, crevices and the sludge pile to the bulk water. Balakrishnan showed that oxidizing conditions in the bulk water during hideout return may cause anions to diffuse more slowly from the crevice regions than cations, thus introducing further uncertainty to the calculation of the hideout MRI (Balakrishnan, 1999; Balakrishnan and Strati, 2005). Balakrishnan proposed that this mechanism might contribute to the elevated sodium-to-chloride molar ratio deduced from hideout return data compared to

[11] Chloride volatility refers to the volatility of HCl in equilibrium with Cl^- in the crevice. Because HCl is not fully dissociated at high temperature, there will be a finite concentration of HCl in equilibrium with Cl^-.

the molar ratio calculated from blow down during operation. Guidelines for applying the MRC methodology to control the crevice MRI to a value close to one based on the analysis of hideout return data are presented in Millett et al. (1995) and Millett (1995).

The effectiveness of the MRI or the sodium-to-chloride ratio as an indicator of crevice pH_T has been tested by looking for correlations between these ratios and the incidence of SCC/IGA originating on the outer surface of SG tubes in plants operating with mill-annealed Alloy 600 SG tubes. The database for SCC/IGA of mill-annealed Alloy 600 suggests that low rates of corrosion should correlate with near-neutral crevices and high rates of corrosion should correlate with either strongly acidic or caustic crevices. Baum et al. compared the SG operating and hideout chemistries of sixteen plants operating with mill-annealed Alloy 600 with the degree of OD-initiated SCC reported for those plants (Baum et al., 1997). No clear correlation was found between the incidence of SCC with either the operating blow down sodium or the operating blow down sodium-to-chloride molar ratio. Evaluation of the prompt hideout return found that neither the hideout sodium-to-chloride molar ratio nor the hideout MRI correlated well with the occurrence of SCC. Most of the plants that were significantly affected by SCC had operating sodium-to-chloride molar ratios that were closer to the target operating molar ratio of 0.3–0.5 (Sawochka et al., 1996) than the plants that were less affected by SCC. Baum et al., however, found that a modified form of the MRI, which they called the Hideout Return Indicator (HRI), provided a better correlation with the incidence of ODSCC than the MRI, where the HRI is defined as:

$$\mathrm{HRI} = (\mathrm{Na} + \mathrm{K} + \mathrm{Ca} + \mathrm{Mg})/(\alpha\mathrm{Cl} + \mathrm{SO_4} + \beta\mathrm{SiO_2}) \tag{10.8}$$

A value of $\alpha = 0.3$ was selected from the presumption that due to its volatility some of the chloride will accumulate on the tube support side rather than the tube side of the crevice, and therefore not contribute to reducing the pH_T on the tube side (Baum, 1996). A value of $\beta = 0.2$ was selected to reflect the fraction of silica return that is believed to originate from the crevice regions. This work suggests that maintaining a relatively high concentration of silica in the blow down may have a beneficial effect at mitigating SCC. It is suggested that the beneficial effect of silica may arise both from its buffering capacity by which it may prevent extremes of pH from developing in the crevice as well as by precipitates of silica physically blocking the penetration of concentrated solution to the tube surface.

Ollar and Viricel-Honorez assessed the results from more than 150 hideout return data sets to develop a better understanding of the chemistry environment within flow-restricted regions and to look for correlations of the chemistry in flow-restricted regions with the incidence of IGA (Ollar and Viricel-Honorez, 1998). No correlation between IGA and the hideout sodium-to-chloride molar ratio was observed, nor was there evidence for a correlation between the incidence of IGA and the pH_T calculated using the hideout return as input data for MULTEQ. Ollar and Viricel-Honorez modified the MRI to include the concentrations of organic species (formate, glycolate, acetate) in the denominator and adjusted the calcium concentration to account for the precipitation of calcium phosphate, but did not observe a good correlation between the modified MRI and the incidence of IGA at French plants.

The corrosion films that form on SG tube surfaces during operation are in thermodynamic equilibrium with their chemistry environment. Therefore, analysis of the composition of these films with reference to the Pourbaix diagrams for iron, chromium, and nickel in high-temperature water should provide valuable information regarding the chemistry conditions under which these films developed. For example, the Pourbaix diagram for nickel at 300°C shows that nickel is thermodynamically stable over a wide range of pH_T from alkaline to caustic conditions in the solid phase, existing as nickel metal at potentials at or below the hydrogen line and as nickel oxide at more oxidizing potentials. In contrast, chromium is thermodynamically stable only as a soluble species under either oxidizing or reducing conditions for highly alkaline to caustic solutions. Iron is thermodynamically stable as the soluble species $HFeO_2^-$ for a band of oxidizing and reducing potentials at high pH_T. Surface examinations of Alloy 600 (Lumsden, 1996a,b; Shoda, 1996) and Alloy 690 (Shoda, 1996) after exposures to a range of high-temperature acidic and caustic solutions and potentials showed that the oxide film after exposure to an alkaline solution is depleted in chromium and enriched in nickel, while exposure to an acidic environment produced an oxide film that was enriched in chromium and depleted in nickel. Exposure of Alloy 600 to a caustic solution resulted in complete removal of the chromium from the outer 1 μm of the surface layer leaving a pure nickel surface. These results are consistent with the high-temperature Pourbaix diagrams for these elements.

To test the hypothesis that the surface film composition should correlate with the local chemistry conditions, SG tubes from the tube/tube-sheet crevice regions that had failed by IGA/SCC were removed from a retired Point Beach SG and the composition of the surface films was examined (Lumsden, 1996a,b). Analysis of sludge removed from the tube-sheet region suggested that the crevices were caustic from prior treatment with phosphate. Analysis of the tube surfaces showed high concentrations of sodium and potassium incorporated into a nickel oxide film. Chromium was completely depleted on the fracture face, and was not found until a depth >1 μm below the surface. Thus, the results from the surface examination are consistent with the caustic environment suggested by the sludge analysis. In another investigation, six SG tubes that had failed by intergranular SCC in the tube-support region were removed from SGs at Trojan NPP in 1991 for surface analysis. Trojan had undergone several changes in chemistry control in its history, but following changes in 1988 the operating sodium-to-chloride molar ratio was 3.14 to 1, suggesting the crevices would be very caustic. Analyses showed that the oxides on five of the six fracture faces examined were depleted in chromium. Two of the fracture faces were completely depleted in chromium and iron near the mouth of the crack. Iron and chromium were not revealed by depth profiling of one of these surfaces until a depth between 0.64 and 1.3 μm. Thus, analysis of the tubes removed from the Trojan SGs suggests that the likely chemistry environment was caustic, consistent with the high operating sodium-to-chloride ratio.

If the composition of the corrosion film on SG tubes in the crevice regions reflects the local crevice chemistry, then so too should the nature and composition of the deposits that form in these flow-restricted regions. Sala et al. have determined compositions of the deposit layers on numerous SG tubes from the tube-support crevice

and free span regions of operating SGs to use as a diagnostic to the local chemistry environment and to investigate the relationship between deposit composition and the risk of local attack by IGA/SCC (Sala et al., 1996a,b, 1998; Cattant et al., 1994). Their investigations found that localized corrosion and cracking occurred primarily under deposits of silicate and an alumino-silicate gel containing nickel and iron. Underneath the gel layer was a nonprotective chromium oxide or hydroxide. It was proposed that nickel and iron from the protective iron-chromium-nickel spinel that normally forms on Alloy 600 SG tubes had diffused into the alumino-silicate gel, leaving behind a nonprotective chromium oxide or hydroxide. They did not find a correlation between cracking and the presence of alkali-forming cations such as sodium and potassium, likely because these cations were present in association with alumino-silicates where their presence is necessary to balance the negative charge. Because silica and alumino-silicate precipitates dissolve in caustic environments, their presence in the crevice indicates that the SG tubes had cracked in an environment that must have been near-neutral to mildly alkaline during operation.

10.4 Plant hideout return studies

10.4.1 Objective of plant hideout return studies

An evaluation of hideout return data is necessary to get a full assessment of SG water chemistry during operation, including crevice chemistry and contaminant inventory. Such an evaluation is called a Hideout Return Study. Before hideout return studies were performed, the correlation of SG chemistry to corrosion observations relied on information collected during normal operation. However, the concentration of boiler contaminants in the blow down during operation represents a steady state between the rate of contaminant ingress to the boilers with the feed water and the rates of removal by a combination of blow down and hideout. SGs with large deposit inventories, or sludge piles, may appear to have excellent water chemistry when in fact most of the contaminant ingress has remained within the boilers in these deposits and in crevices formed between these deposits and the SG tubes. This inventory of contaminants and crevice chemistry can only be evaluated through examining hideout return data.

As noted in Section 10.2, species that concentrate or hide out in crevices and deposits during operation, when there is heat flux and boiling at the surface of the SG tubes, will diffuse from those regions when the heat flux is reduced or removed altogether. When a plant has shut down to zero power, the heat flux and consequently the driving force for hideout is zero. SG blow down samples are taken throughout the time period when the heat flux is zero and the secondary side temperature in the boiler remains within a few degrees of the operating temperature. This period of operation is called a “hot soak.” The period of time after the hot soak when cold feed water enters the boilers to decrease the temperature to ambient or “cold” is called the “cool down to zero power cold.” Samples continue to be taken throughout the “cool down to zero power cold,” where possible.

Hideout return studies were first performed in the 1980s and are now routinely performed by most utilities. In these studies contaminant concentration data are collected during the shut down to zero power hot, and after a hold at zero power hot, throughout the cool down to zero power cold and evaluated to assess crevice chemistry to provide a basis for developing correlations to SG corrosion and establishing molar ratio control programs, if used, and determining the effect of changes in plant equipment or system chemistry. EPRI has published the *Pressurized Water Reactor Hideout Return Sourcebook* (Bates, 2007) to provide guidance to the industry on performing hideout returns and interpreting hideout return data. These guidelines were based on the *PWR Molar Ratio Control Application Guidelines Volume 3* (Brobst and Riddle, 1995) and the development of MULTEQ software to calculate crevice chemistry (Millett and Paine, 1993). Most nuclear utilities have developed in-house procedures consistent with the EPRI guidelines to conduct hideout return studies, and some utilities had these procedures in place (Gonzalez and Pagan, 1990; McKay, 2002) prior to the publication of the EPRI guidelines.

10.4.2 Performing a plant hideout return study

10.4.2.1 Rationale for performing a hideout return study

Hideout return studies provide an assessment of impurity inventory and crevice chemistry during operation. Combined with blow down chemistry during operation, an evaluation of minimum total impurity ingress may be made. The data from hideout return studies are often used in the forensic evaluation of chemistry events and/or the degradation of SG tubes and internals.

To perform a hideout return study, samples of SG blow down are taken when the plant is at zero power hot and during the cool down to zero power cold to provide a baseline of crevice chemistry and impurity ingress for a particular plant. The baseline will be a function of normal feed water chemistry, blow down frequency and efficiency, amount of SG tube sheet deposit and the ingress of contaminants. Hideout return studies provide insights to the effects of changes to chemistry control programs, such as changing the feed water pH additive, changes to the water treatment plant or chemical cleaning. Hideout return studies may also be performed as described above during the plant shut down after an event, if possible. Events such as condenser leaks typically give sufficient notice to plan a hideout return study. Immediate shut downs may be more challenging.

10.4.2.2 Working within plant shutdown procedures

Plant shutdown procedures may dictate the timing and length of sampling in a hideout return study. There may be no, or limited, opportunity for a hot soak, for example. Alternatively, the plant may reduce power and remain at that power level for some time before reducing power to zero power hot. It is important to establish the exact time of power reduction as well as the start and end of zero power hot, and this requires coordination between Chemistry and Operations. Plant Operations personnel need to

be aware of the reasons for performing hot soaks and hideout return studies so that they may be performed effectively.

10.4.2.3 General procedure for performing a hideout return study

During hideout return, samples are taken from individual boilers throughout power reduction, the hot soak at zero power hot, and during cool down. Not all plants may be able to sample throughout the cool down due to insufficient sample line pressure. Typically samples are taken at full power, at any intermediate power holds, and at a frequency of every 15–30 minutes during the power reduction, at zero power hot and during cool down to zero power cold. Plant data are also recorded such as timing of blow downs, blow down flow rate, feed water flow rate, boiler water level (to calculate liquid volume), secondary side temperature (to calculate liquid mass) and pressure. (For pressure >1 atm, the secondary side temperature may be calculated from the SG secondary side pressure.)

10.4.3 Hideout return sampling

10.4.3.1 Species

The species that are typically analyzed in hideout return studies and possible sources of these species are listed in Table 10.5.

Table 10.5 Species analyzed in hideout return studies and possible sources

Species		Examples of possible sources
Cations	Sodium	Condenser leaks, sodium throw from ion exchange resin, contaminant in greases, etc. used in maintenance activities
	Potassium	Condenser leaks, contaminant in greases, etc. used in maintenance activities
	Calcium	
	Magnesium	
	Aluminum	Water treatment plant clarifier, materials used in maintenance activities
Inorganic Anions	Chloride	Condenser leaks, contaminant in greases, etc. used in maintenance activities
	Sulfate	
	Fluoride	Contaminant in greases, etc. used in maintenance activities
	Reactive silica	Condenser leaks, sodium throw from ion exchange resin, contaminant in greases, etc. used in maintenance activities
Organic Anions	Formate	Oil in-leakage, e.g., turbine oil, decomposition of morpholine and other amines used for chemistry control, decomposition of foreign materials
	Acetate	
	Glycolate	

10.4.3.2 Sampling point considerations

The following should be taken into consideration with regard to the sampling point:

- Distance from the boiler with respect to correlation of sampling time with operating parameters such as boiler temperature, blow down flow rate and SG liquid mass at the sampling time.
- Sample line conditioning prior to sampling. A rule of thumb is that sample lines should be open 24 hours prior to the survey and remain open during the entire sampling period. Sample line flow rate should be high enough that the transit time between the boiler and the sampling point is not more than a few minutes.
- Elevation of the sampling point with respect to the boiler. If the sample point is higher than the takeoff from the boiler then it may be difficult to sample during the entire cool down once the boiler pressure drops. Also, once the flow rate decreases significantly, samples may not be representative and there may be difficulty correlating the sample to the exit time for the boiler. Sampling during the entire cool down may not be possible in some plants so a total impurity inventory may be impossible to calculate.

10.4.3.3 Sampling procedures

Typically, samples are taken at equal intervals, the minimum being every 15 minutes and the maximum being 30 minutes, to provide a sufficient number of samples to demonstrate a return profile. The frequency may be influenced by the duration of the hot soak; a longer hot soak may provide enough samples with sampling every 30 minutes.

An example of sampling protocol for hideout return is as follows:

- Sample at 100% reactor power sometime before shut down to establish a baseline.
- Sample at intermediate power if unit is held at an intermediate power prior to shut down. There may be some prompt return of highly soluble species such as Na and Cl at this time.
- Sample as soon as the reactor is shut down. This is essentially the start of zero power hot.
- Sample every 15 minutes during the hot soak. More samples will give a more accurate return profile.
- Hot soaks should be a minimum of 4 hours and longer if there is a deep tube-sheet sludge pile and/or there has been substantial impurity ingress, e.g., condenser leak, resin ingress, during operation. The entire crevice inventory return during hot soak is required to predict crevice chemistry.
- Sample during the entire cool down at a frequency commensurate with duration of cool down, once per hour may be sufficient. These samples are required to determine the total impurity inventory, especially if species with retrograde solubility such as calcium and magnesium sulfate are present.
- Samples may also be taken for hydrazine, pH agent, ammonia, pH and specific conductivity. These are diagnostic parameters that may confirm consistency of analysis. The pH and specific conductivity are real-time indicators of chemistry control and hideout return during the sampling period. Specific conductivity is useful in cases where the hot soak is extended to promote more return since it gives an indication of general return when other chemistry parameters do not change significantly. Monitoring on-line cation conductivity during the hot soak and cool down is more useful for determining if return is continuing since it does not include contributions from chemical additives such as hydrazine and morpholine.

10.4.3.4 Sample preservation and analysis considerations

Boiler ion concentrations measured in today's hideout return studies are typically at least an order of magnitude lower than they were in the 1980s and 1990s. Sample contamination from either sampling personnel or sample bottles can be of concern. The type of sample bottle used may be critical for accurate analysis. It is necessary to prevent contamination from the bottles or adsorption onto bottle surfaces. Table 10.6 is an example of the types of bottles used by one utility. If analysis is immediate, no preservation is required.

10.4.4 Data evaluation and analysis

Once the samples have been analyzed and plant physical data recorded, the total hideout return may be calculated for each boiler ion. If the total return is very small and based on data that are very close to the analytical method detection limits, then any further analysis will likely not be accurate and the data should be retained for trending purposes. If the total return is deemed to be accurate then the crevice pH may be calculated using MULTEQ or an equivalent crevice pH calculation program that calculates chemical equilibria at increasing concentration factors (see discussion in Section 10.3.1.2). The calculated pH can then be compared with corrosion data to determine if the SG tubing could have been degraded during operation. The total return can be compared with operating chemistry to determine the contaminant ingress rate during operation. Data may also be compared with previous hideout return studies to assess the effects of any changes that were made to the chemistry control program.

Emphasis is on hideout return immediately after shut down to zero power hot for crevice chemistry predictions. Data for total shut down evolution are required for impurity source assessments and confirmation of crevice chemistry inferences. All crevice chemistry interpretations are based on mass return, not concentration data.

10.4.4.1 Hideout return calculation methodology

A common methodology for analyzing hideout return employed within the industry is to calculate the cumulative mass return at sampling time t_i by multiplying the blow down concentration at sampling time t_i by the SG liquid water mass at time t_i and

Table 10.6 Example of sample bottle and preservation requirements for hideout return samples

Species	Bottle	Preservation
Organic and inorganic anions	40 mL borosilicate glass vial with 0.125 in. septa-liner	None
Cations	High-density polyethylene (HDPE) 125 mL bottle with poly-lined closure	ULTREX II grade nitric acid to 1%
Reactive Silica	Packard LSC Scintillation Vial (plastic)	None

adding the mass removed by blow down between time t_i and the previous sample taken at time t_{i-1}. This method may result in a somewhat inconsistent hideout return profile if there is an error in any of the parameters, e.g., during the hot soak, species may appear to hide out and then return. The calculated maximum hideout return may not occur at the end of the hot soak, which is inconsistent with the premise that when there is no heat flux contaminants will return to the bulk water. It is imperative to check the consistency of the return profile and use the cumulative hideout return values that are most consistent (usually the highest value during the hot soak) in any calculation of crevice pH.

An alternative method is to evaluate the incremental return during a sampling period, and then integrate all the returns to get the cumulative return at the end of the sampling period. This method ensures that the return is always greater than or equal to zero during a sampling period and that the highest cumulative return is at end of the hot soak (or end of cool down). Anomalies in the analysis are usually resolved by assuming that the real concentration is the average of the concentrations in the samples before and after the anomalous sample.

The hideout return of contaminants during the time interval between samplings at time t_i and time t_{i-1} can be determined from the following equation:

$$R = C_{\mathrm{sgt}(i)} * M_{\mathrm{sgt}(i)} - C_{\mathrm{sgt}(i-1)} * M_{\mathrm{sgt}(i-1)} - F_{\mathrm{fw}} * C_{\mathrm{fw}} \Delta t + F_{\mathrm{s}} * C_{\mathrm{s}} \Delta t + F_{\mathrm{bd}} C_{\mathrm{bd}} \Delta t$$

where:

R = mass returned during the time interval Δt,
$M_{\mathrm{sgt}(i)}$ = mass of liquid water in SG at sampling time t_i,
$M_{\mathrm{sgt}(i-1)}$ = mass of liquid water in SG at time t_{i-1},
$C_{\mathrm{sgt}(i)}$ = mass concentration of contaminant in SG at time t_i,
$C_{\mathrm{sgt}(i-1)}$ = mass concentration of contaminant in SG at time t_{i-1},
Δt = time interval between consecutive samples taken at time t_{i-1} and time t_i,
C_{fw} = average mass concentration of contaminant in feed water during the sampling period,
C_{s} = average mass concentration of contaminant in steam during the sampling period,
C_{bd} = average mass concentration of contaminant in the SG blow down during the sampling period,
F_{fw} = average feed water flow rate during the sampling period,
F_{bd} = average blow down flow rate during the sampling period,
F_{s} = average steam flow rate during the sampling period.

This equation can be simplified during power reduction and hot soak and cool down because the volatility of contaminants is generally zero so that $C_{\mathrm{s}} = 0$, concentrations of contaminants in the feed water are generally far less than in the blow down, and the SG bulk concentration may be said to be equivalent to the blow down concentration.

$$R = C_{\mathrm{bdt}(i)} * M_{\mathrm{sgt}(i)} - C_{\mathrm{bdt}(i-1)} * M_{\mathrm{sgt}(i-1)} + F_{\mathrm{bd}} \left(C_{\mathrm{bdt}(i)} + C_{\mathrm{bdt}(i-1)} \right) / 2 * \Delta t$$

Integrating these incremental increases over the duration of the hot soak then gives the total return, which is then used to estimate the crevice chemistry during operation.

10.4.4.2 Anions

Chloride is highly soluble and usually does not precipitate. It normally returns early during the hot soak and during the power reduction from full power. If there is a significant hold at an intermediate power level, the subsequent return at zero power hot may be very low. Sulfate does not always return during the hot soak; it often returns mainly during the cool down period. Fluoride return is usually minimal. Reactive silica usually returns only during the hot soak.

Organic anions, acetate, formate, and glycolate, may or may not return during the hot soak. In some cases the organic anions may appear to hide out during the hot soak, likely due to adsorption. The interpretation of organic anion behavior may be difficult because it is possible that organic anions may be produced by amine decomposition during the hot soak and that adsorption/desorption occurs.

10.4.4.3 Cations

Sodium and potassium, being highly soluble, usually do not precipitate and return early during the hot soak and during the power reduction from full power. If there is a significant hold at an intermediate power level, the subsequent return at zero power hot may be very low. Calcium, magnesium, and aluminum may return during both the hot soak and cool down.

10.4.4.4 Anion/cation association

When either concentration or cumulative return profiles of an anion and a cation are similar to each other it may mean that they were associated in the crevice solution (e.g., sodium and chloride), existed as a precipitate during operation (e.g., calcium and magnesium sulfates), and/or were associated in impurity ingress (e.g., aluminum sulfate).

10.4.4.5 Impurity source identification

The relative concentrations of anions and cations may be compared with their relative concentrations in the condenser cooling water to determine the contribution from condenser leaks. Other associations such as aluminum and sulfate may indicate a contribution from the water treatment plant clarifier. Improvements in the water treatment plant may result in lower hideout returns. Increases in the concentrations of pH additives may result in increased organic anion returns.

10.4.4.6 Considerations for crevice pH calculation

If the return is minimal, resulting from concentrations that are close to the method detection limit, performing a calculation of crevice pH may not be accurate. In this case the total returns should be trended for future reference. Plants may determine a minimum total hideout return below which crevice pH calculations will not be performed.

Methodologies for estimating crevice pH from the hideout MRI and by using the hideout concentration module in MULTEQ are discussed in Sections 10.3.1 and 10.3.3 and in the original source material (Bates, 2007; Brobst and Riddle, 1995).

Organic anions are sampled routinely by only a few utilities. It was widely believed that organic anions do not play a significant role in crevice chemistry because their parent acids are volatile. However, since the volatility is <1 and measured at about 0.5 in the SG in past studies, and organic anions may be up to 1000 times the concentration of sodium, chloride and sulfate in the bulk SG water during operation, it is possible that organic anions could play a significant role in crevice chemistry when other contaminant ingress is very low.

10.4.5 Case studies

10.4.5.1 PHWR steam generators

In PHWRs the SG secondary side water temperature increases slightly at zero power hot and remains essentially constant throughout the hot soak until cooling is started. Shut down from full power to zero power is almost instantaneous. Some PHWR plants can sample throughout the entire cool down period; others can sample only to the end of the hot soak due to the placement of the sampling stations relative to the blow down lines.

Table 10.7 shows the maximum concentrations of selected species that were observed during hideout return studies at one PHWR unit from 1989 to 2011. This is the most basic evaluation of hideout return and does not differentiate between the hot soak and the cool down phases. The effect of lowering the specification for boiler ions sulfate and chloride from 100 to 20 ppb can be seen in the reduction of return of sulfate and chloride between 1989 and 1992. The effect of chemical cleaning can be seen in the reduction of all species between 1992 and 1995. The effect of better makeup water quality from a new water treatment plant can be seen in the return in 2003 compared to 2000. The increase in organic ions resulting from the increased morpholine specification can also be seen. The hideout return study performed in 2007 was the first hideout return study after a significant water treatment plant resin ingress that resulted in very high sulfate concentrations in the boilers. The effects of the resin cleanup and revised startup procedures to minimize sulfate hideout were successful in that the sulfate return was within the range of previous observations.

Figs. 10.9 and 10.10 are examples of aluminum and sulfate returns from a PHWR plant. The returns are somewhat linear over time throughout the hot soak and cool down. The profiles are similar suggesting that the two species were associated, possibly as $Al_2(SO_4)_3$, which is a clarifying agent that was used in the water treatment plant at that time. The ratio of molar returns of aluminum and sulfate is consistent with $Al_2(SO_4)_3$.

Fig. 10.11 is an example of a typical sulfate return profile from another PHWR plant with the same condenser cooling water source. In this case sulfate return during the hot soak is minimal with most of the return occurring during cool down. There was no cation return associated with the sulfate suggesting desorption from oxide surfaces.

Table 10.7 **Maximum concentrations observed during hideout return study**

	1989	1992	1995	2000	2003	2005	2007	2011
Specifications for SO_4^{2-} and Cl^- (μg/kg)	<100	<20	<10	<10	<10	<10	<10	<10
Notes			1		2		3	
Na	110	160	26	10	3	1	2	8
Ca	520	360	130	65	6	2	6	138
Mg	31	50	20	18	6	3	6	83
SO_4	1540	390	97	100	100	30	50	90
Cl	850	175	12	20	2	2	2	9
Reactive silica	340	2370	88	123	30	30	30	159
Acetate (Note 4)	N/A	N/A	N/A	50	50	50	35	806
Formate	785	260	15	50	180	250	550	890
Glycolate	720	260	35	35	200	300	120	2160

Notes: (1) Post first chemical cleaning. (2) New water treatment plant, post second chemical cleaning morpholine increased to 25–40 ppm. (3) Post resin ingress from water treatment plant. (4) N/A: not analyzed.

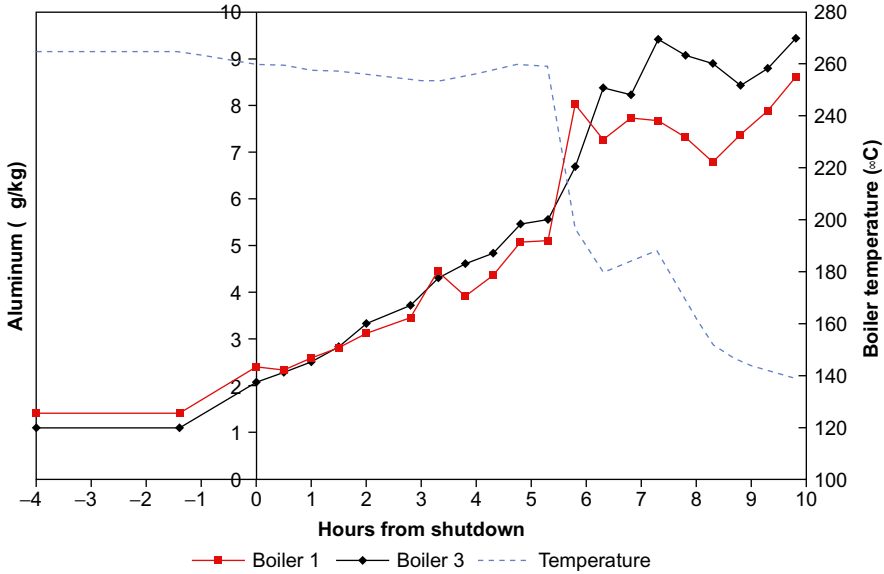

Fig. 10.9 Aluminum from Plant A total return during hot soak ~13 mmol, total return 40 mmol.

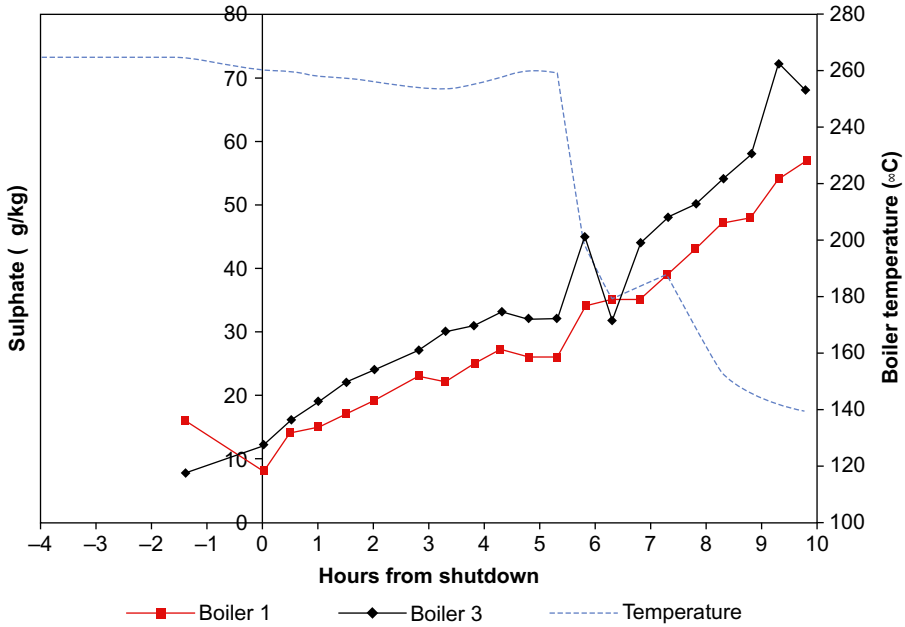

Fig. 10.10 Sulfate Plant A return during hot soak ~22 mmol, total return ~75 mmol.

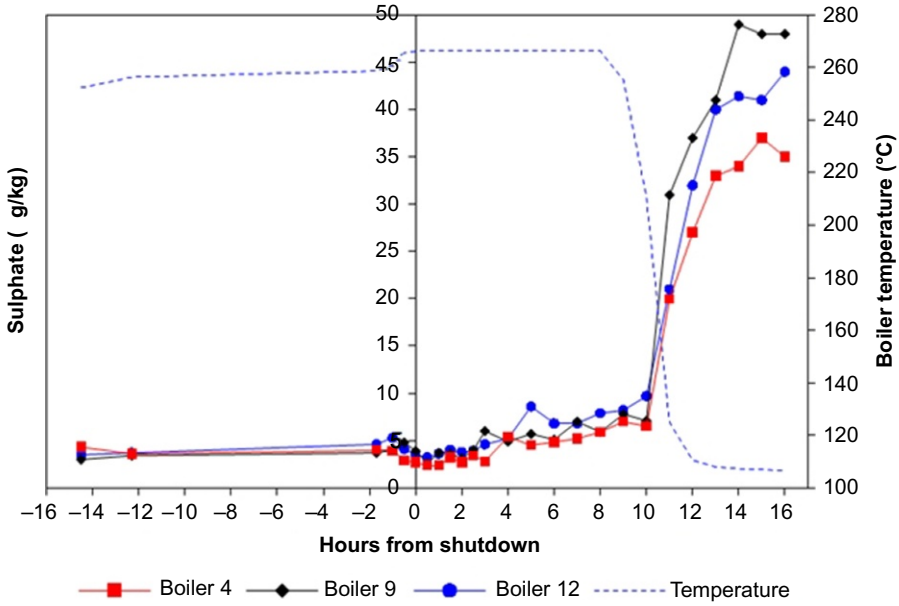

Fig. 10.11 Typical sulfate return profile from Plant B.

10.4.5.2 PWR steam generators

Plant shutdown in PWRs differs from PHWRs in that in PWRs the SG secondary side water temperature decreases throughout the hot soak while in PHWRs the SG secondary side water temperature increases slightly at zero power hot and remains essentially constant through the hot soak until cooling is started. This is illustrated in Fig. 10.12 using data published in the EPRI Hideout Return Sourcebook (Bates, 2007), which show the cumulative returns of the highly soluble ions sodium, potassium, and chloride during a hot soak and cool down.

The return profiles for these species are similar for at-power, zero power hot, and cool down except for chloride that increases during cool down. The reference suggests that this could be a precipitate returning but, because the return is minimal, it could also result from a sampling [lower flow during cool down] or an analytical effect. A possible precipitate was believed to be calcium chloride. The return profiles of calcium and chloride are shown in Fig. 10.13. If the increase in chloride is due to a precipitate return, calcium should respond similarly.

The calcium return is about an order of magnitude greater than the chloride return. It is possible, but not verifiable, that a portion of the calcium return is due to calcium chloride. Another possible calcium precipitate is calcium sulfate. The calcium and sulfate return profiles are shown in Fig. 10.14. Although calcium and sulfate are of the same magnitude, the profiles are different suggesting that calcium and sulfate are not returning as a dissolved deposit.

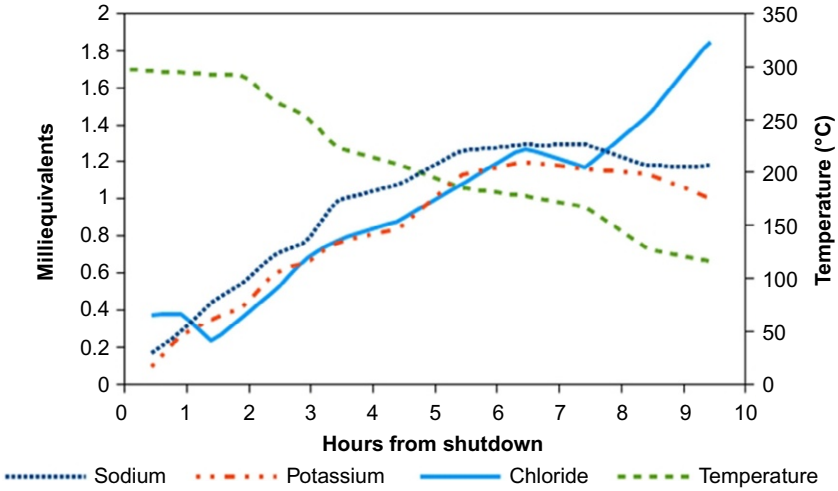

Fig. 10.12 Example of PWR sodium, chloride, and potassium return.
Plotted from data presented in Bates, J., 2007. Pressurized Water Reactor Hideout Return Source Book. Electric Power Research Institute Report EPRI 1014985, December.

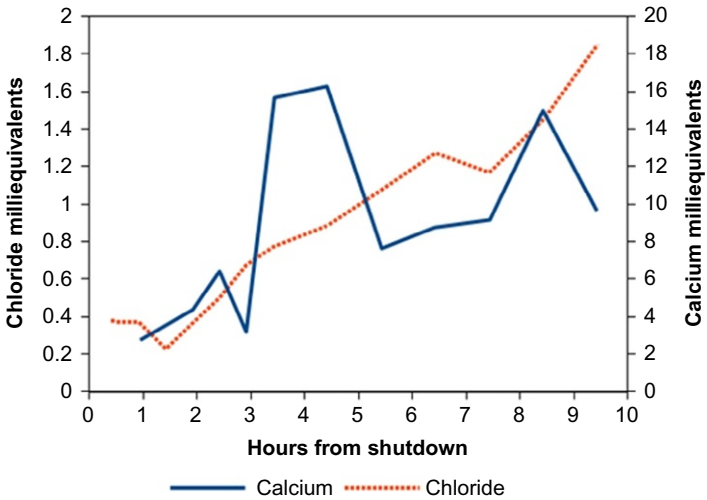

Fig. 10.13 Example of PWR calcium and chloride return.
Plotted from data presented in Bates, J., 2007. Pressurized Water Reactor Hideout Return Source Book. Electric Power Research Institute Report EPRI 1014985, December.

Many US PWR plants do not have holds at zero power hot long enough to perform adequate hideout return studies. Many of those that do perform hideout return studies have minimal returns. Sodium throw from condensate polishers may result in caustic crevice pH predictions.

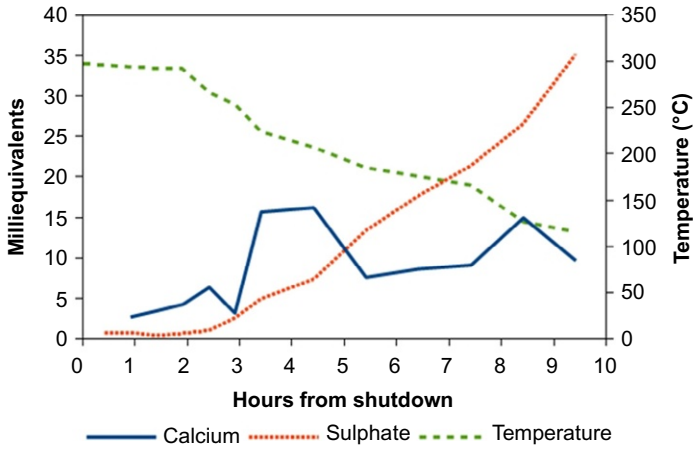

Fig. 10.14 Example of PWR calcium and sulfate return.
Plotted from data presented in Bates, J., 2007**.** Pressurized Water Reactor Hideout Return Source Book**.** Electric Power Research Institute Report EPRI 1014985, December.

10.5 Summary and conclusions

Localized corrosion originating on the outside surface of the SG tubes has been a major cause of SG incapability in the commercial nuclear power industry, with the predominant modes of attack being either SCC or IGA caused by the accumulation of highly concentrated solutions (IAEA, 1997; Staehle and Gorman, 2003; Riznic, 2006). The solutions accumulate in flow-restricted regions on the secondary side of the SG, such as crevices formed at the intersections between the SG tubes and the tube sheet, the tube-support structure and deposits that have accumulated on the tube surface and on the tube sheet. The accumulation of solute in the flow-restricted regions of the SG during operation is called "hideout," and the release of the solute back to the bulk water when the SG is shut down is called "hideout return."

Significant work has been done to understand the thermal and hydraulic processes leading to the accumulation or "hideout" of concentrated solutions in flow-restricted regions (Baum, 1987, 1989). This work led, for example, to an understanding of hydraulically driven and thermally driven concentration processes that are operative under nucleate boiling and transient boiling heat transfer, respectively (Baum, 1987, 1989). The concept of the solubility-superheat ratio helped investigators to understand how a concentrated solution of a highly soluble salt could eventually penetrate a steam-blanketed region and fill the entire region with a highly concentrated, non-boiling solution. Investigators working with heated crevice facilities demonstrated that such processes are operative in deposit-filled crevices (Mann and Castle, 1984; Balakrishnan, 1991; Lumsden et al., 1999) and in the sludge pile that forms on the tube sheet (Gonzalez and Spekkens, 1987). Good agreement was found between experimental data and a model describing heat, mass and momentum transport in a heated crevice filled with porous deposit (Millett and Fenton, 1994).

Deterministic models were developed to calculate the chemistry environment that develops in a highly concentrated solution at SG operating temperatures (Nordmann, 1983; Balakrishnan, 1980; Millett and Paine, 1993), and, in particular, to predict the pH_T that may develop in fouled crevices or under heavy deposits during operation at power. Measurements of the species that precipitate from highly concentrated solutions have provided useful validation data for the chemistry models (Balakrishnan and Strati, 2005; You et al., 1998, 2005). Direct sampling of heated crevices in side-stream model boilers or heated crevice facilities fed with boiler blow down at an NPP have also provided useful data for the validation of crevice chemistry models (Takamatsu et al., 1991; Kawamura and Hirano, 1998; Lumsden et al., 1998; Hojna et al., 2010).

Utilities now routinely perform hideout return analyses to estimate the crevice pH_T during operation at power to assess the risk of localized corrosion of the SG tubes. EPRI has developed guidance to help utilities perform a hideout return analysis (Bates, 2007), and some utilities have developed their own procedures (Gonzalez and Pagan, 1990; McKay, 2002). There are many uncertainties associated with using such an analysis to calculate crevice pH_T, as a result EPRI developed a simplified approach based on the Molar Ratio Indicator (MRI). Attempts to correlate the MRI with the incidence of IGA/SCC, however, have not always been successful (Baum et al., 1997; Ollar and Viricel-Honorez, 1998), and the MRI approach to predicting pH_T is now recognized as being too simplistic (Bates, 2007). Surface analysis of pulled SG tubes (Lumsden, 1996a,b; Shoda, 1996) and analysis of the composition of the deposit layer adjacent to the tube surface (Sala et al., 1996a) can both provide valuable insights to the local chemistry environment based on the assumption that both the corrosion film on the SG tube and the tube deposit layer are in thermodynamic equilibrium with the local chemistry environment.

There will always be uncertainties associated with the prediction of the crevice pH_T in an operating SG. Uncertainties in key properties such as the porosity and permeability of fouled SG crevices limit the ability to model the crevice concentration process with a high degree of certainty. There is evidence that the chemistry within a flow-restricted region is not homogeneous (Baum, 1996, 2002b), and this will affect the prediction of pH_T at the tube surface. Measurements of hideout return under oxidizing conditions highlight the need to account for crevice corrosion and its impact on the rate of return of anionic species relative to cationic species in the calculation of crevice chemistry from hideout return data (Balakrishnan, 1999; Balakrishnan and Strati, 2005). Developments that may improve the accuracy of predictions made by the chemistry models are inclusion of the effect of adsorption of some solute species, such as sulfate (Balakrishnan and Strati, 2005; Sawochka, 2005), and incorporation of the effect of crevice corrosion in the calculation of crevice pH_T (Turnbull and Psaila-Dombrowski, 1996). Combining a numerical model of heat and mass transfer in a porous deposit within a heated crevice (Bajorek and Helton, 2005) with a deterministic model of the high-temperature chemistry conditions that develop under boiling heat transfer may ultimately improve our ability to predict chemistry and the risk of localized corrosion in flow-restricted regions of an operating SG.

References

Abella, J., Balchov, I., Macdonald, D.D., Millett, P.J., 2002. Transport processes in steam generator crevices III: experimental results. Corros. Sci. 44, 191–205.

Adamson, A.W., 1982. The Physical Chemistry of Surfaces, fourth ed. John Wiley & Sons, Inc., New York.

Alexander, J.H., Luu, L., 1989. MULTEQ: Equilibrium of an Electrolyte Solution with Vapour-Liquid Partitioning and Precipitation, Vol. 1: Users Manual (Revision 1): Electric Power Research Institute Report EPRI NP-5561-CCM, May.

Bajorek, S.M., Helton, D.M., 2005. Numerical modelling of steam generator crevice thermal-hydraulics. In: Proceedings of the U.S. EPRI/NRC/ANL Heated Crevice Seminar, Argonne, October 7–11, 2002. NUREG/CP-0189, February 2005.

Balakrishnan, P.V., 1980. Computation of chemical equilibria in steam generator water. In: Proceedings of the 41st International Water Conference, Engineers Society of Western Pennsylvania, Pittsburgh.

Balakrishnan, P.V., 1990. Radiotracer studies on solute concentration within crevices. In: Proceedings of the Conference on Steam Generators and Heat Exchangers Canadian Nuclear Society, Toronto.

Balakrishnan, P.V., 1991. Hideout and Return of Complex Mixtures in Crevices: Electric Power Research Institute Report EPRI NP-7494, September.

Balakrishnan, P.V., 1999. Hideout, hideout return and crevice chemistry in steam generators. In: Proceeding of the 13th International Conference on the Properties of Water and Steam, Toronto.

Balakrishnan, P.V., Strati, G.L., 2005. Laboratory experiments on steam generator crevice chemistry. In: Proceedings of the U.S. EPRI/NRC/ANL Heated Crevice Seminar, Argonne, October 7–11, 2002, NUREG/CP-0189, February.

Balakrishnan, P.V., Turner, C.W., Thompson, R., Sawochka, S., 1995. Hideout of seawater impurities in steam generator tube deposits: laboratory and field studies. In: Proceedings of the 7th International Symposium on Environmental Degradation of Materials in Nuclear Power Systems—Water Reactors, Breckenridge.

Balakrishnan, P.V., Franklin, K.J., Turner, C.W., 1998. Hideout in Steam Generator Tube Deposits: Atomic Energy of Canada Limited Report AECL-11885, May.

Bates, J., 2007. Pressurized Water Reactor Hideout Return Source Book: Electric Power Research Institute Report EPRI 1014985, December.

Baum, A., 1987. Thermal-chemical interactions in restricted regions of steam generators. AIChE Symp. Ser. 257 (83), 97–102.

Baum, A., 1989. Fluid flow, heat and mass transfer—restricted geometries and deposits. In: Cohen, P. (Ed.), The ASME Handbook on Water Technology for Thermal Power Systems. The American Society of Mechanical Engineers, New York (Chapter 6).

Baum, A.J., 1996. Relationships between bulk chemistry and crevice concentration and corrosion processes. In: Staehle, R.W., Gorman, J.A., McIlree, A.R. (Eds.), Control of Corrosion on the Secondary Side of Steam Generators. NACE, Houston. 1996.

Baum, A.J., 2002a. Experimental evaluation of tube support plate crevice chemistry. In: Proceedings of the 10th International Symposium on Environmental Degradation of Materials in Nuclear Power Systems-Water Reactors, Lake Tahoe.

Baum, A.J., 2002b. Relationships between boiling regimes and chemical concentration processes. In: International Conference on Water Chemistry in Nuclear Reactor Systems, Avignon.

Baum, A.J., Greaney, P.K., 1981. Steam Generator Sludge Pile Model Boiler Testing: EPRI NP-1941, July.

Baum, A.J., Prabhu, P.J., Rootham, M.W., Zupetic, N.I., 1997. Development of improved PWR secondary water chemistry guidelines. In: Proceedings of the 8th International Symposium on Environmental Degradation of Materials in Nuclear Power Systems-Water Reactors, Amelia Island.

Bawden, R.J., Mann, G.M.W., Garnsey, R., 1984. Rationale for Chemical Control of Feedwater and Boiler Water, Volume 1: Concentration Models: Electric Power Research Institute Report EPRI NP-3048, January.

Bird, R.B., Stewar, W.E., Lightfoot, E.N., 1965. Transport Phenomena. John Wiley and Sons, Inc., Hoboken, NJ.

Brobst, G.E., Riddle, J.M., 1995. PWR Molar Ratio Control Application Guidelines, Volume 3: Hideout Return Evaluation Guidelines: Electric Power Research Institute Report TR-104811-V3, November.

Campan, J.-L., Brune, J.-P., 1987. Caustic Concentration in Tube Support Plate Crevices of Steam Generators: Electric Power Research Institute Report EPRI NP-5073, March.

Campan, J.L., Shoemaker, C.E., 1987. Sodium hideout studies in steam generator crevices. In: 3rd International Symposium on Environmental Degradation of Materials-Water Reactors, Traverse City.

Cattant, F., Dupin, M., Sala, B., Gelpi, A., 1994. Analysis of deposits and underlying surfaces on the secondary side of pulled out tubes from a French plant. In: SFEN International Symposium, Fontevraud III, Fontevraud Royal Abbey, Chinon.

Cohen, P., 1974. Heat and mass transfer in porous deposits with chimneys. AIChE Symp. Ser. 70, 71–80.

Cohen, P., 1981. Chemical thermal hydraulics of steam generating systems. Nucl. Technol. 55, 105–116.

Dullien, F.A.L., 1988. Two-phase flow in porous media. Chem. Eng. Technol. 11, 407–424.

Engelhardt, G.P., Macdonald, D.D., 1999. Transport processes in steam generator crevices II: a simplified method for estimating impurity accumulation rates. Corros. Sci. 41, 2191–2211.

Engelhardt, G.P., Macdonald, D.D., Millett, P.J., 1999. Transport processes in steam generator crevices I: general corrosion model. Corros. Sci. 41, 2165–2190.

EPRI, 1993. PWR Secondary Water Chemistry Guidelines, Revision 3: Electric Power Research Institute Report EPRI TR-102314, May.

Gaudreau, T., 2005. Status of EPRI software tools for evaluating crevice chemistry. In: Proceedings of the US NRC/EPRI/ANL Heated Crevice Seminar, Argonne National Laboratory, October 7–11, 2002, NUREG/CP-0189, February.

Gonzalez, F., Pagan, S., 1990. Hideout return studies in CANDU steam generators. In: Proceedings of the Canadian Nuclear Society Steam Generator and Heat Exchanger Conference, Toronto.

Gonzalez, F., Spekkens, P., 1987. Concentration processes under tubesheet sludge piles in nuclear steam generators. Nucl. J. Can. 1, 121–140.

Henshaw, J., McGurk, J.C., Sims, H.E., Tuson, A., Dickinson, S., Deshon, J., 2006. A model of chemistry and thermal hydraulics in PWR fuel crud deposits. J. Nucl. Mater. 353, 1–11.

Hojna, A., Karnik, D., Postler, M., Smiesko, I., 2010. Crevice chemistry investigation using crevice model in real plant condition. In: Nuclear Plant Chemistry NPC 2010, Quebec City. 2010.

IAEA, 1997. Assessment and Management of Ageing of Major Nuclear Power Plant Components Important to Safety: Steam Generators: International Atomic Energy Agency Report IAEA-TECDOC-981.

IAEA, 2006. Data processing technologies and diagnostics for water chemistry and corrosion control in nuclear power plants: International Atomic Energy Agency Report TECDOC-1505, June. pp. 70–72.

Kawamura, H., Hirano, H., 1998. Estimation of impurity concentration factor on boiling heat-transfer surface within tube/tube-support plate crevice using corrosion potential measurement technique. In: JIAF International Conference on Water Chemistry in Nuclear Power Plants, Kashiwazaki City.

Lumsden, J.B., 1996a. Insights on local chemistry and IGA/SCC from surface analysis of pulled tubes. In: Proceedings of the 1996 EPRI Surface Chemistry Workshop, Electric Power Research Institute Report TR-112481, March 1999.

Lumsden, J.B., 1996b. Insights on Local Chemistry from Examination of Tubes. In: Staehle, R.W., Gorman, J.A., McIlree, A.R. (Eds.), Control of Corrosion on the Secondary Side of Steam Generators. NACE, Houston. 1996.

Lumsden, J.B., Pollock, G.A., Stocker, P.J., Millett, P.J., Fauchon, C., 1997. Hideout in prototypic tube/tube support plate heated crevices. In: Proceedings of the 8th International Symposium on Environmental Degradation of Materials in Nuclear Power Systems-Water Reactors, Amelia Island.

Lumsden, J.B., Pollock, G.A., Millett, P.J., Takamatsu, H., 1998. Hideout in prototypic tube/tube support plate heated crevices using laboratory feedwater and Ohi-1 blowdown. In: JIAF International Conference on Water Chemistry in Nuclear Power Plants, Water Chemistry '98, Kashiwazaki City.

Lumsden, J.B., Pollock, G.A., Millett, P.J., Torigoe, N., Takamatsu, H., 1999. Effects of the feedwater sodium/chloride ratio and hydrazine on crevice chemistry. In: Proceedings of the 9th International Symposium on Environmental Degradation of Materials in Nuclear Power Systems-Water Reactors, Newport Beach.

Macbeth, R.V., 1971. Boiling on Surfaces Overlaid With Porous Deposit, Heat Transfer Rates Obtained by Capillary Action: United Kingdom Atomic Energy Authority Report AEEW-R711. Winfrith.

Macdonald, D.D., Urquidi-Macdonald, M., 1991a. A coupled environmental model for stress corrosion cracking in sensitized type 304 stainless steel in LWR environments. Corros. Sci. 32, 51–81.

Macdonald, D.D., Urquidi-Macdonald, M., 1991b. An advanced coupled environment fracture model for prediction crack growth rate. In: Parkins Symposium on Fundamental Aspects of Stress Corrosion Cracking, Cincinnati.

Mann, G.M.W., Castle, R., 1983. Salt Concentrations in Heated Crevices and Simulated Scale: Electric Power Research Institute Report EPRI NP-3050, October.

Mann, G.M.W., Castle, R., 1984. Kinetics and processes of solute concentration at crevices in steam generators. In: NEA/CSNI-Unipede Specialist Meeting on Steam Generator Problems, Stockholm.

Mann, G.M.W., Castle, R., 1987. Hideout and Return of Chloride Salts in Heated Crevices Prototypic of Support Plates in Steam Generators: Electric Power Research Institute Report EPRI NP-5015, January.

McKay, A., 2002. Hideout return surveys conducted in Ontario power generation nuclear plants. In: Proceedings of the 4th Canadian Nuclear Society International Steam Generator Conference, Toronto.

Millett, P.J., 1995. PWR Molar Ratio Application Guidelines, Volume 1: Summary: Electric Power Research Institute Report EPRI TR-104811-V1, January.

Millett, P.J., 2004. Advances in High Temperature Water Chemistry and Future Issues. Water Chemistry in Nuclear Reactor Systems, San Francisco.

Millett, P.J., Fenton, J.M., 1989. Transport processes in PWR support structure crevices. In: Proceedings of the 4th Symposium on the Environmental Degradation of Materials in Nuclear Power Systems-Water Reactors, Jekyll Island.

Millett, P.J., Fenton, J.M., 1990. Review of PWR steam generator crevice impurity concentration mechanisms. In: Proceedings of the Canadian Nuclear Society Steam Generator and Heat Exchanger Conference, Toronto.

Millett, P.J., Fenton, J.M., 1991. A detailed model of localized concentration processes in porous deposits of steam generators. In: Proceedings of the 5th Symposium on the Environmental Degradation of Materials in Nuclear Power Systems-Water Reactors, Monterey.

Millett, P.J., Fenton, J.M., 1994. A modelling study of parameters controlling local concentration processes in pressurized water reactor steam generators. Nucl. Technol. 108, 256–265.

Millett, P.J., Paine, J.P., 1993. Improvements in the modeling of crevice chemistry in PWR steam generators using MULTEQ code. In: Proceedings of the 1991 Symposium on Chemistry in High Temperature Aqueous Solutions, Provo, Utah, Electric Power Research Institute Report EPRI-TR-102706.

Millett, P.J., Brobst, G.E., Riddle, J., 1995. A probabilistic approach to controlling crevice chemistry. In: Proceedings of the 7th Symposium on the Environmental Degradation of Materials in Nuclear Power Systems-Water Reactors, Breckenridge.

Nordmann, F., 1983. A computer code (MONA) for pH and chemistry evaluation in secondary system water of PWR. In: Water Chemistry of Nuclear Reactor Systems 3, Bournemouth.

Ollar, P., Viricel-Honorez, L., 1998. Better understanding flow restricted environments from hideout return analyses. In: SFEN Proceedings of the International Symposium Fontevraud 1, Fontevraud Royal Abbey, Chinon.

Oscarson, J., McBride, D., n.d. Unpublished EPRI report.

Paine, J.P.N., Hobart, S.A., Sawochka, S.G., 1991. Predicting steam generator crevice chemistry. In: 5th International Symposium on Environmental Degradation of Materials in Nuclear Power Systems-Water Reactors, Monterey.

Pan, C., Jones, B.G., Machiels, A.J., 1985. Wick boiling performance in porous deposits with chimneys. In: ASME/AIChE/ANS National Heat Transfer Conference Symposium on Multiphase Flow and Heat Transfer Denver.

Pan, C., Jones, B.G., Machiels, A.J., 1987. Concentration levels of solutes in porous deposits with chimneys under wick boiling conditions. Nucl. Eng. Des. 99, 317–327.

Picone, L.F., Taylor, G.R., Cohen, P., 1963. Radiotracer Studies of Hideout at High Temperature and Pressure: United States Atomic Energy Commission Report WCAP-3731. Westinghouse Electric Corporation.

Riznic, J., 2006. Some performance indicators of PWR steam generators. In: Proceedings of the 5th Canadian Nuclear Society International Steam Generator Conference, Toronto.

Sala, B., Combrade, P., Gelpi, A., Dupin, M., 1996a. The use of tube examinations and laboratory simulations to improve the knowledge of local environments and surface reactions in TSPs. In: Staehle, R.W., Gorman, J.A., McIlree, A.R. (Eds.), Control of Corrosion on the Secondary Side of Steam Generators. NACE, Houston.

Sala, B., Henry, K., Lancha, A.M., Dupin, M., Combrade, P., Erre, R., Gelpi, A., 1996b. Analysis of the deposits and surface layers on tubes pulled from PWR French steam generators. In: Eurocorr '96, Paris.

Sala, B., Chevalier, S., Gelp, A., Dupin, M., 1998. Complementary investigations concerning the analysis of deposits and underlying surfaces observed on French PWR steam generators pulled out tubes. In: SFEN International Symposium, Fontevraud IV, Fontevraud Royal Abbey, Chinon.

Sawochka, S.G., 2005. Hideout and hideout return in steam generators: predictions of crevice chemistry. In: Proceedings of the U.S. EPRI/NRC/ANL Heated Crevice Seminar, Argonne, October 7–11, 2002. NUREG/CP-0189, February 2005.

Sawochka, S.G., Choi, S.S., Fruzzetti, K., 1996. Relationships between bulk and local chemistries (hideout return) in molar ratio control and non molar ratio control. In: Staehle, R.W., Gorman, J.A., McIlree, A.R. (Eds.), Control of Corrosion on the Secondary Side of Steam Generators. NACE, Houston. 1996.

Shoda, Y., 1996. Surface film characterization of steam generator tubings. In: Proceedings of the 1996 EPRI Surface chemistry Workshop, Electric Power Research Institute Report TR-112481, March 1999.

Staehle, R.W., Gorman, G.A., 2003. Quantitative assessment of submodes of stress corrosion cracking on the secondary side of steam generator tubing in pressurized water: Part 1. Corrosion 59, 931–994.

Takamatsu, H., Matasueda, K., Kadokami, E., Arioka, K., Tsurtu, T., Okamoto, S., Ueno, T., 1991. Evaluation of steam generator crevice environment by directly sampled method using on-site autoclave facility. In: Proceedings of the 5th International Symposium on the Environmental Degradation of Materials in Nuclear Power Systems-Water Reactors, Monterey.

Tapping, R.L., Turner, C.W., Thompson, R.H., 1991. Steam generator deposits—a detailed analysis and some inferences. Corrosion 47, 489–495.

Tsuruta, T., Okamoto, S., Kitera, T., Takamatsu, H., Matsunaga, T., 1995. IGA/SCC crack propagation rate measurements on alloy 600 SG tubing and evaluation of crevice environments using a side stream model boiler. In: Proceedings of the 7th International Symposium on the Environmental Degradation of Materials in Nuclear Power Systems-Water Reactors, Breckenridge.

Turnbull, A., Psaila-Dombrowski, M., 1996. Modelling of crevice chemistry in the secondary side of nuclear steam generators. In: Staehle, R.W., Gorman, J.A., McIlree, A.R. (Eds.), Control of Corrosion on the Secondary Side of Steam Generators. NACE, Houston.

Turner, C.W., Klimas, S.J., Brideau, M.G., 2000a. Thermal resistance of steam-generator tube deposits under single-phase forced convection and flow-boiling heat transfer. Can. J. Chem. Eng. 78, 1–12.

Turner, C.W., Mitchel, R., Tosello, G., Balakrishnan, P.V., McKay, G., Thompson, M., Dundar, Y., Bergeron, M., Laporte, R., 2000b. ChemAND—a system health monitor for plant chemistry. In: Proceedings of the Canadian Nuclear Society 5th International Conference on CANDU Maintenance, Toronto.

ul Haq, I., Cinosi, N., Bluck, M., Hewitt, G., Walker, S., 2011. Modelling Heat Transfer and Dissolved Species Concentration within PWR Crud. Nucl. Eng. Des. 241, 155–162.

You, D., Lefevre, Y., Feron, D., 1998. A chemical study of concentration processes in steam generator crevices: influence of boron on the hideout of sodium, aluminum and silicon. In: JIAF International Conference on Water Chemistry in Nuclear Power Plants, Kashiwazaki City.

You, D., Lefevre, Y., Feron, D., Vaillant, F., 2005. Experimental study of concentrated solutions containing sodium and chloride pollutants in SG flow restricted areas. In: Proceedings of the U.S. EPRI/NRC/ANL Heated Crevice Seminar, Argonne, October 7–11, 2002, NUREG/CP-0189, February.

This page intentionally left blank

Deposit accumulation in PWR steam generators

11

Robert D. Varrin, Jr.
Dominion Engineering, Inc., Reston, VA, United States

11.1 Overview

Pressurized water reactor (PWR) steam generators (SGs) serve as the boundary between the primary and secondary sides of the plant. As such, the SGs provide both physical and radiological separation between the radioactive primary coolant and the nonradioactive or "clean" secondary feedwater, steam, and condensate. On the primary (tube) side of the SG, hot subcooled primary coolant flows through the SG tubes and transfers energy to the secondary side. On the lower pressure secondary (shell) side, subcooled feedwater is heated and boiled to produce steam.

While plant owners and operators strive to maintain the cleanliness of both the primary side coolant and secondary side feedwater, some impurities inevitably exist in both fluid systems. On the primary side, ionic and particulate corrosion products can lead to activated deposits on fuel and excore surfaces, commonly referred to as *crud* (Berry and Diegel, 1979). On the secondary side, impurities including corrosion products are the precursors to deposits that form in the SGs as the feedwater boils away. These deposits form on both the tubing and internal structures of the SGs, and in the absence of significant primary to secondary side leakage, exhibit only very low levels of activity.

This chapter focuses on the formation, characteristics, and removal of secondary side deposits. Primary side deposits are discussed briefly in Chapter 7.

11.1.1 Formation of secondary side deposits

The accumulation of deposits on the secondary side of SGs leads to a number of side effects that can complicate or compromise the performance, inspection, and maintenance of the SGs in specific and the plant in general. Fig. 11.1 illustrates some of the sources of impurities that transported to the secondary side of a SG (Varrin, 1996). As discussed later in this chapter, the greatest contribution in terms of percentage of impurity ingress is associated with corrosion products. Even at very low concentration of corrosion products such as iron (typically present at 1–5 ppb), hundreds of pounds/kilograms of material can be transported to the SGs in a single year of operation.

While Chapter 10 contains a more detailed discussion of impurity and corrosion product generation and transport, a brief overview of secondary side deposit formation is provided below.

Steam Generators for Nuclear Power Plants. http://dx.doi.org/10.1016/B978-0-08-100894-2.00013-3
© 2017 Elsevier Ltd. All rights reserved.

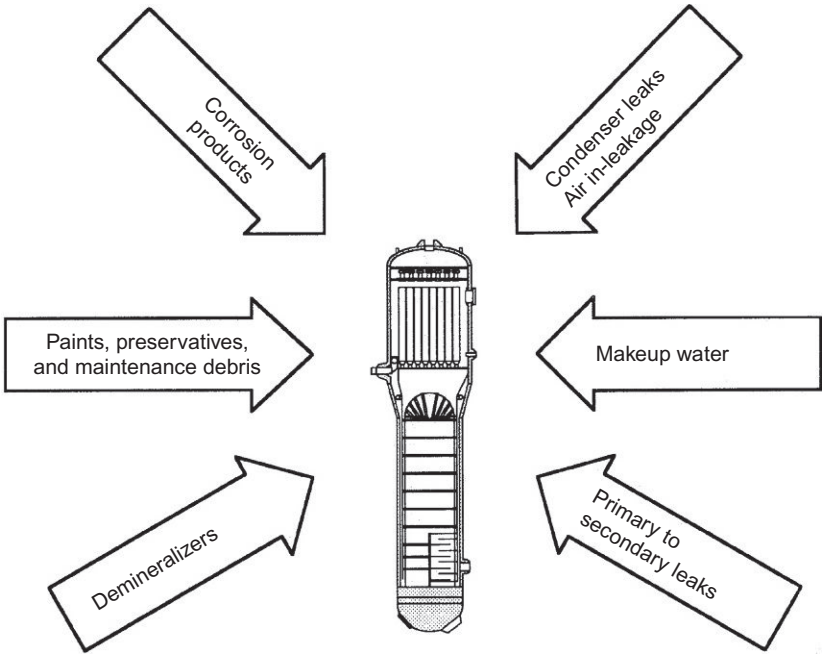

Fig. 11.1 Sources of deposit precursor.

11.1.2 Formation of deposits in RSGs vs OTSGs

In vertically oriented U-tube bundle recirculating SG (RSGs), the most common design in Western-style PWRs, the steam that is produced is dry but saturated. In the once-through steam generators (OTSGs) used at some Western plants, the steam is superheated about 50°F before it exits the SGs. Inside of an RSG, the quality of the steam at the top of the U-tube bundle is about 30%; hence, 70% of the steam/water mixture that exits the bundle is in the form of liquid water (droplets). These droplets are removed from the steam by swirl vane type separators and dryers. The separated water drains by gravity back to the outer annulus of region where it commingles with the incoming colder feedwater. The ratio of the separated to the feedwater flow is known as the circulation ratio (CR), which may range from 3 to about 10 depending on the SG design and power level.

In OTSGs, there is no internal recirculation, and the steam is completely dried and superheated in the uppermost portion of the tube bundle (Figs. 11.2 and 11.3).

To gain an appreciation for the sources on impurities in the secondary side of the plant, it is worth briefly reviewing the operation of the secondary plant with regard to steam generation/power production, condensate collection and purification, and feedwater heating and flow paths.

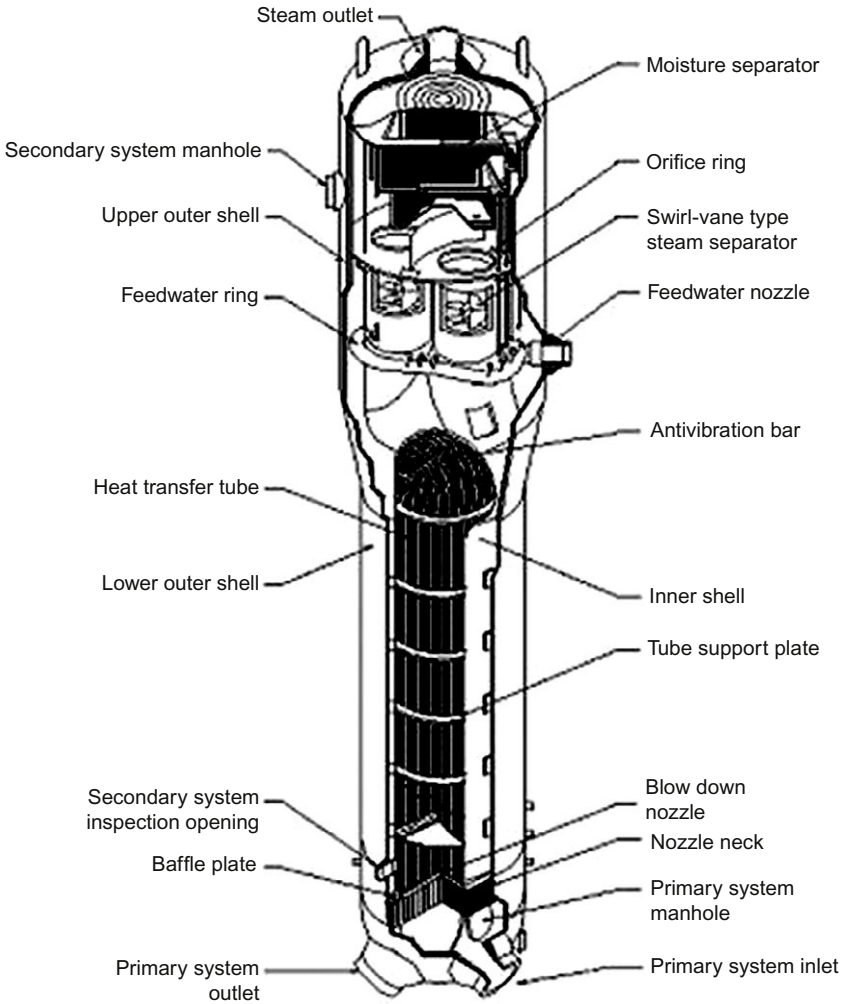

Fig. 11.2 Typical recirculating type steam generator (steam shown in yellow).

11.1.2.1 Steam generation

For both RSG and OTSG designs, almost all of the steam generated in the SGs is directed to the high pressure (HP) turbine to produce electric power. Overall rates of steam generation may range from 4 to 8 million pounds per hour at pressures up to 1200 psig and a temperature of about 570°F (Dahlheimer et al., 1984). A small amount of steam, sometimes called "live steam", is diverted for final feedwater (FW) heating or to reheat wet steam that passes through the moisture separator reheaters (MSRs) (see discussion below). As it exits the SGs, the steam comes in contact with the carbon steel walls of the steam piping system. The flow past the walls of the pipe can lead to erosion/corrosion of these surfaces, the result of which is entrainment of corrosion products into the steam. Eventually, these corrosion

Fig. 11.3 Once-through steam generator (steam shown in yellow).

products will be transported back to the SGs if not removed by the plant's feedwater/condensate cleanup systems. Very little if any of the corrosion products that enter the SG are carried out with the steam.

11.1.2.2 Reheating

Expansion of the steam through the HP turbine results in generation of a significant amount of liquid water in the steam. To avoid excessive erosion/corrosion of downstream piping and components by water droplet impingement, and to optimize the thermodynamic efficiency of the plant, the wet (lower pressure) steam is dried and heated in MSRs, which are generally large horizontal/multizone heat exchangers with integral steam-water separators. After reheating and drying, the steam is then directed to the low pressure (LP) turbines which together with the HP turbine drive the plant's main electrical generator. A significant amount of the steam that passes through the LP turbines is "extracted" to feedwater heaters, the MSRs, deaerators, and other secondary side equipment (e.g., main feedwater pump turbines). Just as with the HP steam, the LP steam in various portions of the secondary plant flows past steam piping walls, and surfaces within the MSRs and FW heaters. This contact results in additional entrainment of corrosion products into the secondary system.

11.1.2.3 Condensate collection and purification

The steam that exits the final stages of the LP turbine(s) is condensed in the main condenser, purified by ion exchange in the condensate polishers, and pumped back to the SGs after being preheated in the feedwater heater system. In this case, the liquid condensate also flows past pipe walls and through the condenser and feedwater heaters. As with the steam, corrosion products generated by slow aqueous corrosion processes can become entrained in the condensate/feedwater flows. At a typical PWR plant, about 70% of the steam generated in the SGs ends up as final condensate in the main condenser hotwell and is therefore purified in the condensate polishing system. A full 30% will have already been pumped back to the SGs without condensate polishing, after having been used for reheating, deaerating, feedwater heating, or driving pump turbines. So even with "full flow" condensate polishing, about one-third of the steam/water that now contains corrosion products and other impurities goes back the SGs.

Finally, within the plant's main condenser, the steam/condensate side is at a lower pressure than the cooling water. As such, small leaks in condenser tubes which contain fresh, brackish or sweater, can be a significant source of deleterious impurities such as chlorides, sodium, and sulfates.

11.1.2.4 Blowdown

In addition, about 1% of the feedwater introduced to RSGs is not used to generate steam but is directed trough the *blowdown* system (Dahlheimer et al., 1984). In an RSG, continuous blowdown of feedwater recirculating in the SGs is one means of reducing the buildup of impurities in the SGs. This is because the internal recirculation of the feedwater causes the impurities to concentrate. In other words, if the incoming concentration of iron is 1 ppb, and the internal recirculation result is a concentration to 100 ppb, then removing 1% by blowdown represents no net accumulation of iron in the SG (theoretically). Usually, the blowdown flow is directed to the plant condenser after cleanup although it can be "overboarded" (disposed of). As discussed elsewhere, OTSG do not use blowdown except perhaps on startup, as there is no concentrating mechanism in an OTSG that would justify blowdown as a means of impurity removal.

11.1.2.5 Makeup

Unless blowdown is overboarded, very little makeup is required in a closed system such as a PWR. Typical makeup water flows are on the order of 100s of pounds per hour as opposed to 16 million pounds per hour steam/feedwater flow at a 1000 MWe plant. Nevertheless, the makeup water flow will inevitably contain some impurities, particularly silica and hardness species.

11.1.3 Deposit precursor source term

Overall, as feedwater, steam, and condensate circulate through the secondary plant, these fluids come in contacts with tens of thousands of square feet of piping, tanks, heat exchanger tubes, and condenser surfaces. The materials of construction used for the secondary plant include carbon steel for piping, and a range of alloys for heat

exchanger tubes (copper alloys owing to their good heat transfer properties, titanium or stainless steel tubing for condenser tubes, copper alloy tubing in many older PWR plant FW heaters, stainless steel tubing for many FW heaters in newer plants, etc.).

Despite diligent efforts to maintain component corrosion rates at extremely low levels, some erosion and corrosion is inevitable in all of these systems. In addition, as discussed earlier, some makeup water is required to compensate for small leaks, sampling flows, and normal leakage. This makeup waiter, while very pure, can also be a source of impurities including silica.

Table 11.1 summarizes some of the sources of deposit precursors, typical transport rates in pounds per year and main chemical/physical forms (Varrin, 1996).

Table 11.1 Summary of major sources of deposit precursors

Source	Type of deposit precursor	Events assocites with generation	Typical pounds per year per SG	Species
Feedwater, condensate, and drain sys	Corrosion products	Normal operation	200–500	*Maior species*: Fe_3O_4, $Fe(OH)_2$, $Fe(OH)_3$, $Cu(OH)^+$, Cu, Ni
		Transients (startups)	100–300	*Minor species*: Lead, sulfur, carbon, phosphorous, silicon, arsenic
Make-up water system	Gases	Performance limitations	(2 ppb)	*Maior species*: Oxygen, silica, harness species, organics
	Soluble species	Performance limitations	10 or more	*Minor species*: Metals
Condenser	Gases		(2 ppb)	*Maior species*: Silica, hardness species, oxygen, organics
	Soluble species	Leaks	Variable	
	Insoluble Species		Variable	*Minor species*: Metals (e.g., copper), carbon dioxide
Condensate polishers and blowdown demineralizers	Resin fines	Throw	>50	*Maior species*: Organics, resin particles, resin breakdown products
	Treatment chemicals	Regeneration	Variable	Oragnic acids, acids, caustic
	Adsorbed impuritie	Over use or chemical upset	Variable	*Minor species*: Metals (e.g., copper), carbon dioxide, iron, hardness

By far, the main impurity in PWR feed and condensate systems is iron. In the early years of PWR operations (e.g., the 1960s and 1970s), it was not uncommon for feedwater iron impurity concentrations to be on the order of 10 ppb with transients of 100 ppb or more, corresponding to transport of thousands of pounds of material to the SGs in just one or two operating cycles. This was particularly troublesome at some early plants that were not equipped with condensate cleanup systems such as condensate polishers (CPs) that use large beds of ion-exchange resin to clean up all or part of the feedwater. Recall that even with CPs, plants return on the order of 30% of the steam that is produced in the SGs back to the SGs primarily via FW heater and MSR condensate drains.

While there is ongoing debate as to the exact ratio of insoluble (particulate) to soluble iron in the feedwater, it is generally accepted that about 90% of the iron as iron oxides exists as colloidal to particulate species with principal diameters ranging from <0.1 μ to a few microns (Varrin, 1996).

At all plants, the ingress of iron species including soluble and insoluble forms of iron is monitored either periodically or semicontinuously. Daily grab samples of feedwater and condensate are taken at "sample sinks" in the secondary chemistry laboratory and analyzed not only for iron but also for other impurities such as silica, sodium, chloride, and sulfate. Longer-term sampling may also be done with corrosion product samplers placed at strategic locations in the feedwater and condensate system, including final feedwater, condensate before or after Cps, and at drains from components such as FW heaters or the MSR. Fig. 11.4 shows and example of one corrosion products samplers (Courtesy NWT Corporation).

Fig. 11.4 On-line corrosion product sampler.

11.1.4 Deposit formation

When impurities enter the SGs with the feedwater, they can: (1) be removed by blowdown, (2) carry out of the SGs with the steam, or (3) remain in the SG and precipitate as deposits. While the original design goal for RSGs was to rely on the blowdown system to remove impurities that enter the SGs, the efficiency of blowdown system has been historically low for two reasons:

- Blowdown works well in many fossil plant designs with mud drums and blowdown worked to a degree in early PWR plants that used phosphate-type water chemistry. Phosphate chemistry results in impurities having a tendency to settle at the bottom of the SGs where suction for blowdown is located. However few if any current PWRs operate with phosphate water chemistry due to the problems associated with tube corrosion such as wastage at the bottom of the SGs (tubesheet region) within insoluble "sludge piles" that form in the low flow areas of the SGs.
- In nonphosphate water chemistry treatment in use today at PWRs ("all volatile treatment" or AVT), the impurities remain volatilized long enough to precipitate/deposit long before they are removed by blowdown. At 1% blowdown, impurities would need to concentrate by a factor of 100 to result in a net zero accumulation. In fact, this extent of concentration is not achieved.

11.1.5 Particulate impurities

Particulate impurities, most notably iron oxide erosion/corrosion products, are typically sub-micron to a few microns in diameter. They represent by far the largest fraction of the material transported to the SGs on a mass basis, corresponding to several hundred pounds per year per SG at some plants.

For iron oxides, very little if any of the ingress is likely to exit the SG with the steam, and studies of blowdown efficiency suggest only about 1% of the oxides are effectively removed via this route (Varrin, 1996).

Note: Since the late 1990s, many plants have begun to introduce organic dispersants in the feedwater, which has increased blowdown efficiency to about 20% or more at some plants.

Once in the SG, some of the particulates are thought to agglomerate or coalesce. The larger agglomerations can settle on horizontal surfaces, particularly in regions where the secondary side liquid velocity is low (less than about one foot per second). Overtime, the particles that settle out of the secondary side can further consolidate into hardened "sludge piles." These sludge piles are commonly found on the bottom tube sheet of vertically oriented U-tube type RSGs. The piles are often found in what is called the "kidney-shaped" region near the center of the hot or cold leg (low flow areas).

Today, a typical distribution of deposits in an RSG would be as follows:

- Approximately 90% of the iron oxides that enter an RSG, if not removed by blowdown, accumulate as scale on the tubing surfaces. This scale may contain up to 10% copper if the secondary plant (so-called balance-of-plant or BOP) contains components fabricated

with copper alloys or brasses. Most plants today have replaced nonferrous components with replacements made with stainless steels or titanium alloys. Newer designed plants rarely contain significant amounts of copper alloys; hence, the tube scale deposits are generally copper free.

- About 5% of the deposits accumulate on structural surfaces of the SGs or on tube supports.
- About 5% of the deposits accumulate or "settle" on the top-of-tubesheet (TTS) in the form of piles. These piles consist of hard agglomerated materials at the base of the tubes known as "collars" and loose powdery material.
- Less than 1% of the deposits form in the tube-to-tube support crevices—these accumulations are particularly important as they act as sites for accumulation of impurities such as sodium and sulfates, the presence for which can raise or lower the local pH and as such increase risk of tubing corrosion.

The formation of tube or *scale* deposits has been an area of significant interest to utilities and research organizations. This is because of the potential that tube deposits can affect the overall efficiency of the SGs and act as sites for impurity concentration if the scale becomes thick enough. There are many models of the lifecycle of tube scale in PWR SGs. One of which is illustrated in Fig. 11.5. In this model, initial scale formation begins as deposition of a thin layer of particulate iron oxides, which gradually thickens. As it thickens, it undergoes a process referred to as ripening where it consolidates, hardens, and becomes less porous. While early in life, the porous nature of the deposits may actually help boiling and heat transfer, thicker denser layers lead to fouling.

At tube supports, deposits are known to accumulate in both RSGs and OTSGs. The consequences of tube support accumtions, particularly at "braoched" or quatrafoil supports, can include thermal hydraulic instabilities and reduction in CR that can lead to a potential for less damping of the tubes and fatgue cracking of vibrating tubes.

Fig. 11.6 shows a pictorial representation of tube support accumulation. Fig. 11.7 shows the typical locations of blockages including some actual secondary side visual inspection images.

Particulates are theorized to be trapped at the eddies that form at the leading edge of tube support plate flow passages, leading to the blockages. In OTSGs, tube support plate blockages cause the water level in the downcomer feedwater annulus to rise which can limit the output of the plant.

As for the TTS, the pattern of accumulation is often referred to as the kidney-shaped region, as illustrated in Fig. 11.8.

Piles can also exist on the flow distribution baffle, if the RSG is equipped with this feature, and on upper "can deck" regions near the swirl vane separators. Some of the newest design SGs include features that are specifically configured to take advantage of this settling behavior in the upper can deck region, using a so-called sludge collector.

Note: In recent years, the terms *sludge* has been used to specifically describe the piles that form on tubesheets, while *deposits* is a more general term for material on the tubesheet, as well as on tubes or tube-to-tube support crevices. Years ago, the term sludge was used in many references as a descriptor for all deposits.

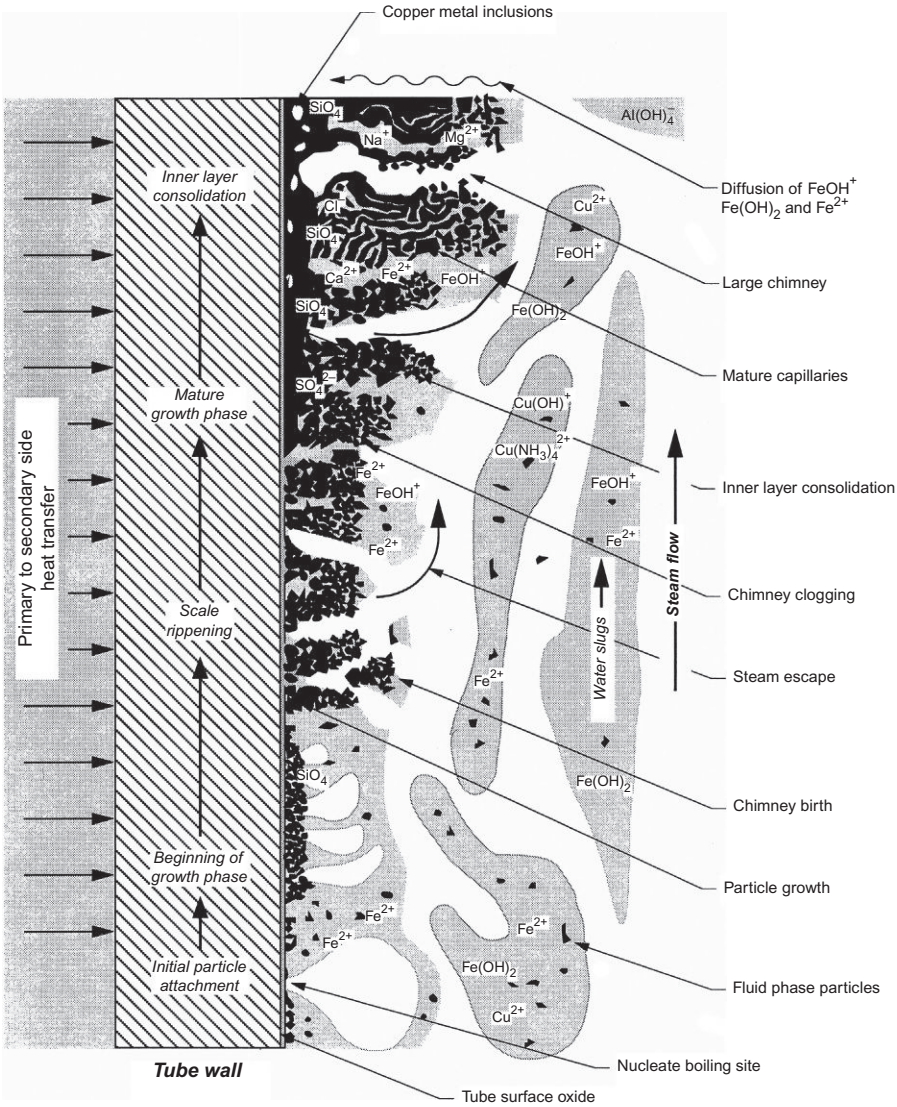

Fig. 11.5 Life cycle of tube scale.

11.1.6 Soluble impurities

While on a mass basis, the transport of particulate species most notably iron as oxides (e.g., Fe_3O_4) dominates the overall mass transport to the SGs (often on the order of hundreds of pounds per SG per year), the ingress of soluble species is also important. Soluble species that are transported to the SGs generally fall into two main categories

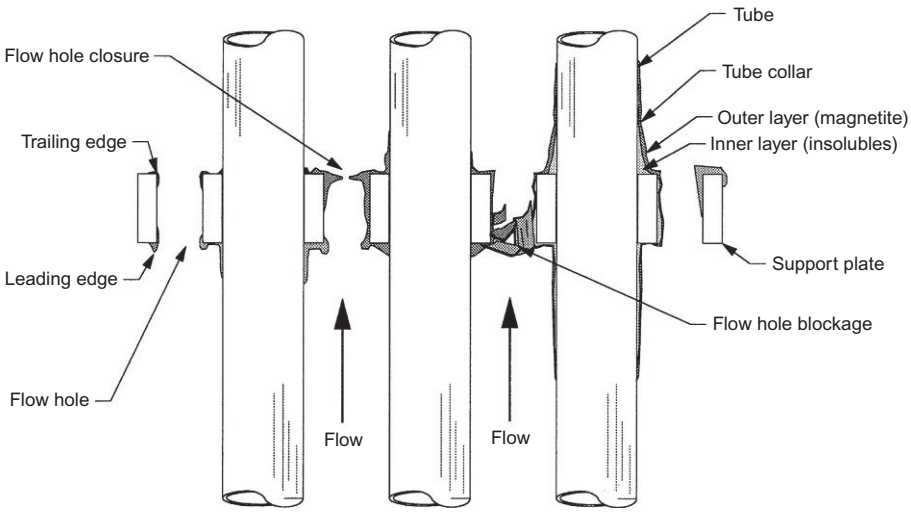

Fig. 11.6 Tube support plate deposit accumulation.

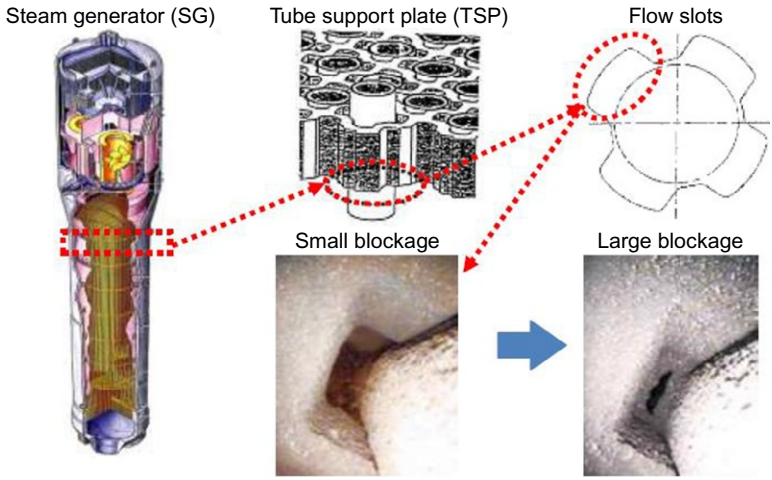

Fig. 11.7 Tube support plate blockages.

– Metallic ions such as Fe^{2+}, Cu^{2+}, and Ni^{2+} which are the result of corrosion of balance of plant components and piping in the feedwater, steam, and condensate systems. These metallic ions may actually be partially hydrolyzed to moieties such as $Fe(OH)^{+}$ or $Cu(OH)^{+}$. In general, as discussed earlier, most PWR plants report that only 5%–10% or more of the iron transported to SGs is soluble (ionic)—as discussed earlier, most iron oxides transported to SGs are believed to be particulate corrosion products.

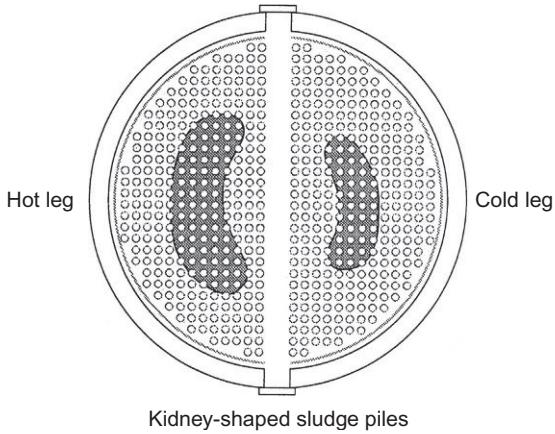

Fig. 11.8 TTS sludge pile patterns (locations of hard collars).

- Ionic impurities including sodium (Na^{2+}), chlorides (Cl^{-}), and sulfates. These particular ionic impurities can concentrate in tube support crevices, within sludge piles, and along tube free spans, particularly within and under tube scale deposits. Like their metal ion counterparts, these ionic species may participate in the chemical mechanisms that consolidate particulate species into tube scale or tube support deposits.
- Ionic species that are loosely referred to as "hardness species" which include not only calcium but also silica (as silicates or silicic acid) and aluminum (probably as aluminate ions).

11.1.7 Organics and gases

Other soluble species such that can be transported to SGs include organics and gases. The main organic species of concern to owners and operators of SGs are organic acids such as acetates, formats, and glycolates, which are breakdown products of feedwater chemistry control additives used for AVT water chemistry treatment, such as morpholine or ethanolamine.

11.1.8 Consequences of deposit accumulation

The consequences of deposit accumulation in PWR SGs are discussed extensively in other chapters of this book (e.g., Chapter 8). Fig. 11.9 summarizes some of the most commonly discussed consequences with regard to SG integrity. Thermal performance effects of deposits are discussed in Chapter 13.

11.2 Deposit characterization

11.2.1 Overview

Far from being generic, the physical and chemical properties of deposits vary from plant to plant. This is because each plant differs with respect to its materials of construction, design, operating history, chemistry control strategy, operating parameters,

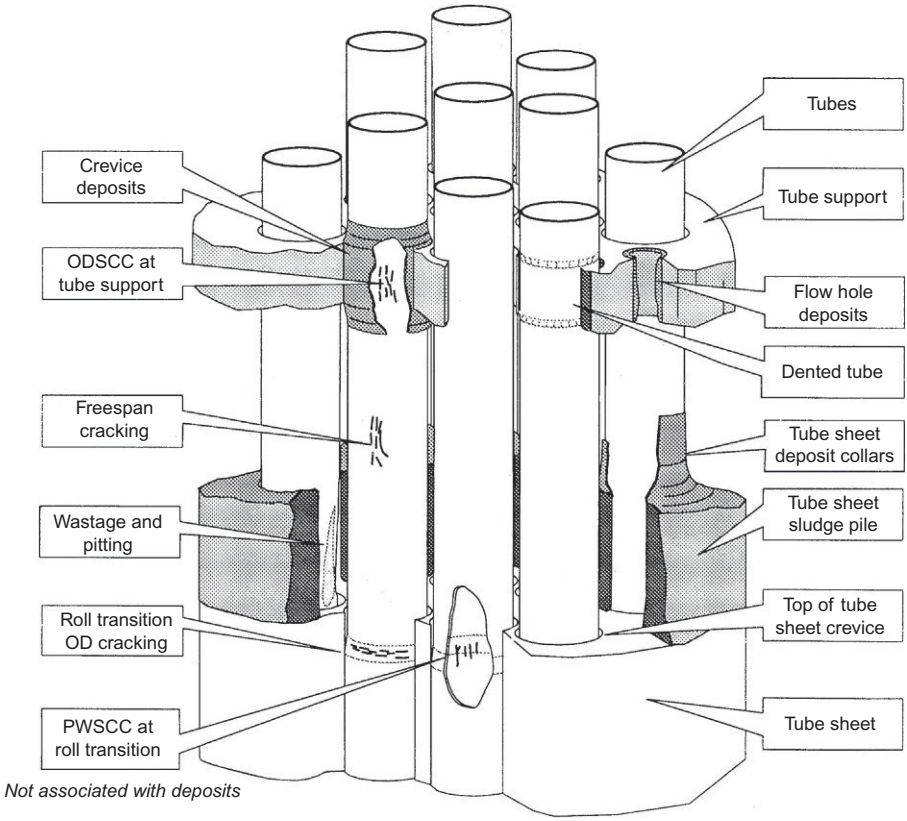

Fig. 11.9 Consequences of deposits in PWR steam generators.

and sources of cooling and makeup water. It is these variables that control the deposit "source term" discussed earlier.

11.2.2 Sample collection

At virtually every PWR plant, plant operators, or chemists will periodically collect samples of deposits that have formed in their SGs. Because access to the inside of the SG is limited, the most common method for collecting deposits is to filter them from the water collected during "sludge lancing," which is a cleaning technique discussed later in this chapter. Samples of powdered deposits can be collected on filters, and tubes scale and harder TTS deposit pieces can be collected in coarse mesh screens (e.g., "grit screens" or y-strainers).

Once collected, the deposit samples can be analyzed by the plant, but it is more common to send them to a vendor who specializes in the analysis of PWR, BWR, or fossil power plant deposits.

This is due in part to the ability of the analysis lab to provide proper interpretation of the results by having access to large databases of deposit characteristics from similar plants.

A typical flowchart for powdered type deposit characterization is depicted in Fig. 11.10. Similar protocols are used for tube scale samples.

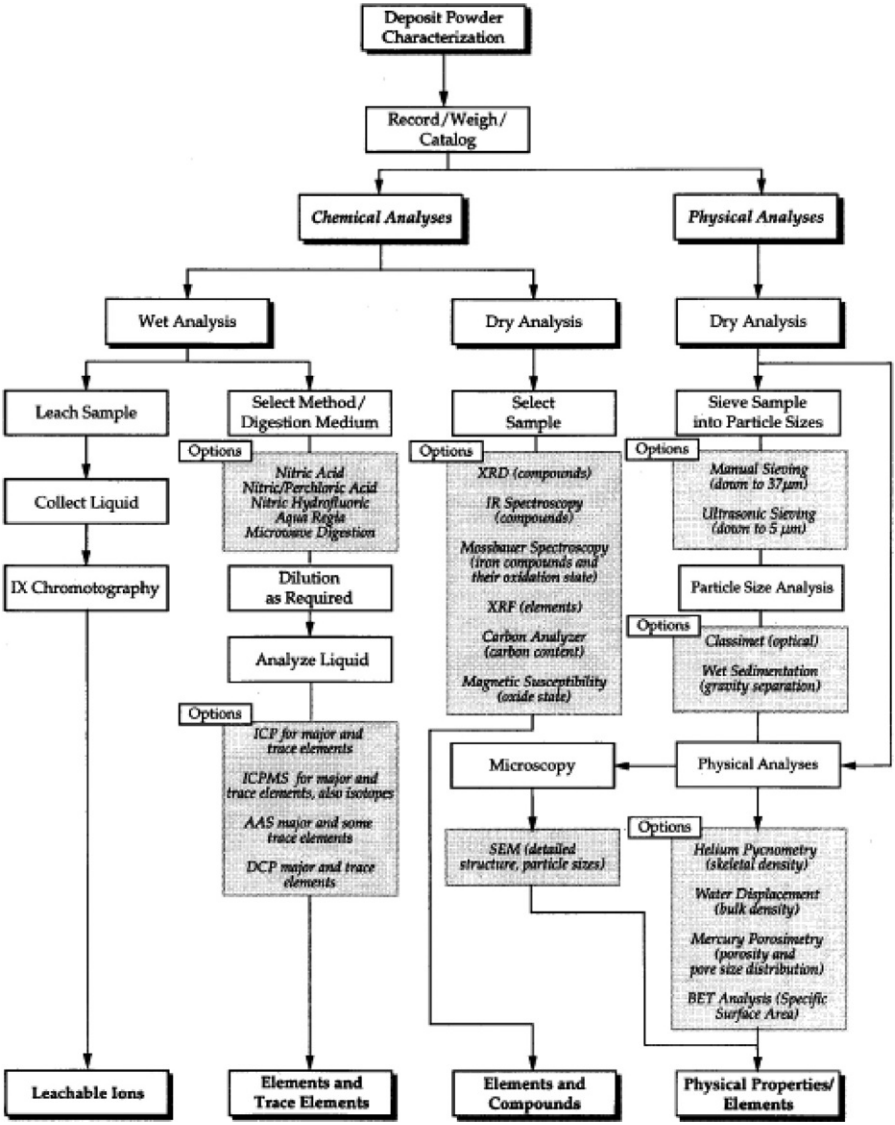

Fig. 11.10 Typical processing of deposit samples for characterization.

The most common techniques used to analyze the deposit samples are:

- Visual observations and segregation/sifting of the samples
- Optical microscopy
- Elemental analysis by inductively coupled plasma spectroscopy (ICP)
- Composition analysis by scanning electron microscopy/energy dispersive spectroscopy (SEM/EDS)
- Compound identification by X-ray diffraction (XRD)

In addition, there are numerous other laboratory techniques that can and have been used by various utilities, research laboratories, and NSSSs to investigate specific properties of deposits. These include, but are not limited to: (1) Mossbauer spectroscopy (iron oxide speciation), (2) pycnometry (bulk and skeletal density), (3) Raman spectroscopy (compound identification), (4) FTIR (compound identification), and (5) ion-exchange chromatography (of water used to leach ionic impurities from the deposits).

The main (most common) techniques listed above are discussed in more detail in the sections below.

11.2.2.1 Visual observations

Upon receipt and drying, samples are typically weighed, inspected, and photographed. Fig. 11.11 shows a typical 25 g sample of deposits collected during a TTS sludge lancing operation. Close inspection of this figure shows a mixture of agglomerations (sometimes called sludge "rocks"), tube scale flakes, TTS collars, and foreign material such as remnants of wire brushes used in plant maintenance.

After photographs are taken, the samples are usually sieved with screens to separate the sample into: (1) finer material (powder that likely had settled to the TTS region), (2) tube scale and TTS collars, and (3) foreign objects (such as the aforementioned brush wires).

Fig. 11.12 shows the appearance of fine powdered deposits separated from the as-received sample.

Of the material present in sample, the two constituents of particular interest to the utilities are: (1) tube scale and (2) hard TTS sludge collars. Figs. 11.13 and 11.14 are examples of the appearance of these materials after separating them from the bulk samples. To distinguish scale from collars, the experience of the analyst plays the greatest role in this task. In general, tube scale pieces are: (1) smaller and thinner (1–6 mils thick) and (2) exhibit distinctive curved shape with the concave inner surface being shiny and the outer convex surface being matte in appearance (typically black as the scale is typically primarily magnetite). The shiny morphology on the inner surface is characteristic of this surface having been previously attached to, but now having spalled from, the smooth SG tubing. The outer surface is matte due to its irregular surface roughness and porosity (see later discussion of cross sectioning of tube scale flakes). Collars, on the other hand, are thicker (up to 100 mils thick or more), exhibit areas that are lighter color, owing to the presence of hardness species such as silica and aluminum compounds. Like tube scale flakes, collars are also curved in shape with an inner (smoother) and rougher (outer) surface.

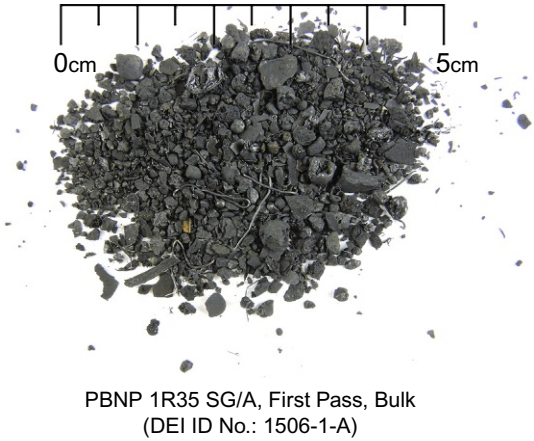

Fig. 11.11 As-received dry deposit sample.
(Courtesy Dominion Engineering, Inc.)

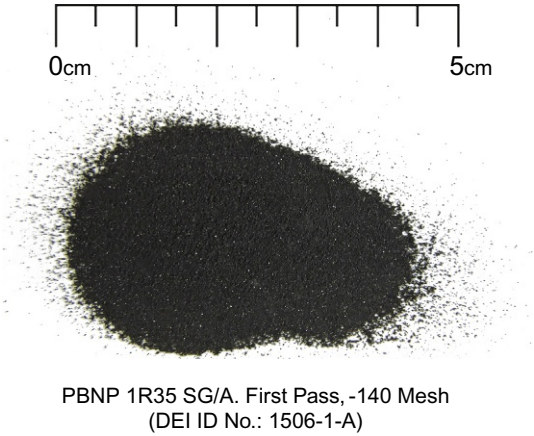

Fig. 11.12 Fine powdered deposits.
(Courtesy Dominion Engineering, Inc.)

11.2.2.2 Optical microscopy and image analysis

Microscopic analysis can be performed on tube scale flakes and TTS collars found in the deposit samples in order to examine and also quantify structural and compositional features. The techniques used to conduct the analysis are cross sectioning followed by optical microscopy and image analysis. These techniques are discussed in detail below.

– *Cross sectioning:* One of the most useful ways to reveal the structure and composition of tube scale and collars is to use cross-sectioning techniques analogous to those used for metallographic examinations. Scale flakes and TTS collars are selected from the deposit sample, mounted in epoxy and polished. These mounts can then be subjected to optical microscopy, image analysis, and SEM/EDS examination.

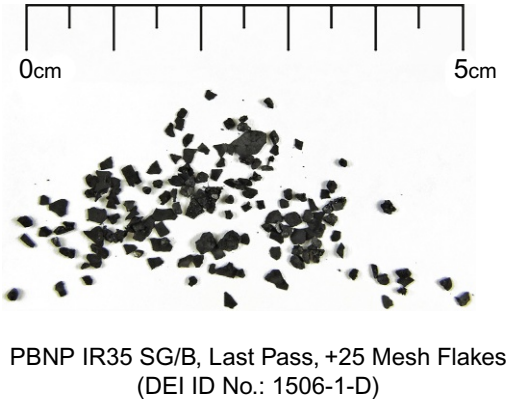

Fig. 11.13 Small tube scale flakes. (Courtesy Dominion Engineering, Inc.)

Fig. 11.14 Hard collar material. (Courtesy Dominion Engineering, Inc.)

- *Optical microscopy:* Optical microscopy images of cross-sectioned deposits are generally taken at medium to high magnification (generally 100–500 ×). Most examinations are performed using bright-field (BF) lighting, which highlights reflective species such as metallic copper. Dark-field (DF) lighting can also be used to reveal optically active species such as silicates and aluminum oxides or hydroxides such as boehmite.
- *Image analysis:* Image analysis is the process of obtaining quantitative information from optical microscopy images. In deposit characterization, image analysis can be used to quantify the following three main characteristics of cross-sectioned deposits:
  - *Porosity:* As discussed previously, tube scale flakes typically contain a significant number of voids or pores. The volume occupied by voids is generally described by a void fraction or porosity, which is a measurement of the net volume fraction occupied by voids within the tube scale structure. Image analysis can be used to obtain a porosity measurement by quantifying the area fraction in the image that is occupied by voids

in cross-sectional view. Standard software routines can be used to make this measurement if there is significant contrast between the voids and the bulk material in the optical photographs. The void fraction is in turn converted to porosity, which is then used to calculate the bulk density of the deposits (e.g., for deposit loading estimates when combined with thickness measurements).

- *Deposit thickness:* Image analysis is often used to determine various distances in a microphotograph by computing the distance in the image relative to an image distance of known length in the actual sample. This is achieved by comparing the length of interest to the known length of a scale bar captured in the optical image. Standard software routines are available to perform the analysis. This data is in turn useful for estimated deposit loading in the SGs, and also to support calculations of heat transfer resistance of the scale (fouling).
- *Phase quantification:* In an optical microscopy image of a cross section of a deposit, various constituents such as magnetite, copper, and zinc oxides will exhibit distinct colors. In this regard, image analysis can be used to provide quantitative information about deposit composition such as percentage copper.

Fig. 11.15 shows a typical optical photomicrograph of a cross section of a tube scale flake. The brighter spots in this cross section are copper metal. The gray phase is magnetite, and the darkest black areas are pores.

Fig. 11.16 is a corresponding image of a TTS collar, with both BF (left side) and DF (right side) images shown. In this case, the right edge of the deposit is the surface that would have been in contact with the tube at the TTS. The bottom flat surface would have been affixed to the tubesheet itself. The BF image shows areas dominated by magnetite, but also small inclusions of foreign objects and other debris. The DF image reveals some optically active areas (white and pink areas) that in this case are silicates and boehmite (γ-AlOOH). This figure can be compared to the illustration shown in Fig. 11.9 for context.

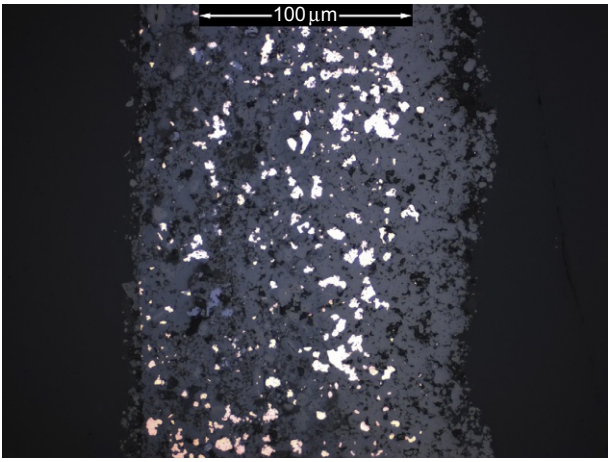

Fig. 11.15 Optical photomicrograph of a tube scale flake (approximate thickness 150 µm). (Courtesy Dominion Engineering, Inc.)

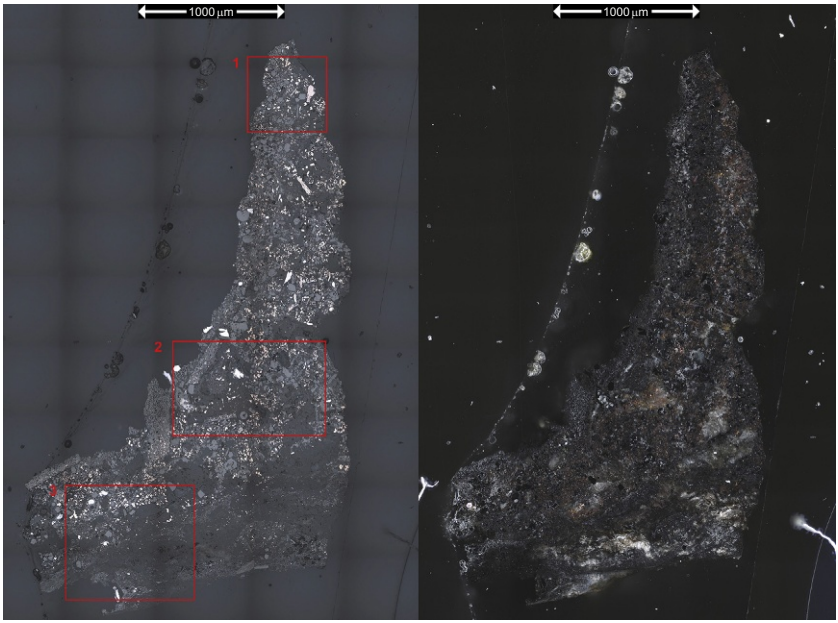

Fig. 11.16 Optical photomicrograph of a TTS collar cross section (approximate width is 3 mm at its base).
(Courtesy Dominion Engineering, Inc.)

11.2.2.3 Elemental analysis by ICP

ICP analysis quantifies the concentration of elements in a solution. This technique is used for analyzing liquid samples, or solids (e.g., deposits) that have been dissolved in a liquid matrix (permitting calculation of the composition of the original solid after adjustment for the matrix composition).

In order to perform ICP analysis on the deposit samples, a small amount of deposit ($\sim$0.1 g) is dissolved in an appropriate acid mixture. Generally, most deposit samples can be dissolved in 10 mL of concentrated nitric/hydrochloric acid solution (aqua regia). Hydrofluoric nitric (i.e., HF-nitric) can also be used if there is a significant ($>$ a few percent) silicates—common in TTS collar deposits. The dissolution is usually performed in a PTFE vessel in a microwave digester. Following dissolution of the deposit sample, the solution is diluted using deionized water. Further dilutions may be made at the time of analysis to bring the concentrations of the elements of interest into the acceptable analysis ranges that can be accommodated by the ICP instrument. This process avoids inadvertent analysis of high elemental concentrations, which can lead to saturation of the ICP detector and inaccurate results. In particular, element-specific dilutions (i.e., different dilutions of the initial solution based on preliminary measurements of elemental concentrations) are made to avoid problems related to saturation. Following analysis with the ICP instrument, the measured concentrations are

corrected by accounting for the composition of the acid solution. The actual composition of the deposit sample is then calculated using assumed oxide forms (e.g., it is assumed that iron is present as magnetite).

11.2.2.4 Scanning electron microscopy/energy dispersive spectroscopy

The SEM is used to examine samples at high magnifications (up to 7000 ×) using a high energy focused beam of electrons. The interactions of electrons with the samples produce secondary electrons, back-scattered electrons, and characteristic X-rays, which subsequently can be detected. The secondary electron detector (SE) and back scatter electron detector (BSE) on SEM provide information about the surface structure and topology of specimen. X-rays are analyzed using EDS in order to obtain detailed information about the chemical composition for a specific spot or area on the specimen. The X-rays released have varying energy levels that depend on the elemental composition of the material. EDS involves the selective sampling of X-rays at different energy levels. The X-ray signal can be measured over a section of the sample for a range of energy levels, generating a correlation between the energy level and the signal strength. Since each energy level corresponds to a specific element in the sample, this spectrum can be used to characterize the elemental composition of the sample, or a small section of the sample, on which the electron beam is focused.

Quantification of the elemental makeup of the sample is performed by deconvolution of the spectrum. This can be performed either automatically or by manually selecting the elements which are of interest.

In order to make the sample electrically conductive, epoxy-mounted cross-sectioned flakes or TTS collars are usually carbon coated prior to SEM/EDS analysis. Flakes, powder, and TTS collars that are not mounted in epoxy can be placed directly in the SEM without coating.

Fig. 11.17, an image taken in an SEM of a tube scale flake, shows the inner smoother surface and the outer porous surface.

Finally, Fig. 11.18 is an example of how EDS dot mapping can be used to assess the distribution of species through the sample. Note that the dot map for carbon corresponds to the epoxy resin used to mount the sample for metallographic polishing.

11.2.2.5 X-ray diffraction

XRD involves bombarding a sample with X-rays and measuring the angle at which those X-rays are diffracted. The angle of diffraction is a function of the fine crystalline structure of the sample. This technique is useful for distinguishing between compounds that have similar chemical formulas but different structures. For example, XRD can be used to distinguish between hematite (Fe_2O_3) and magnetite (Fe_3O_4) (Fig. 11.19).

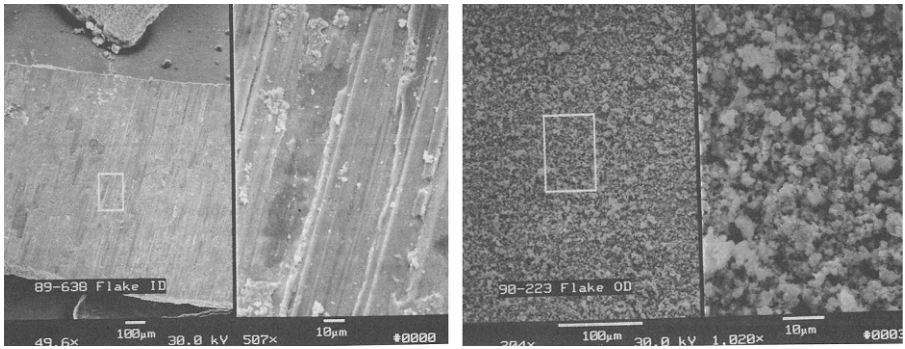

Fig. 11.17 SEM images of tube scale (Varrin, 1996).

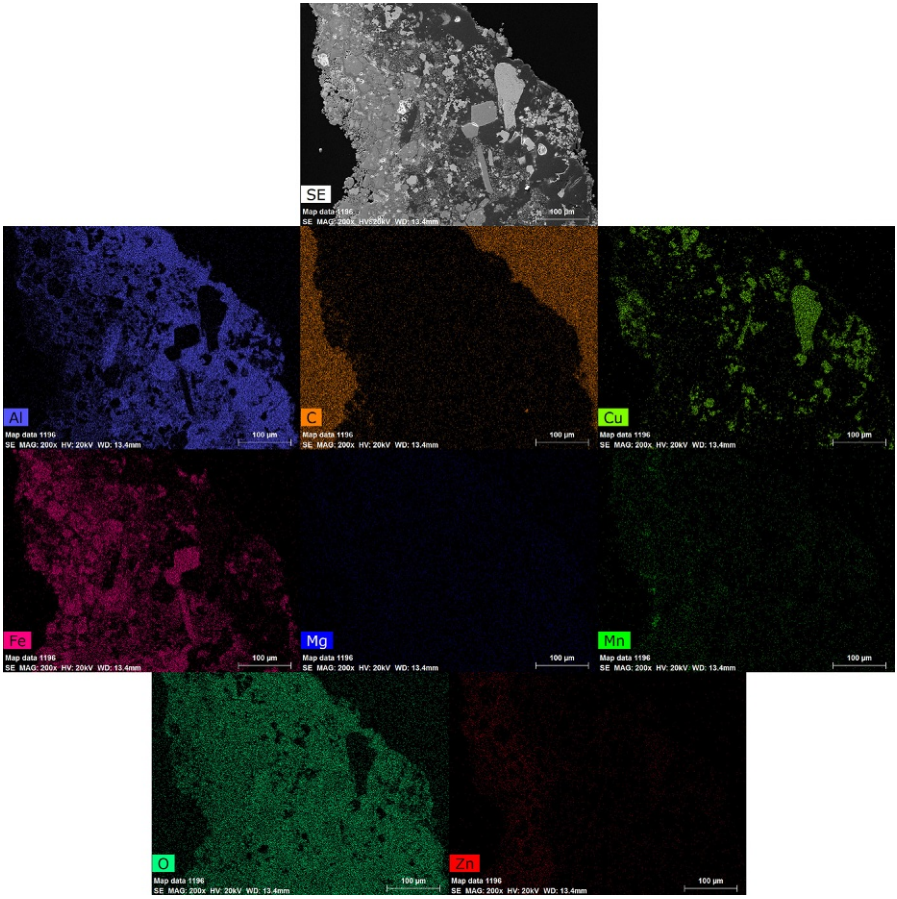

Fig. 11.18 Dot-mapped images of a TTS collar region (Al, Cu, Fe, Mg, Mn, and Zn distributions highlighted).
(Courtesy Dominion Engineering, Inc.)

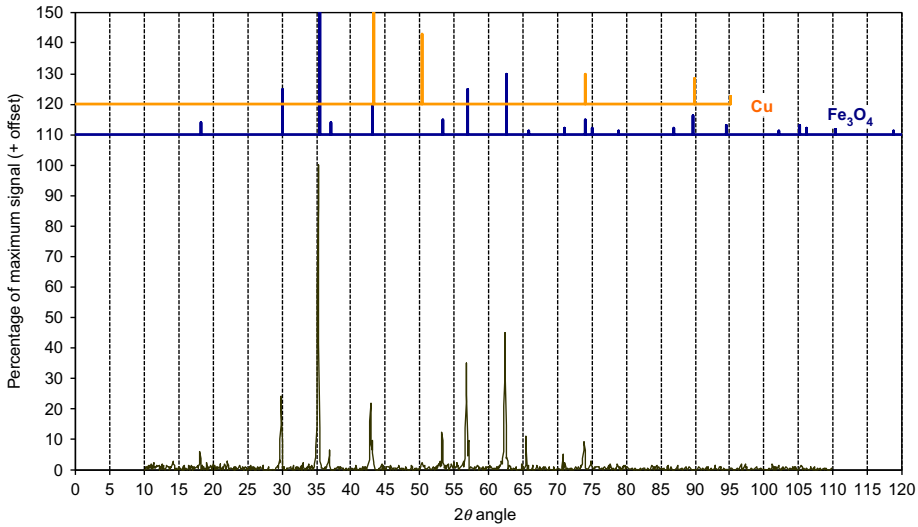

Fig. 11.19 Typical X-ray diffraction pattern for SG deposits showing magnetite and copper phases.
(Courtesy Dominion Engineering, Inc.)

11.3 Deposit management

11.3.1 Overview

As a result of the often undesirable consequences of deposit accumulations (e.g., thermal performance penalties, corrosion, thermal hydraulic instabilities, interference with inspections, etc.), utilities employ a variety of means to periodically remove deposit accumulations from SGs. The specific deposit management activities that are chosen by a utility can include a combination of any or all of the available deposit removal services that are available from vendors. Some deposit removal processes are likely to be used during each and every refueling outage, e.g., tube sheet sludge lancing, while others may only be performed once in the life of the plant, e.g., chemical cleaning.

The approach to deposit management depends first and foremost upon the utility's goals. The goals that often provide a basis for the strategy include:

- Maintain or maximize heat transfer (plant output)
- Reduce risk of secondary side corrosion
- Reduce risk of unwanted thermal hydraulic issues
- Reduce the potential for tube wear and vibration cause by changes in flow patterns or tube fixity conditions

The deposit removal options available to utilities include:

- Mechanical processes for deposit removal
- Chemical cleaning using high concentration cleaning solvents ("hard" chemical cleaning)
- Chemical cleaning using low concentration cleaning solvent ("soft" chemical cleaning)

These methods are discussed in the next sections of this chapter.

11.4 Mechanical cleaning of PWR SGs

11.4.1 Conventional TTS water jet lancing

TTS water jet lancing is a common cleaning processes for RSGs. Also known as "sludge lancing," water jet lancing targets deposits or sludge that has accumulated at the bottom of PWR recirculating type SGs. As discussed earlier, the deposits or sludge on the TTS include: (1) hard consolidated material in the kidney-shaped region of the hot leg and (2) softer powdery sludge that settles on top of the hard deposits and to a lesser extent over the full extent of the tubesheet. Fig. 11.20 shows water jet that are being tested in a partially tubed laboratory mockup.

The overall configuration of equipment used for sludge lancing is shown in Fig. 11.21.

Fig. 11.22 shows one vendor's sludge lancing equipment setup at a handhole. Typical water pressures at the pump range from 1500 to 4500 psi. Actual pressures

Fig. 11.20 Testing of a TTS sludge lancing system.

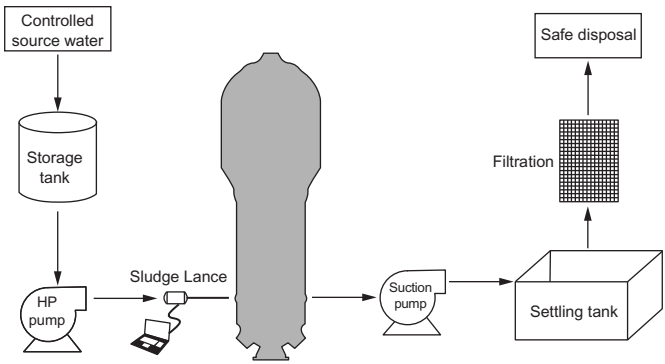

Fig. 11.21 High-pressure water jet lancing system configuration.

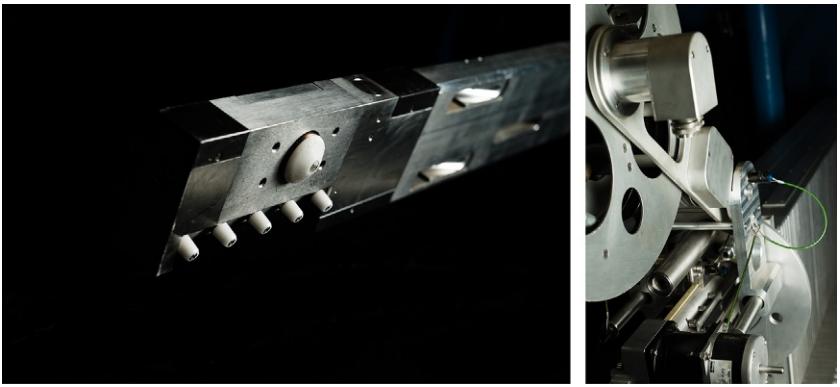

Fig. 11.22 Westinghouse sludge lancing system (handhole equipment on test mockup). (Courtesy Westinghouse Electric Corporation.)

at the nozzles are lower. Total flow rates are on the order of 30 gpm. The jets that remove the deposits are typically 0.035–0.065 in. in diameter at the nozzle, and clean from a distance of a few inches to as much as 100 in. away. The deposits loosened are pushed to the periphery of the tube bundle, where they are collected by suction and filtration systems. The amount of deposit removed from SGs by sludge lancing varies from as little as 25 pounds to as much as several thousand pounds per SG each time the technique is used.

In conventional sludge lancing system, the equipment is mounted to the SGs at secondary side access "handholes" at the TTS elevation, and the cleaning "heads" or nozzles systems are deployed in the blowdown lane or around the periphery of the tube bundle. The cleaning heads are often supported by rails placed along the length of the blowdown lane. In the case of systems that jet from the periphery of the bundle, robotic crawlers are sometimes used to position the water jet deliver system. Total cleaning times vary from plant to plant, but generally the entire process takes between 1 and 2 days per SG.

In addition to high-pressure water jet systems, there are systems that use on low pressure water (<1000 psig) at high flow rates to flush loose deposits from the TTS. Such sludge flush systems are generally simpler from a mechanical design standpoint and can usually remove soft sludge an as little as 8–12 h.

11.4.2 Advanced in-bundle water jet cleaning

While conventional water jet systems spray high pressure water into the tube bundle from outside, there are a number of advanced systems that insert flexible "lances" between the tubes to deliver the water jets directly to the deposit in the interior of the bundle (see Fig. 11.23). The first of these was the Cecil system developed by Foster-Miller, Inc. in the late 1980s under sponsorship of EPRI, ESEERC, and several

Fig. 11.23 In bundle water jet lancing.

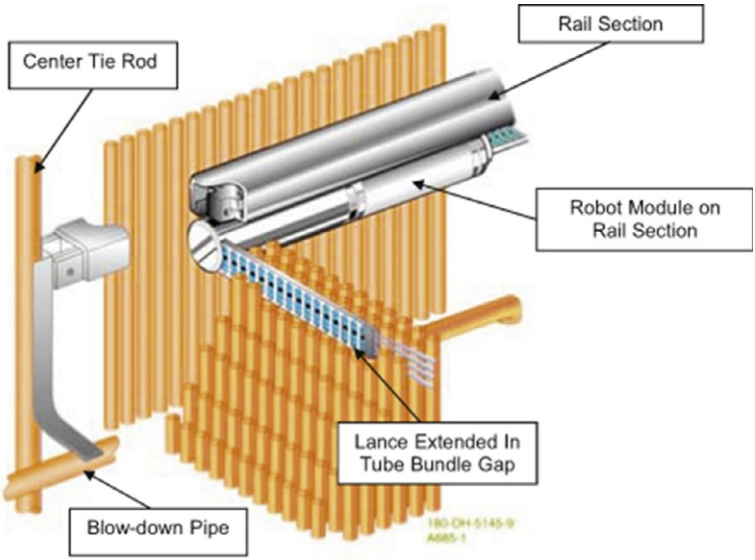

Fig. 11.24 Early CECIL design.
(Courtesy of QinetQ North America 2015.)

US utilities. Cecile systems have since been successfully deployed in the United States, Canada, Korea, and France. Fig. 11.24 shows an early version of a CECIL system. Fig. 11.25 shows a comparable system available from Babcock & Wilcox (B&W).

In addition to the systems that are deployed via the blowdown lane, there are several vendors who offer systems that deliver lances from the bundle annulus. Fig. 11.26 shows one such system.

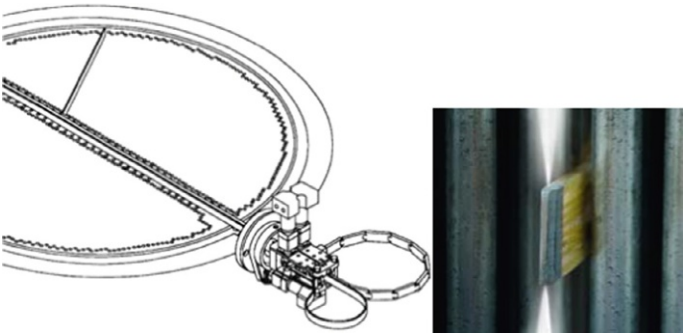

Fig. 11.25 In bundle flexible lance system from B&W. (Courtsey of B&W Canada.)

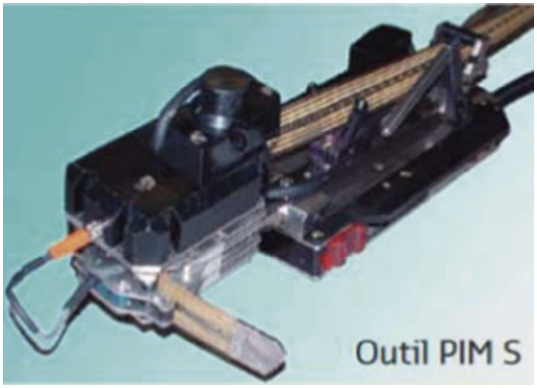

Fig. 11.26 In bundle flexible lancing system deployed from SG bundle periphery.

Finally, in some SG designs, there are access ports at the TTS elevation in addition to the conventional handholes. These access ports, called eye-holes at some plants, have allowed vendors to design and deploy lancing system that go intertube directly from the outside of the SG, as illustrated in Fig. 11.27.

11.4.3 Full bundle mechanical cleaning

Full bundle mechanical cleaning involves extending tube sheet sludge lancing technology to locations higher in the tube bundle. Beginning in the early 1990s, several vendors developed systems that were capable of delivering high pressure water jet cleaning system to the upper bundle of the SGs. Most concepts involved mounting a cleaning fixture on an extensible mast-type deployment system. These systems were quite effective in cleaning deposits from flow passages in broached support plates. However, there use has diminished since about 2000, as more cost-effective chemical cleaning options became available (see later discussion of soft chemical cleaning). An additional disadvantage of the process that it required up to 1 week or more for cleaning the upper support plate regions of a typical RSG.

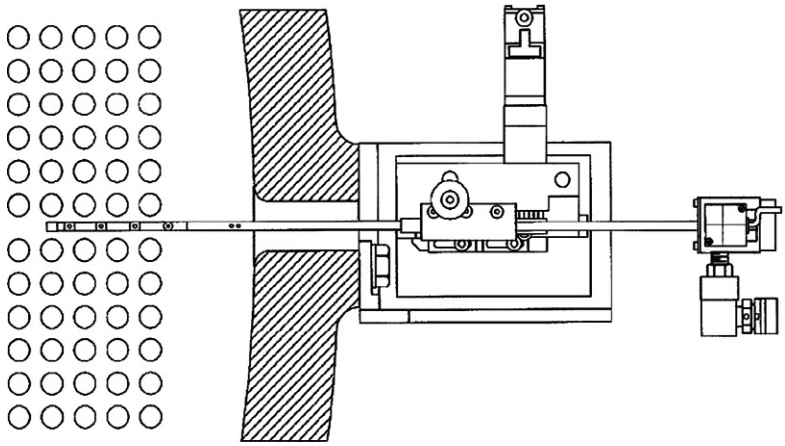

Fig. 11.27 Lance system inserted in-tube from "eye holes".

11.4.4 Pressure pulse cleaning and water slap

In the 1980s, several US plants with OTSGs began experiencing clogging of trefoil broached support plates. This led to increased flow resistance of the steam water flow upward through the bundle and consequence increases in water level in the SG annulus. Rising water level could not be tolerated if the water encroached upon holes in the wrapper known as aspirating ports.

Two remedial measures were used by owners of OTSGs to address this problem. One was chemical cleaning (eventually used at most OTSGS), and water slap cleaning. Water slap cleaning was a process in which bursts of pressurized nitrogen were discharges into the lower regions of the SGs. The water level prior to discharge was held just below the tube supports (Weems and Buford, 1988). The rapid expansion of the nitrogen bubbles pushed the water upward at high velocity where it "slapped" against the TSPs dislodging deposits. Water slap was used at about six plants in the mid-1980s to the early 1990s.

Pressure pulse cleaning (PPC), a process developed by Westinghouse Electric Company, is similar to water slap in principal, which involves underwater expansion of high pressure nitrogen gas charges to dislodge deposits from broached flow passages of RSG tube support plates, and to some extent from tube surfaces. PPC differs in that the pressure of the nitrogen released from the pulsers was significantly higher than that used in the water slap process. At some plants, PPC was combined with chemical cleaning as "chemically enhanced PPC" (Auld et al., 1992).

11.4.5 High volume bundle flushes

In addition to access to the SGs at the TTS level via handholes and other inspection ports, RSGs have larger manways at upper levels above the steam-water separators that allow personnel to gain access to the upper can deck regions of the SGs. This

access allows for water deluge systems known as high volume sludge flushing (HVBF) equipment to be deployed. Tube bundle flushes involve spraying large amounts of low pressure water downward over the top of the tube bundle from the steam-water separator region of the SG. The flow rates can exceed 1000 gpm. HVBF services have been offered by several vendors including Westinghouse and AREVA. Some plants have reported good success at maintaining bundle cleanliness if used routinely in each outage. Other plants have reported little or no deposit removal with HVBF.

11.4.6 Ultrasonic energy cleaning

Ultrasonic energy cleaning (UEC) is a process in which high-powered ultrasonic energy is used to disrupt SG tubesheet deposits (Kaneda et al., 2003). Conceptual designs for full bundle UEC have also been proposed. As ultrasonic energy passes through a fluid (either water or a chemical solution such as ASCA, a soft cleaning solution discussed later in this chapter), acoustic pressure waves cause the bubbles to expand and collapse very quickly, resulting in disruption of SG deposits at surfaces or in sludge piles by cavitation.

UEC is performed when the plant is offline (after plant shutdown). An example system deployment is shown in Fig. 11.28. The typical cleaning sequence involves:

- Installing the transducers through lower hand hole access ports in the SGs. Typically, the transducers are installed in the central no-tube-lane using SG-specific tooling.
- Filling the SG with a cleaning fluid (either water or a cleaning solution such as ASCA or CODE) to ensure that the ultrasonic transducers are submerged. The typical fill height is approximately 18 in. (0.5 m).
- Recirculating the fluid through auxiliary equipment to ensure that temperature and other parameters are controlled within qualified ranges.

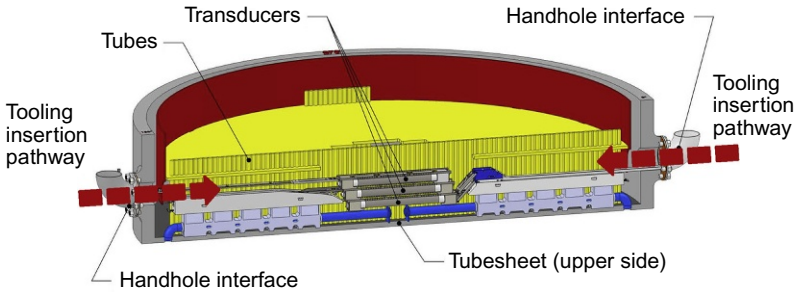

Fig. 11.28 UEC cleaning system deployment.
(Courtesy Dominion Engineering, Inc.)

UEC is usually performed for 12–24 hours. After the cleaning, sludge flushing or sludge lancing is typically perfomed to remove deposuits that have been dislodged and settled to the TTS.

11.5 Chemical cleaning of PWR SGs

11.5.1 Overview

Chemical cleaning involves introducing one or more different chemical solutions into the SGs to dissolve deposits, including iron oxides and copper species (Frenier, 2007). Dissolution of metallic oxides (corrosion products) requires a chemical solution that is chemically "reducing," while copper removal typically requires an "oxidizing" chemical environment. As such, iron oxide removal and copper removal are generally performed with separate cleaning steps. The iron removal process may also include separate steps for removal of the bulk inventory of deposits, and a higher temperature step for cleaning of tight crevices.

Chemical cleaning is a very effective means of deposit removal, historically resulting in the dissolution and removal of as much as 12,000 pounds of deposits from each SG.

Two different types of chemical cleanings are available for PWRs:

11.5.1.1 On-line cleaning

"On-line" cleaning, which can be performed during plant shutdown or startup, involves injection of chemical solutions into the SGs while the plant is in the process of shutting down or starting up. The advantage of on-line cleaning is the potential for reduced schedule impact and overall lower chemical cleaning costs. In on-line cleaning, the heat required to dissolve deposits is supplied by the primary side (decay heat).

11.5.1.2 Off-line cleaning

Off-line cleaning processes are performed during scheduled refueling outages after the plant has been placed in cold shutdown. Off-line processes may or may not affect critical path, depending on the nature of other outage activities.

The principal side-effect of chemical cleaning are the slight corrosion of the carbon and low alloy steel pressure boundary and internal structural materials. The cost of treating, disposing, and storing the chemical cleaning wastes can also be significant.

Fig. 11.29 summarizes the cumulative number of chemical cleanings performed worldwide since 1985 using the two most common process: (1) EPRI/SGOG and (2)AREVA HTCC (Dow, 1994; Gebco Engineering, Inc. & Dominion Engineering, Inc., 1991). Both of these processes are discussed later in this chapter.

11.5.2 EPRI/SGOG process

In the late 1970s PWR operators established a group titled Steam Generator Owner's Group (SGOG) to start a collaborative industry research program managed by the Electric Power Research Institute (EPRI) (Dow, 1994; Jevec and Leedy, 1983;

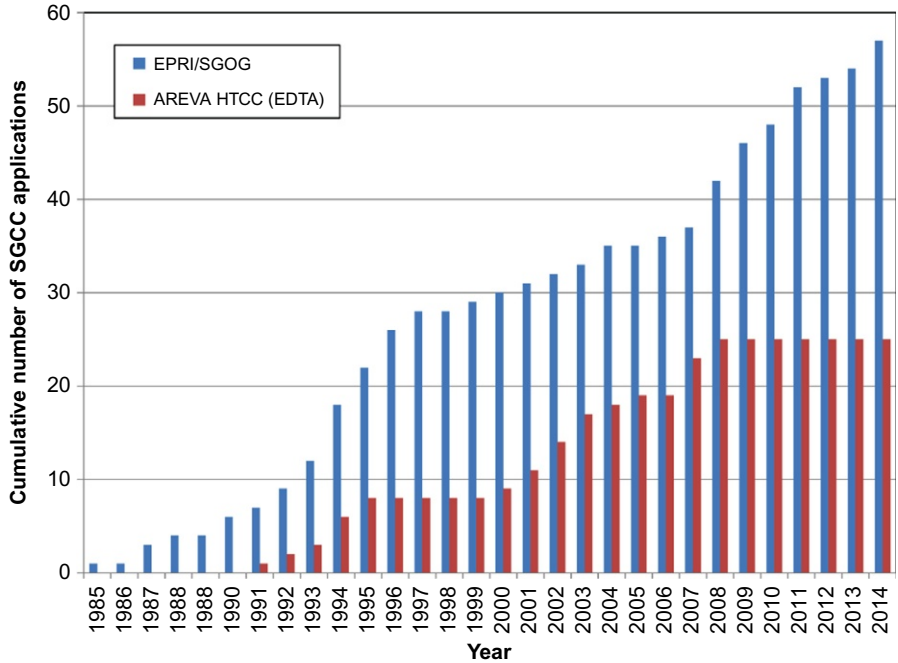

Fig. 11.29 Cumulative number of chemical cleanings performed worldwide.

Schneidmiller and Stiteler, 1983). The goal of the program was to develop a non-proprietary process to chemically remove the corrosion products formed on the secondary side (shell side) of nuclear SGs. The research program's goal was to define the solvents as well as the application techniques required to successfully remove the corrosion products that were distributed throughout the shell side of the SG but also to remove the corrosion products that formed in the tube support plate crevices. All of this cleaning was to be performed with acceptable corrosion on the SG materials of construction (typically less than 10 mils) (Fig. 13.30).

As discussed earlier, the deposits on the secondary side were of particular concern in the 1980s for three main reasons:

- The deposits on the tube surfaces at the often drilled support type-crevices created hide out areas for contaminants that caused corrosion of the Alloy 600 LTMA SG tubes.
- The deposits that built up in the crevice area between the tubes and the early design carbon steel tube support plate (TSP) eventually brought about denting (or squeezing) of the SG tube.
- The deposits that build up on the tubes also resulted in fouling of the steam production of the SG by reducing the heat transfer.

For the above reasons the industry funded a program, managed by EPRI, to develop a low corrosion chemical cleaning process. Not only did the industry need a bulk chemical cleaning process to remove the bulk deposits but also required a process to remove the corrosion deposits in the crevices.

Fig. 11.30 Example of chemical cleaning setup.
Courtesy Westinghouse Electric Company, Inc.

11.5.2.1 Corrosion allowances

Prior to perform a SG chemical cleaning, calculations are performed to determine the maximum corrosion allowance of the SG tube support plates and other critical components or materials used in the construction of the SG. As the area of the tube support plate in contact with the SG tube is corroded, the gap between the tube and tube support plate would increase. If the gap becomes too large the SG tube could be destabilized during power operation resulting in damage to the tube (wear) and therefore loss of capacity of the SG. The crevice area is typically one of the most critical corrosion tolerances. Some weld material can also be identified as a critical tolerance.

11.5.2.2 Corrosion monitoring

During a chemical cleaning, actual corrosion of SG components cannot be measured. However, the corrosiveness of the bulk solvents can be monitored with corrosion probes using galvanic and free corrosion monitoring systems. Generally, only the iron dissolution step in a chemical cleaning processes is corrosive. The copper step causes little or no corrosion.

Mockups of the tubes and TSPs have occasionally been used during the cleaning applications to provide corrosion values following the cleaning, but real-time or in-line corrosion is used to monitor the progression of the cleaning.

When monitoring the corrosion of the carbon steel while cleaning, the initial instantaneous corrosion rates can be very high during the injection of the chemical cleaning solution. This high instantaneous corrosion rate is due to the fracturing of the magnetite corrosion products into ferric (Fe^{+3}) ion and ferrous (Fe^{+2}) ions. The ferric ion will react with the iron in the carbon steel to generate ferrous ions.

$$Fe^{+3} + Fe \rightarrow 2Fe^{+2}$$

The ferric concentration will be the highest upon the injection of the chemical cleaning solution, which drives the equation above to the right resulting in high instantaneous corrosion of the carbon steel. This rate reduces rapidly with time; however the process engineer must monitor the total corrosion while the chemicals are in contact with the SG.

11.5.2.3 Deposit characterization and deposit loading estimates

Prior to performing a chemical cleaning a characterization of the SG deposits is usually be performed. This characterization includes an analysis of the corrosion products as well as a determination of the quantity of deposits in the SG. Care must be taken when determining the analysis of the corrosion products. Typically, the corrosion film obtained for analysis is sludge from the top of the tube sheet or sludge removed by sludge lancing (high-pressure water cleaning of the tube sheet). This sludge may be primarily powder and therefore is a very small percent of the total sludge in the generator and is typically from the lower bundle of the SG. The process engineer must not overestimate some of the minimum constituents in the corrosion film, such as copper. However, there must be enough chemical on-site to remove the deposits in the SG during the chemical cleaning.

An assessment must also be performed of the quantity of deposits in the SG. This quantitative analysis is typically performed by using an average concentration of the deposits in the feedwater during operation. Knowing the feedwater flow rate, the total time of the flow and the concentration of material in the feedwater, the total quantity of material transported into the SG can be calculated. By knowing the corrosion rate of materials in the SG and the length of time the material was exposed to operating conditions the total amount of corrosion material can be determined. By adding the amount of deposit formed in the SG with the amount of deposit transported to the SG the total SG loading can be determined. Knowing the total volume of the SGs, the volume of the cleaning equipment, total quantity of deposit, and type of deposit the correct quantity of chemicals can be purchased.

Prior to a chemical cleaning deposits should be obtained from the specific SGs that will be cleaned. These deposits should be placed in a test facility where the expected process should be applied to the deposits with the expected concentration of solvents vs the expected deposit loading in the SG. This test will provide confidence that the selected process will be successful in dissolving the deposit loading in the SG as well as providing some information on the expected corrosion that may be encountered during the cleaning.

11.5.3 Chemical cleaning solvent chemistries

This section discusses the EPRI-Steam Generator Owners Group solvents (EPRI/SGOG) as well as solvent development by Kraftwerk Union (now AREVA NP, GmbH) (Dow, 1994; Gebco Engineering, Inc. & Dominion Engineering, Inc., 1991). Other groups have developed chemical cleaning solvents with various degrees of success. Information on these solvents can be found in reference.

Several different chemistries are required to completely clean a nuclear SG. The different chemistries dissolve deposits in different areas or different types of deposits. One chemistry is utilized to remove the bulk deposits, another chemistry is utilized to remove the deposits in the crevice region, and finally a different chemistry is utilized to remove copper deposits. This report will discuss all of these chemistries and how they remove the targeted deposits.

All SG-cleaning solvents must meet the following criteria:

- Have acceptable total corrosion, especially in the tube-to-tube support crevice and the solvent must not impact subsequent operations
- Must not be proprietary
- Be applicable for both OTSGs and RSGs
- Efficiently remove all the deposits, including copper deposits, throughout the SG including those in crevices between the tube and the tube support plate leaving no harmful residuals behind

11.5.4 EPRI/SGOG solvents

This section describes the composition of the EPRI/SGOG magnetite solvent, the crevice solvent, the copper solvent, and the passivation solvent. The magnetite solvent is for the dissolution of the bulk deposit. The crevice solution attacks the deposit that is located in the crevice between the tube and the tube support plate. The crevice solution needs some mechanical help in order to replenish the solvent in the crevice area. The copper step dissolves and removes the copper deposits while the passivation step, which is applied after the copper step, puts a small oxide coating on all of the bare carbon steel surfaces in order to reduce the corrosion of the carbon steel during the following startup and operation.

All of the chemical steps are not required for each SG cleaning. The process engineer must identify the goal of the cleaning and design the cleaning steps in order to achieve the goal.

11.5.4.1 Magnetite solvent

The magnetite solvent is composed of the following chemicals:

EDTA	100–250 g/L (10%–25% by weight)
Hydrazine	1% by weight
CCI-801 inhibitor	0.5%–2.5% by volume (5–25 mL/L)
pH	7 adjusted with NH_4OH
Temperature	190–205°F (88–96°C)

These parameters were only finalized after many beaker tests followed by potboiler tests. The pH was selected after the testing of several more acidic solutions. The resultant pH was a compromise of dissolution rate vs the carbon steel corrosion in the SG. Most processes that employ chelates (EDTA) typically require temperatures approaching boiling in order to achieve an acceptable rate of dissolution. How the temperature is achieved will be discussed in a later section.

11.5.4.2 Crevice solvent

The crevice step, which is utilized to dissolve the deposit in the SG crevices, has the following composition:

EDTA	200 g to 250 g/L (20%–25% by weight)
CCI-801 inhibitor	1.0%–2.5% by weight
pH	6–6.2 adjusted with NH_4OH
Temperature	245–255°F (118–124°C)

High temperature is required to allow venting of the SG through the SG pressure relief valve. The boiling results in the expulsion of the depleted solvent in the crevice so that the crevice can be replenished with fresh crevice solvent that has dissolution capability remaining. The venting process will be discussed later on a section on heating and venting SGs.

11.5.4.3 Copper solvent

The copper solvent is employed to remove the copper deposits in the SG and has the following composition.

EDTA	50–100 g/L (5%–10% by weight)
Hydrogen peroxide	2%–3% percent by weight
pH	9.5 (initially adjusted to 7 with NH_4OH then brought to 9.5 with ethylenediamine (EDA))
Temperature	90–110°F (32–43°C)

11.5.4.4 Passivation solvent

As stated earlier the passivation step is utilized to leave the exposed carbon steel in the SG with a "protective" coating on the surface to reduce the corrosion of the carbon steel during startup and initial operation prior to the buildup of the normal operational corrosion film layer. The passivation step is composed of the following:

Hydrazine	0.03% by weight
pH	10 adjusted with NH_4OH
Temperature	195–205°F (91–96°C)
Time	8–10 hours within specification

The generic EPRI/SGOG process was developed and qualified for a well-defined range of application conditions. Any major deviation from these conditions should be specifically qualified in a major test vehicle similar to those used in this qualification program. Plant-specific testing should be done before cleaning to verify process effectiveness and to confirm acceptable corrosion with plant materials of construction. It is recommended that actual plant sludges be used for this testing whenever possible.

11.5.5 EPRI/SGOG process application

The EPRI/SGOG process is utilized to remove the maximum quantity of bulk deposits as well as removing the maximum quantity of corrosion products in the SG crevice area. If a secondary side inspection is performed prior to the cleaning the deposit location in the SG as well as the blockage of the crevices can be determined. Denting of the tubes can be determined from eddy current testing. If denting is not determined by eddy current testing and a visual inspection indicates that the crevices are clear a crevice step can be avoided.

A simplified P&ID for an EPRI/SGOG system is shown in Fig. 11.31. Note that tanks are required for each solvent and depending upon the chosen process the mixing tanks can be utilized for waste tanks if they are not required for further mixing of chemicals.

The amount of EDTA required for the bulk chemical cleaning will be governed by the amount of deposits calculated to be in the SG. For every mole of iron, the process requires 1 mol of EDTA. The other ingredients will not change, only the EDTA. Due to the molecular weight of EDTA and iron, the process requires 5.2 g of EDTA for every gram of iron to be removed. An excess of EDTA must be utilized to act as a driving for the dissolution reaction.

The crevice step EDTA concentration does not change since there is a fixed amount of iron in the crevice area.

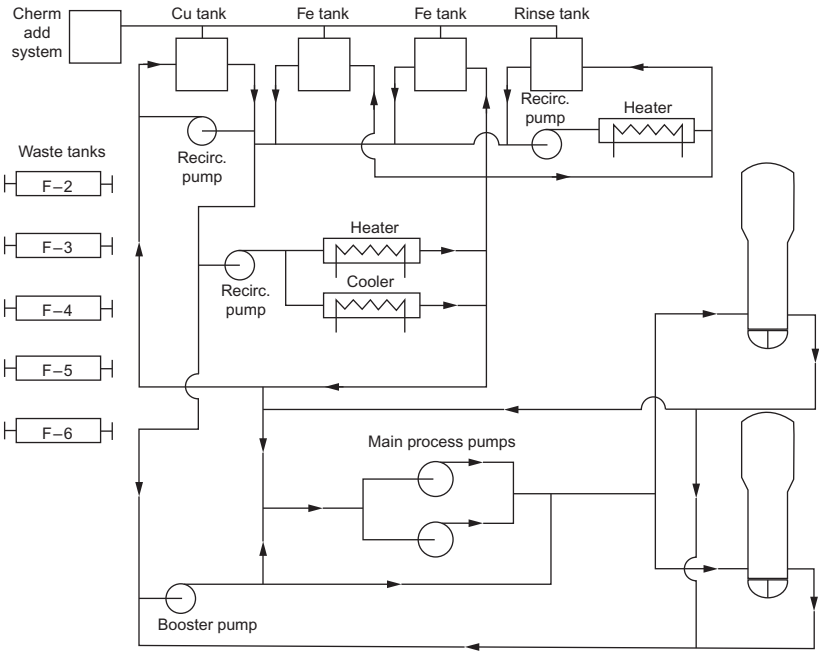

Fig. 11.31 Simplified P&ID for EPRI/SGOG process.

Flow is important to replenish the solvents in order to dissolve the corrosion products. Flow is achieved either by recirculation of the solvent on the shell side of the SG or by filling and draining the SG. The filling and draining technique was typically utilized for OTSGs. For typical bulk cleaning the recirculation method has typically been utilized. This recirculation of the chemical cleaning solvents while continuously heating the solvent between 195 and 205°F resulted in bringing fresh chemical cleaning chemicals to all of the bulk deposits. Unfortunately this recirculation, or bulk cleaning, did not generate significant flow though the tube support plate—SG tube crevice. A high temperature step is required so that the SG relief valves can be opened in order to generate boiling in the SG which resulted in the displacement of the depleted chemical cleaning solvent in the crevice regions to be replenished with solvent that still had dissolution capacity remaining. The depth of boiling in the SG is important for crevice cleaning. If the process engineer overfills the SG the boiling may not be achieved in the lower crevices.

The next step is to select a method for heating the chemicals. The process can utilize either plant heat or external heat. The plant typically determines the method of applying the heat and the time allowed to perform the cleaning during the outage. At least part of the cleaning if not the entire cleaning is on critical path.

If external heat is applied the solvent is heated in external tanks, and then the SG is set up to recirculate the solvent or fill and drain the SG on a regular frequency. If external heat is applied to heat the solvent when the checkout rinse is performed the SG must be heated slowly since there is a requirement that most SGs can only be heated at a rate of 50°/hour. All SG injections must be careful not to exceed a rate of heating or cooling to 50°/hour. Once the checkout rinse is performed and the SG is heated the other steps must be injected, so the rate of temperature range stays within the validation rate in the operational procedure.

More than one bulk iron step or copper step can be performed in the chemical cleaning process. The maximum concentration of EDTA that should be applied in any step is approximately 250 g/L. If more iron is deposited in the SG than can be removed by one iron step, a second step can and should be applied. The step must be applied within the total corrosion allowance determined prior to the start of the actual chemical cleaning.

The equipment required for an EPRI/SGOG process and a large number of other chemical cleaning processes requires a number of tanks, heaters, and pumps. The number of tanks required depends upon the cleaning process, the size (volume) of the SGs, and the size (volume) of the tanks.

11.5.6 KWU/AREVA NP Gmbh chemical cleaning process

In the early 2000s, AREVA NP SA purchased KWU from Siemens, and thus the KWU high-temperature process was renamed as the AREVA NP GmbH high-temperature process. This high-temperature iron removal process is teamed with a low-temperature copper removal process. This process requires plant heat to reach the temperatures required for the process.

Fig. 11.32 shows a simplified P&ID for a KWU/AREVA HTCC process.

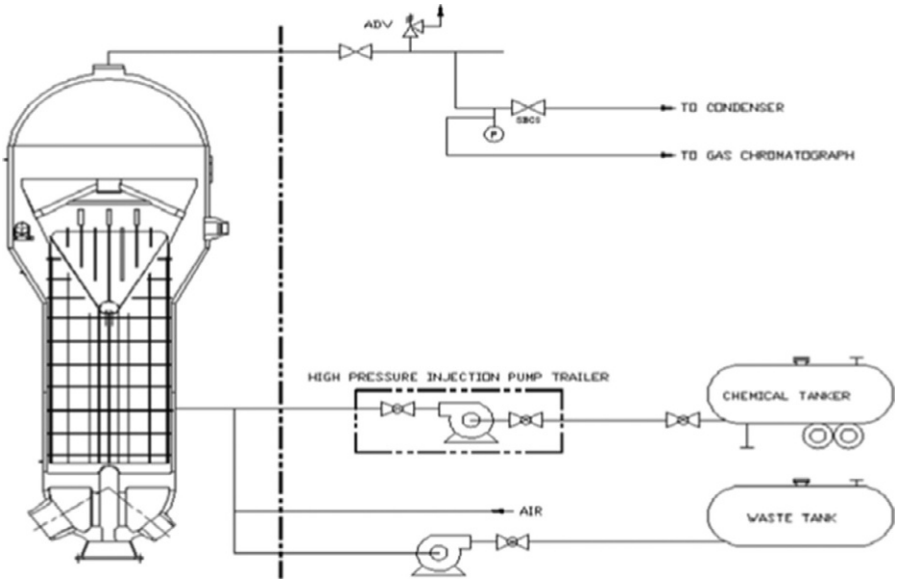

Fig. 11.32 Simplified P&ID for KWU/AREVA process (Dow, 1994).

This process requires temperatures above 250°F for the kinetics to perform at a reasonable rate. The plant-specific temperature should be determined during the qualification program which utilizes specific plant sludge, not simulant sludge. Due to the high temperature applied with this process excess chelant (EDTA) is not required, the high temperature drives the EDTA complex to completion without excess EDTA as in the lower-temperature processes. Once the iron solvent has reacted with the iron oxides it is exhausted and is reported to be essentially benign to the materials of construction.

Operationally the iron solvent is injected to three or four levels in the SG. After each injection the SG is vented and the hydrogen to nitrogen ratio is measured. This ratio gives the process engineer-specific information regarding the success of the process. With this information they may make changes regarding the next injection. The AREVA NP GmbH process simultaneously cleans the bulk deposits as well as the crevice deposits.

11.5.7 High-temperature iron step chemistry

The composition of the AREVA NP GmbH high-temperature process is presented below:

EDTA	90–250 g/L (9%–25% by weight)
Hydrazine	1%–10% by weight
CCI-801 inhibitor	No additional inhibitor
pH	8–10 adjusted with NH_4OH
Temperature	284–392°F (140–200°C)

Copper step: The copper step is composed of the following chemicals:

EDA	10–100 g/L (1%–10% by weight)
Ammonia based	$(NH_4)2CO_3$ amount used is proprietary
pH	9–11 (adjusted with NH_4OH)
Temperature	68–158°F (20–70°C)

Air is utilized to sparge the SG, mixing the solution as well as adding an oxidant to the mixture. This oxidant will oxidize the copper metal to cupric ion, which will then be chelated to the EDA.

11.6 Mild cleaning of PWR SGs

11.6.1 Overview

Since the development of EPRI/SGOG and other SG cleaning processes most SGs in the United States have been replaced with new materials of construction. Water chemistries have also been improved and while deposits still get transported into SGs secondary side the quantity has been reduced. Nuclear utilities have also substantially reduced their outage duration. Thus, new processes needed to be developed that would reduce the time, cost, and complications of an EPRI/SGOG type chemical cleaning (Fig. 11.33).

AREVA NP Inc. and Dominion Engineering Inc. both developed dilute or soft chemical cleaning processes utilizing totally different chelating agents to remove

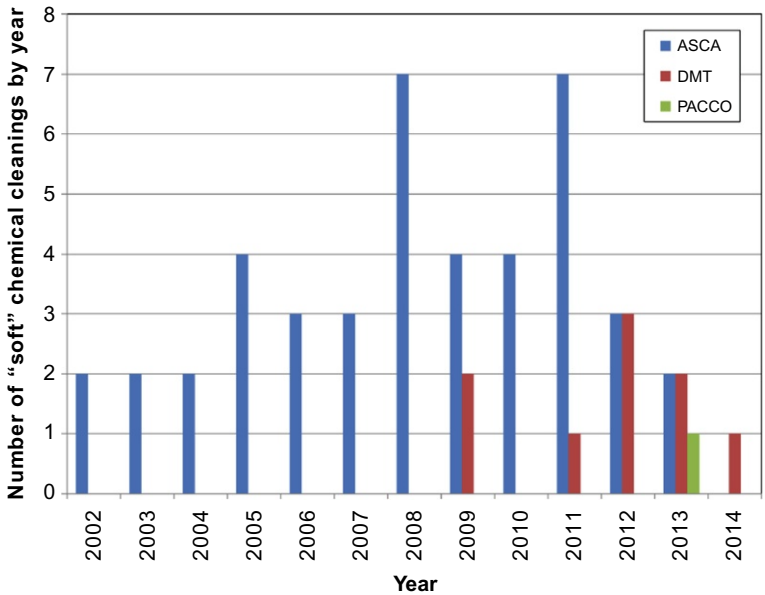

Fig. 11.33 Soft chemical cleaning applications by type (2002–2014).

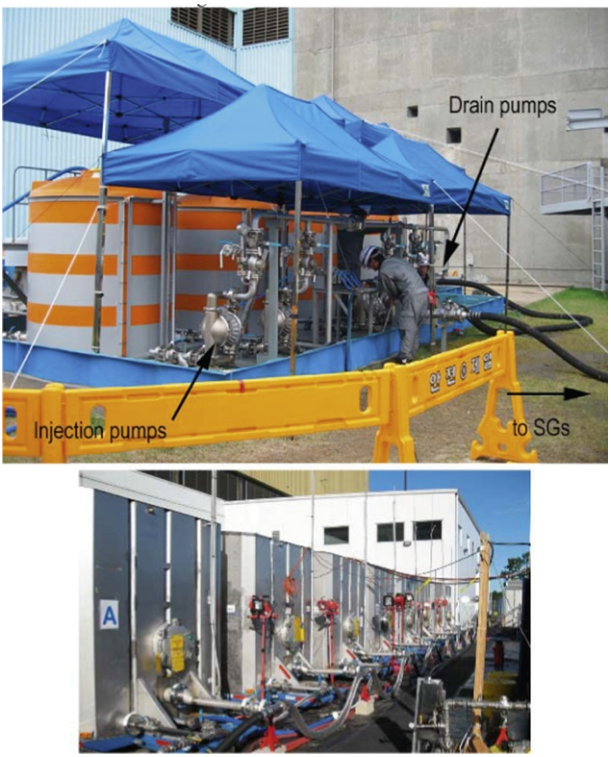

Fig. 11.34 Typical advanced scale conditioning agent setup.
Courtesy Dominion Engineering, Inc.

the iron deposits. AREVA's process uses oxalic acid as the main chelant in their process while Dominion Engineering's process utilizes EDTA as its main ingredient (Little et al., 2014; Alley et al., 2014). Each process is patented and results in minimal corrosion of the SG materials of construction (Fig. 13.34).

These processes are both applied at 95°C and are designed for bulk cleaning. These processes result in minimal cleaning of the tube–tube support plate crevices (Fig. 11.35).

Both of these dilute chemical cleaning approaches were develop to achieve many of the same benefits of the EPRI/SGOG type cleaning at a much lower cost and with simpler equipment. In particular these processes offer a cost-effective method for addressing upper bundle deposit accumulations. Full bundle applications have resulted in deposit removal of up to 2300 pounds per SG.

These dilute chemical cleanings can improve the efficiency of the SGs by:

- Improving the heat transfer efficiency as identified by steam pressure increases
- Reducing the TSP clogging (opening of the tube to tube support plate crevices)
- Removal of deleterious species such as copper and lead
- ASCA has also identified the softening and partial removal of hard TTS sludge

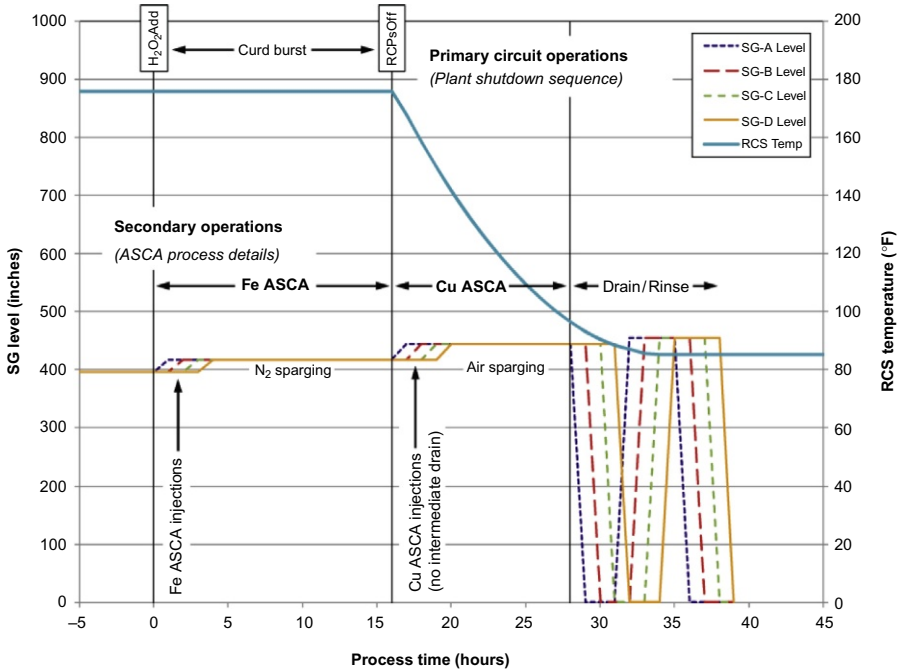

Fig. 11.35 Example application strategy for ASCA process (Little et al., 2014).

Sludge lancing should be performed at the end of either of these processes since the processes dissolve and loosen the upper bundle deposits which result in a rain-down of the deposits to the tube sheet. These rain-down deposits can easily be removed by top of tubesheet sludge lancing. This loose deposit can be 10% or more of the total removed deposits.

During a chemical cleaning, sampling is performed at regular intervals. The main species required to control and monitor the process is iron. Iron should be monitored during the process, and the process needs to be terminated either when the solution is saturated or the increase in iron concentration changes by only a few percent.

11.6.2 Waste processing

Both dilute processes generate reduced amounts of waste compared to EPRI/SGOG type higher concentration processes. The ASCA process treats its waste volume through reverse osmosis, which substantially reduces the volume of the waste volume. The remaining concentrated waste can be absorbed and transported to an industrial landfill, or it can be shipped for further treatment and disposal to a commercial facility.

The DMT process is treated on site with a proprietary method after which the resultant waste volume is passed through a filter followed by mixed bed ion-exchange resin

(Alley et al., 2014). The only waste resulting from the DMT process is ion-exchange resin and several filter cartridges or filter bags. The liquid volume is "pure" water and can be utilized for SG layup volume.

The dilute chemical cleaning processes continue to evolve as they are utilized more. There is a process in the research laboratory called CODE, which has been developed to remove the hard deposits on the top of the SG tube sheet. The CODE process has been designed to remove the oxides of aluminum and silicon that are elements of the hard deposits that form around SG tubes at the top of the tube sheets. This process has not been applied commercially but has shown success in autoclave testing.

Both processes are testing an increase in the concentration of the proprietary chemicals without significantly increasing the corrosion rate during the cleaning which will result in more deposit removal. It is expected that research will continue on these proprietary processes to improve their application that will help to maintain SGs in optimum operating conditions.

References

Alley, M., Jones, D., Evans, S., 2014. Deposit minimization treatment at Robinson Nuclear Plant. Presented at EPRI Steam Generator Secondary Side Management Conference, Baltimore MD.

Auld, G.D., et al., 1992. Chemical cleaning method for steam generators utilizing pressure pulsing. US Patent 5,154,197.

Berry, W.E., Diegel, R.B., 1979. Survey of corrosion product transport and deposition in light water reactors. Electric Power Research Institute, EPRI Report NP-522 (www.epri.com).

Dahlheimer, J.A., et al., 1984. The Westinghouse pressurized water reactor nuclear power plant. Westinghouse Electric Corporation, Water Reactors Division, Pittsburgh, PA.

Dow Jr., B.L., 1994. Utility experience with steam generator chemical cleaning. Electric Power Research Institute, EPRI Report TR-104553.

Frenier, W.W., 2007. Technology for chemical cleaning of industrial equipment. NACE International – The Corrosion Society.

Gebco Engineering, Inc. & Dominion Engineering, Inc., 1991. Guidelines for design of PWR steam generator chemical cleaning systems. Electric Power Research Institute, EPRI Report NP-7384.

Jevec, J.M., Leedy, W.S., 1983. Chemical cleaning solvent and process testing. Electric Power Research Institute, EPRI Report NP-2976.

Kaneda, S., et al., 2003. Ultrasonic Cleaning Method. US Patent 6,572,709.

Little, M., McCree, A., Varrin Jr., R., Pellman, A., Kreider, M., 2014. Advanced scale conditioning agent (ASCA) applications: 2014 experience update, paper no. 10104. In: Presented at NPC 2014 Sapporo: Nuclear Plant Chemistry Conference, Sapporo, Japan.

Schneidmiller, D., Stiteler, D., 1983. Steam Generator Chemical Cleaning Process Development. Electric Power Research Institute, EPRI Report NP-3009.

Varrin Jr., R., 1996. Characterization of PWR steam generator deposits. Electric Power Research Institute, EPRI Report TR-106048 (www.epri.com).

Weems, S., Buford, A., 1988. Water slap steam generator cleaning method. US patent 4,756,770.

This page intentionally left blank

Thermal performance degradation and heat-transfer fouling

12

M. Kreider, G. White
Dominion Engineering, Inc., Reston, VA, United States

12.1 Introduction

12.1.1 Definition of SG thermal performance degradation

As with any heat exchanger, the function of a nuclear steam generator (SG) is compromised by operational changes that increase the resistance to heat transfer between the primary and secondary fluids, lowering the efficiency and leading to thermal performance degradation. Regardless of the underlying causes, which are discussed later in this chapter, it is useful to first specify a working definition for SG thermal performance degradation. For the purposes of this chapter, the definition introduced in a 1996 conference paper on the subject (White et al., 1996) is considered appropriate:

> *Thermal performance degradation can refer to a decrease in SG outlet pressure and/or thermal power, which can be caused by three different [types of] sources:*
>
> - *Decrease in overall tube bundle heat-transfer coefficient,*
> - *other sources within the SG shell, and*
> - *external sources.*

This definition, originally written for pressurized water reactors (PWRs), may be expanded to include increases in reactor inlet header temperature (RIHT) for CANDU units. The remainder of this chapter presents information concerning methods used to quantify this type of performance degradation, the underlying causes, industry experience, plant operational consequences, and the observed effects of fouling remediation techniques.

12.1.2 Background

The thermal-hydraulic designs for SGs typically incorporate an explicit thermal margin to accommodate some level of accumulated heat-transfer fouling, loss in tube surface area as a result of tube plugging, or a combination of both. Early SG designs often included margins in excess of 200 μh-ft^2-°F/Btu (1 μh-ft^2-°F/Btu = 1.76E-04 m^2-K/kW)—a value roughly equivalent to a secondary flow margin of more than 5%. However, as SG vendors sought to improve the thermal capacity of their designs

Steam Generators for Nuclear Power Plants. http://dx.doi.org/10.1016/B978-0-08-100894-2.00014-5
© 2017 Elsevier Ltd. All rights reserved.

in the 1970s and 1980s, margins were reduced, commonly to values of 50–100 μh-ft^2-°F/Btu (roughly 1%–2% on a flow basis). In addition, many plant operators during the last 20 years have implemented thermal power uprates (to boost unit output) or primary temperature reductions (to reduce component corrosion risks) or both. These changes have in many cases decreased operating thermal margins to low levels (~1%), even absent appreciable heat-transfer fouling or losses of tube surface area. In one respect, this is a desirable operating condition that maximizes the thermal capability of the SGs. On the other hand, however, a large fraction of PWR SGs can tolerate only modest decreases in thermal efficiency or tube area before the unit output is compromised (absent other compensating measures).

Beginning in the late 1980s to early 1990s, these reduced margins—coupled with thermal performance decreases that depressed operating PWR SG steam pressures—threatened the ability of several units to generate the rated plant output. As reported in Kreider et al. (2009), such pressure losses commonly reached 10–30 psi (0.07–0.21 MPa) and in some cases exceeded 50 psi (0.34 MPa). US industry evaluations of this issue date to at least the early to mid-1990s (e.g., see EPRI, 1991; Steam Generator Pressure Loss Survey 95-016, 1996).

12.1.3 Objectives

Commercial PWR and CANDU units incorporate a variety of SG types, including both vertical and horizontal recirculating designs, which convert roughly 20%–40% of the liquid passing through the tube bundle to steam, and once-through designs, which convert essentially 100%. This chapter focuses on the thermal performance characteristics of the predominant SG type in use in Western commercial PWR and CANDU nuclear units: the recirculating SG with a vertically oriented tube bundle. Particular emphasis is placed on how SG thermal performance changes during the lifetime of the SG as a result of deposit-induced fouling and other phenomena. Accordingly, it provides a specialized treatment with more in-depth information than can be covered in a general heat-exchanger fouling text (e.g., Bott, 1995).

The primary topics covered in the chapter are:

- Methods for quantifying thermal performance changes in recirculating SGs (Section 12.2).
- Observed industry trends in heat-transfer fouling as reflected by variation in the SG fouling factor (FF) (Section 12.3).
- Causes of SG thermal performance changes (Section 12.4).
- Consequences associated with SG thermal performance degradation (Section 12.5).
- Effects of SG deposit-removal techniques on SG thermal efficiency (Section 12.6).

12.2 Quantifying SG heat-transfer fouling

An accurate quantitative description of the heat-transfer characteristics within recirculating SGs requires detailed three-dimensional two-phase models. Numerous computer codes that reflect implementations of such models have been developed during the last several decades, including EPRI's ATHOS and Triton (EPRI, 1986, 2008a,

2015a), AECL's THIRST (Campagna et al., 1994; Pietralik et al., 1998), Babcock & Wilcox's CIRC (Klarner et al., 1998), and EDF's THYC (Tincq et al., 1994), among others. Although the advanced three-dimensional models implemented with these codes predict the global heat-exchanger performance levels as reflected by the output steam pressure (or the RIHT, as applicable), such models are perhaps more often used to evaluate specific technical concerns than to assess changes in thermal performance level. Examples include the potential for flow-induced vibration (FIV) in some SG designs (see, e.g., EPRI, 2008b, 2010), the degradation of tube lattice-bar ("eggcrate") supports in another SG design [the original San Onofre SGs (NUREG/CR-6754 and BNL-NUREG-52646, 2001)], and enhanced corrosion product deposition and/or component corrosion in localized regions (e.g., upper tube bundle locations in the original Palo Verde SGs per Sweeney et al., 1994), among others.

The original 1985 publication of the EPRI Steam Generator Reference Book, an industry compendium of SG-related technical issues facing nuclear operators (EPRI, 1985), included a chapter on the thermal-hydraulics of SGs. This chapter focused on computer codes of the type referenced in the above paragraph. However, these modeling efforts generally did not address trends in the global heat-transfer behavior of SGs throughout the life cycle of the component. This approach is understandable given the extensive problems with SG material integrity coupled with generally adequate thermal margins characteristic of early SG designs. However, the issue took on increased importance by the 1990s as margins for new units declined and some operating SGs began to exhibit appreciable to substantial net losses in thermal efficiency.

12.2.1 Candidate methods

In addition to a detailed thermal-hydraulic analysis specific to the SG design in question, a number of other approaches can be used to evaluate the SG thermal performance level and its changes over time. As listed in White et al. (1996), alternatives to a three-dimensional SG thermal-hydraulic model include analysis of trends in the following parameters:

- Measured SG steam pressure.
- Measured SG steam pressure, adjusted for variations in primary temperature.
- Calculated heat-transfer effectiveness (NTU approach).
- Global SG FF (i.e., thermal resistance change[1]), where the FF (R_f'') is defined according to the equations below, and where Q is the thermal power transferred from the primary fluid to the secondary fluid, U is the global heat-transfer coefficient, A is the effective (usually OD) tube bundle heat-transfer area, T_{hot} is the flow-averaged primary hot-leg (SG inlet) fluid temperature, T_{cold} is the analogous cold-leg temperature, T_{sat} is the average saturated steam

[1] The fouling factor is not actually a factor, but rather a change in thermal resistance. Thus, the authors consider the term "thermal resistance" (or "change in thermal resistance") to be a better description of this quantity. However, due to its common use in the literature, it is retained in this chapter for continuity and in order to avoid ambiguity.

temperature on the SG secondary side, p_{sat} is the corresponding steam pressure, and R'' is the area-based overall thermal resistance (see Chapter 11 in Incropera and DeWitt (1985) or equivalent text for derivation):

$$Q = \frac{UA(T_{hot} - T_{cold})}{\ln\left(\frac{T_{hot} - T_{sat}(p_{sat})}{T_{cold} - T_{sat}(p_{sat})}\right)} \tag{12.1}$$

$$R''_f = \Delta R'' = R'' - R''_0 = \frac{1}{U} - \frac{1}{U_0} \tag{12.2}$$

Application of the overall heat-transfer equation to a U-tube SG requires a few assumptions as described in detail on p. 4-18ff. in EPRI TR-106048 (EPRI, 1996). Two of these are not strictly satisfied due to changes in the specific heat of the fluid and local overall heat-transfer coefficient resulting from the onset of boiling low in the tube bundle. However, these approximations are judged reasonable given that the secondary boundary-layer resistance is a small fraction of the total thermal resistance (order 10%) and in view of the estimated secondary fluid spatial temperature distribution as illustrated (to scale for one SG design) in Fig. 4-1 of EPRI (1998a)) (see also Fig. 12.1).

12.2.2 Selection of the global fouling factor/thermal resistance

12.2.2.1 Advantages

Of the candidate methods, the SG FF represents the best balance between utility and practicality for evaluating time-varying trends in recirculating SGs. As alluded to in

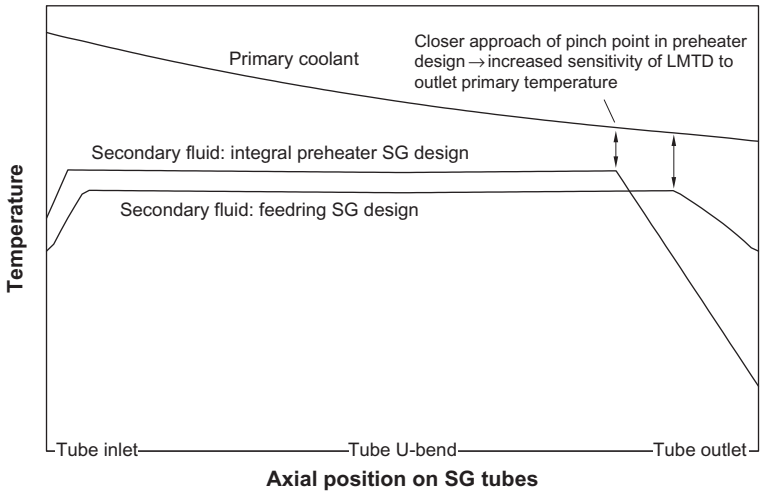

Fig. 12.1 Primary and secondary fluid temperature variations in recirculating SGs.

prior publications (e.g., White, 2001), there are several benefits of using the FF relative to one or more of the alternatives. These include the following:

- All of the necessary inputs for calculating the FF are routinely measured at frequent intervals (many times per day) and recorded in plant computer systems. In contrast, three-dimensional models require many additional quantities that are not typically measured, such as those characterizing spatial distributions of flow and temperature. Consequently, estimates of these additional inputs must be generated or assumed in order to implement the detailed models.
- The method inherently accounts for variations in applied primary temperature, thermal power, and heat-transfer area (e.g., due to tube plugging). Such variations—which to first order have no causal connection to changes in SG thermal efficiency—commonly have an appreciable influence on simpler metrics such as steam pressure readings.
- The physical units associated with thermal resistance facilitate direct comparisons among the SGs at different plants. Such comparisons are more difficult with metrics such as the steam pressure (which can range from 700 to 1100 psi (4.8–7.6 MPa) for different plants) and also with output of three-dimensional thermal-hydraulic models for SGs that reflect substantially different designs.
- Thermal resistance changes may also be directly compared with the properties of tube deposit layers that can be determined independently through theoretical analysis or laboratory measurement.

12.2.2.2 Drawbacks/cautions

On the other hand, care must be taken to address the following issues when using the FF to evaluate SG thermal performance trends:

- Calculated values are subject to uncertainty from a number of independent sources. Any conclusions derived from an analysis based on FF trends must therefore be tempered accordingly. This caution is not unique to the FF but applies to all candidate methods listed earlier (see Section 12.4).
- Computed changes in the FF cannot distinguish among root causes that similarly influence the underlying plant instrument readings. For example, changes resulting from tube-surface heat-transfer fouling can be mimicked by the increased pressure drop associated with deposit-induced clogging of steam separation equipment.
- In a similar fashion, FFs cannot distinguish between fouling-induced changes in the heat-transfer coefficient and those resulting from changes in thermal-hydraulic conditions, such as changes in primary fluid velocity due to tube plugging and variations in the boiling heat-transfer efficiency caused by changes in the recirculation ratio.
- As noted earlier, calculated FFs do not quantify the effects of variations in downcomer subcooling, which affect the true mean temperature difference as well as the distribution of secondary-side heat-transfer coefficients. Based on evaluations completed by the authors for individual utilities, the effects of subcooling variations and changes in thermal-hydraulic conditions (above bullet) are typically small.
- For the minority of units with integral preheaters (economizers), the FF method does not address issues specific to this type of design, such as fouling of preheater baffle plates and the inherent disparity in the meaning of the log-mean temperature difference (LMTD) for preheater SGs compared to feedring designs. Regarding this latter point, note that the LMTD as calculated for preheater SGs is more sensitive to variations in the SG inlet

(cold-leg) temperature due to the onset of boiling higher in the tube bundle as illustrated in Fig. 12.1 (see also pp. 4-5 and 4-6 in EPRI (1998a) for expanded discussion). Nevertheless, the FF method can still be used to reasonably characterize the fouling behavior of preheater-type SGs, albeit with a somewhat higher degree of uncertainty.

- As a global parameter, the FF does not quantify the beneficial effects associated with non-uniform fouling when compared to uniform fouling with the same spatial average. Specifically, more heat is transferred through local regions marked by lower levels of heat-transfer fouling, and less heat is transferred through heavily fouled regions (see Section 12.4.6.3).

12.2.2.3 Industry application

FF evaluations of the SGs at dozens of commercial nuclear units have been completed since the early 1990s, demonstrating the utility of the method. These assessments include a number of graphical FF trends reported in EPRI TR-7524 (EPRI, 1991), five detailed thermal performance case studies in the late 1990s documented in EPRI TR-110018 (EPRI, 1998a), analyses of the startup performance for multiple replacement SG designs conducted in 2003 (Kreider et al., 2003), and additional FF evaluations for the operating histories of various other units as summarized in conference publications and industry studies (Kreider et al., 1997a,b, 1998a; EPRI, 2015b). An overview and statistical evaluation of industry experience based in part on these collective results was published in 2009 (Kreider et al., 2009)—see Section 12.3.3 for further information.

12.2.3 Determining historical FF changes and trends

Although the FF method relies on a single straightforward equation, determining an accurate picture of the past heat-transfer fouling trend at a particular unit is in practice complicated by multiple factors:

- Calculated FF values are subject to inherent scatter as a result of normal fluctuations in the underlying plant instrument readings. As a result, monthly or yearly values are in general insufficient for reliably characterizing the fouling behavior in a typical SG.
- Routine outages and thermal power reductions commonly produce a sharp but transient change in the calculated FF, with the magnitude of the transient effect gradually declining during subsequent operation. These postoutage FF transients apparently have little impact on the long-term fouling behavior of the SGs but can have a sizable short-term effect on the SG thermal margin. This subject is treated in more depth in Section 12.3.2.
- Systematic measurement errors of several types can produce misleading results. See Section 12.4.6 for further discussion.
- Fouling behavior occurring during an initial period—usually a few months to a few years—after startup with clean SGs is often marked by rapid changes in the FF that can be difficult to quantify accurately (see Section 12.2.4).
- Asymmetries among the individual secondary loops can lead to differing fouling behavior among the SGs at a given unit—though this is normally a minor factor.
- Use of the FF as a de facto metric for heat-transfer fouling of the tube surfaces is subject to bias errors associated with confounding causes of SG thermal performance changes (see Section 12.4).

Complete thermal performance evaluations must address each of these issues appropriately on a unit-specific basis.

Example FF histories for the SGs at three different units are shown, respectively, in Figs. 12.2–12.4. In all cases, the curves reflect the trend in the FF average computed for all of the SGs at the subject unit. The effects of scatter in the instrument readings (largely unbiased noise) and postoutage transients (sharp upward spikes followed by

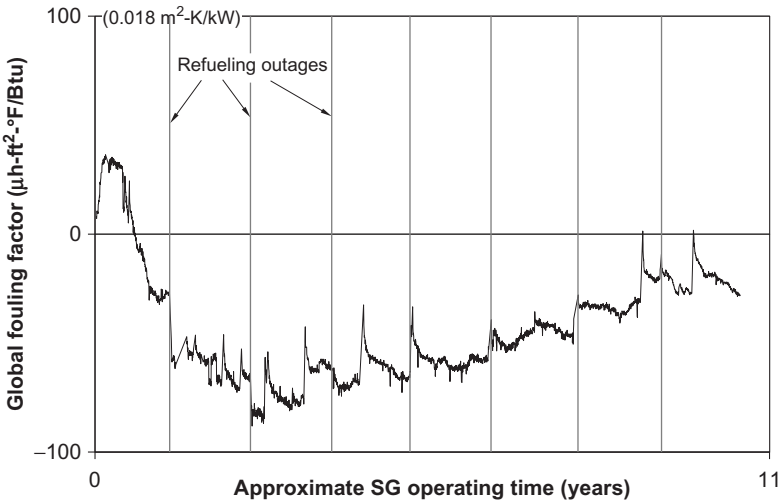

Fig. 12.2 Example recirculating SG FF history: Plant A.

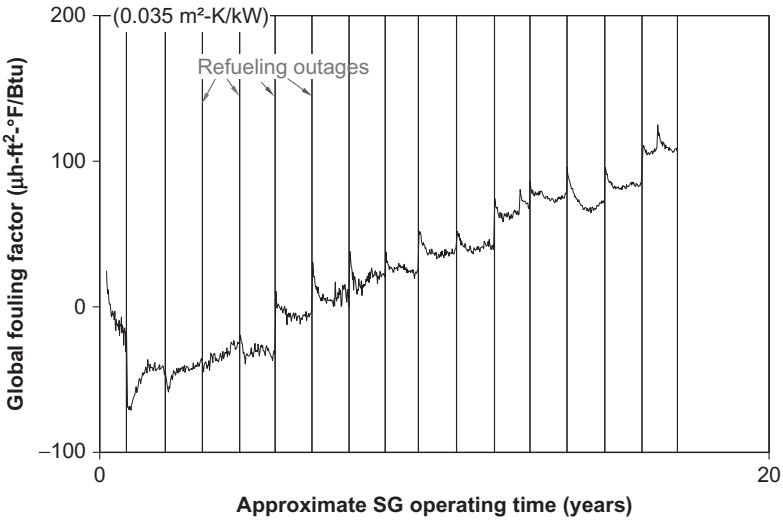

Fig. 12.3 Example recirculating SG FF history: Plant B.

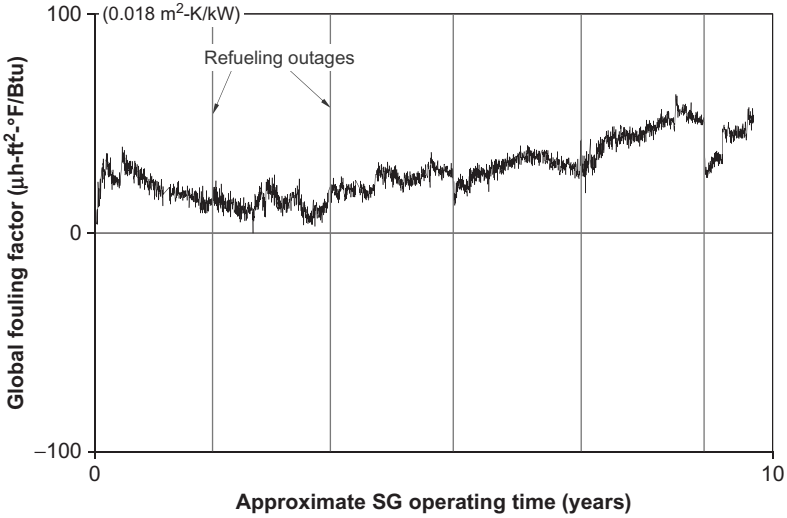

Fig. 12.4 Example recirculating SG FF history: Plant C.

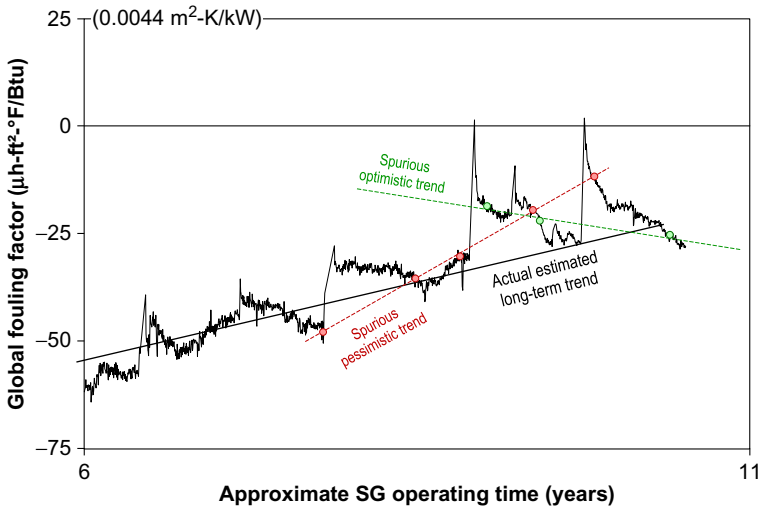

Fig. 12.5 Examples of erroneous fouling rates inferred from infrequent FF values.

gradual declines) are visible in each plot and vary noticeably in magnitude and character from one unit to another. As illustrated in Fig. 12.5—which depicts a portion of the FF history for Plant A—use of a limited number of calculated FF values can lead to substantial errors in estimating the long-term heat-transfer fouling trend. The levels of SG fouling observed among many units in the industry and the associated root causes are addressed in Sections 12.3 and 12.4.

12.2.4 Baseline clean performance level

In order to properly interpret a calculated FF history, quantification of the thermal resistance baseline characteristic of initial clean SG operation is required. Accurate determination of the heat-transfer effects of tube deposit layers—and the potential effects of fouling remediation through cleaning techniques (see Section 12.6)—is strongly dependent on the baseline resistance value. Up to three different sources may be used in a given case:

- *Thermal-hydraulic design*. The SG vendor's thermal design calculations include a specified clean thermal resistance level which is typically based on the results of a three-dimensional code analysis (Section 12.2.1). However, this value is subject to errors associated with the heat-transfer correlations used in the code as well as potential biases due to actual tube wall thicknesses and thermal conductivities that can deviate from nominal values.
- *Industry experience*. Reliable clean SG FF values computed for units with identically designed SGs can serve as a proxy for estimating the clean baseline resistance. However, these estimates, like those based on vendor calculations, are subject to errors associated with unit-specific variations in tube wall thickness and thermal conductivity.
- *Unit-specific calculation*. A baseline value may be determined through FF calculations for the subject unit that reflect operation with clean SGs at prototypical plant operating conditions. Ideally, these calculations reflect initial SG operation (e.g., very early commercial operation or warranty testing), but they may also be performed following complete tube-surface cleaning (e.g., following full-bundle chemical cleaning; see Section 12.6).

Provided that plant instrument data are available from early in the SG operating lifetime (typically within the first few weeks or months), the most accurate of these methods is unit-specific calculation. However, two factors can complicate the use of clean resistance estimates based on early-life FF values: (1) clean SG operation is often marked by a sharp FF increase which may obscure the actual clean baseline if it is not well characterized (see Section 12.3.1.1) and (2) fully clean SG conditions may not apply during initial full-power operation due to prior operation at zero power or reduced power for a period of weeks to months, during which unquantified changes in the heat-transfer coefficient (e.g., due to deposit fouling) can develop.

12.3 Industry trends in SG thermal performance

12.3.1 Idealized thermal resistance curve

Based on the authors' assessments of more than 50 different units, representing approximately 20 SG designs, some common characteristics of SG FF behavior have been observed. These characteristics, which were previously described in Kreider et al. (2009), are illustrated in the idealized curve shown in Fig. 12.6. The three main stages labeled in the figure are clearly identifiable in the actual plant FF histories shown in Figs. 12.2 and 12.4; each stage is discussed further below.

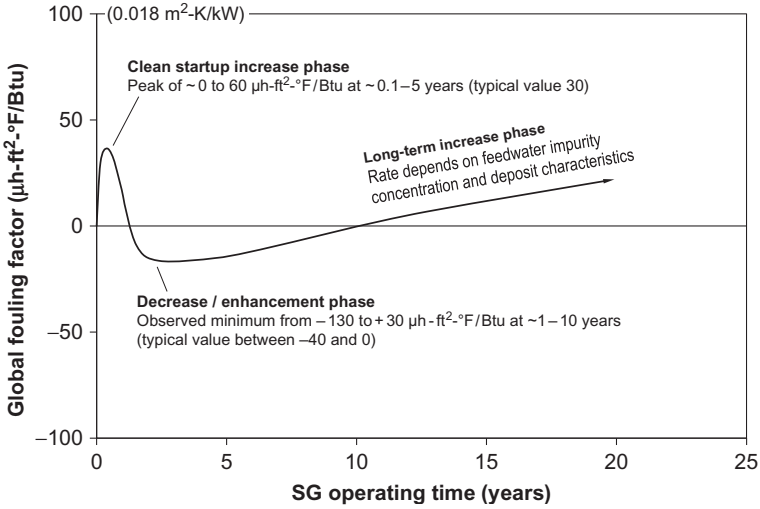

Fig. 12.6 Idealized typical SG fouling factor curve: 1980s–2010s.

12.3.1.1 Phase 1: Clean startup increase

As documented in a 2009 industry conference paper (Kreider et al., 2009), the FF trend for a majority of recirculating SGs includes a sharp increase following initial clean SG operation that reaches a local peak value. Fig. 10 in Kreider et al. (2009) illustrates this pattern for more than a dozen different PWR units, and subsequent analysis of other units since 2009 by the authors has produced results consistent with the pattern. The cause (or causes) of this behavior has not been established. However, based on the discussion in Section 2.4 of Kreider et al. (2009), two points should be noted regarding the underlying phenomenon:

- The magnitude of the increase (averaging 30 µh-ft^2-°F/Btu) is generally much larger than can plausibly be explained by a thermally insulating iron oxide tube scale layer given the limited corrosion product mass transported to the SGs during the relevant operating period and the thermal properties of the deposit constituents.
- The working hypothesis concerning the root cause is that crystallization deposition and/or dissolution of very small quantities of soluble species lead to relatively small decreases (~5%) in the boiling heat-transfer coefficient relative to that applicable for nominally clean SG tubing. This hypothesis was initially proposed by Hu in the 1990s [see Hu, 1997, 1998, 2003, 2006 and the related references (Hospeti and Mesler, 1965; Jamialahmadi and Müller-Steinhagen, 1991, 1993)].

12.3.1.2 Phase 2: Decrease/enhancement

After the conclusion of Phase 1, the following period—typically several months to several years—is marked by a declining trend in the calculated FF. The magnitude of this decrease varies considerably from one unit to another, with some exhibiting almost no change (near-constant FF trend) and others displaying a substantial decrease

to a level more than 150 μh-ft^2-°F/Btu below the peak reached in Phase 1 (representing a flow margin increase of roughly 3%). The primary underlying cause of the FF decrease which marks Phase 2 has been known for nearly 50 years (Macbeth, 1971): an improvement in the heat-transfer coefficient resulting from wick boiling and an increased number of boiling nucleation sites. Further discussion of these phenomena is included in various sources, including EPRI (1991, 1996), Duncan et al. (1997), Pan et al. (1985), and Uhle (1997). See also Section 12.4.1.1 for discussion related to the structure of enhancing tube scale.

12.3.1.3 Phase 3: Long-term increase

Upon reaching a minimum value, the FF at most PWR units begins to increase again, though typically much more gradually than in Phase 1. Prevailing fouling rates during this phase, as measured over several years or more, have typically ranged from 1 to 5 μh-ft^2-°F/Btu per year for the units evaluated by the authors (see Fig. 4 in Kreider et al., 2009). This long-term rate is strongly influenced by the average rate at which iron oxide, the primary constituent of fouling layers, is transported to the SGs. Phase 3 fouling reflects gradual thickening and densification (also termed consolidation or ripening) of the scale layers present on the tube surfaces (see Section 12.4.1.1).

12.3.1.4 Time scale of phase transitions

As indicated in Fig. 12.6, the durations of the three fouling phases generally have been observed to fall within the following approximate ranges:

- Phase 1: 0.1–5 SG operating years.
- Phase 2: 1–10 SG operating years.
- Phase 3: All operation after Phase 2.

As noted in Section 2.4 of Kreider et al. (2009), at least some of the variation in these time scales likely depends on the concentration in the feedwater of the particulates and soluble species which form the tube scale layers, although no systematic evaluation of this hypothesis is known to have been performed.

12.3.2 Postoutage thermal performance transients

The trends discussed in Section 12.3.1 all apply to the smoothed, average behavior of the FF. However, as illustrated clearly in Figs. 12.2 and 12.3, the large majority (if not all) commercial SGs at some point exhibit sharp, transient changes in the calculated FF following plant outages and thermal power reductions. These FF transients have been identified and described since at least the 1980s and are documented in a number of sources (Kreider et al., 2009, 2014; EPRI, 1991, 1998a; Baum, 1996). Accumulated experience with this phenomenon is summarized below:

- In most cases, these transients are marked by an instantaneous FF increase, typically of 10–30 μh-ft^2-°F/Btu, followed by a declining-rate decrease during subsequent weeks to months of continuous plant operation, with the decrease partially or fully offsetting the initial

sharp increase. For PWRs, which control the primary temperature, the FF increase is generally accompanied by a steam pressure decrease. (For CANDU units, which control the steam pressure, the increase in FF is accompanied by a transient increase in the RIHT.) Each occurrence follows restart after a plant outage or upon resumption of full-power operation after a significant power reduction. A typical example is shown in Fig. 12.7.

- Of various candidate causes, the working hypothesis for the sharp transient FF increases shown in Fig. 12.7 is partial exfoliation of secondary scale layers from a small fraction of the tube surface area induced by differential thermal expansion stresses and accompanied by steam blanketing. The gradual FF decreases are believed to reflect complete exfoliation of the partially detached scale during subsequent operation, with the complete detachment occurring at a distribution of times depending on the location as a result of interactions with the secondary flow. This hypothesis, first proposed by Allen Baum in 1996 (Baum, 1996), is illustrated on Slides 9 and 10 in Kreider et al. (2014) and was quantitatively analyzed in Appendix B of EPRI TR-110018 (EPRI, 1998a), demonstrating that it is reasonably plausible. Further detailed discussion regarding this hypothesis and alternatives considered less likely is included in Section 2.5 of Kreider et al. (2009).
- As indicated on Slide 12 of Kreider et al. (2014), variations in the net change following a transient—for example, the increase of 20–15 = 5 μh-ft^2-°F/Btu illustrated in Fig. 12.7—are thought to reflect differences in the collective thermal properties of the scale which is exfoliating. Although net increases in the fouling factor are more common, both increases and decreases have routinely been observed.
- A minority of postoutage transients—less than 10%—reflect changes in the opposite direction: a sharp negative change in the FF followed by a gradual declining-rate increase during subsequent operation. These negative transients most often occur within the first few operating years after clean SG startup (Kreider et al., 2014), though they have also been observed on a few occasions after implementation of online polymeric dispersant addition for SG fouling control [see Section 4.5.4.4 of EPRI 3002005416 (EPRI, 2015b)]. Early

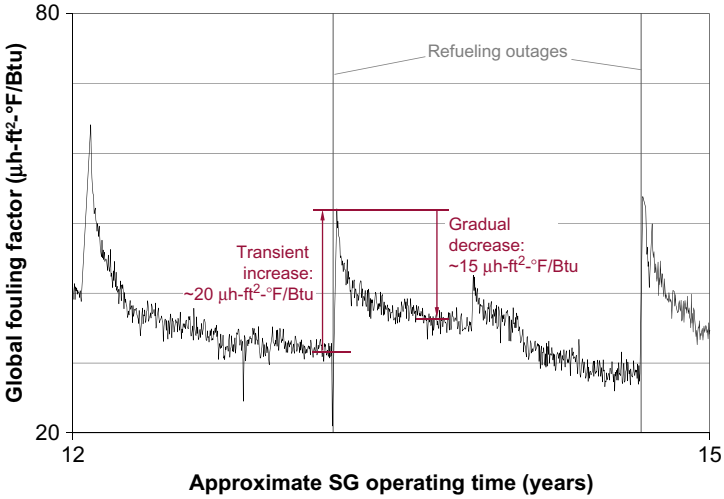

Fig. 12.7 Typical postoutage SG fouling factor transient.

negative FF transients are usually supplanted by the more typical positive transients later in SG life and tend to occur before significant tube scale layers have developed. Consequently, they most likely result from an independent physical or chemical phenomenon—perhaps related to chemical concentration and boiling point elevation and/or crystallization fouling/dissolution (which are plausible even with extremely low levels of tube scale).

- Industry statistics summarizing the FF transients experienced during the lifetime of 34 different PWR units are summarized in Kreider et al. (2014).

12.3.3 Summary of industry experience

Section 2.1 of Kreider et al. (2009) reported numerous summary statistics concerning the collective heat-transfer fouling behavior of the SGs at more than 40 different PWR operating conditions as of 2009. Updated versions of two of these summaries, reflecting analysis of nearly 60 PWR operating conditions for 39 different sets of SGs, are included here as Figs. 12.8 and 12.9. The first plot depicts the distribution of net fouling levels exhibited by the analyzed units over the full operating histories of 1–19 years (since clean SG startup) while the second illustrates the same quantity normalized to account for: (1) the average lifetime feedwater iron concentration, which is a proxy for SG tube deposit mass loading and (2) the SG operating time.

As illustrated in the two plots, a significant number of analyzed units have experienced net heat-transfer improvements. This reflects the fact that the median unit in the analyzed plant data set has operated for 9 years, which is consistent with the idealized curve in Fig. 12.6 that shows near-zero net changes in the FF for this approximate age and enhancing behavior at earlier times (i.e., Phase 2 behavior).

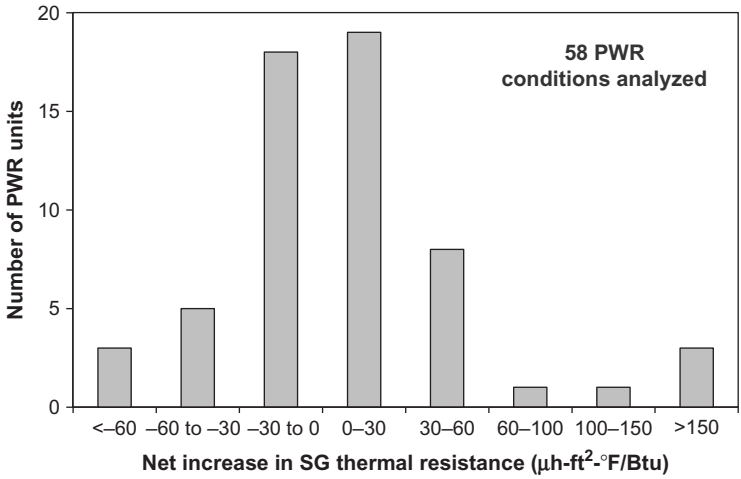

Fig. 12.8 Commercial industry experience with SG heat-transfer fouling.

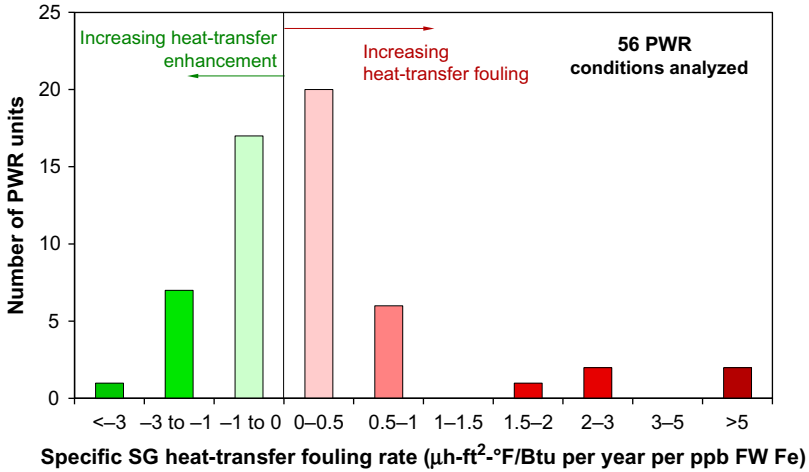

Fig. 12.9 Distribution of industry-observed specific fouling rates.

12.4 Causes of thermal performance changes

12.4.1 Tube deposit layers

12.4.1.1 Secondary scale

Commercial SGs are subject to the formation of fouling layers on tube OD surfaces from corrosion products transported in the secondary circuit. Extensive literature has been published on this subject in the past 20 years, including Bott (1995), EPRI (1996, 2012a, 2014, 2015c), and Varrin et al. (2003) as well as many of the references cited within these sources. Some important observations and generalizations regarding secondary tube scale that are relevant to SG heat-transfer efficiency can be made based on past studies:

- Scale layers form on SG heat-transfer surfaces as a result of multiple deposition mechanisms that vary from unit to unit and from one spatial location to another with an individual SG. Given the action of both particulate mechanisms (e.g., inertial, diffusive, electrophoretic, boiling-enhanced, etc.) and precipitation (crystallization) fouling—as well as variability in the composition and particle size distribution of corrosion products that occur in different plant secondary systems—the physical, chemical, and thermal properties of SG tube deposits vary widely. An even wider range of properties applies to deposits that form on support structures such as the top of the tubesheet (TTS) and tube support plates (TSPs). However, these other types of deposit have little direct influence on SG thermal performance, as they typically cover no more than a very small fraction of the heat-transfer surface.
- Tube scale that forms on freespan surfaces (i.e., at least 1–2 tube diameters away from support structures) is, with few exceptions, composed mainly of iron oxide in the form of magnetite (Fe_3O_4) with lesser fractions of other species. Since the 1980s, the concentration of magnetite in freespan scale has ranged between a lower bound of perhaps 50% up to more than 95%—though improvements in secondary chemistry practices, replacement of

vulnerable secondary materials, and reliability improvements for the integrity of secondary-side components (e.g., leading to fewer condenser leaks) during the past 25 years has raised the typical magnetite concentration to 90%–95% in the scale found in present-day SGs.

- Historically, the tube scale in many PWR SGs contained substantive fractions of metallic copper ranging from a few percent up to as much as 20%–30%. At these higher concentrations, the metallic copper increases the effective thermal conductivity of the fouling layer appreciably, moderating the thermal performance losses that might otherwise be realized. (It is worth mentioning that the presence of copper in the tube scale has adverse effects with regard to tube corrosion risk (see relevant chapter in this book).) In recent years, however, most units operate without copper-containing components in the secondary cycle and therefore produce tube scale with only small concentrations of copper (usually ~1% or less, though not always).
- Even though typically present in small concentrations (collectively just a few percent), hardness minerals, including those containing silicon (e.g., SiO_2), calcium, aluminum, and magnesium, are thought to play a significant role in determining the physical structure and thermal properties of some secondary tube scale layers, in part through crystallization fouling. Although there is limited direct evidence for this hypothesis, it is supported indirectly by prior work conducted by Westinghouse (Hu, 2003, 2006) as well as by unpublished laboratory testing conducted by the authors.
- The thickness of secondary tube scale among the 39 sets of SGs reflected in Figs. 12.8 and 12.9—as averaged over the full tube OD heat-transfer area—ranges from 0.1 mils up to 7.4 mils (2–188 μm). The corresponding influence on the SG FF ranged from −98 μh-ft^2-°F/Btu (strong enhancement) up to +195 μh-ft^2-°F/Btu (severe heat-transfer fouling). The relationship between average thickness and deposit thermal resistance for this plant data set, presented in an earlier form in Kreider et al. (2009) in 2009, is illustrated in updated form in Fig. 12.10. The "typical trend" shown on the figure by the black curve is meant to represent approximately average behavior among the PWR conditions analyzed while the optimistic and pessimistic bounding trends (green and red curves, respectively) were selected to

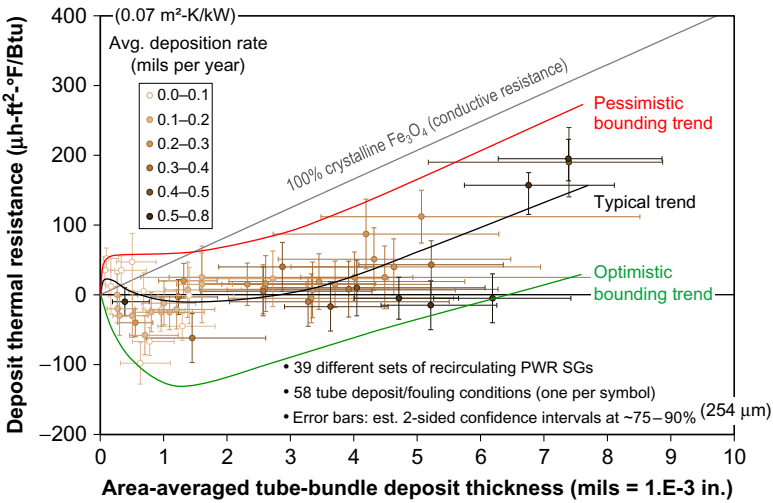

Fig. 12.10 Tube deposit thermal resistance: commercial PWR SG operating experience.

approximately bound the data in the context of relevant theoretical considerations and laboratory experience.

- Tube scale structures frequently include multiple sublayers with distinct properties. Most commonly, the inner part of the scale (closest to the tube-surface interface) exhibits a dense, relatively consolidated morphology that tends to be enriched in nonmagnetite species while the outer part (adjacent to the secondary two-phase flow) displays a more porous morphology. In general, more consolidated morphologies are believed to reflect both particulate deposition as well as crystallization of soluble species while porous scale is dominated by particulate deposition mechanisms. The porous structures permit development of heat-transfer enhancement through wick boiling and an increased density of boiling nucleation sites (see Section 12.3.1.2). Three examples of freespan tube deposits spanning a range of thicknesses are shown to scale in Fig. 12.11. These images are optical microphotographs of individual tube scale flake cross-sections through the thickness which were metallographically mounted and polished. The primary phase in all three images is magnetite (~85%–95% by weight), and the bright inclusions in the two thicker scale flakes comprise metallic copper (3%–10%). Porous structures close to the secondary flow interface on the right are clearly visible in the middle and rightmost cross-sections. Many other structures and compositions have been observed at different units since the 1980s.
- As described in White et al. (1996) and Chapter 5 of EPRI (1998a), the thermal effects of secondary SG tube scale can be effectively modeled by: (1) using Bruggeman's equation (Bruggeman, 1935) to calculate an effective thermal conductivity for consolidated deposit sublayers composed of multiple chemical phases and (2) assigning an appropriate thermal

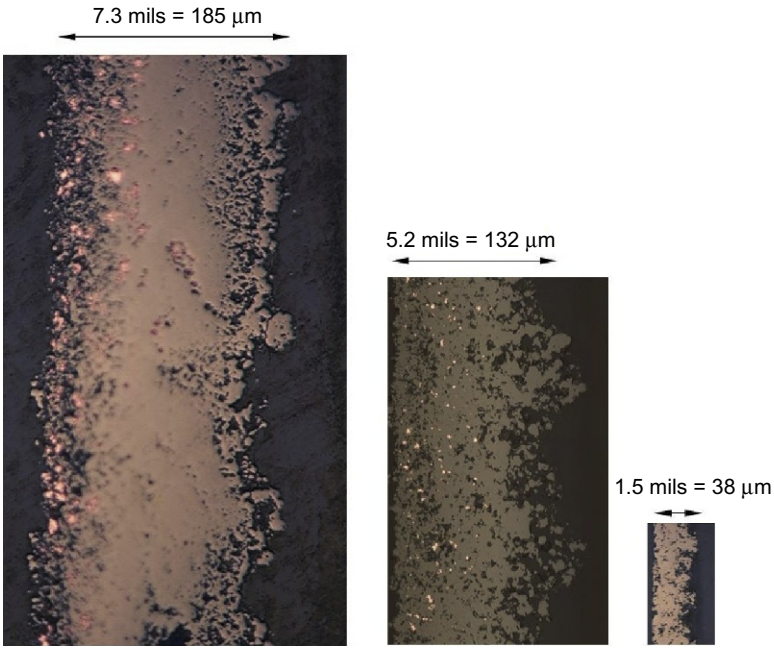

Fig. 12.11 Examples of commercial SG tube scale cross-sections (left = tube interface, right = secondary flow interface).

resistance value for porous sublayers (which are commonly enhancing or near-neutral) in the context of boiling heat-transfer models (Pan et al., 1985; Uhle, 1997) and relevant laboratory data. For consolidated sublayers, the thermal conductivity tends to be predominantly influenced by the value for magnetite, 2.0 Btu/h-ft-°F/Btu (Malgaard and Smeltzer, 1971). Further discussion of heat-transfer modeling for tube scale layers is included in Chapter 4 of EPRI (1996). Successful application of the two-layer modeling approach is demonstrated in Fig. 12.12, which depicts the results of the this approach for several PWR units (solid red circles) compared to calculated resistances for numerous PWR units based on hypothetical uniform zero-porosity scale layers of equivalent total deposit mass (open gray diamonds). As is clear from the figure, the two-layer approach leads to relatively accurate predictions, with some scatter, while the simple zero-porosity model generally overpredicts the thermal resistance.

- Although tube deposits are often nonuniformly distributed spatially within the SG, the effect of this skewed distribution (relative to a uniform distribution of thermal resistance) on the SG thermal efficiency is relatively small (see Sections 12.4.6.3 and 12.4.7).
- While increases in SG heat-transfer fouling are heavily correlated with the rate of iron oxide ingress into the SGs (see Fig. 12.6 and discussion in Section 12.3.1.3), some units have exhibited much higher rates of FF increase than would be inferred from iron ingress rates alone. For example, the average fouling rate at the two San Onofre units in the mid-1990s prior to deposit removal—roughly 25 μh-ft^2-°F/Btu per year per Figs. 14 and 15 in Kreider et al. (2009)—substantially exceeded the rate that would have been associated with deposition of newly incoming iron oxide in a fully consolidated magnetite layer. Instead, one (or both) of the following phenomena most likely occurred: (1) incoming corrosion iron or

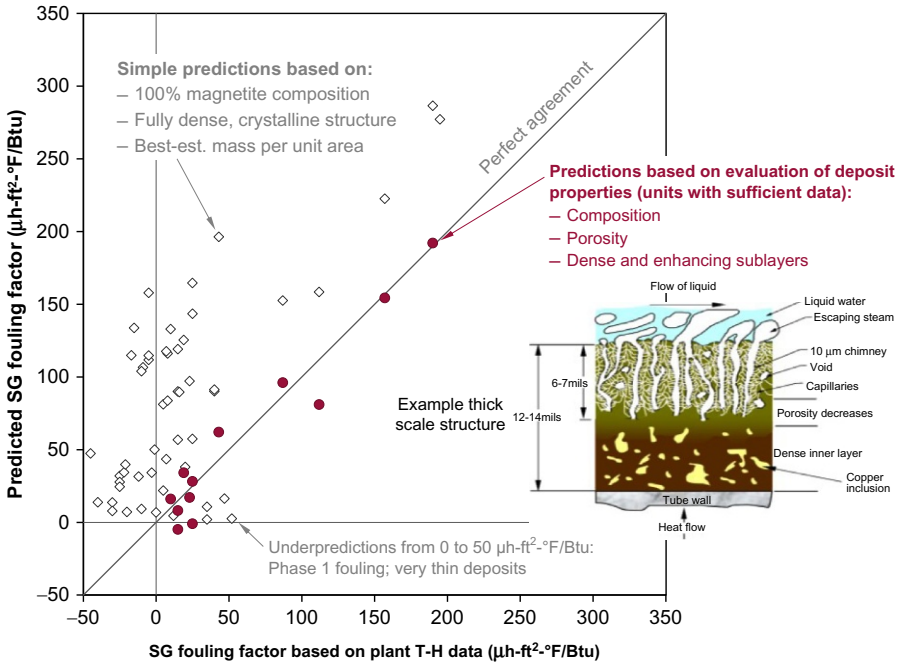

Fig. 12.12 Tube deposit thermal resistance predictions based on two-layer structure.

other species may have deposited within the outermost deposit sublayer, decreasing its porosity and substantially increasing its thermal resistance or (2) existing corrosion iron or other species at other locations within the SG shell or present locally may have been redistributed, leading to a thicker and/or more thermally resistive deposit structure.

- In at least one case, laboratory heat-transfer measurements were conducted on actual plant tube scale samples as documented in EPRI TR-100866 (EPRI, 1992). See Section 12.4.7 for additional discussion.

12.4.1.2 Primary scale

Fouling layers also generally form on the primary side (ID) of the SG tubes, and the effect on heat-transfer efficiency is additive with the effect of secondary scale (see Figs. 4-2 and 4-3 in EPRI, 1998a). An essential difference between the two types of deposit is the fact that primary-side layers form in the presence of subcooled flow (PWRs) or very small steam qualities (CANDU units) while secondary layers form in two-phase flow with substantial levels of boiling. (In recirculating SGs in both PWR and CANDU units, boiling occurs on the secondary side in all regions within the SG except a limited zone of subcooled conditions near the tubesheet and, for relevant designs, within the preheater.) Thus, the properties of primary scale may be expected to differ systematically from the properties of secondary scale. Primary deposits can be divided into two types: those that form in PWR SGs and those that form in CANDU SGs. Each has distinctive properties and is discussed further below.

Primary-side scale layers in PWR SGs form in the presence of corrosion-resistant materials throughout the primary circuit, meaning that the available source term for ID tube deposits is much smaller than for OD deposits. Rather, a stable oxide layer resulting from corrosion of the underlying tube material at low rates is believed to form on the tube ID surfaces during a relatively short period (a few months) at primary operating conditions and to remain essentially unchanged in thickness and properties during subsequent operation. This general view is largely based on data taken during tube pull exams conducted on dozens of tubes extracted from multiple European units aged 8–10 years in the late 1980s [see Appendix E of EPRI TR-110018 (EPRI, 1998a)]. These exams found an average ID deposit thickness of approximately 1 μm (0.04 mils). As reported in EPRI (1998a), the best-estimate effect of a consolidated layer of this thickness composed of typical oxides (magnetite, Cr_2O_3, and NiO) is 2 μh-ft^2-°F/Btu, which is essentially negligible relative to the range of effects occurring due to secondary tube scale.

In CANDU SGs, primary deposit layers typically are much thicker, on average, due to the presence of carbon steel components in the primary circuit, which serve as a source term for iron oxide. A number of publications present industry experience with primary SG deposits in CANDU units during the past two decades, including Burrill and Turner (1994), Yetisir et al. (2000, 2003), Husain and Chew (2006), and Lepine and Obrutsky (2006). These sources indicate the following:

- Per Husain and Chew (2006), the mass loading of primary deposits in the CANDU SGs at several Canadian units examined at different times during the 1990s and early 2000s was measured to be between ~5 g/m^2 and ~500 g/m^2 of tube area. The lowest values were

observed in the initial portion of the hot leg, consistent with the modeling reported in Burrill and Turner (1994). The largest values tended to occur in the U-bend region, the cold leg, and especially the integral preheater (at the applicable units). In general, the heaviest deposits were found in the cold leg and in the integral preheaters.

- Using a nominal density value of 5.2 g/cm^3 (applicable for the dominant phase of magnetite), the mass loadings cited above are equivalent to zero-porosity thicknesses of ~1 and ~100 μm (0.04 and 4 mils). However, additional data in Husain and Chew (2006) indicates an average estimated porosity of ~40% for samples taken from one CANDU unit. Based on this value, primary deposit thicknesses among the CANDU units evaluated ranged from ~2 up to ~160 μm (0.1–6 mils).
- Primary SG tube deposits in CANDU units generally consist of: (1) a dense, grown-in-place sublayer of adherent oxide (typically a Ni-Fe-Cr spinel) resulting from corrosion of the tube base material and (2) a more porous sublayer of deposited magnetite crystals.
- Increases in heat-transfer fouling due to primary-side deposit growth in CANDU SGs have been predicted—with results in reasonable agreement with plant experience—by assuming that the dominant deposition mechanism is precipitation of magnetite due to iron concentrations above the solubility limit, most likely as a result of FAC of outlet feeder piping (Burrill and Turner, 1994). This contrasts with PWR secondary deposits, which form as a result of various contributing deposition mechanisms.
- CANDU SG FFs, calculated in an analogous fashion to those presented in Section 12.3 for PWR SGs, have been observed to exhibit an average rate of increase equal to approximately 0.002 m^2-K/kW per year (equivalent to 12 μh-ft^2-°F/Btu per year) (Yetisir et al., 2000, 2003). Although these FF increases reflect the effects of both primary and secondary tube scale layers (as well as gradual changes in leakage across the SG divider plate), assessments by the authors of the above references suggest that a sizable fraction of the calculated fouling is attributable to primary deposits in the plants studied. In at least one case, this conclusion was supported by the effect of a primary-side cleaning of the SG tubes, after which most of the heat-transfer fouling loss was recovered.
- The calculated long-term fouling rates for three of four analyzed CANDU reactor units were all very close to the value of 0.002 m^2-K/kW per year cited above and were approximately constant (despite significant scatter) during the course of 10–15 operating years, leading to total FF increases of about 0.030 m^2-K/kW (170 μh-ft^2-°F/Btu) (see Fig. 1 in Yetisir et al., 2003). This level of fouling is comparable to the highest FFs calculated for secondary tube deposits developed over similar time frames at many units per Fig. 12.10. (As an aside, it is worth noting that the plant FF data presented in Yetisir et al. (2003) reflect a frequency of roughly once every few months. Accordingly, short-term phenomena, such as the Phase 1 behavior reflected in Figs. 12.2 and 12.4 for PWR secondary deposits, may not be apparent.)
- Based on the average deposit loading values and corresponding estimated thermal resistances shown in Table 1 of Yetisir et al. (2003), the effective thermal conductivity of the CANDU primary-side deposits is apparently significantly lower than that associated with PWR secondary scale. This conclusion is consistent with the absence (or a small level) of boiling enhancement in the primary-side environment.

The consistency of the FFs calculated for CANDU units suggests that the thermal properties of primary layers exhibit less variability, as averaged over the SG, than the thermal properties of secondary scale. This lower variability may be a result of: (a) smaller variability in the deposit chemical and physical properties of CANDU primary scale compared to PWR secondary scale, (b) smaller variability in the *effects* of these deposit property variables on SG thermal efficiency, or (c) both.

12.4.2 Fouling of other SG internal and steam system components

12.4.2.1 Broached tube support plate flow holes

A number of SG designs incorporate broached trefoil or quatrefoil holes in the TSPs. These holes, which contain three or four lobes surrounding the tube (e.g., see Schmitt et al., 2012), provide lateral support to the SG tubes and also permit passage of the two-phase flow vertically through the tube bundle. Compared to other TSP designs (e.g., those using lattice bars or isolated drilled holes), the broached-hole designs have been particularly susceptible to the buildup of corrosion products within the flow openings. A number of studies documenting industry experience, predictive modeling, and laboratory research have been conducted on this phenomenon in the past 30 years (e.g., see Schmitt et al., 2012; EPRI, 2012b; Malaugh et al., 1990; Puzzuoli et al., 1995; Stickel and Miller, 1994; Maanshan, 2005; Corredera et al., 2008; Lee et al., 2009; Barale et al., 2008; Hirano et al., 2010; Guillodo et al., 2009; Moleiro et al., 2010; Oukacine et al., 2012; Vergnault et al., 2008).

Broached-hole deposit accumulation gradually tends to block the secondary flow openings, which can have multiple adverse consequences:

- Instability in the liquid water level within the SG, which requires a power reduction (or deposit removal) in order to suppress the associated level oscillations and permit stable plant operation.
- Tube fatigue and associated cracking as a result of increased flow velocities in specific locations in particular SG designs.
- Reduced SG thermal performance levels.

The last of these effects is relevant to the subject of the current chapter, as it mimics the effects of thermally resistive tube scale by lowering secondary velocities through the tube bundle and, as a result, the recirculation ratio and secondary heat-transfer coefficient. However, as indicated in Kreider et al. (1998b), thermal-hydraulic sensitivity analyses carried out by the authors for different PWR SG designs revealed that this effect tends to be small, even for fairly substantial average blockage fractions (e.g., 50%).

12.4.2.2 Steam separation equipment

Recirculating SGs in both PWR and CANDU units rely on two-stage steam-liquid separation to partition the two-phase flow exiting the tube bundles, which at full power typically has a quality of 20%–40% (consistent with recirculation ratios of 2.5–5). The primary and secondary separator assemblies are usually located inside the SG shell—though some units (e.g., Bruce A) employ an independent steam drum outside the SG. Schematics and descriptions of some of the various designs that have been evaluated and used are included in EPRI (1980, 1983a,b), Prueter and Reed (1994), and Kreider et al. (2015).

A combination of thermal power uprates [which reduce separator operating margins by increasing the steam flow rate through each assembly (Prueter and Reed, 1994)] and deposit fouling have in some cases led to above-design levels of moisture

carryover (MCO) to the high-pressure steam turbine, lowering plant output and increasing risks to material integrity in the steam system. As with TSP blockage, such deposit fouling can lead to an increased pressure drop across the fouled components. From a thermal performance standpoint, as measured by the FF, the effect of this decrease in the steam pressure is indistinguishable from a decrease in SG tube bundle heat-transfer coefficient.

Although industry experience with this issue is not known to have been systematically compiled, a number of PWR units have informally reported out-of-specification MCO levels on the order of 1% or more compared to separator design maximum values of 0.1%–0.25%. The potential effect of separator deposit fouling on SG thermal performance was investigated for two different separator designs:

- Calculations which explore the effect of primary separator flow-path blockage on SG thermal performance are presented as part of a thermal performance root cause study following the Arkansas Nuclear One Unit 2 (ANO-2) dispersant trial. Documented in Appendix F of EPRI (2001a), this study examined whether corrosion product deposits fouling the drain holes of a CE-type primary separator at another station (Calvert Cliffs) could cause a substantial change in the pressure drop across the component. The results showed that a fairly high fraction of the liquid flow area had to be blocked to produce an appreciable increase in the pressure drop (e.g., >70% blockage to produce 1 psi). However, as noted in EPRI (2001a), the analysis involved a number of simplifying assumptions. In addition, data from the utility indicated that cleaning of the Calvert Cliffs separators lowered the MCO substantially and also raised the steam pressure by at least 4 psi, implying that the separator deposits did in fact have a significant effect on SG thermal performance. (Note that a 4 psi steam pressure increase in the original Calvert Cliffs SGs was equivalent to an FF reduction of ~10 μh-ft^2-°F/Btu.) In summary, the various uncertainties concerning this particular plant experience preclude any high-confidence conclusions regarding the role of separator deposits in causing appreciable changes in the SG thermal performance level. However, based on all of the information in EPRI (2001a), it is judged likely that fairly severe deposit fouling levels were necessary for this separator design in order to cause a substantive impact on the SG thermal performance level.
- An analogous investigation was carried out for the secondary separator design employed in the McGuire 2 SGs as documented in EPRI (2007) and Fruzzetti et al. (2008, 2009). This evaluation concluded that deposit buildup on the secondary separator surfaces could have plausibly caused the observed change in pressure drop across these components (roughly 1 psi). For McGuire 2, the equivalent change in SG thermal resistance is between 3 and 5 μh-ft^2-°F/Btu.

Based on both of the above plant experiences, it is concluded that SG heat-transfer efficiency levels are probably fairly tolerant generally to deposit fouling of the steam separation equipment, with adverse effects likely limited to FF increases on the order of 1–5 μh-ft^2-°F/Btu except in cases of severe fouling with concomitant compromises in moisture separation efficiency.

12.4.2.3 SG outlet nozzles/downstream piping

In some plant designs, the secondary steam pressure is measured at taps located on the main steam piping some distance downstream of the SG outlets. These pressure

readings must be used in Eq. (12.1) to calculate the SG FF. As a result, any increased pressure drops upstream of these tap locations would contribute to increases in the calculated FF. Potential locations for such increased pressure drops include primary and secondary steam separators (addressed in Section 12.4.2.2), the SG outlet venturi nozzles, and the steam piping and fittings (elbows, valves, etc.) between the SG outlets and the measurement taps.

A systematic study of fouling of the SG outlet nozzles and steam piping is not known to have been performed for the nuclear power industry—most likely because such fouling has generally been minor and/or has not caused significant operational issues. However, some insight concerning the potential for this type of fouling was developed through the evaluations completed for McGuire 2 following the dispersant trial in 2007 and one of the lead units implementing routine dispersant addition, Byron 1 [see Appendix I of EPRI 1015021 (EPRI, 2007); Fruzzetti et al., 2008, 2009]. Specifically, it was determined that the total pressure drop between a location upstream of the secondary steam separators and a location on the main steam piping downstream of the SG outlet nozzles decreased by ~1 psi at McGuire 2 upon exposure of the SGs to dispersant chemicals. This decline was determined most likely to be the result of dispersant-induced defouling of surfaces within the secondary steam separator cyclones and/or the inlet areas of the SG outlet venturi nozzles. The decrease in differential pressure was equivalent to an apparent reduction in the SG thermal resistance of 3–5 μh-ft^2-°F/Btu.

It follows that the 7 years of operation at McGuire 2 between clean SG startup and the start of dispersant exposure led to gradual fouling of the secondary steam separators, the SG outlet nozzles, or both. The trend in instrument readings showed that the rate of fouling decreased during this 7-year period (see Fig. 3 in Fruzzetti et al., 2009 for Byron 1; a similar trend occurred at McGuire 2). However, a clear asymptote had not been reached, meaning that the effects of fouling were apparently continuing to accumulate at the time of dispersant-induced defouling. Similar data analyzed for several other units following dispersant addition [see Section 7.4.1 of EPRI 1025317 (EPRI, 2012c)] resulted in a similar conclusion: apparent deposit fouling of component surfaces between (and including) the secondary steam separators (of different designs) and the main steam piping downstream of the SG outlet nozzles had historically produced changes in pressure drop believed to be on the order of 1 psi during roughly 10–20 years of prior SG operation.

Based on these experiences, deposit fouling on SG and steam system components in PWRs appears to routinely cause minor increases in the associated pressure drops that are equivalent to SG thermal resistance increases on the order of 5 μh-ft^2-°F/Btu during operating periods of 10–20 years. However, in the absence of a more systematic investigation, larger effects must be considered plausible (e.g., due to unit-specific differences in plant design, corrosion product transport, deposit properties, etc.).

12.4.3 SG divider plate leakage (CANDU units)

As described in Chapter 6 of EPRI TR-110018 (EPRI, 1998a), leakage of primary fluid across the plate which divides the hot-leg side of the SG channel head from

the cold-leg side can cause an unintended reduction in cold-leg temperature (RIHT), an error in T_{cold} measurement, and a slight reduction in the primary-side heat-transfer coefficient. All three effects tend to depress the operating steam pressure (in a PWR) or reduce RIHT margin (in a CANDU unit) and two of the three effects increase the calculated FF.

For PWR SGs, no leakage is known to have occurred through the welded joints used to mount the divider plate. In contrast, CANDU SGs historically have employed bolted connections susceptible to leakage. Per Yetisir et al. (2000, 2003) and Brissette and Lafraniere (1996), this leakage has been identified as a substantial contributor to thermal performance loss as measured by RIHT increases. In the cases quantified in Yetisir et al. (2000), increases in RIHT accumulated over roughly 10 operating years as a result of divider plate leakage for two units were in the range of approximately 3–5°C. This change is very roughly equivalent to an FF increase of 125–250 μh-ft^2-°F/Btu—a sizable performance penalty in comparison to the range of observed thermal resistances for primary and secondary SG tube scale discussed earlier.

12.4.4 Preheater baffle plate fouling/flow distribution

No studies focused on nuclear industry experience with fouling of integral SG preheaters are known to have been published. However, deposit buildup on the preheater baffle plates can potentially compromise SG thermal efficiency, both by reducing flow velocities and through introduction of an insulating fouling layer. Further investigation of this issue, should the industry determine it is warranted, might involve simplified modeling to determine the range of plausible effects and/or characterization of the deposits present in operating units.

Another variable specific to preheater-type SGs that can influence SG thermal efficiency is the fraction of the feedwater flow directed to the preheater inlet compared to that directed to the upper SG internals. As discussed in Appendix D of EPRI TR-110018 (EPRI, 1998a), a decrease in the percentage of flow directed to the preheater—which might be implemented for operational reasons—reduces the SG thermal efficiency.

12.4.5 Changes in SG tube plugging, applied primary temperature, and/or thermal power

Changes in the effective heat-transfer area (typically through tube plugging), the applied primary temperature (for PWRs), or the thermal power all influence the steam pressure produced by the SG and therefore the operating pressure margin for the high-pressure turbine. However, to first order, none of these have a significant influence on the SG thermal resistance. Consistent with this situation, the FF method accounts for changes in these variables, as each appears explicitly in Eq. (12.1). For completeness, it is noted that tube plugging raises primary velocities and therefore lowers the primary-side boundary layer thermal resistance. Also, some common correlations such as that attributed to Thom (Rohsenow et al., 1985) indicate a dependence of

the secondary heat-transfer coefficient on the heat flux, meaning that increases in thermal power would decrease the thermal resistance. In both cases, however, the changes are expected to be very small for typical variations in the relevant variables—though the effect of a substantial power uprate should be considered in any comprehensive SG thermal performance evaluation.

12.4.6 Sources of uncertainty

Evaluations of SG thermal resistance changes as measured by FF calculations per Section 12.2 are subject to several sources of error that lead to uncertainty in the reported results and/or the attribution of a calculated change to the typically presumptive cause—deposit-induced fouling of the tube bundle. The various types of errors and their potential effects on the FF are summarized below.

12.4.6.1 Clean performance level

As described in Section 12.2.4, at least three methods can be used to estimate the clean baseline thermal resistance of an individual set of SGs. However, each approach carries an uncertainty that varies from unit to unit. Based on several dozen analyses conducted by the authors, the unit-specific uncertainty associated with this quantity ranges from about ±20 to ±50 μh-ft^2-°F/Btu (for a two-sided confidence interval estimated roughly at 80%–90%).

12.4.6.2 Plant instrument measurement errors

FF values calculated with Eqs. (12.1), (12.2) depend on a number of measured quantities which have inherent uncertainties. The most important of these (i.e., those with the largest effect on the FF) are typically the main steam pressure, the secondary mass flow rate, and the primary temperatures (e.g., T_{hot} and T_{cold})—though not necessarily in that order. For any given FF value, the computed uncertainty can range from roughly ±20 up to ±60 μh-ft^2-°F/Btu or more [e.g., see Tables 4-2 through 4-5 in EPRI TR-110018 (EPRI, 1998a)]. However, in many cases, the errors are the result of unbiased random fluctuations (noise). For these types of errors, consideration of several FF values calculated using independent data sets recorded at approximately the same time can significantly reduce the effective uncertainty (due to random noise) for determining the performance level at a particular point in time (typically lowering it to values below ±20 μh-ft^2-°F/Btu).

Other types of uncertainty reflect sustained bias errors in one or more of the instrument readings necessary for calculating the FF. Examples of this type of error include transmitter drift, hot-leg streaming (also termed thermal stratification) (EPRI, 1998b), and feedwater or steam flow instrument fouling/defouling, among others (Kreider et al., 2009; EPRI, 1998a). Each type of error can have an appreciable or even substantial impact on the computed FF. Consequently, comprehensive SG thermal performance evaluations address each type of error to ensure that calculated FF values

are representative of actual changes in the SG thermal resistance. Example uncertainty evaluations are included in Chapter 4 of EPRI (1998a).

12.4.6.3 Spatial distribution of fouling layers

In principle, the spatial distribution of tube deposit layers within the SG—irrespective of their spatially averaged thermal resistance—would be expected to have an influence on the net heat-transfer efficiency of the SG. There are two related reasons for postulating an effect of this type: (1) the heat flux varies substantially (by about an order of magnitude) between the hot-leg and cold-leg ends of each SG tube and (2) thermally resistive deposit layers locally depress the heat flux, allowing more heat to be transferred through areas with lower thermal resistance (all other factors being equal). With regard to the first issue, fouling layers prevalent on the hot leg would tend to have a larger effect than those on the cold leg (and by analogy than those on an "average" location). On the other hand, a local concentration of thermal resistance (at any location) would tend to be compensated by a shift of heat transfer to surrounding (less fouled) areas.

The effects of fouling resistance distribution on SG thermal efficiency were evaluated quantitatively in 1998 using a modified version of EPRI's ATHOS software and thermal-hydraulic inputs characteristic of the original San Onofre SGs (Kreider et al., 1998b). In particular, a sensitivity study was performed to investigate the differences in predicted SG steam pressure for various spatial distributions of thermal resistance for two cases: (1) a spatially averaged moderate thermal resistance of 60 μh-ft^2-°F/Btu (a little larger than the overall median FF value shown in Fig. 12.10), and (2) a severe fouling resistance of 200 μh-ft^2-°F/Btu (near the overall maximum FF value in Fig. 12.10). As explained in greater detail in Kreider et al. (1998b), all nonuniform distributions reflected approximately linear variations from low (or high) relative fouling at the TTS to high (or low) relative fouling in the U-bend region. The results of the study showed that the effects of deposit spatial distribution are relatively small. As illustrated in Fig. 12.13, even very extreme spatial distributions (at the two ends of each U-shaped curve on the plot) resulted in fairly modest differences in predicted steam pressure compared to the respective uniform fouling distribution in the middle of each curve (e.g., a difference of 8 psi, or a fouling equivalent of ~20 μh-ft^2-°F/Btu = 10% was calculated for the most extreme nonuniform distribution for the 200 μh-ft^2-°F/Btu case shown on the plot). On the other hand, the nature of the effect—a thermal performance improvement for nonuniform fouling resistance distributions—shows that the beneficial effects of increased heat flux through lightly fouled areas and depressed heat flux in heavily fouled regions outweighs the slight penalty associated with heavy fouling in the areas of highest heat flux. (This penalty is the reason why the left side of each curve is slightly lower than the right side.)

12.4.6.4 Effects of postoutage FF transients

As discussed in Section 12.3.2, virtually all recirculating SGs experience transient changes in the calculated FF, with the most likely cause related to partial detachment

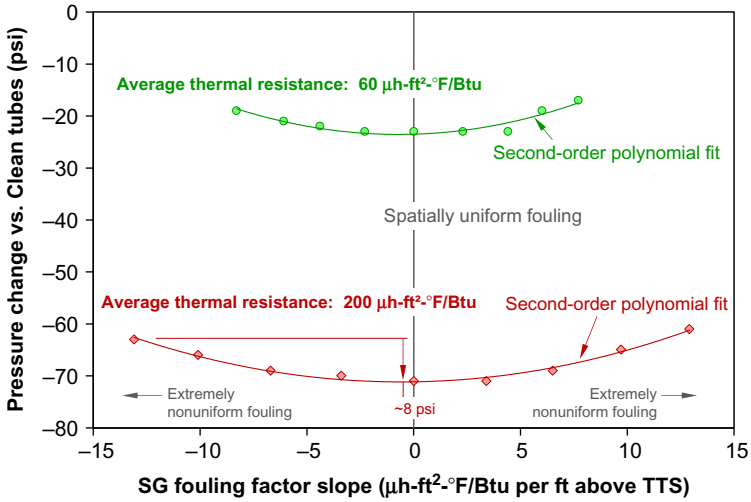

Fig. 12.13 Effect of spatial distribution of fouling resistance on SG thermal performance. Adapted from Kreider, M.A., White, G.A., Varrin Jr., R.D., 1998. A global fouling factor methodology for analyzing steam generator thermal performance degradation. In: Proceedings of the Third International Steam Generator and Heat Exchanger Conference. Canadian Nuclear Society/Société Nucléaire Canadienne, Toronto, Canada, ISBN: 0-919784-59-3, pp. 190–208 (Held in Toronto, Ontario, Canada, June 1998).

of tube scale flakes on a small fraction of the tube bundle. Because these transients routinely alter the short-term behavior of the FF, any determination of fouling changes at a particular unit must consider the context of these transients in order to accurately determine the prevailing medium-term or long-term heat-transfer fouling rate. Further, calculated trends must rely on sufficiently frequent data sets in order to resolve these effects properly (see Figs. 12.2 and 12.5).

12.4.6.5 Fouling of components outside the SG tube bundle

Fouling of nontubing components—such as steam separators and SG outlet nozzles as discussed in Section 12.4.2—can affect the FF calculation and therefore are analogous to the bias errors described in Section 12.4.6.2 from the standpoint of quantifying heat-transfer fouling due to SG tube deposit layers. Accordingly, an estimate of the effect of each potential cause and the associated uncertainty are needed to fully characterize the total FF uncertainty corresponding to a particular fouling condition.

12.4.7 Validation of FF method

As listed below, at least three different methods have been used to confirm that calculated changes in the FF (see Section 12.2) accurately represent the heat-transfer effects of SG tube scale layers. In all cases, sources of SG thermal performance change that are unrelated to the tube deposits must be evaluated on a plant-specific basis and

used to adjust the computed FF value to account for these nontube-fouling effects as appropriate.

- *Theoretical calculation*. Data concerning the composition and structure of the tube scale layers may be used to compute an estimate of the effective thermal conductivity of these layers. The results, coupled with an estimate of the average deposit thickness, may be used to estimate the thermal resistance of the tube scale layers. Provided that other causes of SG thermal performance change are small or are properly accounted for, these theoretical results can serve to confirm the independently calculated FF change, which is based on global plant instrument data and SG tube plugging information. See Section 12.4.1.1 and Chapter 5 of EPRI TR-110018 (EPRI, 1998a) for further details.
- *Postcleaning thermal performance change*. For units that have implemented complete SG secondary tube deposit removal, confirmation of the clean thermal resistance can be provided through calculation of the FF both at the time of initial SG startup as well as immediately upon postcleaning startup. The most effective means to achieve complete deposit removal is hard chemical cleaning (HCC). Accordingly, the FF histories for seven units that carried out chemical cleaning on the full tube bundles were computed and evaluated. The smoothed trends are illustrated in Fig. 12.14, with the pre- and postcleaning values highlighted by a pair of filled circles. The second circle in each pair lies close to the *x*-axis, indicating that the postcleaning thermal resistance is close to the corresponding value computed for early SG operation (at the left side of the plot). In other words, full removal of the deposit layers restored the thermal performance level in each case to that realized at initial clean startup (within a tolerance of about ±25 μh-ft^2-°F/Btu in most cases, which is associated with uncertainty mainly in the early-life calculations). This expected result provides a good measure of validation for the FF approach.

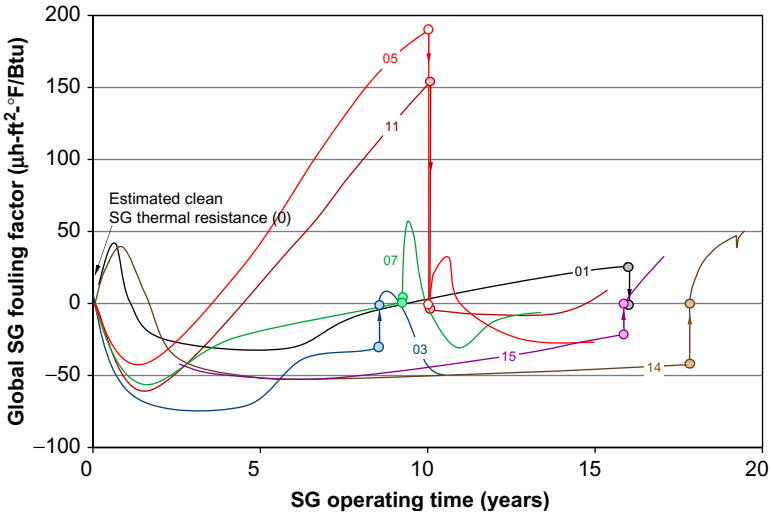

Fig. 12.14 Initial and postcleaning SG thermal resistance: operating experience.
Adapted from Kreider, M.A., Moroney, V.D., White, G.A., Varrin Jr., R.D., 2009. Industry SG heat-transfer fouling trends and probabilistic fouling predictions. In: Paper 4.07P/5.09 Presented at the 6th CNS International Steam Generator Conference Held in Toronto, Ontario, Canada, November 8–11.

- *Laboratory testing of deposit samples*. For the original Ginna SGs, which were heavily fouled with deposits in the early 1990s, sections of a tube were removed and tested in the laboratory both before and after chemically removing the deposits in order to quantify the change in thermal resistance. The result, 225 μh-ft^2-°F/Btu after accounting for differences in the applied heat flux for the fouled and cleaned tube experiments, matches the FF value calculated using plant instrument data and the design thermal resistance value (~190 μh-ft^2-°F/Btu) reasonably closely. In fact, close agreement would not necessarily be expected due to the fact that the tested deposits (from the U-bend region) were likely to have been somewhat thicker than the spatially averaged value.

Of the three methods, comparison of initial startup and postcleaning FF values (as illustrated in Fig. 12.14) provides the highest degree of confirmation because the two thermal resistance values (and therefore the difference) are subject to the smallest uncertainties.

12.5 Consequences of SG thermal performance loss

SG thermal performance declines generally have an adverse impact on unit production. The magnitude of the decrease in production caused any particular performance loss depends on the operating thermal margin. For PWRs, the margin may be defined as the difference between the operating SG steam pressure and the lower steam pressure value (measured at the same physical location) at which the governor valves throttling flow to the high-pressure turbine (in order to provide it with its design mass flow rate) are fully opened ("valves wide open" or "VWO"). The thermal margin may therefore be expressed symbolically as follows:

$$P_{margin} = P_{current} - P_{VWO} \tag{12.3}$$

For CANDU units, the margin would instead be expressed in terms of the increase in RIHT which can be tolerated before reaching the operating limit for that parameter. The margin for either unit may be converted to an equivalent FF change using applicable sensitivity values [e.g., see Section A.3 in Appendix A of EPRI 1002774 (EPRI, 2002)].

For units with substantial thermal margin, decreases in SG thermal efficiency have a modest detrimental effect associated with the decrease in the Carnot cycle efficiency of the secondary system due to the reduction in steam temperature. As the thermal margin nears zero, the steam pressure approaches the VWO value and the change in unit production becomes very nearly flat as gains in thermodynamic availability caused by reduced throttling of the governor valves offsets the decrease in Carnot efficiency. At operating steam pressures below the VWO value, the decreases in unit production are much steeper due to required decreases in the applied thermal power. These trends are illustrated using inputs typical of a PWR in Fig. 12.15. Further discussion is included in Section 2.7 of Kreider et al. (2009).

The economic penalty due to the production loss caused by SG thermal performance declines clearly depends on the particular utility commercial situation.

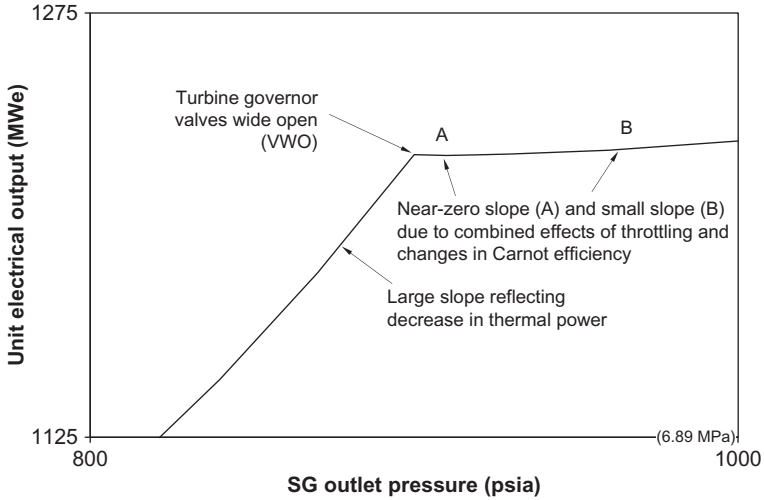

Fig. 12.15 Typical relationship between SG operating pressure and unit production. Adapted from Kreider, M.A., Moroney, V.D., White, G.A., Varrin Jr., R.D., 2009. Industry SG heat-transfer fouling trends and probabilistic fouling predictions. In: Paper 4.07P/5.09 Presented at the 6th CNS International Steam Generator Conference Held in Toronto, Ontario, Canada, November 8–11.

However, it is worth noting that avoiding the performance losses would require deposit removal, which would incur costs, or an increase in the applied primary temperature, which would raise rates of thermally activated corrosion for SG tubing as well as other vulnerable primary system components (e.g., those constructed of Alloy 600). In other words, remedies for counteracting unit production losses caused by SG thermal performance decreases carry offsetting costs or risks. The preferred strategy for managing this type of tradeoff is often determined with the aid of unit-specific economic studies (see Section 12.7).

12.6 Effects of corrosion deposit removal

Thermal performance decreases caused by deposit fouling can be remedied through deposit removal via application of several different techniques. A brief summary of the effects of these cleaning methods on SG heat-transfer efficiency as determined based on accumulated nuclear industry experience is included below.

12.6.1 Hard chemical cleaning

SG HCC involves use of concentrated solvents in processes designed to remove all or nearly all (>95%) of the corrosion product deposit mass present on secondary

freespan SG tube surfaces. With few exceptions among several dozen full-bundle HCC applications in the SGs of PWR and CANDU units, this goal has been achieved. Accordingly, the large majority of the tube heat-transfer surface area is effectively cleaned by HCC processes. As might be anticipated based on this experience, the SG heat-transfer efficiency following HCC has been approximately restored to the level observed during initial clean SG operation. As discussed earlier in Section 12.4.7, several examples of this performance restoration are shown in Fig. 12.14. These examples include units affected by severe heat-transfer fouling (Plants 05 and 11 in the figure) as well as units that were exhibiting heat-transfer enhancement (e.g., Plant 03 in the figure). As a consequence, HCC applications can cause either a thermal performance improvement or a decline, depending on the deposit thermal properties at the time of cleaning. HCC is the most effective means of addressing severe heat-transfer fouling with a single application.

12.6.2 Soft chemical cleaning

Beginning in the early 2000s, alternatives to conventional HCC applications were developed which involve dilute solvents and less complex process equipment and protocols. Frequently termed "soft" cleaning, these alternatives include advanced scale conditioning agents (ASCAs) and deposit minimization treatment (DMT). Full-bundle applications of these techniques are generally capable of removing a significant fraction of the tube-surface deposit loading—though complete removal is generally not an objective. Rather, utilities have typically applied soft cleaning for one or more of the following reasons:

- To prevent long-term increases in deposit accumulation and the associated heat-transfer penalty without the complexity of HCC.
- To avoid the Phase 1 thermal performance penalty (see Section 12.3.1.1 and Fig. 12.6).
- To reduce the degree of TSP broached-hole flow blockage (see Section 12.4.2.1).
- To preferentially remove chemical species such as copper to reduce tube corrosion risks.
- To promote structural modifications in the freespan tube scale that produce changes to the thermal properties of the scale which increase the level of heat-transfer enhancement.

Experience with the effects of soft cleaning on SG thermal performance is summarized below for the two processes that have been commonly applied.

12.6.2.1 ASCA

As documented in EPRI (2015c) and Little et al. (2009, 2010, 2012a,b, 2014), laboratory testing and industry experience with ASCA applications have shown that this type of soft cleaning modifies the scale structure. The result is an increase in the scale porosity through the thickness of the fouling layer and an accompanying increase in the degree of heat-transfer enhancement which improves the net SG thermal performance level. Of the more than 40 completed ASCA applications (EPRI, 2015c), the thermal performance effects are known to have been analyzed for 13. In all of these cases, the thermal performance trend has been marked by a sharp decrease in the FF upon postcleaning startup. This behavior contrasts with a typical postoutage transient

FF *increase* in the absence of the cleaning application as shown in Fig. 12.7. Subsequent operation following ASCA applications has been marked by sustained reductions in the FF relative to precleaning levels. In addition, repeated ASCA applications at the same unit have produced FF reductions which are partially additive. Quantitative results are shown in several of the aforementioned publications. For example, see Figs. 10 and 15 and Table 1 in Little et al. (2010) and Figs. 4-7 through 4-9 in EPRI (2015c).

12.6.2.2 DMT

Experience with DMT applications, documented in EPRI (2015c), Mayer and Jones (2010), Jones et al. (2012), Weiss et al. (2012), and Alley et al. (2014), has included nine applications, with FF analysis results reported for three. One of these three applications resulted in the avoidance of the typical postoutage FF transient observed in the absence of cleaning (Fig. 12.7) and no other discernible short-term change (though a longer-term decreasing trend in the FF observed at this unit could potentially be tied to the DMT deposit removal). A second DMT application was marked by a sharp FF decrease upon postcleaning restart which is comparable to those observed for ASCA applications (see Fig. B-6 in EPRI, 2015c). The third analyzed application did not produce any clear changes in FF behavior. For five of the remaining six applications, the utility reported no significant change in operating steam pressure, but FF evaluations are not known to have been performed for these applications.

12.6.2.3 Long-term effects

Independent of the short-term thermal performance effects, both types of soft cleaning process are expected to confer long-term heat-transfer benefits by substantially reducing the rate of deposit growth. Both types of soft cleaning are also generally expected to allow units to avoid the Phase 1 thermal performance penalty shown in Fig. 12.6 (in contrast to HCC).

12.6.3 Mechanical methods for secondary deposits

An assortment of mechanical techniques for removing secondary SG deposits has been employed over the years (EPRI, 2015c). Most of these have been focused on the TTS region where hardened deposits accumulate. Removal of TTS deposits has a very small or negligible impact on SG thermal performance because it influences only a small fraction of the heat-transfer surface. However, some mechanical cleaning applications, including different types of water-jet lancing, bundle flushes, and pressure pulse cleaning, have focused on removing deposits from the full tube bundle. For many of these applications, a clear effect on SG thermal efficiency was not discernible. However, a systematic evaluation of the effects of mechanical full-bundle cleaning techniques on thermal performance is not known to have been performed.

12.6.4 Polymeric dispersant addition

Online addition of nuclear-grade polyacrylic acid (PAA) dispersant is used for the purpose of increasing the rate of iron oxide removal through the SG blowdown flows. This method was developed and qualified for use in PWR secondary systems in the 1990s and early 2000s (see EPRI, 2001a,b, 2002, 2007). In contrast to the other methods discussed above, the use of online polymeric dispersant addition relies primarily on the ability of these chemical additives to increase the rate at which iron-based corrosion products are removed through the blowdown flow. In other words, dispersants focus primarily on reducing the rate of deposit accumulation rather than removing deposits that have already accumulated. Nonetheless, in some cases dispersant use has also been found to promote the suspension and removal of loosely adherent corrosion deposits present on secondary plant surfaces.

As indicated in Sections 2.5.2.3–2.5.2.4 of EPRI 1025317 (EPRI, 2012c) and in Chapter 4 of EPRI 3002005416 (EPRI, 2015b), the initial exposure of SGs to online dispersant has produced reductions in the calculated FF within a period of weeks to months at a substantial majority of the treated units. Typically, a fraction of the FF reduction (roughly one-third) has been sustained for the succeeding 2–5 years of plant operation (with longer exposures not yet studied). In contrast to the typical plant experience, one unit exhibited an FF increase upon exposure to PAA at concentrations above an apparent threshold value (EPRI, 2001a). In all cases, the thermal performance effects of dispersant exposure are postulated to be the result of dispersant-induced removal of iron-based particles from within the tube deposit structure.

12.6.5 Primary-side cleaning (CANDU units)

As indicated in Section 12.4.1.2, primary-side deposits have generally caused sizable decreases in SG thermal efficiency at CANDU units. Consequently, a number of cleaning efforts focused on these deposits have been carried out. The processes include two mechanical methods that rely on blast media (stainless steel beads) to mechanically remove the deposits: AREVA's Sivablast process and AECL's CANDU Clean process. Application of these methods at six different CANDU units is documented in Husain and Chew (2006). Generally, the processes achieved removal of an estimated 60%–85% of the deposit inventory initially present on the treated tubes. For at least one of the applications, a substantial thermal performance improvement was noted immediately following the cleaning as illustrated in Fig. 1 of Yetisir et al. (2003).

12.7 Conclusion

12.7.1 Key points

This chapter has covered the physical phenomena, main analysis methods, and collective industry experience related to SG thermal performance trends in recirculating SGs

used in commercial nuclear PWR and CANDU units during the past 20–30 years. Some of the key points covered in the chapter include the following:

- SG thermal performance levels are subject to variation as a result of multiple independent causes. These causes include the formation of corrosion deposit layers on both the primary and secondary tube heat-transfer surfaces. They also include fouling of other components within the SG shell, instrument measurement errors, tube plugging, and intentional changes to operating temperatures.
- The most effective method for evaluating SG thermal performance trends—considering both effectiveness and practicality—is the global SG FF based on an overall heat-transfer equation. The basic accuracy of the method has been validated with multiple methods, most notably through comparisons of initial and postcleaning thermal performance levels.
- SG FF analyses conducted for about 60 operating conditions at about 40 different PWR units have revealed a typical pattern marked by three distinct phases of FF behavior: (1) an initial rapid increasing phase, (2) a decreasing/enhancing phase, and (3) a gradual-long term increasing phase. This pattern is illustrated in Fig. 12.6.
- Essentially all commercial SGs are affected at some point by postoutage transient increases in the FF which can affect short-term operating margins but appear to be largely independent of longer-term fouling trends. These transients can have important effects for units operating with small thermal margins.
- For PWR SGs, heat-transfer fouling caused by secondary tube scale (among all known causes of thermal performance changes) generally has the potential for the largest adverse impact on SG thermal performance. However, many different effects have been observed, ranging from −100 to +200 μh-ft^2-°F/Btu as shown in Fig. 12.10. Many units currently have secondary scale which is having a near-neutral effect on thermal efficiency (i.e., they result in an FF near zero), meaning that other causes can collectively have a dominant influence on the SG thermal performance level.
- For CANDU SGs, the largest causes of SG thermal performance loss are generally primary tube deposits and divider-plate leakage, with an apparently smaller (but still significant) contribution in most cases from secondary tube scale.
- The severity of plant production losses (MWe) associated with a given SG thermal performance decrease depends on both the magnitude of the decrease as well as the available operating thermal margin.
- Of the various methods used to remove secondary tube deposit layers, both hard and soft chemical cleaning approaches have been used successfully many times to improve SG thermal performance levels in PWRs.
- For primary fouling deposits in CANDU units, mechanical removal methods that rely on blasting media are capable of removing a large fraction of the deposit mass, resulting in substantial improvements in SG thermal performance in at least one case.

12.7.2 Outlook

Because many units currently operate with intentionally small thermal margins (often ~1%) in order to maximize plant production, even the gradual future SG heat-transfer fouling that occurs at essentially all units can lead to sudden, costly declines in plant production levels (MWe). However, preventing these declines typically involves major cleaning evolutions, changes to the operating temperature that increase the risk

of component corrosion, and/or other remedies that can include costly plant modifications. Typically, the optimal strategy for addressing these tradeoffs is unit-specific. In order to identify the preferred strategy, some utilities carry out technical analysis that include SG FF evaluations, related heat-transfer projections, and associated economic assessments that quantify the costs and benefits of various SG management alternatives (Kreider et al., 2010; Colgan et al., 2010).

References

Alley, M., Jones, D., Evans, S., 2014. Deposit minimization treatment at Robinson Nuclear Plant. In: Paper Presented at the SGMP 2014 Steam Generator Secondary Side Management Conference Held in Baltimore, MD, September 23–25.

Barale, M., Guillodo, M., Brun, C., Clinard, M.-H., Corredera, G., De Bouvier, O., 2008. Preliminary laboratory tests of investigation on the blockage phenomena observed on TSP of French SGs. In: Poster Session Paper No. P2-41 Presented at the International Conference on Water Chemistry of Nuclear Reactor Systems 2008, Held in Berlin, Germany, September 15–18.

Baum, A.J., 1996. Westinghouse experience with performance degradation. In: Paper Presented at the EPRI Performance Degradation Meeting held in Charlotte, NC, February 6.

Bott, T.R., 1995. Fouling of Heat Exchangers. Elsevier, Amsterdam, The Netherlands, ISBN: 0-444-82186-4.

Brissette, D., Lafraniere, P., 1996. Review of operational experience at Gentilly-2 NGS with Reactor Inlet Header Temperatures (RIHT) rise. In: Paper Presented at the 4th Technical Committee Meeting on the Operational Safety Experience of PHWRs, Held in Kyongju, Korea, April 21–26.

Bruggeman, D.A.G., 1935. Ann. Phys. 24, 636–679.

Burrill, K.A., Turner, C.W., 1994. Control of Reactor Inlet Header Temperature (RIHT) rise in CANDU. In: Proceedings of a Conference on Steam Generators and Heat Exchangers, vol. 2. Canadian Nuclear Society/Société Nucléaire Canadienne, Toronto, Canada, ISBN: 0-919784-42-9, pp. 7.125–7.137 (Held in Toronto, Ontario, Canada, June 1994).

Campagna, A.O., Frisina, V.C., Carver, M.B., 1994. Validation of THIRST predictions against the CLOTAIRE experimental data. In: Proceedings of a Conference on Steam Generators and Heat Exchangers, vol. 1. Canadian Nuclear Society/Société Nucléaire Canadienne, Toronto, Canada, ISBN: 0-919784-42-9, pp. 4.1–4.18 (Held in Toronto, Ontario, Canada, June 1994).

Colgan, K., Fleck, J., Cyrus, B., 2010. Steam generator asset management—the future is now. In: Paper Presented at the SGMP 2010 Steam Generator Secondary Side Management Conference Held in San Antonio, TX, March 2–4.

Corredera, G., Alves-Vieira, M., De Bouvier, O., 2008. Fouling and TSP blockage of steam generators on EDF fleet: identified correlations with secondary water chemistry and planned remedies. In: Paper Presented at the International Conference on Water Chemistry of Nuclear Reactor Systems Held in Berlin, Germany, September 15–18.

Duncan, D., Varrin Jr., R.D., White, G.A., 1997. Heat transfer and chemical concentration modeling of porous tube scale deposits. In: Proceedings: Steam Generator Sludge Management Workshop, EPRI No. TR-108047. Electric Power Research Institute, Palo Alto, CA. pp. B6-1–B6-33 (Held in Myrtle Beach, SC, August 1996).

EPRI, 1980. Method of Reducing Carry-Over and Reducing Pressure Drop Through Steam Separators. EPRI, Palo Alto, CA. NP-1607.

EPRI, 1983a. Calibration of Instrumented Steam Separators to Determine Quality and Flow Distribution in an Operating Steam Generator. EPRI, Palo Alto, CA. NP-2805 (available for download at epri.com).
EPRI, 1983b. Numerical Simulation of Steam Separators Used in Nuclear Steam Generators and Reactor Systems. EPRI, Palo Alto, CA. NP-3063. Volume 1: Equations and Numerics.
EPRI, 1985. Steam Generator Reference Book. EPRI, Palo Alto, CA.
EPRI, 1986. ATHOS3: A Computer Program for Thermal-Hydraulic Analysis of Steam Generators. EPRI, Palo Alto, CA. NP-4604-CCM.
EPRI, 1991. Steam Generator Performance Degradation. EPRI, Palo Alto, CA. NP-7524.
EPRI, 1992. Ginna Station Steam Generator U-bend Tube Analysis for Chemical Cleaning Data. EPRI, Palo Alto, CA. TR-100866 (available for download at epri.com).
EPRI, 1996. Characterization of PWR Steam Generator Deposits. EPRI, Palo Alto, CA. TR-106048 (available for download at epri.com).
EPRI, 1998a. Steam Generator Thermal Performance Degradation Case Studies. EPRI, Palo Alto, CA. TR-110018 (available for download at epri.com).
EPRI, 1998b. Feasibility of Analytical Techniques to Quantify Hot-Leg Streaming. EPRI, Palo Alto, CA. TR-107325.
EPRI, 2001a. Dispersants for Tube Fouling Control—Volume 2: Short-Term Trial at ANO-2. EPRI/Entergy Operations, Palo Alto, CA/Russellville, AR. 1003144 (available for download at epri.com).
EPRI, 2001b. Dispersants for Tube Fouling Control—Volume 1: Qualification for a Short-Term Trial at ANO-2. EPRI/Entergy Operations, Palo Alto, CA/Russellville, AR. 1001422 [available for download at epri.com].
EPRI, 2002. Dispersants for Tube Fouling Control—Volume 3: Qualification for a Long-Term Trial in a Replacement Steam Generator Tubed With Alloy 690 TT. EPRI, Palo Alto, CA. 1002774 [available for download at epri.com].
EPRI, 2007. Dispersants for Tube Fouling Control—Volume 4: Long-Term Trial at McGuire Unit 2: Implementation and Results (2005–2006). EPRI, Palo Alto, CA. 1015021.
EPRI, 2008a. ATHOS/SGAP, Version 3.1: Analysis of the Thermal Hydraulics of a Steam Generator/Steam Generator Analysis Package. EPRI, Palo Alto, CA. 1016564.
EPRI, 2008b. Steam Generator Management Program: Thermal-Hydraulic Analysis of Representative Steam Generators with Various Tube Support Plate Blockages. EPRI, Palo Alto, CA. 1018344.
EPRI, 2010. Steam Generator Management Program: Flow-Induced Vibration and Fatigue Analyses of Representative Model 51 Steam Generators with Various Tube Support Plate Blockages. EPRI, Palo Alto, CA. 1020643.
EPRI, 2012a. Steam Generator Management Program: Assessment of the Effect of Deposit Removal Frequency on Sludge Management. EPRI, Palo Alto, CA. 1025127.
EPRI, 2012b. Steam Generator Management Program: Empirical Model for Predicting Recirculating PWR Steam Generator Broached-Hole Blockage. EPRI, Palo Alto, CA. 1025129.
EPRI, 2012c. Dispersants for Pressurized Water Reactor Secondary Side Fouling Control: Sourcebook for Online and Offline Applications: Volumes 1 and 2. EPRI, Palo Alto, CA. 1025317.
EPRI, 2014. Steam Generator Management Program: PWR Steam Generator Deposit Characterization Sourcebook. EPRI, Palo Alto, CA. 3002002794.
EPRI, 2015a. Triton Steam Generator Thermal-Hydraulics Code: Interim Report on Validation Using Experimental Test Results. EPRI, Palo Alto, CA. 3002005513.
EPRI, 2015b. Dispersants for PWR Secondary Side Fouling Control: 2014 Field Evaluations. EPRI, Palo Alto, CA. 3002005416.

EPRI, 2015c. Steam Generator Management Program: Steam Generator Deposit Removal Strategies Sourcebook. EPRI, Palo Alto, CA. 3002005090.

Fruzzetti, K., Rochester, D., Wilson, L., Kreider, M., Miller, A., 2008. Dispersant application for mitigation of steam generator fouling: final results from the McGuire 2 long-term trial and an industry update and EPRI perspective for long-term use. In: Paper Presented at the International Conference on Water Chemistry of Nuclear Reactor Systems Held in Berlin, Germany, September 15–18.

Fruzzetti, K., Kreider, M.A., Anderson, C.E., Marks, C.R., Morey, D.O., Walton, P.R., 2009. 2009 industry update on dispersant use for steam generator fouling control. In: Paper 4.08P Presented at the 6th CNS International Steam Generator Conference held in Toronto, Ontario, Canada, November 8–11.

Guillodo, M., Muller, T., Barale, M., Foucault, M., Clinard, M.-H., Brun, C., Chahma, F., Corredera, G., De Bouvier, O., 2009. Singular deposit formation in PWR due to electrokinetic phenomena—application to SG clogging. In: Paper 4.05 Presented at the 6th CNS International Steam Generator Conference held in Toronto, Ontario, Canada, November 8–11.

Hirano, H., Domae, M., Miyajima, K., Yoneda, K., 2010. Study on the mechanism of flow-hole blockage of steam generator tube support plates under PWR secondary conditions. In: Paper presented at the International Conference on Water Chemistry of Nuclear Reactor Systems 2010, held in Quebec City, Canada, October 3–7.

Hospeti, N.B., Mesler, R.B., 1965. Deposits formed beneath bubbles during nucleate boiling of radioactive calcium sulfate solutions. AIChE J. 11 (4), 662–665.

Hu, M.H., 1997. A new perspective of tube fouling and its effect on steam pressure. In: Proceedings: Steam Generator Sludge Management Workshop, EPRI No. TR-108047. Electric Power Research Institute, Palo Alto, CA. pp. B5-1–B5-27 (Held in Myrtle Beach, SC, August 1996).

Hu, M.H., 1998. Tube micro-fouling, boiling and steam pressure after chemical cleaning. In: Proceedings of the Third International Steam Generator and Heat Exchanger Conference. Canadian Nuclear Society/Société Nucléaire Canadienne, Toronto, Canada, ISBN: 0-919784-59-3, pp. 210–224 (Held in Toronto, Ontario, Canada, June 1998).

Hu, M.H., 2003. A strategic thinking to draw benefit from tube scale for boiling enhancement. In: Proceedings: 2003 Steam Generator Secondary Side Management Conference, EPRI No. 1008468. Electric Power Research Institute, Palo Alto, CA, pp. 727–763 (Held in Savannah, GA, February 2003).

Hu, M.H., 2006. Strategic managements of secondary chemistry and tube scale for enhancing boiling heat transfer of steam generators. In: Paper Presented at the International Conference on Water Chemistry of Nuclear Reactor Systems 2006 Held at Jeju Island, Korea, October 23–26.

Husain, A., Chew, V., 2006. Mechanical cleaning of steam generator primary side tube deposits: assessment of cleaning efficiency based on deposit characteristics. In: Paper Presented at the 5th CNS International Steam Generator Conference Held in Toronto, Ontario, Canada, November 26–29.

Incropera, F.P., DeWitt, D.P., 1985. Fundamentals of Heat and Mass Transfer, second ed. John Wiley & Sons, New York, NY, ISBN: 0-471-88550-9.

Jamialahmadi, M., Müller-Steinhagen, H., 1991. Reduction of calcium sulfate scale formation during nucleate boiling by addition of EDTA. Heat Transfer Eng. 12 (4), 19–26.

Jamialahmadi, M., Müller-Steinhagen, H., 1993. Scale formation during nucleate boiling—a review. Corros. Rev. 11 (1–2), 25–54.

Jones, D., Weiss, S., Schuss, S., Grember, F., 2012. Steam generator preventative chemical cleaning DMT update. In: Paper Presented at the SGMP 2012 Steam Generator Secondary Side Management Conference Held in Atlanta, GA, September 11–13.

Klarner, R., Steinmoeller, F., Millman, J., Schneider, W., 1998. Design and performance of BWC replacement steam generators for PWR systems. In: Proceedings of the Third International Steam Generator and Heat Exchanger Conference. Canadian Nuclear Society/Société Nucléaire Canadienne, Toronto, Canada, ISBN: 0-919784-59-3, pp. 17–46 (Held in Toronto, Ontario, Canada, June 1998).

Kreider, M.A., White, G.A., Varrin Jr., R.D., Srikantiah, G., 1997a. Steam generator thermal performance degradation case studies. In: EPRI Nuclear Plant Performance Improvement Seminar Proceedings, EPRI No. SP-108007-SL, Session III. Electric Power Research Institute, Palo Alto, CA (Held in San Antonio, TX, August 1997).

Kreider, M.A., White, G.A., Varrin Jr., R.D., Schwaebe, M., Matheny, A., 1997b. Predicting the steam pressure recovery following chemical cleaning at San Onofre unit 2. In: EPRI Nuclear Plant Performance Improvement Seminar Proceedings, EPRI No. SP-108007-SL, Session III. Electric Power Research Institute, Palo Alto, CA (Held in San Antonio, TX, August 1997).

Kreider, M.A., White, G.A., Varrin, R.D., Flores, O., Mihalik, M., 1998a. Management of steam generator thermal performance. In: Proceedings: Steam Generator Strategic Management Workshop, EPRI No. TR-111066, Presentation 13. Electric Power Research Institute, Palo Alto, CA (Held in Jackson Hole, WY, June 1998).

Kreider, M.A., White, G.A., Varrin Jr., R.D., 1998b. A global fouling factor methodology for analyzing steam generator thermal performance degradation. In: Proceedings of the Third International Steam Generator and Heat Exchanger Conference. Canadian Nuclear Society/Société Nucléaire Canadienne, Toronto, Canada, ISBN: 0-919784-59-3, pp. 190–208 (Held in Toronto, Ontario, Canada, June 1998).

Kreider, M.A., White, G.A., Varrin, R.D., Whitt, M., Baker, R., Verdin, G., Shaw, J., 2003. Thermal performance trends in replacement steam generators. In: Proceedings: 2003 Steam Generator Secondary Side Management Conference, EPRI No. 1008468. Electric Power Research Institute, Palo Alto, CA, pp. 765–819 (Held in Savannah, GA, February 2003).

Kreider, M.A., Moroney, V.D., White, G.A., Varrin Jr., R.D., 2009. Industry SG heat-transfer fouling trends and probabilistic fouling predictions. In: Paper 4.07P/5.09 Presented at the 6th CNS International Steam Generator Conference Held in Toronto, Ontario, Canada, November 8–11.

Kreider, M.A., Moroney, V.D., White, G.A., Varrin Jr., R.D., 2010. Probabilistic economic evaluation of steam generator management options: development and application at Exelon PWRs. In: Paper Presented at the SGMP 2010 Steam Generator Secondary Side Management Conference Held in San Antonio, TX, March 2–4.

Kreider, M.A., Moroney, V.D., Varrin, R.D., White, G.A., 2014. Steam generator thermal performance transients. In: Proceedings: Steam Generator Management Program 2014 Steam Generator Secondary Side Management Conference, EPRI No. 3002002756, Session 3, Paper No. 7. Electric Power Research Institute, Palo Alto, CA (Held in Baltimore, MD, September 2014).

Kreider, M., Moroney, V., Schmitt, K., White, G., Creegan, P., Valdez, M., Friant, L., 2015. Probabilistic modeling of primary separator degradation in the Byron and Braidwood steam generators. In: Paper Presented at INCC2015, the International Nuclear Components Conference Held in Mississauga, Ontario, Canada, November 1–4.

Lee, J.Y., Kim, H.D., Yoon, D.J., 2009. Prediction of the SG tube support plate flow area blockage rate using SG wide range level measurements and hydrodynamic analysis. J. Nucl. Sci. Technol. 46 (7), 753–762.

Lepine, B., Obrutsky, L., 2006. The impact of magnetite deposits on steam generator inspections. In: Paper Presented at the 5th CNS International Steam Generator Conference Held in Toronto, Ontario, Canada, November 26–29.

Little, M.J., Varrin Jr., R.D., Pellman, A.T., Kreider, M.A., 2009. Advanced Scale Conditioning Agent (ASCA) applications: 2009 experience update. In: Paper 4.03 Presented at the 6th CNS International Steam Generator Conference Held in Toronto, Ontario, Canada, November 8–11.

Little, M.J., Varrin Jr., R.D., Pellman, A.T., Kreider, M.A., 2010. Advanced Scale Conditioning Agent (ASCA) applications: 2010 experience update. In: Paper Presented at the SGMP 2010 Steam Generator Secondary Side Management Conference Held in San Antonio, TX, March 2–4, p. 2010.

Little, M.J., Varrin Jr., R.D., Pellman, A.T., Kreider, M.A., 2012a. SG cleaning with ASCA solutions: 2012 experience update. In: Paper Presented at the SGMP 2012 Steam Generator Secondary Side Management Conference Held in Atlanta, GA, September 11–13.

Little, M.J., Varrin Jr., R.D., Pellman, A.T., Kreider, M., 2012b. Advanced Scale Conditioning Agent (ASCA) applications: 2012 experience update. In: Presented at NPC 2012 Paris: International Conference on Water Chemistry of Nuclear Reactor Systems, September 23–27, Paris, France.

Little, M., McCree, A., Varrin Jr., R., Pellman, A., Kreider, M., 2014. Advanced Scale Conditioning Agent (ASCA) applications: 2014 experience update, paper no. 10104. In: Presented at NPC 2014 Sapporo: Nuclear Plant Chemistry Conference, October 26–31, Sapporo, Japan.

Maanshan Unit 2 Steam Generator Level Oscillation and Cleaning. PowerPoint presentation dated May 31–June 1, 2005, available at the web site www.aec.gov.tw/english/nuclear/files/2005-04.pdf [Taiwan Atomic Energy Council ("Historical"/"Technical")].

Malaugh, J., Ryder, S., St. Louis, D., 1990. Bruce NGS-A support plate inspection and waterlancing. In: Proceedings of a Conference on Steam Generators and Heat Exchangers. Toronto, Canada, Canadian Nuclear Society, ISBN: 0-919784-24-0, pp. 3.51–3.76 (Held in Toronto, Ontario, Canada, 1990).

Malgaard, J., Smeltzer, W.W., 1971. Thermal conductivity of magnetite and hematite. J. Appl. Phys. 42 (9), 3644–3647.

Mayer, T., Jones, D., 2010. DMT applications at Surry Nuclear Power Stations 2009. In: Paper Presented at the SGMP 2010 Steam Generator Secondary Side Management Conference Held in San Antonio, TX, March 2–4.

Macbeth, R.V., 1971. Boiling on Surfaces Overlayed With a Porous Deposit: Heat Transfer Rates Obtainable by Capillary Action. United Kingdom Atomic Energy Authority, Winfrith, UK. AEEW-R.711.

Moleiro, E., Oukacine, F., Adobes, A., 2010. Secondary fouling and TSP flow blockage: a model based on transport equations. In: Paper Presented at the SGMP 2010 Steam Generator Secondary Side Management Conference, March 2–4, 2010, San Antonio, TX.

NUREG/CR-6754, BNL-NUREG-52646, 2001. Review of Industry Responses to NRC Generic Letter 97-06 on Degradation of Steam Generator Internals. Brookhaven National Laboratory and US Nuclear Regulatory Commission, New York, NY and Washington, DC.

Oukacine, F., Prusek, T., Moleiro, E., Touazi, O., 2012. Deposits on steam generator tube support plates: a model to evaluate the local blockage evolution and the global flow

redistribution. In: Paper Presented at the SGMP 2012 Steam Generator Secondary Side Management Conference Held in Atlanta, GA, September 11–13.

Pan, C., Jones, B.G., Machiels, A.J., 1985. Wick boiling performance in porous deposits with chimneys. In: Paper Presented at the ASME/AIChE/ANS National Heat Transfer Conference Symposium on Multiphase Flow and Heat Transfer Held in Denver, CO, August.

Pietralik, J.M., Campagna, A.O., Frisina, V.C., 1998. Validation of the THIRST steam generator thermal hydraulic code against the CLOTAIRE Phase II experimental data. In: Proceedings of the Third International Steam Generator and Heat Exchanger Conference. Canadian Nuclear Society/Société Nucléaire Canadienne, Toronto, Canada, ISBN: 0-919784-59-3, pp. 275–292 (Held in Toronto, Ontario, Canada, June 1998).

Prueter, W.P., Reed, M.J., 1994. Extended steam/water testing of the Babcock & Wilcox separation equipment. In: Paper Presented at the Second International Steam Generator and Heat Exchanger Conference Held in Toronto, Ontario, Canada, June 13–15.

Puzzuoli, F.V., Murchie, B., Allen, S., 1995. Water lancing of Bruce-A Unit 3 and 4 steam generators. In: Third International Conference on CANDU Maintenance Proceedings. Canadian Nuclear Society/Société Nucléaire Canadienne, Toronto, Canada, pp. 189–212 (Held in Toronto, Ontario, Canada, November 1995).

Rohsenow, W.M., Hartnett, J.P., Ganic, E.N. (Eds.), 1985. Handbook of Heat Transfer: Fundamentals, second ed. McGraw-Hill Book Company, New York, NY, ISBN: 978-0070535541 (Chapter 12, including pp. 12–44).

Schmitt, K.P., Kreider, M., Feldman, H., 2012. Development of an empirical model for predicting TSP blockage in recirculating PWR SGs. In: Proceedings: Steam Generator Management Program 2012 Steam Generator Secondary Side Management Conference, EPRI No. 1026545, Presentation No. 4-2. Electric Power Research Institute, Palo Alto, CA (Held in Atlanta, GA, September 11–13, 2012).

Steam Generator Pressure Loss Survey 95-016, 1996. Electric Power Research Institute (EPRI) Plant Support Engineering P^2EP (Plant Performance Enhancement Program). Survey results distributed to survey initiators and respondents in Plant Support Engineering letter dated November 30, 1995. In: Survey Results Also Presented by A. L. Matheny at the Steam Generator Performance Degradation Meeting, Charlotte, NC, February 6.

Stickel, M., Miller, H., 1994. Steam generator water level oscillation due to TSP flow blockage. In: Paper No. 15 in Proceedings: Steam Generator Sludge Management Workshop. EPRI, Palo Alto, CA. TR-104212 (Workshop held in Norfolk, VA, May 10–12, 1994).

Sweeney, K., Melton, M., Radspinner, M., Begley, J., 1994. Free-span IGA/IGSCC at the Palo Verde Nuclear Generating Station. In: Proceedings of a Conference on Steam Generators and Heat Exchangers, vol. 1. Canadian Nuclear Society/Société Nucléaire Canadienne, Toronto, Canada, ISBN: 0-919784-42-9, pp. 1.93–1.104 (Held in Toronto, Ontario, Canada, June 1994).

Tincq, D., David, F., Rascle, P., 1994. THYC, a 3D thermal-hydraulic code for steam generators, heat exchangers and condensers: recent developments and validation tests. In: Proceedings of a Conference on Steam Generators and Heat Exchangers, vol. 1. Canadian Nuclear Society/Société Nucléaire Canadienne, Toronto, Canada, ISBN: 0-919784-42-9, pp. 5.1–5.15 (Held in Toronto, Ontario, Canada, June 1994).

Uhle, J.L., 1997. Boiling heat transfer characteristics of steam generator U-tube fouling deposits. PhD Dissertation, Massachusetts Institute of Technology.

Varrin Jr., R.D., Stanley, R., Gary, G., 2003. Recent experiences with secondary side deposit characterization. In: Proceedings: 2003 Steam Generator Secondary Side Management Conference, EPRI No. 1008468. Electric Power Research Institute, Palo Alto, CA, pp. 433–471 (Held in Savannah, GA, February 2003).

Vergnault, A., Dorel, R., Goux, F., 2008. Steam generator blockage: a thermal-hydraulic approach based on CATHARE 2. In: Proceedings of the 16th International Conference on Nuclear Engineering—2008. American Society of Mechanical Engineers, New York, NY, ISBN: 0-791848-14-0 (Held in Orlando, FL, May 2008).

Weiss, S., Grember, F., Jones, D., 2012. DMT—AREVA's steam generator maintenance cleaning process concept and experiences. In: Presented at NPC 2012 Paris: International Conference on Water Chemistry of Nuclear Reactor Systems, September 23–27, Paris, France.

White, G.A., 2001. Fouling experience of pressurized water reactor nuclear steam generators in the US. In: Proceedings of the 4th International Conference on Heat Exchanger Fouling: Fundamental Approaches & Technical Solutions, vol. 2, Paper 38. United Engineering Foundation, New York, NY, ISBN: 393473605X (Held in Davos, Switzerland, July 8–13, 2001).

White, G.A., Kreider, M.A., Varrin Jr., R.D., 1996. Causes of PWR steam generator thermal performance degradation. In: Paper Presented at the Sixth EPRI PSE Nuclear Plant Performance Improvement Seminar Held in Asheville, NC, September.

Yetisir, M., Turner, C.W., Pietralik, J., 2000. Contribution of SG degradation mechanisms to RIHT behavior. In: Paper Presented at the Fifth CNS International Conference on CANDU Maintenance Held in Toronto, Ontario, Canada, November 19–21.

Yetisir, M., Laroche, S., Turner, C.W., 2003. A technique to infer steam generator fouling factors from tube deposit loading. In: Paper Presented at the Sixth CNS International Conference on CANDU Maintenance Held in Toronto, Ontario, Canada, November 16–18.

Flow-induced vibrations in nuclear steam generators

13

M. Hassan
School of Engineering University of Guelph, Guelph, ON, Canada

13.1 Flow characteristics

Flow characteristics, such as density and velocity, are very important parameters that need to be determined for any successful vibration analysis. Flow velocity distribution is highly dependent on the tube arrangement and tube pitch. Fig. 13.1 shows the basic tube arrangement that is frequently encountered in heat exchangers. The ratio of the tube pitch (P) to the tube diameter (d) is one of the important parameters that affect the flow velocity calculations. The pitch flow velocity (U_p) is often used as the representative velocity in a tube bundle with a pitch-to-diameter ratio of ($P_r = P/d$) and is calculated as follows:

$$U_P = \frac{P_r}{P_r - 1} U_\infty$$

where U_∞ is the upstream flow velocity. The flow distribution in a tube array in terms of flow velocity and density is very important as it is required to estimate the basic flow excitations. However, such calculations are too complex to be carried out analytically or experimentally. Specialized computational fluid dynamics codes are usually used to give an estimate of the flow velocity and the fluid density distributions. An example of the calculated velocity distribution in the U-bend region of a steam generator is shown in Fig. 13.1.

The flow characteristics also affect the tube dynamic parameters. For example, the effective mass of the tube includes the mass of the tube, the internal fluid and the part of the external fluid that vibrates with the tube. The effective mass per unit length is given by:

$$m_t = m_s + m_i + m_a$$

where m_s, m_i, and m_a are the structural, internal, and external added mass, respectively. The internal fluid mass depends on the internal fluid density (ρ_i) and the inside tube diameter $\left(m_i = \frac{\pi}{4} d_i^2 \rho_i\right)$. The external flow added mass is dependent on the array geometry, external flow density (ρ_f), tube diameter (d), and tube pitch (P). It is customary to express the fluid added mass in terms of the added mass coefficient (C_m) which is the ratio of the fluid added mass (m_a) to the fluid displaced by the tube

Steam Generators for Nuclear Power Plants. http://dx.doi.org/10.1016/B978-0-08-100894-2.00015-7
© 2017 Elsevier Ltd. All rights reserved.

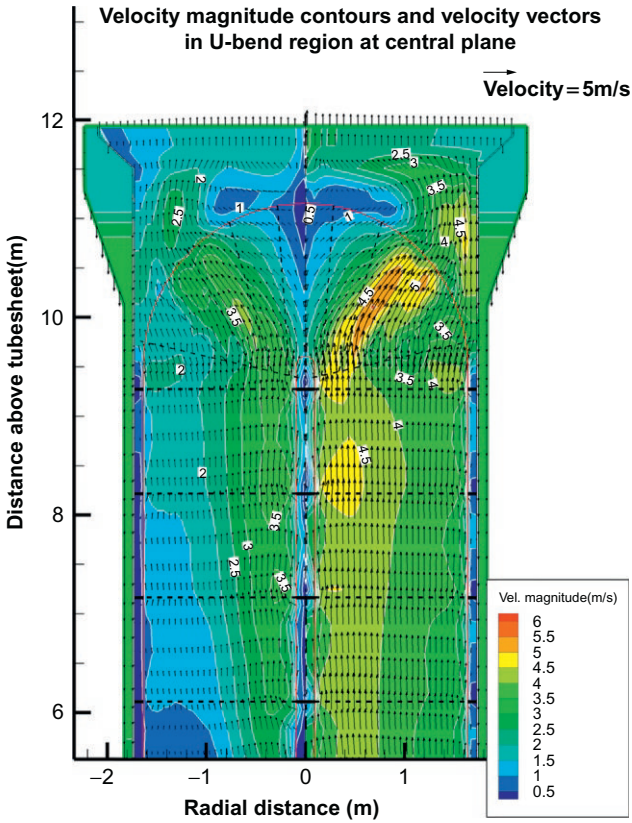

Fig. 13.1 Typical flow distribution in a U-bend tube array.

$\left(m_i = \frac{\pi}{4} d^2 \rho_f\right)$. The added mass coefficient (C_m) can be obtained using the potential flow theory for ideal fluids. Alternatively, one can use the empirical equations.

13.2 Tube vibration characteristics

Vibration analysis aims at ensuring that resonance is absent and that the system is dynamically stable within the intended operating range. Important parameters, such as natural frequencies, mode shapes, and damping, are essential to carry out this analysis. An important step towards this goal is to establish a mathematical model that represents the structure. A typical steam generator tube bundle is shown in Fig. 13.2. The tube structure can be modeled as an Euler-Bernoulli beam:

$$\rho A \frac{\partial^2 w}{\partial t^2} + c \frac{\partial w}{\partial t} + EI \frac{\partial^4 w}{\partial x^4} = F$$

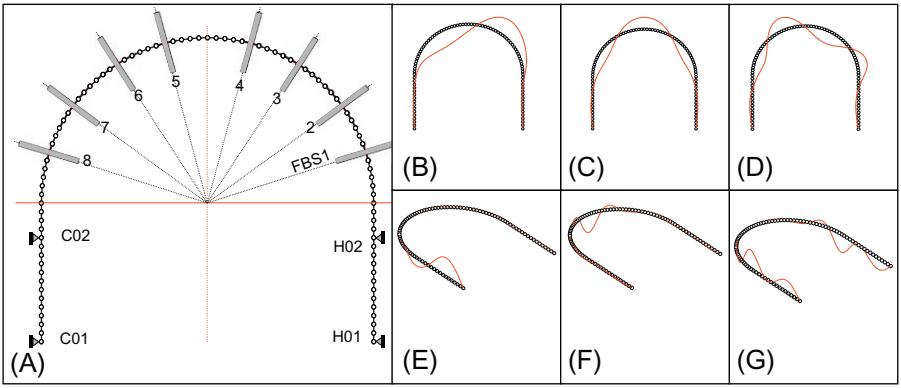

Fig. 13.2 Typical U-bend mode: (A) finite element model, (B–G) mode shapes.

where w, x, and t are the structural response, coordinate, and time, respectively. c, ρ, and EI are the damping, tube density, and the bending stiffness, respectively. The fluid force is represented by F. Standard text books, such as Rao (2016) and Thomson and Dahleh (1997), give a detailed derivation of the above equation. The solution to the above equation is available for simple tube configurations. However, for a U-bend tube bundle the above equation would be rather difficult to use directly to resolve the tube dynamics. Therefore, finite element method is usually utilized. In the finite element frame, the governing equation is expressed as:

$$[M_s]\{\ddot{w}\} + [C_s]\{\dot{w}\} + [K_s]\{w\} = \{F\}$$

where M, C, and K are the structural mass, the stiffness, and the damping matrices, respectively. The eigenvalues and eigen vectors (natural frequencies (f_n) and mode shapes (ϕ)) of the above equation can be easily extracted when the above equation is projected on the modal coordinates. The reduced set of the modal equations of motion are written in terms of the modes as:

$$\left[\widetilde{M}_s\right]\{\ddot{q}\} + \left[\widetilde{C}_s\right]\{\dot{q}\} + \left[\widetilde{K}_s\right]\{wq\} = \left\{\widetilde{F}\right\}$$

where $\widetilde{M}$, $\widetilde{C}$, and $\widetilde{K}$ are modal structural matrices. $\widetilde{F}$ and q are the modal forces and the response, respectively. An example of the mode shapes performed on a reduced U-bend tube model is shown in Fig. 13.2. The model shown in Fig. 13.2A is a reduced model of a U-bend tube where only part of the straight leg is considered. The tube is supported by eight antivibration bars (AVBs) in the U-bend region. These bars prevent tube motion in the out-of-plane direction, i.e., in the direction normal to the U-bend plane.

However, they do not prevent the in-plane motion. Four additional pinned supports are added in the straight part of the tube (H01, H02, C01, and C03). These pinned supports are used to model the straight leg supports. Mode shapes for the first three in-plane and out-of-plane modes are shown in Fig. 13.2B–D. As can be seen, AVBs

are not forcing vibration nodes at the support locations. The out-of-plane modes shown here are estimated by assuming that all the supports are effective in the out-of-plane direction. The effect of the added mass due to both the internal and the external flows is included in the natural frequencies and the mode shapes.

The majority of the commercial finite element packages can be easily utilized to obtain the above calculations of the natural frequencies and mode shapes.

Damping is one of the most important parameters that greatly influence the level of the response and the stability threshold of the system. Several sources contribute to the overall value of damping:

(1) Structural damping (ζ_s): This component represents the capacity of the structure to dissipate vibration energy by internal material friction. This type of damping is usually measured in the air.

(2) Viscous damping ζ_v: This part of damping accounts for the ability of a fluid to absorb the vibration energy. It is normally measured for a vibrating tube in a quiescent fluid. All the surrounding tubes are considered to be rigid. The viscous damping can be estimated using the formula developed by Rogers et al. (1984):

$$\zeta_v = \frac{\pi}{\sqrt{8}}\left(\frac{\rho_f d^2}{m}\right)\left(\frac{2\nu}{\pi f d^2}\right)^{0.5}\left(\frac{1+\left(\frac{d}{D_e}\right)^3}{\left(1-\left(\frac{d}{D_e}\right)^2\right)^2}\right)$$

where ρ_f, ν, f, and D_e are the flow density, viscosity, vibration frequency, and effective diameter, respectively. The effective diameter is dependent on the tube array geometry. For a triangular tube array, $D_e/D = (0.96\ 0.50\ P/D)\ P/D$. Similarly, for a square tube bundle, $D_e/D = (1.7\ 0.56\ P/D)\ P/D$.

(3) Flow velocity-dependent damping ζ_f; This component represents the energy dissipated by the flow as it interacts with the vibrating tube. It is a function of the flow velocity.

13.3 Excitation mechanisms

There are three main mechanisms that account for flow-induced vibrations in heat exchangers. These mechanisms depend on the flow conditions and the structure of the tubes. They are broadly classified as (a) turbulent buffeting, (b) Strouhal periodicity, and (c) fluidelastic instability (Weaver and Fitzpatrick, 1988). These mechanisms arise from the fluid flow on the outside of the tubes. The fluid flow inside the tubes does result in forces that cause vibration. However, the primary flow contributes to the dynamics by adding mass to the total mass of the tube. The tube response resulting from increasing flow velocity is shown in Fig. 13.3 and is often used to explain the signature of these mechanisms. In this figure, the strength/range of action of the three mechanisms is illustrated. The large amplitudes in vibration due to vortex shedding (Strouhal periodicity) take place over a small range of flow velocities. Fluidelastic instability becomes dominant after a

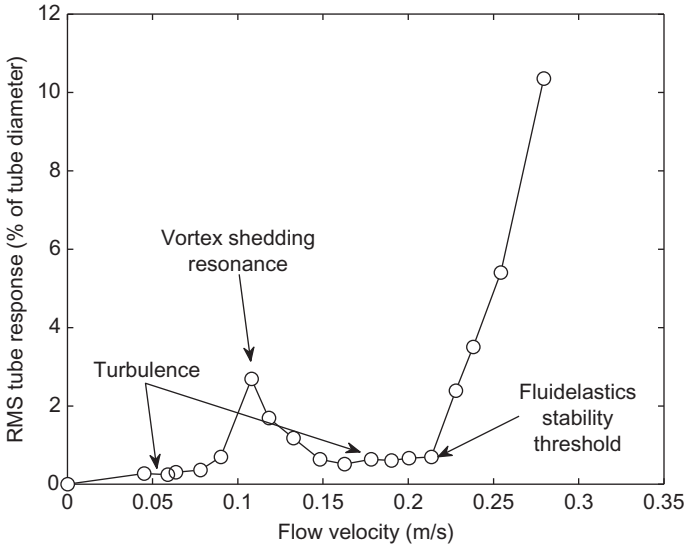

Fig. 13.3 Tube response as a function of the flow velocity.

certain flow (stability threshold) velocity, while turbulence excitation is thought to be active throughout the full range of flow velocities. It should be noted here that the responses due to vortex shedding and fluidelastic instability are very large and should therefore be avoided.

13.3.1 Strouhal periodicity

This mechanism is one of the most studied, especially for isolated cylinders, and has been referred to as vortex shedding, periodic wake shedding, and Strouhal excitation (Weaver and Fitzpatrick, 1988). Strouhal periodicity manifests itself in the tube response as a discrete peak with a frequency that is proportional to the flow velocity:

$$f_s = S_t \frac{U_p}{d}$$

As can be seen, Strouhal frequency is proportional to the flow velocity through the Strouhal number S_t. The problem can be treated as a forced vibration problem as long as the Strouhal frequency is sufficiently removed from the natural frequency of the tube. If the natural frequency is close to the Strouhal frequency, the process becomes locked-on, where the latter synchronizes with the natural frequency of the tube. This results in a large resonant peak in the tube response. The possibility of vorticities occurring in tube arrays has been disputed for some time. These are often mis-characterized as buffeting. However, during the last two decades, studies, such as those of Polak and Weaver (1995) and Ziada and Oengören (1993), have provided ample evidence for the existence of these Strouhal periodicities. In liquid flows,

the consequences of Strouhal periodicity can be severe, especially in cases in which the frequency coincides with the tube's natural frequency. However, for most tube array geometries and mass ratios, a clear resonant peak may not be well-defined as it usually coincides with the fluidelastic instability threshold. The resonance phenomenon may not be of concern at all in gas flows in terms of compromising the tube's structural integrity. However, such frequency coincidences could trigger acoustic resonance (Oengoren and Ziada, 1995).

For design purposes, the lock-in can be avoided by a frequency mismatch between the periodicity (f_s) and the tube's natural frequencies (f_n). As a rule of thumb the frequency ratio should be such that:

$$0.8 > \frac{f_s}{f_n} > 1.2$$

13.3.2 Turbulence excitation

Unlike fluidelastic instability and Strouhal periodicity, turbulence may not cause large-amplitude vibrations in tube bundles, and therefore should not lead to catastrophic tube failure. Turbulence excitation is ubiquitous, leads to small amplitude vibrations, and cannot be avoided. In fact, turbulence is promoted in designs to provide improved heat transfer by choosing certain coolant paths and flow rates. Turbulence results in random vibrations in tube bundles, often referred to as subcritical vibrations as they are dominant in the prestability region. As mentioned earlier, turbulence is usually of much smaller amplitude than that experienced in fluidelastic instability. However, this excitation can supply enough energy to tubes to cause them to impact and rub continuously against their supports. This in turn leads to progressive damage to the tubes in the form of fretting wear. Such excitation determines the long-term integrity of the structure, and it is a very important parameter to consider in aging steam generators.

Turbulence excitation acting on tubes can arise from two sources. The upstream tubes in the inlet region of heat exchangers are excited by the turbulence generated upstream of the inlet nozzle or within the inlet port, baffles, etc. Such excitation is referred to as far-field excitation as it is governed by the upstream components. On the other hand, the interior tubes are excited by the turbulence generated within the bundle. Therefore, the turbulence level is governed by the tube bundle geometry.

The turbulence excitation is random in nature and can be analyzed using a stochastic analysis procedure such as a spectral analysis. The power spectral density (S_f) of the fluid force fluctuations is often utilized as a measure of the turbulence excitation. Several empirically based bounding spectra of turbulence excitation are presented by Pettigrew and Gorman (1973), Axisa et al. (1990), Oengören and Ziada (1998), and Taylor and Pettigrew (2000); for example, the power spectral density (PSD) of the dynamic turbulence force acting on a tube within a normal triangular tube array for various P/D are shown in Table 13.1.

Table 13.1 Turbulence PSD for a triangular array for the lift direction

P/D	Turbulence PSD (lift direction)
1.61	$\phi_L = 4.75 \times 10^{-3} \left(\frac{fd}{U}\right)^{-0.4}$ for $\frac{fd}{U} < 0.43$
	$\phi_L = 1.02 \times 10^{-4} \left(\frac{fd}{U}\right)^{-5}$ for $\frac{fd}{U} > 0.43$
2.08	$\phi_L = 6.34 \times 10^{-3} \left(\frac{fd}{U}\right)^{-0.4}$ for $\frac{fd}{U} < 0.46$
	$\phi_L = 1.80 \times 10^{-4} \left(\frac{fd}{U}\right)^{-5}$ for $\frac{fd}{U} > 0.46$
3.41	$\phi_L = 3.87 \times 10^{-2} \left(\frac{fd}{U}\right)^{-0.4}$ for $\frac{fd}{U} < 0.27$
	$\phi_L = 1.00 \times 10^{-4} \left(\frac{fd}{U}\right)^{-5}$ for $\frac{fd}{U} > 0.27$

Similarly, the bounding spectra for the drag direction was measured and expressed in Table 13.2.

As can be seen, the turbulence PSD in the drag direction is much lower than that in the lift direction. It is also noticed that the PSD is dependent on the *P/D* ratio. The highest level of dynamic forces was found to be in the lower-frequency range ($fd/U < 0.4$). Fig. 13.4 shows the measured turbulence PSD for the inline tube arrays.

The theory of random vibrations provides a powerful tool to develop an equation for the mean square of tube response. The derivation of this equation can be found in various texts and papers such as Pettigrew and Gorman (1978). The expected (mean) square of the tube response can be expressed as:

$$\overline{w_L^2}(s) = \sum_{i=1}^{\infty} \frac{l d S_F(f_i) \phi_i^2(s)}{64\pi^3 f_i^3 m_i^2 \zeta_i} J_{ii}(f_i)$$

$$\overline{w_L^2} = \sum_{l=1}^{\infty}\sum_{k=1}^{\infty} \frac{\phi_i(s)\phi_k(s)}{16\pi^4 f_i^2 f_k^2 m^2} \int_{-\infty}^{\infty} H_i(f) H_k{}^*(f) \int_0^L \int_0^L \phi_i(s)\phi_k(s) S_{F_s F_{\acute{s}}}(s, \acute{s}, f)\, ds\, d\acute{s}\, df$$

where $\phi_i(s)$ and f_i are the ith mode shape and the natural frequency of the tube while $S_F(f)$ is the cross spectral power density of the turbulence excitation, and s is the location on the tube. J is the joint acceptance for the ith mode. The joint acceptance can be expressed as:

$$J_{lk} = \frac{1}{L} \int_0^L \int_0^L \phi_i(\acute{s})\phi_k(s) S_{F_s F_{\acute{s}}}(s, \acute{s}, f)\, ds\, d\acute{s}\, df$$

Table 13.2 Turbulence PSD for a triangular array for the drag direction

P/D	Turbulence PSD (drag direction)
1.61	$\phi_D = 7.35 \times 10^{-4} \left(\frac{fd}{U}\right)^{-0.4}$ for $\frac{fd}{U} < 0.53$
	$\phi_D = 3.96 \times 10^{-5} \left(\frac{fd}{U}\right)^{-5}$ for $\frac{fd}{U} > 0.53$
2.08	$\phi_D = 1.11 \times 10^{-3} \left(\frac{fd}{U}\right)^{-0.4}$ for $\frac{fd}{U} < 0.48$
	$\phi_D = 3.79 \times 10^{-5} \left(\frac{fd}{U}\right)^{-5}$ for $\frac{fd}{U} > 0.48$
3.41	$\phi_D = 9.51 \times 10^{-3} \left(\frac{fd}{U}\right)^{-0.4}$ for $\frac{fd}{U} < 0.38$
	$\phi_D = 1.00 \times 10^{-4} \left(\frac{fd}{U}\right)^{-5}$ for $\frac{fd}{U} > 0.38$

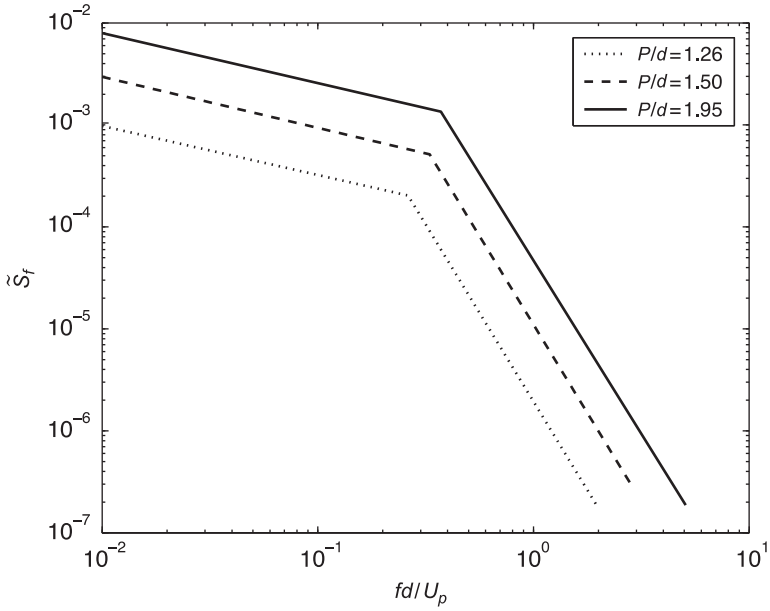

Fig. 13.4 Turbulence bounding PSD for inline tube arrays.

The above equation yields simple expressions when dealing with a single span with a uniform flow over the entire length of the tube. For practical configurations the above analytical expression becomes difficult to use. In this case, the finite element method is used to obtain the response of the system. These forces are usually generated and applied at each finite element.

13.3.3 Fluidelastic instability

Fluidelastic instability is the excitation mechanism with the greatest potential for short term damage to heat exchangers. The complete process leading to this instability is not yet fully understood. Generally, in a tube bundle the fluid forces acting on a tube are affected by both the motion of the tube and its neighbors. This creates an interaction between the fluid forces and the tube motion. Fluidelastic instability forces come into effect when the fluid forces are proportional to the tube displacement and/or are in-phase with the tube velocities. Instability occurs when the amount of energy expended by the tube motion through damping is less than the energy input to the tube. The mechanism is characterized by a critical flow velocity (U_c) below which vibrational amplitudes are small, and above which the amplitudes increase rapidly. Fluidelastic instability is widely acknowledged to be the most complex of these phenomena, since it has the potential to induce large vibration amplitudes when the critical flow velocity is exceeded. This in turn causes severe tube damage, which in certain cases, may be catastrophic. FEI was therefore well researched, leading to considerable amounts of experimental data, which was used to develop empirical models and design guidelines. In addition, a number of theoretical models were developed. These have also contributed to understanding the phenomenon. A detailed description of the available theoretical models can be found in the work of Price (1995). As well, a critical examination of these models with respect to their contributions and deficiencies can be found in a recent paper by Weaver (2008). The available FEI models can predict whether a design is adequate if the flow velocity is below the critical value or inadequate if the flow velocity is above the critical value. The following is a brief overview of the available models.

13.3.3.1 Quasistatic model

In this approach, the steady fluid forces are measured for tube arrays when tubes are displaced relative to one another. The resulting force displacement relationship was used to compute the work done on the tube. An estimation was made of the equivalent periodic force in phase with the tube velocity that would produce the same work done on the tube. The stability threshold was deduced by equating the fluid force energy and the energy dissipated by the structural damping. This approach resulted in the well-known Connors formula, which relates the reduced critical flow velocity $\left(U_{cr} = \frac{U_c}{fd}\right)$ to the mass damping parameter $\left(\mathrm{MDP} = \frac{m_t \delta}{\rho_f d}\right)$ as follows:

$$\frac{U_c}{fd} = k\left(\frac{m_t \delta}{\rho_f d^2}\right)^b$$

where δ and ρ_f are the damping logarithmic decrement and flow density, respectively. K and b are empirical constants. Connors originally proposed values of 9.9 and 0.5 for these constants in the case of a tube row. Extensive experimental investigations were conducted over the last four decades to devise values for these constants suitable for application to tube arrays.

13.3.3.2 Unsteady flow model

In the unsteady flow model, the fluid forces acting on a tube within a group of tubes can be expressed as a linear combination of the response of the tube and the surrounding tubes. These forces were expressed in terms of a number of fluid force coefficients as follows:

$$F_{L_j} = -\frac{\pi\rho_f d^2}{4}\sum_{k=1}^{N}\left(\alpha''_{jk}\ddot{w}_{L_k} + \sigma''_{jk}\ddot{w}_{D_k}\right)$$

$$+\frac{2\pi\rho_f U^2}{f}\sum_{k=1}^{N}\left(\alpha'_{jk}\dot{w}_{L_k} + \sigma'_{jk}\dot{w}_{D_k}\right)$$

$$+\rho_f U^2\sum_{k=1}^{N}\left(\alpha_{jk}w_{L_k} + \sigma_{jk}w_{D_k}\right)$$

$$F_D = -\frac{\pi\rho_f d^2}{4}\sum_{k=1}^{N}\left(\tau''_{jk}\ddot{w}_{L_k} + \beta''_{jk}\ddot{w}_{D_k}\right)$$

$$+\frac{2\pi\rho_f U^2}{f}\sum_{k=1}^{N}\left(\tau'_{jk}\dot{w}_{L_k} + \beta'_{jk}\dot{w}_{D_k}\right) + \rho_f U^2\sum_{k=1}^{N}\left(\tau_{jk}w_{L_k} + \beta_{jk}w_{D_k}\right)$$

where α''_{jk}, σ''_{jk}, τ''_{jk}, and β''_{jk} are the inertial force coefficients, α'_{jk}, σ'_{jk}, τ'_{jk}, and β'_{jk} are the fluid damping coefficients, and α_{jk}, σ_{jk}, τ_{jk}, and β_{jk} are the fluid stiffness coefficients. These force coefficients can be obtained experimentally (Chen, 1983) or numerically (Hassan and Hossen, 2010). Fig. 13.5 shows a sample of these force coefficients.

The FEI forces can be substituted in the right hand side of the equation of motion as an external force vector. Alternatively, the inertial, damping and stiffness components of the FEI force can be moved to the left hand side of the equation as added fluid components. The above equation can be written in matrix form as follows:

$$\left[M_s + M_f\right]\{\ddot{w}\} + \left[C_s + C_f\right]\{\dot{w}\} + \left[K_s + K_f\right]\{w\} = \{0\}$$

where M_f, C_f, and K_f are the fluid contributions to the mass, damping, and stiffness matrices, respectively. Considering the vibrations in the lift direction only, the above equation for a single flexible tube reduces to:

$$\left(M_s + \frac{\pi\rho_f d^2\alpha''_{11}}{4}\right)\ddot{w} + \left(C_s + \frac{2\pi\rho_f U^2\alpha'_{11}}{f}\right)\dot{w} + \left(K_s + \frac{2\pi\rho_f U^2\alpha}{f}\right)w = 0$$

The critical flow velocity can be obtained by equating the total damping to zero:

$$C_s + \frac{2\pi\rho_f U^2\alpha'_{11}}{f} = 0$$

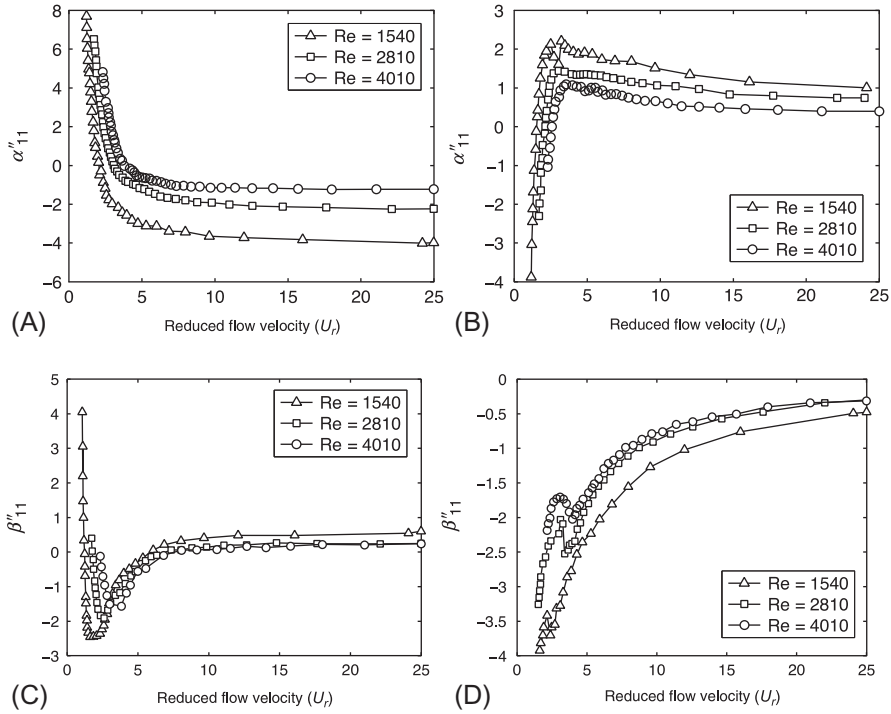

Fig. 13.5 Sample force coefficients for an inline tube array (Hassan and Hossen, 2010): (A,C) fluid damping coefficients, (B,D) fluid stiffness coefficients.

This results in the following stability equation:

$$\frac{U_c}{fd} = \left(\frac{1}{\pi\alpha'_{11}}\right)^{0.5}\left(\frac{m_t\delta}{\rho_f d^2}\right)^{0.5}$$

The above equation is similar to the familiar Connors equation except that the Connors constant K is now a function of the damping coefficient α'_{11}.

13.3.3.3 Quasisteady model

Based on the quasisteady approach, Price and Païdoussis (1984) developed a semiempirical approach. In this model the instantaneous lift and drag forces acting on a tube is similar to those acting on an identical tube moving with a constant velocity equal to the current velocity values. Using this approach and utilizing the symmetry characteristics of fluid forces, the number of force coefficient measurements required is significantly reduced. One of the interesting aspects of this model is the introduction of a time delay in the fluid tube coupling. This time delay allows the tube to extract energy from the flow, and hence the instability becomes possible. This phase between the

tube motion and the resulting fluid forces is attributed to the flow retardation effect. The fluid force can then be expressed as:

$$F_L = \frac{\rho_f d L U^2}{2}\left(C_L - \frac{2d\dot{w}_D}{U}C_L - \frac{d\dot{w}_L}{U}C_D\right)$$

Linearizing the force coefficients about the equilibrium position results in:

$$C_L = C_{Lo} + \frac{\partial C_L}{\partial x}w_D + \frac{\partial C_L}{\partial y}w_L$$

Now for the single DOF, the above can yield a damping type instability only if a phase lag is introduced to account for the flow retardation. This phase lag (τ) is expressed in terms of the flow velocity and diameter $\left(\tau = \mu\frac{d}{U}\right)$. A time lag parameter ($\mu$) value of an order of 1 was found to give reasonable results. The above theory yields the following stability threshold:

$$\frac{U_c}{fd} = \left(\frac{4}{-C_D - \mu d\frac{\partial C_L}{\partial y}}\right)\left(\frac{m_t\delta}{\rho_f d^2}\right)^{0.5}$$

The values of the force coefficients are required for the use of this model. Table 13.3 lists the measured fluid force coefficients for a single tube in an inline and a triangular array. The full set of force coefficients for tube clusters was published by Price and Païdoussis (1984).

13.3.3.4 The Leaver-Weaver model

Based on their flow visualization of the flow pattern inside tube bundles, Lever and Weaver (1982) devised a first-principle model of both the fluid and the structure. In this model, the flow is simplified as one-dimensional and incompressible, and the motion of a single tube in the lift direction was considered. Each tube is attached to two flow channels (see Fig. 13.6). The width (A_o) and length (S_o) of each flow channel is determined by the array type and spacing. The motion of the flexible tube causes a delayed deformation (perturbation) in the channel. The delayed perturbation was thought to result from the flow momentum responding to the tube motion. This results

Table 13.3 Force coefficients for the quasisteady model

Parameter	Inline	Triangular
C_D	5	6.8
$\frac{\partial C_L}{\partial y}$	−73	−243

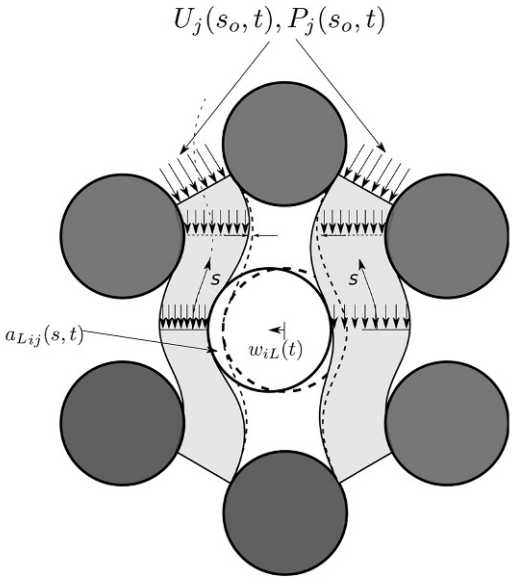

Fig. 13.6 The flow cell model.

in a perturbation in the flow velocity, and was estimated by applying the continuity equation to the flow inside the channel. Using the momentum equation, the pressure field was obtained. The flow fluid force was estimated by integrating the pressure along the tube/channel interface length (D_e). This model requires no measured fluid force coefficients. The interested reader is referred to a series of papers by Lever and Weaver (1982, 1986) and Yetisir and Weaver (1993) for a detailed description of the model. The model yields an expression for reduced critical flow velocity (U_r) as follows:

$$\frac{m_t\delta}{\rho_f d}+\pi C_D\left(\frac{S_o}{d}\right)U_r - 6\pi\left(\frac{D_e S_o^2}{d^3 A_o}\right)U_r^3\left(3\sin\frac{1}{U_r}-\frac{1}{U_r}\cos\frac{1}{U_r}+2h\left[\sin\frac{1}{U_r}+U_r\cos\frac{1}{U_r}-U_r\right]\right)=0$$

The parameter h was introduced to account for the losses due to turbulence. The model seems to capture the essence of the problem and compares reasonably with the experimental data.

13.3.3.5 Design guidelines

All the design guidelines are expressed in terms of the mass damping parameter (MDP). For any value of MDP, the guideline should specify whether the operating flow velocity is safe or not. Because of its simplicity, the guidelines are often expressed in the form of the Connors formula where the constant K has to be suggested. Several excellent guidelines have been published providing lower bound

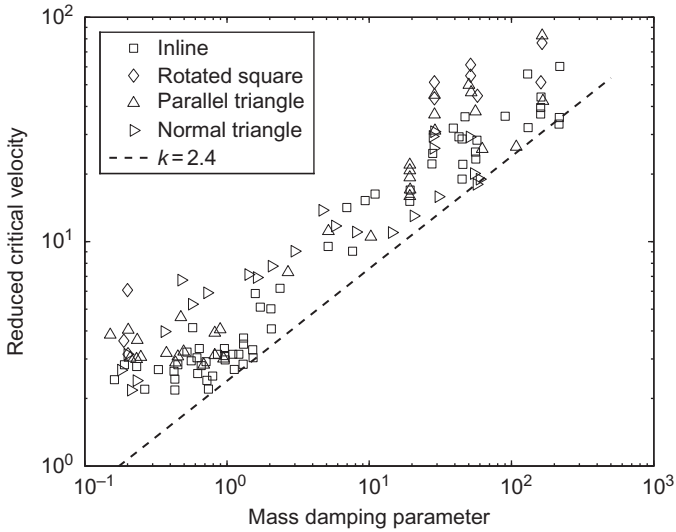

Fig. 13.7 FEI design guidelines considering all data for all tube array geometries.

design curves (Païdoussis, 1983; Chen, 1984; Weaver and Fitzpatrick, 1988; Pettigrew and Taylor, 1991). Fig. 13.7 shows the published data for four types of tube arrays. Based on these data sets, a recommended lower bound value for K is suggested as 2.4. This value also constitutes the basis of the recommendations of the ASME Boiler Code Section III, Appendix N (Au-Yang, 2001). While it is convenient to use a single recommended value, doing so does not incorporate important effects such as tube array type and spacing. Recognizing the important effects of the array type, Weaver and Fitzpatrick (1988) and Schröder and Gelbe (1999) provided lower bound design lines for the standard tube array types. These design guidelines are shown in Fig. 13.8. These alternative guidelines take into account the effect of the low mass-damping parameter region where the stability threshold seems to be insensitive to the mass-damping parameter.

13.3.3.6 Computational fluid dynamics model

The computational fluid mechanics approach has reached an advanced enough level such that it is now being utilized to simulate many complex flows. This level of development has encouraged many researchers to explore the CFD approach to allow for a reliable prediction of the FEI threshold. Two strategies have been pursued: utilizing the CFD to obtain important parameters for the theoretical models, and using coupled fluid/structure simulations. The first strategy involves modeling the tube array with one or more tubes which are forced to either move to a static position or to undergo a prescribed periodic oscillation. Hassan et al. (2011) utilized the latter to extract a number of fluid force coefficients which were then utilized in an unsteady flow model to predict the stability threshold. Utilizing the developed unsteady model, the pitch to

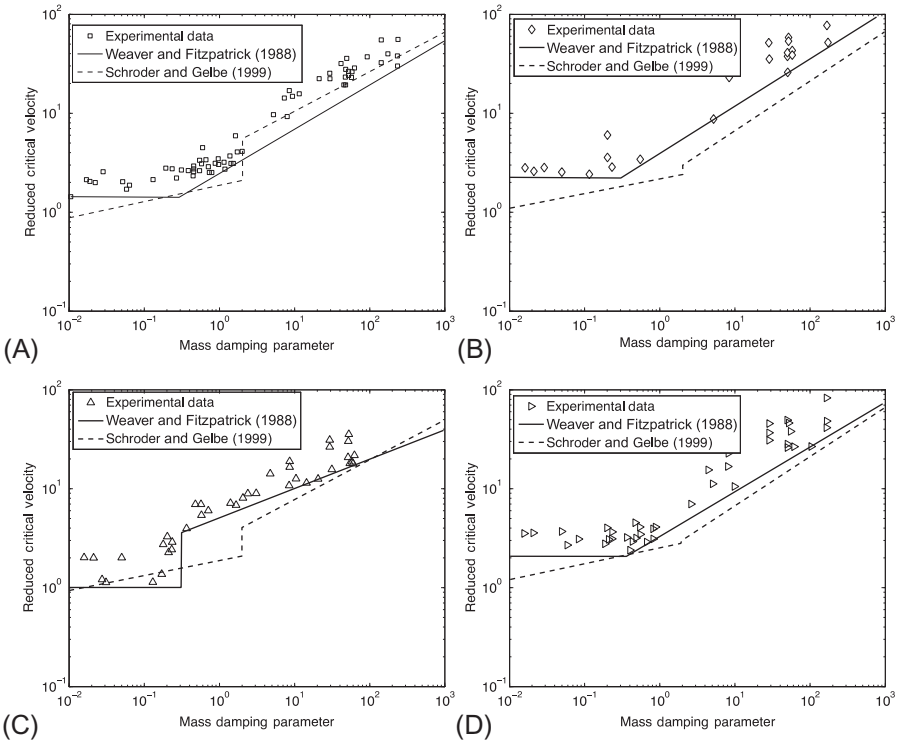

Fig. 13.8 Design guidelines proposed by Weaver and Fitzpatrick (1988) and Schröder and Gelbe (1999) (A) inline square, (B) rotated square, (C) parallel triangle, and (D) normal triangle.

diameter ratio and the Reynolds Number effects on critical velocity were investigated. Khalifa et al. (2013) and El Bouzidi and Hassan (2015) developed numerical techniques to study the flow perturbations and time lag in tube bundles. The obtained time lag was utilized in the semianalytical model of Lever and Weaver (1986) to predict the reduced critical velocity. Anderson et al. (2014) developed a model to account for temporal variations in the flow separation for inline arrays, in which numerical simulations in the separation zone were coupled with a structural model and a far field flow model to obtain the stability threshold.

13.3.3.7 Two-phase FEI

While the characterization of FEI in a single phase flow is still considered a challenging task, characterization of FEI in a two-phase flow is much more difficult to undertake. This is due to the existence of the influence of the two-phase flow regime and the nature of the two-phase flow. Therefore, the nature of FEI in two-phase flow is by far the most complex phenomenon of flow-induced vibrations, and most of its

characteristics are largely unknown. The vast majority of the work done regarding vibrations of tubes in two-phase flow is largely experimental, which makes it much more expensive and difficult to conduct. The typical flow in a steam generator is a steam-water mixture under high pressure and temperature conditions. These conditions are difficult to replicate experimentally. As such, mixtures such as air/water or refrigerants are often used. A water/air mixture is relatively easy to utilize, while the refrigerant often requires much tighter tubing connections, heating elements, and special pumping systems.

Void fraction is an important parameter to characterize the two-phase flow as it controls the estimation of the flow velocity and the two-phase density. The general equation for the void fraction (α) of a two-phase mixture is given by:

$$\alpha = \left[1 + S\frac{\rho_G}{\rho_L}\left(\frac{1}{x} - 1\right)\right]^{-1}$$

where ρ_G, ρ_L, and x are the gas density, the liquid density, and the thermodynamic quality of the mixture respectively. The gas to liquid velocity ratio is given by $S = U_G/U_L$. One of the simplest and widely used methods to determine the void fraction is the homogeneous equilibrium model (HEM). This model assumes that the two fluids (phases) are well mixed, such that the velocity, the pressure, and the temperature of the two phases are equal, i.e., $S = 1$. As a result, the two-phase flow can be modeled by a pseudo fluid whose properties are a weighted average of those of each phase. Therefore, the velocity and density of the assumed pseudo fluid are given by:

$$\rho_H = (1 - \alpha)\rho_L + \alpha\rho_G$$

$$U_H = \frac{\rho_L \dot{V}_L + \rho_G \dot{V}_G}{\rho_H A}$$

where $\dot{V}_L$ and $\dot{V}_G$ are the volume flow rates for the liquid and gas phases, respectively. Using the flow characteristics of the HEM, one can utilize Connors equation to predict FEI in a two-phase flow. In fact, this is the current practice when designing nuclear steam generators. Practitioners justify this approach by assuming that the flow is homogeneous and continuous, such as bubbly flows. As such, a Connors equation with a fluidelastic constant of $K = 3$ is recommended for typical steam generators with a P/D of 1.47 or higher. Fig. 13.9 shows some of the data that supports this approach. However, intermittent flow regimes often lead to bundle reflooding and large flow oscillations. These conditions will not lead to such well-behaved characteristics of the stability curve. In addition, the HEM overestimates the void fraction value. This drawback was overcome with the development of a new model by Feenstra et al. (2000) for predicting the void fraction in upward two-phase flows in tube bundles. The prediction of this model compares remarkably well with other researchers' measurements of void fraction in tube bundles.

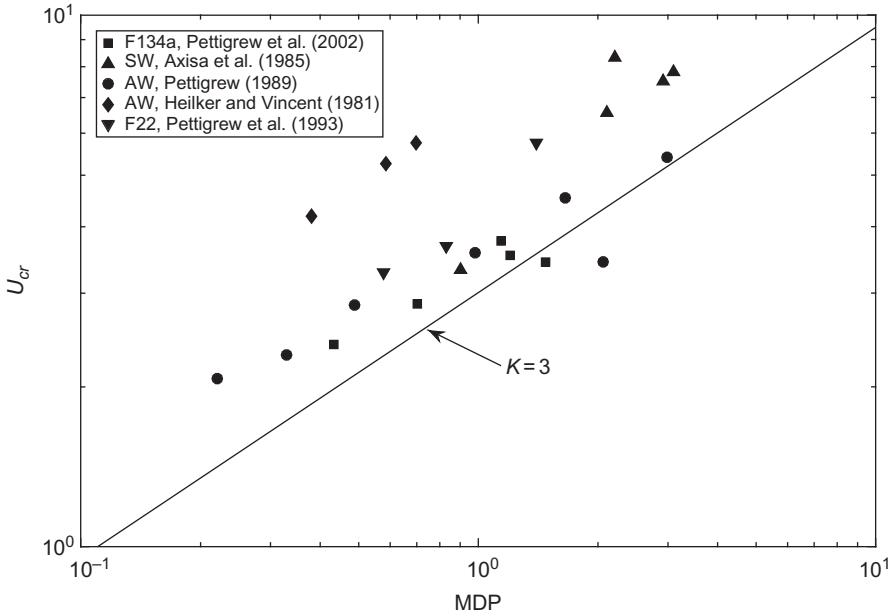

Fig. 13.9 Stability map for two-phase flow data.

13.4 Estimation of tube bundle integrity

Flow-induced vibrations can compromise tube bundle integrity through several mechanisms such as fatigue, cracking, and fretting wear. In nuclear steam generators which are well-designed and operating at safe velocities, turbulence excitation is the dominant mechanism. As such, no catastrophic failures are expected. Wear at the supports is the most likely cause for mechanical degradation in tube bundles over the long term. This section will focus on fretting wear damage.

13.4.1 Fretting wear

Tube wear at the support locations due to flow induced vibrations results from the relative motion between the tube and its supports. The wear mechanisms can be broadly classified as impact wear, sliding wear, and fretting wear.

Impact wear refers to the type of wear resulting from repeated impact between tubes and supports with very little sliding. Impact force induces large contact surface stress, which is a function of the tube/support contact geometry and the amplitude of the vibrations. Problems arise when the surface contact stress exceeds the endurance limit of the tube material, and surface damage takes place.

Sliding wear occurs when tubes are in continuous contact with the supports, and there is a relative sliding motion between the two components. The classical sliding

wear equation can be easily utilized as the volumetric rate ($\dot{V}$) is related to the contact force (F_n) and the sliding distance (w_s) as:

$$\dot{V} = KF_n w_s$$

where K is the wear coefficient and can be obtained experimentally.

Fretting wear includes both impacting and sliding interaction components. The prediction of this mechanism will be discussed in detail in Section 13.5.1.2.

13.4.1.1 Types of supports

Steam generator tubes are characterized as being long and flexible structures. As such, these tubes must be supported along their length to maintain their positions, and to mitigate any destructive flow-induced vibrations due to fluid excitation. A variety of supports has been utilized in the U-bend and the straight regions of the tubes (Fig. 13.10). Tube support plates with drilled or broached holes were used in early steam generator designs (Fig. 13.10A). This support structure is widely recognized as being strong and provides excellent tube support. However, this type of support provides little venting capability in the annular support area around each tube, and as such provides poorly for the release of steam and impurities. In addition, severe flow blockage can take place, particularly when corrosion deposits develop.

A variation of the drilled-hole support can be obtained by using scalloped bars. This configuration can be easily constructed by offsetting alternate half circular bars to create the support hole structure. This support provides a more open configuration to the flow. The radial flexibility of the tube bundle is enhanced by this arrangement.

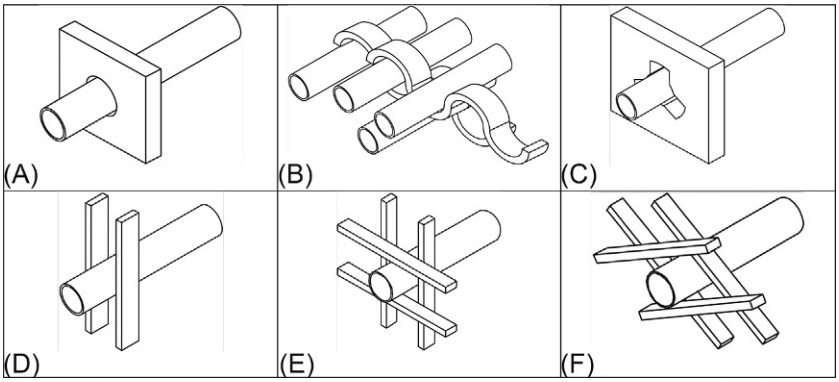

Fig. 13.10 Various support configurations. (A) drilled holes, (B) wiggle bars, (C) broached holes, (D) flat bars, (E) lattice bars *(square array)*, and (F) lattice bars *(triangular array)*.

Flat-bar supports or antivibration bars (AVB), shown in Fig. 13.10D, have proven to be effective in the U-bend region of the tubes. In some designs, the bars drop in and out of the U-bend assembly in a boomerang shape in which both ends of the bars are outside the bundle. Flat bars also provide great flexibility to accommodate differential tube motions in operation due to thermal expansion.

A lattice type of support may be constructed of flat bars to provide a square or a diamond-shaped support space for each tube (lattice network), as shown in Fig. 13.10E and F. This arrangement provides a very open structure to the flow with line contact support. It therefore reduces the potential for the build-up of deposits.

13.4.1.2 Tube/support interaction

Supports are installed to both stiffen and brace the tube structure. However, the tolerance dictated by the manufacturing process and the thermal expansion of the tubes requires that these supports be rather loose. Tubes can therefore vibrate freely in the support space and/or impact against their supports. At the design stage, it is customary to consider the heat exchanger tubes to be simply supported at the tube supports. This assumption simplifies the problem, permitting the application of the linear beam theory to compute the system's natural frequencies and its response to various excitation sources. Under this assumption, the tube will respond as a continuous beam. The supports are assumed to act as knife-edge supports, forcing vibration nodes at the support locations. Such calculations assume that the support is effective, and are shown in Section 13.3.

Linear analysis using the assumption of effective support is suitable as an initial step in predicting the stability threshold of the bundle, and hence predicting the operating flow conditions.

The existence of the clearance allows the tube to vibrate within the support space due to the fluid excitation. When the tube displacement exceeds the support clearance, tube/support contact takes place. During contact, friction force resists the tube motion parallel to the support surface. The average of the product of the normal impact force (F_{CN}) and the sliding displacement (W_s) is called the normal work rate ($\dot{W}_N$):

$$\dot{W}_N = \frac{1}{T}\int_0^T F_{CN}\,dw_s$$

The normal work rate is a very important parameter as it can be used to calculate the fretting wear volume rate ($\dot{V}$) as follows:

$$\dot{V} = C_W \dot{W}_N$$

where C_W is the wear coefficient, which is obtained experimentally. The total tube volumetric loss over a period of time due to fretting wear can then be calculated. This can be done incrementally by assuming that the wear progresses in layers of thickness h_i. The cumulative tube wall loss can be expressed as the summation of these layers.

The tube thickness decreases due to wear and leads to an increase in the tube-to-support clearance. This in turn changes the dynamics of the tube. As a result, the normal

work rate changes with time as the tube wall wears out. In order to obtain the normal work rate and the tube sliding displacement, the time domain nonlinear simulation of the tube/support system must be utilized, which will be described in the next section.

13.4.2 Time domain modeling

13.4.2.1 Contact modeling

Contact modeling is one of the technically challenging problems as it is inherently nonlinear. This is because the condition at the supports is not known a priori. Due to the flow-induced excitation, the tube response could lead to the tube contacting the support or being away from the support. The majority of the available commercial finite element packages are capable of handling general contact problems. These codes can be used to predict the contact forces between tubes and supports. This requires the discretization of both the tubes and the support plates. A typical U-bend tube has over 15 supports, and hence a very large number of elements is required to model the system. Such an approach is very costly considering the number of elements and excitation modeling requirements. Therefore, very specialized codes were developed to simulate loosely-supported tubes subjected to FIV excitations. Examples of these specialized codes include VIBIC (VIbrations of Beams with Intermittent Contacts), H3DMAP (Hydro 3 Dimensional Matrix Analysis Program), GERBOISE (Axisa et al., 1988), and INDAP (Incremental Nonlinear Dynamic Analysis Program). These codes utilize beam elements to model the tubes while treating the tube/support interaction as nonlinearities that are localized, and the contact region is reasonably defined. This greatly simplifies the modeling and results in a very efficient algorithm.

The contact algorithm is described in detail in the work of Axisa et al. (1988), Sauvé and Teper (1987), and Hassan et al. (2002). Briefly, the supports are treated by introducing a spring and a damper at the support location. The effect of these added springs is introduced to the system as pseudo forces. These pseudo forces include spring force (F_{spr}), damping force (F_{dmp}), and friction force. These forces are zero if the tube/support overlap δ_n is negative. The tube/support overlap δ_n is the difference between the tube normal displacement (w_n) at the support and the support clearance (C_r). Negative tube support overlap means there is no contact, while positive overlap indicates that contact takes place. Once contact is confirmed, the spring and damping forces are defined as follows:

$$F_{spr} = k_{spr}\delta_n$$

$$F_{dmp} = -sign\left(\dot{\delta}_n\right)1.5\alpha F_{spr}$$

where k_{spr} and α are the support equivalent contact spring and the impact damping parameter respectively. The friction forces arise in a direction parallel to the support. Several friction models were used in the literature, such as the velocity-limited friction model (VLFM), the spring damper friction model (SDFM), and the force balance friction model (FBFM). A detailed description of these models can be found in the work of Hassan and Rogers (2005).

13.4.2.2 Turbulence modeling

As mentioned in Section 13.4.2, turbulence is a random excitation mechanism that can only be expressed in terms of the spectral parameters, such as the PSD of the distributed force. These empirically-based bounding spectra are obtained using the flow velocity, the tube's diameter, and the array geometry. For the purpose of the time domain estimation, the PSD curve is then transformed into a force-time record using an inverse Fourier transform technique. Typically, one would create two sets of fluctuating forces (one for the lift and one for the drag directions), which are Gaussian in nature with a zero mean value. These two different force records can be used for the entire tube model to gain a conservative estimate. Alternatively, different sets are generated for each tube span or velocity region.

13.4.2.3 FEI modeling

Fluidelastic instability evolves through two mechanisms: damping-controlled instability and stiffness-controlled instability. At a low mass damping parameter, the damping-controlled instability is dominant. Stiffness-controlled instability is dominant at high mass-damping parameters. Through the first mechanism, a single flexible tube is sufficient to represent the FEI. The loss of stability occurs since the net damping deceases as the flow velocity increases, and becomes zero at the stability threshold. Stiffness-controlled instability results as the coupling between the neighboring tubes adds energy to the system, which is greater than the dissipation ability of the tube bundle. The first mechanism is easier to utilize as the bundle dynamics can be represented by a single tube. All of the available approaches exploit this property, and time-domain models of FEI are adaptations of the original stability threshold forms of these models, shown in Section 13.4.3. Detailed descriptions of these time-domain models can be found in Hassan et al. (2011) and Hassan et al. (2011). The following subsections give a brief description of these adaptations.

Connors equation

The Connors equation can be utilized to represent the FEI destabilizing forces. The FEI per unit length (F_L) was expressed by Sauvé (1996) as:

$$F_L = \frac{8\pi^2}{fK^2}\rho_f U^2 \dot{w}_L$$

where K is the Connors constant and $\dot{w}_L$ is tube velocity in the lift direction. Similar to the Connors equation, an equivalent destabilizing force can be derived based on the quasisteady model, as seen in the following subsection.

Quasisteady flow equation

As illustrated in Section 13.4.3, the quasisteady model requires a number of coefficients in addition to the time lag. For a single flexible tube, the time-domain force reduces to the following expression:

$$F_L = \frac{\rho_f dLU^2}{2a^2}\left(\frac{\partial C_L}{\partial y} w_L(t-\tau) - \frac{d\dot{w}_L}{U} C_D\right)$$

The force coefficients are listed in Table 13.3.

Unsteady flow equation

The unsteady flow model (Chen, 1983) can be readily applied since the lift and the drag forces are expressed as a function of the tube response, as described in Section 13.4.3.

Flow cell model

Recent attempts were made by Hassan and Hayder (2008) and Hassan and Mohany (2012) to utilize the flow cell model of Lever and Weaver to model the time domain fluidelastic forces. The complex flow through a tube array is approximated by a number of flow cells, each of which consists of two flow channels. These flow channels are attached to one beam element and a number of boundary fixed elements, as shown in Fig. 13.11. Similar to the original model, the flow in each flow channel is assumed to be a one-dimensional inviscid flow. The flow inside the channel is solved to predict the velocity and the pressure fields that result from the deformation of the flow channels caused by the motion of the tube. The solution algorithm involves decomposing the parameters of the flow channel (channel area A, flow velocity U, and pressure P) into first order terms ($\bar{A}, \bar{U}, \bar{P}$) and second order terms (a, u, p) as follows:

$$\begin{aligned} A(s,t) &= \bar{A}(s) + a(s,t) \\ U(s,t) &= \bar{U}(s) + u(s,t) \\ P(s,t) &= \bar{P}(s) + p(s,t) \end{aligned} \tag{13.1}$$

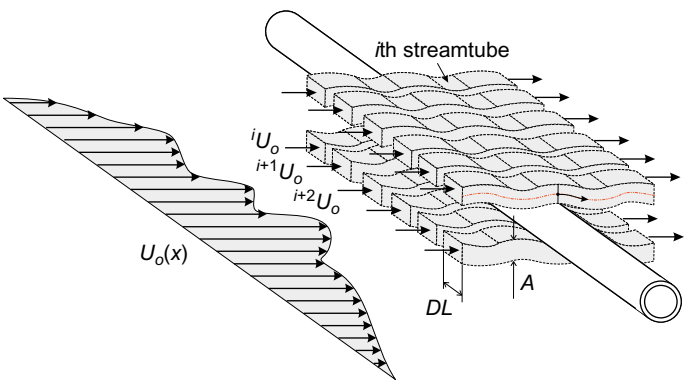

Fig. 13.11 Predictive model for the FEI response using the flow-cell model.

The first order terms (steady) are related to the geometry of the flow channel while the second order terms (perturbations) are related to the motion of the flexible tube. The area perturbation can be directly calculated from the tube vibration time history as follows:

$$a(s,t) = w(t-\tau(s)) \cdot f(s) \tag{13.2}$$

τ is the time lag required for the flow to respond to the tube motion and can be attributed to the process of flow redistribution and momentum. This process is thought to be caused by flow inertia (Lever and Weaver, 1982), flow retardation (Price and Païdoussis, 1984), or vorticity convection and dissipation (Granger and Païdoussis, 1996). Now using the one-dimensional continuity and momentum equations along the length of the flow channel, an expression describing the flow velocity and the pressure perturbations for a fluid of density ρ can be derived as follows:

$$u(s,t) = \frac{-1}{\bar{A} + a(s,t)} \left[U(-S_o) \cdot a(s,t) + \int_{-S_o}^{S} \frac{\partial a(s,t)}{\partial t} ds \right] \tag{13.3}$$

$$p(s,t) = P(-S_o) + \rho \left\{ \frac{1}{2} U(-S_o)^2 - \frac{1}{2} U^2 - \int_{-S_o}^{S} \frac{\partial U}{\partial t} ds \right\} - \rho \left\{ \frac{h}{2S_o} \cdot \int_{-S_o}^{S} U^2 ds \right\} \tag{13.4}$$

Inlet velocity $U(-S_o)$ and pressure $P(-S_o)$ are considered to be constant. Parameter h accounts for the resistance due to viscous losses. Lever and Weaver (1986) presented a good justification for reasonable estimates of this parameter. It was demonstrated that it may be assumed that these parameters do not vary significantly with the Reynolds number, especially in the neighborhood of the critical flow velocity for each array. As such, it is reasonable to select an average value of 0.275. The above model can be further refined by introducing a variable tube-flow channel-contact angle (Anderson et al., 2014).

Fig. 13.12 shows typical simulation results using the above described model. The tube utilized here was greatly simplified into a single degree of freedom system. To produce such a graph, the flow velocity is incremented until the stability threshold is reached. In each increment, the flow velocity value is used to create both turbulence and FEI forces.

These forces are applied to the dynamic system and the response is obtained. While a time domain approach such as this seems to be time consuming and costly compared with the simple Connors equation, it is absolutely essential and irreplaceable for the fretting wear calculations used when predicting the response for a full scale U-bend tube such as the one shown in Fig. 13.13. This model represents the U-Bend tube

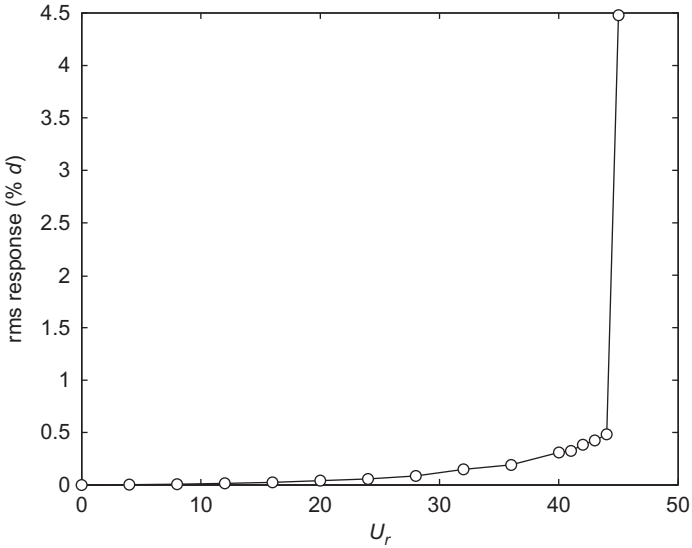

Fig. 13.12 Prediction of the tube response versus flow velocity.

configuration used in the CANDU steam generators at the Bruce Station (Unit 8). The flow velocity and the density distributions obtained from the thermalhydraulics analysis are shown in Fig. 13.13B. The tube is supported by seven broached hole supports along each of the straight legs. Three sets of scallop-bar supports are placed in the U-bend region. Each scallop-bar support set consists of two bars, each of which contains half-circle drilled-hole support space.

Such a tube was discretized via the finite beam element, and the fluid and contact forces were calculated using the models described above. The response is shown in Fig. 13.14B as a function of the velocity ratio. The velocity ratio is the ratio of the current flow velocity to the rated maximum design velocity. The response is for four spans along the U-Bend. The corresponding impact force level and normal work rates are presented in Fig. 13.15. These figures demonstrate the outcome of the predictive methodology for FIV.

While the original formulation of the flow cell model (Lever and Weaver, 1982) assumes that the tube is vibrating at a steady-state amplitude with a frequency close to the natural frequency of the tube, the current model does not have such restrictions and allows the tube to respond to both turbulence and FEI force. This is also suitable in the case of loosely supported tubes, which tend to lack a well-defined natural frequency, complicating the response prediction. For more comprehensive coverage of the fretting wear damage modeling and prediction for U-bend tube bundles the reader is referred to the recent works of Hassan and Riznic (2014) and El Bouzidi et al. (2015).

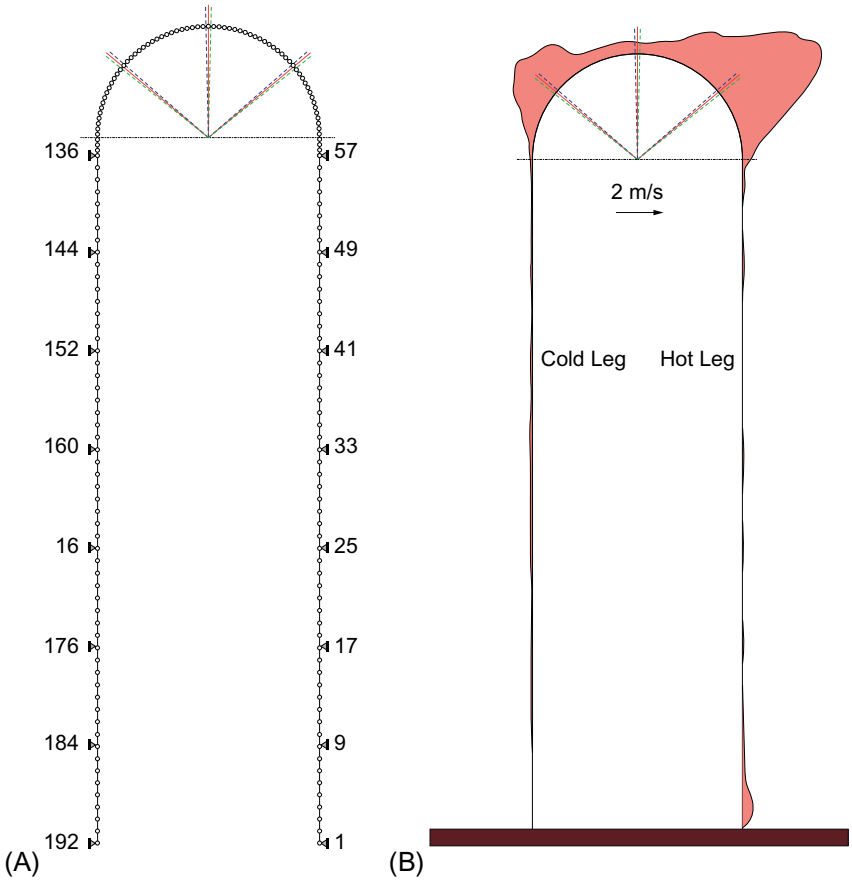

Fig. 13.13 U-bend tube geometry: (A) FEA model and (B) flow distribution.

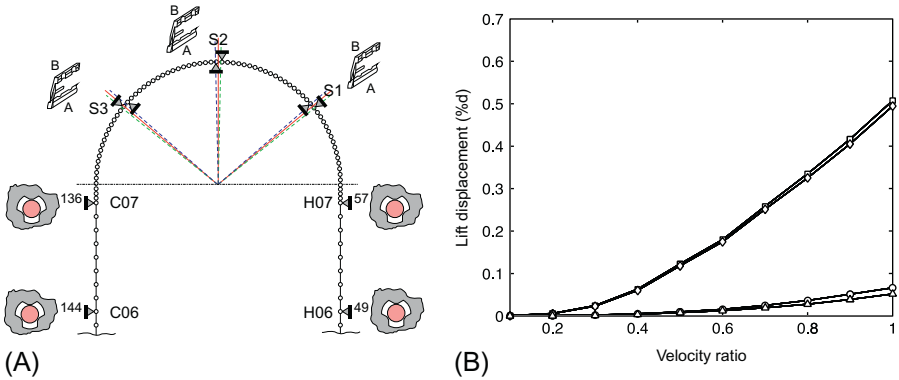

Fig. 13.14 (A) Support configuration and (B) lift response.

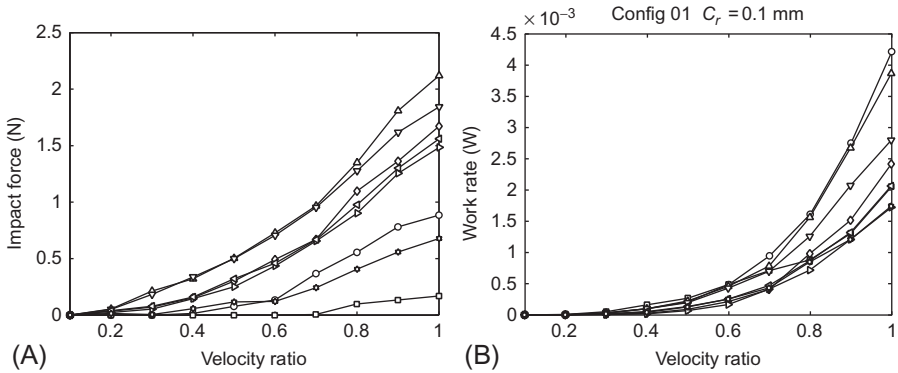

Fig. 13.15 Effect of the flow velocity on (A) impact force and (B) normal work rate.

13.5 Recent challenges

Operating experience and the vast majority of investigative works support the notion that FEI in tube arrays occurs in the direction transverse to the flow direction. This notion has been accompanied by a large body of theoretical studies that have made the same assumption. This assumption has become engrained in design codes and was supported by the vast majority of practitioners. Au-Yang (2001) stated that "the lower in-plane modes of heat exchanger U-tubes have never been observed to be unstable even when the computed theoretical stability margin is well below 1.0." However, recently there have been some indications of the occurrence of FEI in the streamwise direction. These occurrences have been witnessed in experiments (see, e.g., the review in Hassan and Weaver, 2015a,b). However, the design practice has continued its long entrenched methods and assumed that it is sufficient to design against transverse FEI only.

Streamwise (drag) instability was never considered to be of importance in operating steam generators. This belief has been shattered after recent devastating failures in some replacement nuclear steam generators, such as those at SONGS (San Onofre Nuclear Generation Station). These steam generators were designed to last for 40 years and instead, lasted for only 11 months. Investigating these failures has confirmed that streamwise (drag) instability was responsible for the damage caused by tube-to-tube fretting wear and failures. The magnitude of these failures sent shockwaves through the academic and the industrial community. In one plant, the price in terms of equipment damage and lost production costs approached hundreds of millions of dollars. In the wake of these incidents, both the research community and industry have made great efforts to understand this phenomenon. This has resulted in a significant number of research works attempting to understand this phenomenon. A number of recent studies have confirmed beyond any doubt that streamwise FEI can occur. Studies continue to determine the conditions under which this phenomenon prevails. Experiments indicate the importance of fluid

coupling between tubes in the streamwise FEI mechanism (Nakamura et al., 2013; Nakamura, 2014).

Recent experimental evidence (Nakamura et al., 2013; Mureithi et al., 2005; Hirota et al., 2013) has confirmed that the number of flexible tubes, the bundle type, as well as the pitch ratio and the mass-damping parameter strongly influence the streamwise FEI.

Hassan and Weaver (2015a,b) were the first to attempt to build a model from the first principles to predict streamwise FEI. Their model is based on the simple flow cell concept of Lever and Weaver (1982). They extended this concept to cover multiple flexible tubes. The initial results were very promising as the model showed a reasonable agreement with experiments. However, much work is needed to fully understand this phenomenon and to establish better guidelines for new steam generator designs.

13.6 Summary

Flow-induced vibration is an important consideration when dealing with the design and operation of nuclear steam generators. Over the years the technology and the tools have advanced to the extent that problems arising from FIV can be predicted and mitigated at the design stage itself. As the type of flows encountered in operating steam generators are highly unsteady and act on increasingly flexible tubes, this problem is intractable using first principle models. These characteristics have led to a reliance on the empirical models. These empirical models and tools were very successful for designing reliable nuclear steam generators for over five decades. However, recent catastrophic failures in nuclear steam generators have shown that there are still many things to be learnt about this phenomenon.

References

Anderson, B., Hassan, M., Mohany, A., 2014. Modelling of fluidelastic instability in a square inline tube array including the boundary layer effect. J. Fluids Struct. 48, 362–375.

Au-Yang, M.K., 2001. Flow-Induced Vibration of Power and Process Plant Components. ASME Press, New York, NY.

Axisa, F., et al., 1985. Vibration of tube bundles subjected to steam-water cross flow: a comparative study of square and triangular pitch arrays. In: Transactions of the Eighth International Conference on Structural Mechanics in Reactor Technology, Vol. B.

Axisa, F., Antunes, J., Villard, B., 1988. Overview of numerical methods for predicting flow-induced vibration. J. Press. Vessel Technol. 110, 6–14.

Axisa, F., Antunes, J., Villard, B., 1990. Random excitation of heat exchanger tubes by cross flows. J. Fluids Struct. 4, 321–341.

Chen, S.S., 1983. Instability mechanisms and stability criteria of a group of circular cylinders subjected to cross flow. I. Theory. J. Vib. Acoust. Stress. Reliab. Des. 105, 51–58.

Chen, S.S., 1984. Guidelines for the instability flow velocity of tube arrays in cross flow. J. Sound Vib. 93, 439–455.

El Bouzidi, S., Hassan, M., 2015. An investigation of time lag causing fluidelastic instability in tube arrays. J. Fluids Struct. 57, 264–276.

El Bouzidi, S., Hassan, M., Riznic, J., 2015. A comprehensive flow-induced vibration model to predict crack growth and leakage potential in steam generator tubes. Nucl. Eng. Des. 292, 1731.

Feenstra, P.A., Weaver, D.S., Judd, R.L., 2000. An improved void fraction model for two-phase cross-flow through horizontal tube arrays. Int. J. Multiphase Flow 26, 1851–1873.

Granger, S., Païdoussis, M.P., 1996. An improvement to the quasi-steady model with application to cross-flow-induced vibration of tube array. J. Fluid Mech. 320, 163–184.

Hassan, M., Hayder, M., 2008. Modelling of fluidelastic vibrations of heat exchanger tubes with loose supports. Nucl. Eng. Des. 238 (10), 2507–2520.

Hassan, M., Hossen, A., 2010. Time domain models for damping-controlled fluidelastic instability forces in tubes with loose supports. J. Press. Vessel Technol. 132 (4), 041302.

Hassan, M., Mohany, A., 2012. Fluidelastic instability modeling of loosely supported multispan U-tubes in nuclear steam generators. J. Press. Vessel Technol. 135 (1), 011306–011306-9.

Hassan, M., Riznic, J., 2014. Evaluation of the integrity of steam generator tubes subjected to flow induced vibrations. J. Press. Vessel Technol. 136 (5), 051301.

Hassan, M., Rogers, R., 2005. Friction modelling of preloaded tube contact dynamics. J. Nucl. Eng. Des. 235, 2349–2357.

Hassan, M., Weaver, D.S., 2015a. Modelling of streamwise and transverse fluidelastic instability in tube arrays. J. Press. Vessel Technol. 138 (5), 051304. Paper No: PVT-15-1229.

Hassan, M., Weaver, D.S., 2015b. The effect of flat bar supports on streamwise fluidelastic instability in heat exchanger tube arrays. J. Press. Vessel Technol. 137 (6), 061302–061308.

Hassan, M., Weaver, D., Dokainish, M., 2002. A simulation of the turbulence response of heat exchanger tubes in lattice-bar supports. J. Fluids Struct. 16 (8), 1145–1176.

Hassan, M.A., Rogers, R.J., Gerber, A.G., 2011. Damping-controlled fluidelastic instability forces in multi-span tubes with loose supports. Nucl. Eng. Des. 241 (8), 2666–2673.

Heilker, W.J., Vincent, R.Q., 1981. Vibration in nuclear heat exchangers due to liquid and two-phase flow. ASME J. Eng. Power 103 (2), 358–366.

Hirota, K., Morita, H., Hirai, J., Iwasaki, A., Utsumi, S., Shimamura, K., Kawakami, R., 2013. Investigation on in-flow fluidelastic instability of an array of tubes. In: ASME 2013 Pressure Vessels and Piping Conference. paper PVP2013-97163.

Khalifa, A., Weaver, D., Ziada, S., 2013. Modeling of the phase lag causing fluidelastic instability in a parallel triangular tube array. J. Fluids Struct. 43, 371–384.

Lever, J.H., Weaver, D.S., 1982. A theoretical model for the fluidelastic instability in heat exchanger tube bundles. J. Press. Vessel Technol. Trans. ASME 104, 104–147.

Lever, J., Weaver, D., 1986. On the stability of heat exchanger tube bundles, part II: numerical results and comparison with experiments. J. Sound Vib. 107 (3), 393–410.

Mureithi, N.W., Zhang, C., Ruel, M., Pettigrew, M.J., 2005. Fluidelastic instability tests on an array of tubes preferentially flexible in the flow direction. J. Fluids Struct. 21 (1), 75–87.

Nakamura, T., 2014. An analysis of in-flow fluidelastic instability based on a physical insight. In: Proceedings of the ASME PVP2014 Conference, Anaheim, CA. paper PVP2014-28231.

Nakamura, T., Fijita, Y., Sumitani, T., 2013. Study on in-flow fluidelastic instability of circular cylinders caused by air cross flow (triangular arrays). In: Proceedings of the ASME PVP 2013 Conference, Paris, France. paper PVP2013-97111.

Oengören, A., Ziada, S., 1995. Vortex-shedding, acoustic resonance and turbulent buffeting in normal triangular tube arrays. In: Bearman, P.W. (Ed.), Proc., 6th International Conference on Flow-Induced Vibration , London, UK.

Oengören, A., Ziada, S., 1998. An in-depth study of vortex shedding, acoustic resonance and turbulent forces in normal triangle tube arrays. J. Fluids Struct. 12, 717–758.

Païdoussis, M.P., 1983. A review of flow-induced vibrations in reactors and reactor components. Nucl. Eng. Des. 74, 31–60.

Pettigrew, M.J., 1989. Vibration of tube bundles in two-phase cross-flow: part 2—fluid-elastic instability. J. Press. Vessel Technol. 111, 478. http://dx.doi.org/10.1115/1.3265706.

Pettigrew, M.J., Gorman, D.J., 1973. Experimental studies on flow-induced vibration to support steam generator design, part 3: vibration of small tube bundles in liquid and two-phase cross flow. In: Proceedings of UKAEA/NPL International Symposium in Vibration Problems in Industry, Keswick, UK. Paper 426.

Pettigrew, M., Gorman, D., 1978. Vibration of heat exchanger components in liquid and two-phase cross-flow. In: Proceedings BNES International Conference on Vibration in Nuclear Plant.

Pettigrew, M.J., Taylor, C.E., 1991. Fluidelastic instability of heat exchanger tube bundles: review and design recommendations. ASME J. Press. Vessel Technol. 113 (2), 242–256.

Pettigrew, M.J., Taylor, C.E., Janzen, V.P., Whan, T., 2002. Vibration behavior of rotated triangular tube bundles in two-phase cross flows. J. Press. Vessel Technol. 124 (2), 144–153.

Pettigrew, M.J., Taylor, C.E., Yasuo, A., 1993. Vibration damping of heat exchanger tube bundles in two-phase flow. Weld. Res. Counc. Bull. 389, 1–41, New York, NY.

Polak, D.R., Weaver, D.S., 1995. Vortex shedding in normal triangular tube arrays. J. Fluids Struct. 9 (1), 1–17.

Price, S.J., 1995. A review of theoretical models for fluidelastic instability of cylinder arrays in cross-flow. J. Fluids Struct. 9, 463–518.

Price, S., Païdoussis, M., 1984. An improved mathematical model for the stability of cylinder rows subjected to cross-flow. J. Sound Vib. 97 (4), 615–640.

Rao, S., 2016. Mechanical Vibrations, sixth ed. Pearson, United States.

Rogers, R.J., Taylor, C.E., Pettigrew, M.J., 1984. Fluid effects on multispan heat exchanger tube vibration. In: Proceedings of the ASME Pressure Vessels and Piping Conference, San Antonio, pp. 17–26. ASME publication H00316.

Sauvé, R., 1996. A computational time domain approach to fluidelastic instability for nonlinear tube dynamics. In: Pettigrew, M. (Ed.), ASME PVP/ICPVT-8 Conference on Symposium on Flow Induced Vibrations. ASME, Montreal, pp. 551, 111–121.

Sauvé, R., Teper, W., 1987. Impact simulation of process equipment tubes and support plates-a numerical algorithm. ASME J. Press. Vessel Technol. 109, 70–79.

Schröder, K., Gelbe, H., 1999. New design recommendations for fluid elastic instability in heat exchanger tube bundles. J. Fluids Struct. 13 (3), 361–379.

Taylor, C., Pettigrew, M., 2000. Random excitation forces in heat exchanger tube bundles. J. Press. Vessel. Technol. 122, 509–514.

Thomson, W., Dahleh, M., 1997. Theory of Vibrations With Applications, fifth ed. Pearson.

Weaver, D.S., 2008. Some thoughts on the elusive mechanism of fluidelastic instability in heat exchanger tube arrays. Keynote paper, In: Zolotarev, I., Horacek, J. (Eds.), The 9th International Conference on Flow-Induced Vibrations FIV-2008. Institute of Thermomechanics, Academy of Sciences of the Czech Republic, Prague, pp. 21–28.

Weaver, D.S., Fitzpatrick, J.A., 1988. A review of cross-flow induced vibrations in heat exchanger tube arrays. J. Fluids Struct. 2, 73–93. http://dx.doi.org/10.1016/S0889-9746(88)90137-5.

Yetisir, M., Weaver, D., 1993. An unsteady theory for fluidelastic instability in an array of flexible tubes in crossflow. Part 1: theory. J. Fluids Struct. 7, 751–766.

Ziada, S., Oengören, A., 1993. Vortex shedding in an in-line tube bundle with large tube spacings. J. Fluids Struct. 7 (6), 661–687.

Structural integrity assessment of nuclear steam generator

14

S. Majumdar, S. Bakhtiari*, Z. Zeng*, C.B. Bahn†*
*Argonne National Laboratory, Lemont, IL, United States, †Pusan National University, Busan, Republic of Korea

Acronyms

ANL	Argonne National Laboratory
CM	condition monitoring
CNSC	Canadian Nuclear Safety Commission
COD, CTOD	crack opening displacement and crack tip opening displacement, respectively
EC	eddy current
EDM	electro-discharge machining
EPRI	Electric Power Research Institute
ERC	equivalent rectangular crack
FEA	finite-element analysis
ID, OD	inside diameter and outside diameter, respectively
IGSCC	intergranular stress corrosion cracking
INEL	Idaho National Engineering Laboratory
ISI	in-service inspection
MA	mill-annealed
MRPC	motorized rotating probe coils
MSLB	main steam line break
NDE	nondestructive examination
NO	normal operation
NRC	nuclear regulatory commission
OA	operation assessment
ODSCC	outer diameter stress corrosion cracking
PWR	pressurized water reactor
PWSCC	primary water stress corrosion crack
RSG	recirculating steam generator
SBO	station blackout
SCC	stress corrosion cracking
SG	steam generator
SGT	steam generator tube
SGTR	steam generator tube rupture
SIPC	structural integrity performance criteria
TS, TSP	tube sheet and tube support plate, respectively
TT	thermally treated
TW, PTW	throughwall and part-throughwall, respectively

Steam Generators for Nuclear Power Plants. http://dx.doi.org/10.1016/B978-0-08-100894-2.00016-9
© 2017 Elsevier Ltd. All rights reserved.

Symbols

a	Crack depth
$2c$	Crack length
d, d_o	Equivalent crack depths
E, ν	Young's modulus and Poisson's ratio
h	Tube wall thickness
J_{IC},	Critical fracture toughness
k	Flow stress factor
L, L_o	Equivalent crack lengths
m, m_{eff}	Bulging factor and effective bulging factor, respectively
m'	nondimensional constant
m_p, m_{peff}	Stress magnification factor and effective stress magnification factor, respectively
n	Number of circumferential cracks
N	Constant defined in terms of λ and μ
P_b, P_{cr}	Unstable burst pressures of unflawed and flawed tube, respectively
P_{sc}	Ligament rupture pressure
P_{EPRI}	EPRI correlation for rupture pressure
r	Mean radius of tube
R	U-bend radius
t, t_R	Time and time to creep rupture, respectively
t_f	Failure time
T	Temperature
σ_u	Ultimate tensile strength
σ_y	Tensile yield strength
α,β	Factors for defining m_p
δ_c	Critical crack opening displacement
Δp_{NO}	Normal operation pressure differential
Δp_{MSLB}	Differential pressure for main steam line break accident
λ	Constant used in the definition of bulging factor m
μ and κ	Constants
σ, $\overline{\sigma}$	Hoop stress and flow stress, respectively
σ_{cr}	Critical stress for unstable burst
σ_{lig}	Average ligament stress
2θ	Circumferential crack angular length

14.1 Introduction

A historical study of corrosion problems in pressurized water reactor (PWR) steam generator tubing shows that a succession of failure processes have afflicted steam generators (SGs) in the United States and around the world since the early 1960s. All steam generators, but primarily those with Alloy 600 tubing, face three main types of intergranular stress corrosion problems. They are, on the primary side, intergranular stress corrosion cracking (IGSCC), also referred to as primary water SCC (PWSCC), mainly in the transition zone of expanded tubes at the tube sheet (TS); and, on the secondary side, intergranular attack and IGSCC, also referred to as outer-diameter SCC (ODSCC), in crevices and under sludge piles at the tube/TS junctions and tube

support plates (TSPs). Operating experience with PWR steam generators in both the United States and abroad has shown that cracks of various morphologies can and do occur in SG tubes, starting early in life. These may be single cracks that are axial or circumferential, inside or outside diameter (ID or OD) initiated, and part or complete throughwall (TW); they may also be multiple cracks that are parallel or form a network. Tests have shown that, depending on the location and morphology of these cracks, the tubes can be weakened relative to unflawed tubes to various extents.

Since the introduction of improved and stricter water chemistry control and recent industry wide switch of SG tube material from Alloy 600MA to Alloy 690TT, there have been no confirmed incidences of PWSCC or ODSCC in Alloy 690TT tubes. Only a few PWRs with Alloy 600 tubes still exist. In recent years, the US SG tubes are experiencing wear at tube supports (TSs) due to tube vibration.

The SGs in Germany operating with Alloy 800 tubes have now been in service for more than 30 years. Up to now no PWSCC or secondary-side SCC has been observed in the more than 285,000 tubes installed in Siemens/KWU SGs (including recirculating steam generator [RSG]) in 19 PWRs in Europe. During recent SG tubing inspections using eddy current (EC) testing, a few indications were detected within the TS between upper and lower tube expansion. These indications were limited to the outer tube positions. However, the number of affected positions is small (Kilian et al., 2007).

Earlier, Spanish experience (Gomez Briceno et al., 1991) on SG tube degradation in SG materials had shown that SCC resistance of Alloy 690TT in primary water is superior to that of Alloy 800 and Alloy 600MA. However, Alloy 690TT is susceptible to lead caustic environments.

The SGs of the Spanish Almaraz Unit 2 were replaced in 1997 by a newer model with Alloy 800 SG tubes. Denting indications were firstly detected in 2006 in the SG-3 (de Diego et al., 2015). Crack indications were identified in 2009. At the end of 2011, three tubes were recovered from this SG to carry out destructive examination in order to identify the root cause of the tubes degradation. Multiple intergranular cracks were detected at 3 mm above the last contact point between the tube and the TS, in a band of around 5 mm, practically in the whole perimeter of the tube.

The Canadian SG tubes, which are mainly made from Alloy 800 and Monel 400, have been more or less free from ODSCC or PWSCC problem. They have been more prone to fretting damage due to flow-induced vibration of the tubes in the U-bend region. The geometry of the frets is approximately the impression of the unfretted support structure on the tubes, which is a lot simpler than the typical ODSCC or PWSCC geometry.

SG tubes comprise a substantial portion of the reactor coolant pressure boundary, and also play a role in fission product containment. Therefore, any significant breach of the SG tube pressure boundary is a concern for Regulatory Authorities. The US nuclear power industry has established a framework for increasing the reliability of SGs by adopting NEI-97-06, which is the basis for an industry consensus approach to SG integrity assessment by demonstrating the condition of SGs relative to the structural integrity performance criteria (SIPC). Three critical elements—degradation assessment, condition monitoring (CM), and operation assessment (OA)—provide assurance that the SGs will continue to satisfy the appropriate SIPC. CM is backward

looking, in that its purpose is to confirm that adequate SG tube integrity has been maintained during the previous inspection interval. CM involves an evaluation of the as-found condition of the tubing relative to SIPC. OA differs from the CM assessment, in that it is forward looking rather than backward looking. Its purpose is to demonstrate that the tube SIPC will be met throughout the next inspection interval. The SIPC defines the margins to be applied in maintaining adequate tube integrity against gross failure by either burst or plastic collapse. The criteria are to be satisfied with at least a probability of 0.95 at 50% confidence and should include relational uncertainty, material property uncertainty, and nondestructive examination (NDE) measurement uncertainty. The technical bases for the SIPC follow from the design margins implied in Section III of the ASME Boiler and Pressure Vessel Code. SIPC also includes accidental leakage integrity, which is beyond the scope of the present chapter. The reliability of the SG integrity assessment procedure is critically dependent on the accuracy of the structural integrity prediction models because they are used in both the CM and the OA.

In this chapter we have concentrated primarily on a single degradation mechanism—stress corrosion cracks (SCCs)—that have been observed in RSGs using Alloy 600 SG tubes. However, with minor modifications, the failure models can be applied to any other types of SG (e.g., once-through SG) and degradation mechanism (e.g., frets).

14.2 Structural integrity prediction models

US nuclear regulations have evolved over the years from prescriptive to risk-informed and performance-based requirements. In general, tube rupture risk may be considered to arise from three main contributors:

- Spontaneous steam generator tube rupture (SGTR) occurring during normal operation.
- Pressure transient-induced SGTR (resulting from primary-to-secondary differential pressure conditions) caused by a design basis accident.
- Core damage-induced SGTR (resulting from a core damage condition).

In order to improve the accuracy of evaluation of these risks, improved methodologies for predicting SGTR are needed and are under periodic review and reevaluation. Most analytical models for calculating SG tube rupture have been developed for the idealized geometry of single part-throughwall (PTW) and 100% TW rectangular cracks. In Section 14.2, analytical models that are available for predicting rupture and unstable burst of single rectangular cracks are discussed. The challenge of how these models are used to predict rupture of real life SCCs is discussed in Section 14.3.

Generally, any PTW crack in a tube under increasing internal pressure experiences a two-step failure process. First, it experiences ligament rupture at which point the through-thickness ligament at the crack tip ruptures and the crack becomes 100% TW (Fig. 14.1A) and starts leaking. If this event occurs abruptly, the pressure at which

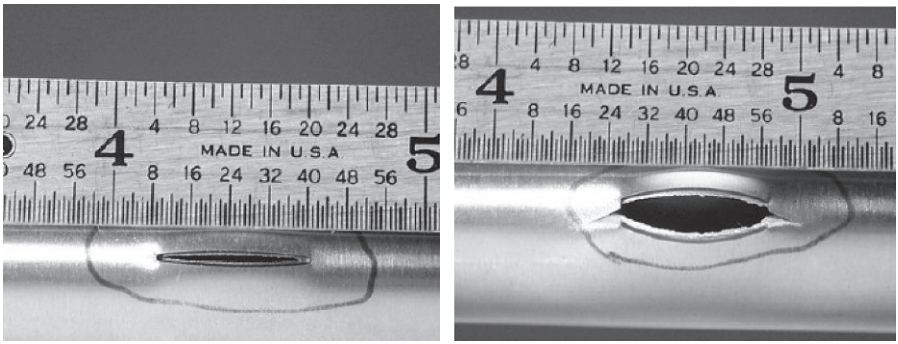

(A) (B)

Fig. 14.1 Surface appearance of notches after (A) ligament rupture and (B) unstable burst showing crack tip tearing into virgin material.

it occurs is defined as the ligament rupture pressure. With increasing pressure the leakage rate increases but the crack remains stable. Finally, the crack experiences burst at which point the tube bulges at the crack location and the crack begins to grow axially at constant pressure in an unstable manner. However, in laboratory tests with pumps of limited flow capacity, the cracks do not propagate significantly as the system rapidly depressurizes but the cracks generally open up significantly (fish-mouth). However, the tell-tale sign of unstable burst in the laboratory is the crack tip tearing into virgin full-thickness material (Fig. 14.1B). In tubes with deep cracks, these two stages occur sequentially. In tubes with shallow cracks, the two stages appear to occur simultaneously. The above sequence of events generally occurs for electro-discharge machining (EDM) notches and SCCs and may be different for other types of flaws, not discussed in this section.

The failure pressure for a defect-free straight tubing of mean radius r and wall thickness h is given by (for small values of h/r)

$$P_b = \frac{\overline{\sigma} h}{r} \tag{14.1a}$$

where $\overline{\sigma}$ is the flow stress, generally defined in terms of the yield (σ_y) and ultimate (σ_u) tensile strengths as

$$\overline{\sigma} = k\left(\sigma_y + \sigma_u\right) \tag{14.1b}$$

Experimentally determined values of k usually vary between 0.5 and 0.6.

There is a loss of about 10%–15% in the flow stress of Alloy 600 between room temperature and the SG operating temperature (~300°C).

14.2.1 Normal operation and design basis accidents

14.2.1.1 Single axial flaws

Throughwall rectangular axial flaws

Unstable burst The critical pressures and crack sizes for the unstable burst of a thin-wall internally pressurized cylindrical shell with a single TW axial crack can be estimated with an equation originally proposed by Folias (1965) and later modified by Hahn et al. (1969) and Erdogan (1976):

$$P_{cr} = \frac{P_b}{m} \tag{14.2a}$$

where

$$\text{Bulging factor } m = 0.614 + 0.48\lambda + 0.386\ \exp(-1.25\lambda) \tag{14.2b}$$

$$\lambda = \left[12\left(1-\nu^2\right)\right]^{1/4} \frac{c}{\sqrt{rh}} = \frac{1.82c}{\sqrt{rh}} \tag{14.2c}$$

$$\nu \text{ is the Poisson's ratio, and} \tag{14.2d}$$

$$2c \text{ is the axial crack length.} \tag{14.2e}$$

A database for unstable burst pressures on 19 mm (0.75 in.) and 22 mm (0.875 in.) diameter Alloy 600 tubes with single, TW, EDM, and laser-cut axial notches has been generated at Argonne National Laboratory (ANL). The rupture data at room temperature and high temperature have been reported by Majumdar et al. (1998), Majumdar et al. (2000), and Majumdar et al. (2001). A critical factor for predicting unstable burst pressure is k, the flow stress factor. The best fit to ANL data on unstable burst of tubes with TW axial notches gives $k = 0.55$. Comparisons of the observed and calculated unstable burst pressures for various heats of Alloy 600 tubes with EDM and laser-cut notches using $k = 0.55$ are shown in Fig. 14.2A and B. For laser-cut notches, the notch lengths were obtained from fractography. In the cases where multiple tests were performed for a given EDM notch length, Fig. 14.2A shows that the unstable burst pressures of the shorter (6 and 9 mm [0.25 and 0.35 in.]) laser-cut notches tend to be at the lower end of the range of burst pressures observed for the EDM notches. However, the burst pressures for the larger (13 mm [0.5 in.]) laser-cut notches were distributed equally above and below those of the EDM notches. Thus, overall, the unstable burst pressures of the EDM and laser-cut notches of equal length are comparable.

Critical crack-tip opening displacement model for unstable burst For predicting the rupture pressures of tubes with 100% TW cracks, a failure criterion based on critical crack tip opening displacement (CTOD), which was originally proposed by Wells (1961) for materials with high fracture toughness (e.g., Alloy 600) where linear elastic fracture mechanics is inapplicable, was used. The method was

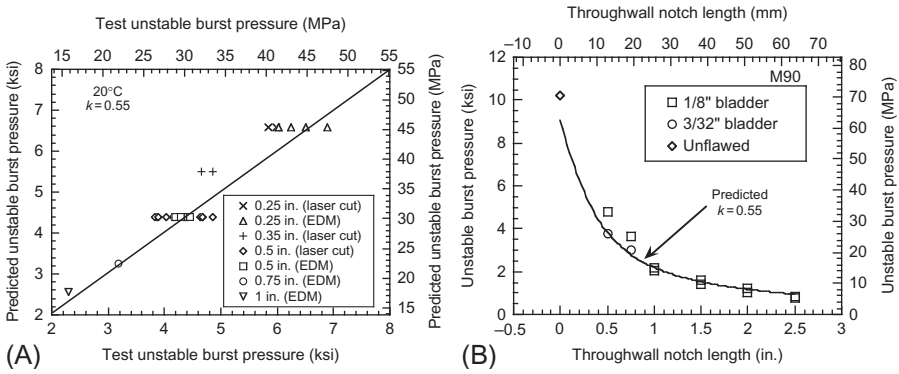

Fig. 14.2 (A) Observed versus predicted unstable burst pressures for tubes with 100% TW EDM and laser-cut notches and (B) predicted versus observed variation of unstable burst pressure with notch length of Heat M90 tubes[1] with 100% TW axial EDM notches.

further expanded by Burdekin and Stone (1966) and Rice (1968) who showed that the critical CTOD δ_c is related to the familiar elastic-plastic plane strain fracture toughness JIC by the following equation:

$$J_{IC} = m'\sigma_y\delta_c \tag{14.3}$$

where m' is a nondimensional constant dependent on the strain hardening property of the material and σ_y is the yield strength.

Internal pressure in the tube causes the 100% TW crack to open up as simulated by finite-element analysis (FEA) in Fig. 14.3. The crack opening displacement (COD) varies along the axial direction, reaching a maximum value at the crack mouth. The COD also increases from the ID to the OD surface of the flaw. For burst calculations, an additional entity called the crack tip opening displacement (CTOD) is often used. CTOD is determined by drawing two straight lines from the mid-section crack tip oriented at ±45° to the crack axis. The value of COD where the two lines intersect the crack flank is defined as the CTOD. Typically, for straight tubes, the following criterion for the onset of unstable burst (crack tip tearing) has been used with reasonable success:

$$\text{CTOD} = \text{critical CTOD} \tag{14.4}$$

where the critical CTOD is, in general, a material and tube geometry dependent property. In the present section, the critical CTOD is assumed equal to the wall thickness of the Alloy 600 tube. For the 0.75 in. (19 mm) diameter, 0.043 in. (1.1 mm) wall

[1] Woods, J.P. (1995), The Effect of Ligament Size on the Burst Pressure of Alloy 600 Tubing Containing Axial Cracks, Master's Thesis, Illinois Institute of Technology.

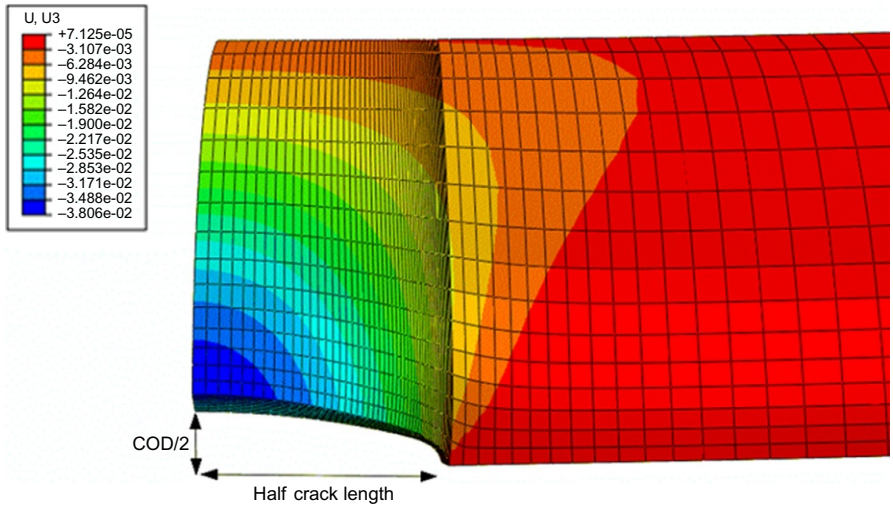

Fig. 14.3 Crack opening geometry of a TW axial crack in a tube due to internal pressure.

thickness Alloy 600 tubes under consideration, critical CTOD is equal to 0.043 in. (1.1 mm). For 0.875 in. (22 mm) diameter, 0.05 in. (1.3 mm) wall thickness Alloy 600 tubes, critical CTOD is equal to 0.05 in. (1.3 mm).

Usually FEA is used to calculate the CTOD. The critical CTOD model for predicting unstable burst pressure has been validated by in-house tests at ANL on straight Alloy 600 tubes with 0.25 in. (6 mm) to 2.5 in. (62 mm) long TW axial cracks, as shown in Fig. 14.4.

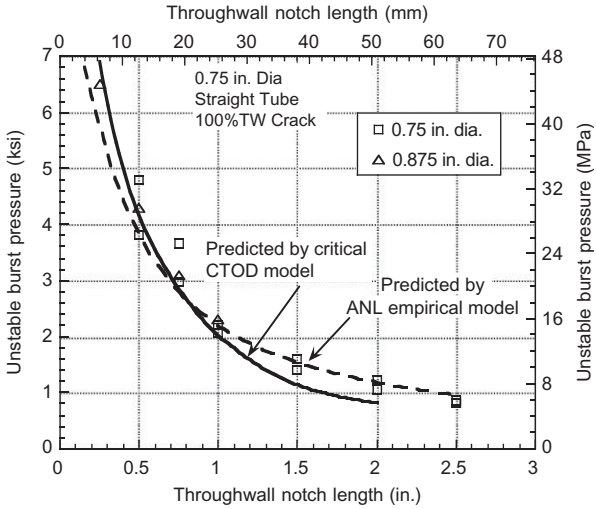

Fig. 14.4 Predicted versus observed unstable burst pressures of straight tubes with 100% TW axial notches. Dashed line represents predicted burst pressures using the empirical Eq. (14.2b). Symbols represent burst pressure test data.

Part-throughwall rectangular axial flaw

A general failure criterion for predicting rupture of the crack tip ligament in a tube with a PTW crack can be expressed as follows:

$$\sigma_{\text{lig}} = \overline{\sigma} \tag{14.5a}$$

where σ_{lig} is the average ligament stress, which for the axial crack is given by

$$\sigma_{\text{lig}} = m_{\text{p}}\sigma \tag{14.5b}$$

where m_{p} is the ligament stress magnification factor (which depends on the axial crack length and depth) and σ is the membrane hoop stress. The pressure at which the ligament ruptures (P_{sc}) can be expressed as

$$P_{\text{sc}} = \frac{P_{\text{b}}}{m_{\text{p}}} \tag{14.5c}$$

Various expressions for m_{p} as a function of crack length and crack depth have been proposed in the literature by Kiefner et al. (1972), Alzheimer et al. (1979), and Flesch and Cochet (1988). Many of the earlier publications did not distinguish between ligament rupture and unstable burst.

A series of burst tests at 600°F on PTW axial EDM slots in Alloy 600 tubes was carried out at Battelle-Pacific Northwest Laboratory and reported by Alzheimer et al. (1979). The tests were conducted in a high-pressure test system with limited flow capacity, which meant that the tests were interrupted immediately after ligament rupture, not necessarily unstable burst. The tests on shallower notches (55%–60% deep) resulted in unstable burst with large crack opening and crack tip tearing. On the other hand, the tests on deeper notches (85%–90% deep) produced ligament rupture (small crack opening) but not unstable burst. The authors of the report correlated all the rupture pressure data with slot length and depth empirically without distinguishing between ligament rupture and unstable burst.

Following a detailed analysis of all the available data and correlations, Majumdar et al. (2001) concluded that the following expression for m_{p} represented the test ligament rupture pressures most accurately:

$$m_{\text{p}} = \frac{1 - \alpha\dfrac{a}{mh}}{1 - \dfrac{a}{h}} \tag{14.6a}$$

where

$$\alpha = 1 + \beta\left(\frac{a}{h}\right)^2\left(1 - \frac{1}{m}\right) \tag{14.6b}$$

with $\beta = 1$.

A number of validation tests conducted on Alloy 600 SG tubes at ANL (Majumdar et al., 2001) showed that the test ligament ruptures can be predicted by Eqs. (14.5a)–(14.5c) reasonably well (Fig. 14.5).

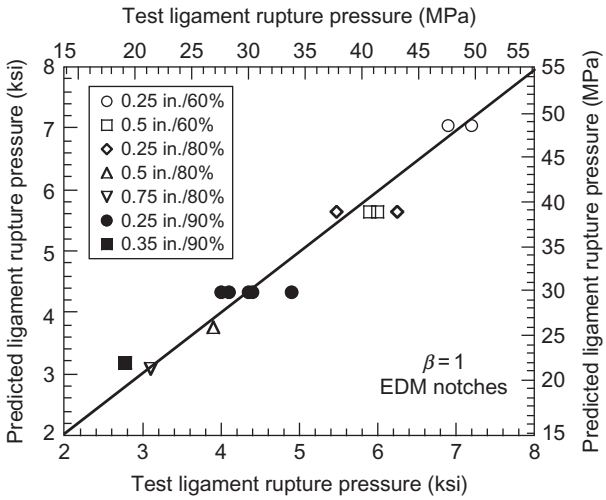

Fig. 14.5 Observed versus predicted ligament rupture pressures for tubes with PTW EDM notches.

Stability criterion for a part-throughwall crack It is postulated that the stability of a PTW crack can be analyzed by using Eqs. (14.2a) and (14.5c). If $P_{cr} > P_{sc}$, the crack is stable after ligament rupture. Although the crack will leak, it will not increase in length without a further increase in pressure. If $P_{cr} < P_{sc}$, the crack will be unstable and will rapidly increase in length without any additional increase in pressure. The problem with many laboratory tests using room-temperature pressurized water on tubes with shallow cracks is that because of limited flow and pressure capability, the system depressurizes immediately after ligament rupture. In such systems, unstable burst will not occur unless the tube is fitted with internal bladder and foil after ligament rupture and the specimen pressurized rapidly. However, in laboratory tests, it is customary to classify failure as unstable burst if the crack tips show evidence of tearing into virgin material (e.g., Fig. 14.1B).

EPRI flaw model EPRI has a model for predicting burst pressures of SG tubes with axial PTW flaws. The model does not distinguish between unstable burst and ligament rupture. It is based on a correlation proposed by Flesch and Cochet (1988) who derived it from burst tests on tubes with axial flaws that are not too deep ($0.2 \le a/h \le 0.85$). The burst pressure reduction factor m_p (EPRI) is given by:

$$\frac{1}{m_p(EPRI)} = \frac{p_{EPRI}}{p_b} = 1 - \left(\frac{2c}{2c+2h}\right)\left(\frac{a}{h}\right) \tag{14.7}$$

where p_{EPRI} is the rupture pressure predicted by the EPRI correlation (Eq. 14.7) and P_b is the burst pressure of virgin, unflawed tube given by Eq. (14.1a).

A comparison of the predicted burst pressure reduction factors using Eq. (14.7) with test burst pressure reduction factors of Alloy 600 tubes with EDM flaws is shown

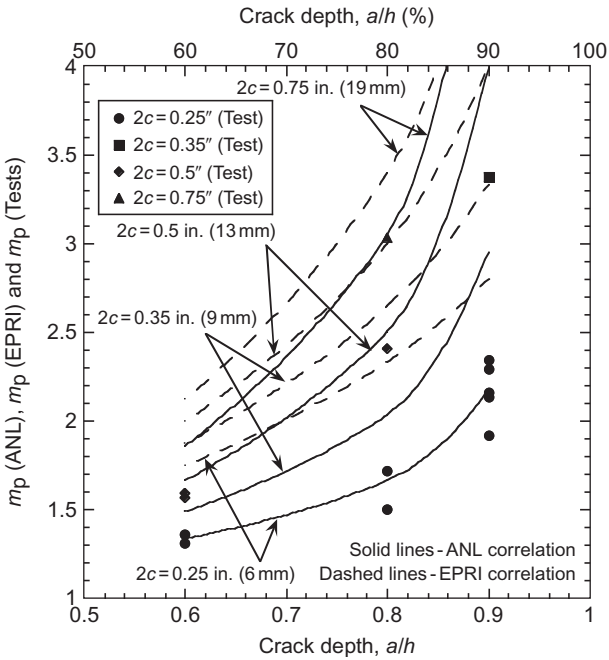

Fig. 14.6 Comparison of ANL test burst pressure reduction factors (symbols) with predicted values (dashed lines) using EPRI correlation (Eq. 14.7). Also included are predicted burst pressure reduction factors m_p (solid lines) using ANL correlation (Eq. 14.5a).

in Fig. 14.6. The predicted burst pressures by EPRI correlation are quite conservative compared to the ANL correlation, which predicts the test results quite accurately.

14.2.1.2 Single circumferential flaws

Throughwall rectilinear circumferential flaws

Unstable burst Failure loads of tubes with a single circumferential crack critically depend on the bending constraint imposed externally on the tubes. The two extremes are the free-bending case and the fully constrained case. In reality, steam generator tubes are partially constrained against bending by the TSs.

Free bending case Failure loads for tubing with throughwall circumferential cracks can be calculated by plastic limit load (collapse) analyses, which are based on beam theory by earlier work of Kanninen et al. (1982) and are described by Ranganath and Mehta (1983). For an unconstrained (free-to-bend) tube with a TW crack of angular length 2θ and no applied primary bending stress, the critical failure pressure is the lesser of the failure pressure of an unflawed tube (Eq. 14.2a) and

$$p_{cr} = 2p_b\left(1 - \frac{\theta}{\pi} - \frac{2\beta}{\pi}\right) \tag{14.8a}$$

where β, the angular location of the neutral axis, is given by

$$\beta = \sin^{-1}\left(\frac{\sin\theta}{2}\right) \tag{14.8b}$$

Fully constrained case Eq. (14.8a) is applicable to one extreme case, where the tube is completely free to bend. In the opposite extreme case of total constraint against bending, a criterion based on maximum shear stress in the net section, as proposed by Cochet et al. (1990), can be used to calculate the instability limit pressure, which for thin shells is:

$$p_{cr} = 2p_b\left(1 - \frac{\theta}{\pi}\right) \tag{14.9}$$

In reality, the TSs offer significant but not total constraint against bending, a condition that tends to increase the failure pressure to somewhere between those predicted by Eq. (14.8a) and those predicted by Eq. (14.9) (Majumdar, 1999).

Part-throughwall rectangular circumferential flaws

Consider a tube with either two symmetrical PTW circumferential flaws or a single PTW circumferential flaw of angular length 2θ and depth a. At low temperatures, where creep effects are negligible, the ligament failure pressure (P_{sc}) is generally expressed in terms of a stress magnification factor (m_p) by equating the magnified axial stress in the ligament to the flow stress,

$$\sigma_{lig} = m_p\frac{p_{sc}r}{2h} = \overline{\sigma} \tag{14.10}$$

The failure pressure for circumferentially cracked tubes (i.e., the value of the magnification factor m_p) depends strongly on the degree of restraint that the tubes are subjected to against bending. The two extreme cases (i.e., the free-bending case and the completely constrained case) are relatively easy to analyze. Generally, steam generator tubes are sufficiently constrained laterally that failure loads are expected to be much closer to the completely constrained case than the free-bending case. The discussion here assumes that the tubes are either fully constrained or are completely free to bend.

Fully constrained case The fully constrained case also includes the case for an unconstrained tube that contains two symmetrical circumferential cracks. In this situation, the whole section that contains the crack (or cracks) is subjected to axial tensile stress, with the ligament (or ligaments) subjected to stress intensification. If the average stress in the ligament (or ligaments) is expressed as $1/m$ times the average stress in the rest of the section that contains the crack (or cracks), the average ligament axial stress (σ_{lig}) can be calculated from a simple equilibrium of axial forces,

$$\sigma_{\text{lig}} = \frac{pr}{2h} \frac{1}{\left[m\left(1 - \frac{2\beta}{\pi}\right) + \left(\frac{n\theta}{\pi}\right)\left(1 - \frac{a}{h} - m\right)\right]} \tag{14.11a}$$

where

$$n = \begin{cases} 1 \text{ for a single crack} \\ 2 \text{ for two symmetrical cracks} \end{cases}$$

Defining m_{p} as the ratio of the average ligament axial stress and the average axial stress in the unflawed tube,

$$m_{\text{p}} = \frac{1}{\left[m + \left(\frac{n\theta}{\pi}\right)\left(1 - \frac{a}{h} - m\right)\right]} \tag{14.11b}$$

Originally, Kurihara et al. (1988) used the empirically obtained expression

$$m = 1 - \left(\frac{a}{h}\right)^{\kappa} \left(\frac{n\theta}{\pi}\right)^{\mu} \tag{14.12}$$

(with $n = 1$). Although Kurihara et al. (1988) recommended values of $\kappa = 2$ and $\mu = 0.2$ for the exponents, the results are almost indistinguishable from those obtained by using $\kappa = 3$ and $\mu = 0.3$. Because the value of m in Eq. (14.12) does not tend to 0 when a/h tends to 1 for all θ, as would be expected intuitively, Eq. (14.9) was modified so as to have the same form as in the case of axial cracks (Eq. 14.6a), that is,

$$m = \frac{1 - \frac{a}{h}}{1 - \frac{a}{Nh}} \tag{14.13a}$$

where

$$N = 1 + \lambda \left(\frac{n\theta}{\pi}\right)^{\gamma} \tag{14.13b}$$

and λ and γ are fitting parameters.

Both the failure modes and moments of the original set of test data from four-point bending failure tests on pressurized, PTW circumferentially cracked, Type 304 stainless steel pipes at room temperature (used by Kurihara et al., 1988) can be predicted somewhat better by the current model with $\lambda = 0.2$ and $\gamma = 0.2$ than by the Kurihara model (Majumdar et al., 2000). Also, this approach led to reasonable predictions of test failure temperatures of pressurized Alloy 600 tubes with two symmetrical PTW circumferential notches subjected to high-temperature ramps (Majumdar et al., 1998).

Free-bending case In the free-bending case, part of the section that contains the flaw will generally be subjected to compressive stress. As a result, Eq. (14.11a) must be replaced by

$$\sigma_{\text{lig}} = \frac{pr}{2h} \frac{1}{\left[m\left(1-\frac{2\beta}{\pi}\right)+\left(\frac{n\theta}{\pi}\right)\left(1-\frac{a}{h}-m\right)\right]} \tag{14.14a}$$

where the angle β that defines the location of the neutral axis is given by

$$\beta = \sin^{-1}\left\{\frac{\sin\theta}{2}\left[1-\frac{1}{m}\left(1-\frac{a}{h}\right)\right]\right\} \; for \; \beta \le \pi - \theta \tag{14.14b}$$

and Eq. (14.11b) must be replaced by

$$m_{\text{p}} = \frac{1}{\left[m\left(1-\frac{2\beta}{\pi}\right)+\left(\frac{n\theta}{\pi}\right)\left(1-\frac{a}{h}-m\right)\right]} \tag{14.14c}$$

with m and N are defined by Eqs. (14.13a) and (14.13b), respectively. This approach led to reasonable predictions of failure temperatures of free-to-bend tubes with a PTW circumferential notch subjected to high-temperature ramps (Majumdar et al., 1998).

Although a detailed analysis comparable to that presented in Majumdar et al. (2000) for TW cracks has not been carried out, it is expected that tubes with PTW circumferential flaws at the top of the TS will behave as though they were fully constrained against bending.

14.2.1.3 Multiple axial flaws

Failure models and validating tests

Unlike single flaws, the literature on rupture of tubes with two or more flaws is rather limited. One can use elastic-plastic nonlinear FEA to predict the inter-crack axial ligament rupture pressure by using a failure criterion (e.g., necking) (Majumdar et al., 2001). An example for the case of two 100% TW axial cracks offset in the circumferential direction (Type 4 cracks) by a 1.27 mm (0.05 in.) thick ligament is shown in Fig. 14.7. An examination of the FEA results shows that the ligament is subjected to high shearing strain and rotation (Fig. 14.7) but relatively low hoop and axial stresses. Average thickness versus pressure plots for this specimen (1.27 mm [0.05 in.] wide ligament), together with one in which the ligament width is 2.5 mm (0.1 in.), are shown in Fig. 14.8. The solid lines end where the FEA fail to converge. The finite deformation analyses are much more in agreement with test results than infinitesimal analyses, because they properly account for the large rotations of the ligament (Fig. 14.7). Although FEA is feasible for notches arranged in a regular array, they are challenging for SCCs which have very complex geometries.

When the individual cracks are of the same size and arranged in a regular array, a simple equivalent rectangular crack method can be used to estimate the radial

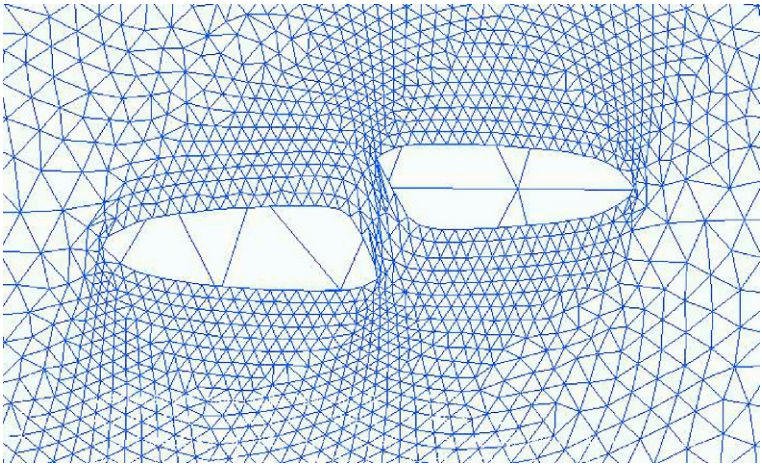

Fig. 14.7 Deformed configuration of two axial cracks offset in the circumferential direction.

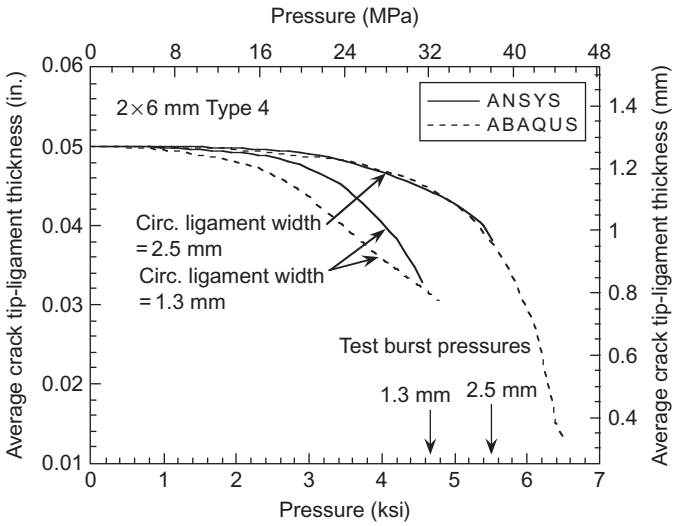

Fig. 14.8 Calculated variation of average circumferential ligament thickness with pressure using finite deformation analyses by ANSYS and ABAQUS for two 6-mm (0.25 in.) long axial flaws separated by a 1.3- and 2.5-mm (0.05 and 0.1 in.) wide circumferential ligament. Vertical arrows denote the test burst pressures.

ligament rupture pressures. The method is illustrated for the simple case of two coaxial flaws in Fig. 14.9. The objective is to replace the two PTW cracks with a single PTW crack of the same overall length by smearing out the solid axial ligament area into the crack tip radial ligament. In this case the predicted ligament rupture pressure of the equivalent crack ($L = 26.7$ mm and heq = 76%) of 21.7 MPa agrees fairly well with the test radial ligament rupture pressure conducted on an Alloy 600 tube with two 13 mm long, 80% deep axial notches.

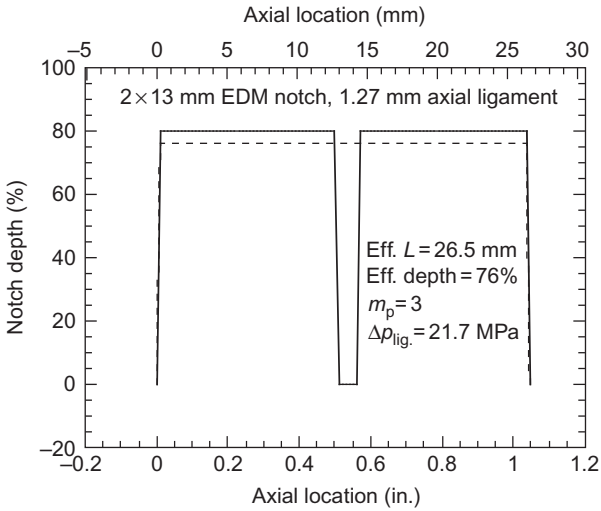

Fig. 14.9 Equivalent rectangular crack for two 13-mm long and 80% deep PTW notches separated by a 1.27-mm wide full-thickness ligament.

A series of tests was conducted on Alloy 600 tubes with 2–6 PTW axial laser-cut notches in various configurations (Types 2–6, Figs. 14.10A–C). The ligament widths were measured by fractography to be 0.13–0.25 mm (0.005–0.010 in.). The equivalent rectangular crack method was used to predict the pressures for through-thickness notch tip radial ligament rupture. Predicted versus observed pressures for through-thickness ligament rupture are shown in Fig. 14.11. The ligament rupture pressures are over-estimated in all cases; however, the overestimation is largest for the tubes with six notches.

Failure maps

SCCs generally consist of multiple cracks separated by ligaments rather than a single, planar crack (Fig. 14.12A).

Although ligament geometry can be very complex, it can be idealized (Fig. 14.12B) as being either radial (PTW cracks), purely axial (Type 2), or purely circumferential (Type 4). During pressurization, the rupture of crack tip radial ligaments results in TW cracks (leading to leakage) and the rupture of axial or circumferential ligaments results in a longer crack that may undergo unstable burst at differential pressures corresponding to normal operation (ΔPNO) or design basis accident condition (ΔPMSLB). Failure maps have been developed (Majumdar et al., 2009) to delineate ranges of crack and ligament sizes that could be susceptible to ligament rupture and/or unstable burst due to pressure differences of ΔPNO, ΔPMSLB, 1.4ΔPMSLB, or 3ΔPNO. The possibility of the presence of 1, 2, 4, or 6 PTW cracks, 80% or 90% deep was considered. Each map shows the ligament widths and overall crack lengths for a number (2, 4, and 6) of axial PTW cracks with a fixed depth that result in failure at pressure differentials of ΔPNO, ΔPMSLB, 3ΔPNO, or 1.4ΔPMSLB. The failures could occur due to a number of mechanisms. The failure mechanisms that were

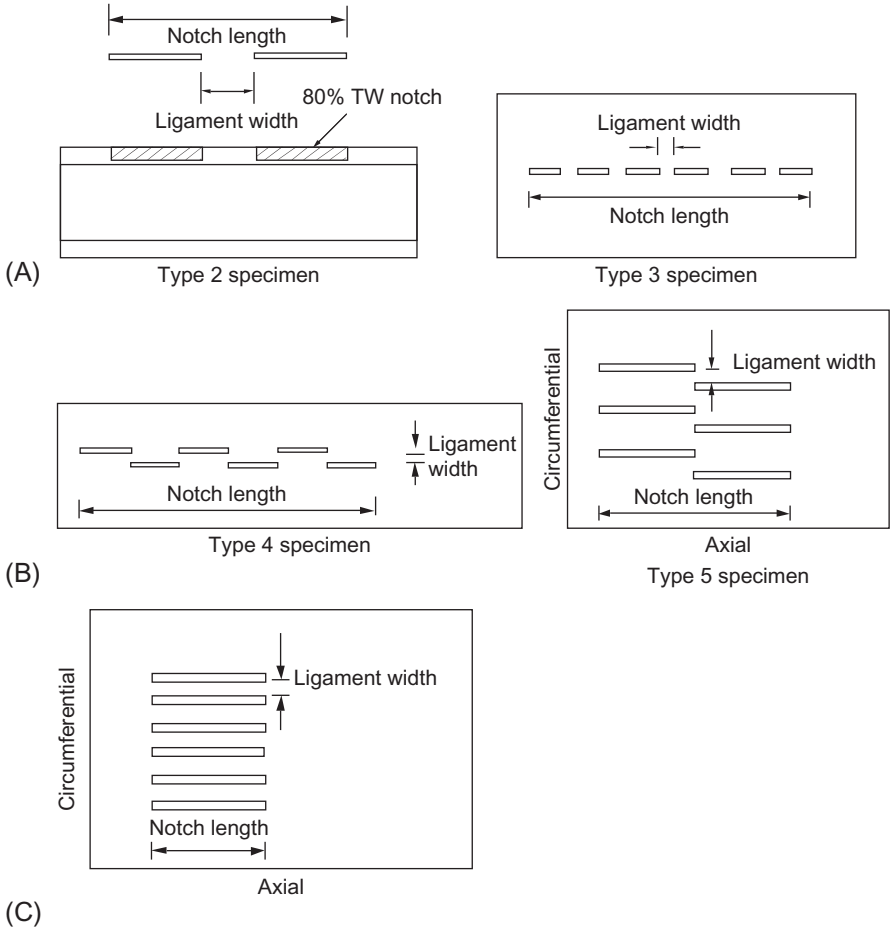

Fig. 14.10 (A) Geometries of types 2 and 3 specimens. (B) Geometries of types 4 and 5 specimens. (C) Geometry of type 6 specimen.

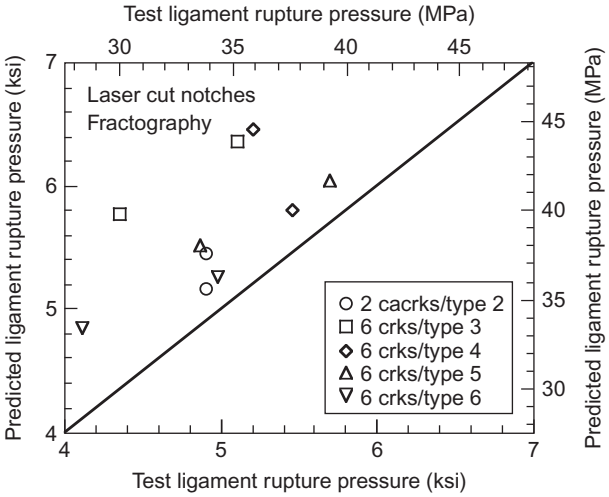

Fig. 14.11 Predicted versus observed ligament rupture pressures for multiple laser-cut notches.

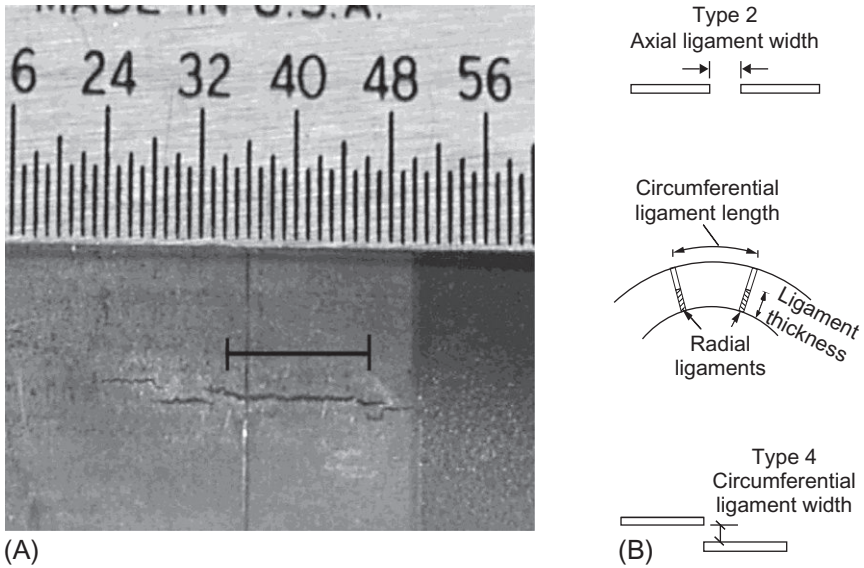

Fig. 14.12 (A) Typical stress corrosion cracks and (B) various idealized ligament configurations.

considered are the rupture of radial ligament (following which leakage occurs), crack coalescence (i.e., rupture of axial or circumferential ligament), and unstable burst. Each map identifies in terms of crack length and ligament width a safe region for which no failure is predicted. Outside this no-failure region, the map delineates in terms of crack length and ligament width the regions of various failure mechanisms (e.g., radial ligament rupture, axial/circumferential ligament rupture, unstable burst).

Failure maps for an Alloy 600 tube with a single axial crack at normal operation and main steam line break condition are shown in Fig. 14.13A and B, respectively.

For multiple cracks, the map can be simple as shown for four 80% deep axial cracks (separated by axial ligaments) in Fig. 14.14A or more complex as shown for the same set of four cracks but 90% deep in Fig. 14.14B.

14.2.2 Severe accident transients

Severe accidents involving significant core damage are unlikely events in nuclear reactors. Even in the unlikely event that such an accident should occur, in most cases any potential risk to the public is mitigated by the presence of a robust containment. The behavior of steam generator tubing during such severe accidents ("high-dry" core damage during so-called station blackout events involving high primary system pressure and dry SGs) is of particular interest, since failure of the SG tubes could create a coolant flow path from the primary side to the secondary side and ultimately outside the containment via various stuck-open valves. As a part of its effort to develop

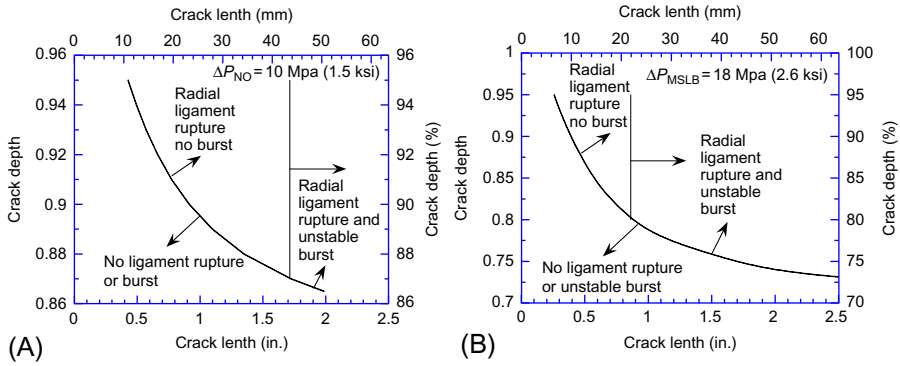

Fig. 14.13 Failure map of a single crack in an Alloy 600 tube at (A) normal operation ΔPNO and (B) main steam line break pressure ΔPMSLB.

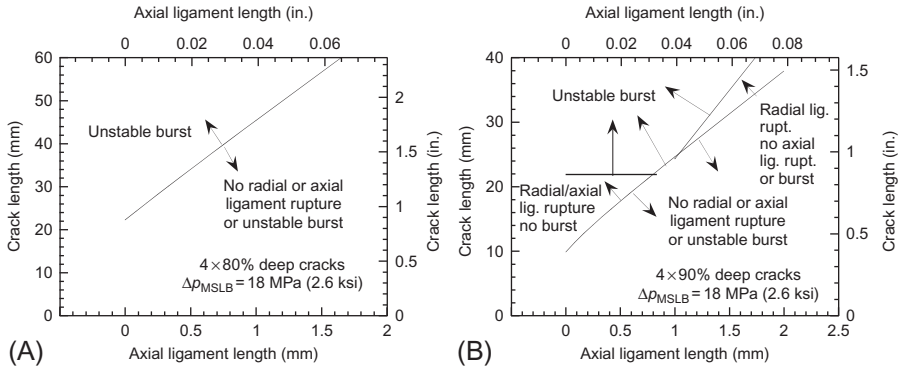

Fig. 14.14 Failure maps for SG tubes with four axial cracks, (A) 80% and (B) 90% deep, separated by three axial ligaments (type C) at main steam line break pressure (ΔPMSLB). "Crack length" denotes the total overall length of the individual cracks and ligaments.

guidance for accident analysis, the NRC and its contractors and EPRI have been investigating the potential for failure of steam generator tubes during severe accidents. The accident sequences that appear to produce the greatest risk of steam generator tube failure are those in which the reactor pressure vessel fails to depressurize, but depressurization does occur on the secondary side.

Analyses of the failure pressure and temperature of tubes under severe accident conditions (i.e., $T > 350°C$) were conducted. The severe accident scenario under investigation involves a total station blackout (SBO) with a stuck-open steam generator secondary-side atmospheric dump valve, resulting in loss of feedwater and secondary-side depressurization. Of all the severe accent scenarios, this transient resulted in the maximum pressure drop across the tube wall. The pressure drops remain relatively constant (~16 MPa [2350 psi]) during the transient. Two time/temperature histories were considered, based upon severe accident analyses by INEL (Ellison et al.,

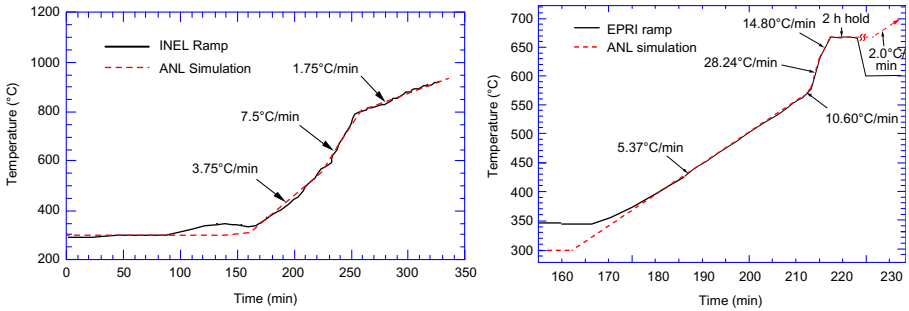

Fig. 14.15 Calculated and ANL simulation of (A) INEL ramp and (B) EPRI ramp for the high-temperature tests.

1995) and EPRI (Fuller et al., 1998). The tests on pressurized tubes simulated the temperature transients closely (Fig. 14.15). Since all of the ruptures occurred at temperatures >600°C where thermal creep is active, it is to be noted that the temperature rates (i.e., strain rates) of the INEL ramp tests were lower (more damaging) than those of the EPRI ramp tests.

At these high temperatures, plastic deformation is likely to be much more extensive than at normal reactor operating temperatures, and creep effects may no longer be negligible. To predict failure times and temperatures under these two hypothetical accident scenarios, two types of predictive models for rupture of the crack tip ligament were evaluated (Majumdar et al., 1998), namely the flow stress model

$$\sigma_{\text{lig}} = \overline{\sigma(T)} \tag{14.15a}$$

where σ_{lig} is the average ligament stress given by Eq. (14.5b), and the creep rupture model

$$\int_0^{t_f} \frac{dt}{t_R\left(T, \sigma_{\text{lig}}\right)} = 1 \tag{14.15b}$$

Comparison of the tests with predicted results showed that the creep rupture model is the more accurate of the two (Majumdar et al., 1998), as shown in Fig. 14.16A and B. Note that the creep rupture model correctly accounts for the increased damage in the slower INEL ramp tests than in the faster EPRI tests.

14.3 Structural integrity of U-bends with flaws

The first reported leakage due to U-bend cracking occurred at Surry in 1976 (Fletcher, 1981). Since then cracking has been observed in U-bends at the inner rows of many steam generators (SGs). Prior to 1980, seven plants reported leakage from U-bend row

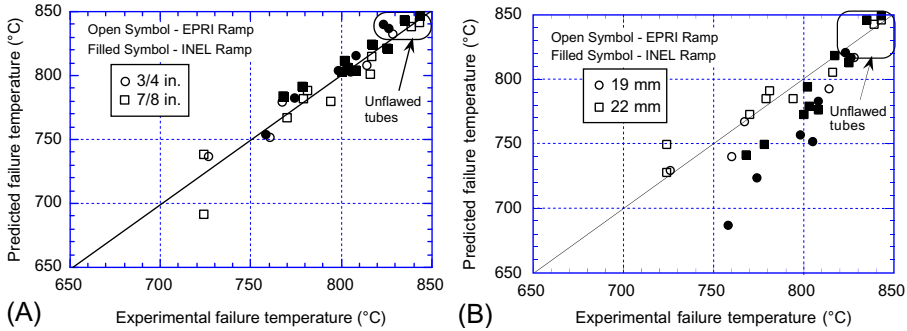

Fig. 14.16 Comparison of observed versus predicted failure temperatures by (A) creep rupture and (B) flow stress models for tests conducted with the INEL and EPRI temperature ramps.

1 cracking (Fletcher, 1981). The cracks were almost equally distributed on the cold and hot leg sides and a few of them occurred at the apex. Since 1980, cracking indications have been reported at both ID (PWSCC) and OD (ODSCC) of U-bends made from mill-annealed Alloy 600 tubes. Cracking has occurred in U-bend regions of tubes made from Alloy 600TT; however, the number of instances has been very limited (1 or 2). In 2009, a plant reported indications in the apex extrados of Alloy 600TT U-bends and small leakages during pressure testing.

In the past, industry determined by a limited number of tests that the burst pressures of U-bends with flaws are higher than those of straight tubes with similar flaws. Therefore, burst and ligament rupture pressure correlations developed for straight steam generator tubes with flaws are assumed to predict the same for U-bends conservatively. The NRC is independently verifying this assumption through a contract at ANL by obtaining prototypic U-bend specimens from a nuclear reactor vendor, developing burst and leakage correlations based on analytical models, and validating them with leak rate and burst tests on U-bends with machined EDM flaws and PWSCC. To this end, ANL procured a number of U-bends with 2.25 in. (57 mm) and 6 in. (152 mm) radius. As a reference, row 1 of Model F and Model 51 Westinghouse SGs have a radius of approximately 2.2 in. (56 mm).

14.3.1 Models for failure of U-bends with a single axial EDM notch

Limited tests have been conducted on U-bends with circumferential notches. Most tests and modeling of U-bends have concentrated on axial notches. Test experience has shown that circumferential notches are inherently more resistant to rupture than axial notches. Consequently, to achieve rupture at normal operation or MSLB pressures, the circumferential cracks have to be unrealistically long (>180°). Production of such long circumferential notches by machining has turned out to be a challenge.

14.3.1.1 100% TW axial notch

The conventional model for predicting unstable burst pressures of straight tubes with 100% TW axial flaws is based on the bulging factor, m (see Section 14.2.1.1). According to the model, the unstable burst pressure P_{cr} is related to the burst pressure of an unflawed tube, P_b, as shown in Eq. (14.2a).

$$P_{cr} = \frac{P_b}{m} \tag{14.2a}$$

Eq. (14.2a) was generalized for representing the unstable burst pressures of U-bends by replacing m by the effective bulging factor m_{eff}. The test unstable burst pressures of flawed U-bends were used to determine m_{eff} as follows:

$$m_{eff} = \frac{P_b}{P_{cr}(\text{Test})} \tag{14.16a}$$

where P_b is the burst pressure of an unflawed straight tube, which is a function of the tube geometry and the flow stress of the virgin tube material. For a straight tube ($R = \infty$) with a TW crack,

$$m_{eff} = m \tag{14.16b}$$

where m is the bulging factor that is dependent only on the tube and crack geometries (Eq. 14.2b) and is independent of the flow stress.

Fig. 14.17A shows effective bulging factors as functions of the bulging factor of the corresponding straight tube. Note that the effective bulging factor of the 6 in. (152 mm) radius U-bend is practically the same as that of the straight tube. Fig. 14.17B, which shows a plot of the predicted versus observed (in-house data) burst pressures, confirms that the burst pressures of all the tests (including those for the flaws located at the intrados and the tangency points) are predicted to within ±95% prediction limits and the uncertainty in the mean is ±200 psi. In-house tests also showed that, if the same correlations for effective bulging factor (Fig. 14.17A) are used for U-bends made from 7/8 in. (22 mm) diameter tube, the test unstable burst pressures are also predicted to within the same ±95% prediction limits.

14.3.1.2 PTW axial notch

An empirical model for predicting ligament rupture pressures of straight tubes with PTW flaws based on m_p factor was presented in Section 14.2.1.1 (Eq. 14.5c). According to the model, the ligament rupture pressure P_{sc} is related to the burst pressure of unflawed tube, P_b, by the following equation:

$$P_{sc} = \frac{P_b}{m_p} \tag{14.5c}$$

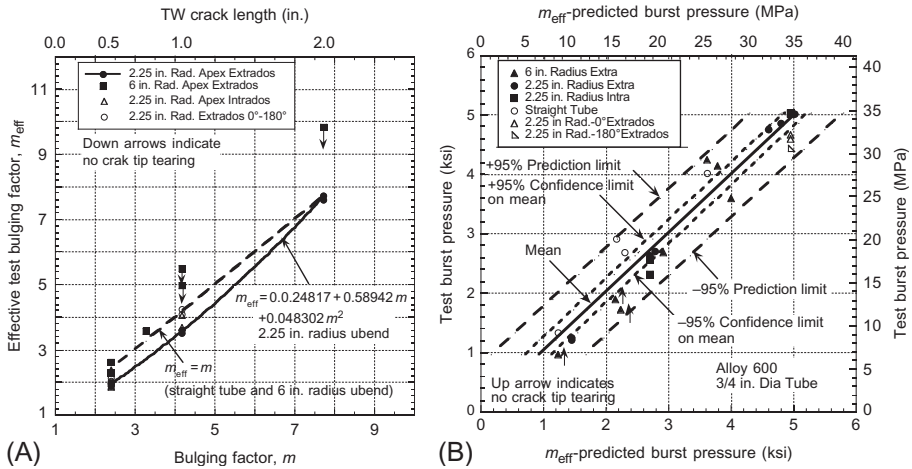

Fig. 14.17 (A) Variation of effective bulging factor for U-bends with the bulging factor of straight tubes and (B) predicted (using m_{eff}) versus observed burst pressures for U-bends.

where m_p is dependent on the crack length and depth as well as the tube geometry but not on flow stress. Since m_p factors are relatively insensitive to the stress-strain curve of the material, they should be applicable to the U-bend which is effectively prestrained during fabrication. An effective m_p factor for U-bends was defined by fitting the ligament rupture pressures predicted by FEA with the following equation:

$$m_{peff} = \frac{P_b}{P_{sc}(\text{FEA})} \tag{14.17}$$

Alternatively, effective m_p factors can also be calculated from the observed (in-house) ligament rupture pressures in tests, as follows:

$$m_{peff} = \frac{P_b}{P_{sc}(\text{Test})} \tag{14.18}$$

The fitted effective m_p factors for all the U-bends with extrados notches are plotted as functions of the m_p factor in Fig. 14.18A. Fig. 14.18B shows that the correlation for effective m_p factors for extrados notches predicts the effective m_p factors for intrados notches as well.

The test ligament rupture pressures (in-house data) of all the U-bends (3/4 in. [19 mm] diameter tube) with PTW axial flaws are compared with the ligament rupture pressures predicted by using the effective m_p factor in Fig. 14.19A. The long-dashed lines in Fig. 14.19A show that all the test ligament rupture pressures (including those for the flaws located at the intrados and the tangency points) are predicted to within

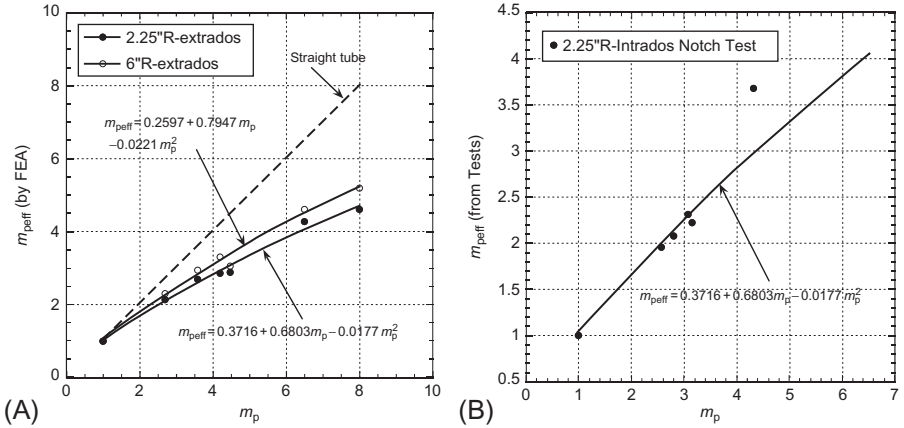

Fig. 14.18 Plots of effective m_p factor (A) calculated by Eq. (14.17) and (B) calculated by Eq. (14.18) for notches at apex intrados as functions of m_p factor for 3/4 in. (19 mm) diameter straight tube.

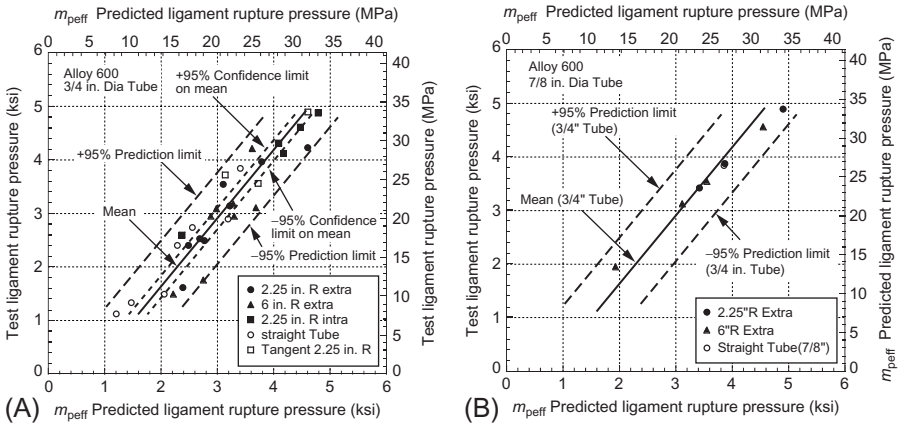

Fig. 14.19 Ligament rupture pressures predicted by m_{peff} factor versus test ligament rupture pressures for U-bends fabricated from (A) 3/4 in. (19 mm) diameter tube and (B) 7/8 in. (22 mm) diameter tube.

±95% prediction limits; the prediction uncertainty is ±1000 psi (±7 MPa). The short-dashed lines show that the uncertainty in the mean is ±200 psi (±1 MPa). Further, if we use the same correlation for effective m_p factor (Fig. 14.18A) as that of the ¾ in. (19 mm) diameter tube, the test ligament rupture pressures of U-bends made from 7/8 in. (22 mm) diameter tube are also predicted to within the same ±95% prediction limits (Fig. 14.19B).

14.4 Application of equivalent rectangular crack method

In contrast to machined notches, which have constant depth and are rectangular in shape, the field or laboratory-grown SCC cracks are irregular in shape and have variable depth along their length. Instead of being a single planar crack, they are often composed of a family of crack segments in closely spaced planes. Typical examples of axial SCC in SG tubes are shown in Fig. 14.20A and B. Depth variations of SCCs with axial location can be measured either nondestructively by EC methods or destructively. The depth estimates from destructive examination (e.g., fractography) are more accurate. Since most analytical models for predicting ligament rupture or burst pressures of SG tubes are based on a rectangular flaw geometry with well-defined length and constant depth, the purpose of the equivalent rectangular crack (ERC) method is to replace the complex SCC depth profile (as measured by EC/NDE or fractography) with a rectangular PTW crack having the same ligament rupture pressure as the SCC.

14.4.1 Eddy current nondestructive examination

Assessment of SG tube structural integrity is commonly based on NDE data obtained during periodic in-service inspections (ISIs). EC testing in its various forms is the primary NDE technique used for inspection of SG tubes. Fig. 14.20 displays some conventional bobbin and rotating probes used for inspection of SG tubes. High-speed bobbin probes are routinely employed for full-length inspection of the SG tube bundle. Intrinsic to its coil design, bobbin probe provides a single circumferentially integrated measurement at each position along the tube axis. The probe therefore is limited in its ability to resolve multiple flaws located at the same axial elevation and in detecting circumferentially oriented crack-like flaws.

Motorized rotating pancake coils (MRPCs) have been developed to overcome the known limitations of bobbin probes. Because of their slow speed, rotating probes are typically employed for the inspection of selected regions of the SG tube (e.g., TS, support plates, U-bend region) or as a supplementary technique for confirmation of signals detected initially by bobbin probe. Rotating probes traverse the tube with a helical

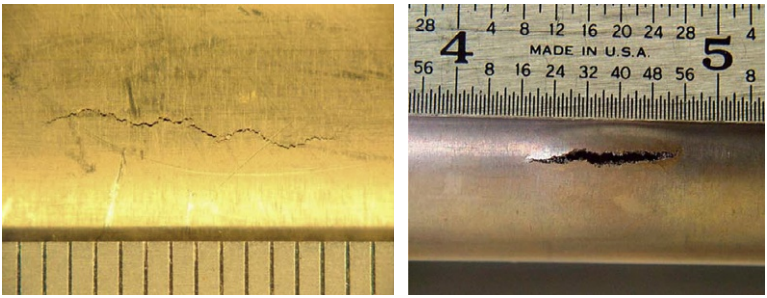

(A) (B)

Fig. 14.20 Surface appearance of stress corrosion cracks in SG tubes after ligament rupture.

motion that results in a complete scan of the tube wall. The probe head assembly may contain single or multiple surface coils that can provide complementary information. Both impedance and transmit-receive probe configurations are available. Directionally sensitive probes are used to more decisively identify the orientation of crack-like indications. One common surface-riding rotating probe design in use today consists of three coils that are integrated into a single probe head: a differential cross wound coil (+Point, Zetec Inc.), an absolute mid-frequency pancake coil, and an absolute high-frequency pancake coil. Because MRPCs in general offer the highest spatial resolution among all EC probe types used for field applications, they are often employed to ultimately resolve and size more complex forms of degradation such as SCCs. More recently, array probes are being deployed for full-length inspection of SG tube bundle. The probe head typically houses parallel bracelets of circumferentially offset elements, either printed circuit or wound coils, which operate in a driver-pickup configuration. The elements are sequentially excited in a multiplexed fashion to provide complete axial and circumferential coverage of the tube. The circumferential resolution of an array probe is essentially dictated by the number of elements used in the probe head assembly. Nonsurface-riding array probes could, in principle, provide comparable inspection speeds to bobbin probes while providing circumferential resolution comparable to rotating probes. Practical constraints, however, limit the circumferential resolution of array probes to less than that obtainable with rotating probes (Fig. 14.21).

Conventional procedures for estimation of flaw size, either for ISI applications or for subsequent engineering assessments, are based primarily on manual analysis of rotating probe data. The process for generating depth profiles in this manner is rather tedious and the results are subject to variability among analysts. Development of computer-aided data analysis tools is a viable approach to help improve the reliability,

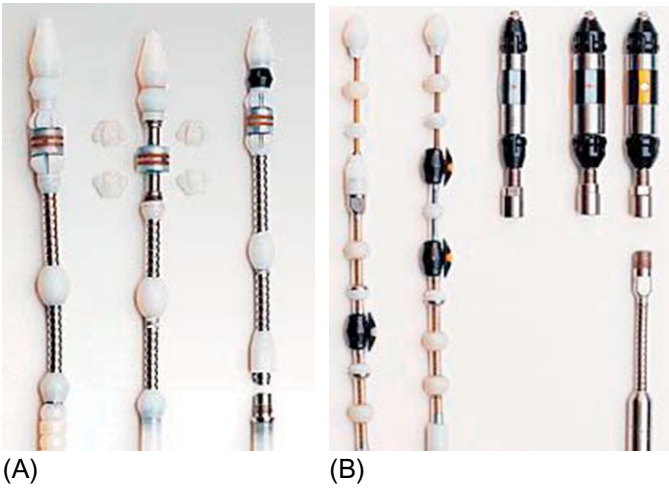

Fig. 14.21 Photograph of various (A) bobbin and (B) motorized rotating eddy current probes used for inspection of SG tubes (Zetec Inc.).

repeatability, and efficiency of flaw sizing based on rotating probe examinations. Evaluation of some alternative methods for estimating crack depth profile using a computer-aided data analysis tool have been reported by Bakhtiari et al. (2009). A discussion on the viability of different sizing methods for cracks in SG tubes has been provided by Bakhtiari and Elmer (2008) and Bakhtiari et al. (2009).

As it has been reported by Bakhtiari and Elmer (2008) and Bakhtiari et al. (2009), a typical calibration standard for rotating probe examination contains machined notches with various depths and orientation. An 18-notch EDM standard made of Alloy 600 tubing material with 0.875-in. (22 mm) OD and 0.05-in. (13 mm) wall thickness containing 0.375-in. (10 mm) long machined flaws was used for calibration of rotating probe data used in this study. The flaws included OD and ID initiated axial and circumferential notches with depths of 20% TW, 40% TW, 60% TW, 80% TW, and 100% TW. Calibration of EC rotating probe data was conducted in accordance with generically qualified examination technique specification sheets (EPRI, 2007; Bakhtiari and Kupperman, 2009).

Calibration and analyses of EC data were all performed offline using software-based tools developed at Argonne (Bakhtiari and Elmer, 2008). For amplitude calibration, the peak-to-peak value of the signal from the 100% TW notch in the EDM notch standard was set to 20 V. For phase-angle calibration, the response from the 40% TW ID EDM notch was set to 15 degrees, resulting in noise associated with probe wobble to be approximately horizontal in the impedance plane. Calibration curves for estimating the depth of cracks were generated at a test frequency of 300 kHz for the mid-range +Point coil and at 400 kHz for the 0.080-in. high-frequency pancake coil of a 3-coil rotating probe. It should be noted that although representative depth profiles based on high-frequency pancake coil data are presented below; for ISI applications, the EC depth profiles for SCCs are more routinely based on data acquired with the +Point coil. Due to their differential coil configuration, orthogonal probes such as +Point are less prone to various sources of noise and provide better directional sensitivity than conventional pancake coils (Bakhtiari et al., 2009).

Local variations in crack depth and geometry are necessarily smoothed out in the EC measurements because of the distribution of induced ECs that are averaged over a finite volume of the material; therefore, the EC data tend to show a relatively smooth variation of crack depth along the crack length. Furthermore, contact across crack faces creates a conducting path for the flow of induced currents, which consequently reduces the secondary fields and thus the EC probe response to tight regions of the crack. This is evidenced by the fact that although many SCC specimens exhibit leakage under low gas pressure prior to testing, the EC probe fails to detect or identify the locations of these TW segments. In the actual tests with water, no leakage is detected until much higher pressures are applied.

14.4.2 Fractography of SCCs

The purpose of fractographic examination is to obtain quantitative data of the SCC depth in steam generator tubes by studying the characteristics of the fractured surface. Generally, intergranular “rock candy features” are typically associated with SCC, as

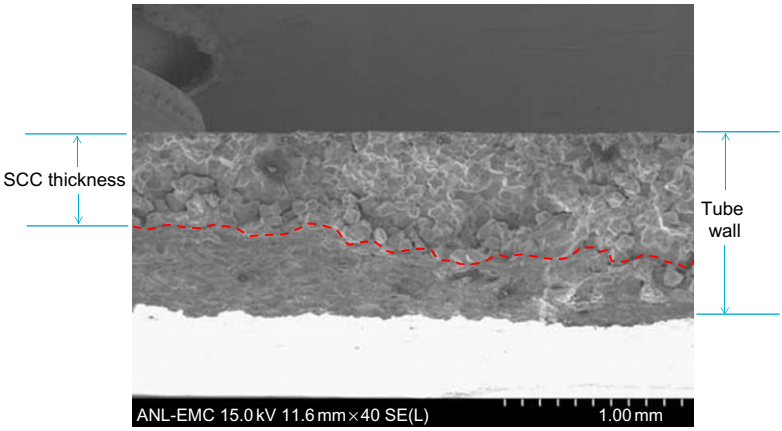

Fig. 14.22 Scanning electronic microscope image of cracking in Alloy 600 tube. The rock candy features that are associated with stress corrosion cracking can be observed above the red line. The rest of the fracture surface below the red line exhibited ductile dimpled features that are typical of overload.

shown in Fig. 14.22. The rest of the fracture surface exhibits ductile dimpled features similar to that caused by overloads. Different types of crack growth (e.g., fatigue, SCC) produce different characteristic features on the surface, which can be used to help identify the failure mode. The depths of SCC of steam generator tubes can be measured from images of the fracture surface by scanning electronic microscopy. The results can be used to compare with the EC testing data and develop analytical models to predict the rupture pressure of SG tubes with SCCs.

14.4.3 Equivalent rectangular crack approximation

No models are currently available for predicting the ligament rupture pressures of cracks with complex geometries. From a plasticity limit analysis viewpoint, it can be argued that the collapse behavior of a crack-tip ligament with an irregular point-by-point variation of crack depth should be similar to a crack with a smoothed out "average" crack depth profile. Therefore, it was assumed that the average profile measured by the +Point probe or fractography is relevant for limit analysis which is the basis for most models to predict ligament rupture pressure of cracks in SG tubes. With this assumption, although the real crack may have short TW segments at a number of locations, the tube behaves as if it has a smoothly varying average ligament thickness (or crack depth) profile. The equivalent crack geometry is determined by the following procedure applied to the depth profile shown in Fig. 14.23A as an example.

1. Choose a crack depth d_o and assume that any crack segment with depth $d < d_o$ does not reduce the crack tip ligament rupture pressure of the tube and can be ignored. In other words, replace the original crack depth profile by a modified crack depth profile in which any crack

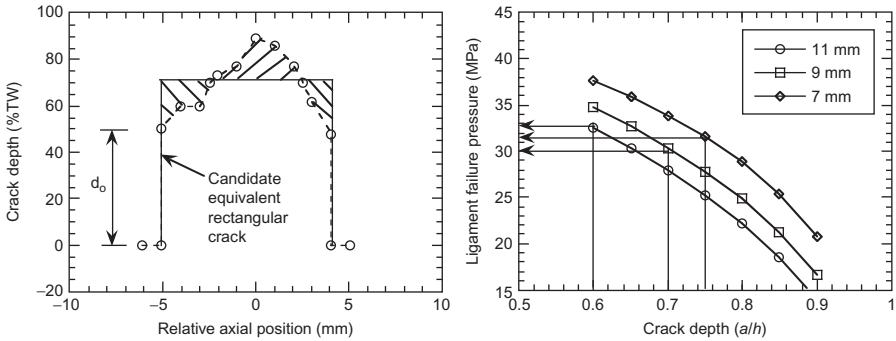

Fig. 14.23 (A) Crack depth profile (symbols) and a candidate ERC and (B) calculated ligament rupture pressures based on three candidate ERCs, showing a minimum ligament rupture pressure of 30 MPa.

segment with depth $d < d_o$ is replaced by $d = 0$ (Fig. 14.23A). The choice of d_o fixes the candidate equivalent rectangular crack length (Lo).

2. The depth of the candidate equivalent rectangular crack is determined by equating its area under the measured depth profile to the area under the modified crack depth profile in Step 1 (Fig. 14.23A). For example, in Fig. 14.23A, the choice of $d_o = 50\%$ fixes the length and depth of the candidate equivalent rectangular crack at 9 mm (0.35 in.) and 70%, respectively.
3. Generate a series of candidate equivalent rectangular cracks by parametrically varying d_o and using the ANL correlation (Eqs. 14.5c, 14.6a, 14.6b) for calculating the ligament rupture pressures for all the candidates. Fig. 14.23B shows the variation of the ligament rupture pressure with the depth d_o in the case of three such candidates.
4. The equivalent rectangular crack corresponds to the crack with the lowest ligament rupture pressure. In the example shown in Fig. 14.23B, the predicted ligament rupture pressure equals 30 MPa (4.4 ksi) corresponding to an equivalent crack length and depth of 9 mm (0.35 in.) and 70%, respectively.

A similar procedure[2], except using Eq. (14.7) instead of Eq. (14.5c) in Step 3, known as the weakest link model has been proposed by EPRI to calculate ligament rupture pressures of SCCs.

14.4.3.1 Validation of ERC method with tests on tubes with ODSCC

A number of specimens with ODSCC were generated at ANL for determining the accuracy of the SCC depth profiles measured by EC/NDE as compared to those measured by fractography as well as for validating the ERC method for predicting ligament rupture pressures. Data for two ODSCC specimens are presented here as typical examples. Fig. 14.24A and B shows the depth profiles of specimen SGL-1 as measured by EC/NDE and fractography, respectively. Similar plots for specimen

[2] Similar equivalent rectangular crack approaches have been used by others, for example, see Report by Aptech Engineering Services, Inc., in Docket No. 50-361, Steam Generator Run Time Analysis for Cycle 9, San Onofre Nuclear Generating Station, Unit 2, September 25, 1997.

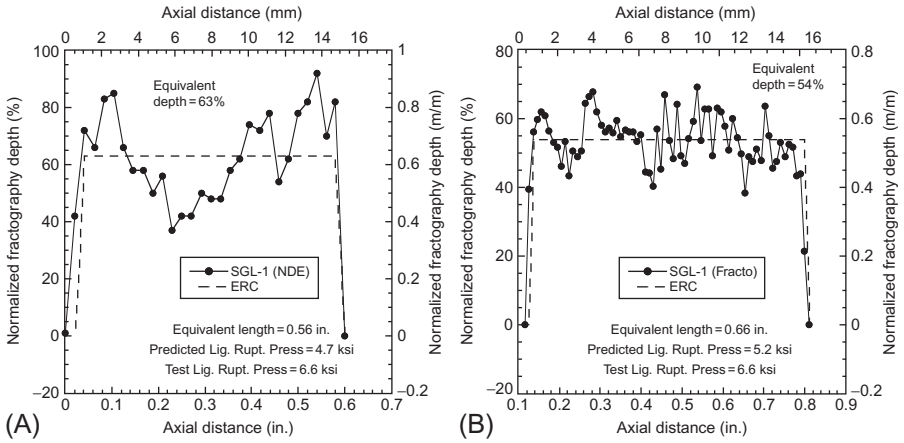

Fig. 14.24 Normalized depth profiles of ODSCC specimen SGL-1 measured by (A) EC/NDE and (B) fractography (in-house data).

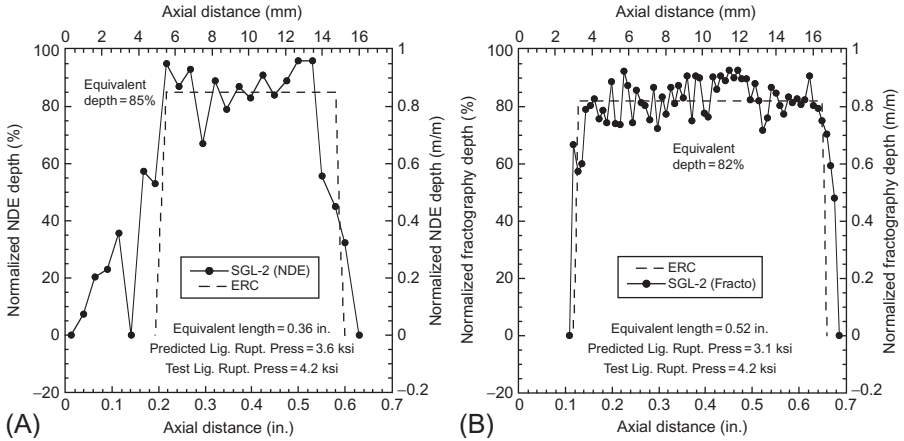

Fig. 14.25 Normalized depth profiles of ODSCC specimen SGL-2 measured by (A) EC/NDE and (B) fractography (in-house data).

SGL-2 are shown in Fig. 14.25A and B, respectively. Note that both the equivalent crack lengths and crack depths based on EC/NDE and fractography profiles are comparable for both specimens. The predicted ligament rupture pressures by EC/NDE and fractography for tests underestimate the test ligament rupture pressures (which is conservative). Comparison of observed ligament rupture pressures of all the ODSCC specimen tests with predicted rupture pressures using the fractography depth profile and the ERC approach is shown in Fig. 14.26. In general, the predicted rupture pressures based on fractography depth profiles underestimate the test ligament rupture pressures (which is conservative). A similar predicted versus observed rupture pressure plot for the same series of tests based on EC/NDE profile currently does not exist.

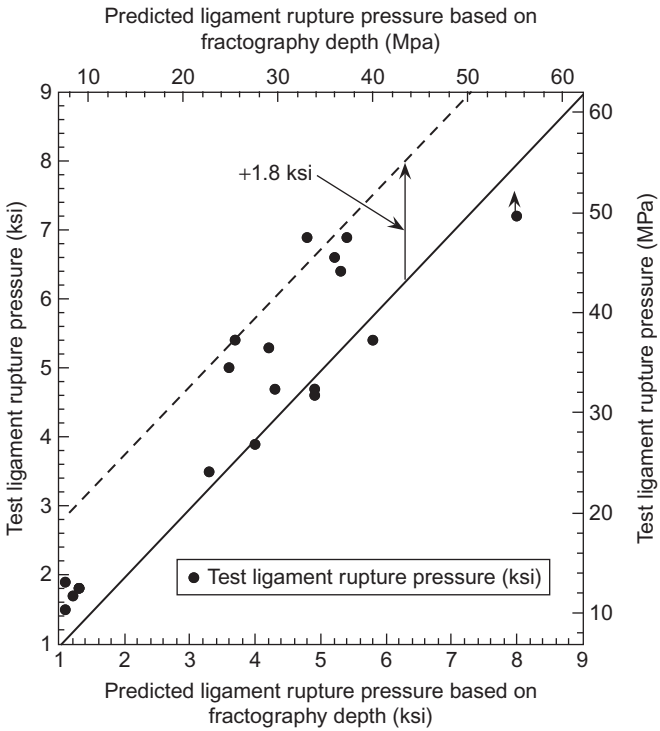

Fig. 14.26 Comparison of test ligament rupture pressures of ODSCC specimens with predicted ligament rupture pressures based on fractography depth profile using the equivalent rectangular crack approach (in-house data).

14.4.3.2 Validation of ERC method with tests on U-bends with PWSCC

A series of U-bend specimens with PWSCC have been prepared and scanned by EC/NDE. Future work may involve pressure testing to rupture, profiling of cracks by fractography, and assessment of the equivalent rectangular crack (ERC) approach for predicting rupture pressures of U-bends with PWSCCs.

14.5 Conclusions and recommendations for future research

Under the sponsorship of US NRC, ANL has been generating a large database on rupture of Alloy 600 SG tubes with flaws due to internal pressure at room temperature as well as high temperature. In this chapter some of the rupture data on straight tubes and U-bends were reviewed. Existing correlations for predicting ligament rupture and unstable burst pressures of Alloy 600 SG tubes at normal operating temperature

and high temperatures have been collected, generalized where needed, and validated by tests.

Steam generator tubes with flaws generally undergo two types of failure: ligament rupture and unstable burst. Ligament rupture occurs when the crack tip radial ligament of a PTW crack ruptures, leading to onset of leakage. Unstable burst occurs when a PTW or 100% TW flaw fails unstably; that is, the 100% TW crack propagates (running crack) unstably under constant pressure. Unstable burst of an SG tube generally leads to very high leakage rates (hundreds of GPM).

Unstable burst pressures (P_{cr}) of straight tubes with axial TW cracks can be correlated with the burst pressure (P_b) of virgin tubing without a flaw by using the bulging factor m. Both burst pressures are controlled by the flow stress of the tube material. The same approach can be used for predicting unstable burst pressures of U-bends with axial TW cracks by replacing the bulging factor m by an effective bulging factor m_{eff}. For straight tubes, $m = m_{eff}$. But for U-bends, m_{eff} is progressively less than m (i.e., burst pressures are higher), the smaller the U-bend radius. However, burst pressures of U-bends having radii $\geq$6 in. (15 mm) are the same as those of straight tubes.

Ligament rupture pressures (P_{sc}) for straight tubes with PTW axial cracks can be correlated with the burst pressure (P_b) of virgin tubing without a flaw by using the stress magnification factor m_p, which is a function of the crack size and the tube thickness and radius. The same approach can be used for predicting ligament rupture pressures of U-bends with axial PTW cracks by replacing the stress magnification factor m_p by an effective stress magnification factor m_{peff}. As in the case of the bulging factor m, for straight tubes $m_p = m_{peff}$. Also, as before, m_{peff} is progressively less than m_p (i.e., ligament rupture pressures are higher), the smaller the U-bend radius and ligament rupture pressures of U-bends having radii $\geq$6 in. (15 mm) are the same as those of straight tubes.

Rupture of straight tubes with a PTW crack during severe accidents at high temperature can be predicted with a cumulative damage summation rule using the same stress magnification factor m_p as at normal operation temperature. The predicted results have been validated with high-temperature tests on Alloy 600 tubes with flaws.

Correlations for predicting failure pressure of rectangular cracks with well-defined length and depth are available and have been validated by tests on SG tubes with EDM flaws. On the other hand, SCCs occurring in the field generally have highly complex geometry with multiple cracks having variable depths, often separated by ligaments. An equivalent rectangular crack approach can be used to define a rectangular crack that has theoretically the same rupture pressure as the SCC from which the ERC depth and length are derived. A limited number of pressure tests on specimens with laboratory-grown SCCs have been tested. The observed rupture pressures have been reasonably predicted using the ERC approach based on depth profiles measured either by pretest EC/NDE or posttest fractography.

Currently ligament rupture pressures of SCC specimens that are relatively simple and without significant ligamentation; that is, they undergo ligament rupture abruptly at a definite pressure can be reasonably predicted. A challenge that remains is in sizing and predicting rupture and leakage of highly ligamented cracks that tend to display increasing leak rate with increasing pressure due to stable ligament tearing. Improving

the spatial resolution of the EC/NDE method and improving computer-aided data analysis techniques so that ligament sizes can be determined accurately may improve the situation. Development of failure and leakage prediction methodologies specifically for highly ligamented SCCs may result in more accurate predictions of tube integrity.

Acknowledgment

This chapter is based on work sponsored by the Office of Nuclear Regulatory Research of the US Nuclear Regulatory Commission and conducted over the last 35 years principally at Argonne National Laboratory.

References

Alzheimer, J.M., Clark, R.A., Morris, C.J., Vagins, M., 1979. Steam Generator Tube Integrity Program Phase I Report: NUREG/CR-0718. Battelle-Pacific Northwest Laboratory, Richland, WA.

Bakhtiari, S., Elmer, T.W., 2008. Technical Letter Report on Development of Flaw Sizing Algorithms for Eddy Current Rotating probe Examinations: 2008, ADAMS Accession No. ML090690837. USNRC, Rockville, MD.

Bakhtiari, S., Kupperman, D.S., 2009. Characterizing Steam Generator Degradation Mechanisms With Eddy Current Technology: ADAMS Accession No. ML090050406. USNRC, Rockville, MD.

Bakhtiari, S., Kupperman, D.S., Shack, W.J., 2009. Assessment of Noise Level for Eddy Current Inspection of Steam Generator Tubes: NUREG/CR-6982 (ANL-05/44). USNRC, Rockville, MD.

Burdekin, F.M., Stone, D.E.W., 1966. The crack opening displacement approach to fracture mechanics in yielding materials. J. Strain Anal. 1, 145–153.

Cochet, B., Engstrom, J., Flesch, B., 1990. PWR Steam Generator Tube and Tube Support Plate Plugging Criteria. EDF, France. Paper 4.1, Steam Generator Tubes Mechanical, LBRB, and Probabilistic Studies.

de Diego, G., Gomez Briceno, D., Maffiotte, C., Baladia, M., Arias, C.J., 2015. Examination of steam generator alloy 800 NG tube from the Almaraz unit 2 NPP. In: Fontevraud 8: Conference on Contribution of Materials Investigations and Operating Experience to LWRs' Safety, Performance and Reliability; Avignon (France); September 15–18, 2014.

Ellison, P.G., Ward, L.W., Dobbe, C., Chavez, S.A., Atwood, C.L., Smith, C.L., Wolfram, L.M., Jones, J.L., Haney, L.N., Reece, W.J., 1995. The Risk Significance of Induced Steam Generator Tube Rupture: INEL-95/0641. Idaho National Engineering Laboratory, Idaho Falls, ID. Rev. 1.

EPRI, 2007. Pressurized Water Reactor Steam Generator Examination Guidelines: Revision 7: EPRI-1013706. Electric Power Research Institute, Palo Alto, CA.

Erdogan, F., 1976. Ductile failure theories for pressurized pipes and containers. Int. J. Pres. Ves. Piping 4, 253–283.

Flesch, B., Cochet, B., 1988. Crack stability criteria in steam generator tubes. In: International Congress on Pressure Vessel Technology, Beijing.

Fletcher, W.D., 1981. Summary of Operating Plant Experience and U-Bends: EPRI WS-80-136. In: Shoemaker, C.E. (Ed.), Proc. U-Bend Tube Cracking in Steam Generator. Electric Power Research Institute, Palo Alto, CA, pp. 3-1–3-6.

Folias, E.S., 1965. A longitudinal crack in a pressurized cylindrical shell. Int. J. Fracture Mech. 1 (2), 104–113.

Fuller, E.L., Kenton, M.A., Epstein, M., Henry, R.E., Cofie, N.G., 1998. Risks From Severe Accidents Involving Steam Generator Tube Leaks or Ruptures: EPRI TR-106194. Electric Power Research Institute, Palo Alto, CA.

Gomez Briceno, D., Lancha Hernandez, A.M.A., Castano Marin, M.L., 1991. Spanish research activities on steam generator tubes degradation. In: Proceedings of the NEA/CSNI-UNIPEDE Specialist Meeting on Operating Experience With Steam Generators, Brussels, September 16–20, 1991.

Hahn, G.T., Sarrate, M., Rosenfield, A.R., 1969. Criteria for crack extension in cylindrical pressure vessels. Int. J. Fracture Mech. 5 (3), 187–210.

Kanninen, M.F., Zahoor, A., Wilkowski, G.M., Abou-Sayed, I., Marschall, C., Broek, D., Sampath, S., Rhee, C., Ahmad, J., 1982. Instability Predictions for Circumferentially Cracked Type 304 Stainless Steel Pipes Under Dynamic Loading. Electric Power Research Institute, Palo Alto, CA. EPRI NP–2347 (Vol. 1: Summary; Vol. 2: Appendices).

Kiefner, J.F., Maxey, W.A., Eiber, R.J., Duffy, A.R., 1972. Failure stress levels of flaws in pressurized cylinders. In: Kaufman, J.G. (Ed.), Progress in Flaw Growth and Fracture Toughness Testing. National Symposium on Fracture Mechanics (6th: 1972: Philadelphia), American Society for Testing and Materials, Committee E–24 on Fracture Testing of Metals. American Society for Testing and Materials, Philadelphia. ASTM Special Technical Publication 536.

Kilian, R., Zimmer, R., Arenz, R., Beck, J., Schoenherr, T., 2007. Operating experience with Alloy 800 SG tubing in Europe. In: Presented at the 13th International Conference on Environmental Degradation of Materials in Nuclear Power Systems, Whistler, BC (Canada), August 19–23, 2007.

Kurihara, R., Ueda, S., Sturm, D., 1988. Estimation of the ductile unstable fracture of pipe with a circumferential surface crack subjected to bending. Nucl. Eng. Des. 106, 265–273.

Majumdar, S., 1999. Failure and leakage through circumferential cracks in a steam generator tubing during accident conditions. Int. J. Pres. Ves. Piping 76, 839–847.

Majumdar, S., Shack, W.J., Diercks, D.R., Mruk, K., Franklin, J., Knoblich, L., 1998. Failure Behavior of Internally Pressurized Flawed and Unflawed Steam Generator Tubing at High Temperatures—Experiments and Comparison With Model Predictions: NUREG/CR–6575. USNRC, Washington, DC.

Majumdar, S., Kasza, K., Franklin, J., 2000. Pressure and Leak–Rate Tests and Models for Predicting Failure of Flawed Steam Generator Tubes: NUREG/CR–6664. USNRC, Washington, DC.

Majumdar, Saurin, Bakhtiari, Sasan, Kasza, Ken, Jang Yul, Park, 2001. Validation of Failure and Leak Rate Correlations for Stress Corrosion Cracks in Steam Generator Tubes: NUREG/CR–6774. USNRC, Washington, DC.

Majumdar, S., Kasza, K., Bakhtiari, S., Park, J., Oras, J., Franklin, J., Vulyak Jr., C., Shack, W.J., 2009. Steam Generator Tube Integrity Issues: Pressurization Rate Effects, Failure Maps, Leak Rate Correlation Models and Leak Rates in Restricted Areas: NUREG/CR-6879. USNRC, Washington, DC.

Nuclear Energy Institute, 2005. Steam Generator Program Guidelines: Nuclear Energy Institute NEI 97-06, Revision 2. Nuclear Energy Institute, Washington, DC.

Ranganath, S., Mehta, H.S., 1983. Engineering methods for the assessment of ductile fracture margin in nuclear power plant piping. Fracture Resistance Curves and Engineering Applications. ASTM International, Philadelphia. ASTM STP 803.

Rice, J.R., 1968. A path independent integral and the approximate analysis of strain concentration by notches and cracks. J. Appl. Mech. 35, 379–386.

Wells, A.A., 1961. Unstable crack propagation in metals: cleavage and fast fracture. In: Proceedings of the Crack Propagation Symposium, Vol. 1, paper 84, Cranefield, UK.

This page intentionally left blank

Nuclear steam generator inspection and testing

15

T. Sollier
Institut de Radioprotection et de Sûreté Nucléaire-IRSN, Paris, France

Acronyms

ASME	American Society of Mechanical Engineers
BPVC	Boiler and Pressure Vessel Code
CFR	Code of Federal Regulations
CSA	Canadian Standards Association
DAC	Distance Amplitude Curve
DMW	Dissimilar Metal Weld
ENIQ	European Network for Inspection and Qualification
EPRI	Electric Power Research Institute
ET	Eddy current Testing
FBH	Flat Bottom Hole (conventional reflector for UT)
FEI	Fluid Elastic Instability
FAC	Flow Accelerated Corrosion
FOSAR	Foreign Object Search and Retrieval
HAZ	Heat-Affected Zone
ISI	In-Service Inspection
JSME	Japan Society of Mechanical Engineers
KEPIC	Korea Electric Power Industry Code
KTA	Kerntechnischer Ausschuss (German Nuclear Safety Standards Commission)
L0	Longitudinal ultrasonic wave with a refraction angle normal to the surface
MT	Magnetic particle Testing
NDT	Nondestructive Testing
NEI	Nuclear Energy Institute
PT	Penetrant Testing
PWHT	Postweld Heat Treatment
PWSCC	Primary Water Stress Corrosion Cracking
RCCM	Règles de conception et de construction des matériels mécaniques des îlots nucléaires REP (Design and Construction Rules for Mechanical Components of PWR Nuclear Islands, French code)
RSEM	Règle de Surveillance en Exploitation des Matériels Mécaniques des Ilots Nucléaires REP (In-Service Inspection Rules for Mechanical Components of PWR Nuclear Islands, French code)
RT	Radiographic Testing
SDH	Side Drilled Hole (often used for UT calibration)
SG	Steam Generator

Steam Generators for Nuclear Power Plants. http://dx.doi.org/10.1016/B978-0-08-100894-2.00017-0
© 2017 Elsevier Ltd. All rights reserved.

TOFD Time of Flight Diffraction ultrasonic technique
TTS Top of Tube Sheet
T45 Transversal (shear) ultrasonic wave with a refraction angle of 45 degrees
UT Ultrasonic Testing
VT Visual Testing

15.1 Introduction

This chapter addresses the in-service inspection (ISI) and testing of steam generators (SGs), excluding the tube bundle inspection which is presented in Chapter 16. It is centered on vertical shell U-tube recirculating evaporators but some techniques may also apply to once-through SGs and horizontal SGs. Utilities have to satisfy domestic regulations with respect to periodic inspections, testing, and qualification or performance demonstration. For example, for US utilities, the requirements for maintenance are given in the Code of Federal Regulation (10 CFR § 50.65 Maintenance Rule). Utilities also refer to industrial codes such as ASME, RSEM, JSME, CSA, KEPIC, or KTA to define ISI and associated maintenance programs. The industry has issued recommendations for the maintenance of steam generators (NEI 97–06, 2011) (EPRI, 1012987). There is also a safety guide edited by the IAEA in 2002 on this topic and an EPRI handbook (Steam Generator Reference Book, 1994).

Steam generators are classified as class 1 component according to nuclear manufacturing codes. The highest quality is expected for manufacturing, operation, and inspection of this equipment. There are differences between US and French codes. For weld fabrication and inspection, these differences have been analyzed in detail by Consonni and Mudge (2012). In addition, a comprehensive comparison of nuclear codes for class 1 nuclear power plant components was prepared by ASME (2012). In this chapter, we introduce the general practice of the industry and we do not intend to compare codes specificities into details. For some specific ISI or testing, we will mention whether it is based on a specific US or French code, regulatory requirements or even industrial practices.

15.2 ISI techniques and qualification methodology

Several nondestructive techniques are used for SG In-Service Inspection:

- Eddy current testing (ET)
- Ultrasonic testing (UT)
- Magnetic particle testing (MT)
- Radiographic testing (RT)
- Visual testing and remote visual testing (VT)
- Penetrant testing (PT)

Most of these techniques are qualified before being applied on site. The qualification process aims to characterize the technique performances and reliability according to the different parameters of the inspection, such as the temperature, the geometry of the

component, and the metallurgical structure (grain size, anisotropy, heterogeneity, etc.). The qualification methodology varies in accordance with domestic regulation, industrial practices, and the specific steam generator component being inspected. The ASME code uses a performance demonstration approach based on the use of statistical tools.

The European regulators have proposed a definition for the qualification of ISI technique:

> *The term NDT qualification is understood in this document as the systematic assessment, by all those methods that are needed, to provide reliable confirmation that the NDT system is capable of achieving the required performance under real inspection conditions.*
>
> *European Commission (1997).*

The European qualification methodology is based on the identification and assessment of all the parameters of the inspection which have an influence on the detection and characterization of the flaws (Chapman et al., 2007). The qualification of ISI techniques according to ENIQ is distinct from the personnel certification for NDT.

With respect to SG maintenance, most ISI techniques are qualified and their performances are characterized on reference flaws. When there is no expected degradation in service, the inspection program is based on a conventional NDT technique. The performances may be characterized on reference flaws such as flat bottom holes or hypothetical planar flaws (notches). In other cases, the performances of ISI techniques have to be characterized for postulated or observed flaws relevant to the expected degradation mechanisms (corrosion, fatigue, wear, etc.).

For SG maintenance, visual testing and remote visual testing are mostly used to detect disorders such as:

- Loose parts in the tube bundle and in the channel head bowl,
- Sludge at the top of tubesheet,
- Degradation of the channel head bowl cladding,
- Degradation of the internals on the secondary side (flow accelerated corrosion, broken support, deposit buildup, blockage of tube support plate flow holes, etc.).

In such cases, when the inspection is not aimed at the detection of flaws, it is acceptable to limit the qualification perimeter to the tool without formal certification from an independent NDT qualification body.

15.3 In-service inspection

The rupture of SG pressure shell or channel head is precluded in safety studies and would have catastrophic consequences with respect to the confinement of the radioactivity in the primary cooling circuit and in the containment building. The steam generator is a class 1 component with respect to nuclear codes requirements. Therefore, only a robust design with large margins and high quality of manufacturing can

ensure the break preclusion needed for this component. The robust design leads to low fatigue usage factor for welds and no degradation is normally expected during the lifetime of SGs. Many inspections of the pressure shells and welds are performed during manufacturing and as a result very few flaws are expected to be present in the pressure shell at the final step of the SG assembly.

Nevertheless, a preservice inspection of the pressure shell is mandatory with respect to nuclear codes and national regulations. The preservice inspection is performed under the responsibility of the utility and is independent of the inspections performed by the manufacturer. Techniques and procedures used by the utility might be significantly different from techniques and procedures used to conduct inspections at fabrication facility. This dual inspection before plant startup responds to the defense-in-depth requirement regarding the high quality in construction (INSAG-10, 1996).

The in-service-inspection of SG pressure shell and internals varies with respect to national regulations, specific nuclear codes and utilities maintenance policy. In this section, a generic in-service-inspection program is discussed. This program is mainly based on the French code RSEM.

15.3.1 Welds inspection

Despite a robust design and extensive manufacturing inspections, an unexpected degradation of the girth weld between the feedwater nozzle shell and the conical shell (see Fig. 15.1) was observed in 1982 at Indian Point Unit 3 (Czajkowski, 1983). A through wall crack was detected in the girth weld. The root cause for the degradation was attributed to corrosion fatigue and/or stress corrosion cracking mechanism. Faulty secondary side chemistry with oxygen ingress during start-up, standby, and shutdown conditions was suspected (Rao, 1990). The postweld heat treatment (PWHT) or stress relief was also nonoptimal. Some similar cases have been reported worldwide, six of them in the USA and two in Europe; please refer to Chapter 7 for detail.

The secondary side chemistry has been improved since these events. According to the RSEM, the girth-weld is inspected during preservice inspection and every 10 years on the full length of the girth weld.

The location of the other pressure shell welds varies according to the SG type. An example of the welds location is given in Fig. 15.1. For older SGs, pressure shells are usually obtained from carbon steel plates that are formed and then welded. Some major welds may be inspected in service periodically (Table 15.1) with a typical time interval of 10 years in France. The inspection coverage includes the volume of the weld and the Heat-Affected Zone (HAZ).

The welds are usually manually inspected from the outer surface of the pressure shell with UT shear wave with angles of refraction of 45 degrees and 60 degrees. The calibration is usually done on side drilled holes (SDH) located at different depths. A distance-amplitude correction (DAC) is used to correct the attenuation of the ultrasonic signal which increases with depth. Considering the defense-in depth approach and no operating experience of flaws propagated in these welds, the performances of the ISI techniques may be characterized conventionally on flat bottom

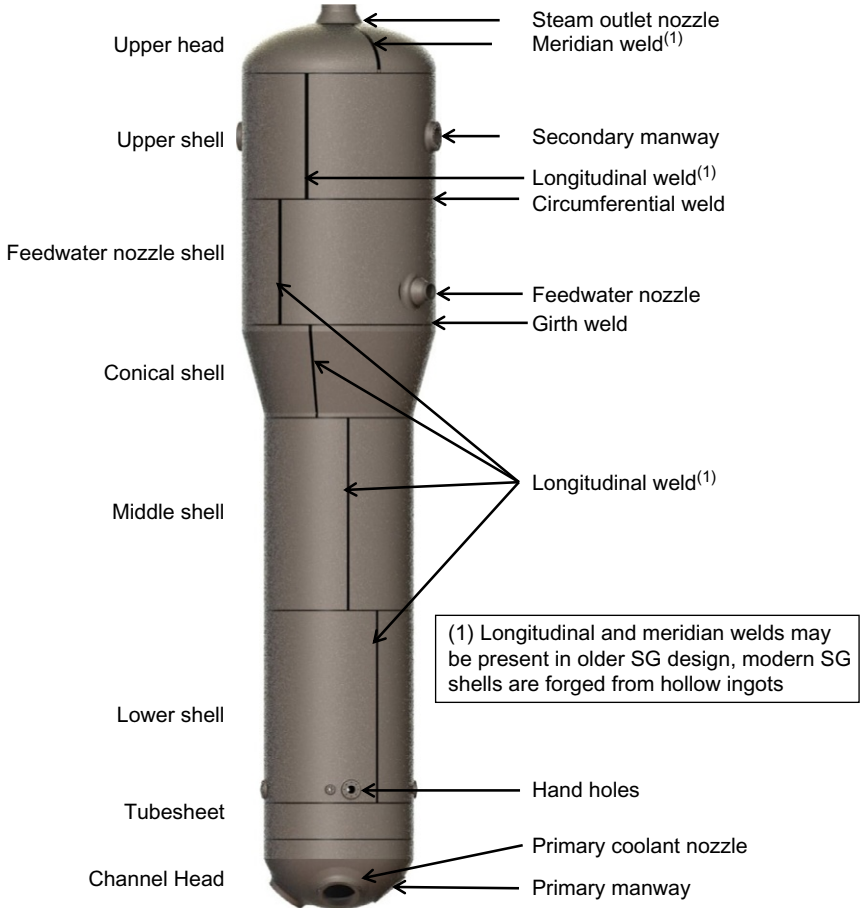

Fig. 15.1 Generic diagram of a U-bend steam generator and locations of main welds for the pressure shell.

Table 15.1 List of major welds for SG pressure shell ISI program (example)

	ISI examples
Channel head—lower shell	UT
Conical shell—feedwater nozzle shell (girth weld)	UT, MT
Feedwater nozzle shell—upper shell	UT
Primary nozzles—safe end (DMW)	RT (+UT for EPR)
Feedwater nozzle shell—Feedwater inlet nozzle	UT, VT
Upper shell—secondary manway	
Steam outlet nozzle—main steam line	UT
Shells longitudinal weld (if relevant)	UT, VT
Upper head meridian weld (if relevant)	UT

holes (FBH). It is however useful to characterize also the performances on planar flaws which are the most threatening flaws for structural integrity. Simulation codes may be used to quantify the performances of UT inspection on planar flaws and to complete tests done on mocks-up. Manual UT testing of welds is done usually in four directions (orientations 1 and 5 perpendicular to the weld seam and orientations 3 and 7 parallel to the weld seam, see Fig. 15.2). At weld seams junction, the inspection is usually performed in eight directions. UT is a volumetric method but, for the mode pulse-echo, a "*dead zone*" is present beneath the transducer. This *dead zone* might be significantly reduced using a miniaturized transducer. If needed, PT, MT, or TOFD might be used for the inspection of the surface and near-surface zone (Fig. 15.3).

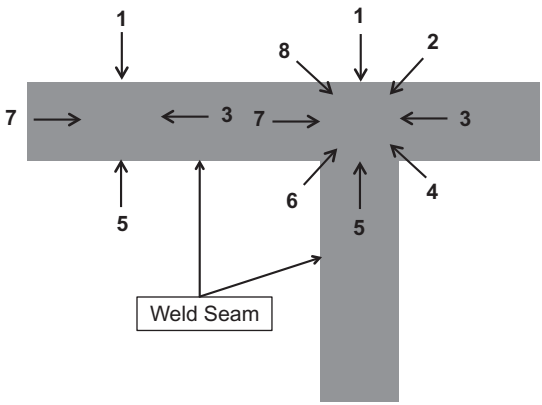

Fig. 15.2 UT oblique shear waves orientations for weld inspection.

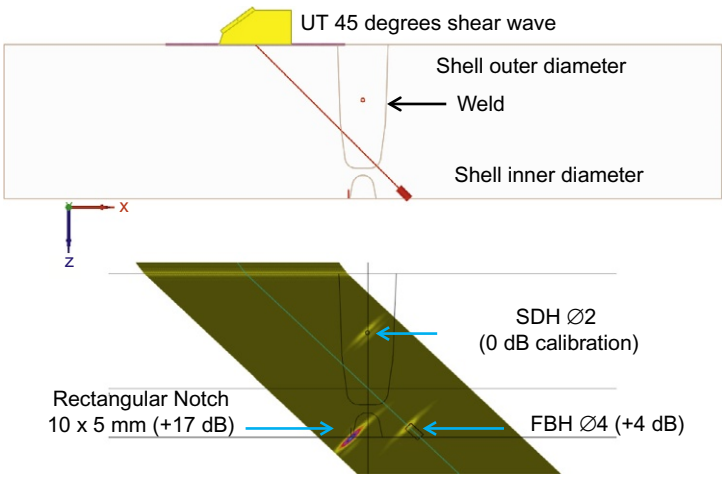

Fig. 15.3 Simulation of the detection of flaws with UT 45 degrees shear waves (CIVA) from left to right: rectangular notch (corner effect), FBH (conventional reflector), SDH (calibration).

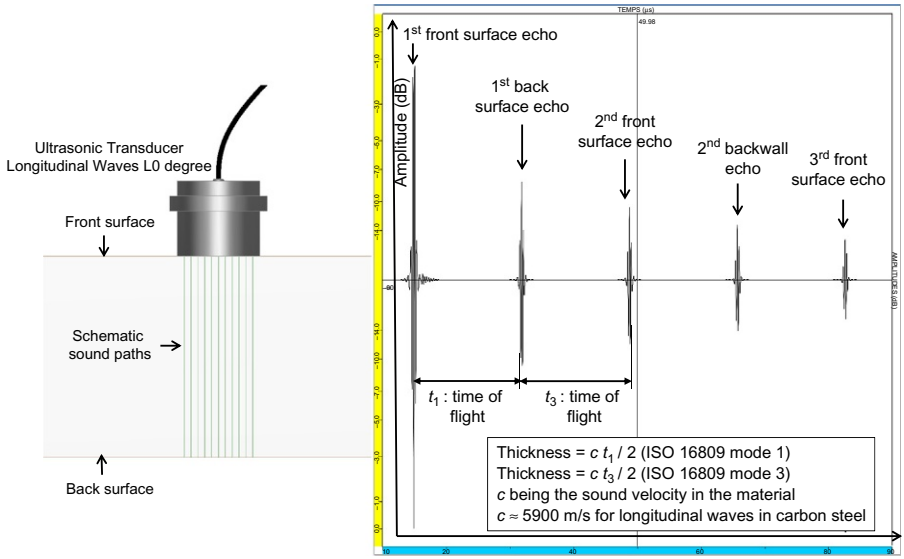

Fig. 15.4 Principle of thickness measurement with UT L0 degree longitudinal waves transducer (*left*) and time of flight measurement (*right*). Both images are produced with CIVA for illustration purposes.

15.3.2 Ultrasonic pressure shell thickness measurement

The secondary side water conditioning minimizes corrosion of the low alloy carbon steel of the pressure shell. The potential for Flow Accelerated Corrosion (FAC) of the pressure shell is also very low considering the velocity of the water in the downcomer and the optimized water conditioning. As part of a defense in depth approach, thickness measurements may be performed on the pressure shell. Manual measurements are based on ultrasonic technique using a contact transducer with longitudinal waves at 0 degree (L0) and a typical frequency of 4 MHz. The measurement methodology is presented in Fig. 15.4 (ISO, 106809:2012). The accuracy of the thickness measurement is approximately ±1 mm for a thickness of the pressure shell ranging from 80 to 90 mm. A specific area of interest is located below the weld from middle shell to conical shell, based on fluid velocity analysis (area of high velocity).

15.3.3 Tube bundle remote visual inspection

The remote visual inspection of the tube bundle at the top of tube sheet (TTS) is a key maintenance operation in order to assess and to maintain the cleanliness of the secondary side. This inspection is used to find and retrieve foreign objects (FOSAR) laying on the TTS. For this purpose, the inspection is mainly performed in the bundle annulus, where the horizontal fluid velocity is higher and therefore the potential for tube wear due to foreign object hammering is higher.

The remote visual inspection may also be performed in-lane inside the tube bundle. In this case, it may also be used for FOSAR operation and to evaluate the quantity of sludge on the TTS and the deposits on the tubes. This operation, performed on a regular basis, is used to assess the efficiency of high pressure sludge lancing. It allows operator to detect hard sludge on TTS and hard collar on tubes, if any, and to take appropriate action (high efficiency sludge lancing, chemical cleaning) to avoid tube denting. Tube denting could have a deleterious effect for corrosion; it increases the tube inner skin axial stress and has been responsible for circumferential and axial PWSCC for alloy 600MA, alloy 600TT (Buisine et al., 2010), and alloy 800NG (Bueno and Garcia, 2012).

The remote visual inspection of the tube bundle periphery may be extended to the lower supports of the bundle wrapper. Some cases of supports cracking have been reported at the weld located on the wrapper side. The root cause may be differential thermal expansion as the wrapper is much thinner than the pressure shell. The thermal transients induced by switches from the high temperature of the main feedwater to the low temperature of the auxiliary feedwater reach thermal equilibrium much faster for the thin wrapper than for the thick pressure shell. In addition, fatigue cracking due to wrapper vibrations is also a potential cause for the observed degradation. This degradation mechanism has only been observed for the older generation of SGs (NRC IN 96-09). The wrapper supports for SGs manufactured after 1990 (approximately) have a full penetration weld instead of a corner weld. This weld is more resistant to fatigue initiation and no degradation has been reported so far.

If there is significant oxide deposits on the TTS, there may be also significant deposit buildup on the tube outside surface (tube fouling) and on the upper face and in the flow holes of the tube support plates (TSPs) as sketched in Fig. 15.5. The blockage of the TSPs flow holes by oxides raises several safety issues (Bodineau and Sollier, 2008):

- Reduction of the thermal hydraulic stability of SGs with a risk of water level oscillations;
- Reduction of the mass of water available at the secondary side for reactor cooling;
- Increased velocity of the water in the tube bundle with a risk of fatigue and fluid-elastic instability (FEI) for U-bends; this risk is increased by a loss of pressure at the secondary side due to tube fouling;
- Increase of TSPs and tie-rods loading in the case of a rapid depressurization of the secondary side such as a main steam line break (Brunin and Deotto, 2009).

Remote visual inspection of the TSPs is a direct way to assess the flow holes blockage severity. The in-service accessibility to TSPs is very limited. The most common way to inspect TSPs is to introduce a tool via a hand hole for the lower TSP or via the secondary manway for the upper TSP. Deposit buildup may also be assessed by a review of eddy current data (Chatellier et al., 2009).

15.3.4 Upper internal visual inspection

The operating experience reveals some potential degradation mechanisms for SGs upper internals:

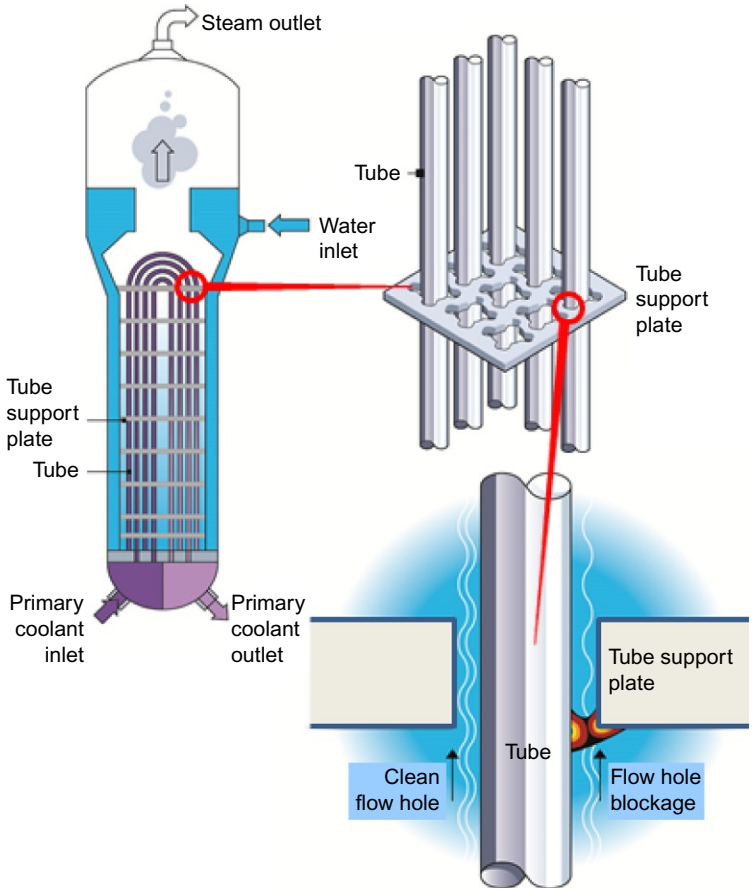

Fig. 15.5 Blockage of tube support plates by oxides deposits.

- Flow accelerated corrosion (FAC) of the swirl vane separators,
- Flow accelerated corrosion of J-tubes made of carbon steel,
- Disconnection of the feedwater distribution ring from the feedwater nozzle due to water hammer effect,
- Loose parts.

The visual inspection is appropriate to detect those potential degradations. In new SGs generation, the J-tubes are made of stainless steel or other corrosion resistant alloys to avoid any FAC degradation. The use of high chromium content steel for the swirl vane separators and a high pH secondary side conditioning reduces the risk of FAC. Water hammer effect remains a threat for the integrity of the feedwater ring. Careful plant operation and longer J-tubes are used to avoid the water hammer transient. The visual inspection is effective for the detection of water hammer effect on the supports (plastic deformation, rupture) (Fig. 15.6).

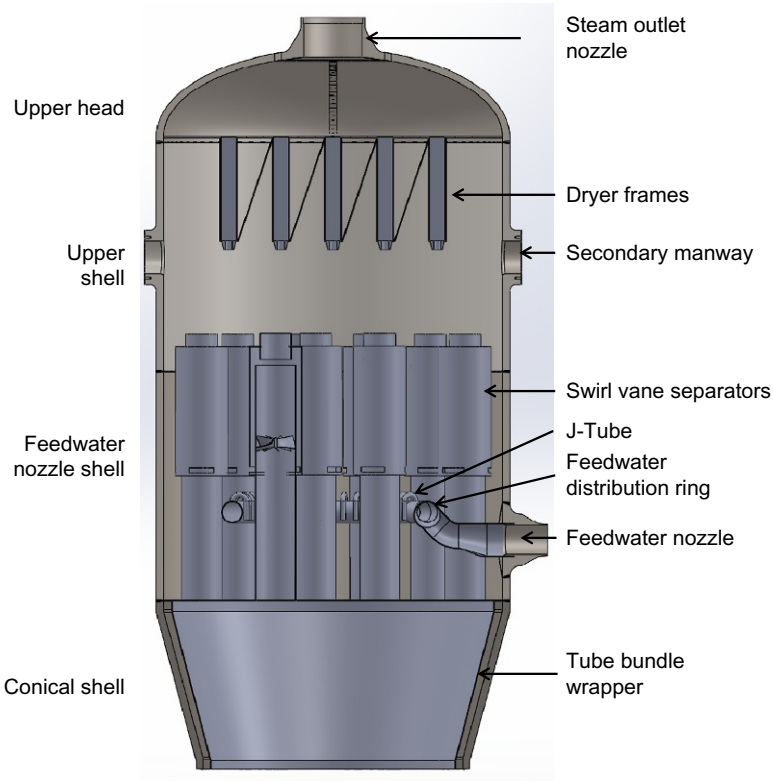

Fig. 15.6 SG upper internals.

15.3.5 Steam outlet and flow restrictor welds inspection

For older SG designs with a welded joint between the steam outlet and the upper head, the weld is inspected in France every 10 years with manual ultrasonic testing from the outside. The weld between the steam outlet and the flow restrictor is inspected in France every 10 years with ultrasonic technique from the outside or with radiographic testing using a gamma-ray source such as Iridium 192.

15.3.6 Feedwater nozzle and thermal sleeve weld inspection

For SG designs with a thermal sleeve welded to the feedwater nozzle, the weld may be inspected every 10 years with ultrasonic technique from the outside. The degradation mechanism identified for the thermal sleeve weld is thermal fatigue due to water stratification during transients when the auxiliary feedwater system is active. Investigations on replaced thermal sleeves confirm the risk of crack initiation and propagation associated with thermal cycles (NRC Bulletin 79-13; Dordonat et al., 1998; Chattopadhyay, 2011).

The ultrasonic testing performed from the outside with shear waves propagating at 45 degrees in the tube wall is efficient for the detection of cracks initiated from the

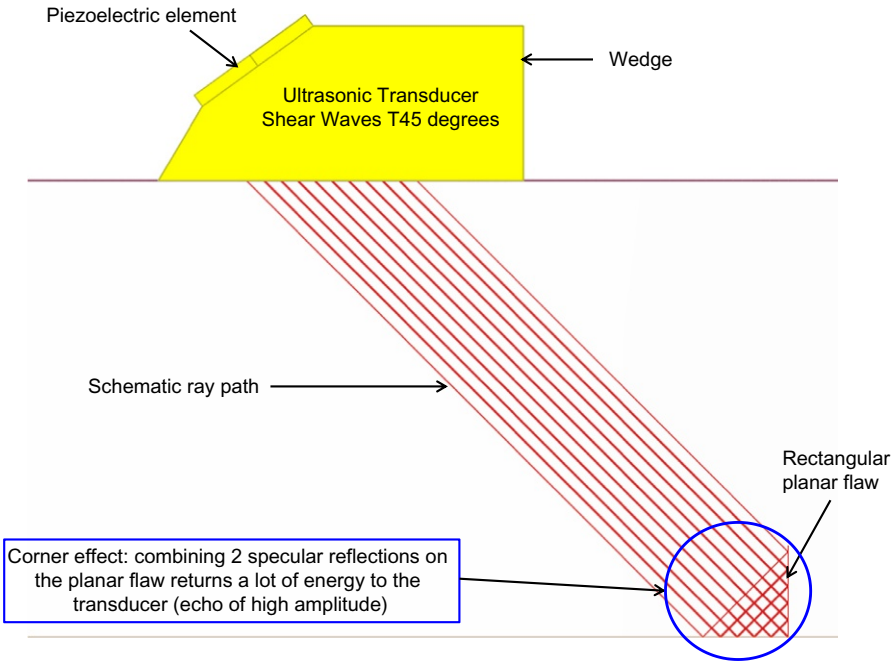

Fig. 15.7 Principle of the corner effect with a UT shear wave 45 degrees transducer. Image produced with CIVA.

inside of the pipe. The corner effect produces high amplitude echoes. The principle of the corner effect is illustrated in Fig. 15.7. The double specular reflection of impinging shear waves on a planar flaw sends back a lot of energy to the transducer.

On the contrary, the diffraction of ultrasonic waves at the tip of a planar flaw produces a much weaker signal. For the example presented in Fig. 15.8, the amplitude of the tip diffraction is much lower than the amplitude of the corner echo. The identification of the tip diffraction is used to characterize the depth of the flaw.

The corner effect may be used for flaw detection with a moderate misorientation (see Fig. 15.9). A variation of ±10 degrees for the tilt angle is not challenging for the detection of a planar flaw. For planar flaws with a larger misorientation, the main energy of the ultrasonic beam is not reflected backward to the transducer. The detection based on the diffraction at the tip of the flaw is in this case more appropriate although the echo is much weaker. The grain size of the ferritic steel of the SG pressure shell is small and the ultrasonic propagation is not affected by a strong attenuation or dispersion. The structural noise for acoustic wave propagation is small and therefore diffraction techniques may be used even for a thick component. If mechanical analysis or operating experience feedback suspect potential planar flaw misorientation, diffraction techniques may be used for detection and characterization. The time of flight diffraction technique (TOFD) is one of these techniques.

The feedwater nozzle may also be inspected by visual testing from the inside using the secondary manway access.

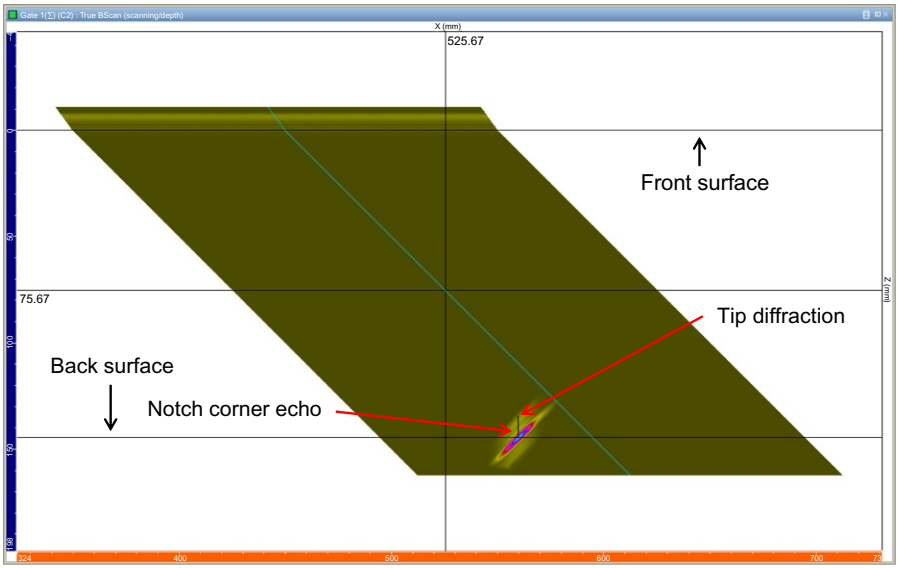

Fig. 15.8 Corner effect and tip diffraction with UT shear wave 45 degrees. Image produced with CIVA.

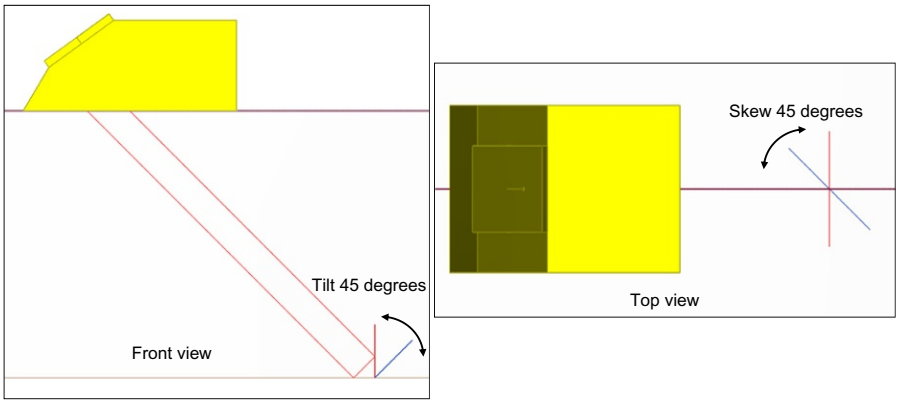

Fig. 15.9 Definition of tilt and skew for the misorientation of a planar flaw. Image produced with CIVA.

15.3.7 Small nozzle inspection

Small nozzles (1″ and 2″) such as the SG secondary drain nozzle, the channel head bowl central drain, if any, and nozzles for instrumentation may be inspected every 10 years with penetrant testing. In the case of alloy 600/182 nozzles, a potential degradation mechanism is stress corrosion cracking. If any repairs were done on site, the inspection period should be reduced since there may be higher residual stresses. Also,

if manufacturing defects are known to have been left in service, the 10 years interval for inspection may be reduced considering fabrication flaws as potential sites for crack initiation.

15.3.8 Channel head inspection

The channel head general design is based on a carbon steel bowl with at least one nozzle for the primary coolant inlet and one nozzle for the outlet nozzle. Some designs such as the AP1000 reactor include two outlet nozzles for the primary coolant cold legs (ML11171A454). The bowl is welded to the tube sheet primary lip and is cladded with stainless steel with some exceptions (CANDU and VVER designs). The water box is separated by a divider plate to form an inlet plenum and an outlet plenum. A majority of SGs has a divider plate welded to the bowl cladding and to a stub runner welded on the primary side of the tube sheet (Fig. 15.10). For divider plates made of alloy 600 and welds made of alloy 182, stress corrosion cracks have been observed on EDF fleet (Deforge et al., 2010). The channel head has also two primary manway for maintenance purposes in the inlet and outlet plenum. The channel head water box drains might be included in the primary nozzles or can be located at the lower point of the bowl.

The degradation mechanisms observed worldwide for the channel head are sorted in the following by main categories:

- Stress corrosion (refer to Chapter 7 for detail)
- Stress corrosion cracking for divider plates and stub runners made of alloy 600 and welds made of alloy 182 (Deforge et al., 2010);
- Stress corrosion cracking for alloy 182 weld of SG bowl drain tap;
- Stress corrosion cracking of primary nozzles dissimilar welds (Shoji et al., 2010);
- Stress corrosion and bulging of the bowl central tube drain for tubes made of alloy 600;

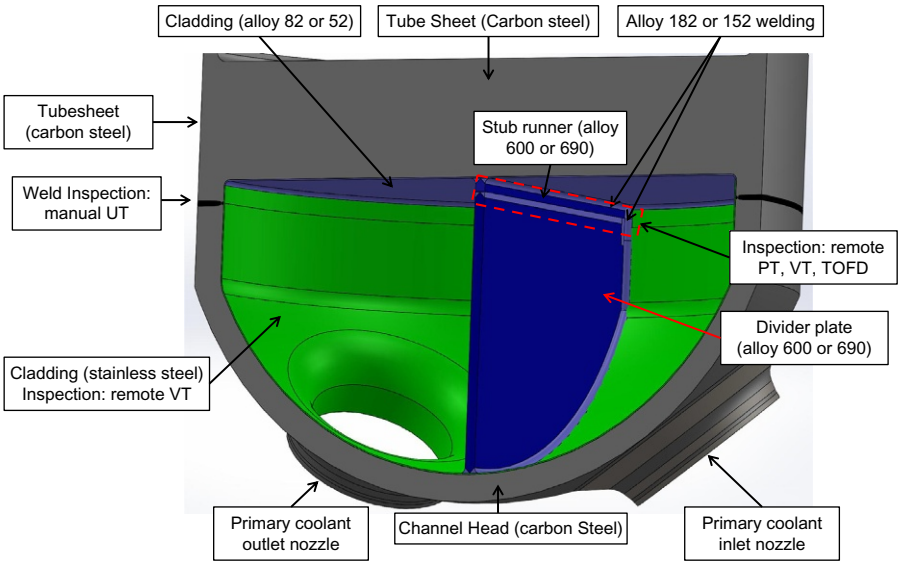

Fig. 15.10 SG channel head. Scheme based on a generic Westinghouse design.

- Corrosion (refer to Chapter 7 for detail)
- FAC for carbon steel divider plates (Tapping et al., 2000);
- Carbon steel corrosion of the channel head bowl concurrent with stainless steel cladding degradation (ML13204A143);
- Mechanical degradation
- Hammering by loose parts in the main coolant system of the channel head cladding, of the tube sheet cladding and of tubes-to-tube-sheet-cladding welds;
- Degradation of threads (primary manway flange and primary nozzle retention ring flange);
- Degradation of primary manway flanges during maintenance operations (scratches);

The inspection program should take into account the active degradation mechanisms, the worldwide operating experience and the safety significance of the degradation. Potential in service inspection items are listed in Table 15.2 with the two main motivations for the inspection: a defense in depth approach when no degradation is anticipated but rupture consequences would be major for safety, operating experience (OPEX) when degradation has been observed. Some references are given in Table 15.2 for degradations reported by utilities. More references and root cause analysis are presented in Chapter 7 of the handbook.

Table 15.2 List of potential inspection targets and techniques for the channel head and tube sheet (example)

Inspection area	NDT selection	Motivations for ISI
Tube sheet to channel head weld	Manual UT from the shell outside diameter	Defense in depth
Tube sheet to stub barrel	Manual UT from the shell outside diameter	Defense in depth
Channel head cladding, tube sheet cladding, tube to tube sheet cladding welds	Remote VT	OPEX (ML13204A143)
Primary manway studs	VT at each opening, UT for crack detection	OPEX
Primary manway nuts	VT at each opening	OPEX
Primary manway ligaments between threads	UT	Defense in depth
Primary coolant nozzle dissimilar welds and safe end welds	RT (Iridium 192), UT, PT from the outer diameter (for intergranular decohesion)	Defense in depth OPEX alloy 82/182 (Shoji et al., 2010)
Tube sheet to blowdown drain weld	VT, PT	OPEX
Primary central bowl drain weld to channel head (if relevant)	VT, PT	OPEX (see Chapter 7)
Divider plate to stub runner weld	Remote VT, remote PT, UT TOFD	OPEX (Deforge et al., 2010)
Tube plugs	Remote VT (detection of boron stain, plugs displacement, missing plugs)	OPEX (NRC Bulletin 89-01; Yeh et al., 1992; Boccanfuso et al., 2010)

15.4 Water tightness of the tube bundle

The steam generator is a physical barrier for the confinement of the radioactive primary coolant. The physical barrier includes the channel head, the tubes wall and the tube-to-tube-sheet cladding weld. It is an industrial coded practice to have a provision in tube wall thickness for corrosion. As a matter of fact, corrosion and wear is common to most industrial heat exchanger tubes so the provision for corrosion represents a significant percentage of the nominal tube thickness required to stand the differential pressure for normal operation and design accidents. Despite this provision for corrosion and periodic nondestructive inspections (refer to Chapter 16 for further details), the degradation of tubes might lead to a leak and eventually a steam generator tube rupture (SGTR) in service. It is therefore a key safety issue to monitor in service the water tightness of the tube bundle and to be able, during an outage for maintenance, to identify a leaky tube.

15.4.1 Water tightness monitoring in operation

The water tightness of the tube bundle is monitored during operation using secondary side radioactivity measurement channels. Several means can be used to detect a leak of radioactive material from the primary circuit to the secondary circuit:

- Radioactivity measurement at the SGs blowdown. The sensitivity and reactivity of this method is considered low because of the large water inventory in the SG secondary part (tens of cubic meters). It is however one of the few methods usable for primary to secondary leak detection when the reactor is in hot standby condition (no production of steam).
- Radioactivity measurement at the condenser for noble gases (^{133}Xe, ^{85}Kr). This method is very sensitive but cannot identify the leaky SG.
- Radioactivity measurement at the main steam line is probably the most sensitive and quickest mean for PWRs to detect a primary to secondary leak. ^{16}N is produced in the pressure vessel by the activation of oxygen atoms by the core neutron fluence. It has a very short half-life period (7 seconds), so it does not build-up in the secondary coolant circuit. A strong gamma emission (6 and 7 MeV) is produced during its decay which can be easily filtered from lower energy radioactive emission from the plant with appropriate shielding. The detection is efficient for a power rating over 20% of the nominal power. The detection sensitivity is less than 1 L/hour.

If a primary to secondary leak is detected, the easiest action to identify the faulty tube is a water test.

15.4.2 Water test

The water test is performed with a SG full of water in the secondary side. The primary coolant system is open at the SG channel head primary manway and a video camera is introduced in the SG bowl. The leaky tube can be identified by direct observation of the continuous water leak. This method is efficient for a large leak. In the case of a small leak due to a tight crack, the helium test is more sensitive and may be used if the water test is not efficient.

15.4.3 Helium test

The helium test is a very sensitive leak test technique because of the small dimension of the helium atom and its diffusivity, its rarity in the atmosphere (5 ppm by volume) and the selectivity of detection with a mass spectrometer. The principle of the helium test for a SG is given in Fig. 15.11. The methodology of the test is based on the following steps:

1. The secondary part of the SG is pressurized with air and a percentage of helium significantly above the natural concentration of helium in the atmosphere;

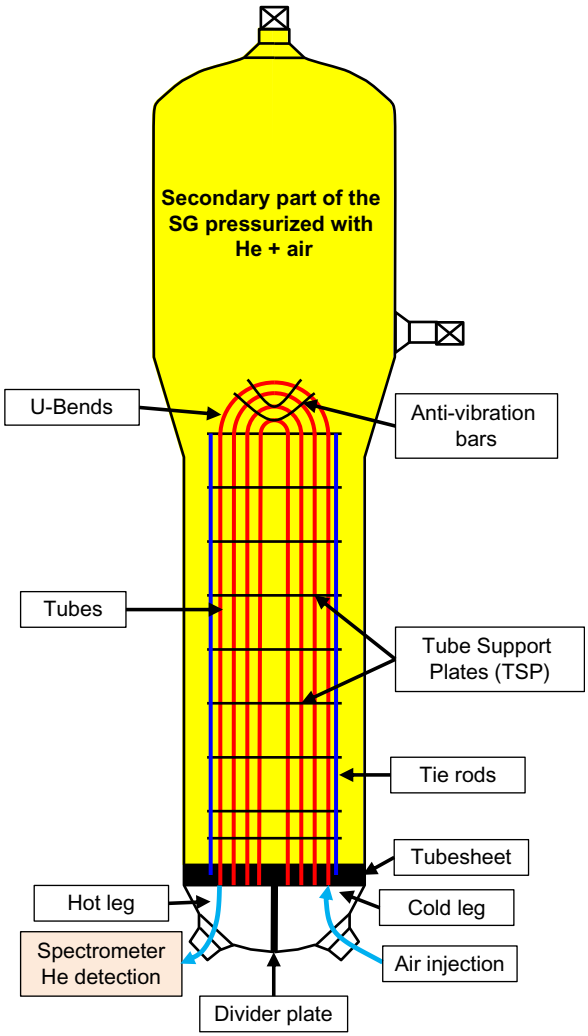

Fig. 15.11 Principle of helium leak test for SGs.

2. An air flow is established at one extremity of a tube, for example at the SG cold leg extremity;
3. A suction tube is introduced in the other extremity of the same tube, in this case at SG hot leg extremity;
4. The suction tube is connected to a helium mass spectrometer. An helium concentration slightly above the natural concentration of helium in the atmosphere can be detected which gives a very high sensitivity to this test for leak detection;
5. Steps 3 to 4 are repeated successively for all the SG tubes to identify the leaky tube(s).

French operator performs a SG helium test every 10 years as part of the regular 10 years outage maintenance program (Brossier et al., 1991). In the event of an unscheduled outage due to a primary to secondary leak, a helium test may be performed if the water test cannot identify the leaky tube.

The helium leak test is also performed at fabrication facility by tube makers. The sensitivity of this technique for through wall pinhole detection in SG tube is unsurpassed by other nondestructive technique such as eddy current or ultrasonic technique. The helium test sensitivity at the fabrication facility can be up to 10^{-5} mbar·L/s which means that a 1 μm diameter hole can be detected for an helium pressure test of 7 bar (Lheureux and Gérard, 2013).

15.5 Hydrostatic pressure test

Hydrostatic pressure test of the primary and of the secondary part of SGs are performed by manufacturer at the end of the manufacturing process. It is a requirement for all the manufacturing codes and also from the regulation. The overpressure coefficient and the temperature of the water may vary according to the reference code and local regulation. The conditions of the hydrostatic pressure test for the equipment should not exceed the yield strength of the material and no permanent deformation should occur. The history of hydrostatic pressure tests shows some occurrences of catastrophic rupture in the piping industry (Cosham et al., 2008) and nonnuclear pressure vessels (Warke, 1992). This feedback shows the usefulness of a global test of resistance for pressure equipment. In the nuclear industry, the author is not aware of catastrophic rupture of class 1 pressure equipment. Some limited leaks due to defective welds in tube to tubesheet cladding have been reported during the preparation of the hydrostatic pressure test. A crack in the weld between the divider plate and the channel head after primary side and secondary side hydrostatic pressure test was detected in San Onofre replacement SG 3B in 2009 (ML 092600513).

15.5.1 Periodic primary and secondary side hydrostatic pressure test

In France, a hydrostatic pressure test is mandatory every 10 years for the primary coolant system and the main secondary coolant system including the secondary part of SGs. All structural welds should be exposed for visual inspection and all

thermal insulation systems should be removed. An acoustic passive receiver system might be used to detect and locate potential leaks. The visual inspection of all welds proved to be very efficient in 1991 at Bugey Unit 3 where the first occurrence of stress corrosion of the weld of a control rod drive mechanism was detected on a closure head in 1991 (Champigny, 2006). The leak was clearly identified by a boric acid stain.

15.5.2 Tube in situ hydrostatic pressure test

Some utilities may perform in situ tube hydrostatic pressure test. In the USA, the regulation requires no tube failure for 1.4 time the design basis accident primary-to-secondary pressure differential and 3 times the normal steady state full power operation primary-to-secondary pressure differential. The in situ pressure test is a way to demonstrate experimentally the integrity of the tubes and the compliance to regulation (EPRI, 1014983). In some cases, the pressure test criteria may not be met. In 2012, some tubes from San Onofre Nuclear Generating Station Unit 3 could not meet the integrity criteria due to severe tube-to-tube wear caused by fluid-elastic instability (ML13263A271; ML15062A125).

15.6 Future trends for recirculating steam generator maintenance and inspection

15.6.1 Recirculating SG manufacturing and design main evolutions

Recirculating SGs design and manufacturing are continuously updated on the basis of operating experience feedback, industry expectation, and regulatory requirements. The evolution in design and manufacturing is generally beneficial with respect to maintenance workload, performances, and safety, with an exception reported in 2013 (ML13263A271). Some evolutions in design and manufacturing are significant for in service inspection. The major evolutions are listed in the following:

- Pressure shells are forged from hollow ingots, avoiding the need for a longitudinal weld (previous technique was to roll and longitudinally weld a plate to form a shell);
- Upper heads are forged (previous technique was to assemble two half-upper head with a meridian weld);
- Channel head is forged (previous manufacturing technique was casting);
- Tubes are made of alloy 690TT[1] or alloy 800NG[2] (both alloys are considered more resistant to corrosion than alloy 600 and stainless steel);
- Tube sheet cladding (if relevant) and divider plates are made from alloy 690/52/152;

[1] TT: Thermally Treated

[2] NG: Nuclear Grade

- Some SGs may have embedded preheater or economizer;
- The support for U-Bends has been improved (more antivibration bars or scallop bars);
- More access to the secondary side is given through additional hand-holes and eye-holes, in particular for TSPs remote visual inspection;
- Some SGs may have a triangular pitch for the tube bundle; the gap between tubes might be reduced compared to older SG designs;
- SG thermal insulator may be easier to remove for the inspection.

Some evolutions such as additional hand-holes and eye-holes clearly facilitate the inspection. Some evolutions are more likely aimed at thermal hydraulic improvements, such as economizer and a triangular pitch for the tube bundle. A compact design for the tube bundle reduces the clearance for tools access and therefore challenges the development and qualification of tools for secondary side maintenance.

The material improvement, in particular for the tubes, may reduce the workload of the maintenance program, provided the secondary side chemistry specifications and maintenance practices are not relaxed.

15.6.2 Maintenance and inspections

The general progress of technology has a positive impact on SG maintenance considering performances and dosimetry. A few technological improvements are listed in the following:

- Maintenance tools enhancement:
  - The reduction in size of high resolution video cameras and LED lighting give the opportunity for better access and high quality video of the tube bundle inner regions. The evaluation of tube fouling, tube support plate blockage, and tube sheet sludge is facilitated. Loose parts can also be identified and retrieved more easily in remote areas (Lecour et al., 2013);
  - More remote operations done with an automatic tool or robotic arm installed in the channel head: tube inspection and repair, divider plate inspection, nozzle dissimilar weld inspection. Robotic arm installation in the channel head is designed to reduce the workers dosimetry;
  - Folding of the nozzle dam for a faster installation and a dosimetry reduction for worker;
- Secondary side cleanliness
  - Availability and positive feedback experience for chemical cleanings (King et al., 2015; Sollier et al., 2015);
  - Improvement of sludge lancing tools with in-bundle access and higher pressure water jet lancing (King et al., 2015);
- Nondestructive testing technology:
  - Availability of array eddy current probes which give an extended inspection coverage of the tubes over their full length (Obrutsky et al., 2009; Mistral et al., 2013);
  - Improvement of eddy current software analysis, including automatic analysis software (EPRI, 1013386);
  - Availability of phased array UT transducers including smart contact transducers for complex geometries such as weld overlays (Cattiaux et al., 2005);
  - Wider use of simulation codes for inspection development, analysis, and qualification (Cattiaux and Sollier, 2010; Truchetti et al., 2012; Maurice et al., 2013).

15.7 Conclusion

Steam generators for PWR are class 1 components according to nuclear manufacturing codes. Their design is very conservative and their manufacturing meets the highest standard. This component needs good operating conditions, careful surveillance and appropriate maintenance for long-term operation.

The first requirement is to avoid aggressive pH and electrochemical potential conditions for the tube bundle and the low alloy carbon steel. Good secondary side chemistry is needed to reduce corrosion issues.

The second requirement is to perform periodic in-service inspections to check for potential unforeseen degradation. The main inspections techniques used by the industry for SG surveillance have been discussed in this chapter. The qualification of these techniques gives assurance in the performances achievable on site.

The third requirement is to maintain the SGs in nominal conditions with periodic maintenance. One of the major maintenance issues is to keep the secondary side as clean as possible and to remove sludge by high pressure water lancing. The potential buildup of corrosion products in the flow holes of the tube support plates should be prevented or cured using chemical cleaning.

For new Steam generators, the main threat for safety is tube wear by loose parts and antivibratory bars. Therefore specific effort should be taken during outages to avoid the ingress of foreign materials in the SGs (Foreign Material Exclusion approach).

Acknowledgments

The author acknowledges many valuable inputs and proofreading from fellow colleagues, many thanks to Gérard Cattiaux, Christine Delaval, Géraldine Graff, Marc le Calvar, Ian de Curières, Emmanuel Viard, Kenneth Karwoski, Patrice Jardet, Olivier Loiseau, and Thierry Payen.

References

10 CFR § 50.65, 2014. Requirements for Monitoring the Effectiveness of Maintenance at Nuclear Power Plants.

ASME, 2012. Code Comparison Report for Class 1 Nuclear Power Plant Components: STP-NU-051. ASME, New York.

Boccanfuso, M., Carrez, J.-M., Fritz, R., Delerablée, Q., 2010. Steam generator mechanical plug failure: a tribologic problem. In: Proceedings of the International Symposium Fontevraud 7, September 26–30, 2010.

Bodineau, H., Sollier, T., 2008. Tube support plate clogging up of French PWR steam generators. In: EUROSAFE, November 3-4, 2008.

Brossier, P., et al., 1991. La sureté d'exploitation des générateurs de vapeur en France. In: NEA/CSNI UNIPEDE, Specialist Meeting on Operating Experience With Steam Generators, Brussels, Belgium, September 16–20, 1991.

Brunin, O., Deotto, G., 2009. Loads applied to clogged steam generators internal structures. In: Proceedings of the ASME 2009 Pressure Vessels and Piping Division Conference, Prague, Czech Republic, July 26–30, 2009.

Bueno, A.G., Garcia, J.J.J., 2012. Almaraz NPP steam generators performances. In: Proceedings of the 9th International Conference on NDE in Relation to Structural Integrity for Nuclear and Pressurized Components, Seattle, May 22–24, 2012.

Buisine, D., de Bouvier, O., Rupa, N., Thebault, Y., Barbe, V., 2010. French steam generator tubes: an overview of degradations. In: Proceedings of the International Symposium Fontevraud 7, September 26–30, 2010.

Cattiaux, G., Sollier, T., 2010. Numerical simulation of nondestructive testing, an advanced tool for safety analysis. In: EUROSAFE, Köln, November 8-9, 2010.

Cattiaux, G., Benoist, P., Poidevin, C., Sollier, T., 2005. IRSN non-destructive testing research relating to the ageing of nuclear installations. In: Symposium NUPEER 2005, Le vieillissement dans les centrales nucléaires, Dijon, June 22–24, 2005.

Champigny, F., 2006. Plant lifetime management and non destructive examinations 10 years experience in France since 1995. In: 9th European Conference on Non-destructive Testing, Berlin, 25–29 September 2006.

Chapman, B., Seldis, T., Eriksson, A. (Eds.), 2007. European Methodology for Qualification of Non-destructive Testing. ENIQ report 31. Office for Official Publications of the European Communities, Luxembourg.

Chatellier, L., Stindel, M., Devinck, J.M., Chavigny, F., De Bouvier, O., 2009. Tube support plate blockage evaluation with televisual examination and eddy current analysis. In: Thompson, D.O., Chimenti, D.E. (Eds.), Review of Quantitative Nondestructive Evaluation, Vol. 28. Plenum Press, New York.

Chattopadhyay, S., 2011. Feed water line cracking in pressurized water reactor plants. In: Tsvetkov, P. (Ed.), Nuclear Power—Control, Reliability and Human Factors. InTech, Rijeka, Croatia, ISBN: 978-953-307-599-0.

Consonni, M., Mudge, P., 2012. Interpretive comparison of the requirements relating to welding and non-destructive examination in the French and US codes for nuclear components. In: Proceedings of the 2012 20th International Conference on Nuclear Engineering, ICONE20-POWER2012, Anaheim, California, USA, July 30–August 3, 2012.

Cosham, A., et al., 2008. A historical review of pre-commisioning hydrotest failures. J. Pipeline Eng., 7, 5–18. 1st Quarter.

Czajkowski, C.J., 1983. Investigation of Shell Cracking on Steam Generators at Indian Point Unit No. 3, NRC Report NUREG/CR 3281.

Deforge, D., Duisabeau, L., Miloudi, S., Thebault, Y., Couvant, T., Vaillant, F., Lemaire, E., 2010. Learnings from EDF investigations on SG divider plates and vessel head nozzles. In: Fontevraud 7, September 26–30, 2010.

Dordonat, M., Le Bon, S., Mazurczak, C., Guttmann, D., Morin, P., 1998. Endommagement par stratification thermique des tuyauteries d'eau alimentaire des générateurs de vapeur. In: Proceedings of the International Symposium Fontevraud IV, September 14–18, 1998.

EPRI, 1994. In: Paine, J.P.N. (Ed.), Steam Generator Reference Book. EPRI, Palo Alto, CA. revision 1.

EPRI, 2006. Steam Generator Integrity Assessment Guidelines: Revision 2: EPRI 1012987. EPRI, Palo Alto, CA.

EPRI, 2007a. Automated Analysis of Rotating Probe Eddy Current Data: EPRI 1013386. EPRI, Palo Alto, CA.

EPRI, 2007b. Steam Generator In Situ Pressure Test Guidelines, Revision 3: EPRI 1014983. EPRI, Palo Alto, CA.

European Commission, 1997. Nuclear science and technology, common position of European regulators on qualification of NDT systems for pre- and in-service inspection of light water reactor components. In: The Nuclear Regulators Working Group, EUR 16802.

IAEA, 2002. Maintenance, Surveillance and In-service Inspection in Nuclear Power Plants: Safety Guide, No. NS-G-2.6. IAEA Safety Standards Series, International Atomic Energy Agency, Vienna, Austria.

INSAG-10, 1996. Defence in Depth in Nuclear Safety, a report by the International Nuclear Safety Advisory Group.

ISO 106809:2012, 2012. Non-Destructive Testing—Ultrasonic Thickness Measurement.

King, P., et al., 2015. Steam generator deposit removal technologies and their applications. In: Proceedings of the International Nuclear Components Conference, Mississauga, Ontario, Canada, November 1–4, 2015.

Lecour, E., et al., 2013. Steam generator secondary side televisual inspections. In: Proceedings of the 10th International Conference on NDE, Cannes, France, October 1–3, 2013.

Lheureux, M., Gérard, P., 2013. Helium leak test in line: enhanced reliability for heat exchanger tubes. In: Proceedings of the 10th International Conference on NDE, Cannes, France, October 1–3, 2013.

Maurice, L., Costan, V., Thomas, P., 2013. Axial probe eddy current inspection of steam generator tubes near anti-vibration bars: performance evaluation using finite element modeling. In: 10th International Conference on NDE in Relation to Structural Integrity for Nuclear and Pressurized Components, Cannes, October 1–3, 2013.

Mistral, Q., et al., 2013. Array probe implementation (SMX) on EDF steam generator tubes. In: Proceedings of the 10th International Conference on NDE, Cannes, France, October 1–3, 2013.

ML 092600513, 2009. San Onofre, unit 3—Root Cause Evaluation for Divider Plate Weld Joint Separation in the Replacement Steam Generators.

ML11171A454, 2011. Westinghouse AP1000 Design Control Document Rev. 19—Tier 2 Chapter 5—Reactor Coolant System and Connected Systems—Section 5.4 Component and Subsystem Design.

ML13204A143, 2013. NRC Information Notice 2013-20: Steam Generator Channel Head and Tubesheet Degradation.

ML13263A271, 2013. San Onofre Nuclear Generating Station—NRC Confirmatory Action Letter Response Inspection 05000361/2012009 and 05000362/2012009.

ML15062A125, 2015. Review of Lessons Learned from the San Onofre Steam Generator Tube Degradation Event.

NEI 97-06, 2011. Nuclear Energy Institute, Steam Generator Program Guidelines.

NRC Bulletin 79-13, 1979. Cracking in Feedwater System Piping.

NRC Bulletin 89-01, 1989. Failure of Westinghouse Steam Generator Tube Mechanical Plugs.

NRC Information Notice 1996-09, 1996. Damage in Foreign Steam Generator.

Obrutsky, L., et al., 2009. Overview of steam generator tube-inspection technology. In: NDT in Canada 2009, London, Ontario, Canada, August 25–27, 2009.

Rao Gutti, V., 1990. Investigation and resolution of steam generator girth weld cracking incidents in pressurized water reactors. In: Proceedings of the International Symposium Fontevraud II, September 10–14, 1990.

Shoji, T., et al., 2010. Effects of cold work and stress on oxidation and SCC behavior of stainless steels in PWR primary water environments. In: Proceedings of the International Symposium Fontevraud 7, September 26–30, 2010.

Sollier, T., et al., 2015. IRSN analysis on steam generators operating experience in France. In: Proceedings of the International Nuclear Components Conference, Mississauga, Ontario, Canada, November 1–4, 2015.

Tapping, R.L., et al., 2000. CANDU steam generator life management. Nucl. Eng. Des. 197, 213–223.

Truchetti, L., Chatellier, L., Peureux, P., 2012. Simulations and impact on NDE development and qualification. In: 18th World Conference on Nondestructive Testing, Durban, South Africa, April 16–20, 2012.

Warke, W.R., 1992. Handbook of Case Histories in Failure Analysis, Vol. 1. ASM International, pp. 143–146.

Yeh, H.-C., Keating, R., Roidt, M., Hochreiter, L., 1992. An analysis for the failed steam generator tube plug. Nucl. Technol. 98, 224–229.

This page intentionally left blank

Nuclear steam generator tube inspection tools

16

L. Obrutsky
B. Eng, CGSB ET Level 3 M&O Tech, Deep River, ON, Canada

16.1 Introduction

A variety of degradation modes may challenge the integrity of steam generator (SG) tubing and therefore the stations' reliability, capacity factor, and cost-effectiveness. Some of these modes generate volumetric material loss due to fretting wear, pitting corrosion, wastage or flaw accelerated corrosion; other modes have directional properties due to intergranular attack (IGA), axial or circumferential outside diameter (OD) stress corrosion cracking (SCC), and primary water (PW) SCC (MacDonald et al., 1996; Nuclear Energy Institute, 2001). One of the key life management components for ensuring tube integrity, and thus protecting the safety of the public and the environment while maintaining cost-effective operation of nuclear power plants (NPP), is inspection and monitoring aimed at timely detection and characterization of the degradation.

SG inspections can be very complex and costly operations. Inspection scope, data acquisition equipment, remote manipulators, probe drives, probe technology, data storage devices, data analysis software, data analysis methods and guidelines, personnel training and qualification, data transmission, data management, tube integrity issues, personnel radiation protection issues, need for tube plugging and their effect in the overall cost of inspections and maintenance are all elements that need to be taken into account when planning SG inspections.

This chapter provides a brief historical perspective regarding the evolution of SG inspections and analyze the motivations behind that evolution. It presents an overview of the inspection technology, the current scope of SG inspections, and regulatory issues.

16.2 Historical perspective

In the late-1970s and early-1980s, in-service inspections of SG tubing were carried out using eddy current testing (ET) bobbin probes connected to analog single-frequency instruments, which rely on storage-type cathode ray tubes to display the eddy current data. In turn, data were recorded using two-channel strip-chart recorders and analog tape recorders and often analyzed in real time or, alternatively, offline by a very slow process of reviewing the strip charts and replaying the tapes. The results were then reported on a sheet of paper with the tube list. The site engineer usually provided

Steam Generators for Nuclear Power Plants. http://dx.doi.org/10.1016/B978-0-08-100894-2.00018-2
© 2017 Elsevier Ltd. All rights reserved.

inspection plans in the form of a short tube listing, and in most cases the inspection scope was aimed at detection of degradation modes such as wastage or fretting wear. The inspection was limited to a small percentage of tubes, typically 3%, and in some cases expanded to no more than 20% of the tubes (Mayes et al., 2006).

Probe-drive technology was slow and unreliable. Remote manipulators required substantial human intervention for their installation inside the SG at the beginning of the inspections and for their repositioning during the inspection that would allow access to different areas of the tubesheet. This resulted in high cost in time and radiation exposure (Mayes et al., 2006).

By the mid-1980s, additional modes of degradation such as pitting corrosion, IGA, axial or circumferential PWSCC and ODSCC, particularly in nonthermally treated Alloy 600 tubing, had to be addressed. The scope, and therefore the cost, complexity, and time of inspections increased significantly. Bobbin probes were inadequate to detect circumferential cracking or to reliably inspect the top-of-tubesheet (TTS) locations; therefore, motorized rotating probes were used to supplement the inspections. These were very slow and prone to failure; consequently, the time and cost of inspections increased significantly.

By the mid-1990s, the number of tubes exhibiting SCC increased dramatically; hence, the need for timely, fast detection and characterization of this and other modes of degradation motivated the development of inspection systems based on advanced probe technology coupled with versatile instruments operated by fast computers and remote communication systems and much improved manipulators and probe drives.

SG inspection systems have progressed through the 1990s, and particularly into this millennium, to a much higher level of automation, efficiency and reliability. The increasingly competitive market of electricity production and the demands of economic globalization required shorter and more cost-effective inspections. Also, the role of nondestructive evaluation (NDE) evolved from simple detection tools to diagnostic tools that provide input into tube integrity assessment decisions, fitness-for-service, and operational assessments. This new role was motivated by tighter regulatory requirements to assure the safety of the public and the environment, better SG life management strategies, and often self-imposed regulations. It led to the development of advanced probe technologies, more reliable and versatile instruments and robotics, better training and qualification of personnel and better data management and analysis systems.

In addition, future SG inspections will likely be challenged by new degradation modes that might emerge as a result of life extension of NPP and their SGs or from new tube materials that are being used in replacement SGs.

16.3 Inspection tools

The bulk of SG tube inspections are carried out using ET probes. Inspection systems consist of ET probes connected to digital, computer-controlled, multichannel, multifrequency instruments that are paired with probe-drive systems, probe manipulators, and mass data-storage units.

Occasionally, additional techniques such as ultrasonic testing (UT) and profilometry probes are deployed for reinspection and characterization.

16.3.1 Equipment technology

The majority of SG inspections are carried out with modern inspection systems having high degree of automation, integration, and versatility. These systems consist of light and compact parts that easily assemble into an integrated single-box system comprising probe pusher, coil reel, probe drive, power supply, electronics, and powerful ET instruments. These systems communicate with the acquisition computer via standard Ethernet connection. They require plant air supply for cooling and/or to assist in probe push operation, and electric power. Fig. 16.1 shows two examples of state-of-the-art Zetec MIZ-80iD system (Burnett et al., 2016) and CoreStar OMNI-200-TIP (CoreStar International Corp, n.d.). These ET instruments are fully digital, support simultaneous or multiplexed multifrequency operation, and use of multiple probes or array probes with channel capabilities of up to 512, 640, or 1024 channels, depending of the configuration. Their high digitation rates permit inspection speeds as fast 40 in./s. The enhanced capabilities of current equipment address the need to continuously reduce inspection costs, shorten outage times, and improve inspection quality. Also, the increase automation aids in reducing levels of radiation exposure for the personnel involved in installing and operating probe manipulators and data acquisition equipment to comply with ALARA (as low as reasonably achievable) objectives.

However, it should be mentioned that, in some cases, SG inspections are still being conducted using legacy inspection systems. These systems consist of multiple heavy and awkward-to-carry individual components, i.e., ET instrument, probe drive and probe-drive controller, power supply, communication system, and manipulator controller. Typically, this equipment is transported into the reactor building by several people. Communication with the computers that are located outside the reactor building requires a large number of cables and adapters, many of them a few hundred meters long. In these cases, inspection systems comprising multiple probe drives operating simultaneously are often used to reduce inspection time, which, in turn, multiplies the overall complexity, time, and dose needed for setup.

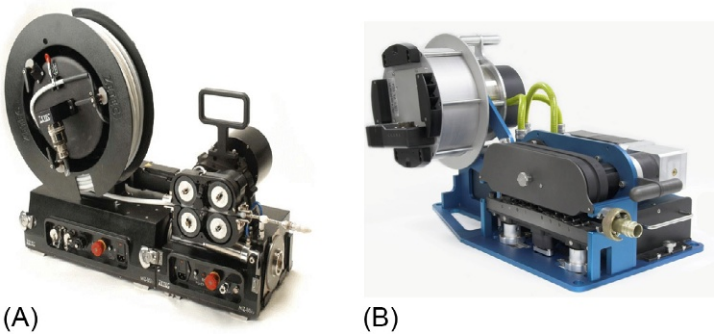

Fig. 16.1 Images of state-of-the-art integrated inspection systems. (A) Zetec MIZ-80iD (Burnett et al., 2016) and (B) CoreStar OMNI-200-TIP (CoreStar International Corp, n.d.).

16.3.2 Probe manipulators

Because of the high radiation fields inside a SG head, data acquisition systems rely on robotics to deliver the probes remotely. The manipulator technology has significantly evolved over the years. Early versions required substantial human intervention as the operator needed to enter the SG head to install and relocate them to cover areas where the manipulators could not reach, called exclusion zones. Also, other manipulators were sometimes needed to perform repairs. This resulted in a very high cost in terms of radiation exposure.

The design of state-of-the-art probe manipulators have addressed many of these issues and, as a result, reduced considerably the radiation exposure of the personnel. They are denoted as minimum-entry or nonentry robots as they are typically installed without the need for the operators to enter the SG. However occasionally, the operators might need to introduce their arms inside the SG head.

Their design eliminates the need to relocate the robot within the generator in order to inspect all tubes and therefore, reduces inspection time. This generation of robots, when coupled with advanced software and hardware, can perform inspections in fully automatic mode. They use vision systems to accurately locate the tubes, ET data to determine probe position and tube end, encoders and information from the robot to go from tube to tube following the inspection plan without the intervention of the operator. Fig. 16.2A–C shows pictures of the Westinghouse ROSA III and AREVA Non-Exclusion Zone RANGER (Westinghouse Nuclear Services, 2016; Wilson, 2011) and BWXT PRIMA 3 Axis Robotic Arm (for inspection of CANDU[1] SGs). Moreover, the robust designs of these robots allow them to perform ET inspections

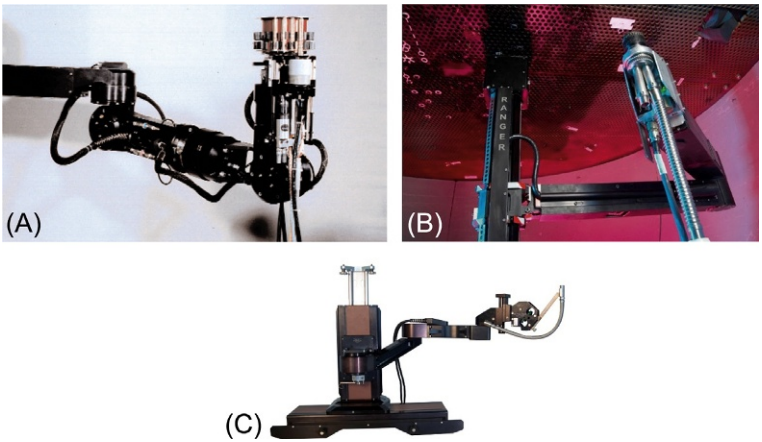

Fig. 16.2 Examples of nonentry manipulators (A) Westinghouse ROSA III (Westinghouse Nuclear Services, 2016), (B) AREVA Non-Exclusion Zone RANGER (Wilson, 2011), and (C) BWXT PRIMA 3.

[1]CANDU is a trade-mark of Atomic Energy of Canada Limited.

as well as the follow-up maintenance and repairs such as tube pulling, plugging, or welding of sleeves with rapid changes of the tool head, minimizing radiation exposure, and total time needed for SG maintenance activities.

A newer generation of nonentry, nonexclusion zone robots are lightweight crawlers such as Westinghouse PEGASYS and Zetec ZR-100. These robots are designed to be mounted on the tubesheet and to navigate it using tube-walking technology. They are lighter and easier to assemble than the previous models, but they can only perform light repairs and consequently are optimal for inspection of replacement SGs that should require very little or no repairs.

Specifically designed versions of older manipulators such as the Zetec SM-23 and ZR-1 are still being used frequently to inspect the CANDU SGs. These smaller SGs require specifically designed robots. The SM-23 mounts on the man-way and is typically dedicated to perform the ET inspections only. It has a computer interface that allows remote semiautomatic operation using specific software. A video camera located on the arm assembly allows the operator to continuously view the guide tube and tubesheet on the remote station monitor and aid in the final tuning of the guide-tube location before inserting the probe in the tube (Zetec Products Alphabetical Listing, 2007).

16.3.3 Probe technology

Bobbin probes (see Fig. 16.3A for typical probes) have been the industry standard for general inspection of SG and heat exchanger tubes for many years. They are quite reliable and provide good general-purpose inspection of the tubes, being able to reliably detect and size volumetric flaws such as fretting wear and pitting corrosion. With the new instrumentation their typical scanning speed is up to about 40 in./s.

However, one of the major limitations of bobbin probes is their inability to detect circumferentially oriented cracks because the induced current in the tube wall circulates parallel to the coil windings and is inherently unaffected by the presence of such cracks. Fig. 16.3B illustrates the limitation of the probe for detecting circumferential cracks. These probes are sensitive to axial cracks at straight tube sections; however, at TTS and the U-bend transition regions, the large signals generated by geometrical tube-wall distortions significantly reduce detectability (Cecco et al., 1981; Cecco and Van Drunen, 1985; Sullivan et al., 1998).

Reliable detection of SCC and further characterization of flaws often requires the use of additional inspection probes.

Motorized rotating pancake coil (MRPC) probe and Plus Point probes are widely used as either reinspection probes or to inspect crack-prone regions such as the TTS. These surface-riding probes are connected to motor units that rotate the probe inside the tube in a helical pattern. They overcome the limitations of bobbin probes since they can detect both axial and circumferential cracks and can also provide information about flaw morphology. Fig. 16.4A illustrates the distortion to the ET pattern generated by a pancake coil in the presence of a circumferential crack. It is this distortion of the magnetic field that gives the ability to detect circumferential cracks. The Plus Point probe comprises two orthogonal coils connected in differential mode crossing

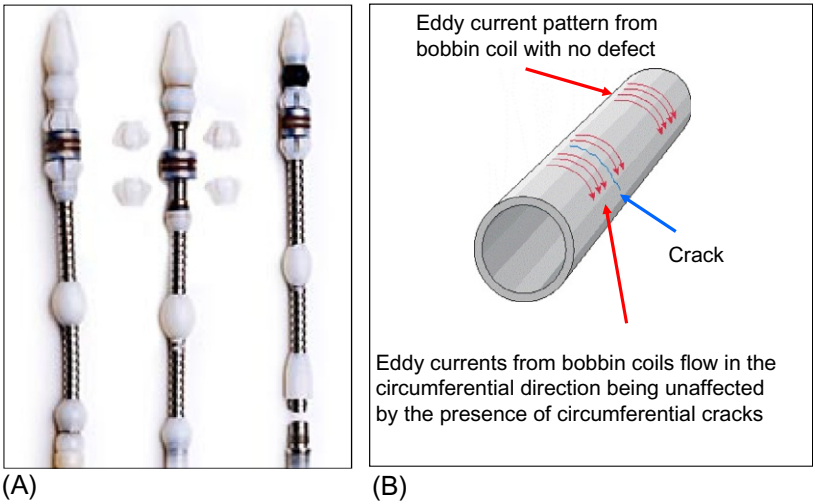

Fig. 16.3 Bobbin probes (A) view of typical bobbin probes for SG tubing inspection and (B) illustration of ET pattern generated by bobbin probes, demonstrating the limitations for detection of circumferential cracks.

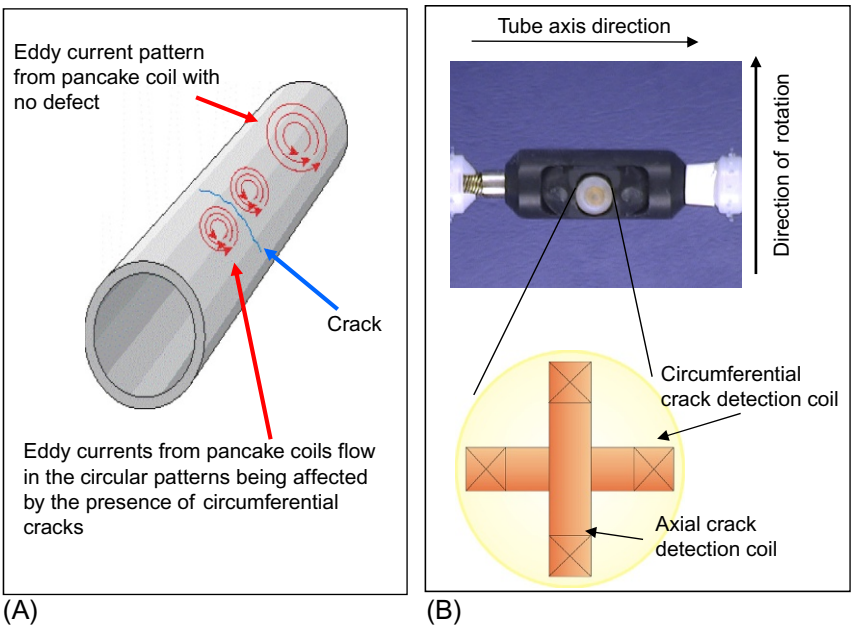

Fig. 16.4 Rotating probes: (A) detection of circumferential cracks with pancake coils and (B) view of Plus Point probe for axial and circumferential crack detection.

at a point so that they are affected simultaneously by material and geometric distortions such as lift-off. This probe has the ability to detect circumferentially and axially oriented cracks as well as discriminate between them. Fig. 16.4B illustrates the coil configuration of a Plus Point probe. In many cases rotating probe heads might incorporate both pancake and Plus Point probes.

The main limitation of rotating probes is, however, their speed. In spite of the use of high speed and high torque motors, rotating probes scanning speed is ~80 times slower than that of bobbin probes. Also, these probes are usually spring loaded to minimize lift-off, which makes them prone to failure. This is especially evident in CANDU reactors where the presence of internal magnetite deposits reduces probe life significantly, and the small diameter of the motors make them more fragile. For that reason, the time required for inspections and thus the cost is significantly higher for stations that are required to inspect a large number of tubes with the plus point probe to address detection of SCC.

Transmit/receive (T/R) array probes were developed in the 1990s, to address specific inspection needs of CANDU SG tubes. These probes take advantage of the superior properties of T/R technology compared to impedance probe technology. They offer a fivefold to tenfold improvement in signal-to-noise ratio, in the presence of lift-off caused by geometrical tube distortions such as U-bend deformations or the tubesheet transition. The array feature makes it unnecessary to have moving parts, which leads to increased probe reliability (Sullivan et al., 1998). Since T/R probes have directional properties, being sensitive primarily to defects in-line with the T/R coil pairs, the probe design can be optimized to maximize response for different crack orientations (Obrutsky et al., 2001).

The X-Probe[2] is a fast single-pass T/R array probe that is currently used world-wide for inspection of SG tubing as a fast alternative to rotating probes. It combines coil pairs aligned for circumferential flaw detection and for axial flaw detection in a single probe-head as shown in Fig. 16.5. The number of coils in each row varies from 8 to 19 depending on the tube diameter. Electronic circuits at the probe head allow the coil pairs to discriminate between axial, circumferential, and volumetric flaws in a single

Fig. 16.5 X-probe for axial and circumferential crack detection (A) view of an X-Probe for 22.3 mm diameter tubing and (B) view of an X-Probe for 12.9 mm diameter tight-radius U-bend tubing.

[2]X-Probe is a registered trademark of Zetec Inc.

Fig. 16.6 View of the Mitsubishi Intelligent probe (EPRI, 2007).

scan. The X-Probe has shown performance equivalent to rotating probes but can run full-length inspections at scanning speeds up to 40 in./s (Davis, 2005). A special design of this probe, shown in Fig. 16.5B, can negotiate tight radius U-bends. When, combined with a bobbin probe, inspection times can decrease significantly, since the need to revisit the tubes with different probes is virtually eliminated (Obrutsky et al., 2001; Davis, 2005).

There are also various versions of T/R array probes becoming available in the market based on similar coil arrangements to that of the X-Probe. Examples of these new probes are the Tecnatom T probe (Ribes et al., 2014) and the Eddyfi DefHi[3] probe (Renaud, 2014).

Another array probe available in the market is the Mitsubishi Intelligent probe shown in Fig. 16.6. This is also a high-speed, high-performance alternative to rotating probe inspections. The Intelligent Probe combines bobbin and array coil technologies to detect all flaw types in a single pass. The nonsurface riding probe design is durable, reliable and allows fast pull speeds. This probe technology combines an inclined drive coil arrangement and thin film pickup coils with traditional bobbin capabilities into one probe. By design, the probe coils are sensitive to all flaw types and provide characterization of indications. Each probe has a build-in electronic preamplifier circuit that optimizes the signal-to-noise ratio and EMI (electromagnetic interference) shielding (ZetecProducts Alphabetical Listing, 2007).

Probe technology and the ET instruments progressed hand-in-hand. The availability of multiple inputs, large number of channels, fast acquisition rates, simultaneous or timeslot multiplexing, and greater bandwidths makes it possible to operate these array probes at high acquisition speeds similar to bobbin probes. Although the initial goal of probe development was to address the need for reliable detection of SCC, the current probe technology not only fulfills that goal but also widens the scope of ET inspections. Current probe technology, in combination with advanced software and hardware, has the ability to characterize flaw types and their morphologies. This information is often used in tube-integrity assessments and root-cause analysis to help identifying degradation mechanisms.

UT probes and inspection systems are occasionally used as reinspection tools. Given the slower scanning speed, scope of inspections is typically limited to a reduced number of tubes and only at the area of interest. The superior sensitivity and sizing accuracy of UT (quoted to be ±3% TW for normal beam) makes it an excellent tool to obtain accurate information about flaw sizes and flaw characterization. It is also often used to detect flaws that are below ET detection to obtain ET "misses" in support of probability of detection (POD) studies (Chen et al., 2008).

[3] DefHi is a registered trademark of Eddyfi Inc.

16.4 Data analysis

Software packages used for analysis of SG data have been designed with the SG application in mind. They permit very quick display of tube data and are extremely versatile having multiple features and production-oriented tools. Some examples of these features are: multiple options for display modes, process channels for multi-frequency mixes and special calibration requirements, landmarks to identify support plate locations, historical data comparison, and built-in reporting capabilities that capture all the important parameters associated with an indication such as signal amplitude and phase, location, extent, depth, built-in codes to identify the type of indication, etc.

Also, before the data can be released for analysis, specific checks are performed to demonstrate that quality standards have been met. The stringent guideline requirements regarding the rigor and number of these verifications necessitate the use of software for automatic checks, denoted as Data Quality Verification (DQV). These checks can be performed in real time at the acquisition station as part of analysis software packages or additional plug-ins, minimizing the cost in time and resources needed for these verifications.

The data analysis process consists of a multilayer system, which provides an in-depth defense scheme that ensures high detection rate and reporting accuracy (EPRI, 2007). Two independent analysts, called primary and secondary, evaluate the data in parallel. Another more experienced analyst, called resolution, compares the reports from primary and secondary, resolves any discrepancies, and confirms the accuracy of the reported indications. A second resolution analyst reviews the results again and dispositions indications that would require further diagnosis.

Often, the primary and secondary analysts operate in a highly demanding production mode, flagging indications, and performing preliminary analysis only. The resolution analysts perform the detail analysis, using more complex characterization procedures and comparing the indications to historical data. An independent analyst, reporting directly to the utility, performs a fourth level of review, verifying that the resolution analysts are consistently resolving calls and providing feedback. This role often involves spot-checking and auditing analysis results. This analyst has access to the data collected with all the probes and therefore can make informed decisions to disposition indications.

The training and qualification requisites for the SG analysis personnel are fairly demanding. In addition to national certification programs, all analysts are required to receive specific SG data analysis training and demonstrate their competence through qualification programs. For instance, in the United States, analysis personnel are required to be certified under the Qualified Data Analyst (QDA) testing program. This is a large database of SG data from multiple NPP and covering multiple degradation modes and also different probes. In addition to this qualification, site-specific training is provided before each inspection to familiarize analysts with the specific details of the SG, operating history of the unit, method of calibration, analysis guidelines, reporting criteria, SG data, technology, and procedures used at the specific site. In turn, they are required to take a site-specific test to demonstrate proficiency. In

addition, during the course of the inspections, analyst performance is verified by the Analyst Performance and Tracking System (APTS), with feedback to the analysts.

16.5 Technique qualification

The information provided by the inspections include characterization of flaw types and quantification of their dimensions, i.e., depth and axial or circumferential extent, as well as distribution and growth rate. The confidence in these results needs to be demonstrated. Electric Power Research Institute (EPRI) Pressurized Water Reactor Steam Generator Examination Guidelines: United States (EPRI, 2007), European Network for Inspection and Qualification (ENIQ) (Martin et al., 2013) in Europe, and CANDU Inspection Qualification Bureau (CIQB) (Baron, 2011) in Canada determine the requirements for qualification of the techniques. POD and sizing accuracy must be established for different techniques, probes and flaw types and geometry combinations. Technical Justifications (CIQB, ENIQ) and Examination Technique Specification Sheets (ETSSs) (EPRI, 2007) provide the basis to determine inspection uncertainties through statistical analysis logical reasoning and knowledge-based assessments. When preparing Technical Justifications or ETSSs, all the parameters that can affect the results and the POD need to be taken into account and assessed. And finally, these documents are subjected to a complex process of review and approval by peers or subject-matter experts.

Once techniques are qualified, all the essential variables and parameters used for probe qualification exercises such as test frequencies, multifrequency algorithms, sizing methods, analysis guidelines, are incorporated in the acquisition and analysis procedures. Also, a site validation process compares signals in the qualification documentation to the signals from the plant being examined to ensure that the performance indices are applicable (Maurer, 2006).

16.6 Data management

Inspections generate enormous amounts of data, which are transmitted from the ET instrument to the acquisition computers via ethernet connections and stored on high-speed large-capacity storage devices. These data are transmitted using high-speed communication lines, to centralized analysis centers that are habitually located off-site and in different parts of the continent.

In the early days of SG testing, the entire acquisition and analysis crew were located at site. To reduce costs it has become the norm to locate the analysis crew at remote sites or at centralized analysis centers. The use of these centralized analysis locations helps reducing costs and improve efficiency of the data analysis portion of the inspections as it makes much better and cost-effective use of the resources. From the human resources point of view, personnel do not need to travel to different sites eliminating inherent travel costs and reducing the head count at site and the number of staff requiring radiation protection training and security verifications for site access.

Time management is also more efficient because analysts can be made available for different jobs instead of being idle waiting for data. It also eliminates the need to transport computers and set up networks for every inspection.

This massive amount of data needs to be managed efficiently and, more importantly, reliably. Dedicated data management systems handle data from thousands of tubes and several SG, in many cases from multiple scans of the same tube performed with one or various probes. Also, historical data are loaded into the database before inspections, so the analysts can use it for comparison purposes.

Typically, primary and secondary analyzes are carried out by different job contractors located at different sites. The data management systems integrate these locations into their network sending data, receiving the reports and frequently operating in parallel with another management system or protocol. These systems also provide inspection plans to the acquisition computers for either semiautomatic or fully automatic acquisition, deal with the reports from multiple levels of analysis, receive the input from DQV, generate rescan lists and help prepare repair and plugging lists. Once data management systems complete processing the information and all the requirements have been fulfilled, the inspection is officially finished and the equipment can be removed.

16.7 Advanced and automatic analysis techniques

The effort required to analyze the large volume of data produced during an inspection can be enormous. Numerous analysts are required to evaluate data at the same rate as are acquired, and often this time pressure can affect their performance and reliability. One approach to reduce costs and analysis time and to improve reliability is to use automatic analysis systems. Typically, autoanalysis software packages consist of threshold and rule-based computerized data-screening methods. Often, they require well trained and experienced analysts to set them up with a fairly good understanding and knowledge of the degradation modes expected on a SG. Site-specific analysis guidelines are used to adjust signal amplitude and phase thresholds and analysis rules that will flag specific types of indications, and their performance has to be demonstrated through the site-specific performance demonstration tests. They are typically used for one level of analysis, either primary or secondary, but they can be used by both teams, provided each one uses different detection algorithms (EPRI, 2007).

These systems have shown good performance when applied in SG with well-known degradation modes and low noise level tubing such as replacement SG. One limitation is the inherent conflict between having excessive false calls if the thresholds are set up too low for detection of very small indications vs the risk of missing flaw indications if these levels are set up too high. Also, they have a high risk of failing to identify new degradation modes. Moreover, they have not been able to replace humans, particularly when identifying indications buried in tube noise, or for indications from multiple sources found at one location.

This type of processing requires sophisticated and flexible algorithms that incorporate the understanding of the electromagnetic phenomena in signal interpretation.

New industry efforts have concentrated in developing and testing automatic analysis systems that make use of different mathematic and multiple computer-based tools. Signal deconvolution and reconstruction, wavelet transform, feature extraction, frequency-domain and spatial-domain analysis, neural networks, fuzzy logic, etc., are some of the methods that the industry is developing to use either individually or in combination with rule-based systems in an attempt to replace analysts (Arunachalam et al., 2006).

16.8 Inspection requirements and scope

Comprehensive SG programs are written to demonstrate that SGs are fit for service and that structural integrity performance criteria (SIPC) that require SGs to be able withstand burst pressure under normal or postulated accident conditions, are satisfied. Degradation assessment, condition monitoring assessment, operational assessment, and primary-to-secondary leakage assessment are important elements of such programs (MacDonald et al., 1996; Canadian Standard Association, 2005). Inspection data and results provide the information needed to establish which degradation modes are active and help determine if any flaws might have failed the SIPC during the last operating period. In this context, inspections not only provide information about flaw size and type, distribution, and growth rate but also need to do this with confidence. As indicated earlier, performance of NDE capabilities needs to be demonstrated. POD and sizing accuracy must be established for different techniques, probes and flaw type and geometry combinations (EPRI, 2007; Behravesh, 2006). Alternatively, technical justifications provide the basis to determine inspection uncertainties (Martin et al., 2013; Baron, 2011; Marmonier and Henaff, 2004).

Operational assessments predict end-of-cycle conditions based on beginning-of-cycle conditions using the NDE information about depth, growth, and uncertainty factors of detected/hidden flaws and sizing. The objective is to estimate if any flaws would grow to exceed the SIPC during the next cycle and, consequently, to determine the length of the next operating period.

Therefore, the process of planning and defining the scope of SG inspection takes into account these requirements, which are normally defined in governing documents issued by national nuclear regulators such as the Nuclear Energy Institute, "Steam Generator Program Guidelines," EPRI "Pressurized Water Steam Generator Examination Guidelines," and Canadian Standard Association, "Periodic Inspection of CANDU Nuclear Power Plant Components" (Nuclear Energy Institute, 2001; EPRI, 2007; Canadian Standard Association, 2005). The planning process also considers other factors such as degradation history of the component and operational experience of similar plants.

A typical inspection scope requires 100% full-length bobbin probe scans. Since this probe can reliably detect and size volumetric flaws such as fretting wear and pitting corrosion and can provide a vast amount of information about the overall condition of the SGs.

However, additional inspections are regularly carried out for detection of crack-like flaws. These inspections are conducted with either rotating probes such as MRPC or Plus Point probe and/or array probes such as X-Probe or similar. This scope usually covers 100% hot leg TTS inspection, 100% of dents or dings larger than a specified voltage threshold, 100% of tubes in tight radius U-bends, typically rows 1–10, 20% cold leg TTS, cold leg periphery, 100% of sleeves (when present). Historical calls with reported depths that were left in-service in previous inspections must be revisited (Mayes et al., 2006). Any unusual or new indications found are reinspected to provide further information that can help its disposition. Furthermore, any new indication that could affect the SIPC generates an expansion to the inspection scope to include adjacent tubes to that with indications. Inspection scope documents normally have clearly defined rules for dealing with expansions.

Moreover, a number of other conditions, new or ongoing that may affect the performance of the SGs, frequently require additional inspections, specialized data analysis techniques or a combination of both. A recent example of a new condition that has required alternative inspection methods is fretting wear found at U-bend regions caused by tube-to-tube contact at U-bend regions and excessive fast growing fretting wear in replacement SGs. In addition to fretting-wear sizing techniques, specific MRPC, X-Probe, and UT techniques have been used to assess the proximity or possible contact between adjacent tubes and to quantify the gap between tubes and tube support plates (Boudreaux, 2012).

Also, data collected during regular inspections with bobbin probes, MRPC, and X-Probe are routinely analyzed for detection and characterization of foreign objects (often referred as loose parts) that are found in proximity to the tubes and to quantify tube damage that these loose parts might have caused. Lastly, bobbin probe data are regularly analyzed to measure the height of secondary-side sludge pile and often to quantify secondary-side deposits in other areas of the SG, and primary-side magnetite deposits in CANDU stations.

ET has been used in cases where tube support plates have shown signs of degradation due to flow-assisted corrosion (Obrutsky et al., 2006). Specific data analysis techniques were applied to bobbin probe and X-Probe data to quantify the remaining amount of support-plate material. This information was then used to assist in the fitness-for-service analysis based on the ability of the structure to still support the tubes.

16.9 Summary/Conclusions

The common wisdom is that one cannot expect exceptionally good quality products or services, to be produced quickly and at a low price because at least one of these three elements excludes the other two.

In the case of SG inspections, undoubtedly the quality has improved enormously over the years. Increased regulatory requirements for flaw detection and characterization, better probe and instrument technology, better analysis guidelines, performance

demonstration requirements of the technology and personnel, noise and data quality measurements, in-depth defense analysis systems, etc., have all contributed to better and more thorough inspections.

In the past, stations were shut down for long periods of time for maintenance and/or refueling, sometimes up to 3 or 4 months. However, the electricity production market has become much more competitive in recent years, and hence stations have been compelled to reduce outage times not only to reduce costs but also to eliminate the lost-opportunity cost associated with the station downtime. As the outages became shorter, there was increased pressure to reduce inspection times as they were frequently in the outage critical path. In addition to the multiplication of resources and equipment deployed at each outage, the industry responded with significant improvements to instrument, manipulator, and probe technology. Also, semi- and fully automatic acquisition systems, faster communication systems for data transmission, better and more versatile and production-oriented analysis software, efficient data management systems, and automatic analysis are all main contributors to more time-effective inspections.

Finally, the costs of inspections have increased by more than an order of magnitude since the early 1980s. This high cost is due to much more demanding regulatory requirements and the presence of active degradation modes that need to be monitored, requiring a much larger inspection scope than in earlier years. However, the trend is to make inspections more cost-effective and to promote reduction in radiation exposure. In fact, remote analysis, single-box instruments, nonentry manipulators that can also perform repairs, automated acquisition and analysis, and single-pass array probes have helped lower both financial and human resource costs. Moreover, shorter and better inspections have a significant economic impact on the overall station's operational cost, since every day of station shutdown represents lost revenue. Thus, shorter inspections and the prevention of unplanned shutdowns help stations save millions of dollars.

Acknowledgments

The content of this chapter is based upon previous publications by the author (Obrutsky et al., 2007, 2009). The contributions from the coauthors of these papers, Joe Renaud, and Richard Lakhan are acknowledged and truly appreciated.

References

Arunachalam, K., Dayana1, R., Al-Sharoa1, E., Ramuhalli, P., Udpa, L., Udpa, S.S., Benson, J., 2006. Development of algorithms for automatic analysis of array probe eddy current data. In: 25th EPRI Steam Generator NDE Workshop, Marco Island, Florida, USA, July.

Baron, J., 2011. Inspection qualification—CIQB experience. In: Smart Materials, Structures & NDT in Aerospace Conference, NDT in Canada Montreal, Quebec, Canada, November 2–4.

Behravesh, M., 2006. Steam generator NDE historical perspective. In: 25th EPRI Steam Generator NDE Workshop, Marco Island, Florida, USA, July.

Boudreaux, M., 2012. Comparative study of NDE techniques for U-bend structure gap measurement. In: 31st EPRI Steam Generator NDE Workshop, Bretton Woods, NH, USA, July 8–11.

Burnett, M., Boudreaux, M., Cardillo, N., Woller, T., 2016. Initial field experiences: MIZ®-80iD integrated eddy current inspection system. In: 25th EPRI Steam Generator NDE Workshop, Marco Island, Florida, USA, July.

Canadian Standard Association, 2005. Periodic Inspection of CANDU Nuclear Power Plant Components, fourth ed. CSA 285.4.

Cecco, V.S., Van Drunen, G., 1985. Recognizing the scope of eddy current testing. In: Sharpe, R.S. (Ed.), In: Research Techniques in Nondestructive Testing, vol. 8. Academic Press Inc., London, pp. 269–301.

Cecco, V.S., Van Drunen, G., Sharp, F.L., 1981. Eddy Current Testing Manual, vol. 1. AECL report AECL-7523, Chalk River, Ontario, Canada.

Chen, Z., Chan, K., Huggins, J., Malkiewicz, T., 2008. Ultrasonic inspection of steam generators at CANDU power plants. In: 17th World Conference on Nondestructive Testing, October 25–28, Shanghai, China.

CoreStar International Corp, Eddy Current Test Equipment and Probes. http://www.corestar-corp.com/equipment/OMNI-200_TIP.shtml.

Davis, K., 2005. X-probe at the Duke plants. In: 6th Steam Generator Inspection Technology Symposium, Zetec, Snoqualmie Ridge Golf Club, Washington, USA, August.

EPRI, 2007. Pressurized water steam generator examination guidelines: revision 7. EPRI Report 1013706 (Final Report), October.

MacDonald, P.E., Shah, V.N., Ward, L.W., Ellison, P.G., 1996. Steam generator tube failures. Idaho National Engineering Laboratory, Lockheed Idaho Technologies Company, Idaho Falls, ID. NUREG/CR-6365, INEL-95/0383, April.

Marmonier, M., Henaff, H., 2004. Qualification of steam generator NDE applications methodology according to French RSE-M rules. In: 23rd EPRI Steam Generator Workshop, Chicago, Illinois, USA, July.

Martin, O., Martin, E., Booler, R., Walker, T., 2013. The European network for inspection and qualification (ENIQ). In: 22nd International Conference "Nuclear Energy for New Europe (NENE2013)" pp. 304.1–304.8.

Maurer, R.S., 2006. Look back at eddy current analysis practices over the last twenty-five years. In: 25th EPRI Steam Generator NDE Workshop, Marco Island, Florida, USA, July.

Mayes, D., Redner, S., Bipes, T., 2006. Utility historical perspective. In: 25th EPRI Steam Generator NDE Workshop, Marco Island, Florida, USA, July.

Nuclear Energy Institute, 2001. Steam Generator Program Guidelines, NEI 97-06 [Rev 1], January.

Obrutsky, L.S., Watson, N.J., Fogal, C.H., Cantin, M., Cecco, V.S., Lakhan, J.R., Sullivan, S.P., 2001. Experiences and applications of the X-probe for CANDU steam generators. In: 20th EPRI Steam Generator NDE Workshop, Orlando, Florida, USA, July.

Obrutsky, L., Cassidy, R., Cazal, M., Sedman, K., 2006. Eddy current assessment of support plate structures degradation in nuclear steam generators. In: 5th CNS International Steam Generator Conference, Canadian Nuclear Society, Toronto, Ontario, Canada, November 26–29.

Obrutsky, L., Renaud, J., Lakhan, R., 2007. Steam generator inspections: faster, cheaper and better, are we there yet? In: 4th Pan-American Conference on NDE, Buenos Aires, Argentina, October.

Obrutsky, L., Renaud, J., Lakhan, R., 2009. Overview of steam generator tube-inspection technology. In: NDT in Canada 2009 Conference and 6th International Workshop for

Advances in Signal Processing for NDE of Materials, London Ontario, Canada, August 24–27.

Renaud, J., 2014. Eddyfi® innovations in steam generator NDE. In: Presented at the 33rd EPRI Steam Generator NDE and Tube Integrity Workshop, Nashville, Tenessee, USA, July.

Ribes, B., Castresana, J.L., Lain, A., Méndez, M., Hernandez, J., Rodrigo, J., 2014. Tprobe: a thin-film eddy current array probe for the inspection of steam generator tubes. In: 33rd EPRI Steam Generator NDE and Tube Integrity Workshop, Nashville, Tenessee, USA, July.

Sullivan, S.P., Cecco, V.S., Obrutsky, L.S., Humprey, D., Smith, S.P., Emde, K.A., 1998. Computer modeling of eddy current transmit-receive probes for tube inspections. In: Thomson, D.O., Chimenti, D.E. (Eds.), In: CP 509, Review of Progress in Quantitative Nondestructive Evaluation, vol. 17A. American Institute of Physics, New York, NY, pp. 283–289.

Westinghouse Nuclear Services, 2016. Steam Generator Services. http://www.westinghousenuclear.com/Operating-Plants/Outage-Services/Steam-Generator-Services, July.

Wilson, S.R., 2011. AREVA's past, present and future steam generator inspection manipulator designs. In: 30th EPRI Steam Generator NDE Workshop, Seattle, Washington, USA, July.

Zetec Products Alphabetical Listing, 2007. SM-23 Remote Fixture, Zetec http://www.zetec.com/pdfs/ds_sm23.pdf, August 28.

Zetec Products Alphabetical Listing, 2007. Intelligent Probe System for Nuclear Steam Generator Inspections, Zetec, http://www.zetec.com/pdfs/ds_intelligent_probes.pdf, August 28.

Nuclear steam generator fitness-for-service assessment

17

L.B. Carroll
Canadian Nuclear Safety Commission, Ottawa, ON, Canada

17.1 Overview

Specific regulatory requirements to establish the fitness-for-service of steam generator tubes may vary among jurisdictions, but there are generally three common requirements in the approaches used:

1. A very low probability of tube rupture during normal operation;
2. A low probability of tube rupture under accident conditions; and
3. Maintaining primary to secondary leakage levels that ensure regulatory dose limits are not exceeded during normal operation and under accident conditions.

Meeting those three requirements ensure that steam generator tubes serve their containment boundary function. Effectively maintaining the fitness-for-service of steam generators involves a program meeting the following objectives (International Atomic Energy Agency, 2011):

- Identification and characterization of material degradation within steam generators.
- Implementation of steam generator inspection program to provide sufficient information concerning specific degradations present in the steam generators.
- Application of steam generator tube fitness for service assessment methods to evaluate condition of steam generators at the end of an inspection interval and to ensure integrity during the subsequent operation period.

17.2 Repair criteria for steam generator tubes

Steam generator tubes may be repaired or removed from service by sleeving or tube plugging when levels of degradation exceed allowable limits established by repair/plugging criteria. Repair/plugging criteria are often expressed in terms of the through wall extent of the degradation. For example, the American Society of Mechanical Engineers (ASME), Boiler and Pressure Vessel Code (BPVC), Section XI, *Rules for Inservice Inspection of Nuclear Power Plant Components* (American Society of Mechanical Engineers, 2015a) considers degradation with depths in excess of 40% of the wall unacceptable unless there is a degradation mechanism specific repair criteria, which has been accepted by the regulatory authority, demonstrating that deeper flaws will not impact the integrity of the affected tube(s). The same criterion

Steam Generators for Nuclear Power Plants. http://dx.doi.org/10.1016/B978-0-08-100894-2.00019-4
© 2017 Elsevier Ltd. All rights reserved.

has been adopted by the Canadian Standards Association (CSA) Standard, N285.4, *Periodic inspection of CANDU nuclear power plant components* (Canadian Standards Association, 2014) and other international standards and practices.

While the 40% through wall criterion has generally been effective in preventing tube ruptures during normal operation and under accident conditions, as inspection technologies improved and flaw sizing has become more accurate it has been recognized that the 40% criterion is often overly conservative, particularly for volumetric forms of degradation such as support plate fretting or pitting. In such cases, implementing the 40% through wall criterion can result in an unnecessary operational penalty if large numbers of tubes are repaired/plugged. Industry has expended significant effort to develop location and degradation mechanism specific repair criteria resulting in deeper allowable flaws as an alternative to the 40% criterion. This criterion may also be difficult to implement for some forms of degradation that cannot be readily characterized in terms of depth using existing inspection methods.

The 40% through wall criterion or other general wall loss criteria are typically established based upon the assumption that the wall loss is uniformly distributed around the circumference of the tube. A plastic limit load analysis is carried out using margins against tube burst of 3 for normal operating loads and 1.43 for design loads (International Atomic Energy Agency, 2011).

Industry has developed location and defect specific criteria that can provide accurate evaluations of the structural integrity of steam generator tubes subjected to localized forms of degradation to take advantage of detailed information provided by nondestructive examination (NDE) techniques and steam generator design features. Some examples are discussed in the following:

Maximum tolerable flaw size (MTFS) (Pagan et al., 2006): The *MTFS* is depth based criteria used for flaws in CANDU steam generator tubes, which accounts for the actual axial and circumferential extent of degradation. This criterion is commonly used to evaluate support fretting flaws but can be applied to other degradation mechanisms when there is sufficient confidence in the sizing accuracy of NDE tools and the axial and circumferential progression of the flaws is predictable. For example, the axial and circumferential extent of the fretting flaw is related to the shape of the support contacting the tube and the depth of the fretting wear. The criterion has been validated through burst tests of tubes containing actual and simulated fretting flaws along with finite element analysis to demonstrate the maximum flaw depth that will maintain structural factors against tube burst comparable to design margins.

P^* and F^* criteria (International Atomic Energy Agency, 2011; Electric Power Research Institute, 1991): The P^* and F^* criteria define allowable depths below the Top of Tubesheet where flaws of any depth can exist within the tubesheet region because of the low likelihood of tube burst (F^*) or pull-out (P^*) due to the structural support from the tubesheet and neighboring tubes.

H^* criterion (Karwoski, 2009): The H^* criterion defines allowable depths below the Top of Tubesheet where flaws of any depth can exist within the tubesheet region because of the low likelihood of tube burst or pull-out due to the structural support from the tubesheet and the interference fit between the tubes and the tubesheet. Unlike the P^* and F^* criteria, the H^* criterion does not depend upon support for neighboring tubes.

Length criteria for PWSCC cracks in roll transition zone (Electric Power Research Institute, 1991): This criterion is based on flaw length instead of flaw depth and has been used

to establish repair criteria for PWR steam generator tubes in the roll transition zone for full or partially expanded tubes. This criterion will allow flaws up to 100% through wall in depth, but places limits on the number of flaws present in the population of steam generator tubes to ensure that limits for primary to secondary leakage are not exceeded.

Voltage based criteria for ODSCC (United States Nuclear Regulatory Commission, 1995): This criterion is based upon a correlation of bobbin coil voltage signals to tube burst and leakage test results for tubes containing axially oriented cracks of known size. The criterion is applied to the evaluation of ODSCC indications at tube support plates. The correlation between the bobbin probe signals and the burst test results permits evaluation of tube structural integrity. Correlations between the bobbin probe signals and the leak test results are used to determine the amount of primary-to-secondary leakage for the total population of tubes to ensure primary to secondary side leakage limits are not exceeded.

The list of alternate repair criteria above is not intended to be exhaustive, but only serves to provide examples of the location and defect specific criteria that have been developed. These criteria may not be accepted for use in all regulatory jurisdictions and is typically contingent upon review/approval by the responsible regulatory authority.

17.3 Steam generator tube degradation assessment

It is necessary to conduct and document a degradation assessment in order to plan preservice and in-service inspections and maintenance activities. In most cases the degradation assessment is carried out as part of the aging management program activities for steam generators and should be updated regularly based upon internal and external operating experience.

The ERPI steam generator integrity assessment guidelines (Electric Power Research Institute, 2008) list the following objectives for a degradation assessment which are also discussed in other documents (International Atomic Energy Agency, 2011; Nuclear Energy Institute, 2011):

- Identify existing and potential degradation mechanisms.
- Identify the limiting structural integrity performance criteria and the appropriate loading conditions for existing and potential degradation mechanisms.
- Identify the condition monitoring limit for all existing and potential degradation mechanisms and the appropriate measurement parameter for each degradation mechanism.
- Select appropriate techniques for detection and sizing and document the NDE measurement uncertainties for each degradation mechanism.
- Document inspection locations, sampling sizes, and expansion criteria.
- Plan for monitoring degradation in tube hardware such as plugs and sleeves and secondary side components such as tube supports and antivibration bars.
- Identify relevant industry operating experience.
- Identify the secondary side activities planned for outages.

The degradation assessment should include a general description of the design of the steam generator including the tube material and dimensions, tube and support designs, and the design of other secondary side components, which is required in order to assess plausible degradation mechanism. Similarities to the design and operation of other

steam generators with known operating history should also be reviewed. The degradation assessment should incorporate a review of factors which can result in tube degradation including temperature and pressure during start-up, shutdown and normal operation, tube manufacturing processes which could generate residual stresses, secondary side water chemistry, and the potential for the introduction of contaminants from the feedwater system such as lead, chlorides, sulfates, and copper which can contribute to tube degradation. Particular attention should be paid to any situations which could lead to degradation that would not be possible under normal operation. These situations could include deviations from normal operating loads, secondary side chemistry conditions or extended periods of exposure to oxygenated conditions during outages.

For plant designs which incorporate carbon steel components in the primary pressure boundary, such as the CANDU design, consideration for the potential deposition of magnetite on the ID of the tubes should also be considered. In itself, magnetite has not been known to contribute to the degradation of steam generator tubes, but it can impact inspection capabilities due to decreased signal to noise ratios.

The degradation assessment should be updated based upon the results of inspection campaigns and operating experience throughout the operational life of the steam generators and used to guide the planning processes for future outages. The degradation assessment may also be useful in establishing guidance for secondary side chemistry control during outages.

The NDE tool requirements, including the probability of detection and required sizing accuracy will be determined from the degradation assessment. The degradation assessment must be thorough to ensure that the correct tooling is used and to identify potential gaps in inspection capabilities that may need to be compensated for using alternative activities, for example pressure testing, to confirm tube structural integrity. Identified gaps in NDE capabilities may also lead to the establishment of specific research activities to advance NDE methods.

The degradation mechanisms identified will establish the basis for the tube repair criteria and the models necessary to conduct condition monitoring and operational assessments (OAs) discussed later in this chapter.

17.4 Performance criteria for steam generator tubes

Steam generator tube performance criteria are established to ensure safe operation and to maintain the safety margins implied in the design and licensing basis for the nuclear pressure boundary for nuclear power plants. Requirements may vary slightly from jurisdiction to jurisdiction, but there are essentially three goals that are common among performance criteria:

- Maintaining structural margins against gross failure under design basis loading;
- Maintaining operational leakage rates at levels to ensure releases during normal operation are below regulatory limits; and
- Ensuring accident-induced leakage would not generate releases in excess of regulatory limits under accident conditions.

The repair criteria discussed in Section 17.2 are intended to ensure that structural margins are maintained under design basis loading conditions, including operational transients and design basis accident loads. Tubes containing detected flaws that do not satisfy these criteria must be repaired or removed from service.

In the United States, the structural integrity performance criteria are defined as (TSTF-510, 2010):

> *All in-service steam generator tubes shall retain structural integrity over the full range of normal operating conditions (including startup, operation in the power range, hot standby, and cool down), all anticipated transients included in the design specification, and design basis accidents.*

In order to achieve this, the following safety factors against tube bursting due to primary-to-secondary pressure differentials are adopted:

- Safety factor of 3.0 for normal steady-state, full power operation
- Safety factor of 1.4 for design basis accidents

Other loads that impact burst must also be considered in combination with pressure loads, using a safety factor of 1.2 for primary loads and a safety factor of 1.0 for axial secondary loads.

Not all regulatory jurisdictions define the requirements for demonstrating structural integrity using the same safety margins, but the general concepts for demonstrating tube structural integrity are similar.

The Canadian CANDU utilities have generated steam generator fitness-for-service guidelines (FFSGs) which establish two possible criteria to demonstrate the structural integrity of steam generator tubes, referred to as the acceptance criteria prohibiting leakage and acceptance criteria permitting leakage (Scarth et al., 1998). Both criteria require the use of safety factors on applied loads equivalent to the design margins inherent in ASME BPVC Section III (American Society of Mechanical Engineers, 2015b) and Section XI (American Society of Mechanical Engineers, 2015a). The prohibiting leakage criteria require a demonstration that a part-through-wall flaw will not propagate through wall. The permitting leakage criteria permit through wall flaw propagation and leakage provided that leak-before-break behavior can be demonstrated for the flaw and that consequential leakage from all flaws during the most limiting postulated upset or abnormal event, including accidents does not result in releases exceeding allowable regulatory limits.

Operational leakage criteria do not provide a direct measure of tube structural integrity, but have been an effective contributor to limiting the frequency of tube ruptures and can be monitored during plant operation (International Atomic Energy Agency, 2011). The proposed operational leakage performance criteria in IAEA documentation are stated as (International Atomic Energy Agency, 2011):

> *The reactor coolant system (RCS) operational primary to secondary leakage through any one steam generator shall be limited to the maximum allowable leak rate (MALR).*

The operational leakage performance criteria in the United States limit leakage for each steam generator to a MALR (Karwoski, 2009). Satisfying the operational leakage requirements using the CANDU FFSGs requires that the operational leak rate limit and leak rate monitoring capabilities are sufficient to provide reasonable assurance of leak-before-break behavior of a degraded tube during normal operation and protection against tube rupture during upset or abnormal loading events (Scarth et al., 1998). Reasonable assurance must be provided that the leak rate contribution resulting from through-wall flaws to the consequential leakage during upset or abnormal loading events is acceptable (Scarth et al., 1998).

Accepted MALRs can vary based upon reactor design and regulatory requirements. In the United States the typical MALR is 23.65 L/h (150 gal/day) (International Atomic Energy Agency, 2011). In Canada it can range from 10 to 15 kg/h depending upon the particular plant design (International Atomic Energy Agency, 2011). In Russia, leakage through a single WWER steam generator is limited to 4 L/h (International Atomic Energy Agency, 2011).

The accident-induced leakage performance criteria based upon US regulations are provided in the following (TSTF-510, 2010):

> *The primary to secondary accident induced leakage rate for any design basis accident, other than a[n] SG [steam generator] tube rupture, shall not exceed the leakage rate assumed in the accident analysis in terms of total leakage rate for all SGs and leakage rate for an individual SG.*

The calculation of leakage during applicable design-basis accidents must be less than that assumed in the accidents (Karwoski, 2009).

The CANDU FFSGs use a similar concept defined as a consequential leakage assessment (Scarth et al., 1998) to determine the potential leakage during upset or normal events considering all degradation mechanisms that is based upon flaw distributions reflecting detected flaws, considering the potential for flaws in uninspected tubes. There must be an adequate margin between the estimated dose arising from consequential tube leakage and the site dose limits.

Under special circumstances, when there is a specific degradation concern, the entire population of tubes at a plant may be inspected during an outage providing a comprehensive dataset to evaluate the current condition of the tubes. Some steam generator fitness-for-service programs may also incorporate in situ pressure tests to demonstrate that structural integrity requirements are achieved for the current condition of the tubes.

Oftentimes steam generator fitness-for-service is demonstrated using a combination of inspection data from a subset of tubes and analysis methods. Inspection programs may target a subset of tubes that are most likely to experience degradation based upon the results of the degradation assessment or inspections may be conducted on a random sample of tubes and this sample could be changed from outage to outage. Targeting the tubes which are most likely to experience degradation can be an effective way to manage steam generator integrity when there is sufficient information to

permit predictions of which tubes may experience a specific degradation mechanism. In situations where information is lacking, it may be appropriate to carry out random sample inspections until gaps in available information are closed. The 1994 edition of CSA Standard N285.4 required plant operators to define a periodic inspection program for steam generator tubes which incorporated targeted and random tube sample sets to combine the benefits and limit the weaknesses of both approaches. CSA N285.4 program requirements have changed in later versions of the standard to now require periodic inspections of the entire tube population over a span of ~40 years (four 10-year inspection cycles). Canadian CANDU operators still implement targeted in-service inspections to monitor tubes known to contain flaws or that are expected to be most susceptible to degradation.

Given that data are not always available concerning the entire tube population and that there are known limitations in the detection and sizing capabilities of inspection tools, analysis methods have been developed to assess the current condition of the tube population using deterministic, statistical, and/or probabilistic approaches. These assessments are often referred to as a condition monitoring assessment (CMA) and an OA. The CMA makes use of collected inspection data to verify that predictions made following a prior outage were conservative. The OA is the forward looking prediction of the condition of the steam generator tubes at a future outage to demonstrate that performance criteria will be met.

17.4.1 Condition monitoring assessment

CMAs are an evaluation of the as-found condition of steam generator tubes using data gathered during an inspection outage before any repairs/plugging are carried out. The current condition of the tubes is evaluated to verify that the performance criteria were satisfied over the operating period since the last OA was completed and to assess the accuracy of the predictions of that OA. Any of the inspected tubes failing to meet the performance criteria for the previous operating period indicates deficiencies in the steam generator fitness-for-service program or the predictive models used to evaluate the progression of the degradation mechanisms. Identification of new degradation not considered in the degradation assessment should trigger corrective actions to update the degradation assessment and revisions to the steam generator inspection and monitoring activities. Alternatively, if CMAs indicate that the OAs regularly overestimate the progression of degradation in the tubes, a case can be made to possibly reduce inspection and monitoring activities associated with that degradation mechanism and ensure that resources are effectively redirected to the most important factors impacting steam generator integrity.

In addition to inspection and maintenance activities, the CSA Standard N285.4 (Canadian Standards Association, 2014) periodic inspection program for CANDU steam generators incorporates a requirement for plant operators to periodically remove steam generator tubes for metallurgical examination. Normally tubes targeted for removal contain NDE indications. Data gathered from the removed tubes have been used to verify the morphology of flaws generated by different degradation

mechanisms, confirm new or unexpected NDE signals and, if enough data are available, to aid in the assessment of the accuracy of NDE tool sizing estimates. Removed tubes may also be included in burst testing programs to aid in the development of, or provide confidence in, defect specific repair/plugging criteria.

CMAs typically require confirmation of the following:

- The growth of previously detected flaws was bounded by the predictions in the OA.
- Previously detected flaws have not grown to a size that would not satisfy the structural integrity performance criteria.
- No unexpected forms of degradation have been detected.
- Predicted accident-induced leakage rates for the population of flaws would not exceed allowable limits.

As an example, Fig. 17.1 presents the steps required in a CMA to satisfy the requirements of the CANDU FFSGs (Scarth et al., 1998).

Inspection program activities must be planned to ensure that sufficient data are gathered to permit a reasonable CMA evaluation. The inspection data obtained must be representative of the population of steam generator tubes and should include flaws expected to have the highest growth rates or that are likely to be closest to failing structural integrity criteria at the time of the inspection. Failure to adequately plan inspection activities could lead to inadequate conclusions regarding the current condition of the steam generator tube population and impact the accuracy of the OA.

17.4.2 Operational assessment

An OA is a forward-looking evaluation to demonstrate that tubes will satisfy performance criteria over the planned operating period until the next scheduled inspection of the steam generator tubes. OA projections are based upon:

- Inspection findings;
- Degradation initiation and growth modeling;
- Tube repair/plugging criteria for each degradation type; and
- The time interval to the next planned inspection outage.

Corrective actions are established based upon the OA. Tubes containing flaws that are not projected to meet performance criteria for the desired operating interval should be repaired or removed from service. Alternatively, operating intervals could be shortened to increase the frequency of inspections for those tubes.

The timing for completion of the OA is regulatory jurisdiction specific. Some jurisdictions may require a complete OA prior to restart of the plant following the inspection outage. In Canada, regulatory requirements allow for the completion of the OA in two steps. A preliminary OA is carried out to identify tubes that require corrective actions in order to satisfy the performance criteria for the planned operating period and must be completed prior to returning the steam generators to operation. A final detailed assessment must be completed within 90 days of restarting the reactor. While the two stage approach will reduce overall outage time and provides additional time

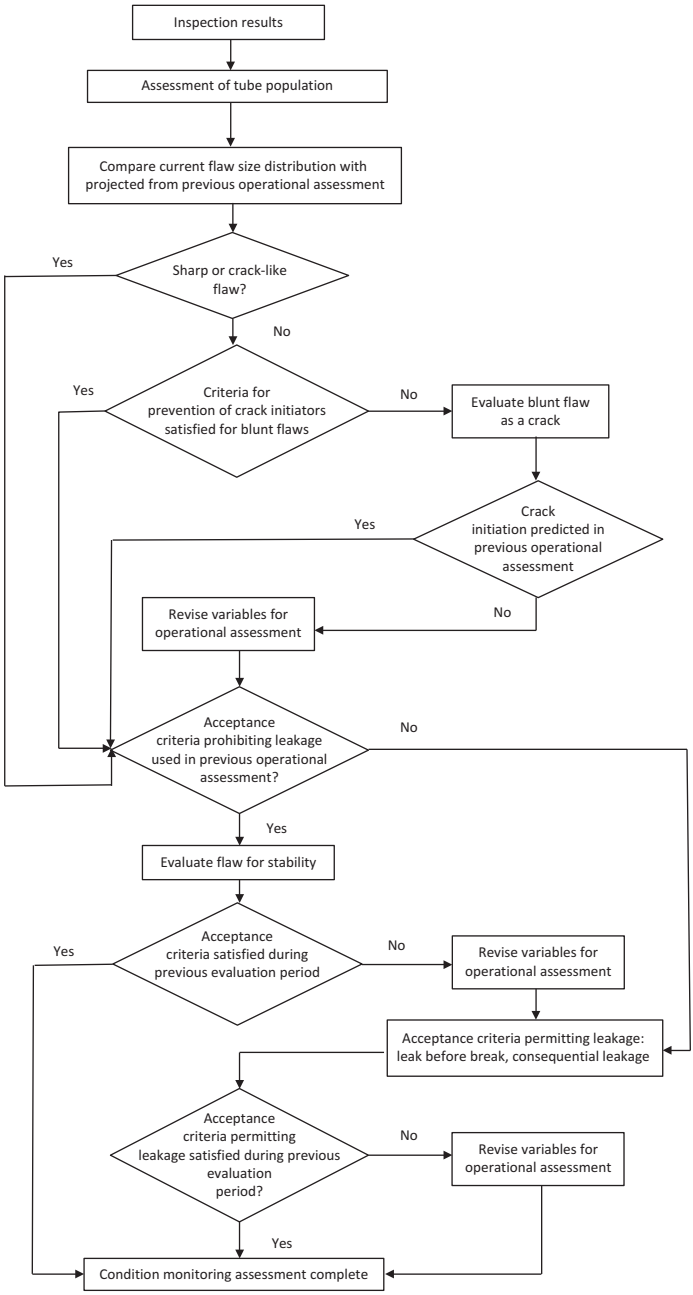

Fig. 17.1 Flow chart for condition monitoring assessments (CMAs) of flaws required by the CANDU fitness-for-service guidelines (Scarth et al., 1998).

for further detailed review of the large amount of inspection data gathered during an outage, there is a potential risk to the plant operator. Should the second stage detailed review identify additional indications that may not satisfy performance criteria for the planned operating interval, it may be necessary to shutdown the plant earlier than planned to carry out the necessary corrective actions.

17.4.3 Structural integrity models

The key to completion of the CMA and OA for steam generator inspection findings are the models used to predict degradation initiation and growth. Degradation modeling normally incorporates deterministic, statistical, or probabilistic modeling methods or combinations of these methods.

Deterministic modeling has traditionally been used for tube integrity evaluations and incorporates the use of bounding parameters representing tube geometry, material properties, NDE tool sizing error estimates, and maximum observed or measured growth rates. The simplest deterministic prediction model would take the form of:

$$\begin{aligned}\text{Flaw depth future outage} = {} & \text{flaw depth current outage} \\ & + \text{NDE tool sizing error} + (\text{annual flaw growth rate} \\ & \times \text{number of years to next outage})\end{aligned}$$

The predicted future flaw depth would be compared against the *MTFS* value for the specific degradation mechanism to determine if it is necessary to carry out a corrective action for the specific flaw. This type of calculation could be carried out for each detected flaw or it could simply be applied to the worst case flaw in the population. Corrective actions would be required for all flaws that do not meet the structural integrity criteria. If only the worst case flaw is analyzed and it does not pass the structural integrity criteria at the next outage, a corrective action (e.g., tube plugging) should be implemented to address the finding and then the next most significant flaw should be evaluated. The process should be repeated until all remaining tubes are assessed as acceptable at the time of the next inspection outage.

Through the use of bounding parameters, deterministic approaches can accumulate significant levels of conservatism. For instance, combining the largest measured NDE tool uncertainty and the fastest observed flaw growth rate in a population is likely to generate very conservative estimates of the population of flaw sizes at the next outage, since for the majority of the population of flaws, these worst case assumptions would not align in reality. The excess conservatism will generally ensure safe operation, but may impose unnecessary operational restrictions and result in a misrepresentation of the safety importance of a specific tube degradation issue, which could divert resources from more significant safety concerns.

When the data available for the input parameters in the tube integrity evaluations are limited, there are few options available but to use a deterministic approach. This is normally the case early in the life of a steam generator when operational experience is limited or when new forms of degradation are detected. Statistical analysis methods

can be used to reduce excess conservatism in deterministic models when more data are available. For instance, instead of using the largest observed NDE tool uncertainties or largest growth rates, 95% upper bound values may be used to reduce the level of conservatism. In order for this approach to be effective standard statistical analysis methods should be employed to verify that the available dataset is reasonably well modeled using a statistical distribution and the associated confidence level in the predicted parameters should be determined so that the confidence in the upper bound prediction is reasonably high. A discussion of statistical modeling methods, acceptable upper bound values, and acceptable confidence limits is beyond the scope of this chapter and should be agreed upon between the plant operator and the regulatory authority.

Statistical models may also be used to estimate the population of flaws in a population of tubes that have not been inspected, through extrapolation of data from the population of inspected tubes. While this approach will not confirm the structural integrity of the tubes that have not been inspected, it can provide insights with respect to the likelihood and expected level of operational or accident-induced leakage from the uninspected tubes. If the likelihood of unacceptable leakage is assessed to be high (the meaning of "high" should be established through regulatory requirements or expectations), then it would be prudent to expand the inspection program activities to capture more data from the uninspected tube population.

Fully probabilistic methods for tube integrity evaluations can, in theory, provide a more realistic assessment of the future condition of steam generator tubes with flaws. The most common approach to probabilistic modeling is the use of Monte Carlo (MC) simulation. Instead of using bounding values in the prediction of flaw growth, statistical distributions would be developed for input parameters that may vary (e.g., NDE, sizing error, and growth rate). Sampling techniques would be used to randomly select values from these distributions and calculations would be repeated for a large number of iterations to generate a distribution of possible flaw sizes at the next planned outage. This distribution would then be used to assess the probability of flaws exceeding structural integrity limits at the end of this evaluation period.

While probabilistic methods have the potential to provide evaluations of the most likely population of flaws in a steam generator at some future time and the resulting likelihood of tube failures, probabilistic modeling does pose challenges, particular when it comes to validation of the probability estimates for rare events. Furthermore, there is not yet a common industry-wide consensus on appropriate probabilistic acceptance criteria. Probabilistic approaches are often successfully adopted in the context of risk-informed decision making, which combines insights from expert judgment, deterministic assessments, and probability estimates in decision making.

A recent report, published by EPRI (Electric Power Research Institute, 2013) provided one approach to evaluate the probability of failure inherent in the design requirements of ASME Section III (American Society of Mechanical Engineers, 2015b) for Class 1 components which was prepared in support of a proposed Section XI (American Society of Mechanical Engineers, 2015a) code case that would be used to define NDE tool detection limits for cast austenitic stainless steel piping. The authors of that report (Electric Power Research Institute, 2013) suggested that the

Table 17.1 Recommended failure probability for each ASME Section III service level and probability of the service level occurring from the 2013 EPRI report (Electric Power Research Institute, 2013)

Service Level	Probability of Occurrence	Conditional Failure Probability
A	1.0	10^{-6}
B	0.1	10^{-5}
C	$<10^{-2}$	10^{-4}
D	$<10^{-2}$	10^{-4}

probability of failure inherent in the Section III design requirements should be equivalent to a value of 1×10^{-6}. They then went on to define the conditional probability of piping failure for each of the Service Level Loads A through D based upon the estimate probability of occurrence of the loading over the life of the plant. The results are presented in Table 17.1 (Electric Power Research Institute, 2013). This example provides one of the avenues of investigation currently underway in the nuclear industry to define probabilistic acceptance criteria applicable to structural integrity applications, but as of yet, there is no internationally agreed upon approach. Given challenges associated with model validation and the development of acceptance criteria, some regulatory jurisdictions do not accept the use of probabilistic methods. Other regulatory jurisdictions are open to the concept, but further work is required for implementation to address issues associated with model validation and the definition of acceptance criteria.

References

American Society of Mechanical Engineers, 2015a. Boiler and Pressure Vessel Code. Section XI, Rules for Inservice Inspection of Nuclear Power Plant Components. American Society of Mechanical Engineers, New York, NY.

American Society of Mechanical Engineers, 2015b. Boiler and Pressure Vessel Code. Section III, Rules for Construction of Nuclear Power Plant Components. American Society of Mechanical Engineers, New York, NY.

Canadian Standards Association, 2014. N285.4-14, Periodic inspection of CANDU nuclear power plant components. Canadian Standards Association, Toronto.

Electric Power Research Institute, 1991. PWR steam generator tube repair limits: technical support document for expansion zone PWSCC in roll transitions. Revision 1, EPRI NP-6864-l, Electric Power Research Institute, Palo Alto, CA December.

Electric Power Research Institute, 2008. Steam generator management program: steam generator integrity assessment guidelines. Revision 3, 1019038, Electric Power Research Institute, Palo Alto, CA. October.

Electric Power Research Institute, 2013. Technical report, Materials reliability program: technical basis for ASME Section XI Code Case on Flaw Tolerance of Cast Austenitic Stainless Steel (CASS) Piping, MRP-362. Electric Power Research Institute, Palo Alto, CA.

International Atomic Energy Agency, 2011. Assessment and management of ageing of major nuclear plant components important to safety: steam generators. IAEA-TECDOC-1668, International Atomic Energy Agency, Vienna. November.

Karwoski, K.J., 2009. Steam generator tube integrity requirements and operating experience in the United States. In: 6th CNS International Steam Generator Conference, Toronto, Canada, November 8–11.

Nuclear Energy Institute, 2011. NEI 97-06, Steam generator program guidelines. Revision 3, Nuclear Energy Institute, Washington, DC. January.

Pagan, S., Mills, B.E., Kozluk, M.J., 2006. Fitness-for-service assessment for steam generator tube fretting at darlington nuclear generating station. In: Proceedings from the American Society of Mechanical Engineers 2006 Pressure Vessels and Piping Conference, Vancouver.

Scarth, D.A., Kozluk, M.J., Cartar, E.E., Mirzai, M., Maruska, C., Nickerson, J.H., Graham, D.B., 1998. CANDU steam generator fitness-for-service guidelines. In: Proceedings From the Third International Steam Generator and Heat Exchanger Conference, Toronto, Canada, June.

TSTF-510, 2010. Revision 2, Revision to steam generator program inspection frequencies and tube sample selection, October 11 (NRC ADAMS accession no. ML110610350).

United States Nuclear Regulatory Commission, 1995. Generic letter 95-05, Voltage based repair criteria for Westinghouse steam generator tubes affected by outside diameter stress corrosion cracking. United States Nuclear Regulatory Commission, Rockville, MD. August 3.

This page intentionally left blank

Regulatory requirements and considerations for nuclear steam generators

18

E.L. Murphy
CONSULTANT, Gaithersburg, MD, USA

18.1 Introduction

Steam generator (SG) tubes comprise a substantial portion of the reactor coolant pressure boundary (RCPB) and also play a role in fission product containment. Their integrity is important to the safe operation of a pressurized-water reactor (PWR). As a result, regulatory authorities around the world have established requirements to ensure SG tube integrity is maintained. Section 18.2 of this chapter focuses on requirements in the United States (US). This chapter provides the background, rationale, and description of new, performance-based regulatory requirements for PWRs in the United States to ensure SG tube integrity. Section 18.3 of this chapter provides a description of regulatory practices and tubing inspection requirements in Canada.

18.2 Regulatory requirements and considerations for nuclear SGs in the United States

18.2.1 NRC regulations governing design and licensing basis

Title 10 of the Code of Federal Regulations (10 CFR) (CFR, n.d.) establishes the fundamental regulatory requirements for RCPB integrity, including the integrity of the SG tubes. Specifically, the General Design Criteria (GDC) in Appendix A to 10 CFR Part 50 state that the RCPB shall have "an extremely low probability of abnormal leakage…and gross rupture" (GDC 14), "shall be designed with sufficient margin" (GDC 15 and 31), shall be of "the highest quality standards possible" (GDC 30), and shall be designed to permit "periodic inspection and testing…to assess…structural and leak tight integrity" (GDC 32). To ensure RCPB integrity in accordance with these regulations, 10 CFR Part 50.55a, "Codes and Standards," requires that the RCPB be designed and constructed in accordance with the American Society of Mechanical Engineers Boiler and Pressure Vessel Code (ASME Code), Section III for Class 1 components (ASME III, n.d.). Also in accordance with 10 CFR 50.55a, the RCPB is subject to the inservice inspection requirements of the ASME Code, Section XI (ASME XI, n.d.).

Steam Generators for Nuclear Power Plants. http://dx.doi.org/10.1016/B978-0-08-100894-2.00020-0
© 2017 Elsevier Ltd. All rights reserved.

In the 1970s, Section XI requirements pertaining to inservice inspection of SG tubing were augmented by additional SG tube surveillance contained in the plant technical specifications (TS), which are part of the plant licensing bases. Today, programmatic requirements for ensuring SG tube integrity reside in exclusively in the technical specifications, as discussed in Sections 18.2.2 and 18.2.3.

As part of the plant licensing basis, applicants for PWR licenses are required to analyze the consequences of postulated design-basis accidents (DBAs), such as an SG tube rupture (SGTR) and main steam line break (MSLB). These analyses consider the primary-to-secondary leakage through the tubing that may occur during these events. The analyses must show that the offsite radiological consequences do not exceed the applicable limits of the guidelines for offsite doses in 10 CFR 50.67, "Accident Source Term," or 10 CFR Part 100, "Reactor Site Criteria"; GDC 19, "Control Room" (in 10 CFR Part 50, "Domestic Licensing of Production and Utilization Facilities," Appendix A, "General Design Criteria for Nuclear Power Plants") for control room operator doses; or some fraction thereof as appropriate to the accident, or the NRC-approved licensing basis (e.g., a small fraction of these limits).

18.2.2 Background: Evolution of current technical specification requirements

On Jan. 20, 2006, the NRC issued NRC Generic Letter 2006-01, "Steam Generator Tube Integrity and Associated Technical Specifications," stating that current plant TS requirements, dating back to initial licensing of each PWR, may not be sufficient to ensure that SG tube integrity can be maintained in accordance with the licensing and design basis. The Generic Letter requested all PWR licensees to provide information addressing the NRC staff's concerns, or adopt new TS requirements acceptable to the NRC that will ensure SG tube integrity.

The then-current standard TS requirements relating to SG tube integrity were developed in the 1970s. Although these requirements were intended to ensure SG tube integrity in accordance with the design and licensing bases, these requirements were prescriptive and operating experience had shown that these requirements, in and of themselves, did not necessarily ensure that facilities would meet the objective of ensuring SG tube integrity. For example, the required minimum tube inspection sample sizes and eddy current test flaw detection performance were sometimes insufficient to ensure the timely detection of flaws before the desired margins against burst and leak tightness were compromised. In addition, eddy current test measurement errors and flaw growth rates sometimes exceeded those considered in development of the tube-plugging criteria. Thus, the surveillance requirements alone did not necessarily ensure that the scope, frequency, and methods of inspection would be sufficient to confirm SG tube integrity.

In view of these shortcomings, licensees experiencing significant degradation problems frequently found it necessary to implement measures beyond minimum TS requirements to ensure the maintenance of adequate tube integrity. Until the 1990s, these measures tended to be ad hoc. In the meantime, the industry and the

NRC staff began initiatives to improve the effectiveness and consistency of the utility programs to ensure SG tube integrity. In 1997, the Nuclear Energy Institute (NEI) issued NEI 97-06, "Steam Generator Tube Integrity Guidelines" (Nuclear Energy Institute, 1997), which provided general, high-level guidelines for a programmatic, performance-based approach to ensuring SG tube integrity. NEI 97-06 references a number of detailed guideline documents from the Electric Power Research Institute for programmatic details concerning SG tube inspections, SG tube integrity assessment, in situ pressure testing, and monitoring of operational primary-to-secondary leakage (EPRI, 2007, 2008, 2011, 2012). The NEI 97-06 approach was inspired by and is similar to an approach developed by the NRC staff in a draft regulatory guide, "Steam Generator Tube Integrity," published as DG-1074 in December 1998 (US Nuclear Regulatory Commission, 1998a). All US PWR utilities committed to NEI to implement the NEI 97-06 initiative no later than the first refueling outage starting after January 1, 1999. Subsequent to the initial issuance of NEI 97-06, the NRC staff worked extensively with the industry to address issues associated with the industry initiative and to identify needed changes to the plant TS to ensure maintenance of tube integrity. These efforts culminated in agreement between the NRC staff and the industry on a generic template for new TS (TSTF, 2005; Federal Register, 2005) incorporating a programmatic, performance-based approach, which was in general alignment with NEI 97-06. NEI subsequently updated NEI 97-06 (Nuclear Energy Institute, 1997) with Revision 2 consistent with the TS generic template. The generic template changes have been incorporated in to the Revision 4 of the Standard Technical Specifications (Standard Technical Specifications, n.d.).

By 2007, new technical specifications in accordance with the generic template (TSTF, 2005) had been approved for all US PWRs. In Federal Register (2011), the NRC staff approved revisions to generic TS template addressing the industry's early implementation experience with the new TS. These revisions can generally be characterized as editorial corrections, changes, and clarifications intended to improve internal consistency, consistency with implementing industry documents, and usability without changing the intent of the requirements. These changes will be included in the next revision to the Standard Technical Specifications.

18.2.3 Technical specifications

The new TS contain three conditions (i.e., LCOs) that require plant shutdown if not met:

1. SG tube integrity shall be maintained.
2. All SG tubes satisfying the tube repair criteria (i.e., tubes with measured flaw sizes that exceed the tube repair criteria) shall be plugged in accordance with the SG Program.
3. Operational primary-to-secondary leakage shall not exceed 555 L/day (150 gal/day) through any one SG.

Condition 1 is a new requirement that makes maintaining tube integrity a direct requirement. It replaces the earlier LCO requirement (in original technical specifications) that the SGs are operable upon completion of specified tube surveillance

actions, which are not directly related to maintaining tube integrity. SG tube integrity shall be verified in accordance with the SG Program. Under the SG Program, as discussed in more detail in Section 18.2.4, tube integrity must be confirmed during each SG inservice inspection under the new requirements through a condition monitoring assessment, and the inspections are to be performed in a manner that ensures the maintenance of tube integrity until the next scheduled inspection.

Condition 2 is equivalent to the earlier requirement that the SGs are operable only after plugging of all tubes found by inspection to satisfy the tube-plugging limit. This condition is somewhat redundant if Condition 1 is met. However, it is included in the TS to ensure that if tubes satisfying the tube-plugging limit are inadvertently not plugged or repaired before plant restart in accordance with the SG Program, the utility will be required to do an analysis within a 7-day period to demonstrate that the affected tubes will maintain their integrity until the next scheduled inspection. If the utility cannot demonstrate this, then the plant must be shut down. If the affected tube is determined to maintain its integrity until the next scheduled inspection, the affected tube must be plugged prior to entering Mode 4 following the next refueling outage or SG tube inspection.

Condition 3 is similar to earlier leakage limit requirements, except with a reduced, more restrictive limit. Earlier limits typically included an 1850 L/day limit per SG and a 5328 L/day limit on total leakage in all SGs. Primary-to-secondary leakage is the only tube integrity indicator, albeit an indirect one, available to the operator while the plant is actually operating. Such leakage may be symptomatic of unanticipated tube degradation or it may indicate that previously identified degradation is proceeding at a rate higher than previously anticipated. Thus, Condition 3 is intended to complement.

Condition 1 providing additional assurance that tube integrity will be maintained. Condition 3 is also intended to ensure that operational primary-to-secondary leakage is maintained at values that ensure that primary-to-secondary leakage during DBAs will be less than is assumed in the licensing basis accident analyses. The accompanying surveillance requirement requires periodic verification that this LCO is met. The frequency of surveillance shall be every 72 h or in accordance with the utility's surveillance frequency control program.

18.2.4 Technical specifications: Steam generator program

The new TS require that an SG Program be established and implemented to ensure the maintenance of SG tube integrity. The TS do not provide specific details on how this objective is to be met; it is the licensee's responsibility to ensure that the program will meet the stated objective. Industry guidelines in NEI 97-06 (Nuclear Energy Institute, 1997) and other industry guidance referenced therein provide a resource to utilities for meeting this objective. However, the TS do define a general programmatic framework for the SG Program, which is discussed in the remainder of this chapter. The programmatic elements that must be included as part of the SG Program include the following:

- performance criteria for SG tube integrity
- provisions for condition monitoring

- provisions for tube repair criteria
- provisions for SG tube inspections
- provisions for monitoring primary-to-secondary leakage

Although the SG Program is fundamentally a performance-based approach for ensuring SG tube integrity, the program includes a number of prescriptive elements to minimize risk in the event of new or unexpected problems.

18.2.5 Steam generator performance criteria

The new TS require that SG tube integrity shall be maintained by meeting the performance criteria for tube structural integrity, accident-induced leakage, and operational leakage. The NRC staff's bases for evaluating the acceptability of these performance criteria are that meeting these criteria is sufficient to ensure that tube integrity is within the plant design and licensing bases and that meeting these criteria in conjunction with implementation of the SG Program ensures no significant increase in risk. The staff also evaluated these performance criteria in the context of the overall SG Program such that if the performance criteria are inadvertently exceeded, the consequences will be tolerable until the facility identifies and corrects the situation. In addition, the performance criteria must be expressed in terms of parameters that are directly or indirectly measurable.

18.2.5.1 Structural integrity performance criteria

The structural integrity criterion is as follows:

> *All inservice steam generator tubes shall retain structural integrity over the full range of normal operating conditions (including startup, operation in the power range, hot standby, and cool down), all anticipated transients included in the design specification, and design basis accidents. This includes maintaining a safety factor of 3.0 against burst under normal steady state full power operation primary-to-secondary pressure differential and a safety factor of 1.4 against burst applied to design basis accident primary-to-secondary pressure differentials. Apart from the above requirements, additional loading considerations associated with design basis accidents, or combination of accidents in accordance with the design and licensing basis, shall also be evaluated to determine if the associated loads contribute significantly to burst or collapse. In the assessment of tube integrity, those loads that do significantly affect burst or collapse shall be determined and assessed in combination with the loads due to differential pressure with a safety factor of 1.2 on the combined primary loads and 1.0 on axial secondary loads.*

The structural integrity performance criteria were developed to maintain consistency with the safety factors embodied in the then-current plant licensing bases, specifically, the safety factors embodied in the TS tube-plugging criteria. The tube-plugging criterion typically specified in plant TS was, and still is, 40% of the initial tube wall thickness. This criterion is typically applicable to all tubing flaws found by inspection, except for certain flaw types at certain locations for which less

restrictive, alternate plugging criteria may be applicable (as specified in the TS) and for certain sleeve repairs (also, as specified in the TS) for which a more restrictive tube repair criterion may be specified.

In 1976 the NRC staff prepared RG 1.121, "Basis for Plugging Degraded PWR Steam Generator Tubes," (NRC Regulatory Guide, 1976) describing an acceptable technical basis for the development of tube repair criteria. This RG is generally cited in licensee and industry documentation as the bases for the TS tube repair criterion in plant TS. The RG includes the following with respect to safety factors:

1. Degraded tubing should retain a factor of safety against burst of not less than three under normal operating conditions.
2. Degraded tubing should not be stressed beyond the elastic range of the tube material during the full range of normal reactor operation. The draft regulatory guide also states that loadings associated with normal plant conditions, including startup, operation in the power range, hot standby, and cool-down, that are included in the design specifications for the plant, should not produce a primary membrane stress in excess of the yield stress of the tube material at operating temperature.
3. Degraded tubes should maintain a margin of safety against tube failure under postulated accidents consistent with the margin of safety determined by the stress limits specified in NB-3225 of Section III of the ASME Code. Note, NB-3225 specifies that the rules in Appendix F of Section III may be used for evaluating these loadings.

The "safety factor of three" criterion stems from Section III of the ASME Code which, in part, limits primary membrane stress under design conditions to one-third of ultimate strength. The performance criteria would limit application of the "safety factor of three" criterion to those pressure loadings existing during normal full power, steady-state operating conditions. Differential pressures under this condition are plant specific, ranging from 1250 to 1500 psi. However, differential pressure loadings can be considerably higher during normal operating transients, ranging between 1600 and 2150 psi during plant heat-up and cool-down. Given a factor of safety equal to three under normal full power conditions, the factor of safety during heat-ups and cool-downs can be as low as about two. The industry stated in a white paper (Memorandum, 1999) that it was not the intent of the 40% depth-based tube-plugging criterion to ensure a factor of safety of three for operating transients such as heat-ups and cool-downs. The industry stated that maintaining a safety factor of three for such transients would lead to a tube-plugging criterion less than the standard 40% criterion for many plants. The NRC staff independently performed calculations that supported the industry's contention that applying the "safety factor of three" criterion to the full range of normal operating conditions would lead to a tube-plugging criterion more restrictive than the 40% criterion that the NRC staff has accepted since the 1970s. The NRC staff concluded that the "safety factor of three" criterion for application to normal full power, steady-state pressure differentials is consistent with the safety margins implicit in then-existing TS tube-plugging criteria and, thus, is consistent with the then-current, and still current licensing basis.

Item 2 above from RG 1.121 is often referred to as the "no yield" criterion. The purpose of this criterion is to prevent permanent deformation of the tube to assure that

degradation of the tube will not occur due to mechanical effects of the service condition. This is consistent with the ASME Code, Section III, stress limits, which serve to limit primary membrane stress to less than yield. The structural integrity criteria above do not explicitly include this "no yield" criterion. The industry stated in its white paper (Memorandum, 1999) that, if a tube satisfies the "safety factor of three" criterion at full power operating pressure differentials, the tube will generally satisfy the "no yield" criterion for the operating transient (e.g., heat-up and cool-down) pressure differentials. The white paper acknowledged that this may not be true for all plant-specific conditions and material properties. For this reason, the EPRI Steam Generator Integrity Assessment Guidelines (EPRI, 2008) state that, in addition to meeting the safety factor of three for normal steady-state operation, the integrity evaluation shall verify that the primary pressure stresses do not exceed the yield strength for the full range of normal operating conditions. The white paper, which has been incorporated as part of the EPRI Steam Generator Integrity Assessment Guidelines, recommends that this be demonstrated for each plant using plant-specific conditions and material properties.

The NRC staff agreed that the "no yield" criterion need not be specifically spelled out in the TS definition of the structural integrity criterion. The NRC staff found that the appropriate focus of the TS criteria should be on preventing burst. The NRC staff calculations confirmed that the proposed "safety factor of three" criterion bounds or comes close to bounding the "no yield" criterion for most of the cases investigated. This is not absolute, however. For once-through steam generators (OTSGs), the NRC staff noted a case where elastic hoop stress in a uniformly thinned tube could exceed the yield strength by 20% under heat-up and cool-down conditions and still satisfy the "safety factor of three" criterion against burst under normal steady-state, full power operating conditions. Such a tube would still retain a factor of safety of two against burst under heat-up and cool-down conditions. The amount of plastic strain induced would be limited to between 1% and 2% based on typical strain hardening characteristics of the material. This is quite small compared to cold working associated with fabrication of tube U-bends and tube expansions. Operating experience shows that this level of plastic strain (i.e., permanent strain caused by exceeding the yield stress) has not adversely affected the stress corrosion cracking resistance of OTSG tubing relative to that expected for nonplastically strained tubing. Thus, the NRC staff concluded that the "safety factor of three" criterion is sufficient to limit plastic strains to values that will not contribute significantly to degradation of the tubing and that the "no yield" criterion need not be specifically spelled out in the structural integrity performance criterion.

The safety factor of 1.4 against burst applied to design basis primary-to-secondary pressure differentials derived from the 0.7 times ultimate strength limit for primary membrane stress in the ASME Code, Appendix F, F-1331.1(a). This criterion is consistent with the stress limit criterion used to develop the standard 40% tube-plugging criterion in the TS and with the safety factor criteria used in the derivation of alternate tube repair criteria in plant TS, such as the voltage-based criterion for outer-diameter stress corrosion cracking. Thus, the criterion is consistent with the historical licensing basis.

Apart from differential pressure loadings, other types of loads may also contribute to burst. Examples of such loads include bending moments on the tubes due to flow induced vibration, earthquake, and loss-of-coolant accident (LOCA) rarefaction waves. For OTSGs, axial loads are induced in the tubes due to pressure loadings acting on the SG shell and tubesheets and due to differential thermal expansion between the tubes and the SG shell. Such nonpressure loads generally produce negligible primary stress during normal operating conditions from the standpoint of influencing burst pressure. In general, such nonpressure loads may be more significant under certain accident loadings depending on SG design, flaw location, and flaw orientation. Such nonpressure sources of primary stress under accident conditions were explicitly considered in the development of the 40% tube repair criterion relative to ASME Code, Appendix F, stress limits.

The above structural criterion requires that, apart from the safety-factor requirements applying to pressure loads, additional loads associated with DBAs, or combination of accidents in accordance with the design and licensing basis, shall also be evaluated to determine whether these loads contribute significantly to burst or collapse. Examples of such additional loads include bending moments during LOCA, MSLB, or safe shutdown earthquake (SSE) and axial, differential thermal loads. "Combination of accidents" refers to the fact that the design and licensing basis for many plants is that DBAs, such as LOCA and MSLB, are assumed to occur concurrently with SSE. Whereas "burst" is the failure mode of interest where primary-to-secondary pressure loads are dominant, "collapse" is a potential limiting failure mode (although an unlikely one, according to industry, based on a recent study (Memorandum, 2004)) for loads other than pressure loads. "Collapse" refers to the condition where the tube is not capable of resisting further applied loading without unlimited displacement. Although the occurrence of a collapsed tube or tubes would not necessarily lead to perforation of the tube wall, the consequences of tube collapse have not been analyzed and, thus, it is both appropriate and conservative to ensure that there is margin relative to such a condition.

Where nonpressure loads are determined to significantly contribute to burst or collapse, the structural criterion requires that such loads be determined and assessed in combination with the loads due to pressure with a safety factor of 1.2 on the combined primary loads and 1.0 safety factor on axial secondary loads. The 1.2 safety factor for combined primary loads was derived from the ratio of burst or collapse load divided by allowable load from Section III of the ASME Code for faulted conditions. Burst or collapse load was assumed to be equal to the material flow stress, assuming Code minimum yield and ultimate strength values and a flow stress coefficient of 0.5. Allowable load was determined from ASME Code, Section III, Appendix F, F-1331.3.a, which defines an allowable primary membrane plus bending load for service level d (faulted) conditions. The 1.0 safety factor for axial secondary loads goes beyond what is required by the design basis in Section III of the ASME Code, since Section III assumes that a one-time application of such a load cannot lead to burst or collapse. However, this is not necessarily the case for tubes with circumferential cracks. The safety factor criterion of 1.0 is conservative for loads that behave as secondary since it ignores the load relaxation effect associated with axial yielding before tube severance (burst) occurs.

Apart from being consistent with the current licensing basis, NRC risk studies at the time the new TS requirements were being evaluated indicated that maintaining the performance criteria safety factors is important to avoiding undue risk, particularly risk associated with severe accident scenarios involving a fully pressurized primary system and depressurized secondary system and where the tubes may heat to temperatures well above design basis values, significantly reducing the strength of the tubes (US Nuclear Regulatory Commission, 1998b).

Based on the above, the structural performance criteria are consistent with the margins of safety embodied in historical plant licensing bases. Exceeding these criteria is not likely to lead to consequences that are intolerable provided that such a condition is infrequent and that, if it occurs, it is promptly detected and corrected so as to ensure that risk is limited. Even if a tube should degrade to the point of rupture under normal operating conditions, such an occurrence is an analyzed condition with reasonable assurance that the radiological consequences will be acceptable. Finally, the structural performance criteria are expressed in terms of parameters that are measurable. Specifically, structural margins can be directly demonstrated through in situ pressure testing or can be calculated from burst prediction models using as input flaw size measurements obtained by inspection.

18.2.5.2 Accident leakage performance criteria

The accident-induced leak rate criterion is as follows:

> *The primary-to-secondary accident induced leakage rate for any design basis accident, other than a SG tube rupture, shall not exceed the leakage rate assumed in the accident analysis in terms of total leakage rate for all SGs and leakage rate for an individual SG. Leakage is not to exceed 3.7 liters/minute (1 gallon/minute) per SG.*

The performance criteria for accident-induced leak rate are consistent with leak rates assumed in the licensing basis accident analyses for purposes of demonstrating that the consequences of DBAs meet the limits in 10 CFR 100 for offsite doses, GDC 19 for control room operator doses, or some fraction thereof as appropriate to the accident, or the NRC-approved licensing basis (e.g., a small fraction of these limits). The criteria does not apply to design basis SGTR accidents for which leakage corresponding to a postulated double-ended rupture of a tube is assumed in the analysis. The criteria ensure that from the standpoint of accident-induced leakage, the plant will be operated within its analyzed condition.

For certain severe accident sequences involving high primary side pressure and a depressurized secondary system ("high-dry" condition), primary-to-secondary leakage may lead to more heating of the leaking tube than would be the case were it not leaking, thus increasing the potential for failure of that tube and a consequent large early release. The proposed (1.0 gpm) limit on total leakage from each SGs during DBAs (other than an SGTR) ensures that the potential for induced leakage during severe accidents will be maintained at a level that will not increase risk.

It is not likely that exceeding this criterion will lead to intolerable consequences provided that such an occurrence is infrequent and that such an occurrence, if it occurs, is promptly detected and corrected so as to ensure that risk is minimized. It should be noted that the criterion applies to leakage that could be induced by an accident in the unlikely event that such an accident occurs. Finally, the accident leakage performance criterion is expressed in terms of parameters that are measurable, both directly and indirectly. Specifically, structural margins can be directly demonstrated through in situ pressure testing or can be calculated using leakage prediction models using flaw size measurements obtained by inservice inspection as input.

18.2.5.3 Operational leakage performance criteria

The operational leakage performance criterion is equivalent to the TS LCO limit on operational primary-to-secondary leakage discussed earlier. Given the TS LCO limit, a separate performance criterion for operational leakage is unnecessary for ensuring prompt shutdown if the limit is exceeded. However, operational leakage is an indicator of tube integrity performance, although it is not a direct indicator. It is the only indicator that can be monitored while the plant is operating. Maintaining leakage within the limit provides added assurance that the plant is meeting structural and accident leakage performance criteria. However, even if within the TS LCO limit, operational leakage may also be an indicator of a new or unexpected condition (e.g., degradation mechanism, flaw grow rates) not anticipated by the operational assessment supporting the current operating interval. Inclusion of the TS leakage limit among the set of tube integrity performance criteria is appropriate from the standpoint of completeness of the performance criteria.

18.2.6 Condition monitoring assessment

The new TS require that the SG Program includes provisions for condition monitoring assessments as follows:

> *Condition monitoring assessment means an evaluation of the "as found" condition of the tubing with respect to the performance criteria for structural and accident induced leakage integrity. The "as found" condition refers to the condition of the tubing during a SG inspection outage, as determined from the inservice inspection results or by other means, prior to the plugging of tubes. Condition monitoring assessments shall be conducted during each outage during which the SG tubes are inspected or plugged to confirm that the performance criteria are being met.*

The requirement for condition monitoring assessments addresses an essential element of any performance-based strategy—the need to monitor performance relative to the performance criteria. Confirmation that the tube integrity criteria are met shows that the plant has achieved the overall programmatic goal of maintaining tube integrity to that point in time. However, failure to meet the tube integrity criteria indicates potential shortcomings in the effectiveness of the utility's SG Program and the need for refinements to the program to ensure the maintenance of tube integrity in the

future. Failure to meet either the structural or accident leakage performance criterion is reportable pursuant to 10 CFR 50.72 and 50.73 in accordance with guidelines in NUREG-1022, "Event Reporting Guidelines 10 CFR 50.72 and 50.73" (US Nuclear Regulatory Commission, 2000). Exceeding the LCO limit on operational primary-to-secondary leakage is similarly reportable. In addition, the NRC regional office would follow up on such a reportable occurrence as appropriate consistent with the NRC Reactor Oversight Program (US Nuclear Regulatory Commission, 2006) and the risk significance of the occurrence.

The technical specifications do not specify the methodologies for performing condition monitoring assessments. Detailed industry guidelines for performing these assessments are contained in the EPRI Tube Integrity Assessment Guidelines (EPRI, 2008), one of several implementing guideline documents referenced in the NEI 97-06 Tube Integrity Guidelines (Nuclear Energy Institute, 1997). These assessments are normally based on estimating remaining burst pressure margins and potential for accident-induced leakage based on evaluation of the eddy current inservice inspection results. These assessments consider eddy current test measurement uncertainties, tube material property variability, and burst pressure and leakage rate predictive model uncertainties to ensure that the condition monitoring assessment is conservative relative to the minimum burst pressure margins and maximum accident-induced leakage potential existing within the SGs. Under the industry integrity assessment guidelines, input parameter and predictive model uncertainties are treated such that the assessment can demonstrate that all tubes meet the tube integrity performance criteria with a probability of at least 0.95.

Condition monitoring assessments may also employ direct pressure tests of individual tubes (i.e., in situ pressure tests) found to contain significant flaws by the inservice eddy current test inspection. These direct pressure tests reduce much of the uncertainty associated with assessments based on the eddy current test results and are often performed when the assessment uncertainties based on the eddy current test results leads to ambiguity as to whether the performance criteria are met or not. Detailed industry guidelines for performing in situ pressure tests are contained in the EPRI Steam Generator In-Situ Test Guidelines (EPRI, 2012), referenced in the NEI 97-06 Tube Integrity Guidelines (Nuclear Energy Institute, 1997).

As will be discussed in Section 18.2.8, operational assessments are conducted to demonstrate that all tubes remaining in service will continue to meet the tube integrity performance criteria until the next scheduled inspection. The results of the condition monitoring assessment performed at that next inspection present the opportunity for refining ("calibrating") the operational assessment methodologies to ensure that they continue to be conservative going forward.

18.2.7 Tube-plugging criteria (i.e., plugging limits)

The new TS retained the TS tube-plugging criteria contained in the old TS requirements. The TS require that tubes found by inspection to contain flaws exceeding these criteria be plugged. These criteria always include a depth-based criterion, typically 40% of nominal tube wall thickness (depending on the plant). The depth-based

criterion at each plant was developed in accordance with NRC Regulatory Guide 1.121 (NRC Regulatory Guide, 1976), and therefore is fully consistent with the tube integrity performance criteria in that flaws not exceeding the tube-plugging criterion satisfy the performance criteria. In addition, the criterion provides an allowance for flaw size measurement error and incremental crack growth between inspections.

The plugging criterion is prescriptive rather than performance based. It supplements the performance-based requirement that the frequency, scope, and methods of inspection must be such as to ensure that the tube integrity performance criteria are satisfied until the next scheduled SG inspection. Utilities sometimes do find it necessary (e.g., if flaw growth rates are unusually high) to plug tubes with flaw depths less than the specified plugging criterion in order to demonstrate by operational assessment that the tube integrity performance criteria will be maintained during this period.

The standard 40% depth-based criterion was developed based on the conservative assumption that the flaw is a uniform thinning of the tube wall over a significant length of the tube. Actual flaws tend to be less damaging for a given depth of penetration than such uniform thinning flaws since they are often more localized in terms of their axial and circumferential extent and/or because the flawed portion of tube may be contained within the tube support plate or tubesheet penetrations preventing an axial burst failure mode. Therefore, the NRC staff has approved on a plant-specific basis a number of "alternate plugging criteria," each applicable to specific flaw types at specific locations. Such alternate criteria can significantly reduce the number of tubes that must be plugged during a given inspection outage and can extend the useful life of the SGs, yet at the same time ensuring that the aforementioned performance criteria will continue to be met.

18.2.8 Inservice inspection

The new TS require that the SG Program includes periodic tube inspections. These TS require that the number and portions of tubes inspected and method of inspection be chosen with the objective of detecting flaws of any type (e.g., volumetric flaws and axial and circumferential cracks) that may be present along the length of the tube, from the tube-to-tubesheet weld at the tube inlet to the tube-to-tubesheet weld at the tube outlet, and that may exceed the applicable tube-plugging criteria. The EPRI Steam Generator Examination Guidelines (EPRI, 2007) provide detailed guidance on how to satisfy this requirement. These guidelines address topical areas such as qualification/performance demonstration of eddy current test techniques (test equipment, coils, and test procedures), personnel (data acquisition and analysis), and automated data analyses for each application (i.e., each degradation type and location) and quality control and quality assurance. To determine which inspection methods should be used and at what locations, the new TS require a degradation assessment to determine the type and location of flaws to which the tubes may be susceptible. Considerations for performing a degradation assessment include, but are not limited to past degradation experience in the subject SGs and SGs of similar design and materials at other plants, accumulated operating time of the SGs, and abnormal occurrences at the subject plant (e.g., water chemistry transients or loose parts occurrences) which may have led to

tube damage. EPRI (2007, 2008) provide industry guidance for performing degradation assessments.

The proposed specification specifically excludes the tubesheet welds and the tube ends beyond the welds from the inspection requirements therein. The NRC staff found this to be consistent with current actual practice and to be acceptable. The tube ends beyond the tube-to-tubesheet welds are not part of the primary pressure boundary.

The new TS include a new performance-based requirement that the scope, methods, and frequency of the inspection ensure the maintenance of SG tube integrity until the next inspection. This is a performance-based requirement that complements the requirement for condition monitoring from the standpoint of ensuring that tube integrity is maintained. The requirement for condition monitoring is backward looking in that it is intended to confirm that tube integrity has been maintained up to the time the assessment is performed. The inspection requirement, by contrast, is forward looking as it is intended to ensure that tube inspections, in conjunction with plugging of tubes, are performed so as to ensure that the plant will continue to meet the performance criteria until the next scheduled SG inspection. Tube inspections would be followed again by condition monitoring at the next SG inspection to confirm that the performance criteria were in fact met, and so on.

The TS bases and the EPRI Steam Generator Integrity Assessment Guidelines (EPRI, 2008) term these forward-looking assessments as "operational assessments." EPRI (2008) guidelines provide detailed guidance for performing operational assessments. Considerations for performing these assessments include the active degradation mechanisms affecting the SGs, the locations within the SGs where these mechanisms are active, the number and size of flaw indications for each degradation mechanism, tubes with flaw indications being removed from service by plugging and tubes with indications that will remain in service until the next scheduled inspection, the flaw growth rate distributions associated with each degradation mechanism, inspection system (technique and personnel) detection and sizing performance for each degradation mechanism, burst pressure and leak rate uncertainties associated with predictive models, and tube material property variability. Under the industry guidelines, input parameter and predictive model uncertainties are treated such that the assessment can demonstrate that all tubes will meet the tube integrity performance criteria at the time of the next scheduled inspection with a probability of at least 0.95.

It should be noted, however, that any assessment or projection of the future condition of the SG tubing based on the existing condition of the tubing and anticipated flaw growth rates can involve significant uncertainty that may be difficult to conservatively and reliably bound or to statistically model in all cases. For this reason, the new TS supplement the performance-based requirement concerning inspection frequencies with a set of prescriptive requirements adding assurance that tube integrity will be maintained. The new prescriptive requirements include the following:

- Inspect 100% of the tubes in each SG during the first refueling outage following SG installation.

  Operating experience has demonstrated that tube degradation mechanisms may initiate as early as the first operating cycle following SG installation. Although most SGs installed at

US plants over the past 25 years have tubing more resistant to stress corrosion cracking than the alloy 600 mill-annealed (MA) tubing in SG installed during the previous era, tube wear from vibration against the tube supports has continued to occur during the first operating cycle in SGs with alloy 600 thermally treated (TT) and alloy 690 TT tubing. Thus, inspections at the first refueling outage are necessary to trend the appearance of flaw indications and their growth rates as input to the operational assessment to ensure that the tube integrity performance criteria will continue to be met until the next scheduled inspection.

- For SGs with alloy 600 MA tubes: After the first refueling outage following SG installation, inspect each SG at least every 24 effective full power months or at least every refueling outage (whichever results in more frequent inspections).
- For SGs with alloy 600 TT tubes: After the first refueling outage following SG installation, inspect each SG at least every 48 effective full power months or at least every other refueling outage (whichever results in more frequent inspections).
- For SGs with alloy 690 TT tubes: After the first refueling outage following SG installation, inspect each SG at least every 72 effective full power months or at least every third refueling outage (whichever results in more frequent inspections).
- For SGs with alloy 600 TT or 690 TT tubes: If crack indications are found in any SG tube, then the next inspection for each affected and potentially affected SG for the degradation mechanism that caused the crack indication shall not exceed 24 effective full power months or one refueling outage (whichever results in more frequent inspections).

The above-mentioned prescriptive requirements for inspection frequency are based on qualitative engineering considerations and experience with stress corrosion cracking. Operating experience has shown that stress corrosion cracking can initiate in alloy 600 MA tubes during the first operating cycle following SG installation and that inspections every 24 months or one refueling cycle are needed to adequately manage tube integrity between inspections. US experience shows that alloy 600 TT tubes may initiate stress corrosion cracks, but generally only after several operating cycles. Alloy 690 TT tubes have been in service for as many as 25 years to date with no reported incidents of stress corrosion cracking. Thus, the 2- and 3-fuel cycle limitations on inspection frequency for alloy 600 TT and alloy 690 TT tubes, respectively, reflect their improved resistance to stress corrosion cracking compared to that of alloy 600 mill-annealed tubing. As previously discussed, operation for 1, 2, or 3 operating cycles between inspections is subject to all tubes being able to meet the performance criteria at the time of the next scheduled inspection.

The new TS also define minimum tube inspection sample sizes. The TS define "inspection periods" over which 100% of the tubing must be inspected. Inspection periods consist of successive multiple inspections as follows:

- For SGs with alloy 600 MA tubes: Inspect 100% of the tubes at sequential periods of 60 effective full power months beginning after the first refueling outage inspection following SG installation.
- For SGs with alloy 600 TT tubes: After the first refueling outage following SG installation, inspect 100% of the tubes during the next 120 effective full power months. This constitutes the first inspection period. During the next 96 effective full power months, inspect 100% of the tubes. This constitutes the second inspection period. During the remaining life of the SGs, inspect 100% of the tubes every 72 effective full power months. This constitutes the third and subsequent inspection periods.

- For SGs with alloy 690 TT tubes: After the first refueling outage following SG installation, inspect 100% of the tubes during the next 144 effective full power months. This constitutes the first inspection period. During the next 120 effective full power months, inspect 100% of the tubes. This constitutes the second inspection period. During the next 96 effective full power months, inspect 100% of the tubes. This constitutes the third inspection period. During the remaining life of the SGs, inspect 100% of the tubes every 72 effective full power months. This constitutes the fourth and subsequent inspection periods
- Each inspection period defined earlier may be extended up to 3 effective full power months to include an SG inspection outage in an inspection period and the subsequent inspection period begins at the conclusion of the included SG inspection outage.
- The minimum number of tubes inspected at each scheduled inspection shall be the number of tubes in all SGs divided by the number of SG inspection outages scheduled in each inspection period.

The requirements also reflect the increase in the potential for cracking with increasing time in service and the particular challenges associated with the management of stress corrosion cracking with respect to satisfying the tube integrity performance criteria.

18.2.9 Provisions for monitoring primary-to-secondary leakage

The new TS require that the SG Program includes provisions for monitoring primary-to-secondary leakage. However, the SG Program requirements in the TS do not include specific requirements in this regard. As discussed in Section 18.2.3, the TS include an LCO limit that operational primary-to-secondary leakage shall not exceed 555 L/day (150 gal/day) through any one SG. The accompanying surveillance requirement requires periodic verification that this LCO is met, but does not specify the specific methodology to be employed to perform the verification. The frequency of surveillance shall be every 72 h or in accordance with the utility's surveillance frequency control program.

There are a variety of approaches available for monitoring primary-to-secondary leakage and for verifying that the LCO limit is met and the NRC staff concluded that there was no need to tie the surveillance to a specific approach. The TS bases states that the primary-to-secondary leakage measurement uses continuous process radiation monitors or radio chemical grab sampling. The EPRI PWR Primary to Secondary Leakage Guidelines (EPRI, 2011) provide extensive, detailed guidance for developing monitoring programs that will provide for effective and timely monitoring.

18.2.10 Performance trends: Steam generator tube integrity

Although the new TS requirements have only been in place since 2005–07, depending on the plant, all PWR licensees have been implementing the basic performance-based elements of these requirements since 1999–2000 following their commitment to the industry's NEI 97-06 initiative. The NEI 97-06 initiative was an evolutionary change in licensee programs for ensuring tube integrity since the effectiveness of these programs have been constantly evolving and improving since the 1970s. Industry guidelines relating to secondary water chemistry control and inservice inspection have been

available since this period and have been frequently updated to reflect research findings, technology developments, and operating experience. In the late 1980s, licensees became sensitized to the need to monitor operational primary-to-secondary leakage on as close to a real-time basis as possible to provide added assurance of plant shutdown before rupture of a leaking tube. Industry guidelines for monitoring and responding to operational primary-to-secondary leakage have been available since the mid-1990s. Another trend dating to the 1970s was an ever-increasing awareness among licensees of the need for their SG programs to address tube integrity in addition to satisfying TS surveillance requirements. Industry guidelines for tube integrity assessment became available in the mid-1990s and led to improved consistency, rigor, and completeness of licensee tube integrity assessments.

In parallel with these SG programmatic improvements, tube integrity reliability appears to have improved significantly since the 1970s. This is evidenced by the sharply declining trends in frequency of forced shutdowns due to SG leakage, as shown in Fig. 18.1, and in SGTR frequency, as shown in Fig. 18.2. The forced outage data in Fig. 18.1 were developed from industry data in Steam Generator Progress Report (2000) (which covers forced outages through 1999) and from unpublished NRC staff data for forced outages after 1999. The SGTR data in Fig. 18.2 were compiled from NUREG/CR-6365 (1996) and also include the SGTR event at Indian Point 2 in 2000 (NRC Special Inspection Report, 2000), which occurred after publication of NUREG/CR-6365 (1996). The use of tubing that is more resistant to stress corrosion cracking (i.e., TT alloy 600 and 690 tubing in lieu of MA alloy 600 tubing used in SGs manufactured through the late 1970s) in new (post-1970s) and replacement SGs has been responsible for some of this improvement as is indicated in these figures. However, as also can be seen in these figures, even plants with alloy 600 MA tubing have experienced sharply improved performance trends in forced outage and SGTR

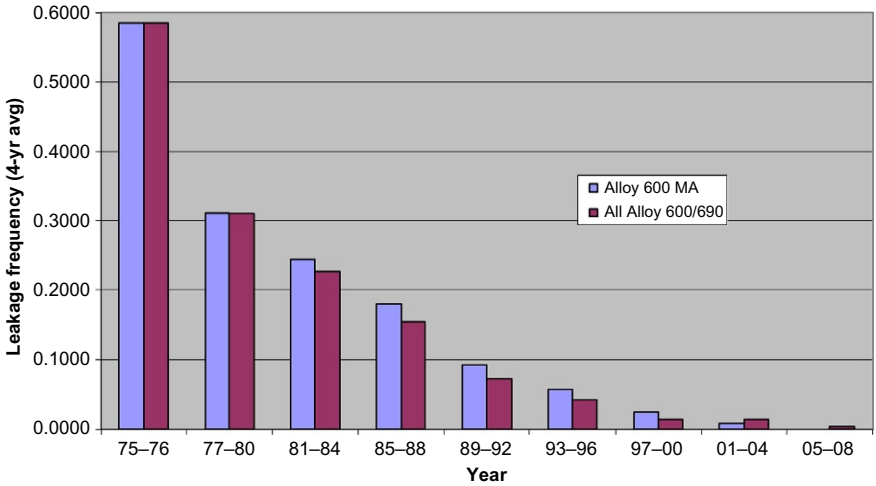

Fig. 18.1 Forced outage frequency due to SG leakage.

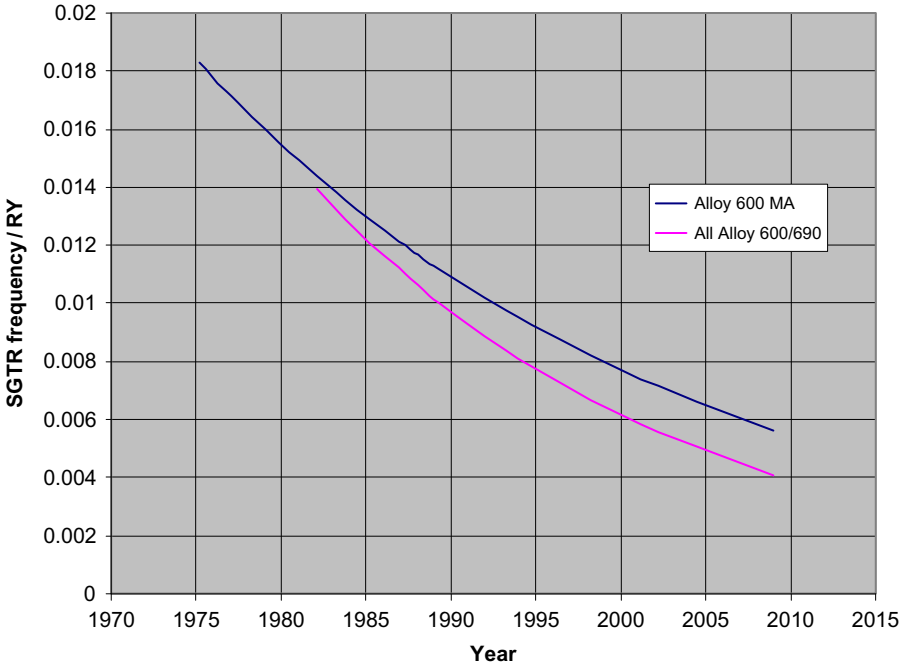

Fig. 18.2 SGTR frequency.

frequencies. The improving trends for the plants with alloy 600 MA tubing are due to a variety of factors relating to tube integrity management programs. These include more effective secondary water chemistry programs and steps taken to control copper and impurity ingress from the feed system. These improvements in water chemistry programs, however, are not the only reason for the improving tube integrity trends since even with the improved water chemistry programs plants with alloy 600 MA tubing have continued to experience extensive degradation, including stress corrosion cracking. As a result, it is clear that improved, more effective inspection programs and tube integrity management have played very important roles in reducing the frequency of forced outages due to SG leakage and SGTRs.

18.3 Regulatory practices and tubing inspection requirements in Canada

The Canadian regulatory requirement governing fitness-for-service assessment for SG tubes and internals (tube supports) is given in the Canadian Standards Association Standard CSA-N285.4, "*Periodic Inspection of CANDU Nuclear Power Plant Components*." The Canadian Standard, CAN/CSA N285.4-09, requires a baseline inspection of 25% of the tubes in each SG after the SG is first installed, but prior

to service. For periodic inspection, there are requirements for volumetric inspection of tubing as follows:

(a) Periodic inspection sample size and extent
The licensee shall
- **(i)** select tubes for inspection from a minimum of 25% of the SGs in a specific unit;
- **(ii)** perform at least one periodic inspection of all SGs by the end of the fourth interval;
- **(iii)** inspect a minimum of 10% of the tubes in the SG(s) selected for periodic inspection during that interval;
- **(iv)** for the random sample, inspect a minimum of 5% of the tubes in each SG of the periodic sample in item (a); and
- **(v)** for the specific sample, inspect a minimum sample of 25 tubes for each specific mechanism that is both postulated and plausible from the degradation assessment.

(b) The random and specific samples require inspection of the full length of the tubes except for the specific sample, where a postulated and plausible degradation mechanism is only applicable to certain sections of the tube then only such sections require inspection.

The licensee shall perform periodic inspections in accordance with the time intervals defined as follows:

Inspection interval[a]	Year since first net power date
Baseline	Preservice
1	4–6
2	10–12
3	16–18
4	22–24
5	28–30

[a]Interval 1 runs from the first day after 3 years of operation to the last day of the sixth year of operation, providing a 3-year window to perform the required inspections.

The standard also allows amended (increased) intervals, when a reactor has been operating derated (including outages) for extended periods of times, if justified and accepted by the regulator. The Canadian Standard requires that the specific sample inspection shall focus on those tubes in regions considered to be at higher risk of inservice degradation, using an inspection method appropriate for the particular degradation mechanism. This may require the use of alternative NDE techniques to detect degradation not readily detected by the standard bobbin coil eddy current inspection technique. Alternative NDE techniques may include the use of specialized eddy current probes such as transmit-receive Cecco probes, motorized rotating pancake coil probes, and transmit-receive X-probes and/or ultrasonic probes.

The Canadian Standard also requires that a section of one tube be removed from one SG for metallurgical examination once every 5 years. This applies to the lead unit in a multiunit station. The results of these periodic destructive examinations are to be used to calibrate the nondestructive examination techniques.

The inspection discussed earlier describes the minimum requirements for Canadian reactors. In practice, the licensees exceed these requirements and prepare specific programs of inspection suited to the individual sites depending on the active and plausible SG degradation mechanisms and life cycle management strategies.

The CSA standard requires disposition of detected volumetric indications predicted to exceed 40% of the SG tube nominal wall thickness before the next inspection and of observations from visual inspections of internals (tube supports) that do not satisfy the acceptance criteria. Indications that do not comply with the acceptance criteria are acceptable provided it has been demonstrated to the regulatory authority that the integrity of the tube(s) or supports are predicted to be adequate at the end of the next inspection interval. The SG and preheater tube fitness-for-service guidelines (FFSG) (COG Report, 2008) provide a method of satisfying the disposition requirements of CSA-N285.4 using inspection results in conjunction with representative, postulated distributions of flaws in the uninspected tubes in the area(s) at risk in each SG to perform an assessment of the condition of all SG tubes. The FFSG do not specify inspection requirements, however, when assessments are performed in accordance with the FFSG; the assessment results may influence inspection requirements beyond the minimum periodic inspection levels specified by CSA N285.4. The FFSG were first developed by Ontario Power Generation (OPG) and submitted to the Canadian Nuclear Safety Commission (CNSC) for trial use in 1999 (Scarth et al., 1998). Since 1999, the FFSG have been revised to consider licensees operating experience and suggestions received from the regulator, to include applicable clauses from the 2005 revision of the CSA N285.4 standard (N285.4-05), and to document them as an industry document, a CANDU Owners Group (COG) report (COG Report, 2008).

The main objectives of the SG and preheater tube FFSG are to provide reasonable assurance that tube structural integrity is maintained, and to provide reasonable assurance that there are adequate margins between estimated accumulated dose and applicable site dose limits. The FFSG provide standard acceptance criteria and evaluation procedures for assessing the condition of SG tubes in terms of tube structural integrity, operational leak rate, and consequential leakage during an upset or accident event. The FFSG require the use of current inspection results to assess fitness for service over the previous operating period (i.e., must pass current and backward-looking condition monitoring assessment) and also for the next future operating interval (i.e., provide forward-looking operational assessment).

Acceptance criteria for degraded tubes in the FFSG are based on the concept of safety-related performance criteria that require that tube structural integrity, with required safety factors, is maintained during the evaluation period, that the operational leak rate is monitored and does not exceed the allowable limit, and that consequential leakage during upset or accident events is acceptable in terms of estimated accumulated dose versus applicable site dose limits.

Due to the presence of tritium in the primary coolant of CANDU plants, low levels of primary-to-secondary leakage (e.g., <1 kg/h) during normal operation can be reliably detected in Canadian plants. The operational leak rate limit requiring shutdown is plant specific but typical values are in the range of 10–20 kg/h.

Two different sets of acceptance criteria for tubing structural integrity and consequential leakage are used in the FFSG.

Acceptance Criteria Prohibiting Leakage requires safety factors on load against through-wall penetration of the flaw for all loading events, where through-wall penetration is considered as ligament failure or "pop-through" of the remaining ligament but does not necessarily lead to tube rupture or burst. The specified safety factors on primary stress in the FFSG range from a value of 3 for Service Level A loads to a value of 1.5 for Service Level D loads. The specified safety factors on secondary stress in the FFSG range from a value of 1.0–1.5 depending upon the characterized depth of the flaw. Therefore, there will be no leakage when these acceptance criteria are satisfied. The Maximum Tolerable Flaw Size (MTFS) is the acceptance standard associated with this *Acceptance Criteria Prohibiting Leakage*. The MTFS defines the maximum size of the part-through-wall flaw that satisfies the acceptance criteria for flaw stability using the specified safety factors on load.

Acceptance Criteria Permitting Leakage allows leakage during one or more loading events provided a leak before break assessment demonstrates that specified safety factors on load against tube rupture (burst) and radiological releases during upset and accident events are maintained. The flaw at risk of leaking (FAROL) is the acceptance standard associated with this *Acceptance Criteria Permitting Leakage*. The FAROL limit is the depth of flaw at the onset of through-wall penetration and is equal to the maximum size of part-through-wall flaw that satisfies the acceptance criteria for flaw stability using a safety factor on load equal to 1.0. Total consequential leakage for all flaws (and all mechanisms) with depth predicted to exceed FAROL must be demonstrated to be acceptable versus the allowable consequential leakage limit established by site-specific dose limits. An additional defense-in-depth requirement imposed by the use the *Acceptance Criteria Permitting Leakage* is that the radiological consequences associated with a consequential tube rupture during the most limiting upset or accident event must be demonstrated to be within the site-specific dose limits.

Acceptance Criteria Prohibiting Leakage has more stringent structural requirements (large safety margin) than *Acceptance Criteria Permitting Leakage*. The general practice in Canada is to apply the MTFS for longer flaws for which the requirement on consequential leakage is limiting. FAROL is applied for shorter flaws provided that adequate margin is demonstrated to exist between the estimated total accumulated dose associated with consequential leakage during all upset and accident.

Reference Kozluk et al. (2002) provides the technical basis for the minimum required safety factors specified in the FFSG as well as for the nonmandatory surface flaw models provided in the FFSG to establish the MTFS and FAROL acceptance standards. Reference Kozluk et al. (2002) used the initial results of OPG's Steam Generator Tube Testing Project (SGTTP) to validate that these surface flaw models conservatively predict ligament failure for different tube sizes, different tube materials, and a wide range of flaw morphologies. As of 2009, the total number of tests conducted under OPG's SGTTP is close to 400 (Pagan et al., 2009); see Kozluk et al. (2002, 2006), Pagan et al. (2007, 2009), and Duan et al. (2008) for the various defect geometries, descriptions of the types of tests, and results for tests performed in the SGTTP. Surveillance tubes are periodically removed from the CANDU SGs. These

are done to meet the requirements of the CSA N285.4 standard; to characterize observed degradation; to validate nondestructive examination (NDE) inspection techniques; and in some cases to support fitness-for-service assessments (Pagan et al., 2009).

When degradation is detected, the FFSG require a series of mandatory, consecutive periodic assessments of the SG tubes to be performed to demonstrate compliance with the acceptance criteria. The tubes are assessed for operation over an evaluation period, which may be the time interval between the current tube inspection and the next schedule inspection. The periodic assessments include four main elements as follows:

- Evaluation of detected flaws and localized tube deformation. The FFSG provide procedures for determining the criteria that is used to assess whether a tube must be repaired, such as plugging.
- Condition monitoring assessment (CMA). This is a current and backward-looking assessment of the entire population of tubes. The CMA evaluates whether the acceptance criteria had been satisfied during the previous evaluation period.
- Operational assessment (OA). This is a forward-looking assessment of the entire population of tubes. The OA considers the projected future condition of the tubes based on the inspection results, NDE uncertainty and the predicted flaw growth rates to the end of the evaluation period.
- Assessment of condition causing leakage (ACCL). If a reactor unit had primary-to-secondary side leakage, an ACCL is performed. The degradation causing the through-wall flaw is assessed in terms of the potential effect on the entire population of SG tubes.

References

ASME III, n.d. Boiler and Pressure Vessel Code (ASME Code), Section III. Nuclear Power Plant Components.

ASME XI, n.d. Boiler and Pressure Vessel Code (ASME Code), Section XI. Rules for Inservice Inspection of Nuclear Power Plant Components.

CFR, n.d. Title 10 of the Code of Federal Regulations. Energy.

COG Report, 2008. Fitness-For-Service Guidelines for Steam Generator and Preheater Tubes, Section I: Evaluation Procedures and Acceptance Criteria, COG Report, COG-07–4089, August 2008.

Duan, X., Kozluk, M.J., Pagan, S., Mills, E., 2008. Structural integrity assessment of steam generator tube by the use of heterogeneous finite element method. J. Press. Vessel. Technol. 130.

Electrical Power Research Institute (EPRI), 2008. Steam Generator Management Program: Steam Generator Integrity Assessment Guidelines: Report No. 1019038. Revision 3, dated October 2008. (NRC ADAMS Accession No. ML100480243 for non-proprietary version only).

EPRI, 2007. Steam Generator Management Program: Pressurized Water Reactor Steam Generator Examination Guidelines: Report No. 1013706. Revision 7, dated October 2007 (NRC ADAMS Accession No. ML080450582 for non-proprietary version only).

EPRI, 2011. Steam Generator Management Program: PWR Primary-to-Secondary Leak Guidelines: Report No. 1022832. Revision 4, dated November 2011. (NRC ADAMS Accession No. ML12065A095 for non-proprietary version only).

EPRI, 2012. Steam Generator Management Program: Steam Generator In Situ Pressure Test Guidelines: Report No. 1025132NP. Revision 4, dated October 2012. (NRC ADAMS Accession No. ML12341A303 for non-proprietary version only).

Federal Register, 2005. Notice of Availability of Model Application Concerning Technical Specification; Improvement to Modify Requirements Regarding Steam Generator Tube Integrity; Using the Consolidated Line Item Improvement Process, vol. 70, p. 24126, dated May 6, 2005.

Federal Register, 2011. Notice of Availability of Models for Plant-Specific Adoption of Technical Specifications Task Force Traveler TSTF-510, Revision 2. Revision to Steam Generator Program Inspection Frequencies and Tube Sample Selection, vol. 76, p. 66763, dated October 26, 2011.

Kozluk, M.J., Scarth, D.A., Graham, D.B., 2002. Technical basis for the CANDU steam generator tube fitness-for-service guidelines. In: Proceedings of the 4th Canadian Nuclear Society International Steam Generator Conference, paper 6-4.

Kozluk, M., Mills, B., Pagan, S., 2006. Darlington steam generator tube fretting fitness-for-service: operating experience and structural and leak rate tests. In: Proceedings of the 5th CNS International Steam Generator Conference, Session 3-A.

Memorandum, 1999. Memorandum dated September 8, 1999, to W.H. Bateman, Chief, EMCB, NRR, NRC from J. W. Anderson, EMCB, NRR, NRC. Summary of August 27, 1999, Senior Management Meeting with NEI/EPRI/Industry to Discuss Issues Involving Implementation of NEI 97-06. This memorandum encloses Industry White Paper entitled, "Deterministic Structural Performance Criterion Pressure Loading Definition."

Memorandum, 2004. Memorandum dated May 19, 2004, from J.L. Birmingham, Project Manager, NRR, NRC to Cathy Haney, Program Director, Policy and Rulemaking Program, Division of Regulatory Improvement Programs, NRR, NRC. Summary of May 14, 2004 Meeting With Nuclear Energy Institute (NEI) on Status of Steam Generator Structural Integrity Performance Criteria, ADAMS Accession No. ML041540500.

NRC Regulatory Guide 1.121, 1976. Bases for Plugging Degraded PWR Steam Generator Tubes, August 1976.

NRC Special Inspection Report, 2000. Letter from W. Lanning (NRC) to A. Blind (Consolidated Edison Company). NRC Special Inspection Report—Indian Point Unit 2 Steam Generator Failure. Report No. 05000247/2000-10. (ADAMS Accession No. ML003746339), dated August 31, 2000.

Nuclear Energy Institute, 1997. Steam Generator Program Guidelines, NEI 97-06 (Original), December 1997 (NRC ADAMS Accession No. 9801050189), Revision 2, May 2005 (NRC ADAMS Accession No. ML052640257), and Revision 3, January 2011 (NRC ADAMS Accession No. ML111310708).

NUREG/CR-6365, 1996. Steam Generator Tube Failures, dated April 1996.

Pagan, S., Lehockey, E.M., Duan, X., Kozluk, M.J., Camacho, F., 2007. Assessment of crack-like flaw in ex-service Monel 400 steam generator tube removed from Pickering Unit 4 steam generator 12. In: Second International Symposium on Nuclear Power Plant Life Management, Shanghai, China, 15–18, October 2007. Paper Number IAEA-CN-155-077.

Pagan, S., Duan, X., Kozluk, M., Mills, B., Gosczynski, G., 2009. Characterization and structural integrity tests of ex-service steam generator tubes at Ontario Power Generation. Nucl. Eng. Des. 239, 477–483.

Scarth, D.A., Kozluk, M.J., Cartar, E.E., Mirzai, M., Maruska, C., Nickerson, J.H., Graham, D.B., 1998. CANDU steam generator fitness-for-service guidelines. In: Proceedings of the 3rd International Conference on Steam Generators and Heat Exchangers, Canadian Nuclear Society, pp. 149–162.

Standard Technical Specifications, n.d. Revision 4. http://www.nrc.gov/reactors/operating/licensing/techspecs/current-approved-sts.html.

Steam Generator Progress Report, 2000. Revision 15, Electric Power Research Institute (EPRI), Palo Alto, CA: 2000, 1000805.

Technical Specification Task Force (TSTF) Traveler—449, 2005. Revision 4, Steam Generator Tube Integrity, April 14, 2005 (NRC ADAMS Accession No. ML051090200).

U.S. Nuclear Regulatory Commission, 1998a. Steam Generator Tube Integrity, Draft Regulatory Guide, DG-1074, December 1998. (NRC ADAMS Accession No. ML003739223) Issued for public comment in Federal Resister, vol. 64, p. 3138, dated January 20, 1999.

U.S. Nuclear Regulatory Commission, 1998b. Risk Assessment of Severe Accident-Induced Steam Generator Tube Rupture. NUREG-1570, March 1998.

U.S. Nuclear Regulatory Commission, 2000. Event Reporting Guidelines 10 CFR 50.72 and 50.73. NUREG-1022, Revision 2, October 31, 2000.

U.S. Nuclear Regulatory Commission, 2006. Reactor Oversight Process, NUREG-1649, Revision 4, December 2006.

This page intentionally left blank

Index

Note: Page numbers followed by *f* indicate figures, *t* indicate tables and *np* indicate footnotes.

A

Acceptance Criteria Permitting Leakage, 544
Acceptance Criteria Prohibiting Leakage, 544
Accident leakage performance criteria, 533–534
Admiral Rickover, 12–13
Advanced Gas Reactor (AGR), 234
Advanced scale conditioning agent (ASCA), 394–395
Aeolipile, 5, 6*f*
All volatile treatment (AVT), 134
  high-AVT chemistry, 134–136, 135*t*
  water chemistry, 159*t*, 167, 334
American Society of Mechanical Engineers (ASME), 10
Ammonia and hydrazine only (High-AVT) chemistry, 134–136, 135*t*
Analyst Performance and Tracking System (APTS), 503–504
ANL. *See* Argonne National Laboratory (ANL)
ANO-2. *See* Arkansas Nuclear One Unit 2 (ANO-2)
Ansaldo, 56
Antivibration bars (AVB), 407–408, 423
APS-1, 13–14
Areva, 56, 161
AREVA Non-Exclusion Zone RANGER, 498–499, 498*f*
AREVA NP GmbH high-temperature process, 358–360, 362*f*
Argonne National Laboratory (ANL), 440, 443, 445*f*
Arkansas Nuclear One Unit 2 (ANO-2), 258–259, 385
ASCA. *See* Advanced scale conditioning agent (ASCA)
Assessment of condition causing leakage (ACCL), 545
Atomic Energy of Canada Limited (AECL), 219
Atom splitting, 11–15
Auxiliary feedwater (AFW), 18
Axial flaws
  multiple, 448–452, 449*f*, 453*f*
  PTW crack, 443–445, 444*f*, 456–458
  single, 440–445, 455–458
  throughwall cracks, 440–442, 441–442*f*, 456

B

Babcock Power, 57
Babcock & Wilcox, 57
Battelle-Pacific Northwest Laboratory, 443
Blake-Kozeny equation, 277–278
Blow down (BD) efficiency
  calculation, 255–256
  DMA effect on, 257
  filming amines, 261
  fouling rate and, 254–256, 256*t*
  polymeric dispersants, 259
  RSGs, 254–255
  for soluble and suspended contaminants, 239
Blowdown system, 327, 330
Bobbin probes, 496, 499, 500*f*
  eddy current nondestructive examination, 459–460, 460*f*
  eddy current testing, 495–496
  limitations, 499
Boiler and Pressure Vessel Code (BPVC), 10
Boiling water reactor (BWR), 13–14, 233
BORAX, 13–14
Boring and Trepanning Association/Single-Tube System (BTA/STS), 62
Bright-field (BF) lighting, 339–340

Bruce Nuclear Generating Station, 221, 229–231, 243
Bruce A, 244–245
Bruce B Unit 7, 231–232*t*
Bruce B Unit 8, 229–231, 229–230*t*
BWXT Canada, 56, 69, 69*f*
BWXT PRIMA 3 Axis Robotic Arm, 498–499, 498*f*

C

Calder Hall I, 14
Calvert Cliffs, 385
Canadian regulatory requirement, 541–545
Canadian SG tube, 437
CANDU Owners Group, 258
CANDU steam generators, 24–26, 26*f*, 366, 382–383
boiling regimes for secondary fluid, 88*f*
FFs calculated for, 383
fitness-for-service guidelines, 543, 545
pressurized heavy water reactor, 221–223, 222*f*, 243, 244*t*
primary and secondary temperature profile, 98*f*
primary deposit layers, 382–383
primary-side cleaning, 396
secondary fluid flow path in, 84–85, 84–85*f*
SG divider plate leakage, 386–387
steam quality, 89*f*
tube deposits in, 383
Carbon and low-alloy steels (C&LAS), 193
environmentally assisted cracking, 205–206
flow-accelerated corrosion, 204–205
generalized corrosion, 204–205
localized corrosion, 205–206
Cation release rate, 193
Cecil system, 346–347, 347*f*
Central electricity generation stations, 10–11
Channel head, in-service inspection, 483–484, 483*f*, 484*t*
Chemical cleaning, 144–145, 351
deposit loadings removed by, 241*t*
dilute process, 361–363
EPRI/SGOG process, 351–354, 357–358, 357*f*
EPRI/SGOG solvents, 355–356
high-temperature iron step chemistry, 359–360
KWU/AREVA NP Gmbh process, 358–359, 359*f*
off-line cleaning, 351, 352*f*
on-line cleaning, 351
operations, 246–249, 248*t*
results of, 262
solvent chemistries, 354–355
water lancing and, 242, 247–249
ChemSolv, 292–294, 292*np*, 294*t*
Chicago Pile Experiment, 12
Circulation ratio (CR), 86, 324
Circumferential crack, 445–448
PTW, 446–448
throughwall, 445–446
unstable burst, 445–446
C&LAS. *See* Carbon and low-alloy steels (C&LAS)
Cleaning technique, PWR SGs, 351
advanced in-bundle water jet cleaning, 346–348, 347–349*f*
EPRI/SGOG process, 351–354, 357–358, 357*f*
EPRI/SGOG solvents, 355–356
full bundle, 348
high-temperature iron step chemistry, 359–360
HVBF, 349–350
KWU/AREVA NP Gmbh process, 358–359, 359*f*
off-line cleaning, 351, 352*f*
on-line cleaning, 351
pressure pulse cleaning, 349
solvent chemistries, 354–355
TTS water jet lancing, 345–346, 345–346*f*
UEC, 350–351, 350*f*
waste processing, 362–363
water slap cleaning, 349
Cockerill, 56
CODE process, 363
Combustion engineering (CE), 46, 57, 155–159
Commercial nuclear power, 13–14
Computational fluid dynamics (CFD) model, 418–419
Concentration processes, in flow-restricted regions, 274–282, 275*t*, 277*f*
Condensate extraction pump (CEP), 229–231

Condensate polishers (CPs), 327, 329
Condensate polishing system (CPS), 136
Condition monitoring assessment (CMA), 517–518, 519*f*, 534–535, 545
Condition monitoring (CM), SIPC, 437–438
Connors equation, 415, 420, 425
Contact modeling, 424
Cooper, Peter, 8
Copper alloys, 223, 233–234, 262
Copper solvent, 356
CoreStar OMNI-200-TIP, 497, 497*f*
Corner effect, 480–481, 481–482*f*
Corrosion films, on SG tube, 302–303, 316
Corrosion product transport
  anisokinetic sampling, 237–238
  vs. feedwater chemistry, 235–236*t*
  measurements, 242
  mitigation, 233–237
  Mossbauer analyses, 225
  origin, 221–227
  phase composition of, 230*t*, 232*t*
  PLGS, 223–225, 224*t*, 228–231, 228*t*, 237
  sampling systems, 237–238
  during start-up, 228–233
Coupled environment boiling crevice model (CEBCM), 281–282
Crack-tip opening displacement (CTOD) model, 440–442, 442*f*
Creep rupture model, 454, 455*f*
Crevice chemistry, 273–274
  calculation of, 292–293
  ChemSolv, 292–294, 292*np*, 294*t*
  by direct measurement, 296–299
  inferring from experimental/operating data, 299–303
  MULTEQ, 292*np*, 294–296
  pH calculation, 309–310
  using deterministic models, 291–296
Crevice concentration model, 281–282, 284–285, 287
Crevice solvent, 356
Crud burst, 228–229
Crystal River-3 nuclear power station, 244–245, 290–291
CTOD model. *See* Crack-tip opening displacement (CTOD) model

D

Damping, 408
Darcy's law, 278
Dark-field (DF) lighting, 339–340
Data analysis process
  hideout return, 307–310
  SG inspection systems, 503–504
Data management, SG inspection systems, 504–505
Data Quality Verification (DQV), 503, 505
Degradation modes, 495–496, 505–506
Denting
  Alloy 600MA and Alloy 600SR tubing, 172
  Alloy 800NG tubing, 172
  consequences, 166–167
  corrosion fatigue, 174–176
  horizontal steam generators with stabilized stainless steel tubing, 173–174
  IGA (*see* Intergranular attack (IGA))
  locations, 165, 202
  materials and design features, 166
  pitting, 168–169
  primary side corrosion, 177
  secondary side corrosion, 177–178
  secondary side fatigue, 174–176
  secondary side IGA/SCC, 173–174
  SG tube bundle, 201–203
  steam generators affected by, 166–167
  at tube support plate, 165*f*
  vertical steam generators with Alloy 600TT tubing, 172–173
  wastage occurrences, 167–168
  wear in horizontal steam generators, 176–177
  wear in vertical steam generators, 176
Deposit minimization treatment (DMT), 395
Design-basis accidents (DBAs), 526
Deterministic models, crevice chemistry using, 291–296
Dimethylamine (DMA), 137–138, 257
Dispersant injection, 145–146
Dissolved hydrogen (DH), 190
Distance-amplitude correction (DAC), 474–476
Divider plates
  channel head and, 483
  leakage, 89–90, 386–387

DMT. *See* Deposit minimization treatment (DMT)
Dodecylamine (DDA), 261
Doosan/Doosan Babcock, 55
DQV. *See* Data Quality Verification (DQV)
Drum shell, 64–65, 66*f*

E

Eddy current testing (ECT), 117, 117*f*
  bobbin probes, 495–496, 499, 500*f*
  instruments, 497, 502, 504
  nondestructive examination, 459–461, 459–460*f*
  tube inspections, SG, 496–502
Edison, Thomas, 10–11
EDS. *See* Energy dispersive spectroscopy (EDS)
Electricite de France (EdF), 245
Electric Power Research Institute (EPRI), 219, 260, 316
  ANL simulation and, 453–454, 454*f*
  database, 27–31
  flaw model, 444–445, 445*f*
  hideout return, 299–300, 304
  integrity assessment guidelines, 513
  observed *vs*. predicted failure temperatures, 455*f*
  weakest link model, 463
Electrochemical corrosion potential (ECP), 201, 219
Electro-discharge machining (EDM), 455–458
  PTW axial, 443, 444*f*
  unstable burst, 440
Energy dispersive spectroscopy (EDS), 342
Energy dispersive X-ray (EDX) analysis, 290–291
ENSA, 56
Environmentally assisted cracking (EAC), 205–206
EPRI-Steam Generator Owners Group (EPRI/SGOG) process, 351–354
  application, 357–358
  copper solvent, 356
  corrosion allowances, 353
  corrosion monitoring, 353–354
  crevice solvent, 356
  deposit characterization/loading estimates, 354
  magnetite solvent, 355
  passivation solvent, 356
  simplified P&ID for, 357*f*
Equivalent rectangular crack (ERC) method, 459–465
  approximation, 462–465, 463*f*
  eddy current nondestructive examination, 459–461, 459–460*f*
  fractography of SCC, 461–462, 462*f*
  ODSCC, 463–464, 464–465*f*
  PWSCC, U-bend with, 465
Ethanolamine (ETA), 136–138
Euler-Bernoulli beam, 406–407
Examination Technique Specification Sheets (ETSSs), 504

F

FAC. *See* Flow-accelerated corrosion (FAC)
FEA. *See* Finite-element analysis (FEA)
Feedwater distribution system, 116
Feedwater (FW) heaters, 216–217
  Bruce B Unit 7, 231–233, 231–232*t*
  Bruce B Unit 8, 229–231, 229–230*t*
  copper-bearing alloys in, 233–234
  corrosion products removed from, 226, 228–229
  designs of, 221–223
  FAC, 234
  PHWRs, 223–225
  PWRs, 223–225
FEI. *See* Fluidelastic instability (FEI)
FF. *See* Fouling factor (FF)
Film-forming amines, 146–147, 146*f*
Filming amines, 260–262
Finite-element analysis (FEA)
  CTOD model, 441–442
  elastic-plastic nonlinear, 448
  PTW axial notch, 456–457
Fitness-for-service assessment
  accident-induced leakage performance criteria, 516
  ASME Section III, 521–522, 522*t*
  condition monitoring assessment, 517–518, 519*f*
  degradation assessment, 513–514
  deterministic modeling, 520–521

H* criterion, 512
MTFS, 512
ODSCC, voltage based criteria for, 513
operational assessment, 518–520
operational leakage criteria, 515–516
P* and F* criteria, 512
performance criteria, 514–522
probabilistic methods, 521
PWSCC, length criteria, 512
repair criteria, 511–513
requirements, 511
statistical models, 521
structural integrity models, 520–522
structural integrity performance criteria, 515
FIV. *See* Flow-induced vibration (FIV)
Flat-bar supports, 423
Flow-accelerated corrosion (FAC), 134, 221, 223*np*
carbon steel, 233–234, 243
C&LAS, 204–205
pressure shell, 477
in steam cycle, 260–261
Flow cell model, 426–429, 426*f*
Flow characteristics, 405–406
Flow-induced vibration (FIV), 221, 366–367
challenges, 430–431
design guidelines, 417–418
excitation mechanisms, 408–420
flow characteristics, 405–406
tube bundle integrity, 421–429
tube vibration characteristics, 406–408
U-bend tube array, 406*f*
Flow-restricted regions
chemistry environment, 291–303
ChemSolv, 292–294, 292*np*, 294*t*
concentration processes, 274–282, 275*t*, 277*f*
hideout and hideout return, 274–291
MULTEQ, 292*np*, 294–296
thermal hydraulic and chemical concentration process in, 275*t*
Flow stress model, 454, 455*f*
Flow velocity-dependent damping, 408
Fluidelastic instability (FEI), 408–409, 413–420
modeling, 425–429
two-phase FEI, 419–420
using flow-cell model, 426*f*
Fouled crevice, 282–287, 283–285*f*
Fouling
alternative amines, 257, 258*f*
and BD efficiency, 254–256, 256*t*
deposit loading and distribution, 239–240, 241*t*
effect on SG performance degradation, 218–221
filming amines, 260–262
of horizontal SGs, 249, 249*t*
polymeric dispersants, 258–260
sludge collector process, 261–262
tube bundle, 240–243, 244*t*, 250–252
tubesheet, 246–249, 246*t*, 248*t*, 254
tube-support plate, 220–221, 243–245, 253–254, 253*f*
Fouling factor (FF), 367*np*
advantages, 368–369
calculated for CANDU units, 383
drawbacks/cautions, 369–370
historical changes and trends, 370–372, 371–372*f*
idealized thermal resistance curve, 373–375, 374*f*
industry application, 368–369, 373, 377, 377–378*f*
postoutage transient, 375–377, 376*f*, 389–390
recirculating SGs, 370–372, 371–372*f*
validation method, 390–392
Fractography, 461–462, 462*f*
Fretting wear, 421–424
Full bundle mechanical cleaning, 348
FW heaters. *See* Feedwater (FW) heaters

G

General Electric, 14
Gentilly-2 Nuclear Generating Station, 220–221, 237, 240, 242–243, 245
Grover Shoe Factory, 10
Gundrilling, 62

H

Hard chemical cleaning (HCC), 391, 393–394
Heated crevices, 274–275
carbon-fiber packed, 280, 283–284, 284*f*
crevice chemistry, 298–299

Heated crevices *(Continued)*
deterministic equilibrium models, 299
facility, 298–299
hideout and hideout return, 283*f*
under nucleate boiling, 284–285*f*
packed with diamond dust, 287
sodium accumulation, 285–286
Heat-transfer fouling, 365–367
advantages, 368–369
baseline clean performance level, 373
candidate methods, 367–368
drawbacks/cautions, 369–370
historical changes and trends, 370–372, 371–372*f*
idealized thermal resistance curve, 373–375, 374*f*
industry application, 368–369, 373, 377, 377–378*f*
postoutage transient, 375–377, 376*f*, 389–390
Heavy water (D_2O), 91
Helium test, SGs, 486–487, 486*f*
Hematite, 225–227, 233, 256*t*
Heron of Alexandria, 5–7
Hideout process, 219, 273
flow-restricted regions, 273–291
fouled crevice, 282–287, 283–285*f*
molar ratio index, 299–301
sludge pile and tube deposit, 287–291, 288*f*, 289*t*
species analyzed in, 305, 305*t*
Hideout return, 273
calculation methodology, 307–308
of contaminants, 308
data evaluation and analysis, 307–310
flow-restricted regions, 273–291
fouled crevice, 282–287, 283–285*f*
general procedure for performing, 305
maximum concentrations observed during, 311*t*
objective of, 303–304
rationale for performing, 304
samples, 305–307, 307*t*
sludge pile and tube deposit, 287–291, 288*f*, 289*t*
species analyzed in, 305, 305*t*
working within plant shutdown procedures, 304–305
Hideout Return Indicator (HRI), 301
High-AVT chemistry. *See* Ammonia and hydrazine only (High-AVT) chemistry
High volume bundle flushes (HVBF), 349–350
Homogeneous equilibrium model (HEM), 420
Horizontal steam generator (SG), 217–218, 249, 249*t*
Hydrostatic pressure test, 487–488

I

Idaho National Engineering Laboratory (INEL), 453–454, 454–455*f*
IGA. *See* Intergranular attack (IGA)
Image analysis, 339
IMGB company, 56
IMPSA company, 56
In-bundle water jet cleaning, 346–348, 347–349*f*
Inductively coupled plasma (ICP), 341–342
Industrial Revolution, 6–7
INEL. *See* Idaho National Engineering Laboratory (INEL)
Inner-bundle lancing, 144
In-service inspections (ISIs), 459–461, 472
channel head inspection, 483–484, 483*f*, 484*t*
European qualification methodology, 473
maintenance, 489
nondestructive techniques, 472
performances, 473
qualification methodology, 472–473
small nozzle inspection, 482–483
techniques, 472–473
tube bundle remote visual inspection, 477–478, 479*f*
ultrasonic pressure shell thickness measurement, 477, 477*f*
upper internal visual inspection, 478–479, 480*f*
welds inspection, 474–476, 475*f*, 475*t*, 480–481, 481*f*
In situ tube hydrostatic pressure test, 488
Inspection systems, 495
advanced and automatic analysis techniques, 505–506
bobbin probes, 499, 500*f*
CoreStar OMNI-200-TIP, 497, 497*f*
data analysis process, 503–504

data management, 504–505
equipment technology, 497
historical perspective, 495–496
independent analysts, 503
Mitsubishi Intelligent probe, 502, 502*f*
motorized rotating pancake coils probe, 499–501
national nuclear regulators, 506
nonentry manipulators, 498–499, 498*f*
plus point probes, 499–501
probe manipulators, 498–499
requirements and scope, 506–507
resolution analyst, 503
rotating probes, 500*f*, 501
technique qualification, 504
T/R array probes, 501–502
ultrasonic testing probes, 502
X-Probe, 501–502, 501*f*
Zetec MIZ-80iD system, 497, 497*f*
Intergranular attack (IGA), 295, 301
Alloy 600, 196–197*f*
Alloy 800NG tubes, 171
Alloy 600SR tube, 170*f*
at French plants, 301
new steam generators, 171
operating experience, 194–199
OTSGs, 170
PHWR Alloy 600 steam generators, 171
state-of-the-art, 199–201
Intergranular stress corrosion cracking (IGSCC), 170–171, 436–437
ISIs. *See* In-service inspections (ISIs)

K

Kinetic limits, 276
Korean recirculating steam generator, 21*f*
Kurihara model, 447
KWU/AREVA NP Gmbh process, 358–359, 359*f*

L

Larson and Toubro, 56
Leak test technique, helium, 486–487, 486*f*
The Leaver-Weaver model, 416–417
Lepidocrocite, 225–227, 233
Ligament rupture pressure, 438–439
ERC, 462–464, 463*f*
inter-crack axial, 448
observed *vs*. predicted, 444*f*, 451*f*
PTW flaws, 456–457
surface appearance of notches, 439*f*
Live steam, 325–326
Log-mean temperature difference (LMTD), 369
Loss-of-coolant accident (LOCA) rarefaction waves, 532
Low potential stress corrosion cracking (LPSCC). *See* Primary water stress corrosion cracking (PWSCC)

M

Macroscopic mass-balance model, 280
Magnetite
BD efficiency, 255–256, 256*t*
in corrosion product, 225, 225*t*, 233
deposit profiles of, 243
fouling rate of, 261
preparation, 226–227
solvents, 355
MAN company, 56
Manhattan Project, 11–13
Mass damping parameter (MDP), 417–418
Maximum tolerable flaw size (MTFS), 512, 544
McGuire 2 SGs, 385–386
Mechanical cleaning, 144
advanced in-bundle water jet cleaning, 346–348, 347–349*f*
full bundle, 348
HVBF, 349–350
pressure pulse cleaning, 349
thermal performance, 395
TTS water jet lancing, 345–346, 345–346*f*
UEC, 350–351, 350*f*
water slap cleaning, 349
Methyl-propanol-amine (MPA), 137–138
Mill-annealed Alloy 600, 156, 161–162, 299, 301
Mitsubishi Heavy Industries (MHI), 56
Mitsubishi Intelligent probe, 502, 502*f*
Moisture separator drain (MSD), 223–225, 233–237
Moisture separator reheater (MSR), 223, 228–229, 234, 257
Molar ratio control (MRC), 299–301
Molar ratio index (MRI), 299–301

Morpholine, 136–138
Mossbauer spectroscopy, 229–231
Motorized rotating pancake coils (MRPCs), 459–460, 460*f*, 499–501, 507
Mount Vernon, 57
MULTEQ code, 292*np*, 294–296, 299
Multiple axial flaws, 448–452
  failure maps, 450–452, 453*f*
  failure models and validating tests, 448–450, 449–450*f*

N

New Production Reactor, 156
Nondestructive examination (NDE), 496, 512–514
  eddy current testing, 459–461, 460*f*
  ODSCC, 463–464, 464–465*f*
  role of, 506
Nondestructive testing (NDT)
  in-service inspection, 473
  technology, 489
Nonwetting fluid, 278–279
Normal work rate, 423
Nuclear Energy Institute (NEI) 97-06, 526–527
Nuclear industry, 15, 255, 258
Nuclear Nonproliferation Treaty (NPT), 14
Nuclear power
  commercial, 13–14
  emergence, 11–15
Nuclear Power Demonstration (NPD) reactor, 14
Nuclear-powered submarines, 12–13
Nuclear power plants (NPPs), 3–4
Nuclear reaction, energy from, 12
Nuclear steam generator design
  ASME code, 50
  boiling film temperature, 39, 40*f*
  bolted closures, 50–51
  broached plate, 47, 47*f*
  CANDU steam generators, 36, 46–47
  circulation, 41–46, 45–46*f*
  feedwater inlet, 49–50
  fluid-elastic instability, 48
  hydrostatic pressure, 44
  integral preheaters, 48–49, 49*f*
  lattice grid, 47, 47*f*
  layout, 40–41, 41*f*
  mass flow, 42
  natural circulation, 42
  pressure boundary design, 50–52, 51–52*f*
  recirculating steam generators, 41
  Russian reactors, 41
  Siemens designs, 48–49
  single-phase flow, 42
  sizes in PWR and CANDU plants, 53*f*
  specifications, 35
  steam-water separators, 47–48
  stress analysis, 50
  temperature diagram, 38*f*
  tube bundle, 36–40
  tube supports, 42–43, 46–49, 47*f*, 220–221, 220*f*
  turbulent buffeting, 48
  two-phase flow, 39, 47
  U-bend supports, 48–49
  void fraction, 42
  vortex shedding, 48
  wrapper, 41–42
Nucleate boiling, 127–128, 274, 280–281, 283, 284–285*f*

O

Octadecylamine (ODA), 260–261
ODSCC. *See* Outer Diameter Stress Corrosion Cracking (ODSCC)
Off-line cleaning, 351, 352*f*
Once-through steam generator (OTSG), 4, 216–217, 218*f*, 220–221, 243–244, 290, 326*f*
  with Alloy 600SR tubing, 161–162
  Crystal River plant, 244
  flow-affected phenomena, 103
  flow paths, 101
  heat transfer, 101–103
  IGA affecting, 170
  primary and secondary fluid flow paths, 102*f*
  RSGs *vs.*, 324–327
  temperature profile, 103*f*
  theoretical approach to solving, 103–104
On-line cleaning, 351
On-line corrosion product, 329*f*
Operational assessment (OA), 437–438, 518–520, 545
Operational leakage performance criteria, 534

Optical microscopy, 338–340
OTSG. *See* Once-through steam generator (OTSG)
Outer diameter stress corrosion cracking (ODSCC), 436–437
  in alloy 600, 196–197*f*
  in Alloy 690TT tubes, 437
  ERC method, 463–464, 464–465*f*
  operating experience, 194–199
  state-of-the-art, 199–201
  U-bends, 437, 454–455
Oxygenated water chemistry, 140–142
Oxygen dosing, 139–142

P

Papin, Denis, 7–8
Part-throughwall (PTW) crack
  axial flaw, 443–445, 444*f*, 456–458
  circumferential flaws, 446–448
  internal pressure, tube failure process, 438–439
  stability criterion for, 444
Passivation solvent, 356
Patent Law, 8
Pearl Street Station, 10–11
PHWR. *See* Pressurized heavy water reactor (PHWR)
Pitch flow velocity, 405
Pitting
  horizontal VVER steam generators, 169
  vertical PHWR steam generators, 169
  vertical PWR steam generators, 168
PLGS. *See* Point Lepreau Nuclear Generating Station (PLGS)
Plus point probes, 499–501, 507
POD. *See* Probability of detection (POD)
Point Lepreau Nuclear Generating Station (PLGS), 223–225, 224*t*, 228–231, 228*t*, 237, 240, 242–243, 255–256
Polyacrylic acid (PAA) dispersants, 258–260
Polymeric dispersants, 258–260, 396
Pourbaix diagrams, 302
Power Reactor Information System (PRIS), 3–4, 17*t*
Power spectral density (PSD), 410–411, 411–412*t*, 412*f*
PPC. *See* Pressure pulse cleaning (PPC)
Preheaters
  axial flow preheaters, 91–92, 92*f*
  crossflow preheaters, 93, 93*f*
Preheater thermal plate leakage, 90
Preservice inspection, 474
Pressure boundary design, nuclear SG, 50–52, 51–52*f*
Pressure pulse cleaning (PPC), 349
Pressurized heavy water reactor (PHWR), 4, 159–161
  Alloy 600 steam generators, IGA affecting, 171
  CANDU, 24–26, 26*f*, 221–223, 222*f*, 243
  case studies, 310–312, 312–313*f*
  pitting in, 169
  PWRs and, 223–225, 225*t*
Pressurized water reactor (PWR), 4, 134, 221–223, 222*np*, 238, 323, 365–366
  advanced in-bundle water jet cleaning, 346–348, 347–349*f*
  Alloy 600MA tubes, 156
  Alloy 600TT tubes, 157
  Alloy 690TT tubes, 158
  Alloy 600 tubes, 436–437
  AVT water chemistry, 159*t*
  boiling regimes for secondary fluid, 87*f*
  B&W advanced series, 22*f*
  and BWR, 233
  calcium and sulfate return, 315*f*
  case studies, 313–314, 314–315*f*
  chemical cleaning, 351
  consequences of deposit accumulation, 334, 335*f*
  corrosion modes, 157*f*, 158–159*t*
  deposit formation, 330
  deposit precursor source term, 324*f*, 327–329, 328*t*
  EPRI/SGOG process, 351–354, 357–358, 357*f*
  EPRI/SGOG solvents, 355–356
  full bundle, 348
  high-temperature iron step chemistry, 359–360
  HVBF, 349–350
  KWU/AREVA NP Gmbh process, 358–359, 359*f*
  of KWU/Siemens/AREVA type with Alloy 800NG tubing, 161
  during main steam line break, 452, 453*f*

Pressurized water reactor (PWR) *(Continued)*
mechanical cleaning, 345–351
mild cleaning, 360–362, 360*f*
nonpreheat unit, 155–156
during normal operation, 440–452
off-line cleaning, 351, 352*f*
once-through steam generators, 20–22
on-line cleaning, 351
organics and gases, 334
OTSGs with Alloy 600SR tubing, 161–162
particulate impurities, 330–331, 332–334*f*
PHWR and, 223–225, 225*t*
pitting in, 168
during power operation, 225*t*
preheater, 155–156
pressure pulse cleaning, 349
primary fluid, 81–82, 82*f*
primary-side scale layers, 382–383
recirculating, 19*f*
RSGs *vs.* OTSGs, 324–327
secondary fluid, 83–86, 83*f*
secondary side deposits, 323, 334–344
soluble impurities, 332–334
solvent chemistries, 354–355
with stainless steel tubes, 156
TTS water jet lancing, 345–346, 345–346*f*
tube deposit thermal resistance, 379, 379*f*
UEC, 350–351, 350*f*
vertical steam generators, 16–20, 155–159
VVER, 23–24, 23*f*, 162
waste processing, 362–363
water slap cleaning, 349
Western-style, 324
Primary head sub-assembly, 62–64, 63*f*
Primary water stress corrosion cracking (PWSCC), 21–22, 156, 160*f*, 436–437
in Alloy 690TT tubes, 437
component-scale modeling, 191–192
conditions required for occurrence, 164
consequences, 164–165
damage modeling, 189–190
engineering basic tools, 190
internal oxidation model, 190
partition plates, 185–186
safety nozzles welds, 188–189
SG tube bundles in alloy 600, 184–185
shot-peening process, 188–189
steam generator bowl drains, 186–187
steam generators affected and locations affected by, 163–164
U-bends with, 437, 454–455, 465
Probability of detection (POD), 119, 502, 504, 506
Probe-drive technology, 496
PWR. *See* Pressurized water reactor (PWR)

Q

Qualified Data Analyst (QDA) testing program, 503–504
Quasistatic model, 413
Quasisteady flow equation, 425–426
Quasisteady model, 415–416

R

Reactor inlet header temperature (RIHT), 365, 386–387, 392
Recirculating steam generator (RSG), 216, 219–221, 240, 325*f*, 366, 384
at Bruce A plant, 244
design and manufacturing, evolution in, 488–489
fluid temperature variations in, 368*f*
fouling behavior, 252, 255–256
fouling factor, 370–372, 371–372*f*
with integral preheater, 217*f*
vs. OTSGs, 324–327
separation equipment, 384–385
Recirculation ratio (RR), 86
Regulatory requirements and considerations, for nuclear SGs, 525–541
accident leakage performance criteria, 533–534
in Canada, 541–545
condition monitoring assessment, 534–535
inservice inspection, 536–539
NRC regulations, 525–526
operational leakage performance criteria, 534
primary-to-secondary leakage, monitoring, 539
steam generator performance criteria, 529–534
steam generator tube integrity, 539–541
structural integrity performance criteria, 529–533

TS (*see* Technical specifications (TS))
tube-plugging criteria, 535–536
Remote visual inspection, 477–478, 479*f*
The Requirements of a Perfect Steam Boiler (Babcock and Wilcox), 9
RIHT. *See* Reactor inlet header temperature (RIHT)
RSG. *See* Recirculating steam generator (RSG)
Rutherford, Ernest, 11–12

S

Savery, Thomas, 5–6
Scanning electron microscopy (SEM), 342, 343*f*
SCC. *See* Stress corrosion cracking (SCC)
SCOPUS database, 4, 27–28, 29*f*
Secondary shell assembly, 64, 65*f*
Secondary side deposits, PWR SGs
characterization, 334–335
EDS, 342
formation, 323
ICP analysis, 341–342
management, 344
optical microscopy and image analysis, 338–340, 340–341*f*
reasons for, 352
RSGs *vs*. OTSGs, 324–327
sample collection, 335–343, 336*f*
SEM, 342, 343*f*
visual observations, 337, 338–339*f*
XRD, 342–343, 344*f*
SGHWR. *See* Steam Generating Heavy Water Reactor (SGHWR)
SGTR. *See* Steam generator tube rupture (SGTR)
Shanghai Nuclear Electric power Co., 55
Shippingport, 156
Single axial flaws, 440–445, 441*f*
U-bends failure, models for, 455–458
Single circumferential flaws, 445–448
SIPC. *See* Structural integrity performance criteria (SIPC)
Sludge collector process, 261–262
Sludge lancing, 345–346
Sludge pile, 273, 287–291, 288*f*, 289*t*
Small nozzle, in-service inspection, 482–483
Soft chemical cleaning, 360*f*, 394–395
ASCA, 394–395
DMT, 395
long-term effects, 395
Solubility-superheat ratio, 315
Spanish Almaraz Unit 2, 437
Spanish SG tube, 437
Steam boiler explosions, 9–10
Steam engine, 5–8
Steam Generating Heavy Water Reactor (SGHWR), 238, 238*np*
Steam generators (SGs), 3–4
accident leakage performance criteria, 533–534
APR 1400, 20
bowl drains, 186–187
circulation, thermalhydraulics for (*see* Thermalhydraulics, for steam generators circulation)
corrosion products release, 192–193
drum/separator assembly, 74*f*
drum shell, 64–65, 66*f*
features of, 16–26
filet and flush seal welds, 72, 72*f*
final assembly and preparation for shipment, 73–77, 75*f*
forgings, 78
history of, 5–11
inspection and testing, 78–79
Korean recirculating steam generator, 21*f*
literature survey, 27–31
magnetic particle, 78–79
major assemblies, 68–73
manufacturers, 55–58
material purchasing, 59–60
“no yield” criterion, 530–531
objectives, 57
operational leakage performance criteria, 534
patents, 29–31, 30*f*
plate, 78
pressure boundary welds, 78–79
pressure vessel, 58
primary head sub-assembly, 62–64, 63*f*
QA requirements, 57–58
radiographic examination, 73
RT examination, 78–79, 79*f*
safety-critical roles, 215
“safety factor of three” criterion, 530–531

Steam generators (SGs) *(Continued)*
scheduling, 58–60
secondary shell assembly, 64
separator sub-assembly, 66–67, 67*f*
shipment, 79–80
stress reliefs, 77–78
structural integrity performance criteria, 529–533
tubesheet/thick shell assembly, 60–62, 61*f*
tube supports and shrouds, 67, 68*f*
tubing, 71*f*, 78
U-bend support, 72
welding process, 60–64, 72–73, 78–79
Steam generator tube rupture (SGTR), 438
Steam Generator Tube Testing Project (SGTTP), 544–545
Steam locomotive, 8–9
Steam-water cycle chemistry
alternative amines, 136–138
ammonia and hydrazine only, 134–136, 135*t*
calculated iron solubility, 139*f*
chemical cleaning, 144–145
condensate polishing system, 136
conservation specifications, 143*f*
control by additives, 145–147
copper-alloy plants, 130–131
degradation mechanism, 127–130
denting, 128
dispersant injection, 145–146
dissociat constants, 133*f*
distribution coefficients, 133*f*
Fe ion corrosion, 131*f*
film-forming amines, 146–147, 146*f*
flow-accelerated corrosion, 131, 132*f*
guidelines, 149
high-pressure feedwater heater, 140, 140*f*
historical evolution, 134
long-term feedwater iron concentration, 136*f*
mechanical cleaning, 144
minimization of impurities, 147–149
NPP Isar Unit 2, 140, 141*f*
nucleate boiling site, 127–128, 128*f*
objective, 127
oxygen dosing, 139–142
oxygen injection, 140–142
pH-value, 130–133
plant layup and start-up, optimization, 142–143
quatrefoil tube support structure, 129*f*
reheater condensate, 140, 141*f*
removal, 143–145
SG clogging, 129, 130*f*
SG fouling, 129
surveillance, 149–150
transport, 142*f*
tube denting mechanism, 147*f*
VGB guideline, 149
Steam-water separation, 90
Stephenson, George, 8
Stevens, John Cox, 8
Stiffness-controlled instability, 425
Stress corrosion cracking (SCC)
fractography of, 461–462, 462*f*
inspection systems, steam generator, 496, 499, 501–502
surface appearance, 459*f*
typical, 452*f*
Stress reliefs, 77–78
Strouhal periodicity, 408–410
Structural damping, 408
Structural integrity, 520–522
condition monitoring, 437–438
multiple axial flaws, 448–452, 449*f*, 453*f*
operation assessment, 437–438
prediction models, 438–454
severe accident transients, 452–454
single axial flaws, 440–445, 441*f*, 455–458
single circumferential flaws, 445–448
U-bends with flaws, 454–458, 457–458*f*
Structural integrity performance criteria (SIPC), 437–438, 506–507, 529–533
Surface-active agents, 252, 258–262
filming amines, 260–262
polymeric dispersants, 258–260

T

Technical specifications (TS), 526
alternate plugging criteria, 536
condition monitoring assessment, 534–535
conditions of, 527–528
evolution, 526–527
inservice inspection, 536–539

steam generator performance criteria, 529–534
steam generator program, 528–529
tube-plugging criteria, 535–536
Tesla, Nikola, 10–11
Thermal concentration process, 274–277
Thermalhydraulics, for steam generators circulation
axial flow preheaters, 91–92, 92*f*
carryover and carryunder, 91
cavitation erosion, 94
crossflow preheaters, 93, 93*f*
divider plate leakage, 89–90
fatigue, 95
flow-accelerated corrosion, 95–96
flow-induced vibrations, 95
fouling, 88–89
heat transfer, 86–90
high concentration rate, 94
high fouling rates, 93
preheater thermal plate leakage, 90
primary fluid and, 81–82, 91
secondary fluid and, 83–86
sludge accumulation on tubesheet, 94
steam-water separation, 90
theoretical approach to solving, 96–101
tube plugging, 90
water level oscillations, 94–95
Thermalhydraulics, OTSGs
flow-affected phenomena, 103
flow paths, 101
heat transfer, 101–103
primary and secondary fluid flow paths, 102*f*
temperature profile, 103*f*
theoretical approach to solving, 103–104
Thermally treated (TT) condition, 156–159
Thermal performance degradation, 219
broached tube support plate flow holes, 384–386
CANDU units, 386–387
clean performance level, 388
consequences loss, 392–393
definition, 365
hard chemical cleaning, 393–394
heat-transfer behavior (*see* Heat-transfer fouling)
idealized thermal resistance curve, 373–375, 374*f*
industry experience, 377, 377–378*f*
mechanical cleaning techniques, 395
objectives, 366
plant instrument measurement errors, 388–389
polymeric dispersant addition, 396
postoutage transients, 375–377, 376*f*, 389–390
preheater baffle plate fouling/flow distribution, 387
primary-side cleaning, 396
SG outlet nozzles/downstream piping, 385–386
soft chemical cleaning, 394–395
spatial distribution of fouling layers, 389, 390*f*
steam separation equipment, 384–385
tube deposit layers, 378–383, 379–381*f*
validation of FF method, 390–392
Thermal sleeve, welds inspection, 480–481, 481–482*f*
Thermodynamic limit, 280–281, 284–287
Thermophoresis, 238*np*
Throughwall (TW) rectangular cracks
axial flaws, 440–442, 441–442*f*, 456
circumferential flaws, 445–446
Time domain modeling, 424–429
Title 10 of the Code of Federal Regulations (10 CFR), 525
Top-of-tubesheet (TTS)
dot-mapped images, 343*f*
sludge pile patterns, 334*f*
water jet lancing, 345–346, 345–346*f*
Transmit/receive (T/R) array probes, 501–502
Trojan NPP, 302
Tube bundle
denting, 201–203
EAC, 205–206
fouling, 240–243, 244*t*, 250–252
integrity, estimation, 421–429
ODSCC/IGA, operating experience, 194–199
ODSCC/IGA, state-of-the-art, 199–201
wastage, 203–204
water tightness, 485–487
Tube deposits
in free span, 249
sludge pile on, 273, 287–291, 288*f*, 289*t*

Tube deposits *(Continued)*
spatial distribution, 389, 390*f*
thermal performance changes, 378–383, 379–381*f*
Tube fouling, 88–89
Tube plugging, 90, 535–536
Tubesheet fouling, 246–249, 246*t*, 248*t*, 254
Tubesheet lancing, 144
Tubesheet/thick shell assembly, 60–62, 61*f*
Tube structural integrity, 409–410
Tube/support interaction, 423–424
Tube support plates (TSPs), 18–19, 216–217
blockage rates, 245, 333*f*
broached-hole designs, 384
crevice, 285
deposit accumulation, 253–254, 333*f*
fouling, 220–221, 243–245, 253–254, 253*f*
"lips" protruding from, 244
remote visual inspection, 478, 479*f*
U-bend supports, 245
Tube vibration, 406–408
Turbulence excitation, 410–412
Turbulence modeling, 425
Two-phase FEI, 419–420

U

U-bends
with flaws, structural integrity, 454–458, 457–458*f*
outer diameter stress corrosion cracking, 437, 454–455
with PWSCC, 465
tube array, flow distribution, 406*f*
tube support plates, 245
Ultrasonic energy cleaning (UEC), 350–351, 350*f*
Ultrasonic testing (UT) probes, 502
Unstable burst
conventional model for, 456
CTOD model, 440–442, 442*f*
single axial flaws, 440
single circumferential crack, 445–446
tell-tale sign, 438–439
throughwall notch length and, 442*f*
Unsteady flow equation, 426
Unsteady flow model, 414–415
Upper bundle flushing, 144

V

Valves wide open (VWO), 392
Velocity ratio, 428
Vena contracta, 253
Viscous damping, 408
Visual inspection
tube bundle remote, 477–478, 479*f*
upper internal, 478–479, 480*f*
Vodo-Vodyanoj Energeticheskij Reaktor (VVER), 4, 23–24, 23*f*
pitting in, 169
with stabilized stainless steel tubes, 162
Void fraction, 111, 420

W

Wastage, SG tube bundle, 203–204
Water jet lancing
high-pressure, system configuration, 345*f*
in-bundle, 346–348, 347–349*f*
top-of-tubesheet, 345–346, 345–346*f*
Water lancing
and chemical cleaning, 242, 247–249
tubesheet deposit removed by, 240, 246–249, 246*t*, 248*t*
Water slap cleaning, 349
Water test, SGs, 485
Water tightness, tube bundle
helium test, 486–487, 486*f*
monitored during operation, 485
radioactivity measurement, 485
water test, 485
Watt, James, 5–7, 7*f*
Wear
fretting, 421–424
in horizontal steam generators, 176–177
long-term effects of, 176–177
in vertical steam generators, 176
Weibull method, 191
Welds inspection, 474–476, 476*f*
dead zone, 474–476
feedwater nozzle and thermal sleeve, 480–481, 481–482*f*
pressure shell, 474, 475*f*, 475*t*
steam outlet and flow restrictor, 480
UT oblique shear waves orientations, 476*f*
Westinghouse electric (WE), 155–159
Westinghouse ROSA III, 498–499, 498*f*

Wetted length, 280–281, 282*f*, 289
Wetting fluid, 278–279
Wick boiling, 279, 290–291
World Intellectual Property Organization's (WIPO) Patentscope database, 4
World Nuclear Association, 240
WWER steam generators
  blowdown, 115, 115*f*
  burst pressure, 118
  chemical composition, 107, 109*t*
  cold collector, 107, 110*f*
  cold feedwater flow, 116–117
  collector weld, 114*f*
  crack growth *vs*. time, 120*f*
  degradation, 107–113
  description, 107, 108*f*
  dissimilar shell, 114*f*
  ECT indication *vs*. real crack depth, 117*f*
  elastic and plastic deformation, 119*f*
  erosion-corrosion damage, 107–109
  feedwater distribution system, 116
  hazard function, 123*f*
  heat exchange tubes integrity, 117–124
  hot collector, 107, 110*f*
  impurities distribution, 114
  measurement, 112*f*
  modifications, 113–117
  parameters, 107, 108–109*t*
  POD curve, 119–120, 120*f*
  salt corner, 115
  sampling points, 116
  simplified model, 110*f*
  test results, 118*f*
  threaded holes bottom, 113*f*
  tube defects under support plates, 123*f*
  tubes damage, cumulative probability, 122*f*
  two-phase flow rate, 116–117

X

X-probe, 501–502, 501*f*, 507
X-ray diffraction (XRD), 342–343, 344*f*

Z

Zetec MIZ-80iD system, 497, 497*f*

This page intentionally left blank

WOODHEAD PUBLISHING SERIES IN ENERGY

Key features

- Includes case studies which demonstrate the most up-to-date technology and industry practices
- Analyses what can be learnt through operational experience
- Written by a team of expert contributors from a range of backgrounds including manufacturers, vendors and technical support organizations, as well as academics from research institutes and universities.

Steam Generators for Nuclear Power Plants examines all phases of the life cycle of nuclear steam generators (NSGs) and components which are essential for the efficient and safe operation of light water reactors (LWRs). Edited by Riznic and with contributions from various experts from different backgrounds, this book presents a comprehensive analysis of all phases of the nuclear steam generator life cycle, from the design, manufacturing, operation and maintenance, to fitness-for-service and long term operation. It also considers fundamental engineering aspects and phenomena, as well as very applied, practical content and direction which typically does not appear in the literature already available.

This book is an invaluable resource for students, academics, researchers and professionals involved in all phases of the NSG life cycle; from those working in and researching power generation and utilities operations, to technical service providers.

Jovica R Riznic, PhD., P.Eng., FASME, is a Technical Specialist with the Canadian Nuclear Safety Commission (CNSC), working on regulatory analysis and assessment of technical issues with operating nuclear power plants (NPP). He served CNSC on various position, including nuclear safety analysis and managing the CNSC Research and Support Program. He served as an adjunct professor/thesis advisor at the University of Waterloo, Mc Master, and Purdue Universities and currently is on faculty at Algonquin College in Ottawa in the School of Business and the Centre for Continuing and Online.

ELSEVIER
WP WOODHEAD PUBLISHING
An imprint of Elsevier
elsevier.com/books-and-journals

ISBN 978-0-08-100894-2
9 780081 008942